Inhibition of Protein-Nucleic Acid Interactions Mediated by Viral and Bacterial Proteins via Fragments and Peptides

Dissertation

Zur Erlangung des Grades des Doktors der Naturwissenschaften der Naturwissenschaftlich-Technischen Fakultät der Universität des Saarlandes

Vorgelegt von:

Dipl.-Chem. Valentin Jakob

Saarbrücken 2021

Tag des Kolloquiums:	3. August 2021
Dekan:	Prof. Dr. Jörn Erik Walter
Berichterstatter:	Prof. Dr. Rolf W. Hartmann Prof. Dr. Claus-Michael Lehr
Vorsitz:	Prof. Dr. Uli Kazmaier
Akad. Mitglied:	Dr. Charlotte Dahlem

Die vorliegende wissenschaftliche Arbeit entstand im Zeitraum Juli 2016 bis April 2021 unter Anleitung von Herrn Dr. Martin Empting und Univ.-Prof. Dr. Rolf W. Hartmann in der Fachrichtung Pharmazeutische und Medizinische Chemie der Naturwissenschaftlich-Technischen Fakultät der Universität des Saarlandes, sowie am Helmholtz-Institut für Pharmazeutische Forschung Saarland (HIPS) in der Abteilung Drug Design and Optimization (DDOP).

Acknowledgements

Gerne möchte ich mich ganz besonders bei Herrn **Dr. Martin Empting** für das Überlassen des interessanten Forschungsthemas bedanken. Insbesondere danke ich für die vielen angenehmen Diskussionen, welche sehr hilfreich waren und die Zeit, die er sich dabei gelassen hat.

Auch **Prof. Dr. Rolf W. Hartmann** möchte ich herzlich danken, dass ich die Möglichkeit bekam, in seiner Abteilung eine Doktorarbeit anzufertigen. Als Erstgutachter gab es einige sehr konstruktive Gespräche mit ihm.

Herrn **Prof. Dr. Claus-Michael Lehr** danke ich für die hilfreichen Momente als wissenschaftlicher Begleiter und die Übernahme des Zweitgutachtens.

Besonderer Dank geht an **Prof. Dr. Michael Hust** und **Saskia Helmsing** aus der Abteilung Biotechnologie der TU Braunschweig, welche mir ermöglicht haben, ein Hands-on Training in Phagen Display bei Ihnen zu machen. Auch aus der Ferne waren sie stehts eine große Unterstützung.

Ein weiterer Dank geht an **Prof. Dr. Uli Kazmaier** aus der Organische Chemie der Universität des Saarlandes für die interessante Zeit in seiner Graduiertenschule und der Möglichkeit in seinem Arbeitskreis einen Peptidsynthesizer zu benutzen. Insbesondere **Andreas Siebert**, der uns gezeigt hat, wie man mit dem Peptidsynthesizer arbeitet, möchte ich dafür danken.

Ausdrücklich möchte ich mich bei **allen Mitarbeitern** des gesamten Arbeitskreises, insbesondere bei meinen Laborkolleginnen und Kollegen **Ben Zoller**, **Yingwen Wu**, **Julia Rinkes** und **Aylin Berwanger** für die gute und angenehme Zusammenarbeit bedanken. **Dr. Philine Kirsch** danke ich ganz besonders für die unvergessliche Zeit – auch mit Bürohund Molly – und unserem gemeinsamen Erfolg im LANA-Projekt. **Dr. Andreas Kany** danke ich für die vielen kleinen aber nützlichen Tipps rund um die praktische und theoretische Arbeit.

An dieser Stelle möchte ich mich auch bei den **TA's** Simone Amann, Jeannine Jung, Dennis Jener und Selina Wolter bedanken, die im Labor stehts eine große Hilfe waren und nebenher noch für gute Laune gesorgt haben.

Ebenso möchte ich mich bei den **Sekretärinnen** Julia Mohr, Lisa Andre und Annette Herkströter für die Erledigung organisatorischer Aufgaben, welche im Forschungszeitraum angefallen sind, bedanken.

Unserer hauseigenen **IT-Abteilung** mit Michael Roth und Mark Caspari gebührt ein besonderer Dank für die schnelle Unterstützung in computertechnischen Aufgaben.

Auch Frank Jakob und Michael Zeuner aus dem **Facility Management** danke ich für die kontinuierliche Arbeit in der Warenannahme und hausmeisterlichen Tätigkeiten.

Ein herzliches Dankeschön geht außerdem an **meine Eltern**, welche mir meine Promotion ermöglicht und mich in all meinen Entscheidungen unterstützt haben. Auch bei meinem **Lebenspartner** möchte ich mich bedanken für die mentale Unterstützung und wertvolle Zeit neben der Arbeit.

Summary

Some infectious diseases can be still challenging for the entire population because sometimes no specific medication is available. One opportunity is addressing new target modalities to inhibit viral and bacterial proteins. Important approaches in this regard are protein-nucleic acid interactions, on which many pathogenic processes rely. Intervening in and inhibiting these interactions can be particularly challenging, as the targets as well as the interactions are often not sufficiently understood.

The latency-associated nuclear antigen (LANA) is the major factor in the latent persistence of the Kaposi's sarcoma-associated herpesvirus (KSHV). In this thesis, a simple method to express a LANA mutant is described. In addition, a functional fluorescence polarization assay was established to test inhibitors generated from a fragment-based approach for LANA-DNA interaction inhibition. Another target is the RNA-binding, post-transcriptional carbon storage regulator A (CsrA), which is highly conserved in many bacterial species. Using a self-designed peptide library, a cloning method and a phage display specialized for CsrA were successfully developed. This led to a first hit, a disulfide-cyclized heptapeptide as a highly potent CsrA-RNA inhibitor. Using fluorescence polarization assay, structure-activity relationships of this hit were further explored. Also, redox-stable triazole-bridged disulfide peptide mimetics, which can inhibit the CsrA-RNA interaction from various bacterial species, were generated.

Zusammenfassung

Einige Infektionskrankheiten stellen nach wie vor eine große Herausforderung für die gesamte Bevölkerung dar, weil oft keine gezielte Medikation verfügbar ist. Eine Chance besteht in der Adressierung neuer Targetmodalitäten zur Hemmung viraler und bakterieller Proteine. Wichtige Ansätze hierfür sind Protein-Nukleinsäure-Interaktionen, auf welchen zahlreichen krankmachende Prozessen beruhen. Besonders herausfordernd ist es, in diese Interaktionen einzugreifen und diese zu hemmen, da die Targets als auch die Interaktionen häufig nicht hinreichend erforscht sind.

Das latenz-assoziierte nukleäre Antigen (LANA) ist der Hauptfaktor für die latente Persistenz des Kaposi's Sarkom-assoziierten Herpesvirus (KSHV). In dieser Arbeit wird eine einfache Methode beschrieben, wie ein LANA-Mutant exprimiert werden kann. Außerdem wurde ein funktionaler Fluoreszenzpolarisations-Assay etabliert, mit welchem Inhibitoren, die aus einem Fragment-basierten Ansatz entstanden sind, auf LANA-DNA-Interaktions-Hemmung geprüft wurden. Ein weiteres Target ist der RNA-bindende, post-transkriptionelle *carbon storage regulator A* (CsrA), welcher hochkonserviert in vielen Bakterienspezies vorkommt. Mittels einer selbst designten Peptidbibliothek konnte erfolgreich eine Klonierungsmethode und ein auf CsrA spezialisiertes Phagen-Display entwickelt werden. Dies führte zu einem ersten Hit, einem disulfidzylisierten Heptapeptid als hochpotenter CsrA-RNA-Inhibitor. Mittels Fluoreszenzpolarisations-Assay wurden Struktur-Aktivitätsbeziehungen dieses Hits weiter vertieft. Auch redoxstabile Triazol-verbrückte Disulfid-Peptid-Mimetika, welche die CsrA-RNA-Interaktion verschiedener Bakterienspezies hemmen, wurden generiert.

Publications Included in this Thesis

Publication 1: Philine Kirsch, Valentin Jakob, Kevin Oberhausen, Saskia C. Stein, Ivano Cucarro, Thomas F. Schulz and Martin Empting; Fragment-Based Discovery of a Qualified Hit Targeting the Latency-Associated Nuclear Antigen of the Oncogenic Kaposi's Sarcoma-Associated Herpesvirus/Human Herpesvirus 8; **2019**, *J. Med. Chem, 62,* 3924-3939.

Publication 2: Philine Kirsch, Valentin Jakob, Walid A. M. Elgaher, Christine Walt, Kevin Oberhausen, Thomas F. Schulz and Martin Empting; Discovery of Novel Latency-Associated Nuclear Antigen Inhibitors as Antiviral Agents Against Kaposi's Sarcoma-Associated Herpesvirus; **2020**, *ACS Chem. Biol., 15,* 388-395 **[shared first authorship / P.K. and V.J. contributed equally]**.

Publication 3: Philine Kirsch, Saskia C. Stein, Aylin Berwanger, Julia Rinkes, Valentin Jakob, Thomas F. Schulz and Martin Empting; Hit-to-Lead Optimization of a Latency-associated Nuclear Antigen Inhibitor against Kaposi's Sarcoma-associated Herpesvirus Infections; **2020**, *Eur. J. Med. Chem., 202*, 112525.

Publication 4: Valentin Jakob, Saskia Helmsing, Michael Hust and Martin Empting in *Genotype Phenotype Coupling*, Springer US, New York, NY, **2020**, pp. 95–113. Restriction-Free Construction of a Phage-Presented Very Short Macrocyclic Peptide Library.

Publication 6: Valentin Jakob, Ben G. E. Zoller, Julia Rinkes, Yingwen Wu, Alexander F. Kiefer, Michael Hust, Saskia Helmsing, Andrew M. White, Peta J. Harvey, Thomas Durek, David J. Craik, Andreas Siebert, Uli Kazmaier and Martin Empting; Phage Display-based Discovery of Cyclic Peptides against the Broad Spectrum Bacterial Anti-Virulence Target CsrA; submitted on April 8th, **2021** to *Angew. Chem. Int. Ed.*

Contribution Report

Publication 1:

- Expression optimization of LANA1008-1146
- Expression and purification of LANA1008-1146
- Establishment of the fluorescence polarization assay for LANA
- Wrote parts of the supporting info

Publication 2:

- Performed parts of the FP-based assay
- Expression and purification of LANA1008-1146

Publication 3:

- Expression of LANA

Publication 4:

- Performed all experiments
- Wrote the manuscript

Publication 5:

- Performed phage display
- Performed fluorescence polarization assay and MST assay
- Synthesis of some peptides
- Wrote main parts of the manuscript and supporting info

Abbreviations

AIDS: acquired immunodeficiency syndrome
BSA: bovine serum albumin
CsrA: carbon storage regulator A
CTD: *C*-terminal domain
CuAAC: copper-catalyzed azide-alkyne 1,3-dipolar cycloaddition
DBD: DNA-binding domain
DNA: desoxyribonucleic acid
EBNA1: Epstein–Barr nuclear antigen 1
EBV: Epstein–Barr virus
EMSA: electrophoretic mobility shift assay
FBDD: fragment-based drug design
FP: fluorescence polarization
HHV-8: human gammaherpesvirus 8
HPV: human papillomavirus
IC_{50}: half-maximal inhibitory concentration
KS: Kaposi's sarcoma
KSHV: Kaposi's sarcoma-associated herpesvirus
LANA: latency-associated nuclear antigen
LBS: LANA binding site
mRNA: messenger RNA
MST: microscale thermophoresis
NMR: nuclear magnetic resonance
ORF: open reading frame
PAGE: polyacrylamide gel electrophoresis
PROTAC: proteolysis targeting chimeras
RNA: ribonucleic acid
RsmA: regulator of secondary metabolites A
RuAAC: ruthenium-catalyzed azide-alkyne 1,3-dipolar cycloaddition
SAR: structure-activity relationship
scFv: single-chain variable fragment
SPPS: solid phase peptide synthesis
SPR: surface plasmon resonance

STD-NMR: saturation-transfer difference NMR

TR: terminal repeat

tRNA: transfer RNA

TSA: thermal shift assay

wt: wild type

Table of Contents

1 Introduction

1.1 Protein-Nucleic Acid Interactions and their Inhibition

Protein-nucleic acid interactions belong to biological macromolecule-macromolecule interactions.[1] Especially in physiological and pathological processes, biomacromolecules and their interactions are necessary and involved in biological processes throughout the organism.[2–3] A function of most cellular proteins is only given in complex with other macromolecules.[4] This complexation regulates e.g. substance transport, molecular switches, molecular pumps, catalysts, growth factors, and signal transduction receptors.[5] More concrete examples include the interaction of ribosomes with RNA,[6] tRNAs (transfer RNA) with aminoacyl-tRNA synthase during translation,[7] RNA with ribonucleoprotein particles in post-transcriptional regulation[8] and also antibodies with antigens.[9]

Biological macromolecules include proteins such as enzymes or antibodies and nucleic acids such as DNA or RNA, but also polysaccharides such as starch or cellulose belong to it.[10] A common characteristic of these macromolecules is a composition of individual building blocks such as amino acids, nucleotides or monosaccharides.[10] The molecular mass of biomacromolecules may well be above 10 kda.[11]

In the context of this work, we will focus on interactions of proteins with the nucleic acids DNA and RNA, which have been increasingly studied for more than 30 years.[12] In the process of molecular recognition, these interactions are (mostly) non-covalent.[13] Main interactions are elicited through hydrogen bonds, which can also be mediated by water molecules, and non-polar Van der Waals forces, both through base and backbone contacts.[14–15]

As far as protein-DNA interactions are concerned, it is known on the basis of calculations, that 5 to 33 % of the protein surface is available for DNA binding.[16] The 33 % usually referring to proteins that form this bond as a dimer or higher oligomer. Involved are one to two hydrogen bonds per 100 $Å^2$, while protein dimers often have a larger gap between protein and DNA compared to monomers.[16] The major groove on the DNA is usually considered as the binding site for nucleic acid binding proteins.[14]

Computational chemistry analyses have also been published for protein-RNA complexes.[15] The number of often encountered hydrogen bonds is similar to that of protein-DNA complexes. However, an RNA is less polar than DNA and only half as many water molecules contribute to

the water-mediated hydrogen bonds. Due to possible more complex secondary structures of RNA, the gap between protein and RNA is larger on average.[15]

Of course, there are also unwanted processes of such interactions, which are responsible for diseases, especially by the introduction of foreign proteins into the body by pathogens such as viruses or bacteria.[17–18] A central component of medicinal chemistry is the displacement of nucleic acids from the protein by other molecules (e.g. small molecules, fragments, peptides, antibodies) that have a higher affinity for the protein than the nucleic acid itself.[19] An example of such DNA/RNA binding proteins that are undesirable in the host is the viral latency-associated nuclear antigen (LANA), which is able to bind DNA. Furthermore, the bacterial carbon storage regulator (CsrA), which is able to bind RNA, is a key virulence modulator in Gram-negative bacteria. Both proteins and their interaction with nucleic acid are described in more detail below.

1.2 The Latency-Associated Nuclear Antigen

The latency-associated nuclear antigen (LANA) is the most prominent virulence factor of Kaposi's sarcoma-associated herpesvirus (KSHV), formerly called human herpesvirus-8 (HHV-8).[20] KSHV is one of nine known human herpesviruses.[21–22] Like all herpesviruses, these cause a latent infection in the host organism and remain there for life after infection.[23] To date, there is still no way to eliminate these viruses from the host.[24–25] Up to now, only antiviral drugs for symptomatic treatment of Kaposi's sarcoma (KS) exist.[26]

Following human transmission of KSHV, which usually occurs via saliva or other body fluids, mainly B lymphocytes, endothelial and primary mesenchymal stem cells become infected.[27–28] The appearance of this disease is called Kaposi's sarcoma (KS), which is a type of cancer and named after Moritz K. Kaposi (1872).[29–30] Initially, it is an angioproliferative dysfunction affecting the skin and in advanced stages, mucous membranes, lymph nodes, lungs, and gastrointestinal tract can be involved.[31–32] However, KSHV is not pathogenic for healthy individuals with intact immune systems. Outbreaks may occur in severely immunosuppressed patients with existing acquired immunodefiency syndrome (AIDS) or transplant recipients.[33–34]

The latent persistence of infected cells is caused by a specific region on the KSHV episome (140 kb), the so-called latency-associated region, which is also shown in **Figure 1**. MicroRNAs

(miRNAs), kaposins and the open reading frames (ORFs) 71-73 (v-FLIP, v-cyclin and LANA) form a latent gene cluster there.[27,35–36] As already mentioned, LANA, as the most prominent viral protein in this context, plays a crucial role in persistence and will therefore be examined in more detail.

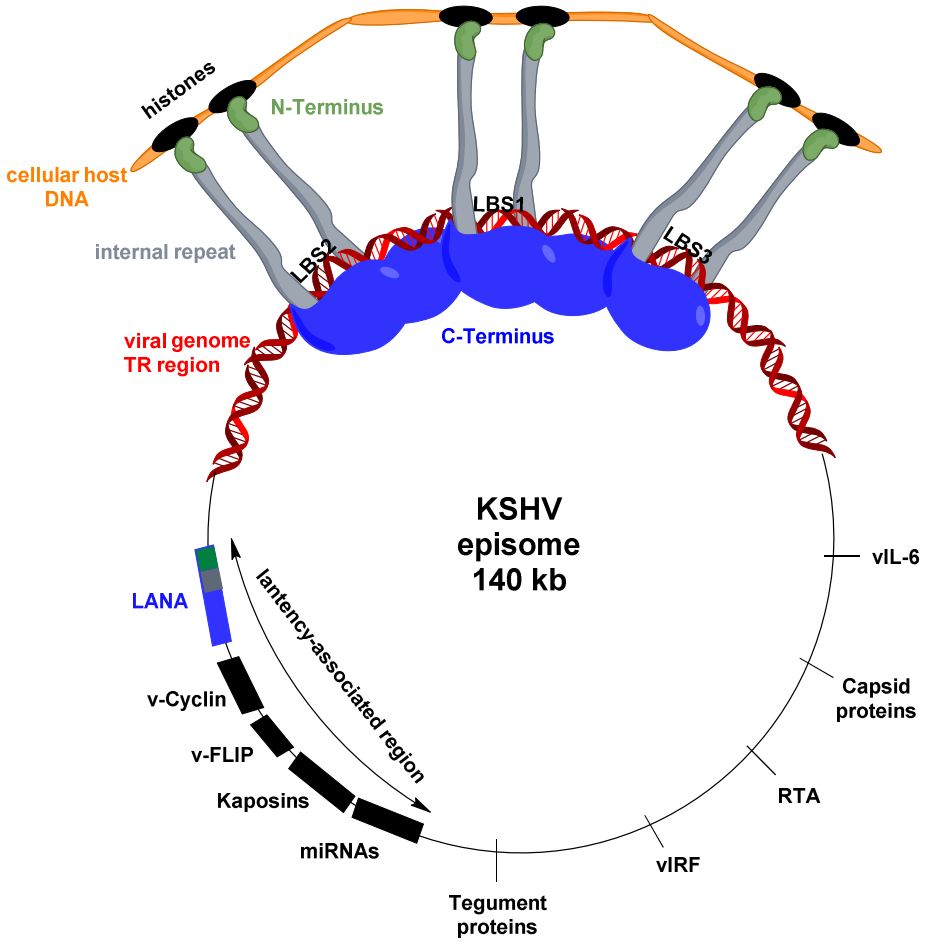

Figure 1: LANA captures latent persistence. LANA dimers bind with the C-terminus to the viral DNA of the TR region at LBS1, 2 and 3 and connect via the N-terminus to the host DNA. The TR is located on the KSHV episome, which is also the site of the latency-associated region that among others encodes for LANA.

In solution, LANA forms dimers and consists of 1162 amino acids with a molecular weight of 222-234 kDa.[37–39] Such a LANA dimer has a sequence-specific DNA-binding domain (DBD) at the *C*-terminal domain, which is highly ordered and binds to the viral DNA within the viral terminal repeat (TR). In total, the TR consists of 78 bp and has three so-called LANA binding sites (LBS1,2,3). Each of these LBS can bind a LANA dimer with different affinity. LBS1 has the highest affinity for LANA, while LBS3 has a 100-fold lower affinity.[40] The nucleotide sequences differ slightly and have a length of 20 bp (**Figure 2**).[40] In contrast, the *N*-terminal domain is highly disordered and links the viral DNA to the human host nucleosome via the

internal repeat.[41–42] This linkage is illustrated in **Figure 1**. Thus, transferring the viral episome into the dividing daughter cells and linking the two genomes are major functions of LANA for ensuring latent persistence.[43–44] To survive in the host cell, other functions include targeting tumor suppressors, chromatin modification and the transcriptional control, and latent viral replication.[39,45]

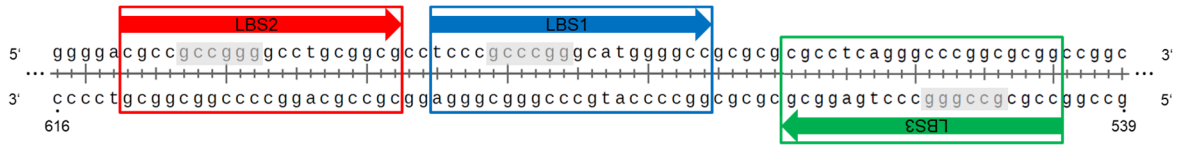

Figure 2: Localization of the three LBS on the TR region.[40] Primary DNA recognition sites are highlighted in grey.

In addition to LANA, there are existing other viral DNA-binding proteins that have a very similar structure and function. These include Epstein-Barr nuclear antigen 1 (EBNA1) of Epstein-Barr virus (EBV) and the E2 protein of human papillomavirus (HPV).[46–47]

Since LANA is responsible for latent persistence in the host and there are no drugs available yet to defeat this persistence, it is an interesting drug target.

1.3 The Carbon Storage Regulator A

In 1995 Liu *et al.* found the carbon storage regulator (Csr) as a global, post-transcriptional regulatory system.[48] It can control for example the carbon metabolism in *E. coli*.[49] The carbon storage regulator A (CsrA), alternatively named regulator of secondary metabolites A (RsmA) in *Pseudomonas*, is a bacterial protein, which is a prominent virulence factor in many bacterial species.[50] These proteins can be seen as the key players of the Csr/Rsm system.[19]

CsrA consists of 61 amino acids and forms a symmetrical homodimer.[51–52] As an RNA-binding effector protein, both identical binding surfaces are able to bind an mRNA strand each.[53] Each monomer consists of five β-strands and one α-helix (**Figure 4**).[54] *In vitro*, the Arg44 residue located at the *N*-terminus of the α-helix on CsrA seems to be important for RNA binding (**Figure 4**).[54] These facts have been confirmed by X-ray crystallography and nuclear magnetic resonance (NMR) solution studies.[55] The mRNA which will be recognized by CsrA must have the characteristic and highly conserved GGA core binding motif in its sequence, which is

usually present in a hair pin loop.[53] A model of a CsrA homodimer in complex with RNA and the specific GGA motif is shown in **Figure 3**.

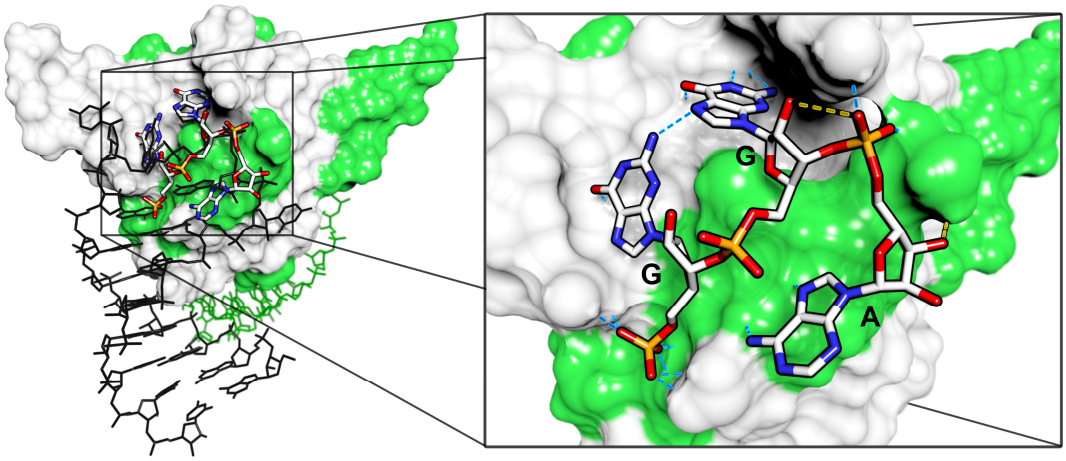

Figure 3: CsrA dimer (white and green represents a monomer each) in combination with two RNA molecules (black/green) and zoomed-in view of the essential GGA motif, based on X-ray and NMR structure of, among *Pseudomonas fluorescens*, RsmA from *Yersinia enterocolitica*.[19]

CsrA/RsmA shows similar sequences in several bacterial species. While there is a lack in eukaryotes, CsrA is widespread among Gram-negative bacteria and also highly conserved there.[56–57] There is a remarkable homology in several human pathogens. For example *E. coli*, *Yersinia* species, *Helicobacter pylori* and *Pseudomonas aeruginosa* are producing nearly identical variants of CsrA/RsmA.[58–59] An amino acid sequence comparison of these four important bacterial pathogen species is illustrated in **Figure 4**.

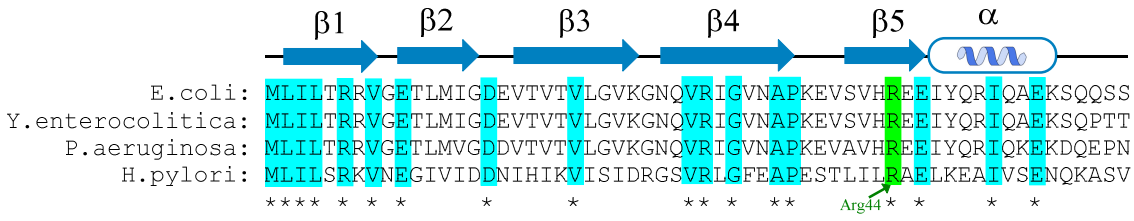

Figure 4: Comparison of CsrA/RsmA sequences of different human pathogenic species.[59] Identic sequence parts are marked in blue. The sequences of *E. coli*, *Y. enterocolitica* and *P. aeruginosa* are strongly conserved, whereas *H. pylori* contains more divergence. The assignment of the β-sheets and α-helix is provided. Arg44, which is putative for binding to RNA, is marked in green.

In mouse model studies with CsrA/RsmA deficient mutants of *P. aeruginosa* and *H. pylori* a significantly lower virulence could be proven.[60–61] The protein acts via binding and regulating mRNA and, thus exerting pleiotropic effects on the bacterial transcriptome.[62] It can regulate both positively (mostly while acute infection) and negatively (mostly after chronic infection). To mention a few regulation examples, there can be recognized a repression of glycogen biosynthesis, gluconeogenesis, peptide transport and biofilm formation and on the other hand an activation of glycolysis, acetate metabolism, motility, host colonization and invasion.[59,63–66]

In more detail, an example for positive regulation is the binding of CsrA to *E. coli flhDC* (encodes for flagellum) mRNA[67], which leads to transcript stabilization and preventing RNase degradation (**Figure 5B**). This results in activating the *flhDC* expression leading to increased motility to escape from stressful microenvironments.[66,68]

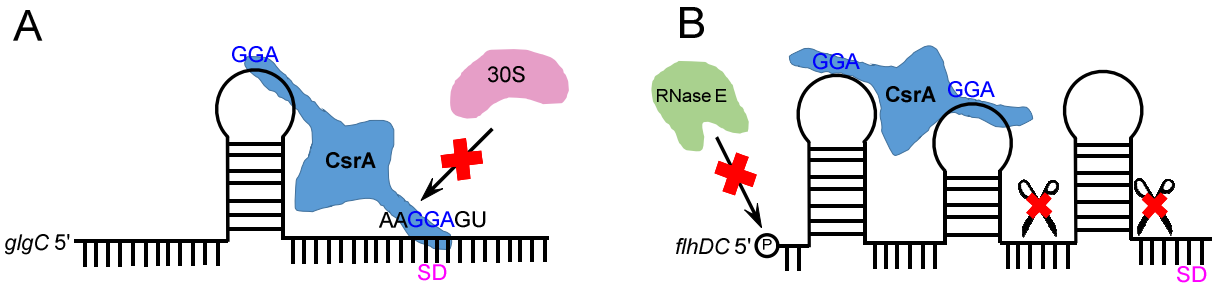

Figure 5: How CsrA impacts gene expression in *E. coli*.[69] (**A**) Negative regulation of *glgC* expression through repression of translation. CsrA homodimer binds to GGA motif of hairpin loop and GGA of Shine Dalgarno (SD) sequence on ribosomal binding site, preventing the 30S unit of the ribosome from binding to mRNA. (**B**) Positive regulation of *flhDC* expression by mRNA transcript stabilization. CsrA homodimer binds to two GGA motifs in hairpin loops, preventing RNase E from mRNA degradation (cleavage) and mRNA turnover.

In negative regulation a repression of translation is observed.[70] There, CsrA competes with the ribosome, while binding to the ribosome binding site of the mRNA, which leads to a modulation of bacterial virulence.[19] Peptide uptake via carbon starvation gene *cstA* (a permease encoding hydrophobic polypeptide) by blocking ribosome access to the *cstA* transcript can be mentioned in this context.[52] In a similar way, CsrA is able to bind *glgC* mRNA (**Figure 5A**) which reduces the energy of the cells.[49,71] This was shown by Romeo *et al.*, where a 20-fold increase in glycogen level was observed after inhibiting CsrA.[62,72]

Due to the fact that CsrA strongly influences gene expression and is also present in numerous human pathogenic bacterial species, it is an interesting drug target as well.

1.4 Fluorescence Polarization Assay

When a fluorophore is irradiated with linear polarized light, molecules whose transition dipole moment is oriented in parallel to the electric field of the irradiated light are excited. The emitted light is then also polarized to a certain degree.[73] Perrin *et al.* first described fluorescence polarization in 1926.[74] In 1952, Laurence *et al.* studied the binding of fluorescein and bovine serum albumin (BSA), establishing a method for monitoring the binding of small molecules to proteins.[75]

An application of this principle is the fluorescence polarization assay (FP assay), which is an important biochemical assay for the characterization of binding affinities of fluorophores to macromolecules. Especially ligand-receptor,[76] protein-protein,[77] protein-peptide[78] and protein-nucleic acid[79] interactions can be observed. In particular, it can be used for competition experiments in which a ligand (e.g., nucleic acid) competes with another ligand (e.g., peptide) for binding to a receptor (e.g., protein). In this process, a fluorescence-labeled ligand binds to a receptor and competes with an unlabeled molecule.[80] Fluoresceine is a commonly used fluorescence label.[81]

Measurements are taken in special plate readers. The light emitted from a monochromatic light source passes through a vertical polarizer. The resulted vertically polarized excitation energy passes through the sample. Only those fluorescence-labeled molecules, which are in the vertical layer are able to absorb the vertically polarized excitation light. These molecules are now in the excited state and emit light. The resulting emission energy is now depolarized to some degree. For quantification, a rotatable polarizer is used to measure in the vertical and horizontal planes. Thus, the proportion of the vertical (parallel, remaining polarized part) and horizontal (perpendicular, depolarized part) emission can be detected.[82] The decisive factor here is the polarization value *P*, which is calculated from ratios of light intensities *I*.[83]

$$P = \frac{I_{parallel} - I_{perpendicular}}{I_{parallel} + I_{perpendicular}} \qquad (1)^{83}$$

For a measurement at constant temperature and viscosity, the polarization is directly proportional to the molecular volume.[84] If a labeled ligand is excited with linearly polarized light, it starts to rotate and the resulted emitted light is depolarized. If this labeled ligand is now bound to a receptor, the molecular volume increases and the rotation speed is slowed down

considerably, resulting in a higher polarization value.[85] The polarization change is illustrated in **Figure 6**.

If an inhibitor is active in competition experiments and polarization is plotted as a function of the logarithmic concentration of the analyte, the result shows up as a sigmoidal curve.[19] This allows the determination of the half-maximal inhibitory concentration (IC_{50}) value in its inflection point, which can classify the activity of the analyte.[86] This phenomenon is also shown in **Figure 6**.

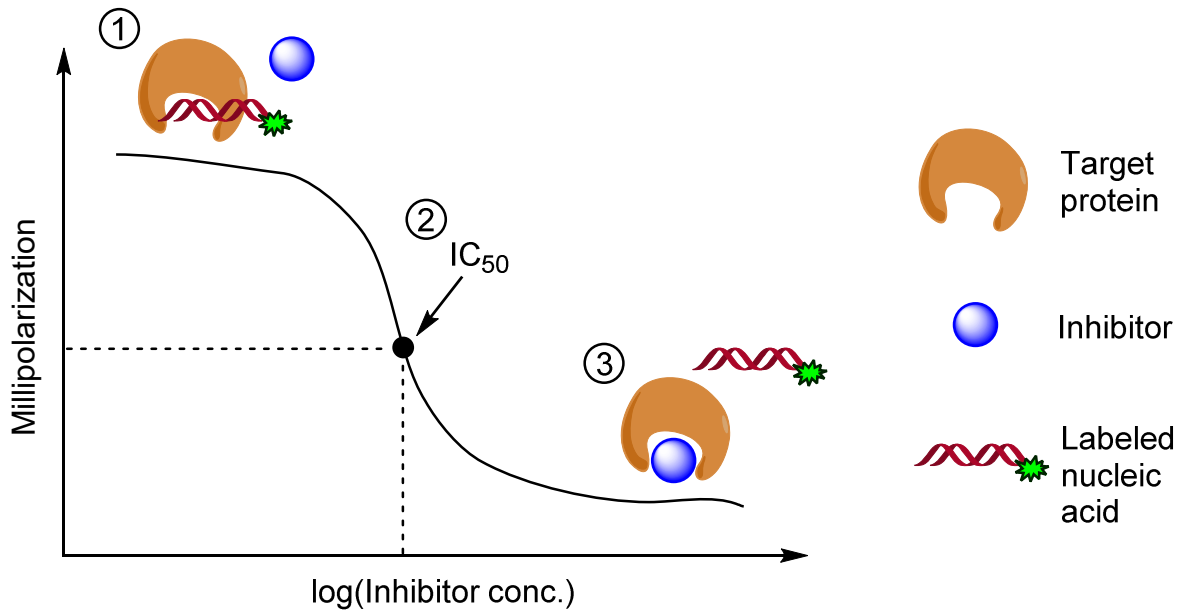

Figure 6: Sigmoidal inhibition curve for a competition experiment in which an inhibitor competes with a nucleic acid for binding at the target. Polarization (millipolarization mP) is plotted against the logaritmic inhibitor concentration. (**1**) At low inhibitor concentrations, the labeled nucleic acid remains on the target and the inhibitor is free. Upon irradiation of polarized excitation light, slow rotation of the target-nucleic acid complex occurs, resulting in polarization retention of the emitted light (high mP value). (**2**) 50 % of the nucleic acid is replaced by the inhibitor, resulting in the important medicinal chemistry parameter, the IC_{50} for determining binding affinity. (**3**) At high inhibitor concentration, the labeled nucleic acid is completely displaced by the target. Due to the rapid rotation of the relatively small labeled nucleic acid, the emitted light is highly depolarized (low mP value).

In addition to the determination of IC_{50} values of individual compounds, it is possible to perform high throughput screenings. In this case, numerous compounds can be tested at a specific concentration on a target.[87] Another point is the dissociation constant (K_d value) which can be determined with a saturation experiment.[88]

1.5 Phage Display

There are several types of so-called "display" technologies existing, including mRNA,[89] ribosome,[90] and CIS displays.[91] However, one of the most commonly used display strategies is phage display.[92] Here, a phage presents its appendage of choice to a target, usually an immobilized protein. It is a method for selecting potential binders for such a protein. Binders can be, for example, peptides[92] or antibodies[93]. Accordingly, these phage displays are then termed peptide display[94] and antibody display[95], respectively. The oligopeptide display method was first described by George P. Smith in 1985.[96] In 2018, George P. Smith and Sir Gregory P. Winter received the Nobel Prize for the peptide and antibody display process, in which genetically modified phages are used to generate new biopharmaceuticals.[97]

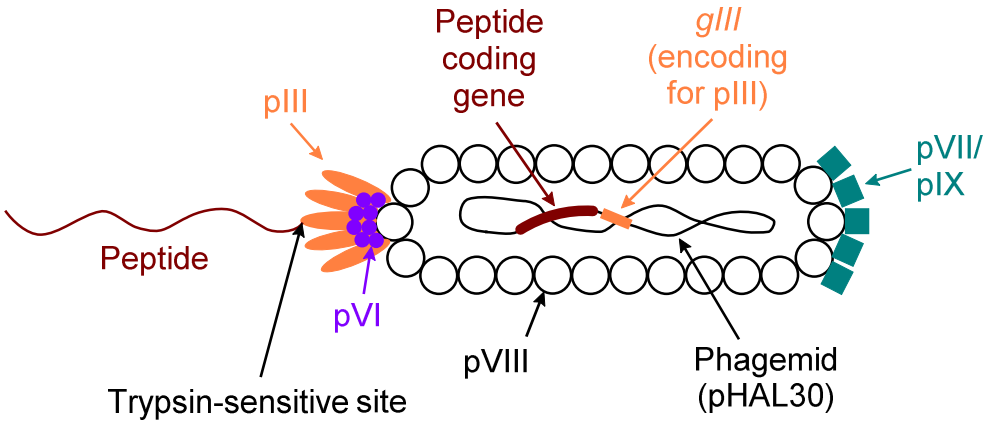

Figure 7: Schematic representation of an M13 phage presenting a peptide (modified according to Kügler *et al*. 2013).[98] This consists of several capsid proteins (pIII, pVI, pVIII, pVII/pIX), whereby pVIII forms the actual envelope in which the phagemid is enclosed, which codes for the peptide to be presented, as well as for pIII, to which the peptide is linked. Here we can also see how genotype and phenotype are coupled: Coding gene and translated peptide are present on the phage at the same time. To separate the genome-bearing phage from the target-binding peptide during panning, there is a trypsin cleavage site between the peptide and pIII. This phage is not capable of replication on its own because the remaining surface proteins (capsid proteins) are not encoded in the phagemid. These are supplied by an additional helper phage.

Different types of phages can be used for phage display, e.g. phage T7,[99] phage lambda[100] or filamentous phages f1, fd, M13.[96] Filamentous phages, in particular M13 phage will now be examined in more detail and is schematically shown in **Figure 7**. M13 has different surface proteins to which the appendage to be displayed can be bound. Possible are so-called capsid proteins (pVII/pIX, pVIII, pVI, pIII) which are located on the surface of an M13 phage. In our case, the pIII protein was used for connection of the appendage to phage, which is also regularly applied for the binding of peptides or antibodies.[101–102]

The principle of phage display is based on genotype-phenotype coupling, where the peptide gene and peptide is quasi linked.[103] The coding gene is located inside the phage (genotype) and simultaneously the translated gene is presented by the phage fused to pIII protein on the phage surface (phenotype). [96]

To be able to map numerous peptides at the same time, so-called libraries are used. A library is a bundle of different gene sequences that are supposed to code for e.g. different peptides.[104] Billions of different combinations,[92] which determine the diversity of a library, are possible and can be screened simultaneously in the phage display for potential binders to any target.[105]

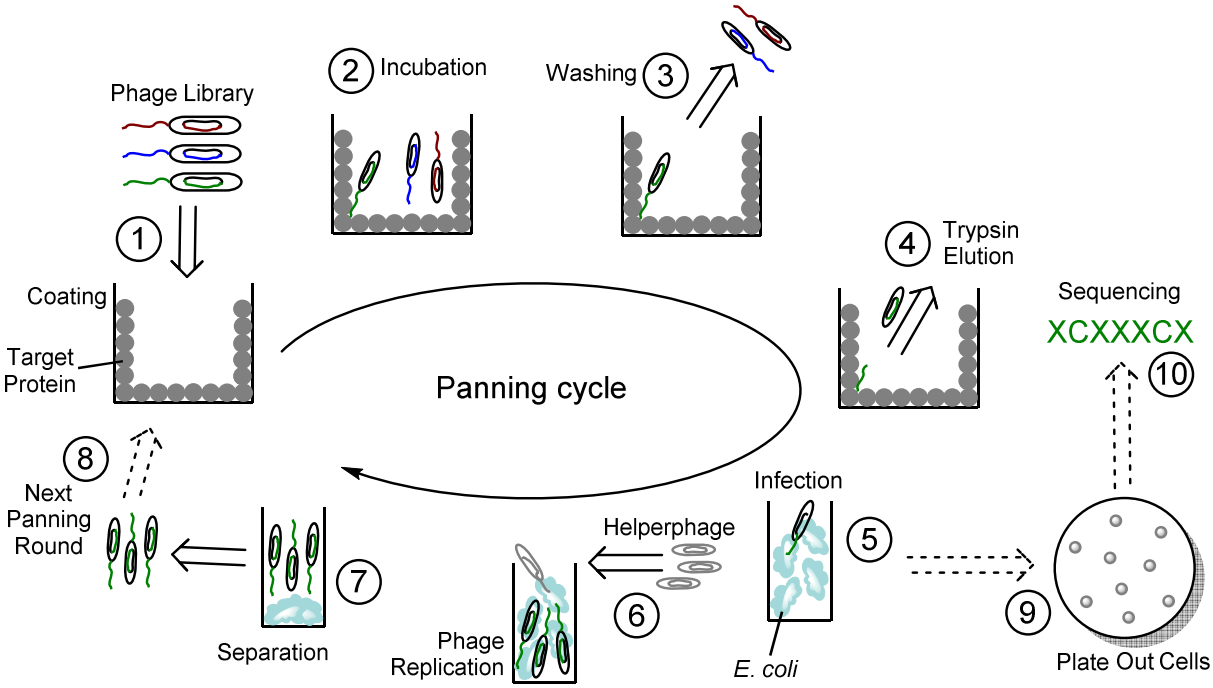

Figure 8: Schematic representation of a phage display panning.[106] (**1**) A microtiter plate well is coated with the target protein and the phage library is subsequently added. (**2**) The phages are left on the target for a period of time and the peptides are presented to the target, some of which bind and some of which do not. (**3**) The well is washed out and thus non-binding phages are removed. (**4**) After addition of trypsin, the peptide-encoding phage is separated from the peptide. (**5**) In a deep well, an *E. coli* culture is infected with the eluted phages. (**6**) The phages are not replicated until a helper phage is added. (**7**) The newly formed phages are separated from *E. coli*. (**8**) These phages are now the library enriched with potential binders, which can be used for the next round of panning. (**9**) After any round of panning, clones can be separated on agar plates. (**10**) The clones are sequenced to determine which peptide the potential binders encode.

After the design of a library of interest, it is cloned into a special vector, which in this context is also called a phagemid. A phagemid is the name for vectors that code for filamentous phages.[107] The phagemid also contains the sequence encoding the surface protein pIII.[108] In this work pHAL30[109] is used. The library cloned into the phagemid is then packaged into M13 phage and is then ready for panning, a process in which potential binders are enriched.[106,110] After the

target of interest has been immobilized in microtiter plate wells, incubation with the packaged library is performed.[111] Here, the presented peptides have a chance to bind to the target, whereas weak binders and non-binders are subsequently eliminated by washing the wells with a plate washer, the binders remain in the well binding to the target. Between peptide and pIII is a trypsin cleavage site. After incubation with trypsin, the phage is separated from the peptide. The peptide remains on the target, and the phage encoding this peptide is reused for the next step. *E. coli* cultures are treated with this phage and thereby infected. However, these phages cannot replicate themselves because the phagemid lacks the building blocks to produce intact phages. For this purpose, a co-infection with a helper phage is required, which provides all capsid proteins.[108,112] The result is a library enriched with binders, which can be used for the next round of panning.[113] After several rounds of panning and thus enrichment of binders, it is worthwhile to plate out and thus separate some clones and sequence them to observe the gene sequence of these binders. The whole panning process is shown in **Figure 8**.

Phage display is a tool which offers the possibility of a high throughput screening to rapidly and effectively identify potential binders for any protein target.[114] In practice, this is often applied to antibody display in the discovery of single-chain variable fragments (scFvs) for any antigen.[105,109,115] These scFvs contain only a minimal functional part of a full antibody, where the light chain (V_L) and heavy chain (V_H) are connected via an amino acid linker.[116–117]

Another application is peptide display, which can be applied analogously to the antibody display above and was also used in this thesis.[92,98,106] Thus, for any given protein, there is the possibility of finding peptides that can act as potential binders.[118] Heinis *et al.* describes the procedure with small bicyclic peptides (< 1.5 kDa), which gain increased stability in intestinal environments by this cyclization.[119–120]

2 Aim and Scope

Numerous viral and bacterial targets are underexplored. In particular LANA, a disease-causing protein of the KSHV, is only poorly studied with regard to antiviral agents. KSHV as a disease is still not curable because there is no specific drug that can interrupt the latent phase of this virus. On the other hand, CsrA as a bacterial target, whose sequence is wide spread and highly conserved among bacteria, the first small molecules have only recently been discovered as inhibitors. This makes it even more important to study both targets in detail and to develop new methods to identify antiviral or antibacterial agents.

The aim of this thesis was the evaluation of new protein-nucleic acid inhibitors for the viral target LANA and the discovery of new peptides hits for the bacterial target CsrA. A fluorescence polarization assay should be established as SAR driver. Furthermore, phage display was established and used as an approach to find further hit structures.

In the first part of this work, based on previous studies, the expression of LANA mutants should be optimized. Hits of a fragment-based approach, an in-house library screening and a hit-to-lead optimization should be characterized by biophysical assays. For this purpose, a functional fluorescence polarization-based LANA-DNA interaction inhibition assay should be established. These efforts are shown in **Chapter A**, **B** and **C**.

In the second part of this work a phage display methodology should be established, enabling to find binding peptides for any target. First, an oligomer coding for a peptide library should be designed. Subsequently, this library should be cloned into a vector and packaged in phage. This library should then be used in the phage display, where the individual peptides are presented to the target in disulfide cyclized form. A special goal was to optimize this panning as much as possible to obtain plausible potential binders for *Yersinia* CsrA. These procedures were described in **Chapter D**.

In the third part of this work a peptide-based approach should be used to identify CsrA-RNA interaction inhibitors. For this purpose, the established and optimized phage display procedure against *Yersinia* CsrA should be performed and potential CsrA binders should be characterized by sequencing. The discovered hit sequences should then be resynthesized and confirmed by a functional fluorescence-based CsrA-RNA interaction inhibition assay, which has been established in a previous work for CsrA. This hit should be further characterized by microscale thermophoresis (MST). Additionally, structure-activity relationships of this hit should be investigated by synthesizing a number of peptide derivatives by solid phase peptide synthesis.

Furthermore, it should be shown that the disulfide bridge is essential and an alanine scan should be performed to identify important interaction hotspots. In a final step, disulfide mimetics should be found, which enabling to protect the macrocyclic motif from reductive cleavage while retaining activity. The whole process was described in **Chapter E**.

3 Results

3.1 Chapter A: Protein-DNA Interactions (Part I)

Title:

Fragment-Based Discovery of a Qualified Hit Targeting the Latency-Associated Nuclear Antigen of the Oncogenic Kaposi's Sarcoma-Associated Herpesvirus/Human Herpesvirus 8

Authors:

Philine Kirsch, Valentin Jakob, Kevin Oberhausen, Saskia C. Stein, Ivano Cucarro,

Thomas F. Schulz, and Martin Empting

Bibliographic Data:

Journal of Medicinal Chemistry,

Volume 8, Issue 62, Pages 3924-3939,

March 19, 2019,

DOI: 10.1021/acs.jmedchem.8b01827

Graphical Abstract:

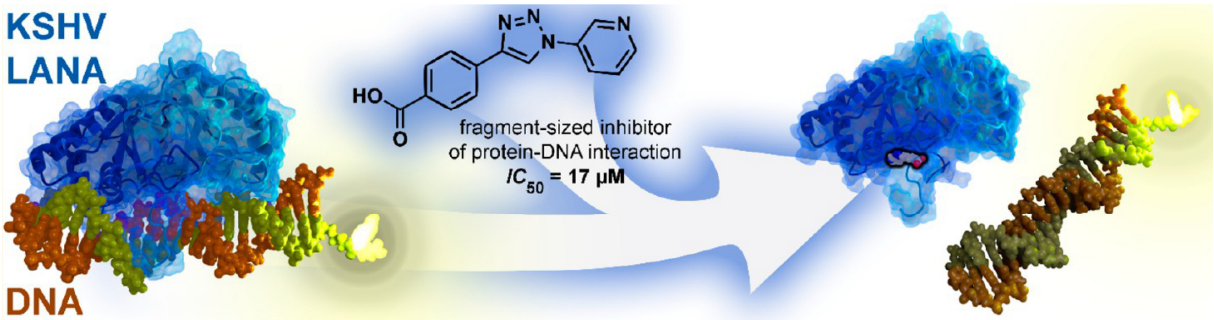

Journal of Medicinal Chemistry

Article

Cite This: J. Med. Chem. 2019, 62, 3924−3939

pubs.acs.org/jmc

Fragment-Based Discovery of a Qualified Hit Targeting the Latency-Associated Nuclear Antigen of the Oncogenic Kaposi's Sarcoma-Associated Herpesvirus/Human Herpesvirus 8

Philine Kirsch,[‡,§,∥] Valentin Jakob,[‡,§] Kevin Oberhausen,[‡,§] Saskia C. Stein,[∥,⊥] Ivano Cucarro,[‡,§] Thomas F. Schulz,[∥,⊥] and Martin Empting*[,‡,§,∥]

[‡]Department of Drug Design and Optimization (DDOP), Helmholtz-Institute for Pharmaceutical Research Saarland (HIPS)-Helmholtz Centre for Infection Research (HZI), Campus E8.1, 66123 Saarbrücken, Germany

[§]Department of Pharmacy, Saarland University, Campus E8.1, 66123 Saarbrücken, Germany

[∥]German Centre for Infection Research (DZIF), Partner Site Hannover-Braunschweig, 66123 Saarbrücken, Germany

[⊥]Institute of Virology, Hannover Medical School, Carl-Neuberg-Strasse 1, 30625 Hannover, Germany

Supporting Information

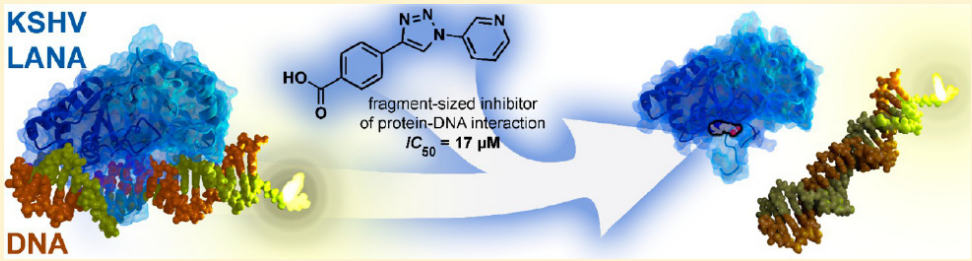

ABSTRACT: The latency-associated nuclear antigen (LANA) is required for latent replication and persistence of Kaposi's sarcoma-associated herpesvirus/human herpesvirus 8. It acts via replicating and tethering the virus episome to the host chromatin and exerts other functions. We conceived a new approach for the discovery of antiviral drugs to inhibit the interaction between LANA and the viral genome. We applied a biophysical screening cascade and identified the first LANA binders from small, structurally diverse compound libraries. Starting from a fragment-sized scaffold, we generated optimized hits via fragment growing using a dedicated fluorescence-polarization-based assay as the structure−activity-relationship driver. We improved compound potency to the double-digit micromolar range. Importantly, we qualified the resulting hit through orthogonal methods employing EMSA, STD-NMR, and MST methodologies. This optimized hit provides an ideal starting point for subsequent hit-to-lead campaigns providing evident target-binding, suitable ligand efficiencies, and favorable physicochemical properties.

INTRODUCTION

Kaposi's sarcoma-associated herpesvirus (KSHV; taxonomic name human herpesvirus 8) is a human gammaherpesvirus and is classified as a carcinogenic agent Group I by the World Health Organization.[1,2] It was identified as the etiological agent of Kaposi sarcoma (KS) and lymphoproliferative disorders. After a first infection, it establishes a lifelong latent infection in the host organism. KSHV is usually not pathogenic in healthy individuals, but AIDS-related Kaposi's sarcoma (AIDS-KS), KS in transplant recipients, and endemic KS in East/Central Africa cause significant morbidity and mortality in affected patients.[3] In latently infected cells, KSHV expresses only a limited set of proteins, which are important for its persistence. One of these is the latency-associated nuclear antigen (ORF73/LANA).[4,5] LANA plays an important role for the latency and regulation of the viral genome in the host organism. Previous studies have shown that LANA exerts several functions in the host cell like cell survival, transcriptional control, latent viral DNA replication, and stable episome segregation during mitosis.[6] The *C*-terminal domain of LANA binds to the terminal repeat (TR) region of the viral genome in a sequence-specific manner.[7,2] The TR consists of three adjacent LANA binding sites (LBS), which are referred to as LBS1, LBS2, and LBS3 (Figures 1 and 2).[7] The *N*-terminal domain of LANA is very poorly structured and is tethered to the host nucleosome.[8,9] It is separated by a large internal repeat sequence from the *C*-terminal DNA-binding domain (Figure 1).[10,11]

To date, the options for treating KSHV-associated diseases are limited.[12] While several inhibitors of herpesviral DNA polymerases are active against KSHV productive replication, they are not effective against KS or other KSHV associated

Received: November 22, 2018
Published: March 19, 2019

DOI: 10.1021/acs.jmedchem.8b01827
J. Med. Chem. 2019, 62, 3924−3939

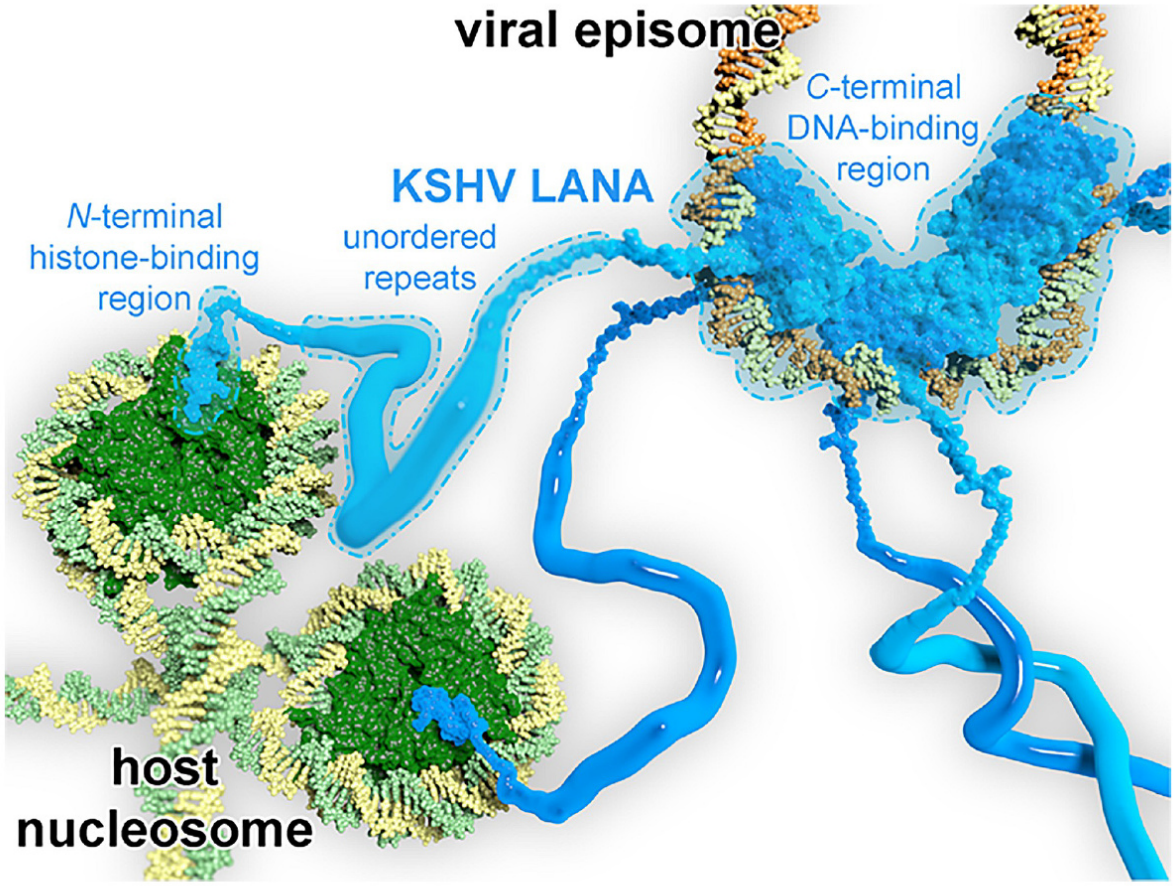

Figure 1. Illustration of molecular interactions between KSHV LANA, viral episome, and host nucleosome, rationalizing the C-terminal DNA-binding domain of KSHV LANA as an antiviral drug target as it links viral DNA (yellow and orange) to host histones (dark green) and attached host DNA (yellow and green). Three KSHV LANA dimers (blue) are shown, and unordered repeats are displayed as tubes. Illustration was modeled using coordinates of PDB entries 1zla, 4uzb, and 4uzc.

malignancies.[12] LANA represents a very promising target for the discovery and development of new anti-KSHV drugs that, in contrast to currently available compounds, would interfere with the latent phase of the viral life cycle. Based on the knowledge that LANA is involved in binding to viral latent episomal DNA and tethering it to host nucleosomes[7,6] we conceived a new approach for the discovery of specific KSHV inhibitors. Our concept aims at the inhibition of the interaction between LANA and the viral genome. This should ultimately prevent latent persistence of KSHV, which could result in the gradual loss of infected cells and in a decrease in viral load in infected individuals. In the present work, we present our efforts to exploit this strategy through identification of the first functional LANA−DNA-interaction inhibitors by using fragment-based drug design. As a first step, we made use of different biological and biophysical methods to screen fragment libraries for identification of LANA binders. Subsequently, we established a fluorescence polarization (FP)-based assay to determine the inhibitory activities of our hits, and we used it for further optimization steps. Furthermore, we confirmed target binding of our best compound via orthogonal assays using saturation-transfer difference (STD) NMR and microscale thermophoresis (MST) methodologies. Finally, we qualified the optimized hit scaffold for future lead-generation campaigns in an orthogonal interaction inhibition assay, namely, the electrophoretic mobility shift assay (EMSA). This provides an ideal starting point for subsequent medicinal chemistry efforts toward specific anti-KSHV agents. To the best of our knowledge, this study is the first report of inhibitors targeting the DNA-binding domain of LANA. A similar approach, however, has been previously applied to the EBNA1 protein, the functional homologue of LANA in Epstein−Barr virus (EBV).[13] However, these conceptually related studies as well as experiments with a DNA-binding site mutant of LANA provide a sufficient basis for the validity of this antiviral drug target.[14]

■ RESULTS AND DISCUSSION

Screening and Hit Identification. To discover the first small molecules that can bind to LANA, we used orthogonal biophysical methods to screen two different small-molecule libraries from synthetic and natural sources.[15,16] For the primary selection, we used two protein binding assays, surface plasmon resonance (SPR) and differential scanning fluorimetry (DSF), due to their high sensitivity and low protein

DOI: 10.1021/acs.jmedchem.8b01827
J. Med. Chem. 2019, 62, 3924−3939

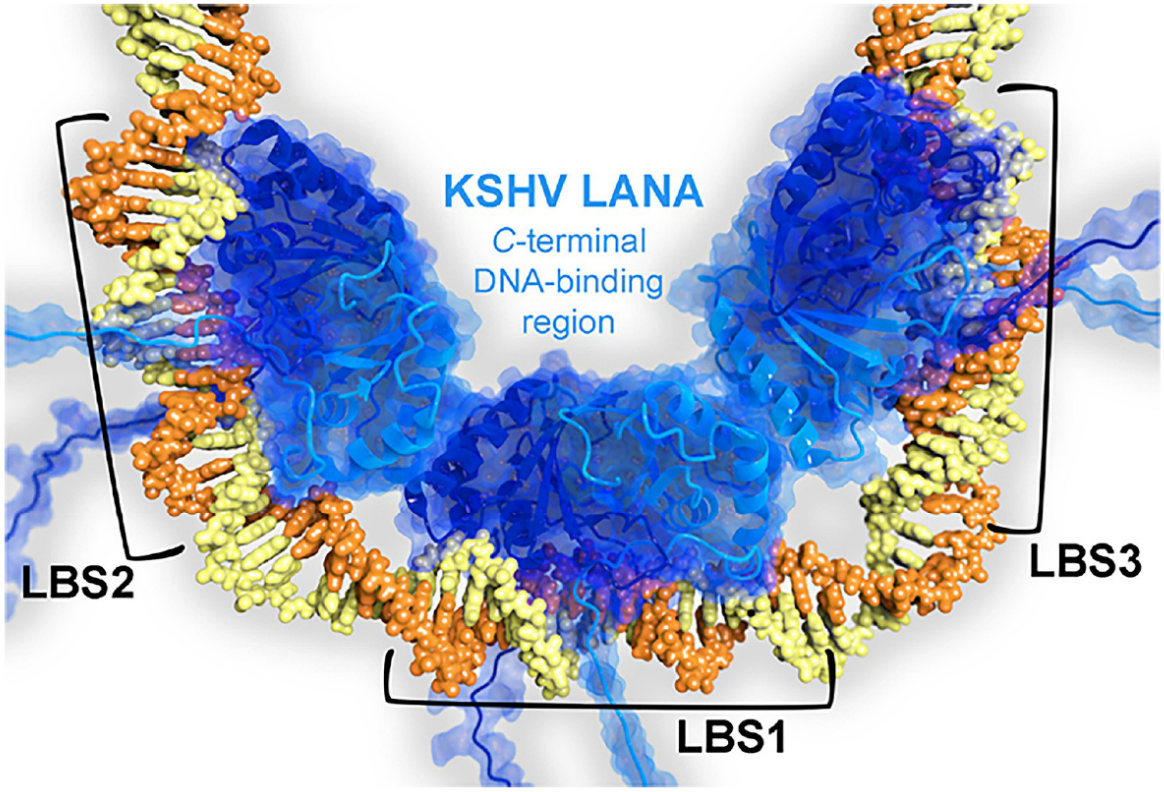

Figure 2. Model of the C-terminal DNA-binding domain of three KSHV dimers bound to adjacent LANA-binding sites LBS1, 2, and 3. Protein chains are shown as ribbon representations (chain A: blue, chain B: light blue). Viral DNA (yellow orange) is shown in space-filling representation. The model was generated using pdb entries 4uzb and 4uzc.

consumption. First, we conducted SPR screening at a constant concentration to preselected putative LANA binders. Subsequently, we applied DSF (thermal shift assay, TSA) as a secondary filter.

This methodology enabled us to select 20 compounds for further testing. In order to test for functionalities of our LANA binders in vitro, we established an FP-based assay, which allows for the quantitative evaluation of the LANA−DNA interaction and its inhibition by small molecules. In this manner, we identified three promising small molecule hit scaffolds for further consideration. In this report, we will focus on our hit optimization efforts, starting from the fragment-sized hit **1** (Figure 3).

SPR- and DSF-Based Primary Screening. Two different libraries, containing a total of 720 highly structurally diverse hit-like small molecules with molecular weights below 398 g/mol, were screened.[15,16] We started with SPR spectroscopy using the wild-type LANA C-terminal domain (CTD) as the ligand and the library compounds at a constant concentration of 500 μM. Compounds that showed a response higher than 9 μ-refractive index units were selected from this screening, which yielded 52 primary binders (for detailed results, see the Supporting Information Figure S1). In a second step, we employed DSF experiments as a secondary filter. This assay quantifies a change in thermal denaturation temperature of the wild-type LANA C-terminal domain by binding to a compound. Generally, an increase of melting temperature

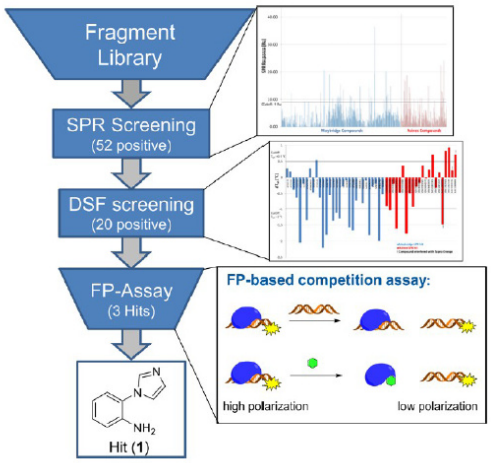

Figure 3. Screening procedure using two different fragment libraries targeting LANA. In total, 720 compounds were screened using SPR experiments, followed by DSF. An FP-based assay was used to identify promising interaction inhibitors, which resulted in three promising hits.

indicates a stabilization of the protein due to binding of a small molecule. Our experiments showed for almost all compounds a decrease in melting temperature for LANA. A decrease of

DOI: 10.1021/acs.jmedchem.8b01827
J. Med. Chem. 2019, 62, 3924−3939

Scheme 1. Synthesis of Hit I and 1*H*-Imidazole-1-yl Derivatives[a]

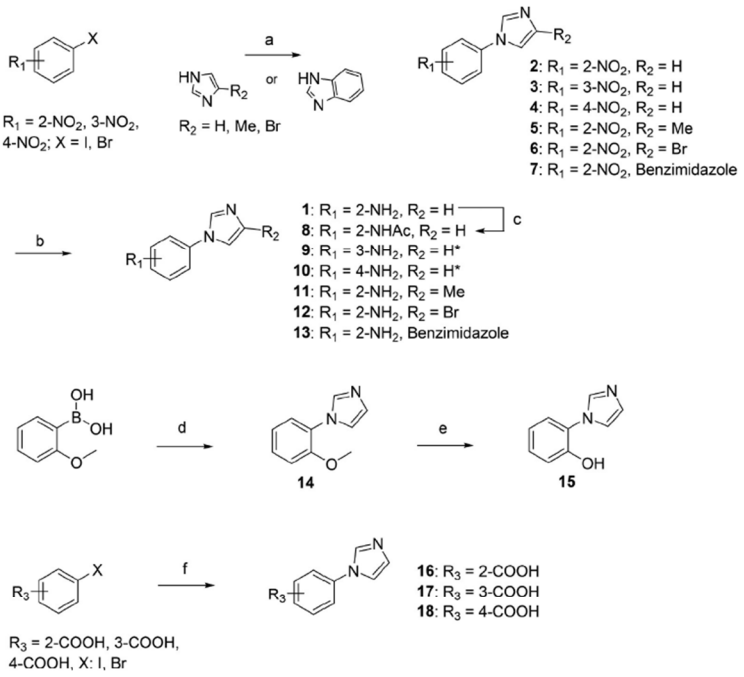

[a]Reagents and conditions: (a) K_3PO_4, CuI abs. DMF, 110 °C, 24 h; (b) $SnCl_2$, EtOH, 80 °C, 30 min; (c) H_2SO_4, AcOH, Ac_2O, rt, 16 h; (d) imidazole, CuCl, MeOH, 80 °C, 16 h; (e) 48% aq HBr, 100 °C, 16 h; (f) K_2CO_3, CuCl, *N*,*N*′-dimethylmethanediamine, DMF, 120 °C, 24 h.

melting temperature may indicate a destabilization of the protein by compound binding. Although usually an increase in protein stability and, thus, increase in melting temperature are observed for target binders, also negative shifts are commonly considered as binding events.[17] As a consequence, we selected 20 compounds that showed significant thermal shifts $T_M \geq +0.5$ °C and $T_M \leq -1.0$ °C for further investigations (for detailed results see the Supporting Information, Figure S2).

Establishment of FP Assay. For further characterization and optimization, our compounds were tested for inhibition of the DNA−LANA interaction using an FP-based competition assay. The FP assay is a rapid and quantitative method for identification of small molecular macromolecule−macromolecule interaction inhibitors.[18] For this process we used a mutant of the KSHV LANA *C*-terminal DNA-binding domain (DBD) (aa1008-1146) that lacked the ability to form oligomers of LANA DBD dimers.[7] In previous studies it was observed that the wild-type LANA *C*-terminal domain (LANA CTD (aa934-1162)) precipitated readily following the addition of either specific or unspecific DNA.[19] It has the ability to form higher-order oligomers, which contribute to the low solubility in the presence of DNA. For avoiding these solubility problems, multiple point mutations were inserted into the basic patch and the oligomerization interface of LANA DBD; none of these mutations are located at the specific DNA-binding site of LANA, while the basic patch mutations suppress unspecific DNA binding. This *C*-terminal LANA mutant with the amino acid mutations K1055E, K1138S, K1140D, K1141D, R1039Q, R1040Q, A1121E, K1109A, and D1110A shows a high solubility also in the presence of oligonucleotides representing the viral LANA-binding sites (LBS) in the viral terminal repeat subunit.[19,7,14]

A fluorescence-labeled DNA sequence was employed as a competitive binding partner, which corresponds to LANA-binding site 2 (LBS2) in a KSHV terminal repeat subunit.[7] We chose LBS2 as the fluorescence probe because of its lower affinity for the LANA DBD and used varying concentrations of unlabeled LBS1, LBS2, and LBS3 to validate and optimize our assay conditions (see the Supporting Information, Figures S3 and S4). In accordance with previous reports, we obtained a difference in affinity between the LBS sequences.[7]

FP-Based Functional Screening. In order to assess the effect of identified screening hits on LANA−DNA-interaction inhibition we tested them in our FP-based assay using LBS2 as the fluorescent probe. Due to their high solubility, the compounds could be tested at high concentrations (1 mM or 500 μM), allowing for the identification of even weak inhibitory effects usually observed with fragment-like scaffolds. Each compound was measured in duplicate and in two independent experiments. Three of the 20 tested compounds showed promising results (Table S9, Supporting Information). In this paper we will present the hit optimization and validation for hit **1**. Despite its fragment-like size with a molecular weight of only 159.08 g/mol, this compound showed an inhibitory effect of 25 ± 9% at 1 mM (Figure 3; SPR at 500 μM: 15.69 ± 9.3 RU; DSF at 500 μM: T_M −1.80 ± 1.41 °C). Considering the large interaction site between LANA and its target DNA sequence, this result was promising and encouraged medicinal chemistry optimization of this fragment hit.

DOI: 10.1021/acs.jmedchem.8b01827
J. Med. Chem. 2019, 62, 3924−3939

Scheme 2. Synthesis of Azide Intermediates and Reaction of Aryl Azides with Different Alkynes Using Click Chemistry and Derivatives[a]

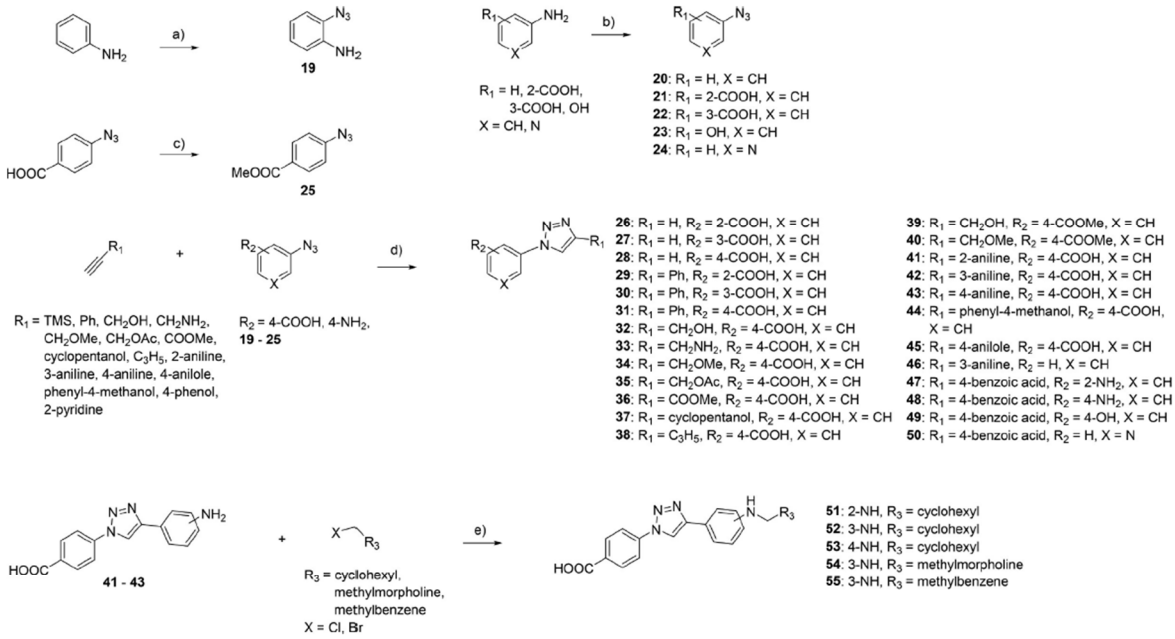

[a]Reagents and conditions: (a) $TMSN_3$, CuBr, TBHP, MeCN, 0 °C → rt, 16 h; (b) concd H_2SO_4 or concd HCl, $NaNO_2$, NaN_3, H_2O, 0 °C, 1.5 h; (c) $SOCl_2$, MeOH, 0 °C → rt, 16 h; (d) $CuSO_4 \cdot 5H_2O$, sodium ascorbate, H_2O/*tert*-BuOH (1:1), DIPEA, rt, 16 h; (e) Cs_2CO_3, DMF, 5 h, 90 °C.

The fragment-like structure of hit **1** provided reasonable opportunities for fragment-growing strategies toward generating drug like LANA−DNA inhibitors. Unfortunately, no X-ray or NMR structure was available when starting this hit optimization endeavor. Hence, structure-guided fragment-linking or -merging approaches were not feasible.

Chemistry. The synthesis of hit **1** was carried out starting from commercially available 2-iodonitrobenzene in two steps. Hit **1** and further imidazole derivatives **9**−**13** were synthesized via an Ullmann-type coupling reaction with a halogen nitrobenzene and the appropriate imidazole.[20] In a second step, the nitro group was reduced with tin(II) chloride to the amine to yield the target compounds **1** and **9**−**13**.[21] The *N*-acetyl derivative **8** was obtained by acetylation with acetyl anhydride. Furthermore, the 2-methoxyphenyl imidazole (**14**) was synthesized via copper salt catalyzed coupling of imidazole with (2-methoxyphenyl)boronic acid[22] and by cleaving the methyl group with aqueous HBr, affording the hydroxyl derivative **15**.[23] The synthesis of the benzoic acid derivatives was done by copper catalyzed coupling with the appropriate halo-benzoic acid and 1*H*-imidazole in a one-step reaction (Scheme 1).[24] Generation of 1-azidoaniline (**19**) was achieved by copper catalyzed C−H activation of aniline.[25] The azido intermediates (**20**−**24**) were synthesized from the corresponding anilines using standard azidation methods (concd H_2SO_4 or concd HCl, $NaNO_2$, NaN_3 in H_2O).[26] Methyl azidobenzoate (**25**) was synthesized by activation with thionyl chloride followed by treatment with methanol.[27] The 1,2,3-triazoles (**26**−**50**) were synthesized using standard copper(I)-catalyzed click reaction conditions. The appropriate alkyne was dissolved in 1:1 *tert*-butanol/water and treated with DIPEA, $CuSO_4 \cdot 5H_2O$, and sodium ascorbate under an argon atmosphere, followed by the addition of the corresponding azide. Amino-phenyl-substituted compounds (**51**−**55**) were synthesized from the appropriate amino-phenyl scaffold by treatment with different halogen alkyl analogues under basic conditions in DMF (Scheme 2).

Stepwise Hit Optimization and Biological Evaluation. For measuring the inhibitory effect of our compounds, we performed dose−response experiments using constant concentrations of the mutated LANA DBD (aa1008-1146) and fluorescence-labeled LBS2 with varying concentrations of the test compound. To exclude false positives through interaction with DNA or via fluorescence quenching, we conducted the dose-dependent experiments with and without addition of LANA. We did not observe any noticeable assay-interfering effect for any of the compounds. The results obtained with our FP-based interaction inhibition assay are listed in Table 1.

The aim of this first series of derivatives was to identify possible growth vectors to increase size and potency of the compound. Hence, substituents at the imidazole (R1) as well as the phenyl ring (R2) were introduced. Notably, moieties of different sizes (**11**−**13**) were tolerated at R1. In particular, the methyl derivative **11** showed an improved inhibitory effect of 91 ± 8% at 1 mM. We concluded that position R1 should be further explored (vide infra) as a possible growth vector. Regarding R2, we first varied the position of the amino group at the phenyl ring and investigated the effect of acetylation (compounds **8**−**10**). However, these modifications did not improve the inhibitory effect on the DNA−LANA interaction significantly. Hence, we introduced different hydrophilic moieties like nitro (**2**−**4**), methoxy (**14**), hydroxyl (**15**), and carboxy (**16**−**18**) groups instead. To our surprise, the presence of a carboxylic acid on the aromatic moiety was tolerated. For

DOI: 10.1021/acs.jmedchem.8b01827
J. Med. Chem. 2019, 62, 3924−3939

Table 1. Inhibitory Activities of 1*H*-Imidazole-1-yl Derivatives in FP Assay at 1 mM

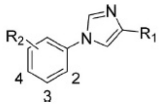

Cpd	R_1	R_2	inhibition [%] at 1 mM or IC_{50} [μM] (LBS2)
1	H	2-NH_2	25 ± 9 %
11	Me	2-NH_2	91 ± 8 %
12	Br	2-NH_2	13 ± 4 %
13	Benzimidazole	2-NH_2	32 ± 9 %
8	H	2-NHAc	32 ± 16 %
9	H	3-NH_2	n. i.
10	H	4-NH_2	n. i.
2	H	2-NO_2	74 ± 16 %
3	H	3-NO_2	21 ± 16 %
4	H	4-NO_2	22 ± 16 %
14	H	2-OMe	15 ± 12 %
15	H	2-OH	51 ± 13 %
16	H	2-COOH	333 ± 59 μM[a]
17	H	3-COOH	19 ± 9 %
18	H	4-COOH	13 ± 1 %

[a]Maximum effect was 50% displacement.

compound **16** we were able to plot a full sigmoidal inhibition curve providing an IC_{50} value of 333 ± 59 μM, with a restriction that the maximum effect leveled out at 50% displacement. Considering the rather basic interaction surface at the DNA-binding domain of LANA, the effectiveness of the acidic moiety in compound **16** was indeed a plausible finding in hindsight. Furthermore, it rendered an unfavorable compound−DNA interaction as the cause for the observed activity in the FP assay very unlikely.

These initial findings inspired us to conduct a combinatorial chemistry approach exploiting the copper(I)-catalyzed alkyne-azide cycloaddition as a straightforward synthetic method for the rapid generation of a reasonable number of new derivatives. This prototypic click chemistry provides very efficient and robust reactions under mild conditions and has become a powerful tool in drug discovery.[28] Assuming that the replacement of the imidazole moiety by a triazole core is tolerated, this strategy would dramatically accelerate the establishment of structure−activity relationships. Further considerations for the design of the click library were the envisioned fragment growth in the direction of residue R1 (Figure 4) as well as the switch from the amino to the carboxylic group in the western part of the molecule. Hence, we first checked whether this strategy was valid by synthesizing compounds **26**−**31** (Table 2).

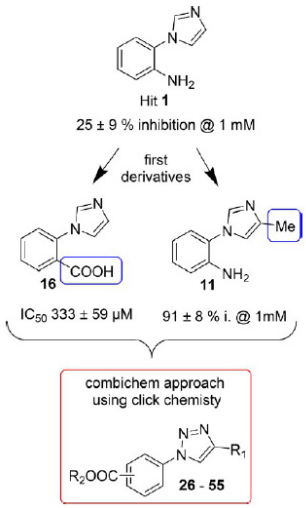

Figure 4. From our initial screening hit **1** first derivatizations lead to compounds **11** and **16**, which served as a starting point for a CombiChem approach using click chemistry.

Table 2. Inhibition of the First Series of 1,2,3-Triazole Compounds in FP Assay

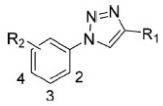

Cpd	R_1	R_2	IC_{50}(LBS2) [μM] or Inhibition [%][a]
26	H	2-COOH	12 ± 10 %
27	H	3-COOH	98 ± 1 %
28	H	4-COOH	35 ± 3 %
29		2-COOH	13 ± 1 %
30		3-COOH	43 ± 17 %
31		4-COOH	232 ± 10 μM

[a]Inhibition (%) at 1 mM.

Indeed, by comparing the carboxylic acid imidazole compounds (**16**−**18**) and the carboxylic acid triazole analogues (**26**−**28**), the introduction of a 1,2,3-triazole was accepted, although the preference for the orientation of the carboxylic acid was shifted from position 2 to 3. This trend even continued when introducing a bulky phenyl moiety in the eastern part of the molecule (**29**−**31**). In this case, position 4 was favored for the carboxylic group implying a shift in interaction geometries and/or binding modes between LANA and the inhibitors when moving from imidazolyl to triazolyl to enlarged triazolyl compounds. Derivative **31** showed reasonable potency (IC_{50} value of 232 ± 10 μM) with a significant improvement over inhibitor **16** and additionally provided the

DOI: 10.1021/acs.jmedchem.8b01827
J. Med. Chem. 2019, 62, 3924−3939

Table 3. Inhibitory Activities of Further 1,2,3-Triazole Derivatives in FP Assay

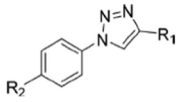

Cpd	R_1	R_2	IC_{50} (LBS2) [μM]	Cpd	R_1	R_2	IC_{50} (LBS2) [μM]
32		COOH	79 ± 2	**42**	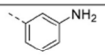	COOH	109 ± 3
33		COOH	30 ± 2	**43**	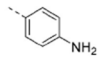	COOH	14 ± 1
34		COOH	210 ± 31	**44**	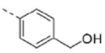	COOH	27 ± 4
35		COOH	n. i.	**45**		COOH	20 ± 3 % [a]
36		COOH	163 ± 30	**46**		H	n. i.
37		COOH	159 ± 2	**51**	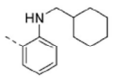	COOH	n. i.
38		COOH	694 ± 41	**52**	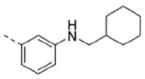	COOH	n. i.
39		COOMe	84 ± 53	**53**	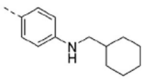	COOH	n. i.
40		COOMe	237 ± 33	**54**	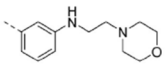	COOH	n. i.
41		COOH	28 ± 1	**55**	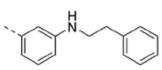	COOH	n. i.

[a]Inhibition (%) at 500 μM.

opportunity for further modifications replacing the newly introduced bulky phenyl ring. Consequently, we chose this scaffold as the basis for the click library design (Table 3) keeping the carboxylic acid in the *para* position at the aromatic ring in the western part and varying the substituents on the eastern side of the molecule.

A rather general observation when varying the residue R1 was that introducing hydrogen-bond-donating groups gave a boost in potency. In detail, direct attachment of a primary hydroxyl or amino group to the triazole core could improve the inhibitory effect by 3- to 4-fold (**32**: IC_{50} 79 ± 2 μM, **33**: IC_{50} 30 ± 2 μM). A methyl ether (**34**) or methyl ester (**36**), on the other hand, showed just a small potency enhancement compared to compound **29**, while the acetylated analogue **35** resulted in a complete loss of activity. Moving from the primary (**32**) to a tertiary alcohol (**37**) by addition of a cyclopentyl motif led to a decrease in activity. However, this derivative shows that obviously bulkier substituents could be tolerated at this position. Also, a rather hydrophobic cyclopropyl residue (**38**) did not yield a potent compound. In parallel, we synthesized two additional compounds with a methyl ester instead of the carboxylic acid at the aromatic ring, **39** and **40**. By comparing compound **32** with **39** and **34** with **40** it seems that also a methyl ester is well accepted, which certainly provides opportunities for future optimization efforts. Additionally, it becomes clear that the beneficial effect of the carboxylic group is not fully relying on a possible ionic interaction with the protein surface. As laid out above, our aim was to explore R1 as a growth vector. Hence, we synthesized aniline derivatives (**41**−**43**). Introducing the amino group in the *ortho* (**41**) or *para* (**43**) position resulted in the most active compounds to date with IC_{50} values in the low double-digit micromolar range. A loss of activity was observed with *m*-aniline (**42**) and *p*-anisole (**45**). Also, the phenyl methanol analogue (**44**) showed a rather potent IC_{50} value of 27 ± 4 μM. Keeping the aniline residue and deleting the carboxylic acid at the aromatic region we observed a total loss in activity (**46**). In order to further grow the LANA inhibitor, compounds substituted at the aniline (**51**−**55**) were synthesized. Unfortunately, none of these derivatives were active regardless

DOI: 10.1021/acs.jmedchem.8b01827
J. Med. Chem. 2019, 62, 3924−3939

of the position of the attached substituent. Probably these residues incorporated in **37**−**41** are too bulky and are, thus, not tolerated. Nevertheless, more research should be done in this area of the molecule when moving the project into the lead-generation phase. Finally, we synthesized a series of compounds with an inverted orientation of the 1,2,3-triazole core using 4-ethyl carboxylic acid and an array of azido benzenes. Compounds **47** and **48** were similar to the previous compounds **41** and **43** showing good IC_{50} values in the same range. Modifying the *para* aniline analogue to a *para* phenol (**49**) resulted in slight loss of activity. Besides that, for the 2-pyridine derivative **50** we observed an IC_{50} of 17 ± 1 μM (Table 4).

Table 4. Inhibitory Activities of Compounds with Inverted Orientation of the 1,2,3-Triazole Core in FP Assay

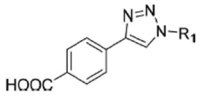

Cpd	R_1	IC_{50} (LBS2) [μM]
47		18 ± 3
48	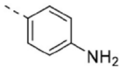	19 ± 1
49	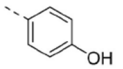	52 ± 3
50		17 ± 1

Qualification of Obtained Optimized Hits. *Comparison of the Inhibition of the Interaction between LANA and LBS1, 2, and 3.* In order to investigate whether inhibitors of the LANA−LBS2 interaction would also interfere with protein binding to the other LANA binding sites, we modified our FP assay protocol to also include labeled LBS1 and LBS3 sequences as fluorescent probes. We selected six compounds (**37**, **41**−**43**, **47**, **50**) with differing activities against LBS2 for this assessment, and the determined IC_{50} values are summarized in Table 5. Notably, we observed IC_{50} values in a similar range compared to the inhibition against the LBS2 probe. Additionally, we calculated the log *P* value and the ligand efficiency (LE) for these compounds to provide a metric for comparing the most potent hits taking potency and molecular weight into account.[29] The log *P* value is defined as the partition coefficient of a given compound between octanol and water. It provides information about its hydrophobicity, and log *P* values below 3 are found generally in an aqueous medium (e.g. blood serum).[30] The LE value is defined as the binding energy of a compound for its target divided by its number of heavy atoms, and hence, it enables to identify those hits, which interact efficiently with most of their atoms. In practice, an LE of 0.3 or greater is considered to characterize a suitable hit for the optimization to a drug-like compound.[31] Notably, compounds **41**, **43**, **47**, and **50** displayed an LE value of 0.3 or higher and log *P* values below 3, hence, are suitable scaffolds for further optimization efforts. Considering that these hits have to compete with a macromolecule (DNA) upon binding to a rather flat interaction surface, these results are encouraging.

EMSA (Electrophoretic Mobility Shift Assay) as Orthogonal Interaction Inhibition Assay. As an orthogonal interaction inhibition assay, EMSA was used to probe the ability of these six selected compounds to inhibit the DNA−LANA interaction (Figure 5). In this assay, solutions of protein, nucleic acid, and inhibitor were combined and the resulting mixtures were subjected to electrophoresis under native conditions.[32] We evaluated the effects of the compounds using fixed concentrations of DNA probes of 20 nM, LANA DBD mutant of 200 nM, and compounds of 500 μM. The probes were Dy-682-modified, and a purified GST protein was used as the control. We performed the EMSA with two different DNA probes: An oligonucleotide representing only LBS1 for comparing the results with the results of our previous FP assay (Figure 5A) and a longer oligonucleotide containing both of the LBS1 and LBS2 sequences (Figure 5B). The latter also forms trimeric complexes with LANA (Supporting Information, Figure S6). In both experiments, we observed that the compounds with IC_{50} values in the triple-digit micromolar range have no specific effect on the DNA−LANA interaction at the concentration used. Importantly, the aniline analogue having an IC_{50} value in the lower double-digit micromolar range caused a significant decrease in the intensity of the DNA−LANA complexes and an increase in the intensity of the band representing the free DNA probe. This clearly indicated that these compounds inhibit the interaction of the LANA DBD mutant with LBS1 and/or LBS1 + 2.

The most effective inhibitor was the pyridine analogue (**50**, IC_{50} 17 ± 1 μM). The single LBS1 probe (Figure 5A) could be displaced almost completely and the combined LBS1-LBS2 probe (Figure 5B) to a significant extent. Additionally, we performed further dose-dependent EMSA experiments with the most efficient compound **50** using LBS1 as the probe and the LANA DBD mutant as well as the wild-type LANA C-terminal domain (CTD) (aa934-1162) as the protein (for more information see the Supporting Information, EMSA gels: Figures S9 and S10; calculated IC_{50} values see Figure S11, IC_{50} (LANA DBD mutant) 426 ± 2 μM and IC_{50} (LANA CTD wild-type) 435 ± 6 μM).

MST and STD NMR Studies for Further Characterization of Ligand Binding. We used MST to quantify the binding affinity of compound **50** to the LANA DBD mutant and determined the dissociation constant K_D.[33] The binding assay was performed using the labeled LANA DBD mutant protein at a concentration of 50 nM and starting the dose−response curve with a ligand concentration of 1 mM. The calculated K_D for the binding of compound **50** to LANA was determined to be 23 ± 1 μM. The detected binding curve is shown in Figure 6A. We also attempted to perform crystallography on the LANA DBD−inhibitor complex but have so far not been successful. With the aim to gather information on the mode of binding, we performed ligand-observed STD NMR studies with compounds **41**, **47**, and **50**. The STD NMR can provide information on the putative orientation of a given binder to the target of interest in the absence of any structural data of the protein. In this assay, protons that are closest to the protein upon binding show the strongest STD effect. In our

DOI: 10.1021/acs.jmedchem.8b01827
J. Med. Chem. 2019, 62, 3924−3939

Table 5. Comparison of IC_{50} Values Obtained by Using LBS1, 2, or 3 as Fluorescent Probes, *c* log *P*, and LE

Cpd	structure	IC_{50} LBS1	IC_{50} LBS2	IC_{50} LBS3	clogP	LE
37	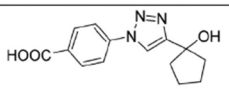	104 ± 33 μM	159 ± 2 μM	39 ± 4 μM	1.80	0.26
42	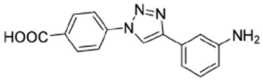	136 ± 27 μM	109 ± 3 μM	106 ± 32 μM	2.78	0.26
41	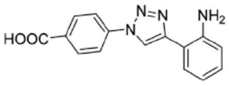	25 ± 1 μM	28 ± 1 μM	26 ± 1 μM	2.78	0.30
43	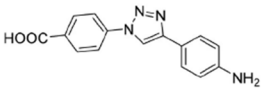	19 ± 55 μM	14 ± 1 μM	12 ± 1 μM	2.78	0.32
47	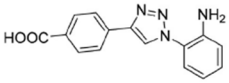	25 ± 1 μM	18 ± 3 μM	26 ± 1 μM	2.78	0.32
50	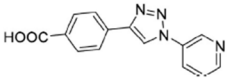	20 ± 3 μM	17 ± 1 μM	19 ± 3 μM	2.00	0.33

measurement, samples contained a 40-fold excess of the compound (1 mM) relative to the LANA DBD mutant (25 μM) and were recorded at 298 K (Figure 6B). The STD effects (I/I_0) were measured and calculated for each proton of the ligand. The STD effect of compound **50** is shown in Figure 6B. The overlaid spectra were normalized to the signals of H-1 and H-2, which gave the strongest enhancement and, hence, can be assumed to interact the most with the protein surface. These observable variations of the STD effects suggest that the compound binds in a defined orientation to the protein where the pyridine moiety faces the protein surface with its aromatic nitrogen. It can be assumed that this motif acts as a hydrogen bond acceptor. STD effects of H-3 and H-4 (53 and 61% of H-3 and H-4, respectively) suggest that these protons are not in direct contact with the protein and should be further investigated as potential growth vectors. Indeed, inactive compounds **51**−**55** were already grown in this direction and led to abolished activities.

However, the introduced residues were rather large leaving the option of smaller less bulky substituents to be tried. The four protons referred to by H-8 and H-9 presumably divide into two populations: two hydrogens, which are closer to the protein surface, and two, which are more remote (see Figure 6B). As these are indistinguishable in the STD NMR experiment, the observed effect should be a mean of the signals from both populations. As a consequence, growth of the compound breaking this ambiguity is a potential path forward in future optimization efforts.

For compounds **41** and **47** we observed similar STD effects (see Figure S12, Supporting Information). The protons from the aniline next to the amino group gave the strongest enhancement. This also implies that the NH_2 plays an important role as a hydrogen bond acceptor or donor for binding.

Molecular Docking. In order to generate a possible binding mode of the optimized hit **50** to LANA, we performed docking experiments taking the STD-NMR data into account. Importantly, we specifically searched for target−ligand complex geometries, which are in line with the gathered experimental data. As we demonstrated that this compound binds to LANA (FP assay, MST, STD NMR) and is able to displace the DNA (FP assay, EMSA), we directed our docking experiment to the DNA-binding site of the target (Figure 7A). This approach intentionally neglects a possible allosteric mechanism of our compound, which we consider to be rather unlikely due to the rigidity of the DNA-binding domain.

In order to identify the initial docking site, we selected those LANA residues, which were in close proximity (4.5 Å) to the DNA atoms found in PDB entry 4uzb.[7] Docking to this large interaction surface yielded three distinct clusters (Figure 7A). We searched for a binding pose of our inhibitor capable of prominently displacing the DNA from the protein. In general, cluster site 2 was located at the center of the LANA−nucleic acid interaction and would enable to disrupt major as well as minor groove interactions. Sites 1 and 3 were located on the peripheral areas of the LANA−DNA interface. Hence, we selected cluster site 2 for a more focused redocking experiment and screened the yielded binding poses for compliance with the STD NMR data (see Figure 6B). We selected the highest scoring pose, which met the criterion of bringing protons 1 and 2 as well as one pair of protons 8 and 9 into close proximity to the protein surface, while exposing protons 3, 4, and 5 as well as the other 8 and 9 pair (Figure S13, Supporting Information and Figure 6B). This pose was further refined through local

DOI: 10.1021/acs.jmedchem.8b01827
J. Med. Chem. 2019, 62, 3924−3939

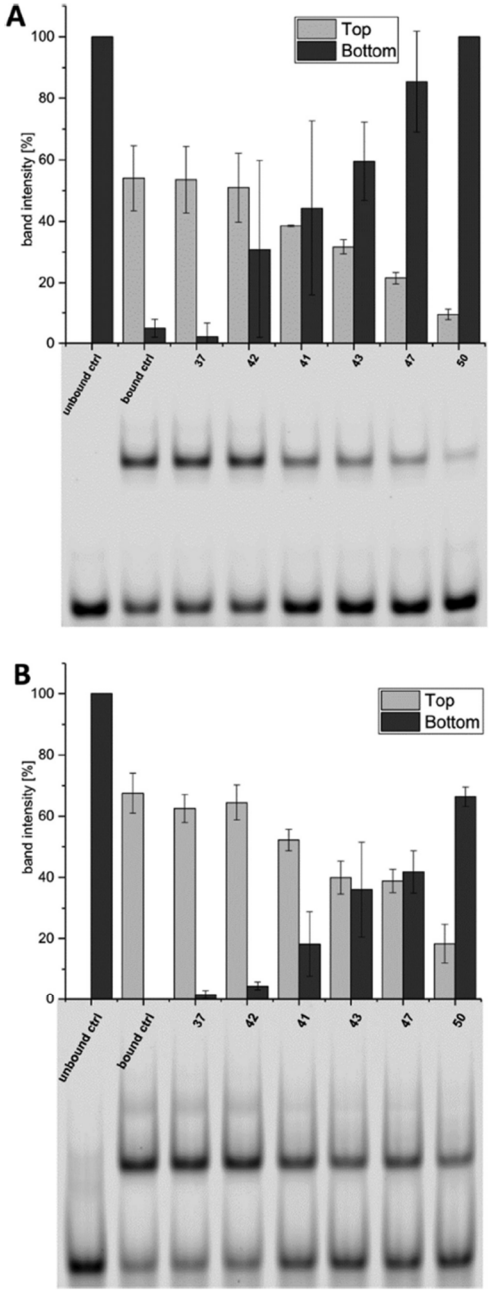

Figure 5. EMSA analysis of compounds **37**, **41**, **42**, **43**, **47**, and **50** using (A) LBS1 and (B) LBS1 + 2 as probes. Representative EMSA gels of one independent experiment are shown containing unbound control (GST + LBS1 or LBS1 + 2), bound control (DMSO + LANA + LBS1 or LBS1 + 2), and compounds (Cpd + LANA + LBS1, or LBS1 + 2). Bar graphs are shown with normalized data points (inhibition from 0−100%) representing mean intensities of top band values (LANA−LBS complex) and bottom band values (single LBS). The experiment was performed in duplicate, and the standard deviations were given; each compound was used at 500 μM, proteins were used at 200 nM, and DNA probe concentration was 20 nM.

energy minimization and is depicted in Figure 7B,C. A very prominent interaction partner suggested by this pose is Gln1015. Due to the symmetrical assembly of the LANA dimer, each Gln1015 from either of the two protein chains can contribute to inhibitor binding by acting as hydrogen-bond donors to the carboxyl group. Furthermore, Gln1073 and Val1019 form hydrogen-mediated interactions with the pyridine motif of **50**. As seen from the 2D interaction profile (Figure 7C), the proton at position 2 is detected as "solvent exposed" although it was in van der Waals contact with the protein (see Figure S13, Supporting Information). However, this is in agreement with the observation that introduction of an aniline motif is tolerated in this position (**43**). Finally, we postulate a possible cation−π interaction between nearby Lys1069 and the central triazole motif, which would further add to the attractive forces between LANA and the inhibitor. At this point, we would like to stress that the preferential docking pose is hypothetical and needs further validation through wet lab experiments, for example, via single-amino acid mutation of the strongly interacting Glu1015. Nonetheless, it is in line with currently available data and, hence, a plausible binding mode to base structure-guided modifications on. Next optimization efforts will be directed toward exploration of the proposed growth vectors (Figure 6B). The surface of LANA at the DNA-binding site is densely covered with possible hydrogen-bonding donors and acceptors, which could be exploited for further attractive interactions.

■ CONCLUSIONS

In this study, we successfully obtained a qualified fragment-sized hit capable of displacing a viral nucleic acid sequence from the DNA-binding domain of the latency-associated nuclear antigen (LANA)−a potential antiviral drug target to treat Kaposi's sarcoma herpesvirus (KSHV) infections. We achieved this by means of fragment-based drug design employing biophysical screening via SPR and DSF as two orthogonal selection filters followed by functional evaluation through fluorescence polarization (FP). FP also guided hit optimization toward low micromolar activity. Favorable ligand efficiency (>0.3) and low lipophilicity combined with additional EMSA, MST, and STD NMR experiments corroborating specific target interaction qualify hit **50** as a suitable starting point for a follow-up lead-generation campaign. Future optimization efforts will be aided by a wet lab-informed docking pose and amenability of the described scaffold to facilitate CombiChem-driven derivatization via click chemistry. In parallel, continuing efforts are underway to identify a suitable crystallographic system for the generation of protein−ligand complex structures, which would ultimately enable structure-based drug design. The ability to inhibit a nucleic-acid-involving macromolecule−macromolecule interaction by a small molecular scaffold is encouraging. The same is true for the promise to break the latent replication cycle of a herpesviral infection. In our opinion, both concepts are challenging yet worthwhile endeavors.

■ EXPERIMENTAL SECTION

Materials and Methods. All reagent-grade chemicals were obtained from commercial suppliers and were used as received. All reactions were carried out under an argon atmosphere. Automated column flash chromatography (CombiFlash Rf + von Teledyne ISCO, Lincoln, NE, USA) was performed on silica gel (Axel Semrau, Sprockhövel, Germany). Preparative high pressure liquid chromatog-

DOI: 10.1021/acs.jmedchem.8b01827
J. Med. Chem. 2019, 62, 3924−3939

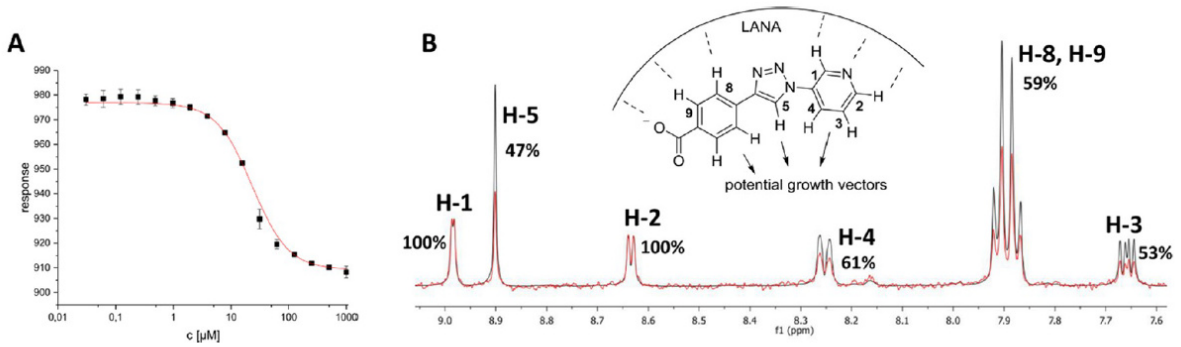

Figure 6. (A) Dose-dependent MST interaction curve of compound 50 with LANA DBD mutant. (B) STD experiments of compound 50 in complex with LANA DBD mutant. The reference spectrum is displayed in black (STD-off) and STD difference spectra (STD-on) in red. Overlaid spectra were normalized to the signals for H-1 and H-2, which showed the strongest enhancement.

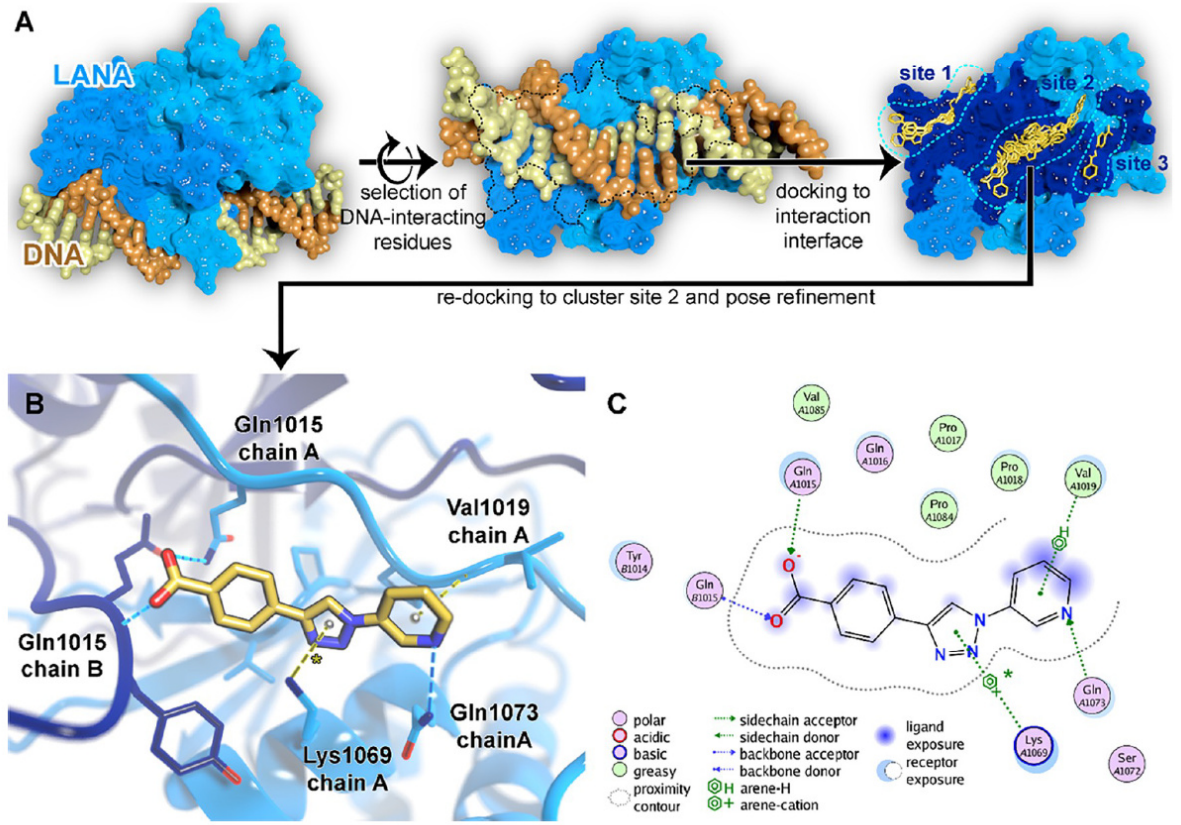

Figure 7. Design (A) and result (B,C) of STD-NMR-informed docking study performed on 50. (A) Docking was conducted using PDB entry 4uzb (left). Residues that make up the docking site were selected based on proximity (4.5 Å) to DNA in complex structure (dashed black lines, middle; dark blue surface, right). First docking resulted in three distinct clusters (light blue dashed lines; right). Cluster site 2 was selected for redocking and subsequent pose refinement. (B) 3D and (C) 2D representation of the plausible binding pose of 50. A putative cation−π interaction mediated by Lys1069 is shown and marked with an asterisk.

raphy (HPLC, Ultimate 3000 UHPLC+ focused, Thermo Scientific) purification was performed on a reversed-phase column (C18 column, 5 μm, Macherey-Nagel, Germany). For gradient elution a mobile phase consisting of acetonitrile containing 0.05% formic acid (FA) (v/v) and water containing 0.05% FA (v/v) was used. The syntheses were not optimized regarding yields. ^{1}H and ^{13}C NMR were recorded on a Bruker Fourier spectrometers (300/500 or 176/126/75 MHz). Chemical shifts (δ) are reported in parts per million (ppm) relative to each reference solvent. The chemical shifts recorded as δ values in ppm units by reference to the hydrogenated residues of the deuterated solvent as the internal standard. Coupling constants (J) are given in hertz (Hz), and splitting patterns are designated as follows: s, singlet; d, doublet; dd, doublet of doublets; t, triplet; m, multiplet; br., broad signal. Purity of all final compounds was measured on the UV trace

DOI: 10.1021/acs.jmedchem.8b01827
J. Med. Chem. 2019, 62, 3924−3939

recorded at a wavelength of 254 nm and was determined to be >95% by a reversed-phase liquid chromatography mass spectrometer (LCMS). High resolution mass spectra of all final compounds were measured on a Thermo Scientific Q Exactive Focus (Germany) equipped with a DIONEX ultimate 3000 UHPLC+ focused and can be found in the Supporting Information.

*Procedure I: General Synthesis of 1-(Nitrophenyl)-1H-imidazole **2**–**7***. The appropriate halo-nitrobenzene (1 equiv) was dissolved in DMF and treated with K_2CO_3 (1.2 equiv), CuI (0.1 equiv), and substituted 1*H*-imidazole (1.2 equiv) or 1*H*-benzoimidazole (1.2 equiv) under an argon atmosphere. The mixture was stirred at 120 °C for 24 h. After cooling to room temperature, the solids were filtered off and washed with ethyl acetate (3×). The combined filtrate was concentrated under reduced pressure. The resulting product was purified by column chromatography. Experimental details can be found in the Supporting Information. Compound **2** is presented as an example. 1-(2-Nitrophenyl)-1*H*-imidazole **2** was prepared according to general procedure I using 2-iodonitrobenzene (100 mg, 0.40 mmol), K_2CO_3 (66 mg, 0.48 mmol), CuI (7.5 mg, 0.04 mmol), 1*H*-imidazole (33 mg, 0.48 mmol), and DMF (3 mL). The obtained crude was purified by column chromatography (PE:EE 1:9) to yield the title compound (36 mg, 0.19 mmol, 49%). ^{1}H NMR (300 MHz, $CDCl_3$) δ ppm: 7.10 (s, 1 H), 7.25 (s, 1 H), 7.48 (dd, J = 7.82, 1.21 Hz, 1 H), 7.57–7.71 (m, 2 H), 7.71–7.79 (m, 1 H), 8.01 (dd, J = 8.06, 1.35 Hz, 1 H); ^{13}C NMR (75 MHz, $CDCl_3$) δ ppm: 125.35, 128.65, 129.62, 130.66, 133.70, 137.23.

*Procedure II: General Synthesis of (1H-Imidazol-1-yl)anilines **1** and **9**–**13***. 1-(Nitrophenyl)-1*H*-imidazole derivatives (1 equiv) were dissolved in ethanol and treated with tin(II) chloride (5 equiv). The mixture was refluxed for 30 min, and after cooling to room temperature, the solids were filtered off and washed with ethanol. The filtrate was combined, and the solvent was removed under reduced pressure. The crude was dissolved in ethyl acetate and extracted with saturated $NaHCO_3$ solution. The combined organic layers were dried over sodium sulfate and concentrated under reduced pressure. The products were purified by flash chromatography or by reversed-phase HPLC and were dried at a lyophilisator. Experimental details can be found in the Supporting Information. Compound **1** is presented as an example. 2-(1*H*-Imidazol-1-yl)aniline **1** was prepared by the general procedure II using 1-(2-nitrophenyl)-1*H*-imidazole **2** (150 mg, 0.79 mmol), $SnCl_2$ (890 mg, 3.96 mmol), and ethanol (20 mL). The obtained crude was purified by flash column chromatography (gradient elution, DCM/MeOH 95:5–90:10) to yield the target compound (108 mg, 0.67 mmol, 68%). ^{1}H NMR (300 MHz, $CDCl_3$) δ ppm: 3.80 (br. s, 2 H), 6.91–7.02 (m, 2 H), 7.20–7.31 (m, 2 H), 7.34–7.43 (m, 2 H), 7.79 (s, 1 H); ^{13}C NMR (75 MHz, $CDCl_3$) δ ppm: 116.35, 118.54, 120.09, 123.25, 127.11, 129.79, 129.92, 137.64, 141.90.

*N-(2-(1H-Imidazol-1-yl)phenyl)acetamide (**8**)*. 2-(1*H*-Imidazol-1-yl)aniline **1** (50 mg, 0.31 mmol) was dissolved in a mixture of acetic acid (4 mL) and acetic acid anhydride (2 mL). One drop of sulfuric acid was added, and the solution was stirred at room temperature for 16 h. The reaction mixture was neutralized with aqueous 10% NaOH solution and extracted with DCM (2×). The combined organic phases were dried over sodium sulfate and concentrated under reduced pressure to give the crude, which was purified by HPLC (reversed-phase, mobile phase consisting of acetonitrile containing 0.05% FA (v/v) and water containing 0.05% FA (v/v), gradient elution: 5:95–60:40) to yield the target compound (8 mg, 0.04 mmol, 13%). ^{1}H NMR (300 MHz, $CDCl_3$) δ ppm: 2.12 (s, 3 H), 7.06–7.11 (m, 1 H), 7.19 (d, J = 1.02 Hz, 1 H), 7.23 (s, 1 H), 7.24 (s, 1 H), 7.43–7.51 (m, 1 H), 7.51–7.54 (m, 1 H), 7.74 (s, 1 H), 8.25 (d, J = 8.20 Hz, 1 H); ^{13}C NMR (75 MHz, $CDCl_3$) δ ppm: 24.28, 120.20, 123.78, 124.99, 126.79, 129.83, 130.30, 133.36, 137.63, 168.90.

*1-(2-Methoxyphenyl)-1H-imidazole (**14**)*. (2-Methoxyphenyl)-boronic acid (150 mg, 0.98 mmol), 1*H*-imidazole (80 mg, 1.18 mmol), and CuCl (5 mg, 0.05 mmol, 5 mol %) were dissolved in methanol (10 mL) and refluxed for 16 h. After cooling to room temperature the solvent was removed under reduced pressure, and the obtained crude was dissolved in ethyl acetate and extracted with water. The combined organic phases were dried over sodium sulfate and concentrated under reduced pressure to give the crude. The crude was purified by column chromatography (DCM/MeOH 95:5) to yield the title compound (70 mg, 0.40 mmol, 41%). ^{1}H NMR (300 MHz, methanol-d_4) δ ppm: 3.87 (s, 3 H), 7.01–7.13 (m, 2 H), 7.22 (d, J = 8.29 Hz, 1 H), 7.30–7.48 (m, 3 H), 7.88 (s, 1 H); ^{13}C NMR (75 MHz, methanol-d_4) δ ppm: 56.58, 113.90, 122.15, 122.30, 126.91, 127.62, 128.75, 130.77, 139.18, 154.33.

*2-(1H-Imidazol-1-yl)phenol (**15**)*. 1-(2-Methoxyphenyl)-1*H*-imidazole **14** (50 mg, 0.28 mmol) was dissolved in 48% hydrobromic acid in water (6 mL) and refluxed for 16 h. The mixture was neutralized with saturated $NaHCO_3$ solution and extracted with ethyl acetate (2×). The combined organic phases were dried over sodium sulfate and concentrated under reduced pressure to give the crude, which was purified by column chromatography (DCM/MeOH 95:5) to yield the title compound (40 mg, 0.25 mmol, 90%). ^{1}H NMR (300 MHz, DMSO-d_6) δ ppm: 6.91 (td, J = 7.59, 1.40 Hz, 1 H), 6.98–7.11 (m, 2 H), 7.16–7.26 (m, 1 H), 7.33 (dd, J = 7.87, 1.63 Hz, 1 H), 7.45 (s, 1 H), 7.94 (s, 1 H), 10.27 (br. s, 1 H); ^{13}C NMR (75 MHz, DMSO-d_6) δ ppm: 116.90, 119.54, 124.75, 125.25, 128.47, 150.23.

*Procedure III: General Procedure of (1H-Imidazol-1-yl)benzoic Acids **16**–**18***. The appropriate halo-benzoic acid (1 equiv) was dissolved in DMF (0.1 M) and treated with *N*1,*N*2-dimethylethane-1,2-diamine (0.2 equiv), K_2CO_3 (2.2 equiv), CuCl (0.1 equiv), and 1*H*-imidazole (1.5 equiv) under an argon atmosphere. The mixture was stirred at 120 °C for 24 h. After cooling to room temperature the solids were filtered off and washed with ethyl acetate. The combined filtrate was concentrated under reduced pressure. The resulting product was purified using preparative HPLC (reversed-phase, mobile phase consisting of acetonitrile containing 0.05% FA (v/v) and water containing 0.05% FA (v/v); gradient elution, 5:95–90:10) to yield the target compound. Experimental details can be found in the Supporting Information. Compound **16** is presented as example. 2-(1*H*-Imidazol-1-yl)benzoic acid **16** was prepared according to general procedure III using 2-iodobenzoic acid, *N*1,*N*2-dimethylethane-1,2-diamine, K_2CO_3, CuCl, 1*H*-imidazole, and DMF. ^{1}H NMR (500 MHz, DMSO-d_6) δ ppm: 7.40 (br. s, 1 H), 7.57 (br. s, 1 H), 7.59–7.72 (m, 2 H), 7.72–7.84 (m, 1 H), 7.99 (br. s, 1 H), 8.51 (br. s, 1 H); ^{13}C NMR (126 MHz, DMSO-d_6) δ ppm: 119.23, 120.21, 123.52, 126.37, 127.64, 130.14, 130.25, 135.58, 138.45, 166.53.

*2-Azidoaniline (**19**)*. Aniline (500 mg, 5.4 mmol) was dissolved in acetonitrile (100 mL). *tert*-Butylhydroperoxide (1.5 mL, 8.1 mmol) and copper(I) bromide (77 mg, 0.5 mmol) were added, and the mixture was cooled to 0 °C. At 0 °C $TMSN_3$ (1.4 mL, 10.7 mmol) was added dropwise, and the reaction mixture was stirred at room temperature overnight. The solvent was removed under reduced pressure, and the crude product was purified by flash chromatography (PE:EE, gradient elution, 1:0–9:1) to yield the target compound (230 mg 1.72 mmol, 32%). ^{1}H NMR (300 MHz, $CDCl_3$) δ ppm: 7.05 (d, 1 H, J = 9 Hz), 6.97 (dd, 1 H, J = 7.5 Hz), 6.80 (dd, 1 H, J = 7.5 Hz), 6.71 (d, 1 H, J = 3 Hz), 3.81 (br. s, 2 H); ^{13}C NMR (75 MHz, $CDCl_3$) δ ppm: 138.1, 125.6, 125.2, 119.1, 118.3, 115.8.

*Azido Benzene (**20**)*. Aniline (364 mg, 4.0 mmol) was dissolved in ethyl acetate (8 mL) and cooled to 0 °C, and water (1 mL) and concentrated HCl (2.4 mL) were added. Sodium nitrite (469 mg, 6.8 mmol, 1.7 equiv) dissolved in water (1 mL) was added slowly. The reaction mixture was stirred for 30 min at 0 °C. Subsequently, sodium azide (442 mg, 6.8 mmol, 1.7 equiv) in water (1 mL) was added slowly at 0 °C. After stirring at room temperature for 1.5 h, TLC indicated full conversion and the mixture was neutralized and extracted with ethyl acetate (2×). The combined organic phases were dried over sodium sulfate and concentrated under reduced pressure to give the crude. The crude product (300 mg) was used as obtained in the next step without further purifications.

*2-Azidobenzoic Acid (**21**)*. Anthranilic acid (300 mg, 2.2 mmol) were dissolved in a mixture of water (10 mL) and sulfonic acid (2 mL) and cooled to 0 °C. Sodium nitrite (151 mg, 2.2 mmol) was dissolved in water (1 mL) and added dropwise. The reaction mixture was stirred for 15 min at 0 °C. Subsequently, sodium azide (172 mg,

DOI: 10.1021/acs.jmedchem.8b01827
J. Med. Chem. 2019, 62, 3924–3939

2.6 mmol) in water (1 mL) was added slowly at 0 °C. After stirring at room temperature for 2 h, TLC indicated full conversion and the mixture was diluted with water and extracted with ethyl acetate (2×). The combined organic phases were dried over sodium sulfate and concentrated under reduced pressure to give the crude. The crude product (250 mg) was used as obtained in the next step without further purifications. MS (ESI−) m/z 162 (M − H).

*3-Azidobenzoic Acid (**22**).* 3-Aminobenzoic acid (300 mg, 2.2 mmol) was dissolved in a mixture of water (10 mL) and sulfonic acid (2 mL) and cooled to 0 °C. Sodium nitrite (151 mg, 2.2 mmol) was dissolved in water (1 mL) and added dropwise. The reaction mixture was stirred for 15 min at 0 °C. Subsequently, sodium azide (172 mg, 2.6 mmol) in water (1 mL) was added slowly at 0 °C. After stirring at room temperature for 2 h, TLC indicated full conversion and the mixture was diluted with water and extracted with ethyl acetate. The combined organic phases were dried over sodium sulfate and concentrated under reduced pressure to give the crude. The crude product (220 mg) was used as obtained in the next step without further purifications. MS (ESI) m/z 162 (M−H).

*4-Azido Phenol (**23**).* 4-Aminophenol (436 mg, 4.0 mmol) was dissolved in 6 M HCl (15 mL). Sodium nitrite (469 mg, 6.8 mmol, 1.7 equiv) was dissolved in water (3 mL) and added. The reaction mixture was stirred for 30 min at 0 °C. Subsequently, sodium azide (442 mg, 6.8 mmol, 1.7 equiv) in water (1 mL) was added slowly at 0 °C. After stirring at room temperature for 1.5 h, TLC indicated full conversion and the mixture was neutralized and extracted with ethyl acetate (2×). The combined organic phases were dried over sodium sulfate and concentrated under reduced pressure to give the crude. The crude product (290 mg) was used as obtained in the next step without further purifications.

*3-Azido Pyridine (**24**).* 3-Aminopyridine (376 mg, 4.0 mmol) was dissolved in ethyl acetate (8 mL) and cooled to 0 °C, and water (1 mL) and concentrated HCl (2.4 mL) were added. Sodium nitrite (469 mg, 6.8 mmol, 1.7 equiv) dissolved in water (1 mL) was added dropwise. The reaction mixture was stirred for 30 min at 0 °C. Subsequently, sodium azide (442 mg, 6.8 mmol, 1.7 equiv) in water (1 mL) was added slowly at 0 °C. After stirring at room temperature for 1.5 h, TLC indicated full conversion and the mixture was basified with saturated Na_2CO_3 solution (pH 10) and extracted with ethyl acetate (2×). The combined organic phases were dried over sodium sulfate and concentrated under reduced pressure to give the crude. The crude product (280 mg) was used as obtained in the next step without further purifications.

*Methyl 4-Azidobenzoate (**25**).* 4-Azidobenzoic acid (300 mg, 1.8 mmol) was dissolved in methanol (10 mL) and cooled to 0 °C. Thionyl chloride (297 μL, 4.14 mmol) was added dropwise at 0 °C, and the reaction mixture was stirred at room temperature overnight. The solvent was removed, and the obtained crude was purified by flash chromatography (PE:EE, gradient elution, 1:0−95:5) to yield the product (305 mg, 1.7 mmol, 94%). MS (ESI+) m/z 178 (M + H).

*Procedure IV: General Synthetic Procedure for (1H-1,2,3-Triazol-1-yl)benzoic Acids **26**−**28**.* Ethynyltrimethyl silane (1.0 equiv) was suspended in 1:1 mixture of water and methanol under an argon atmosphere. Copper sulfate heptahydrate (0.5 equiv) and sodium ascorbate (0.5 equiv) were added. After addition of the corresponding azide (1.0 equiv) the mixture was stirred for 24 h at room temperature. After full conversion (TLC control) the mixture was acidified with 1 M HCl for cleaving the TMS group and extracted with dichloromethane (2×). The combined organic phases were dried over sodium sulfate and concentrated under reduced pressure to give the crude. The crude product was purified using preparative HPLC (reversed-phase, mobile phase consisting of acetonitrile containing 0.05% FA (v/v) and water containing 0.05% FA (v/v); gradient elution, 5:95−90:10) and dried on a lyophilizer to yield the target compound. Experimental details can be found in the Supporting Information. Compound **26** is presented as example. 2-(1*H*-1,2,3-Triazol-1-yl)benzoic acid **26** was synthesized according to procedure IV using 2-azidobenzoic acid and ethynyltrimethylsilane as starting materials. ^{1}H NMR (500 MHz, DMSO-d_6) δ ppm: 7.60 (s, 1 H), 7.63−7.70 (m, 1 H), 7.73−7.79 (m, 1 H), 7.91 (d, J = 8.70 Hz, 2 H), 8.51 (s, 1 H); ^{13}C NMR (126 MHz, DMSO-d_6) δ ppm: 126.47, 126.53, 129.84, 130.38, 132.29, 133.35, 135.36, 166.62.

*Procedure V: General Synthetic Procedure for Synthesis of Copper Catalyzed Click Reaction of Alkynes and Azides (Compounds **29**−**50**).* Under an argon atmosphere the appropriate alkyne (1.0 equiv) was suspended in a 1:1 mixture of water and *tert*-butanol. DIPEA (2.0 equiv), copper sulfate heptahydrate (0.5 equiv), and sodium ascorbate (0.5 equiv) were added. After addition of the corresponding azide (1.0 equiv) the mixture was stirred for 16 h at room temperature. After full conversion (TLC control) the mixture was acidified with 1 M HCl and the product was precipitated. The solids were collected, washed with water, and dried under vacuum to obtain the crude product. The products were purified by preparative HPLC (reversed-phase, mobile phase consisting of acetonitrile containing 0.05% FA (v/v) and water containing 0.05% FA (v/v); gradient elution, 5:95−90:10) and dried on a lyophilizer. The reactions and purification steps were not optimized regarding yields. Experimental details can be found in the Supporting Information. Compound **31** is presented as an example. 4-(4-Phenyl-1*H*-1,2,3-triazol-1-yl)benzoic acid **31** was synthesized according to procedure V using 4-azidobenzoic acid and ethynyl benzene as starting materials. ^{1}H NMR (300 MHz, DMSO-d_6) δ ppm: 7.39 (dd, J = 7.39 Hz, J = 7.39 Hz, 1 H), 7.50 (dd, J = 7.50 Hz, J = 7.50 Hz, 2 H), 7.95 (d, J = 7.45 Hz, 2 H), 8.16 (s, 3 H), 9.41 (s, 1 H); ^{13}C NMR (75 MHz, DMSO-d_6) δ ppm: 119.65, 125.37, 128.38, 129.01, 129.99, 139.46, 147.56, 167.52.

*Procedure VI: General Procedure for 4-(4-(((Cyclohexylmethyl)-amino)phenyl)-1H-1,2,3-triazol-1-yl)benzoic Acid **51**−**53**.* The appropriate 4-(4-(aminophenyl)-1*H*-1,2,3-triazol-1-yl)benzoic acid (30 mg, 0.11 mmol, 1 equiv), cesium carbonate (107 mg, 0.33 mmol, 3 equiv), and (bromomethyl)cyclohexane (39 mg, 0.22 mmol, 2 equiv) were dissolved in DMF (5 mL) and stirred at 90 °C for 5 h. After cooling to room temperature 1 M HCl was added and the mixture was extracted with DCM (2×). The combined organic phases were dried over sodium sulfate and concentrated under reduced pressure to give the crude. Purification was done by flash column chromatography (DCM/MeOH, gradient elution, 95:5−90:10) to yield the target compound. Experimental details can be found in the Supporting Information. Compound **51** is presented as example and was obtained with 72% (29 mg, 0.08 mmol) yield. ^{1}H NMR (500 MHz, $CDCl_3$) δ ppm 1.03−1.16 (m, 2 H) 1.19−1.35 (m, 4 H) 1.73 (d, J = 12.05 Hz, 1 H) 1.77−1.83 (m, 2 H) 1.83−1.90 (m, 2 H) 4.20 (d, J = 6.26 Hz, 2 H) 5.48 (br. s., 1 H) 6.73−6.86 (m, 2 H) 7.15−7.23 (m, 1 H) 7.46 (dd, J = 7.71, 1.30 Hz, 1 H) 7.92 (d, J = 8.54 Hz, 2 H) 8.18−8.33 (m, 3 H); ^{13}C NMR (126 MHz, $CDCl_3$) δ ppm 25.68, 26.35, 29.76, 34.68, 37.24, 70.54, 112.96, 116.93, 117.54, 117.56, 119.99, 127.89, 129.59, 130.78, 131.36, 139.93, 145.30, 149.43, 165.47.

*4-(4-(3-((2-Morpholinoethyl)amino)phenyl)-1H-1,2,3-triazol-1-yl)benzoic Acid (**54**).* 4-(4-(3-Aminophenyl)-1*H*-1,2,3-triazol-1-yl)-benzoic acid **42** (30 mg, 0.11 mmol, 1 equiv), cesium carbonate (107 mg, 0.33 mmol, 3 equiv), and 4-(2-chloroethyl)morpholine (331 mg, 0.22 mmol, 2 equiv) were dissolved in DMF (5 mL) and stirred at 90 °C for 5 h. After cooling to room temperature the solvent was removed under reduced pressure and purified by flash column chromatography (DCM/MeOH, gradient elution, 95:5−90:10) to yield the target compound (16 mg, 0.04 mmol, 36%). ^{1}H NMR (500 MHz, $CDCl_3$) δ ppm: 2.57−2.63 (m, 4 H), 2.81 (t, J = 5.87 Hz, 2 H), 3.72−3.76 (m, 5 H), 3.81 (br. s, 2 H), 4.52 (t, J = 5.87 Hz, 2 H), 6.72 (dt, J = 7.52, 1.74 Hz, 1 H), 7.21−7.26 (m, 2 H), 7.36 (s, 1 H), 7.92 (d, J = 8.54 Hz, 2 H), 8.22 (s, 2 H), 8.24 (s, 1 H); ^{13}C NMR (126 MHz, $CDCl_3$) δ ppm: 53.88, 57.08, 62.69, 66.97, 112.36, 115.38, 116.15, 117.24, 119.85, 129.93, 130.20, 130.77, 131.39, 140.17, 147.00, 148.94, 165.32.

*4-(4-(3-(Phenethylamino)phenyl)-1H-1,2,3-triazol-1-yl)benzoic Acid (**55**).* 4-(4-(3-Aminophenyl)-1*H*-1,2,3-triazol-1-yl)benzoic acid **42** (30 mg, 0.11 mmol), cesium carbonate (107 mg, 0.33 mmol, 3 equiv), and (2-bromoethyl)benzene (41 mg, 0.22 mmol, 2 equiv) were dissolved in DMF (5 mL) and stirred at 90 °C for 5 h. After cooling to room temperature 1 M HCl was added and the mixture

DOI: 10.1021/acs.jmedchem.8b01827
J. Med. Chem. 2019, 62, 3924−3939

was extracted with DCM (2×). The combined organic phases were dried over sodium sulfate and concentrated under reduced pressure to give the crude. Purification was done by flash column chromatography (DCM/MeOH, gradient elution, 95:5−90:10) to yield the target compound (20 mg, 0.05 mmol, 45%). ^{1}H NMR (500 MHz, $CDCl_3$) δ ppm: 3.13 (t, J = 6.94 Hz, 2 H), 3.81 (br. s, 1 H), 4.59 (t, J = 6.94 Hz, 2 H), 6.72 (d, J = 7.63 Hz, 1 H), 7.21−7.26 (m, 2 H), 7.28−7.33 (m, 3 H), 7.35 (d, J = 7.63 Hz, 3 H), 7.89−7.92 (m, 2 H), 8.18−8.21 (m, 2 H), 8.22 (s, 1 H); ^{13}C NMR (126 MHz, $CDCl_3$) δ ppm: 35.19, 65.86, 112.36, 115.36, 116.14, 117.26, 119.81, 126.70, 128.57, 128.60, 128.90, 128.94, 129.91, 130.29, 130.78, 131.33, 131.36, 137.67, 140.10, 147.00, 148.90, 165.32.

Expression and Purification of His-Tagged Oligomerization-Deficient Mutant of the KSHV LANA C-Terminal DNA-Binding Domain (DBD; aa1008−1146). For the expression of KSHV His-tagged oligomerization-deficient LANA DBD (aa1008−1146) protein pETRO1.01 vector BL21 (DE3) cells were used.[7] The His-tagged LANA DBD target protein was purified by Ni-NTA affinity chromatography (HisTrap HP column) using ÄKTAxpress (GE Healthcare). For more details see the Supporting Information.

Screening Library. The screening library contained 220 diverse fragment compounds from Asinex (Winston-Salem, NC, USA) and 500 from Maybridge (Loughborough, U.K.). The compounds possessing molecular weights (MWs) from 142 to 398 g/mol and were dissolved in DMSO to 10 or 20 mM stocks.

Surface Plasmon Resonance (SPR) Screening. SPR experiments were performed in running buffer (10 mM PBS, pH = 7.4, 5% DMSO (v/v), 0.05% Tween20 (v/v)) using a Reichert SR7500 biosensor (Buffalo, NY, USA) with research-grade CMD-500 M sensor chips provided by XanTec Bioanalytics (Düsseldorf, Germany) at 18 °C. All experiments were performed in two independent experiments. Scrubber 2 software (Version 2.0c 2008, BioLogic Software) was used for processing and analyzing the data. Changes in the refractive index due to DMSO-dependent solvent effects were corrected by using a calibration curve (seven solutions, 4.75−5.75% DMSO in buffer).

We immobilized the wild-type LANA C-terminal domain (LANA CTD (aa934−1162))on CMD500 sensor chips using standard amine coupling with ddH_2O as immobilization buffer at 25 °C. The carboxymethyl dextran surface was first prepared with sodium borate (1 M, pH 9.5) (5 injections) and was activated with a 7 min injection of a 1:1 ratio of 0.4 M 1-ethyl-3-(3-dimethylaminopropyl)-carbodiimide hydrochloride (EDC) to 0.1 M *N*-hydroxysuccinimide (NHS). LANA CTD was diluted into sodium acetate (10 mM, pH 4.5) to 10 mM solution and coupled to the surface with a 1.5 min injection. Remaining activated groups were blocked with a 7 min injection of 1 M ethanolamine (pH 8.5).

Binding experiments were performed at a constant flow rate of 20 μL/min, and before starting the experiments, 12 warm-up blank injections were done. Zero-buffer blank injections were included for referencing. For SPR screening, all compounds were tested at 500 μM. Each sample was injected twice on two different sensor chips. To collect the binding response the sample was dissolved in running buffer and injected for 120 s association and 300 s dissociation. Compounds that showed a response higher than 9 RU were selected from the first screening (52 compounds). Results are shown in Figure S1.

Differential Scanning Fluorimetry (DSF) Screening. DSF experiments were performed in running buffer (10 mM PBS, pH = 7.4, 5% DMSO (v/v), 0.05% Tween20 (v/v)) using a StepOne Plus Real Time PCR System (Biosystem, Life Technologies Corporation), StepOne Software (StepOne and StepOne Plus Real Time PCR System Version 2.3) as collecting data software, and Applied Biosystem (Protein Thermal Shift Software Version 1.1) as analyzing software. Final concentrations of 20 μM wild-type LANA C-terminal domain (LANA CTD (aa934−1162)) and 500 μM compounds were used. The 52 positive compounds from SPR screening were tested. Compounds showing T_M > + 0.5 °C and T_M < −1 °C were selected for further investigations. Results are shown in Figure S2.

Fluorescence Polarization (FP) Assay. FP was recorded in black 384 well microtiter plates (Greiner Bio-One, catalog number 781900) using a CLARIOstar microplate reader (BMG LABTECH, Ortenberg, Germany) with an extinction filter at 485 nm and emission filter at 520 nm. Gain adjustment was performed before starting each measurement to achieve maximum sensitivity. The FP values were measured in millipolarization units (mP). The experiments were performed in two independent experiments, and each sample was tested in duplicate. In all experiments the inhibitor and His-tagged oligomerization-deficient LANA DBD (aa1008−1146) mutant (final concentration 200 nM) were preincubated for 60 min. After addition of fluorescent labelled DNA (LBS1_flc, LBS2_flc, or LBS3_flc, final concentration 10 nM) the samples were incubated for 90 min. The assay was performed in FP-Buffer (10 mM HEPES, 150 mM NaCl, 0.005% (v/v) Tween20, DEPC water) with 5% DMSO. Assay optimization studies can be found in Figure S3.

Microscale Thermophoresis (MST). According to the MST (nanotemper-technologies.com) guided procedure, the His-tagged oligomerization-deficient LANA DBD (aa1008−1146) mutant was labeled using the Monolith NTTM His-Tag Labeling Kit RED-tris NTA. The binding assay was performed as described in the MST guided procedure, and MST-Buffer (10 mM HEPES, 150 mM NaCl, 2 mM DTT, 0.005% (v/v) Tween20, DEPC water) with 5% DMSO was used.

Electrophoretic Mobility Shift Assay (EMSA). The EMSA was carried out with slight modifications as described in Hellert et al.[14] The His-tagged oligomerization-deficient LANA DBD (aa1008−1146) mutant protein (200 nM final) was incubated with the compounds (500 μM final) for 1 h at RT in the dark in a reaction volume of 15 μL. The reaction buffer consisted of 30 mM Tris HCl pH 7.5, 50 mM KCl, 10 mM $MgCl_2$, 1 mM DTT, 1 mM EDTA, 10% glycerol, 0.25% Tween 20, 0.5 mg/mL BSA, and 0.05 mg/mL poly(dI-dC). After the initial incubation period the 5′-Dy682-labeled double stranded DNA probe (IBA Lifesciences) (20 nM final) was added to the reaction and incubated for another 30 min at RT in the dark. 10 μL of the reaction was run on a pre-run native 5% acrylamide gel for 45 min at 100 V with tris-borate-EDTA buffer. Images of the gels were acquired with the Odyssey (Licor) using the Image Studio software. Raw data can be found in Figures S7 and S8.

Saturation-Transfer Difference (STD) NMR. The STD experiments were recorded at 298 K on a Bruker Fourier spectrometer (500 MHz). The samples contained a 40-fold excess of compound (1 mM final) relative to the C-terminal His-tagged oligomerization-deficient LANA DBD (aa1008−1146) mutant (25 μM final). The control spectra were recorded under the same conditions containing the free compound to test for artifacts. The STD buffer considered 20 mM bis-tris-Cl, 300 mM NaCl, 2 mM DTT, pH 6.5 in D_2O containing 5% DMSO-d_6. The experiments were recorded with a carrier set at 0 ppm for the on-resonance and −40 ppm for the off-resonance irradiation. Selective protein saturation was carried out at 2 s by using a train of 50 ms Gauss-shaped pulses, each separated by a 1 ms delay. The difference in intensity due to saturation transfer was quantified using $STD_{effect} = (I_0 - I_{sat})/I_0$ and constitutes an indication of binding. I_{sat} is the intensity of a signal in the on-resonance NMR spectrum, and I_0 is the intensity of one signal in the off-resonance or reference NMR spectrum.

Molecular Docking. All docking experiments were performed with MOE 2018.01 (Molecular Operating Environment, Chemical Computing Group),[34] while graphic processing for manuscript figures was done using YASARA structure (YASARA Biosciences GmBH)[35] and POV-Ray 3.7.0. First, 4uzb was loaded into MOE. LANA residues in 4.5 Å proximity to DNA atoms were selected and used as initial docking sites. Then compound **50** was docked in its deprotonated form to this site ignoring solvent, using "Triangle Matcher" as the placement method and "London dG" as the scoring function with 300. Refinement was done using the "Induced Fit" method and "GBVI/WSA dG" scoring function with 50 poses. Amber10:EHT was used as the force field. For the redocking experiment we used the 14 ligand poses found in cluster 2 as docking sites ignoring solvent, using Triangle Matcher as the placement method and London dG as the

DOI: 10.1021/acs.jmedchem.8b01827
J. Med. Chem. 2019, 62, 3924−3939

scoring function with 100. Refinement was done using the Induced Fit method and GBVI/WSA dG scoring function with 10 poses. Amber10:EHT was used as the force field. The proposed binding pose depicted in Figure 7 was selected from the resulting array of poses based on the following criteria: (1) compliance to STD-NMR data (see also Figure S12); (2) docking score; and (3) number of occurrence. The highest score of the selected pose was position 35, and it occurred eight times within the 140 generated poses. Refinement of the selected pose was done using the built-in "QuickPrep" function with standard parameters and the Amber10:-EHT force field.

■ ASSOCIATED CONTENT

Supporting Information

The Supporting Information is available free of charge on the ACS Publications website at DOI: 10.1021/acs.jmedchem.8b01827.

Synthetic procedures and characterizations of compounds **3**−**7**, **11**−**13**, **17**, **18**, **27**−**30**, **32**−**50**, **52**, and **53**, high resolution mass spectra of all final compounds, more details to SPR screening results, DSF screening results and FP assay condition optimizations as well as concentration-dependent FP experiments of compounds **37**, **41**−**43**, **47**, and **50**, EMSA row data for compounds **37**, **41**−**43**, **47**, and **50**, concentration-dependent EMSA for compound **50** and further STD NMR spectra for compounds **41** and **47** (PDF).

Docking was performed only with PDB entry 4uzb (PDB)

Docking was performed only with PDB entry 4uzb (PDB)

Molecular formula strings and some data (CSV)

■ AUTHOR INFORMATION

Corresponding Author

*E-mail: Martin.Empting@helmholtz-hzi.de. Phone: +(49) 681 988062031.

ORCID

Martin Empting: 0000-0002-0503-5830

Author Contributions

All authors have given approval to the final version of the manuscript.

Funding

This work was financial supported by the German Centre for Infection Research (DZIF) and the DFG Collaborative Research Centre 900, project C1.

Notes

The authors declare no competing financial interest.

■ ACKNOWLEDGMENTS

We thank Prof. Dr. Rolf W. Hartmann for his continuous support and guiding expertise. For the help with the SPR and DSF screening we thank Dr. Elisabeth Weidel, and for helping with the establishment of the FP-based assay, Dr. Christine Maurer and Dr. Jan Hellert.

■ ABBREVIATIONS

AcOH, acetic acid; Ac_2O, acetic anhydride; AIDS-KS, acquired immune deficiency syndrome-related Kaposi's sarcoma; CTD, C-terminal domain; DCM, dichloromethane; DMSO, dimethylsulfoxide; DNA, deoxyribonucleic acid; DBD, DNA-binding domain; DMF, dimethylformamide; DIPEA, diisopropylethylamine; DSF, differential scanning fluorimetry; EBV, Epstein−Barr virus; EBNA1, Epstein−Barr nuclear antigen 1; EDC, 1-ethyl-3-(3-dimethylaminopropyl) carbodiimide hydrochloride; EE, ethyl acetate; EtOH, ethanol; EMSA, electrophoretic mobility shift assay; FA, formic acid; FP, fluorescence polarization; HPLC, high pressure liquid chromatography; HHV-8, human herpesvirus 8; KS, Kaposi Sarcoma; KSHV, Kaposi's sarcoma-associated herpesvirus; LANA, latency associated nuclear antigen; LBS, LANA binding site; LE, ligand efficiency; LCMS, liquid chromatography mass spectrometer; MeCN, acetonitrile; MeOH, methanol; MST, microscale thermophoresis; NHS, *N*-hydroxysuccinimide; PBS, phosphate-buffered saline; PE, petroleum benzene; STD NMR, saturation transfer difference nuclear magnetic resonance; SPR, surface plasmon resonance; TBHP, *tert*-butyl hydroperoxide; *tert*-BuOH, *tert*-butanol; $TMSN_3$, trimethylsilyl azide; TSA, thermal shift assay; TR, terminal repeat

■ REFERENCES

(1) World Health Organization - International Agency for Research on Cancer. *A Review of Human Carcinogens*; World Health Organization: Lyon, France, 2012; Vol *100 B*.

(2) Weidner-Glunde, M.; Mariggiò, G.; Schulz, T. F. Kaposi's sarcoma-associated herpesvirus latency-associated nuclear antigen: replicating and shielding viral DNA during viral persistence. *J. Virol.* **2017**, *91*, No. e01083-16.

(3) Mariggiò, G.; Koch, S.; Schulz, T. F. Kaposi sarcoma herpesvirus pathogenesis. *Philos. Trans. R. Soc., B* **2017**, *372*, 21060275.

(4) Rainbow, L.; Platt, G. M.; Simpson, G. R.; Sarid, R.; Gao, S. J.; Stoiber, H.; Herrington, C. S.; Moore, P. S.; Schulz, T. F. The 222- to 234-kilodalton latent nuclear protein (LNA) of kaposi's sarcoma-associated herpesvirus (human herpesvirus 8) is encoded by orf73 and is a component of the latency-associated nuclear antigen. *J. Virol.* **1997**, *71*, 5915−5921.

(5) Kedes, D. H.; Ganem, D.; Ameli, N.; Bacchetti, P.; Greenblatt, R. The prevalence of serum antibody to human herpesvirus 8 (kaposi sarcoma-associated herpesvirus) among HIV-seropositive and high-risk HIV-seronegative women. *JAMA* **1997**, *277*, 478−481.

(6) Verma, S. C.; Lan, K.; Robertson, E. Structure and function of latency-associated nuclear antigen. *Curr. Top. Microbiol. Immunol.* **2007**, *312*, 101−136.

(7) Hellert, J.; Weidner-Glunde, M.; Krausze, J.; Lünsdorf, H.; Ritter, C.; Schulz, T. F.; Lührs, T. The 3D structure of kaposi sarcoma herpesvirus LANA C-terminal domain bound to DNA. *Proc. Natl. Acad. Sci. U. S. A.* **2015**, *112*, 6694−6699.

(8) Barbera, A. J.; Chodaparambil, J. V.; Kelley-Clarke, B.; Joukov, V.; Walter, J. C.; Luger, K.; Kaye, K. M. The nucleosomal surface as a docking station for kaposi's sarcoma herpesvirus LANA. *Science* **2006**, *311*, 856−861.

(9) Chodaparambil, J. V.; Barbera, A. J.; Lu, X.; Kaye, K. M.; Hansen, J. C.; Luger, K. A charged and contoured surface on the nucleosome regulates chromatin compaction. *Nat. Struct. Mol. Biol.* **2007**, *14*, 1105−1107.

(10) Alkharsah, K. R.; Schulz, T. F. A role for the internal repeat of the kaposi's sarcoma-associated herpesvirus latent nuclear antigen in the persistence of an episomal viral genome. *J. Virol.* **2012**, *86*, 1883−1887.

(11) Russo, J. J.; Bohenzky, R. A.; Chien, M.-C.; Chen, J.; Yan, M.; Maddalena, D.; Parry, J. P.; Peruzzi, D.; Edelman, I. S.; Chang, Y.; Moore, P. S. Nucleotide sequence of the kaposi sarcoma-associated herpesvirus (HHV8). *Proc. Natl. Acad. Sci. U. S. A.* **1996**, *93*, 14862−14867.

(12) Coen, N.; Duraffour, S.; Snoeck, R.; Andrei, G. KSHV targeted therapy: an update on inhibitors of viral lytic replication. *Viruses* **2014**, *6*, 4731−4759.

(13) Li, N.; Thompson, S.; Schultz, D. C.; Zhu, W.; Jiang, H.; Luo, C.; Lieberman, P. M. Discovery of selective inhibitors against EBNA1

DOI: 10.1021/acs.jmedchem.8b01827
J. Med. Chem. 2019, 62, 3924−3939

via high throughput in silico virtual screening. *PLoS One* **2010**, *5*, No. e10126.
(14) Hellert, J.; Weidner-Glunde, M.; Krausze, J.; Richter, U.; Adler, H.; Fedorov, R.; Pietrek, M.; Rückert, J.; Ritter, C.; Schulz, T. F.; Lührs, T. A structural basis for BRD2/4-mediated host chromatin interaction and oligomer assembly of kaposi sarcoma-associated herpesvirus and murine gammaherpesvirus LANA proteins. *PLoS Pathog.* **2013**, *9*, No. e1003640.
(15) Maurer, C. K.; Fruth, M.; Empting, M.; Avrutina, O.; Hoßmann, J.; Nadmid, S.; Gorges, J.; Herrmann, J.; Kazmaier, U.; Dersch, P.; Müller, R.; Hartmann, R. W. Discovery of the first small-molecule CsrA-RNA interaction inhibitors using biophysical screening technologies. *Future Med. Chem.* **2016**, *8*, 931−947.
(16) Weidel, E.; Negri, M.; Empting, M.; Hinsberger, S.; Hartmann, R. W. Composing compound libraries for hit discovery-rationality-driven preselection or random choice by structural diversity? *Future Med. Chem.* **2014**, *6*, 2057−2072.
(17) Cimmperman, P.; Baranauskienė, L.; Jachimovičiūtė, S.; Jachno, J.; Torresan, J.; Michailoviene, V.; Matulienė, J.; Sereikaitė, J.; Bumelis, V.; Matulis, D. A quantitative model of thermal stabilization and destabilization of proteins by ligands. *Biophys. J.* **2008**, *95*, 3222−3231.
(18) Lea, W. A.; Simeonov, A. Fluorescence polarization assays in small molecule screening. *Expert Opin. Drug Discovery* **2011**, *6*, 17−32.
(19) Hellert, J.; Krausze, J.; Schulz, T. F.; Lührs, T. Crystallization, room-temperature X-ray diffraction and preliminary analysis of kaposi's sarcoma herpesvirus LANA bound to DNA. *Acta Crystallogr. F Struct. Biol. Commun.* **2014**, *70*, 1570−1574.
(20) Wang, X.; Jin, Y.; Zhao, Y.; Zhu, L.; Fu, H. Copper-catalyzed aerobic oxidative intramolecular C-H amination leading to imidazobenzimidazole derivatives. *Org. Lett.* **2012**, *14*, 452−455.
(21) Campiani, G.; Morelli, E.; Gemma, S.; Nacci, V.; Butini, S.; Hamon, M.; Novellino, E.; Greco, G.; Cagnotto, A.; Goegan, M.; Cervo, L.; Dalla Valle, F.; Fracasso, C.; Caccia, S.; Mennini, T. Pyrroloquinoxaline Derivatives as High-Affinity and Selective 5-HT_3 Receptor Agonists: Synthesis, Further Structure−Activity Relationships, and biological studies. *J. Med. Chem.* **1999**, *42*, 4362−4379.
(22) Lan, J.-B.; Chen, L.; Yu, X.-Q.; You, J.-S.; Xie, R.-G. A simple copper salt catalysed the coupling of imidazole with arylboronic acids in protic solvent. *Chem. Commun.* **2004**, 188−189.
(23) Pratt, D. A.; Pesavento, R. P.; van der Donk, W. A. Model studies of the histidine-tyrosine cross-link in cytochrome C oxidase reveal the flexible substituent effect of the imidazole moiety. *Org. Lett.* **2005**, *7*, 2735−2738.
(24) He, Z.; Bae, M.; Wu, J.; Jamison, T. F. Synthesis of highly functionalized polycyclic quinoxaline derivatives using visible-light photoredox catalysis. *Angew. Chem. Int. Ed Engl.* **2014**, *53*, 14451−14455.
(25) Tang, C.; Jiao, N. Copper-catalyzed C-H azidation of anilines under mild conditions. *J. Am. Chem. Soc.* **2012**, *134*, 18924−18927.
(26) Hu, M.; Li, J.; Yao, S. Q. In situ "click" assembly of small molecule matrix metalloprotease inhibitors containing zinc-chelating groups. *Org. Lett.* **2008**, *10*, 5529−5531.
(27) Addy, P. S.; Erickson, S. B.; Italia, J. S.; Chatterjee, A. A chemoselective rapid azo-coupling reaction (CRACR) for unclickable bioconjugation. *J. Am. Chem. Soc.* **2017**, *139*, 11670−11673.
(28) Hou, J.; Liu, X.; Shen, J.; Zhao, G.; Wang, P. G. The impact of click chemistry in medicinal chemistry. *Expert Opin. Drug Discovery* **2012**, *7*, 489−501.
(29) Mortenson, P. N.; Murray, C. W. Assessing the lipophilicity of fragments and early hits. *J. Comput.-Aided Mol. Des.* **2011**, *25*, 663−667.
(30) Shargel, L.; Wu-Pong, S.; Yu, A. B. C. *Applied Biopharmaceutics & Pharmacokinetics* 5. ed; McGraw-Hill Medical Publ. Division: New York, NY, 2005.
(31) Erlanson, D. A.; Jahnke, W., Eds. *Fragment-based Drug Discovery;* Wiley-VCH Verlag GmbH & Co. KGaA: Weinheim, 2016.
(32) Hellman, L. M.; Fried, M. G. Electrophoretic mobility shift assay (EMSA) for detecting protein-nucleic acid interactions. *Nat. Protoc.* **2007**, *2*, 1849−1861.
(33) Jerabek-Willemsen, M.; André, T.; Wanner, R.; Roth, H. M.; Duhr, S.; Baaske, P.; Breitsprecher, D. Microscale thermophoresis: interaction analysis and beyond. *J. Mol. Struct.* **2014**, *1077*, 101−113.
(34) *Molecular Operating Environment (MOE), 2013.08* Chemical computing group ULC 2018.
(35) Krieger, E.; Koraimann, G.; Vriend, G. Increasing the precision of comparative models with YASARA NOVA-a self-parameterizing force field. *Proteins* **2002**, *47*, 393−402.

DOI: 10.1021/acs.jmedchem.8b01827
J. Med. Chem. 2019, 62, 3924−3939

3.2 Chapter B: Protein-DNA Interactions (Part II)

Title:

Discovery of Novel Latency-Associated Nuclear Antigen Inhibitors as Antiviral Agents Against Kaposi's Sarcoma-Associated Herpesvirus

Authors:

Philine Kirsch,† Valentin Jakob,† Walid A. M. Elgaher, Christine Walt, Kevin Oberhausen, Thomas F. Schulz, and Martin Empting [†shared first authorship]

Bibliographic Data:

ACS Chemical Biology,

Volume 15, Pages 388-395,

2020

DOI: 10.1021/acschembio.9b00845

Graphical Abstract:

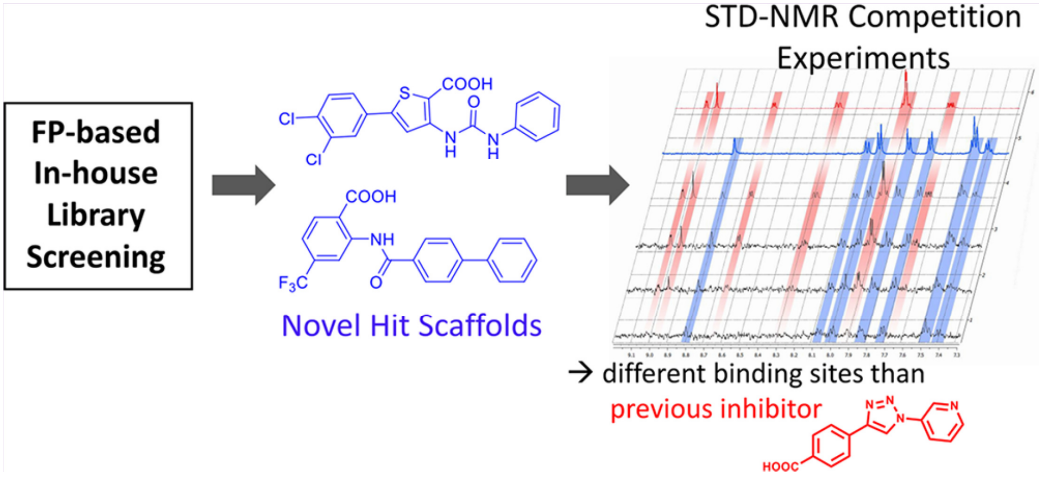

pubs.acs.org/acschemicalbiology

Articles

Discovery of Novel Latency-Associated Nuclear Antigen Inhibitors as Antiviral Agents Against Kaposi's Sarcoma-Associated Herpesvirus

Philine Kirsch,[⊥] Valentin Jakob,[⊥] Walid A. M. Elgaher, Christine Walt, Kevin Oberhausen, Thomas F. Schulz, and Martin Empting*

Cite This: *ACS Chem. Biol.* 2020, 15, 388−395

Read Online

ACCESS | Metrics & More | Article Recommendations | Supporting Information

ABSTRACT: With the aim to develop novel antiviral agents against Kaposi's Sarcoma Herpesvirus (KSHV), we are targeting the latency-associated nuclear antigen (LANA). This protein plays an important role in viral genome maintenance during latent infection. LANA has the ability to tether the viral genome to the host nucleosomes and, thus, ensures latent persistence of the viral genome in the host cells. By inhibition of the LANA−DNA interaction, we seek to eliminate or reduce the load of the viral DNA in the host. To achieve this goal, we screened our in-house library using a dedicated fluorescence polarization (FP)-based competition assay, which allows for the quantification of LANA−DNA-interaction inhibition by small organic molecules. We successfully identified three different compound classes capable of disrupting this protein−nucleic acid interaction. We characterized these compounds by IC_{50} dose−response evaluation and confirmed the compound−LANA interaction using surface plasmon resonance (SPR) spectroscopy. Furthermore, two of the three hit scaffolds showed only marginal cytotoxicity in two human cell lines. Finally, we conducted STD-NMR competition experiments with our new hit compounds and a previously described fragment-sized inhibitor. Based on these results, future compound linking approaches could serve as a promising strategy for further optimization studies in order to generate highly potent KSHV inhibitors.

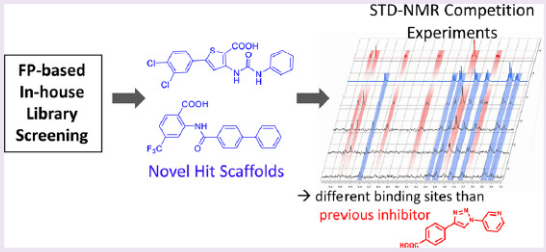

Kaposi's sarcoma herpesvirus (KSHV, also known as HHV-8) is a human γ_2-herpesvirus that was identified as the etiological agent of Kaposi's sarcoma (KS) and two lymphoproliferative disorders, primary effusion lymphoma (PEL) and the plasma cell variant of multicentric Castleman's disease (MCD).[1] Most of the disease burden caused by KSHV occurs in immunocompromised individuals, mainly patients suffering from the acquired immunodeficiency syndrome (AIDS) and transplant recipients. In contrast, KSHV-associated disease is infrequent in otherwise healthy individuals; however, KSHV also causes "classic" KS mainly in elderly men from KSHV-endemic areas and "endemic" KS in East and Central Africa.[2−5] No specific treatments directed against the latent phase of the KSHV life cycle and KSHV-associated diseases are available.[6] For the latent persistence and the regulation of KSHV in the human host, the latency-associated nuclear antigen (LANA) plays an important role.[7−9] All KSHV-infected tumor cells express LANA, which is hence used as a biomarker for diagnostics by immunohistochemistry.[10,11] It functions as an origin-binding protein via tethering the viral genome with its *C*-terminus and the host nucleosome with its *N*-terminus.[12−14] LANA ensures a stable and latent persistence of the viral genome in the human cells.[15] There are three adjacent LANA binding sites (LBSs) located in the terminal repeat (TR) region on the viral genome, which are referred to as LBS1, LBS2, and LBS3.[13,16] Previous studies showed that disruption of LANA expression leads to a reduction of viral DNA copies.[17] On the basis of these findings, we aim to prevent latent KSHV persistence and reduce the viral load of infected cells through inhibition of the interaction between LANA and the viral genome.[18] In a previous work, we discovered first inhibitors that interfere with the LANA−DNA interaction using a fragment-based drug-discovery approach.[12] The functional activity of our LANA−DNA interaction inhibitors was evaluated using a fluorescence polarization (FP)-based competition assay as a rapid and quantitative method. The most promising fragment-sized inhibitor **I** showed an IC_{50} value of 17 ± 1 μM (Figure 1). Additionally, target binding was confirmed via microscale thermophoresis (MST) and saturation transfer difference (STD)-NMR experiments as well as in an electrophoretic mobility shift assay (EMSA) measuring the interaction between the LANA DNA-binding domain (DBD) and DNA oligonucleotides representing LBS1 and LBS2.[12]

Received: October 21, 2019
Accepted: January 16, 2020
Published: January 16, 2020

https://dx.doi.org/10.1021/acschembio.9b00845
ACS Chem. Biol. 2020, 15, 388−395

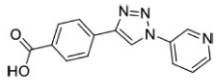

Inhibitor I

IC_{50}(LBS2): 17 ± 1 μM

Figure 1. Previously discovered LANA−DNA interaction inhibitor **I** using a fragment-based approach.

In this present study, we exploit our FP-based competition assay as a new screening tool to search our in-house HIPS library for compounds with the ability to disturb the LANA−DNA interaction. In order to exclude assay artifacts, we used surface plasmon resonance (SPR) spectroscopy to confirm target binding and affinity of the screening hits and assessed their applicability by determining their cytotoxic potential. Moreover, with the view to compare the novel hit scaffolds with inhibitor **I**, we performed STD-NMR-based competition experiments. By this means, we were able to demonstrate nonoverlapping binding sites for two of our novel scaffolds with inhibitor **I**. Our screening protocol served as an effective strategy for the discovery of LANA−DNA interaction inhibitors and the identification of novel scaffolds for future medicinal chemistry campaigns.

RESULTS AND DISCUSSION

General Screening Protocol and Hit Evaluation. In order to identify new potential scaffolds, we decided to screen our in-house HIPS-library (670 compounds) comprising various chemical classes of small molecules with diverse biological activities. We used an FP-based competition assay, which we have established and described previously.[12] By this assay, we are able to quantitatively assess the functional activity of compounds in terms of LANA−DNA interaction inhibition. We employ a mutant of the C-terminal DBD of LANA, which is multimerization deficient. A fluorescence-labeled double-stranded DNA oligomer is used as the probe. Hit identification was done in two steps as shown in Figure 2A. The first screening step was carried out at a single fixed concentration (100 μM) for preselection. Then, a three-point dose-dependency test was performed for evaluating the activity profiles. This procedure resulted in nine hits that can be clustered into three classes according to their chemical structure (Figure 2B). Subsequently, we determined the IC_{50} values using our FP-based competition assay and confirmed target binding via SPR measurements of the hit compounds. Moreover, we investigated the binding mode of the most promising inhibitors using STD-NMR competition experiments with the inhibitor **I**.

Library Screening Using FP-Based Assay. To apply our FP-based competition assay as a medium-to-high throughput screening method, we modified assay conditions slightly. For the primary screening, we used the same concentrations of LANA DBD mutant and LBS2 probe as described before.[12] The library compounds were screened in two independent experiments at a final concentration of 100 μM. Additionally, we used a high control (HC) comprising samples with LANA DBD mutant, LBS2 probe, and DMSO in buffer without any compound and low control (LC) containing the same components without LANA DBD mutant in each screening plate. Compounds that contained strong chromophores or precipitated under assay conditions were neglected to exclude false positives. Compounds showing an inhibitory effect greater than 50% were defined as hits. According to these criteria, we selected 86 compounds out of 670 (hit rate 12.8%) for further investigations (Figure S1). Next, we tested the 86 primary actives in a concentration-dependent three-point test in two independent FP-based experiments at final concentrations of 100 μM, 50 μM, and 10 μM (Figure S2−S4). By this means, we were able to focus on well-behaved compounds that can display a concentration-dependent inhibition of the LANA−DNA interaction and avoid being misguided by a strong initial effect in the spot test. The largest of the three classes (class I) comprises 64 2-ureidothiophene-3-carboxylic acid derivatives.[19,20] This scaffold was previously described as a dual

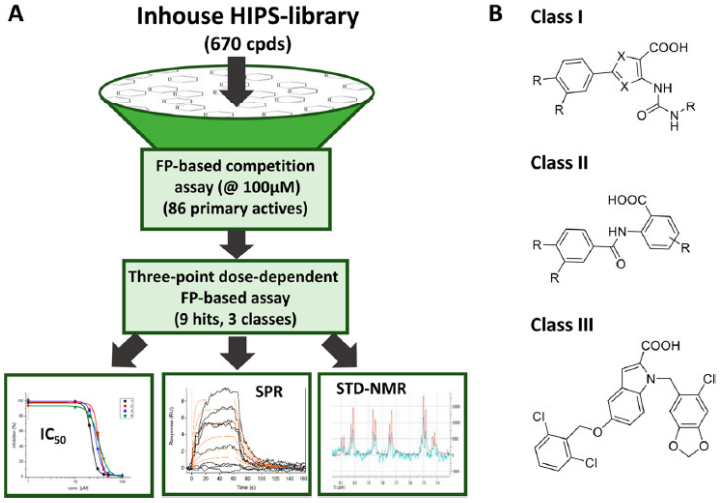

Figure 2. (A) Flowchart illustrating the screening procedure and the following hit evaluation methods. Using FP-based primary screening for identification of LANA−DNA interaction inhibitors and dose-dependent screening as secondary filters. IC_{50} determination, SPR, and STD-NMR experiments were performed for hit characterization and to confirm target binding. (B) Core structures of our screening hit compound classes.

https://dx.doi.org/10.1021/acschembio.9b00845
ACS Chem. Biol. 2020, 15, 388−395

Table 1. Characterization of Hit Compounds 1−9

Compd	Structure	MW [g/mol]	IC_{50} [μM] (FP assay)	Response [RU] at 100 μM (SPR)	K_D [μM] (SPR)
1	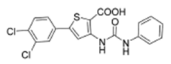	407.27	24 ± 1	9.5 ± 0.7	131.0 ± 9.0
2	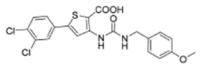	437.29	33 ± 1	14.4 ± 0.6	n.d.[a]
3	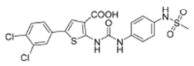	500.37	26 ± 2	8.6 ± 0.1	n.d.
4	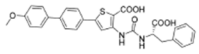	516.57	31 ± 2	42.3 ± 0.8	n.d.
5	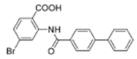	396.24	33 ± 5	22.1 ± 1.2	n.d.
6	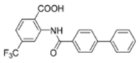	385.34	30 ± 2	12.2 ± 0.6	9.9 ± 0.4
7	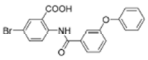	412.24	38 ± 1	10.1 ± 0.5	n.d.
8	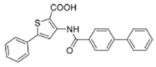	399.46	11 ± 2	21.2 ± 1.1	n.d.
9	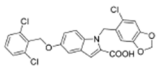	504.74	11 ± 1	9.1 ± 0.7	9.3 ± 0.4

[a]Not determined.

antibacterial and antiviral inhibitor for methicillin-resistant *Staphylococcus aureus* (MRSA) and human immunodeficiency virus type 1 (HIV-1) co-infections.[21] The antibacterial activity can be attributed to the inhibition of RNA polymerase (RNAP) activity, which is an essential enzyme for bacterial viability. RNAP is responsible for the transcription of double-stranded DNA into single-stranded RNA. Antiviral potency of these compounds was rooted in their ability to inhibit the HIV-reverse transcriptase (HIV-RT), which reversibly transcribes the single-stranded viral RNA to double-stranded DNA.[21] Obviously, there is a certain degree of functional relationship between these two targets and our target LANA, as all three possess the ability to interact with DNA or RNA (nucleic acids). The second class (class II) consists of 21 carboxamido benzoic acid derivatives, which were also identified as bacterial RNAP inhibitors.[22] Additionally, we identified a unique compound in our LANA−DNA interaction inhibition assay possessing an indole-2-carboxylic acid scaffold (class III).

Based on these results, we selected representative examples from class I (compounds **1**−**4**, Table 1) and class II (compounds **5**−**8**, Table 1), which show suitable concentration-dependent activity and structural diversity in addition to the single member of class III (compound **9**, Table 1) for further investigations.

Hit Characterization. Selected hits were further characterized for their relative potency and target affinity. We carried out dose-dependent FP-assay experiments using serial dilutions up to 100 μM or 125 μM with and without addition of LANA DBD mutant. Importantly, for none of our hit compounds we observed fluorescence quenching or enhancement. Representative curves show the results of compounds **1**−**9** (Figures 3A−C and S6−S14). Curves were fitted to a four-parameter dose−response model using OriginPro 2018 to calculate IC_{50} values. Generally, the observed IC_{50} values are in the low micromolar range (Table 1). Importantly, we carried out SPR experiments to confirm that our hits are real target binders and not interfering with the DNA. We screened the hit compounds at a final concentration of 100 μM for binding to an immobilized LANA DBD mutant. For all hit compounds, we observed a significant binding response (Figure S16A−I). The bar diagram (Figure 3D) shows the mean of SPR response values in RU normalized to the molecular weight (MW) of the compounds. These results indicate that protein−DNA-interaction inhibition is most probably due to LANA binding rather than DNA or florescence-interfering effects.

Within class I (**1**−**4**), compound **1** showed the lowest IC_{50} value of 24 ± 1 μM and the lowest MW (Table 1). The IC_{50} values of hits **2**−**4** are in the same low micromolar range. However, bulkiness and complexity are increased compared to hit **1**. In the SPR study, compounds **1**−**3** displayed reproducible responses between 9−14 RU and their sensorgrams showed clear association and dissociation phases indicating a typical reversible binding to LANA (Figure S16A−C). Hit **4** showed a relatively high response value (42

https://dx.doi.org/10.1021/acschembio.9b00845
ACS Chem. Biol. 2020, 15, 388−395

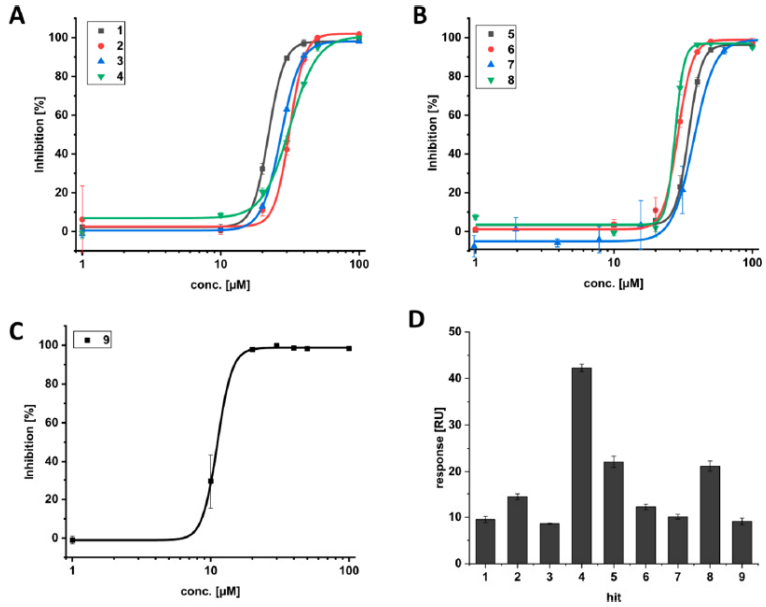

Figure 3. (A−C) Dose-dependent FP-based competition experiments for hit compounds 1−9. Curves were based on normalized data points (inhibition from 0−100%) from FP values of duplicates ± standard deviation; (D) Mean of SPR response values (RU) of duplicates ± standard deviation of the screened compounds at 100 μM injected over an immobilized LANA DBD mutant.

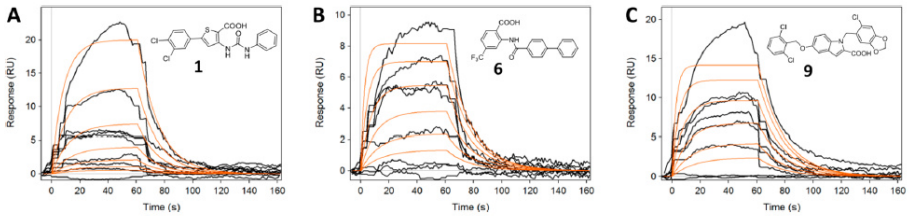

Figure 4. SPR sensorgrams (black) of the hit compounds 1 (A), 6 (B), and 9 (C) at concentrations of 1.6−100.0 μM using immobilized LANA. Global fitting of the association and dissociation curves (red).

RU), which may indicate unspecific binding because of the two carboxylic acid motifs. Based on these results, we picked out hit **1** showing the lowest MW, least structure complexity, best IC_{50} value, and good SPR response for further characterization. For class II (**5**−**8**), hit compound **8** showed the highest inhibitory activity (IC_{50} value, 11 ± 2 μM). Moreover, all hits displayed prominent SPR responses and binding curves (Figure S16E−H). Interestingly, sensorgram of compound **6** revealed a slow dissociation interaction with LANA among this set compounds (**5**−**8**) and a potential high affinity. Accordingly, we choose compound **6** for further evaluation as it represents class II preferably, having the lowest MW, low IC_{50} value (30 ± 2 μM), and favorable binding kinetics. Furthermore, compound **6** showed the highest solubility in our assay conditions. In addition, compound **9** (class III) showed also high activity (IC_{50} value, 11 ± 1 μM), as well as binding response, and was selected for further investigations.

Next, we evaluated compounds **1**, **6**, and **9** for affinity to LANA and determined binding kinetics using SPR. Compounds **6** and **9** showed high affinity to LANA (K_D values, 9−10 μM) and about 13-fold stronger than compound **1** (K_D value, 131 μM) (Table 1 and Figure 4). The on-rate of compounds **6** and **9** was 1 order of magnitude faster than that of compound **1**, while all compounds displayed a comparable off-rate (see Figure S17−S19 and Table S2 for detailed results including Langmuir isotherms and kinetic parameters). The dissociation rate constant (k_{off}) and the ligand−protein residence time ($1/k_{off}$) are known to play a major role in potency, efficacy, and duration of effect.[23] Interestingly, we found that the inhibitory activities (IC_{50} values) obtained from the FP assay show a better correlation with the off-rates of the compounds rather than the binding affinities (K_D values). Such a correlation is known to be target-specific and was observed previously for other protein targets.[23,24] These results indicate that the dissociation rate and consequently the duration of binding seem to be the driving force for the activity on LANA.

Saturation Transfer Difference (STD) NMR Competition Experiments. As the new hits were able to compete with the DNA in the FP-based competition experiments, they seem to bind to the DNA binding site of LANA. Having confirmed compound−LANA binding by the SPR study, we were interested in studying the LANA−ligand interactions and

https://dx.doi.org/10.1021/acschembio.9b00845
ACS Chem. Biol. 2020, 15, 388−395

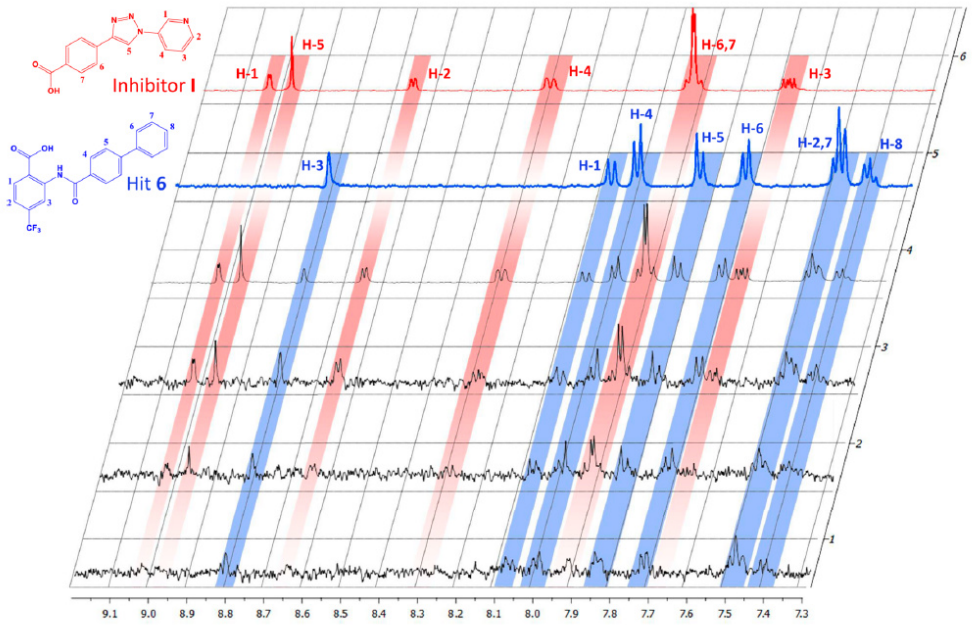

Figure 5. STD-NMR competition experiments with inhibitor **I** and hit **6** in complex with LANA DBD mutant. The respective protons of each compound are highlighted with a corresponding color, inhibitor **I** in red and hit **6** in blue; spectrum 6 (red), off resonance spectrum of inhibitor **I** with final concentration of 250 μM; spectrum 5 (blue), off resonance spectrum of hit **6** with final concentration of 250 μM; spectrum 4, off resonance spectrum of inhibitor **I** mixed with hit **6**, each with a final concentration of 250 μM; spectrum 3, STD spectrum of inhibitor **I** mixed with hit **6**, inhibitor **I** with a final concentration of 500 μM and hit **6** with a final concentration of 250 μM; spectrum 2, STD spectrum of inhibitor **I** mixed with hit **6**, each with a final concentration of 250 μM; spectrum 1, STD spectrum of inhibitor **I** mixed with hit **6**, inhibitor **I** with a final concentration of 125 μM and hit **6** with a final concentration of 250 μM.

getting insights into the mode of binding. To this end, we performed ligand-observed STD-NMR studies using compounds **1**, **6**, and **9** in a competition experiment with our previously discovered inhibitor **I** (Figure 1). STD-NMR competition experiments can provide important information on the putative binding of the hit compounds to the target in the absence of any structural data of the protein.[25] In our previous work, we observed a defined binding orientation for inhibitor **I** to LANA where the pyridine moiety of inhibitor **I** interacts strongly with the LANA surface.[12] A competition experiment should allow for evaluating whether the new hit compounds bind at the same binding site as inhibitor **I** or if they bind simultaneously at different binding regions. For the STD studies, we used a fixed concentration (250 μM) of compound **1**, **6**, or **9** and different concentrations (125 μM, 250 μM, and 500 μM) of inhibitor **I**. The observed STD spectra for hit **6** in competition to inhibitor **I** is shown in Figure 5. Spectrum 6 (red) shows the off resonance spectrum of inhibitor **I**, and spectrum 5 (blue) shows the off resonance spectrum of compound **6**. The next spectrum (4) is the off resonance spectrum of inhibitor **I** mixed with **6**. The spectra 1−3 show the STD signals with fixed concentration of 250 μM of compound **6** and increasing concentrations of inhibitor **I**. The observed STD effects indicate that both compounds can bind simultaneously to the LANA surface as signals for compound **6** have identical peak intensities regardless any concentration of inhibitor **I**. The STD signals for inhibitor **I** increase with increasing concentration of inhibitor **I** as expected. For the STD competition experiments with compound **1** and inhibitor **I**, we observed similar results (see Figure S26). Unfortunately, we were not able to observe STD-NMR data for compound **9**.

It is quite possible that compounds **1** and **6** bind in different binding modes and on different binding sites of LANA considering the huge DNA binding interface of LANA. Another explanation could be that the hit compounds have an allosteric effect on LANA, which could prevent the LANA−DNA interaction. Importantly, with the STD-NMR competition experiments, we demonstrated that different and non-overlapping binding sites for our novel scaffolds do exist compared to inhibitor **I**.

Cytotoxicity. We complemented our hit characterization by testing the compounds for cytotoxicity. Hit **1** and **6** showed only a marginal cytotoxicity on Hek293 and HepG2 cells, whereas compound **9** seems to be highly toxic (Table 2). Cytotoxicity assessment is very important in prospect of testing cell-based activities of antiviral compounds, which renders hit **6** the most promising starting point for subsequent optimization efforts as it showed the lowest cytotoxic potential.

Table 2. Cytotoxicity Data of Compounds 1, 6, and 9

	relative viability after 48 h [%] at 100 μM	
hit	HepG2	Hek293
1	114 ± 42	43 ± 3
6	147 ± 12	85 ± 3
9	20 ± 9	7 ± 6

https://dx.doi.org/10.1021/acschembio.9b00845
ACS Chem. Biol. 2020, 15, 388−395

However, also scaffolds found in classes I (**1**) and III (**9**) might provide valuable structural motifs to be exploited in compound merging studies.

Conclusion. We have identified three chemical scaffolds as novel LANA−DNA interaction inhibitors by screening our in-house library using a dedicated FP-based competition assay. These new LANA inhibitors were found to inhibit the LANA−DNA interaction with IC_{50} values in the low micromolar range providing a very good starting point for medicinal chemistry optimization. Additionally, we applied SPR to confirm target binding and exclude DNA interaction in the FP assay. All hit compounds displayed a significant binding to LANA, and the obtained affinity (K_D) results were comparable to the inhibitory activity (IC_{50} values). Furthermore, we performed STD-NMR competition experiments with previously discovered inhibitor **I**. We found that compounds **1** and **6** are binding at a different binding site on the LANA surface than inhibitor **I**. Cytotoxicity was also evaluated for one representative compound from each class, whereby compounds **1** and **6** only show a marginal cytotoxicity and in contrast compound **9** was highly toxic. Importantly, our study demonstrated that our FP-based competition assay can be used as a fast and simple method to identify new LANA−DNA interaction inhibitors, which can open up avenues for further studies. Moreover, the results obtained in this study can serve as a starting point for further development of LANA−DNA interaction inhibitors with greater potency and selectivity as future therapeutic agents against latent KSHV infections.

METHODS

Expression of His-Tagged Oligomerization-Deficient LANA DBD (aa1008−1146) Mutant. The expression of His-tagged oligomerization-deficient LANA DBD (aa1008−1146) mutant was done as described previously.[12,13]

FP-Based Library Screening. The in-house HIPS small molecule library contained 670 compounds dissolved in DMSO to 10 mM stock solutions. The fluorescence polarization assay was performed as described previously[12] with slight modifications. All experiments were performed in two independent experiments and each sample was tested in duplicate. The primary spot-test screening was performed with a final concentration of 100 μM of each compound. The three-point secondary screening was carried out with final compound concentrations of 10 μM, 50 μM, and 100 μM. LANA DBD mutant was used with a final concentration of 200 nM, and fluorescent-labeled LBS2 oligomer was used with a final concentration of 10 nM.[12] IC_{50} determination of the final screening hits was performed as described previously.[12] Curves were fit to a four-parameter dose−response model using OriginPro 2018 to calculate IC_{50} values. For data reliability, high control (HC) comprising 24 samples with LANA DBD mutant, LBS2 probe, and DMSO (5% [v/v] final) in buffer without any compound and low control (LC) comprising 24 samples containing the same components without LANA DBD mutant were distributed over each screening plate.

Binding Studies Using Surface Plasmon Resonance (SPR). The SPR experiments were performed using a Reichert SR7500DC surface plasmon resonance spectrometer (Reichert Technologies, Depew, NY, USA), and medium density carboxymethyl dextran hydrogel CMD500 M sensor chips (XanTec Bioanalytics, Düsseldorf, Germany). Double distilled (dd) water was used as the running buffer for immobilization. Phosphate-buffered saline (PBS) buffer (10 mM Na_2HPO_4, 1.8 mM KH_2PO_4, 137 mM NaCl, 2.7 mM KCl, 0.05% [v/v] tween 20, pH 7.4) containing 5% [v/v] DMSO was used as the running buffer for binding study. All running buffers were filtered and degassed prior to use. The LANA 1008−1146 (17.653 kDa) was immobilized in one of the two flow cells by amine coupling procedure. The other flow cell was left blank to serve as a reference. The system was initially primed with borate buffer 100 mM (pH 9.0); then the carboxymethyldextran matrix was activated by a 1:1 mixture of *N*-ethyl-*N*′-(3-(dimethylamino)propyl)carbodiimide hydrochloride (EDC) 100 mM and *N*-hydroxysuccinimide (NHS) 100 mM at a flow rate of 10 μL min^{-1} for 7 min. The LANA protein (aa1008−1146) was diluted to a final concentration of 50 μg mL^{-1} in 10 mM sodium acetate buffer (pH 4.0) and was injected at a flow rate of 10 μL min^{-1} for 7 min. Nonreacted surface was quenched by 1 M ethanolamine hydrochloride (pH 8.5) at a flow rate of 25 μL min^{-1} for 3 min. A series of 7 buffer injections was run initially on both reference and active surfaces to equilibrate the system resulting in a stable immobilization level of approximately 5000 micro-refractive index units (μRIU). Binding experiments were performed at 20 °C. Compounds dissolved in DMSO were diluted with PBS buffer (final DMSO concentration of 5% [v/v]) and were injected (in duplicate) at a flow rate of 30 μL min^{-1}. Single-cycle kinetics were applied for K_D determination. The association time was set to 60 s, and the dissociation phase was recorded for 120 s. Ethylene glycol 80% in the running buffer or 10 mM glycine hydrochloride (pH 2.0) was used for regeneration of the surface. Differences in the bulk refractive index due to DMSO were corrected by a calibration curve (nine concentrations: 3−7% [v/v] DMSO in PBS buffer). Data processing and analysis were performed by Scrubber software (version 2.0c, 2008, BioLogic Software). Sensorgrams were calculated by sequential subtractions of the corresponding curves obtained from the reference flow cell and the running buffer (blank). SPR responses are expressed in resonance units (RU). Concentration-dependent SPR experiments were performed at final compound concentrations of 100 μM, 50 μM, 25 μM, 12.5 μM, 6.25 μM, and 3.125 μM. The K_D values were calculated by global fitting of the kinetic curves.

Saturation-Transfer Difference (STD) NMR. The STD experiments were recorded at 298 K on a Bruker Fourier spectrometer (500 MHz). The samples contained 5 μM (final concentration) C-terminally His-tagged oligomerization-deficient LANA DBD (aa1008−1146) mutant and different compound concentrations. The control spectra were recorded under the same conditions containing the free compound to test for artifacts. The STD buffer for experiments using compound **1** and inhibitor **I** consisted of 5 mM HEPES, 125 mM NaCl, pH 8.5, in D_2O containing 10% [v/v] DMSO-d_6. The experiments were recorded with a carrier set at −1 ppm for the on-resonance and −40 ppm for the off-resonance irradiation. Selective protein saturation was carried out at 1 s using a train of 50 ms Gauss-shaped pulses, each separated by a 1 ms delay. For all experiments, a constant concentration of 250 μM of **1** was used combined with different concentrations of inhibitor **I** (125 μM, 250 μM, and 500 μM). The STD buffer for experiments using compound **6** and inhibitor **I** consisted of 20 mM Tris-Cl, 150 mM NaCl, pH 7.4, in D_2O containing 10% [v/v] DMSO-d_6. The experiments were recorded with a carrier set at −2 ppm for the on-resonance and −40 ppm for the off-resonance irradiation. Selective protein saturation was carried out at 1.5 s using a train of 50 ms Gauss-shaped pulses, each separated by a 1 ms delay. For all experiments, a constant concentration of 250 μM of **6** was used combined with different concentrations of inhibitor **I** (125 μM, 250 μM, and 500 μM).

Cytotoxicity Assay. HepG2 and Hek193 cells (2×10^5 cells per well) were seeded in 24-well flat bottom plates. The procedure for culturing the cells, incubation times, and OD measurements were performed as described previously[26] with slight modifications. Twenty-four hours after seeding the cells, the compounds were added (final DMSO concentration of 1%) and incubated for 24 h. The living cell mass was determined after 24 h. Each compound was tested in two independent experiments.

ASSOCIATED CONTENT

Supporting Information

The Supporting Information is available free of charge at https://pubs.acs.org/doi/10.1021/acschembio.9b00845.

https://dx.doi.org/10.1021/acschembio.9b00845
ACS Chem. Biol. 2020, 15, 388−395

Data of primary and secondary FP-based library screening, concentration-dependent FP experiments, SPR response curves, information on K_D determination via SPR, STD-NMR spectra, and cytotoxicity assay data (PDF)

AUTHOR INFORMATION

Corresponding Author

Martin Empting − *Department of Drug Design and Optimization (DDOP), Helmholtz-Institute for Pharmaceutical Research Saarland (HIPS) - Helmholtz Centre for Infection Research (HZI), 66123 Saarbrücken, Germany; Department of Pharmacy, Saarland University, 66123 Saarbrücken, Germany; German Centre for Infection Research (DZIF), Partner Site Hannover-Braunschweig, 66123 Saarbrücken, Germany;* orcid.org/0000-0002-0503-5830; Phone: +49681-98806 2031; Email: Martin.Empting@helmholtz-hips.de

Authors

Philine Kirsch − *Department of Drug Design and Optimization (DDOP), Helmholtz-Institute for Pharmaceutical Research Saarland (HIPS) - Helmholtz Centre for Infection Research (HZI), 66123 Saarbrücken, Germany; Department of Pharmacy, Saarland University, 66123 Saarbrücken, Germany; German Centre for Infection Research (DZIF), Partner Site Hannover-Braunschweig, 66123 Saarbrücken, Germany*

Valentin Jakob − *Department of Drug Design and Optimization (DDOP), Helmholtz-Institute for Pharmaceutical Research Saarland (HIPS) - Helmholtz Centre for Infection Research (HZI), 66123 Saarbrücken, Germany; Department of Pharmacy, Saarland University, 66123 Saarbrücken, Germany; German Centre for Infection Research (DZIF), Partner Site Hannover-Braunschweig, 66123 Saarbrücken, Germany*

Walid A. M. Elgaher − *Department of Drug Design and Optimization (DDOP), Helmholtz-Institute for Pharmaceutical Research Saarland (HIPS) - Helmholtz Centre for Infection Research (HZI), 66123 Saarbrücken, Germany;* orcid.org/0000-0002-8766-4568

Christine Walt − *Department of Drug Design and Optimization (DDOP), Helmholtz-Institute for Pharmaceutical Research Saarland (HIPS) - Helmholtz Centre for Infection Research (HZI), 66123 Saarbrücken, Germany*

Kevin Oberhausen − *Department of Drug Design and Optimization (DDOP), Helmholtz-Institute for Pharmaceutical Research Saarland (HIPS) - Helmholtz Centre for Infection Research (HZI), 66123 Saarbrücken, Germany*

Thomas F. Schulz − *German Centre for Infection Research (DZIF), Partner Site Hannover-Braunschweig, 66123 Saarbrücken, Germany; Institute of Virology, Hannover Medical School, 30625 Hannover, Germany*

Complete contact information is available at: https://pubs.acs.org/10.1021/acschembio.9b00845

Author Contributions

⊥P.K. and V.J. contributed equally.

Funding

This work was financial supported by the German Centre for Infection Research (DZIF) and the DFG Collaborative Research Centre 900, project C1.

Notes

The authors declare no competing financial interest.

ACKNOWLEDGMENTS

We thank Prof. Dr. R. W. Hartmann for his continuous support and guiding expertise. For the help with the STD NMR experiments, we thank Dr. J. Zapp.

ABBREVIATIONS

AIDS, acquired immune deficiency syndrome; DMSO, dimethyl sulfoxide; DBD, DNA binding domain; EDC, 1-ethyl-3-(3-(dimethylamino)propyl) carbodiimide hydrochloride; FP, fluorescence polarization; HHV-8, human herpesvirus 8; HIPS, Helmholtz Institute for Pharmaceutical Research Saarland; KS, Kaposi sarcoma; KSHV, Kaposi's sarcoma-associated herpesvirus; LANA, latency-associated nuclear antigen; LBS, LANA binding site; MST, microscale thermophoresis; NHS, *N*-hydroxysuccinimide; PBS, phosphate-buffered saline; STD NMR, saturation transfer difference nuclear magnetic resonance; SPR, surface plasmon resonance; TR, terminal repeat

REFERENCES

(1) Schulz, T. F. (2006) The pleiotropic effects of Kaposi's sarcoma herpesvirus. *J. Pathol. 208*, 187−198.

(2) Greene, W., Kuhne, K., Ye, F., Chen, J., Zhou, F., Lei, X., and Gao, S.-J. (2007) Molecular biology of KSHV in relation to AIDS-associated oncogenesis. *Cancer Treat. Res. 133*, 69−127.

(3) Zlatkovskaia, N. M., Penner, I. D., Sosnova, M. A., Abramova, V. A., and Duovitskaia, N. F. (1975) Clinical characteristics of intestinal coli infection in the city of Frunze. *Zdravookhr Kirg*, 23−27.

(4) World Health Organization - International Agency for Research (2012) Biological agents. Volume 100 B. A review of human carcinogens. *IARC Monogr. Eval. Carcinog. Risks. Hum. 100*, 1−441.

(5) Bouvard, V., Baan, R., Straif, K., Grosse, Y., Secretan, B., El Ghissassi, F., Benbrahim-Tallaa, L., Guha, N., Freeman, C., Galichet, L., and Cogliano, V. (2009) A review of human carcinogens–Part B: biological agents. *Lancet Oncol. 10*, 321−322.

(6) Coen, N., Duraffour, S., Snoeck, R., and Andrei, G. (2014) KSHV targeted therapy: an update on inhibitors of viral lytic replication. *Viruses 6*, 4731−4759.

(7) Bhutani, M., Polizzotto, M. N., Uldrick, T. S., and Yarchoan, R. (2015) Kaposi sarcoma-associated herpesvirus-associated malignancies: epidemiology, pathogenesis, and advances in treatment. *Semin. Oncol. 42*, 223−246.

(8) Rainbow, L., Platt, G. M., Simpson, G. R., Sarid, R., Gao, S. J., Stoiber, H., Herrington, C. S., Moore, P. S., and Schulz, T. F. (1997) The 222- to 234-kilodalton latent nuclear protein (LNA) of Kaposi's sarcoma-associated herpesvirus (human herpesvirus 8) is encoded by orf73 and is a component of the latency-associated nuclear antigen. *J. Virol. 71*, 5915−5921.

(9) Kedes, D. H., Ganem, D., Ameli, N., Bacchetti, P., and Greenblatt, R. (1997) The prevalence of serum antibody to human herpesvirus 8 (Kaposi sarcoma-associated herpesvirus) among HIV-seropositive and high-risk HIV-seronegative women. *JAMA 277*, 478−481.

(10) Mariggiò, G., Koch, S., and Schulz, T. F. (2017) Kaposi sarcoma herpesvirus pathogenesis. *Philos. Trans. R. Soc., B 372*, 20160275.

(11) Yamada, M., Katano, H., Yotsumoto, M., Hashimoto, H., Muramatsu, T., Shiotsuka, M., Fukutake, K., and Kuroda, M. (2014) Unique expression pattern of viral proteins in human herpesvirus 8-positive plasmablastic lymphoma: a case report. *Int. J. Clin. Exp. Pathol. 7*, 6415−6418.

(12) Kirsch, P., Jakob, V., Oberhausen, K., Stein, S. C., Cucarro, I., Schulz, T. F., and Empting, M. (2019) Fragment-Based Discovery of a Qualified Hit Targeting the Latency-Associated Nuclear Antigen of the Oncogenic Kaposi's Sarcoma-Associated Herpesvirus/Human Herpesvirus 8. *J. Med. Chem. 62*, 3924−3939.

https://dx.doi.org/10.1021/acschembio.9b00845
ACS Chem. Biol. 2020, 15, 388−395

(13) Hellert, J., Weidner-Glunde, M., Krausze, J., Lünsdorf, H., Ritter, C., Schulz, T. F., and Lührs, T. (2015) The 3D structure of Kaposi sarcoma herpesvirus LANA C-terminal domain bound to DNA. *Proc. Natl. Acad. Sci. U. S. A. 112*, 6694−6699.
(14) Barbera, A. J., Chodaparambil, J. V., Kelley-Clarke, B., Joukov, V., Walter, J. C., Luger, K., and Kaye, K. M. (2006) The nucleosomal surface as a docking station for Kaposi's sarcoma herpesvirus LANA. *Science 311*, 856−861.
(15) Chodaparambil, J. V., Barbera, A. J., Lu, X., Kaye, K. M., Hansen, J. C., and Luger, K. (2007) A charged and contoured surface on the nucleosome regulates chromatin compaction. *Nat. Struct. Mol. Biol. 14*, 1105−1107.
(16) Weidner-Glunde, M., Mariggiò, G., and Schulz, T. F. (2017) Kaposi's Sarcoma-Associated Herpesvirus Latency-Associated Nuclear Antigen: Replicating and Shielding Viral DNA during Viral Persistence. *J. Virol. 91*, No. e01083-16.
(17) Verma, S. C., Lan, K., and Robertson, E. (2007) Structure and Function of Latency-Associated Nuclear Antigen. *Curr. Top. Microbiol. Immunol. 312*, 101−136.
(18) Hellert, J., Weidner-Glunde, M., Krausze, J., Richter, U., Adler, H., Fedorov, R., Pietrek, M., Rückert, J., Ritter, C., Schulz, T. F., and Lührs, T. (2013) A structural basis for BRD2/4-mediated host chromatin interaction and oligomer assembly of Kaposi sarcoma-associated herpesvirus and murine gammaherpesvirus LANA proteins. *PLoS Pathog. 9*, No. e1003640.
(19) Elgaher, W. A. M., Fruth, M., Groh, M., Haupenthal, J., and Hartmann, R. W. (2014) Expanding the scaffold for bacterial RNA polymerase inhibitors: design, synthesis and structure-activity relationships of ureido-heterocyclic-carboxylic acids. *RSC Adv. 4*, 2177−2194.
(20) Sahner, J. H., Empting, M., Kamal, A., Weidel, E., Groh, M., Börger, C., and Hartmann, R. W. (2015) Exploring the chemical space of ureidothiophene-2-carboxylic acids as inhibitors of the quorum sensing enzyme PqsD from Pseudomonas aeruginosa. *Eur. J. Med. Chem. 96*, 14−21.
(21) Elgaher, W. A. M., Sharma, K. K., Haupenthal, J., Saladini, F., Pires, M., Real, E., Mély, Y., and Hartmann, R. W. (2016) Discovery and Structure-Based Optimization of 2-Ureidothiophene-3-carboxylic Acids as Dual Bacterial RNA Polymerase and Viral Reverse Transcriptase Inhibitors. *J. Med. Chem. 59*, 7212−7222.
(22) Hinsberger, S., Hüsecken, K., Groh, M., Negri, M., Haupenthal, J., and Hartmann, R. W. (2013) Discovery of novel bacterial RNA polymerase inhibitors: pharmacophore-based virtual screening and hit optimization. *J. Med. Chem. 56*, 8332−8338.
(23) Copeland, R. A. (2016) The drug-target residence time model: a 10-year retrospective. *Nat. Rev. Drug Discovery 15*, 87−95.
(24) Doornbos, M. L. J., Cid, J. M., Haubrich, J., Nunes, A., van de Sande, J. W., Vermond, S. C., Mulder-Krieger, T., Trabanco, A. A., Ahnaou, A., Drinkenburg, W. H., Lavreysen, H., Heitman, L. H., Ijzerman, A. P., and Tresadern, G. (2017) Discovery and Kinetic Profiling of 7-Aryl-1,2,4-triazolo4,3-apyridines: Positive Allosteric Modulators of the Metabotropic Glutamate Receptor 2. *J. Med. Chem. 60*, 6704−6720.
(25) Lepre, C. A., Moore, J. M., and Peng, J. W. (2004) Theory and applications of NMR-based screening in pharmaceutical research. *Chem. Rev. 104*, 3641−3676.
(26) Haupenthal, J., Baehr, C., Zeuzem, S., and Piiper, A. (2007) RNAse A-like enzymes in serum inhibit the anti-neoplastic activity of siRNA targeting polo-like kinase 1. *Int. J. Cancer 121*, 206−210.

https://dx.doi.org/10.1021/acschembio.9b00845
ACS Chem. Biol. 2020, 15, 388−395

3.3 Chapter C: Protein-DNA Interactions (Part III)

Title:

Hit-to-lead optimization of a latency-associated nuclear antigen inhibitor against Kaposi's sarcoma-associated herpesvirus infections

Authors:

Philine Kirsch, Saskia C. Stein, Aylin Berwanger, Julia Rinkes, Valentin Jakob, Thomas F. Schulz, and Martin Empting

Bibliographic Data:

European Journal of Medicinal Chemistry,

Volume 202, 112525,

2020

DOI: 10.1016/j.ejmech.2020.112525

Graphical Abstract:

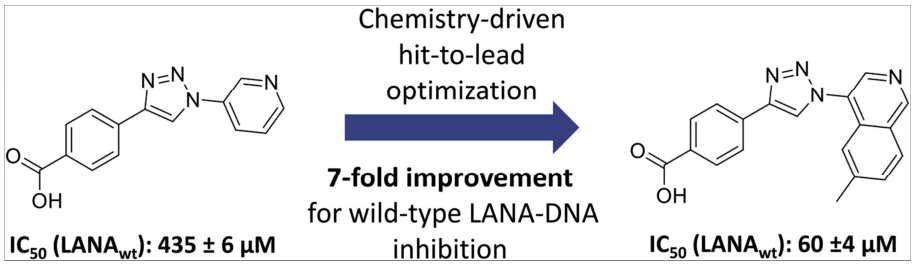

European Journal of Medicinal Chemistry 202 (2020) 112525

Contents lists available at ScienceDirect

European Journal of Medicinal Chemistry

journal homepage: http://www.elsevier.com/locate/ejmech

Research paper

Hit-to-lead optimization of a latency-associated nuclear antigen inhibitor against Kaposi's sarcoma-associated herpesvirus infections

Philine Kirsch [a, b, c], Saskia C. Stein [c, d], Aylin Berwanger [a, b, c], Julia Rinkes [a, b, c], Valentin Jakob [a, b, c], Thomas F. Schulz [c, d], Martin Empting [a, b, c, *]

[a] Department of Drug Design and Optimization (DDOP), Helmholtz-Institute for Pharmaceutical Research Saarland (HIPS) - Helmholtz Centre for Infection Research (HZI), Campus E8.1, 66123, Saarbrücken, Germany
[b] Department of Pharmacy, Saarland University, Campus E8.1, 66123, Saarbrücken, Germany
[c] German Centre for Infection Research (DZIF), Partner Site Hannover-Braunschweig, 66123, Saarbrücken, Germany
[d] Institute of Virology, Hannover Medical School, Carl-Neuberg-Strasse 1, 30625, Hannover, Germany

ARTICLE INFO

Article history:
Received 11 February 2020
Received in revised form
25 May 2020
Accepted 30 May 2020
Available online 28 June 2020

Keywords:
Hit-to-lead optimization
Latency-associated nuclear antigen (LANA)
Kaposi's sarcoma herpesvirus (KSHV)
Fluorescence polarization (FP)-Based interaction inhibition assay
Electrophoretic mobility shift assay (EMSA)
CuAAC
STD-NMR

ABSTRACT

The Latency-associated nuclear antigen (LANA) plays a central role for the latent persistence of the Kaposi's Sarcoma Herpesvirus (KSHV) in the human host and helps to establish lifelong infections. Herein, we report our efforts towards hit-to-lead generation starting from a previously discovered LANA-DNA inhibitor. By tethering the viral genome to the host nucleosomes, LANA ensures the segregation and persistence of the viral DNA during mitosis. LANA is also required for the replication of the latent viral episome during the S phase of the cell cycle. We aim to inhibit the interaction between LANA and the viral genome to prevent the latent persistence of KSHV in the host organism. Medicinal chemistry-driven optimization studies and structure-activity-relationship investigation led to the discovery of an improved LANA inhibitor. The functional activity of our compounds was evaluated using a fluorescence polarization (FP)-based interaction inhibition assay and electrophoretic mobility shift assay (EMSA). Even though a crystal structure of the ligand protein complex was not available, we successfully conducted hit optimization toward a low micromolar protein-nucleic acid-interaction inhibitor. Additionally, we applied STD-NMR studies to corroborate target binding and to gain insights into the binding orientation of our most potent inhibitor, providing opportunities for further rational design of more efficient LANA-targeting anti KSHV agents in future studies.

1. Introduction

Kaposi's Sarcoma Herpesvirus (KSHV) is a human gamma herpesvirus and establishes a lifelong latent infection in B-cells and endothelial cells [1,2]. The virus was identified as the etiological agent of Kaposi's Sarcoma (KS) and is involved in two other neoplastic diseases, multicentric Castleman's disease and pleural effusion lymphoma [1,3]. In healthy individuals, KSHV-associated diseases are rare. However, in immunosuppressed patients, e.g., transplant recipients or patients with the acquired immunodeficiency syndrome (AIDS), KSHV is highly oncogenic [4,5]. However, classic KS mainly can also occur in elderly men especially from KSHV-endemic areas and endemic KS in East and Central Africa [6]. The main key player for the establishment and maintenance of the latent infection is the latency-associated nuclear antigen (LANA) [7–9]. It is an origin-binding protein, whose *C*-terminal domain binds to the viral genome and whose *N*-terminal region interacts simultaneously with host nucleosomes [10–12]. This allows the segregation of latent viral episomes during mitosis and their partitioning to daughter cells [13]. LANA has also additional functions like latent viral replication, transcriptional control and survival in the host cell [14–16]. The *C*-terminal DNA-binding domain (DBD) of LANA binds the viral genome in a sequence-specific manner [17]. Located on the terminal repeats (TRs) are three specific LANA binding sites (LBS), LBS1, LBS2 and LBS3. LBS1 has a hundred fold higher affinity to LANA compared to LBS2 and LBS3 [17]. In the majority of KSHV-associated cancer cells the viral genome is present and LANA is expressed [18]. It has been shown, that the

* Corresponding author. Department of Drug Design and Optimization (DDOP), Helmholtz-Institute for Pharmaceutical Research Saarland (HIPS) - Helmholtz Centre for Infection Research (HZI), Campus E8.1, 66123, Saarbrücken, Germany..
E-mail address: Martin.Empting@helmholtz-hzi.de (M. Empting).

https://doi.org/10.1016/j.ejmech.2020.112525

Abbreviations

AIDS	acquired immune deficiency syndrome
CTD	*C*-terminal domain
DCM	dichloromethane
DMSO	dimethylsulfoxide
DBD	DNA binding domain
DMF	dimethylformamide
DIPEA	diisopropylethylamine
EE	ethyl acetate
EtOH	ethanol
EMSA	electrophoretic mobility shift assay
FA	formic acid
FP	fluorescence polarization
HPLC	high pressure liquid chromatography
HHV-8	human herpesvirus 8
KS	Kaposi Sarcoma
KSHV	Kaposi's sarcoma-associated herpesvirus
LANA	latency-associated nuclear antigen
LBS	LANA binding site
LCMS	liquid chromatography mass spectrometer
MeCN	acetonitrile
MeOH	methanol
MST	microscale thermophoresis
PBS	phosphate-buffered saline
PE	petroleum benzene
STD NMR	saturation transfer difference nuclear magnetic resonance
SPR	surface plasmon resonance
TR	terminal repeat
wt	wild-type

persistence of viral DNA is affected by disturbing or influencing LANA [15]. The inhibition of the interaction between LANA and viral DNA could lead to a reduction or loss of viral genomes in the infected cells. Today's treatment of KSHV and KSHV-associated diseases is difficult and still limited [19,20]. It is clear, that there is an urgent need for specific drugs, which interfere with novel steps in the KSHV lifecycle. In view of its central role during latent viral persistence, LANA is considered to be a very promising target for the development of specific antiviral therapeutics against KSHV.

In a study previously published by us in 2019, we described the discovery of first inhibitors, which interfere with the LANA-DNA interaction [11]. Further inhibitor scaffolds have been identified using a functional screen and an in-house compound library [21]. Starting with a fragment-based drug discovery approach, we successfully developed a fragment-sized inhibitor **I** capable to compete with the viral DNA (Fig. 1). For the evaluation of functional activity of our compounds, we used a fluorescence-polarization (FP)-based assay and electrophoretic mobility shift assay (EMSA) experiments. For our most promising fragment-sized inhibitor **I,** we observed an IC_{50} value of 17 ± 1 μM in our FP-assay using a LANA DNA binding domain (DBD) mutant and 435 ± 6 μM in the EMSA studies using the wild-type LANA *C*-terminal domain (CTD).

We confirmed target binding using microscale thermophoresis (MST) and saturation transfer difference (STD)-NMR experiments. Additionally, the STD-NMR experiments and molecular docking studies provided important information on the putative orientation of Inhibitor **I** when bound to LANA. Based on the STD-NMR studies and docking results we suggested that the nitrogen at the pyridine core acts as a hydrogen bond acceptor and protons 2, 3 and 4 are not in direct interaction with the protein surface, hence these positions should be further investigated as potential growth vectors. Furthermore, two glutamines are presumably involved in hydrogen-bond interactions with the carboxyl group. However, it was not clear whether the carboxylic acid function is necessary for binding [11].

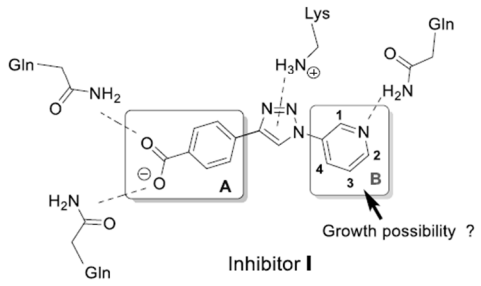

Fig. 1. Previously described LANA-DNA interaction inhibitor **I** and its predicted binding mode which provides the basis for structural optimization by rational design and growth vector exploration.

Based on these findings, we embarked on structure-activity relationship (SAR) studies and further medicinal chemistry optimization to improve the potency of our hit compounds. Herein, we report our recent advances in improving our LANA-DNA-interaction inhibitors using compound **I** as a starting point. Unfortunately, our efforts in solving a co-crystal structure of inhibitor **I** in complex with LANA have not been successful to date. This renders unambiguous experiment-supported structure-based optimization unfeasible. Therefore, we systematically investigated the LANA-DNA-interaction inhibition of new synthesized compounds using FP-based competition assay and EMSA experiments as the SAR drivers.

2. Design concept

Based on the previously applied STD-NMR and docking studies we modified Inhibitor **I** in a step-by-step manner. Inhibitor **I** was divided in two regions, the benzoic acid part **A** and the pyridine core **B** (Fig. 1). The triazole core was not yet modified in order to exploit the robust and facile Copper(I)-catalyzed azide-alkyne cycloaddition (CuAAC) click chemistry. First, region **A** was modified and variations of the carboxylic acid were introduced. As a second step, we have modified the pyridine moiety, region **B**. From our previous results we assumed that the nitrogen at the pyridine motif is essential for binding and functions as hydrogen bond acceptor. STD-NMR data revealed that Proton 1 interacts tightly with LANA while proton 2 is also in close proximity to the protein surface. However, our docking studies suggested that the latter might be at least partially solvent exposed. In contrast, protons at position 3 and 4 did not show direct contact with the LANA surface according to their weak STD-NMR effects. These observations inspired us to investigate positions 2, 3 and 4 as potential growth vectors in the presented study.

3. Results and discussion

3.1. Chemistry

3.1.1. Modifications of region A

3-azidopyridine **2** was generated by a standard azidation method using 3-aminopyridine **1**, $NaNO_2$ and NaN_3 in a mixture of EtOAc and 6M HCl [11,22]. In a second step, as depicted in Scheme 1, various commercially available ethynylbenzene derivatives were used in a standard copper-catalyzed CuAAC reaction with 3-azidopyridine to provide the triazoles **3**–**5, 8, 10, 11**, and **13** [11].

The ethyl ester **6** and amide **7** analogue were generated from the carboxylic acid **3** by thionyl chloride-mediated activation and subsequent treatment with ethanol or aq. ammonia solution. The hydrolysis of 3-chloro-4-methylester intermediate **8** with NaOH in ethanol produced the corresponding acid **9**. The *N*-acetyl analogue **12** was synthesized from amine **11** with acetyl chloride under basic conditions.

3.1.2. Modifications of region B

Compound **16** bearing an additional CH_2-linker between triazole and pyridine core was synthesized starting from (bromomethyl)benzene **14**, which was converted to the azide **15** using NaN_3 in DMSO [23], followed by a click reaction with 4-ethynylbenzoic acid. Different arylazides **17a-n** and **20** decorated with various substitutions were generated by reaction of the corresponding commercially available amines **18a-n and 21** with $NaNO_2$ and NaN_3 in 6 M HCl and EtOAc (Scheme 2). The subsequent CuAAC click reaction with 4-ethynylbenzoic acid provided the target molecules **19a-n and 22**. The hydroxypyridine **19o** analogue was generated from the methoxypyridine **19k** by treating with 48% aqueous HBr solution at 80 °C.

As depicted in Scheme 3, the syntheses of target compounds via Suzuki coupling was achieved using two different synthetic routes. In route 1, Suzuki coupling with different commercially available boronic acids and halogenated pyridine-3-amines **23, 27 and 28** in presence of $Pd(P(Ph_3)_4$ achieved phenyl-substituted pyridine amines **24a-b and 29a-b** in the first step. Subsequently, the amines were converted to the corresponding azides **25a-b and 30a-b** followed by a CuAAc click reaction with 4-ethynylbenzoic acid to obtain the target compounds **26a-b and 31a-b**. In parallel, the alternative route 2 was established for late stage modifications via Suzuki coupling. First, halogenated pyridine-3-amines **32a-b** were converted to the corresponding azide **33a-b**, followed by click reaction with 4-ethynylbenzoate to obtain the corresponding triazole intermediates **34a-b**. Subsequently, phenyl-substituted compounds **35a-k** were achieved via Suzuki coupling using corresponding boronic acids and $Pd(P(Ph_3)_4$.

Finally, the hydrolysis of the esters with NaOH in methanol produced the target carboxylic acid compounds **36a-k**. As depicted in Scheme 4, for the synthesis of the series of pyridine-phenoxy target compounds **40a-e**, cupper-catalyzed Ullmann reaction was used in the first step using 6-bromo-4-methylpyridin-3-amine **37**, the corresponding phenol derivative or thiophenol, Cs_2CO_3 and CuI to obtain the aminopyridine-phenoxy intermediates **38a-e**.

The obtained amines were transformed into the corresponding azides **39a-e** as described above. Last step was a CuAAC reaction of azides with 4-ethynylbenzoic acid to obtain the target compounds **40a-e**. The isoquinoline **43** and quinoline **46** analogue were synthesized starting from isoquinoline-4-amin **41** and quinoline-3-amin **44** by standard azidation to **42** and **45**, followed by CuAAC click reaction with 4-ethynylbenzoic acid. Further isoquinoline derivatives **50a-c** were synthesized in a 3 step procedure (Scheme 5). A direct transformation of bromo isoquinolines **47a-c** into the corresponding azides using NaN_3, Cu(I) and Na_2CO_3 at 85 °C over night as described in literature was not efficient [24]. LCMS-guided reaction monitoring showed the formation the primary amine and other side products. For this reason, we extended the reaction time until we detected full conversion into the corresponding primary amine **48a-c** with the aim to subsequently transform these intermediates into the corresponding azides. Indeed, we achieved successful azidation (intermediates **49a-c**) and CuAAC coupling, respectively, using amines **48a-c** and the conditions described above yielding the desired isoquinoline products **50a-c**.

3.2. Functional evaluation using LANA-DNA interaction inhibition assays and SAR studies

The target compounds were tested for functional activity in the FP-based LANA-DNA interaction inhibition assay using LBS2 as the probe and an oligomerization-deficient LANA DBD mutant [11]. This oligomerization-deficient *C*-terminal LANA mutant (aa1008-1146) has nine amino acid point mutations: K1055E, K1138S, K1140D, K1141D, R1039Q, R1040Q, A1121E, K1109A, and D1110A. For this mutant, also in presence of oligonucleotides, which represent the viral LANA-binding sites LBS1, LBS2 or LBS3, a high water solubility was shown [10,11,17,25]. All compounds showing an IC_{50} values less than 250 μM were further tested in an orthogonal LANA-DNA interaction inhibition assay employing EMSA methodology, the same LANA DBD mutant and LBS1 as probe. As described above, the latter oligo has a higher affinity to the target rendering the EMSA experiment a more stringent read out for compound efficacy.

For the first series of compounds, we investigated the significance of the carboxylic acid in the Western part of the molecule (region A) by varying its position, attaching additional groups or substituting it by other polar functional groups capable of

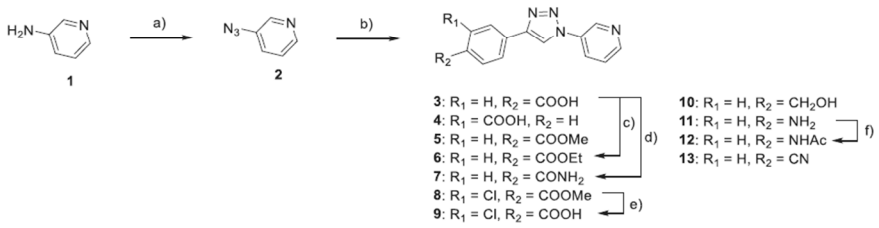

Scheme 1. Modification of region A.[a]

[a]Reagents and conditions: a) $NaNO_2$, NaN_3, EtOAc, 6M HCl, 0 °C → rt, yield 50%, 2 h; b) corresponding ethynylbenzene, $CuSO_4 \bullet 5H_20$, Na-Ascorbate, DIPEA, MeOH, H_2O, rt, 16 h, yield 60–82%; c) 1. $SOCl_2$, DMF, 60 °C, 1 h, 2. EtOH, DIPEA, rt, 16 h, yield 53%; d) 1. $SOCl_2$, DMF, 60 °C, 1 h, 2. NH_4OH, rt, 16 h, yield 27%; e) 2 M NaOH, MeOH, rt, 16 h, yield 66%; f) Actyl chloride, Et_3N, DCM, DMF, rt, 16 h, yield 14%.

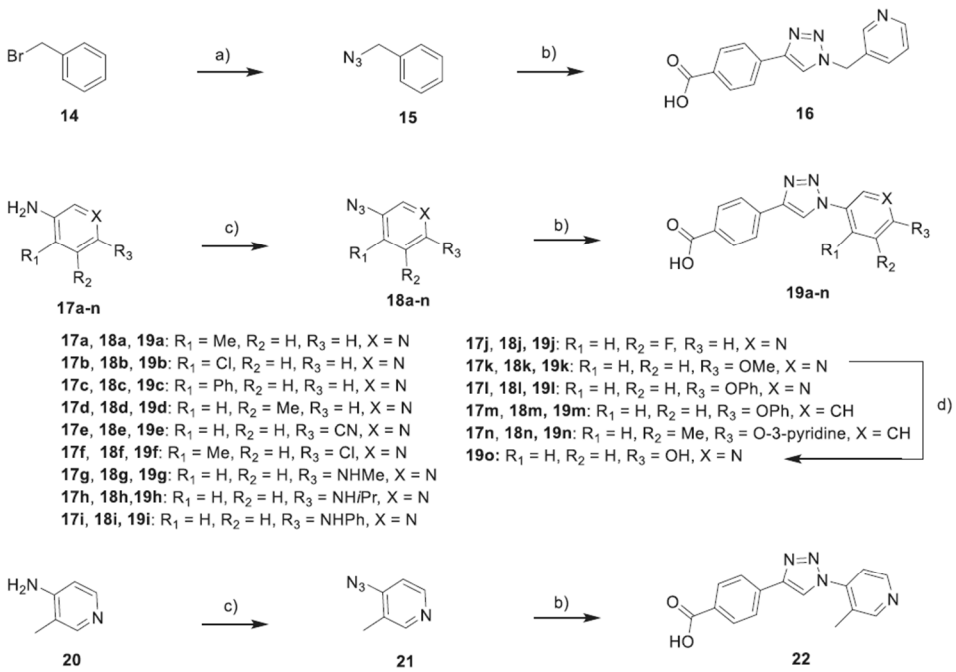

Scheme 2. Azide synthesis and CuAAC click reaction.[a].
[a]Reagents and conditions: a) NaN_3, Et_3N, DMSO, rt, 16 h, yield 78%; b) 4-ethynylbenzoic acid, $CuSO_4 \bullet 5H_20$, Na-Ascorbate, DIPEA, MeOH, H_2O, rt, 16 h, yield 20–90%; c) $NaNO_2$, NaN_3, EtOAc, 6M HCl, 0 °C → rt, 2 h, yield 4–98%; d) 48% aq. HBr, 80 °C, 12 h, yield 86%.

participating in hydrogen bonding. The results are shown in Table 1.

Moving the carboxylic acid from para (inhibitor **I**) to *meta* position (**4**) decreases the activity significantly. Also an additional chlorine atom attached in *meta* position (**9**) lead to a complete loss of activity. The replacement of the carboxylic acid by a methyl ester (**5**), ethyl ester (**6**) or amide (**7**) was also detrimental. Furthermore, moving from the carboxylic acid to the methyl alcohol (**10**), amine (**11**), acetamide (**12**) or nitrile (**13**) also resulted in inactive compounds. These results indicate that the carboxylic acid in *para* position in region A is essential for inhibitory activity. Therefore, we kept the *p*-carboxylic acid in region A fixed for further optimization studies and focused on the modifications at the pyridine core in region B. First, we examined the effect on inserting a short linker between the triazole and the pyridine core (**16**).

This, however, resulted in loss of activity. As described before, from previous STD-NMR and molecular docking experiments we expected, that growing the fragment-sized Inhibitor **I** in different positions at the pyridine core (region B) would potentially increase potency.

To explore the influence of larger structural motifs at the pyridine core in position 4 we introduced a variety of residues. As listed in Table 2, growing in this position is accepted and resulted in moderate to potent inhibitory effects in FP assay ranging from IC_{50} values of 86 ± 6 μM (**19a**) to 18 ± 4 μM (**19c**). The size of the introduced residue seems to play an important role. While a small methyl group is not favorable, but accepted (**19a**, IC_{50} 86 ± 6 μM), further increasing the size from chlorine (**19b**) to phenyl (**19c**) improves IC_{50} values to 29 ± 1 μM μM and 18 ± 4 μM, respectively. This observation might hint at a steric *ortho* effect. The additional bulky phenyl ring strongly hinders the rotation of the bond between triazole and pyridine and, therefore, might fix the nitrogen in the pyridine core in a more favorable orientation. In EMSA experiments, 4-substituted compounds **19b** (EMSA: 94% inhibition @ 500 μM) and **19c** (EMSA: 100% inhibition @ 500 μM) showed a higher efficiency compared to Inhibitor **I** (EMSA: 83% inhibition @ 500 μM) [11]. Additionally, we shifted the nitrogen of the pyridine core from *meta* (**19a**) to para position (**22**) which resulted in an inactive compound. The improvements in the EMSA assay for compounds **19b-c** over our initial hit compound **I** were not perfectly mirrored by the FP IC_{50} values, which presumably is rooted in the usage of different DNA probes (LBS1 vs LBS2, respectively).

Nevertheless, the results for compounds **19b** and **19c** were a major step towards achieving LANA inhibitors suitable for cellular assays and encouraged us to explore the potential of growing the hit scaffold in this direction even further.

In the next series of compounds, Inhibitor **I** was grown in position 3 at the pyridine core by introducing a variety of aromatic rings. As listed in Table 3, a small methyl residue in position 3 (**19d**, IC_{50} of 45 ± 5 μM; EMSA: 78% inhibition @ 500 μM) is tolerated, but the fluorinated analogue **19j** and most of the phenyl substituted compounds **36a-d**, **36f-i**, and **31a** showed a complete loss or only moderate activity.

However, compounds with an additional hydroxyl function attached to the phenyl ring (**36e,** IC_{50} of 153 ± 7 μM, EMSA: 20% inhibition @ 500 μM) showed moderate activity.

Moving from a phenyl **36a** to a smaller and more polar furanyl residue **36j** the potency was restored (IC_{50} of 19 ± 2 μM). Unfortunately, in EMSA experiments we observed only a weak effect (34% inhibition @ 500 μM) for this compound. Interestingly, by attaching an additional chlorine atom in position 4 and having a phenyl in position 3 (**31b**) resulted in a highly potent compound with IC_{50} of

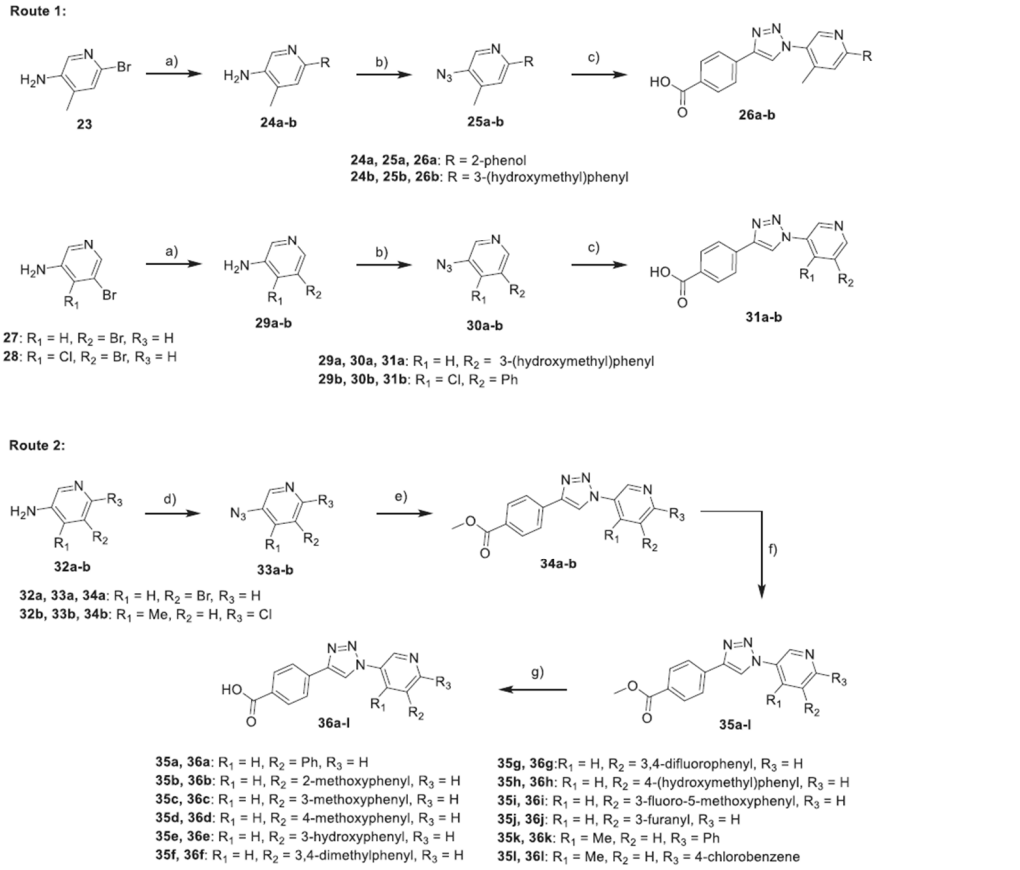

Scheme 3. Synthesis of target compounds via Suzuki coupling using two different routes.[a].
[a]Reagents and conditions: a) corresponding boronic acid, Na_2CO_3, $Pd(P(Ph_3)_4$, 1,4-dioxan, H_2O, 90 °C, 16 h, yield 21–75%; b) $NaNO_2$, NaN_3, EtOAc, 6M HCl, 0 °C → rt, 2 h, yield 86–99%; c) 4-ethynyl benzoic acid, $CuSO_4 \bullet 5H_20$, Na-Ascorbate, DIPEA, MeOH, H_2O, rt, 16 h, yield 36–76%; d) $NaNO_2$, NaN_3, EtOAc, 6M HCl, 0 °C → rt, 2 h, yield 34–80%; e) 4-ethynyl benzoate, $CuSO_4 \bullet 5H_20$, Na-Ascorbate, DIPEA, MeOH, H_2O, rt, 16 h, yield 63–80%; f) corresponding boronic acid, Na_2CO_3, $Pd(P(Ph_3)_4$, 1,4-dioxan, H_2O, 90 °C, 16 h, yield 20–90%; g) 2 M NaOH, MeOH, rt, 16 h, yield 16–83%.

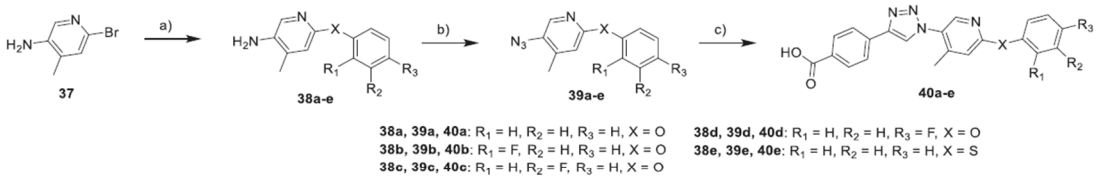

Scheme 4. Synthesis of target compounds via Ullmann Reaction.[a].
[a]Reagents and conditions: a) corresponding phenol or thiophenol, Cs_2CO_3, CuI, DMF, 130 °C, 16 h, yield 28–94%; b) $NaNO_2$, NaN_3, EtOAc, 6M HCl, 0 °C → rt, 2 h, yield 70–99%; c) 4-ethynyl benzoic acid, $CuSO_4 \bullet 5H_20$, Na-Ascorbate, DIPEA, MeOH, H_2O, rt, 16 h, yield 45–93%.

38 ± 3 μM and full inhibition in FP and EMSA assays, respectively. These results further corroborate the notion of a beneficial *ortho* effect.

To explore the influence of growing inhibitor **I** at the pyridine core in position 2, a set of different target compounds was synthesized (Tables 3 and 4). The direct attachment of a nitrile group to the pyridine was tolerated (**19e**: IC_{50} 52 ± 37 μM, EMSA: n. i.). Moving to chlorine, hydroxy or methoxy group we observed a significant loss in activity (**19f**: IC_{50} > 250 μM; **19o:** IC_{50} 214 ± 24 μM and **19k:** IC_{50} 218 ± 192 μM). Also in EMSA experiments **19j** (75% inhibition @ 500 μM) and **19k** (11% inhibition @ 500 μM) did not show a significant effect. An increase in activity was observed by introducing bulkier substituents and an additional methyl group for R_1. In detail, an unpolar bulky phenyl or *p*-

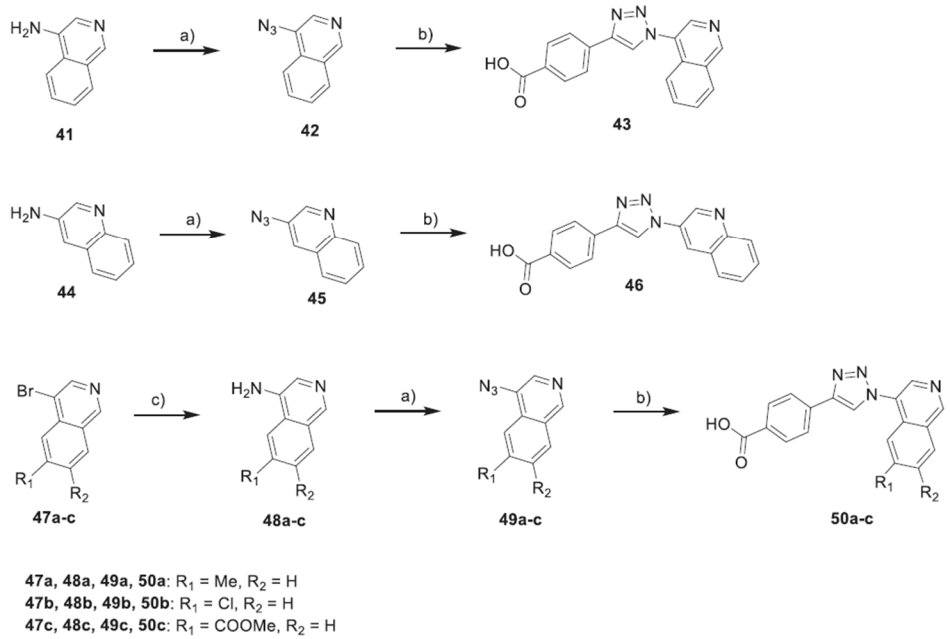

Scheme 5. Synthesis of isoquinoline derivatives.[a].
[a]Reagents and conditions: a) $NaNO_2$, NaN_3, EtOAc, 6M HCl, 0 °C → rt, 2 h, yield 68–91%; b) 4-ethynyl benzoic acid, $CuSO_4 \bullet 5H_20$, Na-Ascorbate, DIPEA, MeOH, H_2O, rt, 16 h, yield 25–90%; c) NaN_3, Na_2CO_3,$CuSO_4 \bullet 5H_20$, Na-Ascorbate, L-proline, DMF, H_2O, 85 °C, 24 h, yield 88–97%.

Table 1
Inhibition activities of compounds with modification in region A.

Cpd	R	FP Assay (LBS2)[a] IC_{50}	Cpd	R	FP Assay (LBS2) IC_{50}
Inhibitor I		17 ± 1 μM	**9**		n.i.
4		>250 μM	**10**		n.i.
5		n.i.[b]	**11**		>250 μM
6		n.i.	**12**		n.i.
7		n.i.	**13**		>250 μM

[a] Fluorescence-polarization assay using LBS2 as probe, data representing average of duplicates ± standard deviation.
[b] No inhibition at 500 μM.

chlorophenyl was accepted in position 2 and we observed IC_{50} values of 36 ± 5 μM for **36k** and 58 ± 7 μM for **36l** and moderate inhibition in EMSA. Analogues **26a** and **26b** with polar hydroxyl groups attached at the phenyl showed good potency with IC_{50}

Table 2
Inhibitory activities of analogues modified in position 4 – observing higher efficiency for 4-substituted compounds.

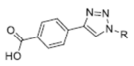

Cpd	R	FP Assay (LBS2)[a] IC_{50}	EMSA (LBS1)[b] inhibition @ 500 μM
Inhibitor I		17 ± 1 μM	82%
16		>250 μM	n.d.[d]
19a		86 ± 6 μM	39%
19b		29 ± 1 μM	94%
19c		18 ± 4 μM	100%
22		n.i.[c]	n.d.

[a] Fluorescence-polarization assay using LBS2 as probe, data representing average of duplicates ± standard deviation.
[b] Electrophoretic mobility shift assay using LBS1 as probe.
[c] No inhibition at 500 μM.
[d] Not determined.

Table 3
Inhibitory activities of analogues modified in position 3. Most derivatives substituted in this position (R_2) showed a significant decrease in activity.

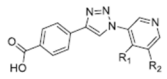

cpd	R_1	R_2	FP Assay (LBS2)	EMSA (LBS1)
			IC_{50}	Inhibition @ 500 μM
Inhibitor I	H	H	17 ± 1 μM	82%
19d	H	Me	45 ± 5 μM	78%
19j	H	F	n. i.	n. d.
36a	H		>250 μM	n. d.
36f	H		n.i.	n. d.
36g	H		>250 μM	n. d.
36b	H		n. i.	n. d.
36c	H		110 ± 32 μM	n. i.
36d	H		n. i.	n. d.
36i	H		n. i.	n. .d
36e	H		153 ± 7 μM	20%
31a	H		>250 μM	n. d.
36h	H		>250 μM	n. d.
36j	H		19 ± 2 μM	34%
31b	Cl		38 ± 3 μM	100%

[a]Fluorescence-polarization assay using LBS2 as probe, data representing average of duplicates ± standard deviation.
[b]Electrophoretic mobility shift assay using LBS1 as probe.
[c]No inhibition at 500 μM.
[d]Not determined.

values of 21 ± 3 μM and 25 ± 1 μM, respectively. Furthermore, the efficiency of these two analogues in our EMSA studies was high with a full inhibition @ 500 μM. By attaching methylamine (**19g**), isopropylamine (**19h**) and anilino (**19i**) at position 2 we observed an increase in activity from small to bigger size, whereby the methylamine compound **19g** was completely inactive and the

Table 4
Inhibitory activities of analogues modified in position 2. Attaching polar hydroxyl benzene groups increases inhibitory activity.

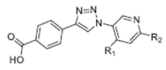

cpd	R_1	R_2	FP Assay (LBS2)	EMSA (LBS1)
			IC_{50}	Inhibition @ 500 μM
Inhibitor I	H	H	17 ± 1 μM	82%
19e	H	CN	52 ± 37 μM	n.i.
19f	Me	Cl	>250 μM	n.d.
19o	H	OH	214 ± 24 μM	75%
19k	H	OMe	218 ± 192 μM	11%
36k	Me		36 ± 5 μM	36%
36l	Me		58 ± 7 μM	30%
26a	Me		21 ± 3 μM	100%
26b	Me		25 ± 1 μM	100%
19g	H		n.i.	n.d.
19h	H		>250 μM	n.d.
19i	H		110 ± 20 μM	29%

[a]Fluorescence-polarization assay using LBS2 as probe, data representing average of duplicates ± standard deviation.
[b]Electrophoretic mobility shift assay using LBS1 as probe.
[c]No inhibition at 500 μM.
[d]Not determined.

anilino analogue **19i** showed a moderate activity of IC_{50} of 110 μM and 29% inhibition in EMSA.

Additionally, a series of compounds was synthesized with a more flexible and bulky phenoxy group in position 2 (Table 5). The phenoxy analogue **19l**, similar to the aminophenyl compound **19i**, was inactive, indicating that an amino linker between pyridine and phenyl is more suitable for activity compared to the oxygen linker. By attaching an additional methylgroup in position 4 (R_1) at the pyridine core **40a** an increase in activity compared to **19l** was observed leading to a moderate IC_{50} of 198 ± 8 μM. The fluorinated analogues **40b-d** also showed moderate activities like compound **40a** while the *o*-fluoro analogue **40b** possessed the best IC_{50} of 64 ± 2 μM. For the *m*- (**40c**) and *p*-fluoro (**40d**) derivatives IC_{50}s of 122 ± 3 μM and 134 ± 2 μM were observed, respectively. Unfortunately, all these compounds showed no effect in EMSA experiments.

Exchanging the oxygen linker by a sulfur (**40e**, IC_{50} 175 ± 10 μM) was tolerated (compare with **40a**, IC_{50} 198 ± 8 μM). As expected, by removing the nitrogen in the pyridine core resulted in an inactive compound (**19m**). Astonishingly, moving the nitrogen to the phenoxy residue (**19n**) yielded a highly potent compound with an IC_{50} of 19 ± 1 μM showing also full inhibition in the EMSA experiments.

Intrigued by the notion that fragment growing in position 3 was possible in combination with *ortho*-substituents, we focused our efforts on further exploring these two positions by installing a connected structural motif. To this end, we designed and synthesized isochinoline analogues (Table 6). In general, isoquinoline analogues were pleasingly effective. The unsubstituted isochinoline

Table 5
Inhibitory activities of Phenoxy analogues. Shifting nitrogen to the phenoxy residue improves inhibitory efficiency.

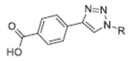

cpd	R_2	FP Assay (LBS2)	EMSA (LBS1)
		IC_{50}	inhibition @ 500 μM
Inhibitor I		17 ± 1 μM	82%
19l	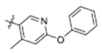	n. i.	n. d.
40a	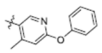	198 ± 8 μM	n. i.
40b	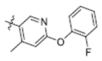	64 ± 2 μM	n. i.
40c	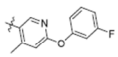	122 ± 3 μM	n. i.
40d	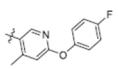	134 ± 2 μM	n. i.
40e	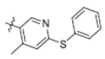	175 ± 10 μM	n. i.
19m		n.i.	n. d.
19n	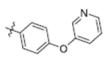	19 ± 1 μM	100%

[a]Fluorescence-polarization assay using LBS2 as probe, data representing average of duplicates ± standard deviation.
[b]Electrophoretic mobility shift assay using LBS1 as probe.
[c]No inhibition at 500 μM.
[d]Not determined.

43 showed an FP IC_{50} value of 33 ± 1 μM and 96% inhibition in EMSA experiments. Moving from isoquinoline to quinoline **46** resulted in a slight loss in activity compared to **43** (**46,** IC_{50} 70 ± 34 μM, 61% inhibition in EMSA).

Attaching an additional methyl (**50a**) or chlorine (**50b**) at the isoquinoline motif was beneficial for the inhibitory effect. Noteworthy, **50a** showed the lowest FP IC_{50} of 8 ± 1 μM reported to date, while **50b** also possessed a decent IC_{50} of 17 ± 1 μM. Furthermore, in EMSA experiments 100% inhibition was detected for both compounds at 500 μM. Finally, an isoquinoline methylester analogue **50c** was inactive, however.

3.3. Further characterization and EMSA studies using wild-type LANA

For further evaluation and characterization the most promising compounds were selected. On the bases of our results, we chose compounds **19c**, **31b**, **26a-b**, **19n**, **50a**, and **50b**, which possessed the best IC_{50} values in the FP-based assay and showed strong inhibitory effects at 500 μM in EMSA using the oligomerization-defizient LANA DBD mutant (aa1008-1146).

Table 6
Inhibitory activities of Isoquinoline derivatives. Adding an annulated ring structure in direction of identified growth vector results in the most efficient inhibitors to date.

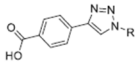

Cpd	R	FP Assay (LBS2)	EMSA (LBS1)
		IC_{50}	inhibition @ 500 μM
Inhibitor I		17 ± 1 μM	82%
43		33 ± 1 μM	96%
46		70 ± 34 μM	61%
50a		8 ± 1 μM	100%
50b		17 ± 1 μM	100%
50c		>250 μM	n. d.

[a]Fluorescence-polarization assay using LBS2 as probe, data representing average of duplicates ± standard deviation; [b]Electrophoretic mobility shift assay using LBS1 as probe; [c]No inhibition at 500 μM; [d]Not determined.

First, these compounds were initially tested for inhibition at 250 μM using LANA DBD mutant (Fig. 2, A) to see if they are also able to disturb the LANA-DNA interaction at a lower concentration in EMSA and compared these results also with inhibitor **I**. Inhibitor **I** and the compounds **19c**, **31b**, and **26b** showed no inhibitory effect on the $LANA_{mut}$-DNA interaction at 250 μM. However, strong inhibitory effects were observed at this concentration for compounds **26a**, **19n**, **50a**, and **50b** as observed by the disappearance of the bands for the $LANA_{mut}$-DNA complex (upper band, Fig. 2A).

We also determined the inhibitory activity of our best compounds against the interaction between wild-type LANA CTD (aa934-1162) and viral LBS1 (Fig. 2, B) in EMSA. Our wild-type LANA CTD construct is longer compared to the LANA DBD mutant and has no mutations and still shows a sufficient solubility in aqueous medium also in presence of viral LBS1. The compounds were also tested at 250 μM. Unfortunately, no inhibitory effect was observed for compounds **I**, **19c**, **31b**, **26a-b**, **19n**, and **50b**. However, Compound **50a** showed a significant effect and was able to inhibit the interaction between wild-type LANA CTD and LBS1.

Furthermore, we titrated the compounds showing an effective inhibition in EMSA using the LANA DBD mutant (Fig. 2, A), in EMSA experiments using the LANA DBD mutant and LBS1 as a probe to determine the IC_{50} values. The results are listed in Table 7 and detailed information can be found in the supporting information.

As reported earlier by us, inhibitor **I** showed an IC_{50} in FP assay (LBS2) of 17 ± 1 μM and an IC_{50} in EMSA of 426 ± 2 μM using LANA DBD mutant [11]. The observed IC_{50} values using LBS2 for the most promising inhibitors were basically in the same range. Additionally, we also tested the most promising inhibitors

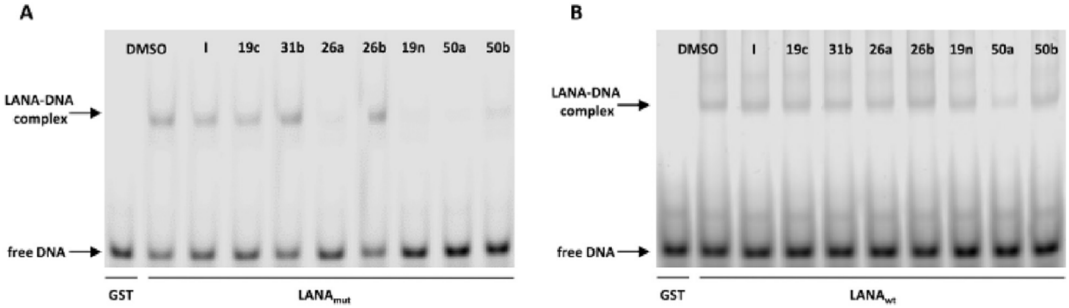

Fig. 2. EMSA gels with inhibitor **I**, **19c**, **31b**, **26a-b**, **19n**, **50a-b**. Compounds were tested at a final concentration of 250 μM and LBS1 was used as probe. (**A**) Using an oligomerization-deficient LANA DBD mutant, a strong inhibitory effect (disappearance of LANA-DNA complex band) was observed for compounds **26a**, **19n** and **50a-b** (**B**) Using wild-type LANA CTD, a significant inhibitory effect for compound **50a** was observed.

Table 7
Comparison of most efficient LANA-DNA inhibitors.

Cpd	Structure	FP-Assay[a] IC_{50} (LBS2) ($LANA_{mut}$)	FP-Assay IC_{50} (LBS1) ($LANA_{mut}$)	FP-Assay IC_{50} (LBS3) ($LANA_{mut}$)	EMSA[b] IC_{50} (LBS1) ($LANA_{mut}$)
Inhibitor I	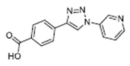	17 ± 1 μM	20 ± 3 μM	19 ± 3 μM	426 ± 2 μM
19c	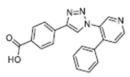	18 ± 4 μM	52 ± 2 μM	42 ± 3 μM	n.i. at 250 μM[c]
31b	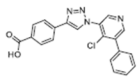	38 ± 3 μM	55 ± 7 μM	45 ± 4 μM	n.i. at 250 μM
26a	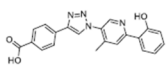	21 ± 3 μM	30 ± 2 μM	34 ± 3 μM	156 ± 27 μM
26b	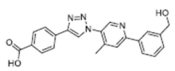	25 ± 1 μM	64 ± 1 μM	63 ± 8 μM	n.i. at 250 μM
19n	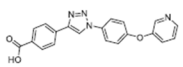	19 ± 1 μM	15 ± 1 μM	25 ± 1 μM	64 ± 12 μM
50a	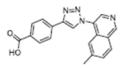	8 ± 1 μM	9 ± 2 μM	8 ± 1 μM	53 ± 43 μM
50b	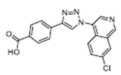	17 ± 1 μM	14 ± 1 μM	15 ± 1 μM	93 ± 8 μM

[a] Fluorescence-polarization assay using LBS1, LBS2 and LBS3 as probe, data representing average of duplicates ± standard deviation.
[b] Electrophoretic mobility shift assay using LBS1 as probe.
[c] No inhibition at 250 μM.

in FP assay using LBS1 and LBS3, respectively. Compound **50a** showed a 2-fold better IC_{50} of 8 – 9 μM against all LBS compared to **I**. Furthermore, we could increase the inhibitory activity in EMSA experiments using LBS1 by 7-fold. As a consequence compounds **19n** and **50a** are the most potent LANA-LBS1-inhibitors reported so far (IC_{50} values of 64 ± 12 μM and 53 ± 3 μM). Interestingly, compounds showing increased IC_{50} values of 50–60 μM against LBS1 and LBS3 in FP assay were also not effective in EMSA at 250 μM. Excepted is however inhibitor **I**, which showed also IC_{50} values around 20 μM against LBS1 and LBS3, but no effect at 250 μM in EMSA.

As described above, only compound **50a** showed an inhibitory effect at a concentration of 250 μM in EMSA using wild-type LANA CTD (Fig. 3 A). A dose-response EMSA experiment with wild-type LANA CTD yielded an IC_{50} value of 60 ± 4 μM (Fig. 3 B).

These results indicate that compound **50a** is equally potent against wild-type LANA CTD and the oligomerization-deficient LANA DBD mutant. In comparison to inhibitor **I** (IC_{50} of

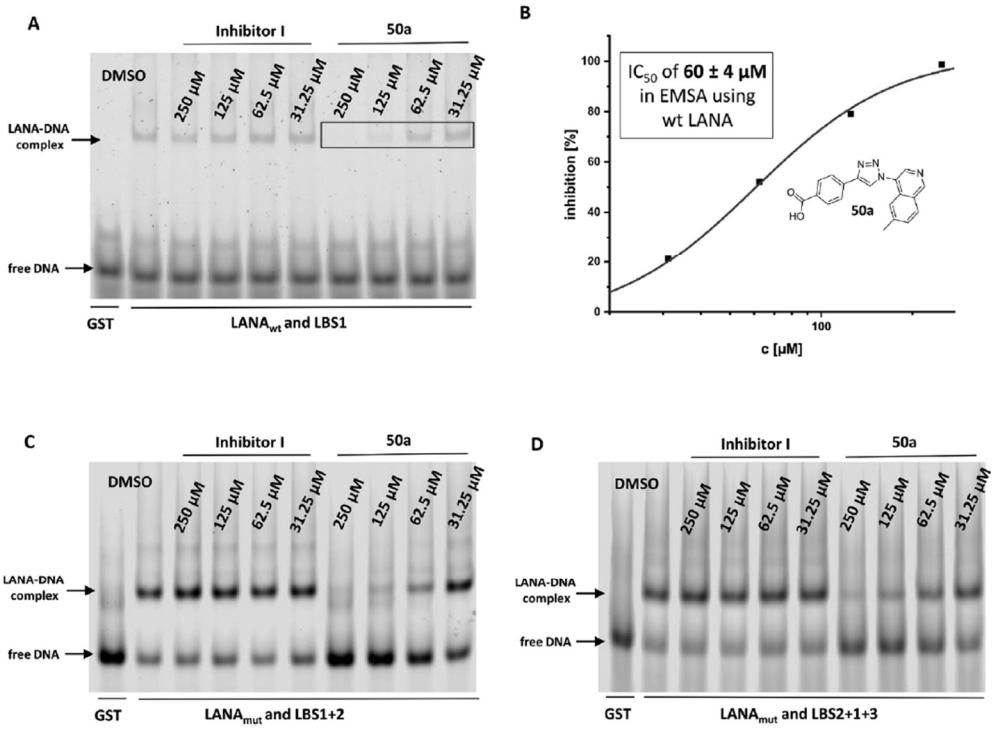

Fig. 3. (**A**) Dose-dependent EMSA experiment using wild-type LANA CTD, LBS1 as probe and Compound **50a**. (**B**) Curve shows normalized data points (inhibition from 0 to 100%) representing intensities of LANA-DNA-complex bands (Fig. 3 (A), upper bands, marked in red) from dose-dependent EMSA experiment. IC_{50} value was calculated using a four-parameter dose-response model. (**C**) Dose-dependent EMSA experiment using LANA DBD mutant, a combination of LBS1+2 as probe and Inhibitor **I** and Compound **50a**. (**D**) Dose-dependent EMSA experiment using LANA DBD mutant, a combination of LBS2+1 + 3 as probe and Inhibitor **I** and Compound **50a**. (For interpretation of the references to colour in this figure legend, the reader is referred to the Web version of this article.)

435 ± 6 µM against wild-type LANA CTD in EMSA) these results represent a huge potency improvement [11]. Furthermore, we tested if compound **50a** is also able to disturb the LANA-DNA interaction when using longer oligonucleotides comprising LBS1+2 as well as LBS2+1 + 3, in an arrangement that is present on the viral KSHV genome [17]. Each LBS is able to associate with one LANA dimer. Hence, LANA and the LBS1+2 oligomer can form a trimeric complex while the LBS2+1 + 3 oligomer gives rise to a quaternary complex. In order to test the efficacy of our inhibitors against the formation of these higher-order aggregates, dose–dependent EMSA experiments using LBS1+2 and LBS2+1 + 3 with the LANA DBD mutant were performed (Fig. 3C and D). We compared the effects of inhibitor **I** and Compound **50a** in this setup. As expected, inhibitor **I** showed no inhibitory effects in both experiments. However, Compound **50a** was still able to significantly inhibit the LANA LBS1+2 interaction at a concentration of 62.5 µM (Fig. 3, C) and additionally inhibited the LANA LBS2+1 + 3 interaction at 125 µM (Fig. 3, D). These results provide a basis for testing these inhibitors in cell based assays in the future.

The similar IC_{50} values of compound **50a** observed against wild-type LANA and LANA DBD mutant corroborates our hypothesis that our inhibitor binds at the DNA binding interface and is able to compete with the DNA. The DBD mutant involves nine point mutations, which are all located outside of the DNA binding site [25]. The goal of generating and using this mutant was to disturb the higher oligomerization in solution, which resulted in improved handling characteristics of the protein and better solubility of LANA-DNA complexes. Fig. 4 illustrates the LANA DBD surface (blue) and its single point mutations (yellow) bound to double-stranded DNA (red). The distribution of these mutations distant from the DNA-interaction interface combined with the observed similar IC_{50} values of our compound against wild-type and DBD mutant provide strong evidence, that we are targeting the LANA DNA interaction interface and that we do not unintentionally target one of the mutated regions on the LANA surface.

Taken together, compound **50a** is the most effective inhibitor against LANA DBD mutant and wild-type LANA CTD reported to date. To complement our studies, we applied STD-NMR experiments in order to identify further growth vectors.

3.4. STD-NMR studies for insight on ligand binding modes

Finally, we complemented our lead generation campaign by STD-NMR experiments with the aim to gather information on the binding orientation and to identify further growth vectors. In parallel, we attempted to solve co-crystal structures of our inhibitors in complex with LANA, unfortunately without success. However, we could successfully confirm previous STD-NMR and molecular docking results for inhibitor **I** by the obtained SAR in the present study and we were able to enlarge inhibitor **I** in the suggested direction. In order to inform our next optimization steps, we again performed STD-NMR experiments of our best inhibitor **50a**.

The protons of the tested compound, which are in closest proximity to the protein surface upon binding, are showing the

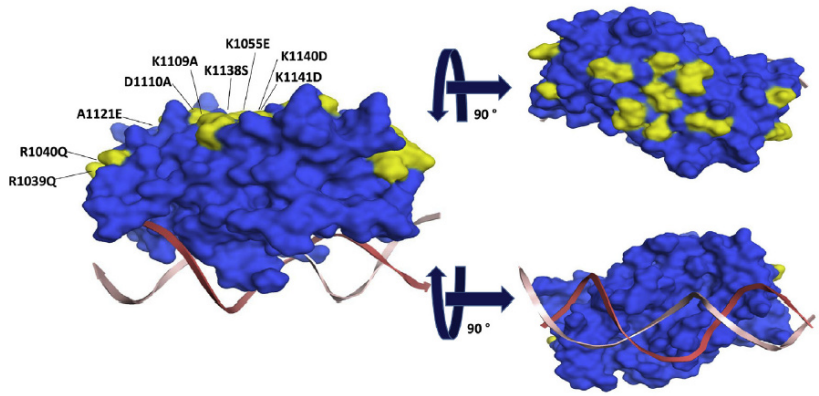

Fig. 4. Illustration of the nine single point mutations (yellow) of oligomerization interface and basic patch LANA mutant (blue) bound to DNA (red) assuming that our inhibitors bind at the LANA-DNA interaction interface. (For interpretation of the references to colour in this figure legend, the reader is referred to the Web version of this article.)

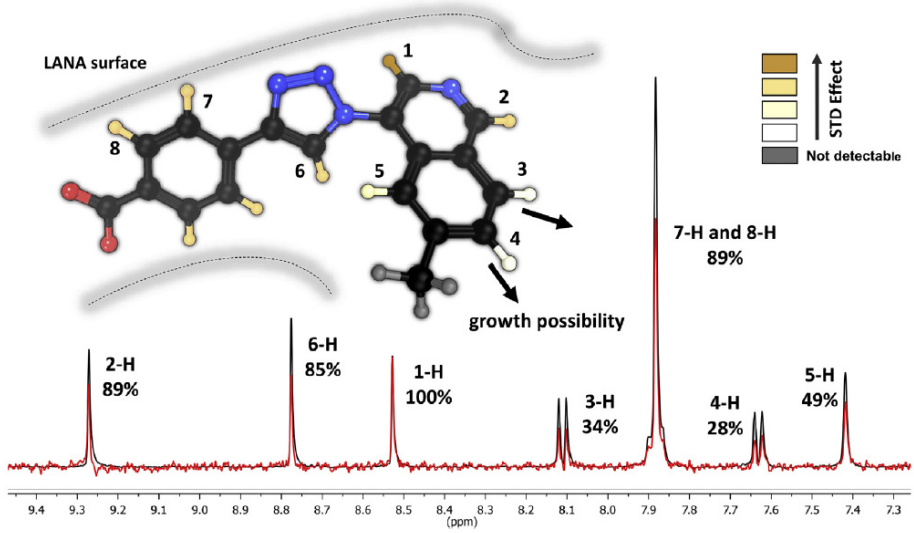

Fig. 5. STD experiments of compound **50a** in complex with LANA DBD mutant. The reference spectrum is displayed in black (STD-off) and STD difference spectra (STD-on) in red. Overlaid spectra were normalized to the signal for 1-H, which showed the strongest enhancement. (For interpretation of the references to colour in this figure legend, the reader is referred to the Web version of this article.)

strongest STD effects. In Fig. 5 an overlay of the on- (red) and off- (black) resonance STD-NMR spectra of the aromatic region are shown. The spectra were normalized to the strongest signal, which was observed for proton 1. The STD effects were calculated for each proton of inhibitor **50a** ($Effect_{STD} = I/I_0$). The results suggest that compound **50a** has a binding orientation to LANA similar to that of inhibitor **I** [11].

The nitrogen of the pyridine ring presumably acts as a proton acceptor and thereby anchors proton 1 close to the LANA surface. The proton in position 2 showed also a strong STD effect of 89%. The corresponding proton in inhibitor **I** showed a slightly stronger effect of 100% [11]. The bulky isoquinoline moiety and the additional methyl group cause an *ortho* effect, which hinders the rotation of the bond between the triazole core and the isoquinoline. We hypothesize, that this effect brings the nitrogen in an even more favorable orientation to the LANA surface and in turn leaves proton 2 now slightly more exposed. Furthermore, proton 6 located in the triazole core shows a stronger STD effect of 85% (47% in inhibitor **I**) [11], which leads us to suspect that the triazole is also now interacting more favourably with LANA. The four protons at the benzoic acid moiety, 7-H and 8-H, were found under one signal displaying a prominent STD effect of 89%. In contrast, the protons at the second ring of the isoquinioline motif showed a significantly lower STD effect (3-H: 34%, 4-H: 28% and 5-H: 49%). Hence, we conclude that these protons are not in direct contact with the protein and should be further investigated as potential secondary growth vectors. Unfortunately, the STD effect of the methyl group could not be determined, because signals of buffer ingredients were in the same

chemical shift range. For future medicinal chemistry optimization studies, further growing of the isoquinoline analogues in positions 3, 4 and 5 should be investigated. Additionally, a combination of the isoquinoline **50a** and compounds elongated in position 2 (see **19n** and **26a**) should be attempted.

4. Conclusion

In this study we synthesized a series of new derivatives of our LANA inhibitor **I** [11] and evaluated them for LANA-DNA interaction inhibition in an FP-assay and in EMSA experiments in order to generate more potent LANA-DNA inhibitors. Based on the previously discovered fragment-sized inhibitor **I**, medicinal chemistry optimization lead to new inhibitors with improved potency. In particular, the replacement of the pyridine core (inhibitor **I**) by a methyl-isoquinoline (**50a**) led to an increase of inhibitory potency of 7-fold against the wild-type LANA CTD interaction with viral LBS1. Moreover, compound **50a** was also able to inhibit the interaction between LANA DBD mutant and LBS1+2 and LBS2+1 + 3, respectively, in the lower micromolar range. Additionally, step-by-step modification studies gave new and important SAR insights for future medicinal chemistry optimizations towards lead structures. Furthermore, STD-NMR measurements of the most potent inhibitor **50a** in complex with LANA revealed important details about the binding orientation and allowed for the identification of a new potential growth vector. The ability to inhibit the wild-type LANA DNA interaction in a low micro molar range (IC_{50} 60 ± 4 μM) with such a small molecule scaffold is striking as such a macromolecule-macromolecule-interaction is usually considered to be highly challenging, if not "undruggable". Unexpectedly, we were able to significantly improve the inhibitory effects of our inhibitors using a chemistry-driven approach without having any structural information from a co-crystal about the binding mode and location on the LANA surface. Our results pave the way for the generation of a LANA-targeting anti-KSHV agent.

5. Experimental section

All reagent-grade chemicals were purchased from commercial suppliers and were used as received. The purifications were performed using automated column flash chromatography (CombiFlash Rf+, Teledyne ISCO, Lincoln, NE, USA) on silica gel 0.04–0.063 mm (RediSep Rf Kartuschen, Axel Semrau, Spocklhövel, Germany) or using preparative high performance liquid chromatography (HPLC, Ultimate 3000 UHPLC + focused, Thermo Scientific) on a reversed-phase column (C18 column, 5 μm, Macherey-Nagel, Germany). The solvents used for column flash chromatography were EtOAc and cyclohexane or DCM and MeOH. The solvents used for HPLC were water (containing 0.05% [v/v] FA) and MeCN (containing 0.05% [v/v] FA) (gradient elution, MeCN:H_2O 1:9 → 9:1). Reaction progress was monitored by TLC on TLC Silica Gel 60 F_{254} plates (Merk, Darmstadt, Germany) or by a reversed-phase liquid chromatography mass spectrometer (LCMS). ^1H and ^{13}C NMR were recorded on a Bruker Fourier spectrometers (500 or 126 MHz). Chemical shifts (δ) were reported in parts per million (ppm) relative to the corresponding reference solvent. The chemical shifts recorded as δ values in ppm units by reference to the hydrogenated residues of the deuterated solvent as the internal standard. Coupling constants (J) are given in hertz (Hz) and splitting patterns are designated as follows: s, singlet; d, doublet; dd, doublet of doublets; t, triplet; m, multiplet; br., broad signal. Purity of all final compounds was measured on the UV trace recorded at a wavelength of 254 nm and was determined to be >95% by a reversed-phase liquid chromatography mass spectrometer (LCMS). Representative ^1H and ^{13}C spectra of all final compounds can be found in the supporting information. High resolution mass spectra of all final compounds were measured on a Thermo Scientific Q Exactive Focus (Germany) equipped with a DIONEX ultimate 3000 UHPLC + focused and can be found in the supporting information. The reactions and purification steps were not optimized regarding yields.

General procedure for azide formation (GP1) for Compounds 2, 18a-n, 21, 25a-b, 30a-b, 33a-b, 39a-e, 42, 45, 49a-c: The appropriate aryl amine (1 eq.) was dissolved in EtOAc, cooled to 0 °C and 6 M HCl was added. Sodium nitrite (1.7 eq.) was dissolved in water and added slowly. The reaction mixture was stirred for 30 min at 0 °C. Subsequently, sodium azide (1.7 eq.) in water was added slowly at 0 °C. The mixture was stirred at room temperature for 2 h. TLC control indicated full conversion and the mixture was basified with saturated $NaHCO_3$ solution and was extracted with EtOAc (2 ×). The combined organic layers were dried over sodium sulfate and concentrated under reduced pressure to give the crude. The crude product was used as obtained in the next step without further purifications. Compound **2** is presented as an example. 3-azidopyridine (**2**): The azide was synthesized according to **GP1** using pyridin-3-amine **1** (376 mg, 4 mmol), sodium nitrite (1.7 eq., 469 mg, 6.8 mmol), sodium azide (1.7 eq., 442 mg, 6.8 mmol), EtOAc (8 mL), 6 M HCl (5 mL). The crude product (245 mg, 2 mmol, 50%) was used as obtained in the next step without further purifications. R_f = 0.37 (PE/EtOAc 7:3).

General procedure for synthesis of amino isoquinolin derivatives (GP2) for compounds 48a-c: Under argon atmosphere the appropriate bromo isoquinolin (1 eq.), L-proline (0.1 eq.), sodium azide (1.3 eq.) and sodium carbonate (1.3 eq.) was dissolved in a 2:1 mixture of DMF and water. Subsequently, sodium ascorbate (1.3 eq.) and copper sulfate hepta hydrate (1 eq.) were added and the reaction mixture was stirred over night at 85 °C. After full conversion (LCMS control) the mixture was cooled to room temperature and EtOAc and sat. aqueous $NaHCO_3$ solution were added. The mixture was extracted with EtOAc (3x), the combined organic layers were dried over sodium sulfate and concentrated under reduced pressure to obtain the crude. The obtained products were used as obtained without further purification. Compound **48a** is presented as an example. 6-methylisoquinolin-4-amine (**48a**): The amino isoquinolin was synthesized according to **GP2** using 4-bromo-6-methylisoquinoline **47a** (100 mg, 0.46 mmol), L-proline (0.1 eq., 0.05 mmol, 5 mg), sodium azide (1.3 eq., 0.60 mmol, 34 mg), sodium carbonate (1.3 eq., 0.60 mmol, 64 mg), sodium ascorbate (1.3 eq., 0.60 mmol, 119 mg), copper sulfate heptahydrate (1 eq., 0.46 mmol, 115 mg), DMF (4 mL) and water (2 mL). The crude product (70 mg, 0.44 mmol, 97%) was used as obtained in the next step without further purifications. MS (ESI+) m/z 159 (M + H).

General procedure for copper catalyzed click reaction (GP3) for compounds 3–11, 13, 16, 19a-n, 22, 26a-b, 31a-b, 34a-b, 40a-e, 50a-c: Under argon atmosphere the appropriate alkyne (1 eq.) was suspended in a 1:1 mixture of water and MeOH. Subsequently, DIPEA (2.0 eq.), copper sulfate hepta hydrate (0.5 eq.) and sodium ascorbate (0.5 eq.) were added. After addition of the corresponding azide (1.2 eq.) the mixture was stirred for 16 h at room temperature. After full conversion (LCMS control) the mixture was acidified with 1 M HCl and the product was precipitated. The solids were collected, washed with water, and dried under vacuum to obtain the crude product. The products were purified using preparative HPLC. The solvents used were water (containing 0.05% [v/v] FA) and MeCN (containing 0.05% [v/v] FA) (gradient elution, MeCN:H_2O 1:9 → 9:1). Compound **4** is presented as an example. 3-(1-(pyridin-3-yl)-1*H*-1,2,3-triazol-4-yl)benzoic acid (**4**): The triazole was synthesized according to **GP3** using 3-ethynylbenzoic acid (92 mg, 0.64 mmol) and 3-azidopyridine **2** (1.3 eq., 100 mg, 0.83 mmol) as starting materials. The crude was obtained as a white solid (110 mg,

0.41 mmol, 64%). Purification was done using preparative HPLC. ^{1}H NMR (500 MHz, DMSO-d_6) δ ppm 7.66 (br. s., 1 H) 7.68–7.79 (m, 1 H) 7.88–8.06 (m, 1 H) 8.19 (d, J = 7.63 Hz, 1 H) 8.41 (d, J = 8.24 Hz, 1 H) 8.53 (s., 1 H) 8.76 (s., 1 H) 9.25 (s., 1 H) 9.55 (s, 1 H) 13.23 (br. s., 1 H); ^{13}C NMR (126 MHz, DMSO-d_6) δ ppm 120.56, 124.96, 127.82, 129.40, 141.24, 146.80, 149.81, 167.30.

General procedure for Suzuki coupling (GP4) for compounds 24a-b, 29a-b, 35a-l: Under argon atmosphere the appropriate aryl halide 1 (eq.) was dissolved in water and 1,4-dioxane (1:1). Sodium carbonate (3 eq.), the corresponding boronic acid (1.2 eq.) and tetrakis (triphenylphosphine) palladium (0.1 eq.) were added. The reaction mixture was heated to 90 °C for 16 h. After full conversion (LCMS control) the mixture was cooled to room temperature and EtOAc and sat. aqueous $NaHCO_3$ solution were added. The mixture was extracted with EtOAc (3x), the combined organic layers were dried over sodium sulfate and concentrated under reduced pressure to obtain the crude. The purification was done using automated flash chromatography (cyclohexane/EtOAc 1:0 → 0:1). Compound **24a** is presented as an example. 2-(5-amino-4-methylpyridin-2-yl)phenol **(24a)**: The coupling was done according to **GP4** using 6-bromo-4-methylpyridin-3-amine **23** (130 mg, 0.69 mmol), (2-hydroxyphenyl)boronic acid (1.2 eq., 113 mg, 0.83 mmol), sodium carbonate (3 eq., 218 mg, 2.08 mmol) and tetrakis (triphenylphosphine) palladium (0.1 eq., 78 mg, 0.07 mmol) in 1,4-dioxan:water (1:1, 6 mL). **24b** was obtained as yellow solid (103 mg, 0.52 mmol, 75%). MS (ESI+) m/z 201 (M + H).

General procedure for hydrolysis of methyl ester (GP5) for compounds 36a-l: The appropriate methyl ester was dissolved in MeOH and aqueous 0.5 M NaOH solution (1:1). The mixture was stirred at room temperature for 16 h. After full conversion (LCMS control) the mixture was acidified with 1 M HCl and the product was precipitated. The solids were collected, washed with water, and dried under vacuum to obtain the crude product. The products were purified using preparative HPLC. Compound **36a** is presented as an example. 4-(1-(5-phenylpyridin-3-yl)-1*H*-1,2,3-triazol-4-yl) benzoic acid **(36a)**: The synthesis was done according to **GP5** using methyl 4-(1-(5-phenylpyridin-3-yl)-1*H*-1,2,3-triazol-4-yl)benzoate **35a** (20 mg, 0.06 mmol). The crude was obtained as a white solid (13 mg, 0.04 mmol, 66%). Purification was done using preparative HPLC.^{1}H NMR (500 MHz, DMSO-d_6) δ ppm 7.49–7.54 (m, 1 H) 7.56–7.61 (m, 2 H) 7.84–7.95 (m, 2 H) 8.02–8.16 (m, 4 H) 8.65 (t, J = 2.21 Hz, 1 H) 9.07 (d, J = 1.98 Hz, 1 H) 9.22 (d, J = 2.29 Hz, 1 H) 9.64 (s, 1 H); ^{13}C NMR (126 MHz, DMSO-d_6) δ ppm 121.41, 125.29, 125.57, 127.30, 128.97, 129.30, 130.22, 133.38, 133.97, 135.68, 136.49, 139.93, 146.65, 147.70, 167.01.

General procedure for Ullmann reaction (GP6) for compounds 38a-e: Under argon atmosphere 6-bromo-4-methylpyridin-3-amine (1 eq.) was dissolved in DMF and the appropriate phenol derivative (1.2 eq.), cesium carbonate (3 eq.) and CuI (0.05 eq.) were added. The mixture was stirred for 16 h at 130 °C. LCMS control indicated full conversion and the mixture was cooled to room temperature. EtOAc and sat. aqueous $NaHCO_3$ solution were added. The mixture was extracted with EtOAc (3x), the combined organic layers were dried over sodium sulfate and concentrated under reduced pressure to obtain the crude. Compound **38a** is presented as an example. 4-methyl-6-phenoxypyridin-3-amine **(38a)**: The aryl ether was synthesized according to **GP6** using 6-bromo-4-methylpyridin-3-amine **37** (100 mg, 0.53 mmol), phenol (1.2 eq., 0.60 mmol, 70 mg), cesium carbonate (3 eq., 1.61 mmol, 523 mg) and CuI (0.1 eq., 0.05 mmol, 9 mg) in DMF (3 mL). The product was purified using automated flash chromatography (DCM/MeOH 1:0 → 9:1). Yield: (30 mg, 0.15 mmol, 28%) MS (ESI+) m/z 201 (M + H).

Protein expression and purification: The expression and purification of His-tagged oligomerization-deficient LANA DNA binding domain (DBD; aa1008–1146) mutant and GST-tagged KSHV LANA C-terminal domain (CTD; aa934-1162) were described previously and the protocol was adopted [10,11].

Fluorescence Polarization (FP) assay: The FP assay was performed, analyzed and evaluated as described previously [11].

Electrophoretic mobility shift assay (EMSA): The EMSA was performed, analyzed and evaluated as described previously [11].

Saturation-Transfer Difference (STD) NMR: The STD experiments were recorded at 298 K on a Bruker Fourier spectrometer (500 MHz). The samples contained 10 μM (final concentration) His-tagged oligomerization-deficient LANA DBD (aa1008–1146) mutant and a final compound concentration of 500 μM. The control spectra were recorded under the same conditions containing the free compound to test for artifacts. The STD buffer for experiments consists of 10 mM HEPES, 150 mM NaCl, pH 7.4 in D_2O containing 10% [v/v] DMSO-d_6. The experiments were recorded with a carrier set at −1 ppm for the on-resonance and −40 ppm for the off-resonance irradiation. Selective protein saturation was carried out at 2 s by using a train of 50 ms Gauss-shaped pulses, each separated by a 1 ms delay.

Declaration of competing interest

The authors declare that they have no known competing financial interests or personal relationships that could have appeared to influence the work reported in this paper.

Acknowledgments

The authors acknowledge the financial support by the German Centre for Infection Research (DZIF) and the DFG Collaborative Research Centre 900, project C1.

Appendix A. Supplementary data

Supplementary data to this article can be found online at https://doi.org/10.1016/j.ejmech.2020.112525.

References

[1] M. Weidner-Glunde, G. Mariggiò, T.F. Schulz, Kaposi's sarcoma-associated herpesvirus latency-associated nuclear antigen: replicating and shielding viral DNA during viral persistence, J. Virol. 91 (2017), https://doi.org/10.1128/JVI.01083-16.

[2] L. Wang, B. Damania, Kaposi's sarcoma-associated herpesvirus confers a survival advantage to endothelial cells, Canc. Res. 68 (2008) 4640–4648, https://doi.org/10.1158/0008-5472.CAN-07-5988.

[3] P. Purushothaman, P. Dabral, N. Gupta, R. Sarkar, S.C. Verma, KSHV genome replication and maintenance, Front. Microbiol. 7 (2016) 54, https://doi.org/10.3389/fmicb.2016.00054.

[4] G. Mariggiò, S. Koch, G. Zhang, M. Weidner-Glunde, J. Rückert, S. Kati, S. Santag, T.F. Schulz, Kaposi Sarcoma Herpesvirus (KSHV) Latency-Associated Nuclear Antigen (LANA) recruits components of the MRN (Mre11-Rad50-NBS1) repair complex to modulate an innate immune signaling pathway and viral latency, PLoS Pathog. 13 (2017), e1006335, https://doi.org/10.1371/journal.ppat.1006335.

[5] D.H. Kedes, E. Operskalski, M. Busch, R. Kohn, J. Flood, D. Ganem, The seroepidemiology of human herpesvirus 8 (Kaposi's sarcoma-associated herpesvirus): distribution of infection in KS risk groups and evidence for sexual transmission, Nat. Med. 2 (1996) 918–924, https://doi.org/10.1038/nm0896-918.

[6] L. Yan, V. Majerciak, Z.-M. Zheng, K. Lan, Towards better understanding of KSHV life cycle: from transcription and posttranscriptional regulations to pathogenesis, Virol. Sin. 34 (2019) 135–161, https://doi.org/10.1007/s12250-019-00114-3.

[7] L. Rainbow, G.M. Platt, G.R. Simpson, R. Sarid, S.J. Gao, H. Stoiber, C.S. Herrington, P.S. Moore, T.F. Schulz, The 222- to 234-kilodalton latent nuclear protein (LNA) of Kaposi's sarcoma-associated herpesvirus (human herpesvirus 8) is encoded by orf73 and is a component of the latency-associated nuclear antigen, J. Virol. 71 (1997) 5915–5921.

[8] T. Uppal, S. Banerjee, Z. Sun, S.C. Verma, E.S. Robertson, KSHV LANA–the master regulator of KSHV latency, Viruses 6 (2014) 4961–4998, https://

doi.org/10.3390/v6124961.
[9] F. Juillard, M. Tan, S. Li, K.M. Kaye, Kaposi's sarcoma herpesvirus genome persistence, Front. Microbiol. 7 (2016) 1149, https://doi.org/10.3389/fmicb.2016.01149.
[10] J. Hellert, M. Weidner-Glunde, J. Krausze, U. Richter, H. Adler, R. Fedorov, M. Pietrek, J. Rückert, C. Ritter, T.F. Schulz, et al., A structural basis for BRD2/4-mediated host chromatin interaction and oligomer assembly of Kaposi sarcoma-associated herpesvirus and murine gammaherpesvirus LANA proteins, PLoS Pathog. 9 (2013), e1003640, https://doi.org/10.1371/journal.ppat.1003640.
[11] P. Kirsch, V. Jakob, K. Oberhausen, S.C. Stein, I. Cucarro, T.F. Schulz, M. Empting, Fragment-based discovery of a qualified hit targeting the latency-associated nuclear antigen of the oncogenic kaposi's sarcoma-associated herpesvirus/human herpesvirus 8, J. Med. Chem. 62 (2019) 3924–3939, https://doi.org/10.1021/acs.jmedchem.8b01827.
[12] K.R. Alkharsah, T.F. Schulz, A role for the internal repeat of the Kaposi's sarcoma-associated herpesvirus latent nuclear antigen in the persistence of an episomal viral genome, J. Virol. 86 (2012) 1883–1887, https://doi.org/10.1128/JVI.06029-11.
[13] A. de Leo, Z. Deng, O. Vladimirova, H.-S. Chen, J. Dheekollu, A. Calderon, K.A. Myers, J. Hayden, F. Keeney, B.B. Kaufer, et al., LANA oligomeric architecture is essential for KSHV nuclear body formation and viral genome maintenance during latency, PLoS Pathog. 15 (2019), e1007489, https://doi.org/10.1371/journal.ppat.1007489.
[14] R.K. Singh, Z.L. Lamplugh, F. Lang, Y. Yuan, P. Lieberman, J. You, E.S. Robertson, KSHV-encoded LANA protects the cellular replication machinery from hypoxia induced degradation, PLoS Pathog. 15 (2019), e1008025, https://doi.org/10.1371/journal.ppat.1008025.
[15] S.C. Verma, K. Lan, E. Robertson, Structure and function of latency-associated nuclear antigen, Curr. Top. Microbiol. Immunol. 312 (2007) 101–136.
[16] F. Wei, J. Gan, C. Wang, C. Zhu, Q. Cai, Cell cycle regulatory functions of the KSHV oncoprotein LANA, Front. Microbiol. 7 (2016) 334, https://doi.org/10.3389/fmicb.2016.00334.
[17] J. Hellert, M. Weidner-Glunde, J. Krausze, H. Lünsdorf, C. Ritter, T.F. Schulz, T. Lührs, The 3D structure of Kaposi sarcoma herpesvirus LANA C-terminal domain bound to DNA, Proc. Natl. Acad. Sci. U.S.A. 112 (2015) 6694–6699, https://doi.org/10.1073/pnas.1421804112.
[18] C. Parravicini, B. Chandran, M. Corbellino, E. Berti, M. Paulli, P.S. Moore, Y. Chang, Differential viral protein expression in Kaposi's sarcoma-associated herpesvirus-infected diseases : Kaposi's sarcoma, primary effusion lymphoma, and multicentric Castleman's disease, Am. J. Pathol. 156 (2000) 743–749.
[19] N. Coen, S. Duraffour, R. Snoeck, G. Andrei, KSHV targeted therapy: an update on inhibitors of viral lytic replication, Viruses 6 (2014) 4731–4759, https://doi.org/10.3390/v6114731.
[20] C. Hoffmann, M. Sabranski, S. Esser, HIV-associated kaposi's sarcoma, Oncol. Res. Treat. 40 (2017) 94–98, https://doi.org/10.1159/000455971.
[21] P. Kirsch, V. Jakob, W.A.M. Elgaher, C. Walt, K. Oberhausen, T.F. Schulz, M. Empting, Discovery of novel latency-associated nuclear antigen inhibitors as antiviral agents against kaposi's sarcoma-associated herpesvirus, ACS Chem. Biol. (2020), https://doi.org/10.1021/acschembio.9b00845.
[22] J. Cui, L'A. Hu, W. Shi, G. Cui, X. Zhang, Q.-W. Zhang, Design, synthesis and anti-platelet aggregation activity study of ginkgolide-1,2,3-triazole derivatives, Molecules 24 (2019), https://doi.org/10.3390/molecules24112156.
[23] D. Dou, G. He, Y. Li, Z. Lai, L. Wei, K.R. Alliston, G.H. Lushington, D.M. Eichhorn, W.C. Groutas, Utilization of the 1,2,3,5-thiatriazolidin-3-one 1,1-dioxide scaffold in the design of potential inhibitors of human neutrophil proteinase 3, Bioorg. Med. Chem. 18 (2010) 1093–1102, https://doi.org/10.1016/j.bmc.2009.12.057.
[24] Y. Liu, Q. Xiao, Y. Liu, Z. Li, Y. Qiu, G.-B. Zhou, Z.-J. Yao, S. Jiang, Biological evaluation of new mimetics of annonaceous acetogenins: alteration of right scaffold by click linkage with aromatic functionalities, Eur. J. Med. Chem. 78 (2014) 248–258, https://doi.org/10.1016/j.ejmech.2014.03.062.
[25] J. Hellert, J. Krausze, T.F. Schulz, T. Lührs, Crystallization, room-temperature X-ray diffraction and preliminary analysis of Kaposi's sarcoma herpesvirus LANA bound to DNA, Acta Crystallogr. F Struct. Biol. Commun. 70 (2014) 1570–1574, https://doi.org/10.1107/S2053230X14019906.

3.4 Chapter D: Phage Display

Title:

Restriction-Free Construction of a Phage-Presented Very Short Macrocyclic Peptide Library

Authors:

Valentin Jakob, Saskia Helmsing, Michael Hust, and Martin Empting

Bibliographic Data:

Genotype Phenotype Coupling,

Methods in Molecular Biology

Volume 2070, Pages 95-113,

Springer Nature 2020

DOI: 10.1007/978-1-4939-9853-1_6

Chapter 6

Restriction-Free Construction of a Phage-Presented Very Short Macrocyclic Peptide Library

Valentin Jakob, Saskia Helmsing, Michael Hust, and Martin Empting

Abstract

Phage display is a commonly used technology for the screening of large clonal libraries of proteins and peptides. The construction of peptide libraries containing very short sequences, however, poses certain problems for conventional restriction-based cloning procedures, which are rooted in the necessity to purify restricted library oligos. Herein, we present an alternative cloning method especially suitable for such very short sequences of about only 21 base pairs resulting in a 60 bp insert. The employed restriction-free hot fusion cloning strategy allows for facile library construction bypassing the need for purification of the small oligo. The library includes one well-defined disulfide bridge rendering the displayed macrocyclic peptide sequences as attractive scaffolds for novel active principles.

Key words Library construction, Hot fusion cloning, Restriction-free cloning, Macrocyclic oligopeptide phage display, Panning

1 Introduction

Recently, the use of macrocyclic peptides as pharmaceutical agents has regained scientific interest [1]. In general, these circular amino acid sequences are more rigid and stable than their linear counterparts [2]. This usually results in better pharmacokinetics and dynamics and, hence, renders them more suitable for the application in an organism [3]. However, larger peptides and medium-sized ones (>10 amino acids) intrinsically exceed the criteria posed by the Lipinski's rule of five for oral bioavailability by a huge extend [4]. Hence, it might be worthwhile investigating small macrocyclic peptide scaffolds at the borderline of the Lipinski's space or just slightly beyond. This requirement directly leads us to a peptide size of about five to seven amino acids resulting in a molecular weight of at least 303 g/mol (five glycines) to a maximum of 1321 g/mol (seven tryptophans). With the aim in mind to include a simple and straightforward macrocyclic motif, this sequence should include two cysteines in order to form a disulfide bond. This alters the

Stefan Zielonka and Simon Krah (eds.), *Genotype Phenotype Coupling: Methods and Protocols*, Methods in Molecular Biology, vol. 2070, https://doi.org/10.1007/978-1-4939-9853-1_6,

minimal and maximal molecular weights of the resulting macrocycles to 393 g/mol and 1153 g/mol, respectively. In our opinion, this provides a suitable range to probe the "near Lipinski's space" for novel peptide-based active agents.

Phage display is a very powerful method to identify target-binding peptides [5, 6] in general and disulfide-bridged macrocycles [7] in particular. A variety of libraries [8–10] and panning methods [8, 11, 12] has been described in literature. One particular difficulty we encountered in this context was the construction of a phage-presented peptide library based on a very short randomized DNA oligo. Particularly, the cloning of such a peptide library into the appropriate phagemid was challenging. Cloning of short (library) genes with less than 100 bp is rarely described in literature, and in general, it is not common to clone such small DNA fragments into a vector. Conventional cloning procedures make use of restriction and purification steps applied to both phagemid and randomized library oligo prior to ligation [13]. However, gene purification like PCR cleanup for small oligos is very difficult and results at best in low yields. The usage of special kits for the gene extraction out of agarose gels is often advised, but these are usually recommended only down to 40 bp. Another applicable method is PAGE purification, which can also be used for small DNA fragments [14]. In this case, the small oligo has to be extracted out of a polyacrylamide gel after electrophoresis and manual excision. This procedure is rather time-consuming, and large quantities of product will also get lost even if extraction was successful. Notably, a reasonable yield of purified randomized DNA oligo is required to ensure that the desired library is completely incorporated in the phagemid and presented on the phages in the end.

An efficient method to circumvent these problems represents restriction enzyme- and ligase-free hot fusion cloning [15]. It also avoids the necessity for cleanup steps as a whole. Given an adequate primer design, it allows the unlabored assembly of very short DNA fragments and cloning into a library phagemid of choice. With this method, we were able to reduce the oligo size of our library to only 60 bp, which contains the 21 bp relevant library sequence. This sequence encodes for a peptide library, which will be presented by the phage and contains five randomized amino acids (except cysteine) and two cysteines at fixed places, which can form a macrocycle under oxidative conditions. Hence, it includes the features of the envisioned very short macrocyclic peptide sequences described above, which we wanted to screen via phage display.

The protocol presented herein describes how to design and clone such a small peptide library into a phagemid with the usage of the hot fusion technology and how to optimize the number of positive library-containing clones. Importantly, previously reported methods of library packaging [16] and the phage panning [17] are compatible with this procedure of library construction.

2 Materials

Prepare all solutions using H_2O Milli-Q.

2.1 Amplification of the Library Oligomer

1. Lyophilized library oligomer.
2. dNTPs.
3. Forward and reverse primers (in this study HF_PhageLib_01_-for and HF_PhageLib_01_rev, Table 1).
4. Q5 HF DNA polymerase and 5 × Q5 reaction buffer (NEB).
5. PCR tubes.
6. Thermocycler.
7. Agarose.
8. TAE buffer 50× (instant).
9. Electrophoresis chamber.

2.2 Linearization of the Phagemid Over PCR

1. Phagemid (in this protocol pHAL30 [18]).
2. dNTPs.
3. Forward and reverse primers (in this study: HF_lin_-pHAL_01_for and HF_lin_pHAL_01_rev, Table 2).
4. Q5 HF DNA polymerase and 5 × Q5 reaction buffer (NEB).
5. PCR tubes.
6. Thermocycler.
7. Agarose.
8. TAE buffer 50× (instant).
9. Electrophoresis chamber.

Table 1
Primers for PCR amplification of the library oligomer: The overlapping part with the oligomer is written in capital letters

Oligonucleotide primer	Sequence 5′-3′
HF_PhageLib_01_for	ctgctggcagctcagccggcAGCTCAGCCGGCCATG
HF_PhageLib_01_rev	agatcagcttttgttcagaacctgccTGTTCAGAACCTGCGGCCG

Table 2
Primers for PCR linearization of the phagemid pHAL30

Oligonucleotide primer	Sequence 5′-3′
HF_lin_pHAL_01_for	gcaggttctgaacaaaagctgatct
HF_lin_pHAL_01_rev	gccggctgagctgccag

2.3 Hot Fusion Reaction

1. Amplified library.
2. Linearized phagemid (pHAL30).
3. 5× ISO buffer: 3 mL 1 M Tris–HCl pH 7.5, 150 µL 2 M $MgCl_2$, 240 µL 100 mM dNTP mix, 300 µL 1 M DTT, 1.5 g PEG-8000, 300 µL 100 mM NAD, up to 6 mL H_2O Milli-Q. Store in aliquots at −20 °C.
4. 2× hot fusion mix: 100 µL 5× ISO buffer, 0.8 µL 1:5 diluted 10 u/µL T5 exonuclease (NEB), 6.25 µL 2 u/µL Q5 HF polymerase (NEB), up to 250 µL H_2O Milli-Q. Store in aliquots at −20 °C.
5. Thermocycler.
6. PCR tubes.
7. Dialysis plates (Merck).
8. 8.5 cm petri dishes.
9. 10% (v/v) glycerol.

2.4 Transformation and Titration

1. Electrocompetent *E. coli* ER2738.
2. Desalted hot fusion product.
3. 0.1 cm electroporation cuvette.
4. Electroporator.
5. Recovery medium (Lucigen).
6. Thermomixer.
7. Centrifuge for 1.5 mL tubes.
8. 2× YT medium pH 7.0: 1.6% (w/v) tryptone, 1% (w/v) yeast extract, 0.5% (w/v) NaCl.
9. 2× YT-GAT agar: 2× YT medium, 100 mM glucose, 100 µg/mL ampicillin, 20 µg/mL tetracycline, 1.2% (w/v) agar-agar.
10. 8.5 cm petri dishes.
11. Polystyrene dish with lid (245 mm × 245 mm × 25 mm).
12. Single-use Drigalski spatulas.
13. Rocking shaker.
14. 50 mL falcon tubes.
15. Cryotubes.
16. Glycerin.
17. Liquid nitrogen.

2.5 Library Quality Control

1. Forward and reverse primers (in this study MHLacZ-Pro_f and MHgIII_r (Table 3)).
2. 2× DreamTaq™ Green PCR Master Mix (Thermo Fisher Scientific).

Table 3
Primers for library quality control and sequencing

Oligonucleotide primer	Sequence 5′-3′
MHLacZ-Pro_f	GGCTCGTATGTTGTGTGG
MHgIII_r	CTAAAGTTTTGTCGTCTTTCC

3. Thermocycler.
4. Agarose.
5. Electrophoresis chamber.

2.6 Library Packaging

1. 2× YT-GA: 2× YT medium, 100 mM glucose, 100 μg/mL ampicillin.
2. Shaker/incubator.
3. 50 mL Falcon tubes.
4. M13K07 helper phage (NEB).
5. Falcon centrifuge.
6. 2× YT: 1.6% (w/v) tryptone, 1% (w/v) yeast extract, 0.5% (w/v) NaCl.
7. 86% (v/v) glycerol.
8. 2 mL cryotubes.
9. Liquid nitrogen.
10. 2× YT-AK: 2× YT, 100 μg/mL ampicillin, 50 μg/mL kanamycin.
11. PEG/NaCl mix: 20% (w/v) PEG 6000, 2.5 M NaCl.
12. Phage dilution buffer: 10 mM Tris–HCl pH 7.5, 20 mM NaCl, 2 mM EDTA.
13. 0.45 μm filter.

2.7 Titration of the Amplified Library

1. 2× YT-T: 2× YT, 20 μg/mL tetracycline.
2. XL1-Blue MRF′ (Agilent Technologies).
3. Phage dilution buffer.
4. 2× YT-GA agar plates: 2× YT medium, 100 mM glucose, 100 μg/mL ampicillin, 1.2% (w/v) agar-agar.
5. Single-use Drigalski spatulas.

2.8 Coating of Microtiter Plate Wells, Panning, and Phage Titration

1. 96-Well ELISA plates.
2. PBS pH 7.4: 8.0 g NaCl, 0.2 g KCl, 1.44 g $Na_2HPO_4 \times 2H_2O$, 0.24 g KH_2PO_4 in 1 L.
3. Streptavidin 1 μg/μL in PBS.

4. Panning block: 1% (w/v) skim milk powder, 1% (w/v) BSA in PBST, prepare fresh.
5. PBST: PBS, 0.05% (v/v) Tween-20.
6. 2% (w/v) BSA in PBST.
7. Target protein (in this study: CsrA [19]).
8. TG1 cells (Lucigen).
9. 2× YT.
10. Shaker/incubator also for well plates.
11. Rocking shaker.
12. ELISA-plate washer (e.g., Tecan Hydroflex).
13. Trypsin 10 μg/mL in PBS.
14. 96-Well deep-well plate.
15. 10× GA: 1 M glucose, 1 mg/mL ampicillin.
16. M13K07 helper phage.
17. Centrifuge for well plates.
18. 2× YT-AK.
19. XL1-Blue MRF′.
20. 2× YT-GA agar plates.
21. Single-use Drigalski spatulas.

2.9 Gene Extraction and Sequencing

1. 2× YT-GA.
2. 2× YT-GA agar plates.
3. Incubator/shaker.
4. Plasmid miniprep kit.
5. Primer for sequencing, here MHLacZ-Pro_f (Table 3).

3 Methods

3.1 Design of the Peptide Library

1. Design the library oligomer in a way that there will be two cysteines in it (*see* Table 4).
2. Between these two cysteines, there should be two or three variable amino acids (three in this example). Before the first

Table 4
Sequence of the designed oligomer and the resulting peptide sequence

Designed oligonucleotide	AGCTCAGCCGGCCATGGCC**XXX TGT XXX XXX XXX TGT XXX**GCGGCCGCAGGTTCTGAACA
Resulting peptide	**X C X X X C X**

Restriction sites NcoI and NotI are underlined; the relevant library sequence is shown in bold

Table 5
Encoding possibilities for XXX (DNA codon) and resulting amino acid X (single letter code)

	XXX		X
Lys	AAA	5.26	**K**
Asn	AAC	5.26	**N**
Thr	ACT	5.26	**T**
Ile	ATC	5.26	**I**
Met	ATG	5.26	**M**
Gln	CAG	5.26	**Q**
His	CAC	5.26	**H**
Pro	CCG	5.26	**P**
Arg	CGT	5.26	**R**
Leu	CTG	5.26	**L**
Glu	GAA	5.26	**E**
Asp	GAT	5.26	**D**
Ala	GCA	5.26	**A**
Gly	GGT	5.26	**G**
Val	GTT	5.26	**V**
Tyr	TAC	5.26	**Y**
Ser	TCT	5.26	**S**
Cys	TGC	–	**C**
Trp	TGG	5.26	**W**
Phe	TTC	5.26	**F**
	Sum	99.94	

and after the second cysteine, there should be one variable amino acid. XXX can encode for every amino acid X except cysteine (Table 5) (*see* **Note 1**).

3. Before and after this peptide encoding sequence, there should be enough nucleotides for amplification.
4. Include the two restriction sites NcoI before and NotI after the essential library sequence (*see* **Note 2**).
5. Every translated amino acid X, there should have the same probability (*see* **Note 3**).
6. Ensure that the coding for XXX does not include the restriction sites (here: NcoI and NotI) so that these do not occur in the library coding sequence (*see* **Note 4**).

Table 6
PCR components for the oligomer amplification

Solution or component	Volume
5× Q5 reaction buffer	10 µL
dNTPs (10 mM)	4 × 1 µL
HF_PhageLib_01_for (10 µM)	2.5 µL
HF_PhageLib_01_rev (10 µM)	2.5 µL
Template (Library Oligo)	1 ng
Q5 HF DNA polymerase	0.5 µL
H_2O Milli-Q	Up to 50 µL

Table 7
PCR program for the library oligomer amplification

PCR step	Temperature	Duration
Initial denaturation	98 °C	30 s
Denaturation	98 °C	10 s
Annealing	72 °C (NEB calc.)	20 s
Elongation	72 °C	25 s/kbp
Final elongation	72 °C	2 min

3.2 Amplification of the Library Oligomer

1. Solve the lyophilized oligomer 100 µM in H_2O Milli-Q.
2. Design the two primers which allow the amplification of the sequence, and prepare it for the hot fusion reaction (*see* **Note 5**).
3. Amplify the library oligomer by means of a PCR using the designed library oligomer: like in Table 6, pipet 10 µL 5× reaction buffer, 1 µL of each dNTP with a concentration of 10 mM, 2.5 µL forward and 2.5 µL reverse primer (10 µM each) and about 1 ng of the solved library oligomer as template. Fill up to 49.5 µL with H_2O Milli-Q, add 0.5 µL Q5 HF DNA polymerase, and mix gently by pipetting up and down.
4. Run PCR in a thermocycler based on the program from Table 7. Use about 30 cycles of denaturation, annealing, and elongation. Calculate the annealing temperature with the help of the NEB calculator (*see* **Note 6**) and elongation time. For example, oligo: 3 s (25 s/kbp × 0.106 kbp).
5. Check the amplified PCR product via agarose gel electrophoresis, and quantify the product (*see* **Note 7**).

Table 8
PCR components for the phagemid linearization

Solution or component	Volume
5× Q5 reaction buffer	10 µL
dNTPs (10 mM each)	4 × 1 µL
HF_lin_pHAL_01_for (10 µM)	2.5 µL
HF_lin_pHAL_01_rev (10 µM)	2.5 µL
Template (pHAL30)	1 ng
Q5 HF DNA polymerase	0.5 µL
H_2O Milli-Q	Up to 50 µL

Table 9
PCR program for the phagemid linearization

PCR step	Temperature	Duration
Initial denaturation	98 °C	30 s
Denaturation	98 °C	10 s
Annealing	68 °C (NEB calc.)	25 s
Elongation	72 °C	25 s/kbp
Final elongation	72 °C	2 min

3.3 Linearization of the Phagemid Over PCR (See Note 8)

1. Design primers that create an overlap to the amplified library (Subheading 3.2).
2. Pipette the PCR reaction like in Table 8 (*see* **Note 9**).
3. Run PCR in a thermocycler based on the program from Table 9. Use about 30 cycles of denaturation, annealing, and elongation. Calculate the annealing temperature with the help of the NEB calculator and 25 s/kbp for the elongation step. For pHAL30, 2 min 5 s (30 s/kbp × 4175 kbp).
4. Check the PCR product via agarose gel electrophoresis (*see* **Note 10**).
5. Purify the PCR product over a PCR cleanup kit, elute with 30 µL H_2O Milli-Q
   pH 8–8.5, and determine the concentration with a Nanodrop (*see* **Note 16**).

3.4 Hot Fusion Reaction

1. Mix 10 µL 2× hot fusion mix with 0.06 pmol linearized phagemid (pHAL30) with 0.14 pmol amplified library oligomer, and fill up to 20 µL with H_2O Milli-Q (*see* **Note 11**).

2. Hot fusion reaction: Hold a temperature of 50 °C for 1 h in a thermocycler and then cool down to 20 °C within 5 min (0.1 °C/s).
3. Desalt the HF product for about 30 min via dialysis plates against 10% glycerol.

3.5 Transformation and Titration

Transformation and titration are based on Zantow et al. [16] (Subheading 3.5).

1. Thaw 25 µL *E. coli* ER2738 electrocompetent cells on ice. Add 5 µL of the desalted HF product. Transfer these 30 µL to a precooled 0.1 cm electroporation cuvette, and avoid air bubbles (*see* **Note 12**).
2. Perform electroporation for bacteria (1.8 kV; pulse ~3.5–4.5 ms). Immediately add 1 mL prewarmed (37 °C) recovery medium, and resuspend three times before transferring the mixture into a prewarmed (37 °C) Eppendorf tube.
3. Incubate at 37 °C for 1 h and 600 rpm.
4. Centrifuge the tubes for 5 min at 5000 × *g*.
5. Remove about 30 µL of the supernatant, and resuspend the pellet in the remaining medium (*see* **Note 13**).
6. Make a 1:100, 1:1000, and a 1:10,000 dilution in recovery medium with 10 µL of the suspension in a volume of 150 µL, and spread them out on 2× YT-GA 8.5 cm agar plates.
7. Plate the remaining 990 µL of the transformation onto a 245 × 245 × 25 mm 2× YT-GA agar plate.
8. Incubate all plates at 30 °C overnight (*see* **Note 14**).
9. Perform the colony counting on the 8.5 cm plates.
10. Add 20 mL of 2× YT to the 245 × 245 × 25 mm plate, and incubate on a rocking shaker for 20 min.
11. Carefully scrape the cells from the medium surface with a Drigalski spatula. Collect the liquid-containing cells with a serological pipette in a 50 mL tube, supplement with 20% (v/v) glycerol, and distribute 1 mL in each of 6 cryovials.
12. Flash freeze the cells in liquid nitrogen and store the tubes at −80 °C.

3.6 Library Quality Control

The library quality control is based on Zantow et al. [16] (Subheading 3.6).

1. Pick at least 12 colonies from the plate used for colony counting to perform a colony PCR with the help of the DreamTaq™ PCR mastermix polymerase (Table 10). Use the empty phagemid as a negative control (*see* **Note 15**).
2. Send positive clones for sequencing, to check whether the peptide library is cloned properly. Additionally, this provides a first hint at the diversity of the library (*see* **Note 16**).

Table 10
Composition of the colony PCR

Solution or component	Volume
2× DreamTaq™ mastermix	25 µL
MH_LacZ-Pro_f	1.5 µL
MHgIII_r	1.5 µL
H_2O Milli-Q	22 µL

3.7 Library Packaging

Library packaging is based on Zantow et al. [16] (Subheading 3.7).

1. Inoculate 400 mL 2× YT-GAT with a gently thawed 1 mL glycerol stock (Start OD600 < 0.1).
2. Incubate at 37 °C, 250 rpm until an OD600 of 0.4–0.5 is reached. Transfer 25 mL of this culture (1.25×10^{10} bacteria, OD600 of $1 = 1 \times 10^9$) in a 50 mL falcon tube, and infect with the M13K07 helper phage (MOI 1:20).
3. Incubate at 37 °C for 30 min without shaking and 30 min at 250 rpm.
4. Distribute the rest of the culture (375 mL) to eight falcons, centrifuge for 10 min at 3220 × *g*, discard the supernatant, and resuspend each pellet in 800 µL 2× YT.
5. For storage at this point, transfer the suspension into 2 mL cryotubes, add 200 µL 86% glycerol, shock freeze in liquid nitrogen, and store at −80 °C.
6. Pellet the bacteria at 3220 × *g* for 10 min, discard the supernatant, carefully resuspend the pellet in a little amount 2× YT, and take up in 400 mL 2× YT-AK. Incubate over night at 30 °C, 250 rpm.
7. Centrifuge the bacteria for 20 min at 10,000 × *g* at 4 °C in two containers. Transfer the supernatant in two new containers, and precipitate the phage by adding 1/5 volume ice-cold PEG/NaCl, mix it, and incubate on ice on a rocking shaker for 1 h.
8. Resuspend the two pellets in 10 mL phage dilution buffer.
9. Centrifuge for 10 min, 20,000 × *g* at 4 °C.
10. Filter the supernatant through 0.45 µm in two fresh centrifugation tubes.
11. Precipitate the phage by adding 1/5 volume ice-cold PEG/-NaCl, mix it, and incubate on ice on a shaker for 20 min.
12. Centrifuge for 30 min, 20,000 × *g* at 4 °C, and discard the supernatant.

13. Place the centrifuge tubes upside down on a paper towel (*see* **Note 17**).
14. Resuspend each pellet in 1 mL phage dilution buffer, and centrifuge for 1 min, 16,000 × *g* at 4 °C to remove the rest of the bacteria. Transfer the supernatant into an Eppendorf tube.

3.8 Titration of the Amplified Library

Titration of the amplified library is based on Zantow et al. [16] (Subheading 3.7).

1. Inoculate 5 mL 2× YT-T with XL1-Blue MRF′ cells, and incubate over night at 37 °C, 200 rpm.
2. On the next day, inoculate 50 mL 2× YT-T with 500 µL overnight, culture, and grow to an OD600 of 0.5 (~5×10^8 bacteria/mL).
3. Make a 10^{-2}, 10^{-4}, 10^{-6}, 10^{-8}, 10^{-10}, and 10^{-12} dilution of this culture by mixing 990 µL phage dilution buffer with 10 µL phage solution.
4. Add 10 µL of this dilutions to 50 µL ready-grown XL1-Blue MRF′ cells.
5. Incubate for 30 min at 37 °C without shaking.
6. Streak out each dilution containing the XL1-Blue MRF′ on 2× TY-GA agar plates, and incubate at 37 °C overnight (*see* **Note 18**).
7. Determine the titer in pfu/mL by counting the colonies.
8. Pick at least 12 colonies by performing a colony PCR.
9. Save the plates to perform a DNA extraction for Subheading 3.11.

3.9 Panning Procedure for a Biotinylated Protein

The panning procedure is based on Russo et al. [17] (Subheading 3.1).

Day 1:

1. Coating: Prepare a solution of 998 µL PBS + 2 µL 1 µg/µL streptavidin in PBS (2 µg), and fill up two ELISA wells with this mixture (*see* **Note 19**). Fill up the third ELISA well with panning block (fresh). Incubate for 2 h at 4 °C without shaking.
2. Blocking: Empty the first two ELISA wells, wash three times with PBST, and fill up the wells with 2% BSA (fresh) in PBST. Incubate for 2 h at 4 °C without shaking.
3. Adding target (protein): Empty the first two ELISA wells and wash three times with PBST. Add 4 µg in 150 µL of the protein in his storage buffer in the first well (*see* **Notes 20** and **21**). Fill up the second well with PBS. Incubate over night at 4 °C without shaking.

4. TG1 culture: Inoculate 15 mL 2× YT with TG1 cells. Incubate o/n at 200 rpm and 37 °C.

Day 2:

1. Adding phage: Empty the third well of the ELISA plate, and add a mixture of 75 µL of the amplified library (normally about 5×10^{11} pfu/mL) + 70 µL panning block + 5 µL 1 µg/µL (5 µg) streptavidin in PBS to this well. Incubate for 1 h at room temperature on a shaker.
2. Transferring phage I: Empty the second well and wash three times with PBST. Transfer the 150 µL phage solution from the third well into the empty second well. Incubate for 1 h at room temperature on a shaker.
3. Transferring phage II: Empty the first well and wash three times with PBST. Transfer the 150 µL phage solution from the second well into the empty first well. Incubate for 1.5–2 h at room temperature on a shaker.
4. Washing step: Empty the first well and wash ten times with PBST with a plate washer.
5. Phage elution: Add 150 µL (10 µg/mL in PBS) trypsin to the empty first well. Incubate for 30 min at 37 °C without shaking.
6. Transfer the 150 µL eluted phage into a well of a 96-well deep-well plate (*see* **Note 22**).
7. Grow a TG1 culture (by inoculating with the o/n culture) to an OD600 of 0.5 (can be done earlier and stored on ice at this OD till the next step).
8. Add 150 µL ready-grown TG1 cells (OD600 = 0.5) to the deep well containing the eluted phage. Incubate 30 min at 37 °C without shaking and 30 min at 37 °C with 450–650 rpm (*see* **Note 23**).
9. Coating: Choose three new ELISA wells. Prepare a solution of 998 µL PBS + 2 µL 1 µg/µL streptavidin in PBS (2 µg), and fill up two ELISA wells with this mixture (*see* **Note 19**). Fill up a third ELISA well with panning block (fresh). Incubate for 1 h at room temperature without shaking.
10. Blocking: Empty the first two ELISA wells, wash three times with PBST, and fill up the wells with 2% BSA (fresh) in PBST. Incubate for 1 h at room temperature without shaking.
11. Adding target (protein): Empty the first two ELISA wells and wash three times with PBST. Add 4 µg in 150 µL of the protein in his storage buffer in the first well (*see* **Notes 20** and **21**). Fill up the second well with PBS. Incubate over night at 4 °C without shaking.

12. Add 1 mL 2× YT + 150 µL 10× GA to the deep well containing 300 µL eluted phage in 2× YT. Incubate for 1 h at 37 °C and 450–650 rpm.
13. Add 10^{11} pfu M13K07 helper phage to the deep well. Incubate for 30 min at 37 °C without shaking and 30 min at 37 °C, 450–650 rpm.
14. Centrifuge the deep-well plate for 10 min, 3220 × *g* at room temperature. Discard the supernatant carefully.
15. Resuspend the pellet in 950 µL 2× YT-AK. Incubate o/n at 30 °C and 450–650 rpm.
16. TG1-culture: Inoculate 15 mL 2× YT with TG1 cells. Incubate o/n at 200 rpm and 37 °C.

Day 3:

1. Centrifuge the deep-well plate for 10 min, 3220 × *g* at room temperature. Transfer the supernatant in the neighbored deep well and resuspend for a few times.
2. Adding phage: Empty the third well of the ELISA plate, and add a mixture of 95 µL panning block + 5 µL 1 µg/µL (5 µg) streptavidin in PBS + 50 µL amplified phage from the deep well (**step 1**) to this well. Incubate for 1 h at room temperature on a shaker.
3. Transferring phage I: Empty the second well and wash three times with PBST. Transfer the 150 µL phage solution from the third well into the empty second well. Incubate for 1 h at room temperature on a shaker.
4. Transferring phage II: Empty the first well and wash three times with PBST. Transfer the 150 µL phage solution from the second well into the empty first well. Incubate for 1.5–2 h at room temperature on a shaker.
5. Washing step: Empty the first well and wash 20 times with PBST with a plate washer.
6. Phage elution: Add 150 µL (10 µg/mL in PBS) trypsin to the empty first well. Incubate for 30 min at 37 °C without shaking.
7. Transfer the 150 µL eluted phage into a 96-well deep-well plate (*see* **Note 22**).
8. Grow a TG1 culture (by inoculating with the o/n culture) to an OD600 of 0.5 (can be done earlier and stored on ice at this OD till the next step).
9. Add 150 µL ready-grown TG1 cells (OD600 = 0.5) to the deep well containing the eluted phage. Incubate for 30 min at 37 °C without shaking and 30 min at 37 °C with 450–650 rpm (*see* **Note 23**).

10. Coating: Choose three new ELISA wells. Prepare a solution of 998 µL PBS + 2 µL 1 µg/µL streptavidin in PBS (2 µg), and fill up two ELISA wells with this mixture (*see* **Note 19**). Fill up a third ELISA well with panning block (fresh). Incubate for 1 h at room temperature without shaking.
11. Blocking: Empty the first two ELISA wells, wash three times with PBST, and fill up the wells with 2% BSA (fresh) in PBST. Incubate for 1 h at room temperature without shaking.
12. Adding target (protein): Empty the first two ELISA wells and wash three times with PBST. Add 4 µg in 150 µL of the protein in its storage buffer in the first well (*see* **Notes 20** and **21**). Fill up the second well with PBS. Incubate over night at 4 °C without shaking.
13. Add 1 mL 2× YT + 150 µL 10× GA to the deep well containing 300 µL eluted phage in 2× YT. Incubate for 1 h at 37 °C and 450–650 rpm.
14. Add 10^{11} pfu M13K07 helper phage to the deep well. Incubate for 30 min at 37 °C without shaking and 30 min at 37 °C, 450–650 rpm.
15. Centrifuge the deep well plate for 10 min, 3220 rpm at room temperature. Discard the supernatant carefully.
16. Resuspend the pellet in 950 µL 2× YT-AK. Incubate o/n at 30 °C and 450–650 rpm.

Day 4:

1. Centrifuge the deep-well plate for 10 min, 3220 × *g* at room temperature. Transfer the supernatant in the neighbored deep well and resuspend for a few times.
2. Adding phage: Empty the third well of the ELISA plate, and add a mixture of 95 µL panning block + 5 µL 1 µg/µL (5 µg) streptavidin in PBS + 50 µL amplified phage from the deep well (**step 1**) to this well. Incubate for 1 h at room temperature on a shaker.
3. Transferring phage I: Empty the second well and wash three times with PBST. Transfer the 150 µL phage solution from the third well into the empty second well. Incubate for 1 h at room temperature on a shaker.
4. Transferring phage II: Empty the first well and wash three times with PBST. Transfer the 150 µL phage solution from the second well into the empty first well. Incubate for 1.5–2 h at room temperature on a shaker.
5. Washing step: Empty the first well and wash ten times with PBST with a plate washer.

6. Phage elution: Add 150 µL (10 µg/mL in PBS) trypsin to the empty first well. Incubate for 30 min at 37 °C without shaking.
7. Save the sample with the eluted phage for titration and further steps.

3.10 Phage Titration

The phage titration is based on Russo et al. [17] (Subheading 3.3).

1. Inoculate 30 mL 2× YT-T in a 100 mL with XL1-Blue MRF′ and grow overnight at 37 °C and 250 rpm.
2. Inoculate 50 mL 2× YT-T with 500 µL overnight culture and grow at 250 rpm and 37 °C up to OD600 = 0.5.
3. Make serial dilutions of the phage suspension in PBS.
4. Infect 50 µL bacteria with 10 µL phage dilution and incubate for 30 min at 37 °C (*see* **Note 24**).
5. Plate the 60 µL infected bacteria on 2× YT-GA agar plates (8.5 cm petri dishes).
6. Incubate the plates overnight at 37 °C.
7. Count the colonies and calculate the cfu/mL titer according to the dilution.

3.11 Gene Extraction and Sequencing

1. Inoculate up to 50 cultures of 15 mL 2× YT-GA with colonies from the titration plate from the third panning round and up to 50 cultures of 15 mL 2× YT-GA with colonies from Subheading 3.8 (packed library before panning).
2. Inoculate all cultures at 37 °C, 200 rpm overnight.
3. Extract the DNA from each culture using a DNA miniprep kit.
4. Use the MHLacZ-Pro_f primer for sequencing each DNA.
5. Compare the peptide encoding sequences before the panning with the sequences after the third panning round.
6. Determine the enrichment of peptide sequences from the sequencing result after the third panning round (*see* **Note 25**).

4 Notes

1. 19 canonical amino acids without cysteine at 5 different positions result in about 2.5×10^6 variants in the library.
2. These two restriction sites are only for the case if you want to use restriction cloning. They will not be used for the hot fusion cloning. When using the restriction sites, only 30 bp will be left. This will probably cause problems for performing a purification step.

3. The oligomer was synthesized by ELLA Biotech GmbH, which is specialized on the synthesis of randomized oligonucleotides using trinucleotides.
4. This is only necessary if you plan to do a restriction cloning instead of a hot fusion.
5. We recommend using a program like SnapGene to make the design of primers for hot fusion much easier. If the program has no function for hot fusion, it is possible to use the Gibson assembly function for the design.
6. 72 °C is the maximum from NEB Tm-calculator, and in our case, due to the primer design, the Tm-difference between the two primers is greater than the recommended limit of 5 °C (here: 7 °C difference).
7. We recommend using a low-molecular-weight ladder-like N3233S from NEB. The PCR product does not need to be further purified for the hot fusion reaction. The purification of such small genes (in this case about 100 bp) will result in an insufficient recovery. This is also a reason to decide for hot fusion than restriction cloning, because further purification is not necessary.
8. It is also possible to linearize the phagemid via restriction enzymes, for pHAL30 with NcoI and NotI. In addition to these two enzymes, HindIII and MluI can be used to make the restriction-digested DNA fragment smaller. Unfortunately, the efficiency of this procedure was not high in our case, and it seemed that restriction was not quantitative, because in a hot fusion reaction, the library oligomer with the restriction-linearized pHAL30 often was less than 10% positive clones.
9. It is important to have a nearly quantitative linearization of the phagemid, so less than 1 ng of template will be even better.
10. It is possible that more than one band will occur on the gel (three bands in our case), but if the strongest band is the desired product, it will work nevertheless.
11. Sometimes it is necessary to try different ratios to achieve a successful hot fusion reaction. Consider doing more than one of those reactions in parallel. Combining several reactions after transformation will result in a higher propensity to get library-containing clones.
12. Consider doing more than one transformation in parallel. It will be effective to combine the reactions after transformation. Keep also in mind that the transformation efficiency can vary.
13. If using more than one transformation sample, this will be the point to combine these. Be sure to have in total a volume of about 1 mL remaining media in the supernatant, because this will be the ideal volume to streak out on the plates.

14. We recommend incubating at 30 °C instead of 37 °C because the ER2738 is growing very fast.
15. Typical rates are about 9/12 (75%) up to 11/12 (92%) positive clones.
16. Due to the lengths of the pHAL30 (>4000 bp), the linearization via PCR even with the Q5 HF polymerase can cause several point mutations in the backbone of the pHAL30. However, in most cases, this will have no effect on the presented peptide and the functionality of the phage presenting it.
17. The PEG/NaCl solution should be completely removed.
18. It is not necessary to add tetracycline to the culture/plates even though the MRF′ has a tetracycline resistance.
19. For non-biotinylated proteins, see also the instructions from Subheading 3.1 (Russo et al. [17]).
20. When using biotinylated proteins, it does not matter, if there is DTT or glycerol in the buffer. For non-biotinylated proteins, it is necessary to remove such components from the buffer.
21. The needed amount depends on the protein. If you can estimate how well your protein immobilizes, it will be possible to adjust the amount for every panning round.
22. Collect 10 μL of the eluted phage after each panning round for titration and further steps.
23. If you do not have a plate shaker/incubator, use a conventional shaker/incubator with a plate holder at maximum speed, i.e., the Thermo MaxQ 4000, and use 400–500 rpm.
24. Make the titration for every stock of the collected eluted phage from each panning round. Using droplets of just PBS with XL1-Blue MRF′ and droplets of just XL1-Blue MRF′ as a negative control on a separate plate is recommended. This will show if the PBS and the XL1-Blue MRF′ are contamination-free. XL1-Blue MRF′ is used for titration and for following single-clone analysis, because the phagemid is more stable in these bacteria compared to TG1.
25. The more frequently a sequence occurs, the higher is the probability that this is a desired binder for the used target protein.

Acknowledgments

This review contains updated and revised parts of former protocols by Zantow et al. [16] and Russo et al. [17]. We thank Rolf W. Hartmann for his continuous support.

References

1. Craik DJ, Lee M-H, Rehm FBH et al (2018) Ribosomally-synthesised cyclic peptides from plants as drug leads and pharmaceutical scaffolds. Bioorg Med Chem 26(10):2727–2737. https://doi.org/10.1016/j.bmc.2017.08.005
2. Bogdanowich-Knipp SJ, Chakrabarti S, Siahaan TJ et al (1999) Solution stability of linear vs. cyclic RGD peptides. J Pept Res 53 (5):530–541. https://doi.org/10.1034/j.1399-3011.1999.00052.x
3. Diao L, Meibohm B (2013) Pharmacokinetics and pharmacokinetic-pharmacodynamic correlations of therapeutic peptides. Clin Pharmacokinet 52(10):855–868. https://doi.org/10.1007/s40262-013-0079-0
4. Lipinski CA (2004) Lead- and drug-like compounds: the rule-of-five revolution. Drug Discov Today Technol 1(4):337–341. https://doi.org/10.1016/j.ddtec.2004.11.007
5. Brown T, Brown N, Stollar EJ (2018) Most yeast SH3 domains bind peptide targets with high intrinsic specificity. PLoS One 13(2): e0193128. https://doi.org/10.1371/journal.pone.0193128
6. Sidhu SS, Lowman HB, Cunningham BC et al (2000) [21] Phage display for selection of novel binding peptides. In: Applications of chimeric genes and hybrid proteins—part C: protein-protein interactions and genomics, vol 328. Elsevier, Amsterdam, pp 333–IN5
7. Sakamoto K, Sogabe S, Kamada Y et al (2017) Discovery of high-affinity BCL6-binding peptide and its structure-activity relationship. Biochem Biophys Res Commun 482(2):310–316. https://doi.org/10.1016/j.bbrc.2016.11.060
8. Rentero Rebollo I, Heinis C (2013) Phage selection of bicyclic peptides. Methods 60 (1):46–54. https://doi.org/10.1016/j.ymeth.2012.12.008
9. Diderich P, Heinis C (2014) Phage selection of bicyclic peptides binding Her2. Tetrahedron 70(42):7733–7739. https://doi.org/10.1016/j.tet.2014.05.106
10. Ryvkin A, Ashkenazy H, Weiss-Ottolenghi Y et al (2018) Phage display peptide libraries: deviations from randomness and correctives. Nucleic Acids Res 46(9):e52. https://doi.org/10.1093/nar/gky077
11. Watters JM, Telleman P, Junghans RP (1997) An optimized method for cell-based phage display panning. Immunotechnology 3(1):21–29. https://doi.org/10.1016/S1380-2933(96)00056-5
12. Nguyen X-H, Trinh T-L, Vu T-B-H et al (2018) Isolation of phage-display library-derived scFv antibody specific to *Listeria monocytogenes* by a novel immobilized method. J Appl Microbiol 124(2):591–597. https://doi.org/10.1111/jam.13648
13. Hust M, Meyer T, Voedisch B et al (2011) A human scFv antibody generation pipeline for proteome research. J Biotechnol 152 (4):159–170. https://doi.org/10.1016/j.jbiotec.2010.09.945
14. Dretzen G, Bellard M, Sassone-Corsi P et al (1981) A reliable method for the recovery of DNA fragments from agarose and acrylamide gels. Anal Biochem 112(2):295–298. https://doi.org/10.1016/0003-2697(81)90296-7
15. Fu C, Donovan WP, Shikapwashya-Hasser O et al (2014) Hot Fusion: an efficient method to clone multiple DNA fragments as well as inverted repeats without ligase. PLoS One 9 (12):e115318. https://doi.org/10.1371/journal.pone.0115318
16. Zantow J, Moreira GMSG, Dübel S et al (2018) ORFeome phage display. Methods Mol Biol 1701:477–495. https://doi.org/10.1007/978-1-4939-7447-4_27
17. Russo G, Meier D, Helmsing S et al (2018) Parallelized antibody selection in microtiter plates. Methods Mol Biol 1701:273–284. https://doi.org/10.1007/978-1-4939-7447-4_14
18. Frenzel A, Schirrmann T, Hust M (2016) Phage display-derived human antibodies in clinical development and therapy. MAbs 8 (7):1177–1194. https://doi.org/10.1080/19420862.2016.1212149
19. Maurer CK, Fruth M, Empting M et al (2016) Discovery of the first small-molecule CsrA-RNA interaction inhibitors using biophysical screening technologies. Future Med Chem 8 (9):931–947. https://doi.org/10.4155/fmc-2016-0033

3.5 Chapter E: Protein-RNA Interactions

Title:

Phage Display-based Discovery of Cyclic Peptides against the Broad Spectrum Bacterial Anti-Virulence Target CsrA.

Authors:

Valentin Jakob, Ben G. E. Zoller, Julia Rinkes, Yingwen Wu, Alexander F. Kiefer, Michael Hust, Saskia Helmsing, Andrew M. White, Peta J. Harvey, Thomas Durek, David J. Craik, Andreas Siebert, Uli Kazmaier and Martin Empting

Bibliographic Data:

This part has been submitted to *Angew. Chem. Int. Ed*. on April, 8th 2021.

Graphical Abstract:

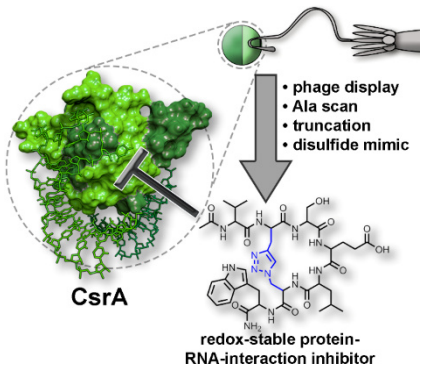

Size matters: Inhibition of protein-nucleic acid interactions can require the use of extended structural space with MW > 500 Da. Here, we identified a redox-stable ultrashort macrocyclic peptide containing a disulfide mimic. The parent disulfide-bridged peptide was selected by phage display against the attractive antiinfective target CsrA.

WILEY-VCH

COMMUNICATION

Phage Display-based Discovery of Cyclic Peptides against the Broad Spectrum Bacterial Anti-Virulence Target CsrA.

Valentin Jakob,[a,†] Ben G. E. Zoller,[a,†] Julia Rinkes,[a] Yingwen Wu,[a] Alexander F. Kiefer,[a] Michael Hust,[b]Saskia Helmsing,[b] Andrew M. White,[c] Peta J. Harvey,[c] Thomas Durek,[c] David J. Craik,[c] Andreas Siebert,[d] Uli Kazmaier[d] and Martin Empting*

[*] Dr. M. Empting
Department of Drug Design and Optimization (DDOP)
Helmholtz-Institute for Pharmaceutical Research Saarland (HIPS) - Helmholtz Centre for Infection Research (HZI)
Campus E8.1, 66123 Saarbrücken, Germany
E-mail: martin.empting@helmholtz-hips.de

[a] V. Jakob,[†] B. G. E. Zoller,[†] J. Rinkes, Y. Wu, Dr. A. F. Kiefer
Department of Drug Design and Optimization (DDOP)
Helmholtz-Institute for Pharmaceutical Research Saarland (HIPS) - Helmholtz Centre for Infection Research (HZI)
Campus E8.1, 66123 Saarbrücken, Germany
Department of Pharmacy
Saarland University
Campus E8.1, 66123 Saarbrücken, Germany

[b] Prof. Dr. M. Hust, S. Helmsing
Abteilung Biotechnologie
Technische Universität Braunschweig, Institut für Biochemie, Biotechnologie und Bioinformatik
Spielmannstr. 7, 38106 Braunschweig, Germany

[c] Dr. A. M. White, Dr. Peta J. Harvey, Dr. T. Durek, Prof. D. J. Craik
ARC Centre of Excellence for Innovations in Peptide and Protein Science
Institute for Molecular Bioscience
The University of Queensland, Brisbane, QLD, 4072, Australia
E-mail: t.durek@uq.edu.au
d.craik@imb.uq.edu.au

[d] A. Siebert, Prof. Dr. U. Kazmaier
Institut für Organische Chemie
Saarland University
Campus C4.2, 66123 Saarbrücken, Germany

[†] These authors contributed equally to this work.

Supporting information for this article is given via a link at the end of the document.

Abstract: Small macrocyclic peptides are promising candidates for new anti-infective drugs. To date, such peptides have been poorly studied in the context of anti-virulence targets. Using phage display and a self-designed peptide library, we identified a cyclic heptapeptide that can bind the carbon storage regulator A (CsrA) from *Yersinia pseudotuberculosis* and displace bound RNA. The initial disulfide-bridged peptide, showed an IC_{50} value in the low micromolar range. Upon further characterization, cyclization was found to be essential for its activity. To increase metabolic stability, a series of disulfide mimetics were designed and a redox-stable 1,4-disubstituted 1,2,3-triazole analogue displayed activity in the double-digit micromolar range. Further experiments revealed that this triazole peptidomimetic is also active against CsrA from *Escherichia coli*. This study is an ideal starting point for medicinal chemistry optimization of this macrocyclic peptide and might pave the way towards broad-acting virulence modulators.

WILEY-VCH

COMMUNICATION

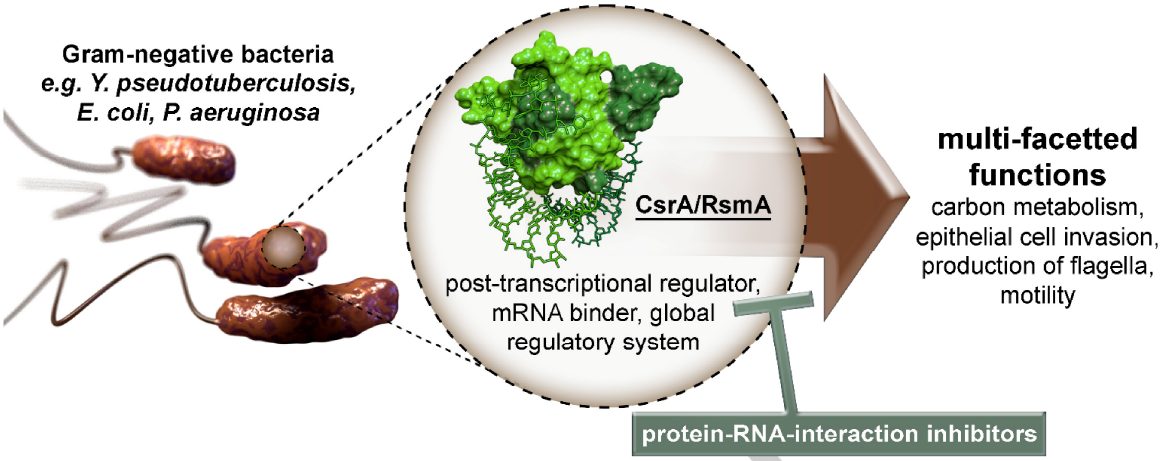

Figure 1. CsrA/RsmA as a promising drug target for multi-pathogen virulence modulation by disruption of an essential protein-RNA interaction.

For years, researchers have warned about the antimicrobial resistance (AMR) crisis.[1] The rampant spread of multi-drug resistant bacterial pathogens combined with the lack of novel treatment options, especially against Gram-negative species, poses a great threat for our modern healthcare systems.[2] For this reason, the discovery of new anti-infective candidates with novel and innovative mechanisms-of-action will be needed. We consider the carbon storage regulator A (CsrA; in some species also called the regulator of secondary metabolites, RsmA)[3] as an attractive, yet underexplored, virulence-modulating target.[4] It is widespread in Gram-negative pathogens[5] where its sequence and function is highly conserved.[6] Knock-out studies in *Pseudomonas aeruginosa*, *Yersinia pseudotuberculosis* and *Helicobacter pylori*[7] have demonstrated its critical role in bacterial virulence and highlighted its potential as a therapeutic target.[8] The CsrA/RsmA protein is a post-transcriptional regulator[9], that binds and regulates translation of mRNA and, thus exerts pleiotropic effects on the bacterial transcriptome (Figure 1).[10] Through its mRNA binding activity it is involved in the regulation of quorum sensing,[11] motility,[12] carbon metabolism,[13] peptide uptake *via* cstA[14] and biofilm development.[15] To disrupt the function of CsrA/RsmA at the molecular level, protein-RNA interaction inhibitors need to be devised. CsrA usually occurs as a homodimer,[16] with two identical RNA-binding sites.[17]

In a previous study using *Yersinia* CsrA and a short piece of RNA that contained the important core binding motif GGA, it was shown that this RNA can be displaced by small molecules.[7,18] In the present work, we sought to find novel lead molecules within the extended Lipinski space (MW between 500 and 1000 Da).[19,20] These molecules should provide a suitable basis for disrupting macromolecule-macromolecule interactions while still retaining the potential for membrane permeability and oral bioavailability.[20,21] To this end, we devised a strategy to screen a library of disulfide-constrained heptapeptides covering a mass range between 548 – 1193 Da via phage display (Scheme 1).[22] The use of phage-encoded libraries displaying millions of compound variants[23] has proven to be an excellent method for finding novel binders for several targets.[24] An important example is the search for small antibody fragments, so called single-chain variable fragments (scFvs) for any desired target.[25] Phage display can also be transferred to libraries encoding for short peptides.[24,26] This method allows screening of whole peptide libraries for one target to find potential binders.[27]

Our self-designed phage library encodes for a peptide library with the general structure XCXXXCX ($2.48 \cdot 10^6$ variants).[22] It contains two cysteines at fixed positions, which form a disulfide bond under oxidative conditions; X encodes for any amino acid except cysteine. We screened this library against immobilized *Yersinia* CsrA (biotinylated and His-tagged CsrA construct CsrA_biot_His_6; more details on phage display and CsrA expression can be seen in Supporting Information and a published protocol)[22] bound to a streptavidin-coated ELISA well. After three rounds of panning, phage binding with high affinity were separated on agar plates. After sequencing of 32 clones, we identified one sequence as a potential CsrA binder. The criteria for selection were intact sequences and avoidance of a high tryptophan content (more than two Trp), which usually leads to unspecific binding.[28] Noteably, the selected sequence contained a glutamic acid residue - a feature we deemed plausible as anionic carboxyl groups should be of benefit for binding the positively charged surface of CsrA possessing a high content of basic amino acids.

This peptide hit (**1**) was synthesized by solid phase peptide synthesis (SPPS) in disulfide-cyclized, *N*-terminally acetylated and *C*-terminally amidated forms. These modifications were chosen because the sequence is presented within a peptide backbone extending beyond its *N*- and *C*-termini on the phage during the panning experiment. The peptide was characterized by LC-MS, HRMS and NMR (Supporting Information). Using an established fluorescence polarization assay[7] (Supporting Information), peptide **1** was tested for its ability to displace mRNA from CsrA. In this assay a fluorescein (flc)-labeled RNA (5'-UUCACGGAGAA[flc]) and CsrA_biot_His_6 were used to probe the protein-RNA interaction. The labeled RNA was successfully displaced by peptide **1** with an IC_{50} value in the micromolar range (6.9 ± 1.3 µM, Figure 2). This peptide is one of the most potent compounds discovered against CsrA to date and is readily synthetically accessible. Previously identified natural products such as MM14 and tubulysin Ar-672, have shown similar potency

(4 ± 1 µM and 11 ± 1 µM, respectively),[7] but are much more challenging to synthesize.

When the assay was conducted in the presence of 5 mM DTT, peptide **1** lost its activity almost completely. Under these conditions the disulfide bond is reduced and the macrocycle linearized. Thus, we concluded that the conformational constraint induced by the disulfide bond is essential for activity. This observation also supports a conformation-specific (structure-dependent) interaction between the peptide and CsrA. Additionally, a microscale thermophoresis (MST) assay was performed with peptide **1** and CsrA_biot_His_6 yielding a K_d of 10.5 ± 1.4 µM (Supporting Information). This assay further supports a direct specific interaction between the peptide and CsrA.

To gain further insights into the underlying structure-activity relationships (SAR) of peptide **1** we synthesized an array of derivatives by Fmoc-SPPS, oxidized them with DMSO and tested for inhibitory activity in the fluorescence polarization assay. The resultant IC_{50} values are listed in Table 1.

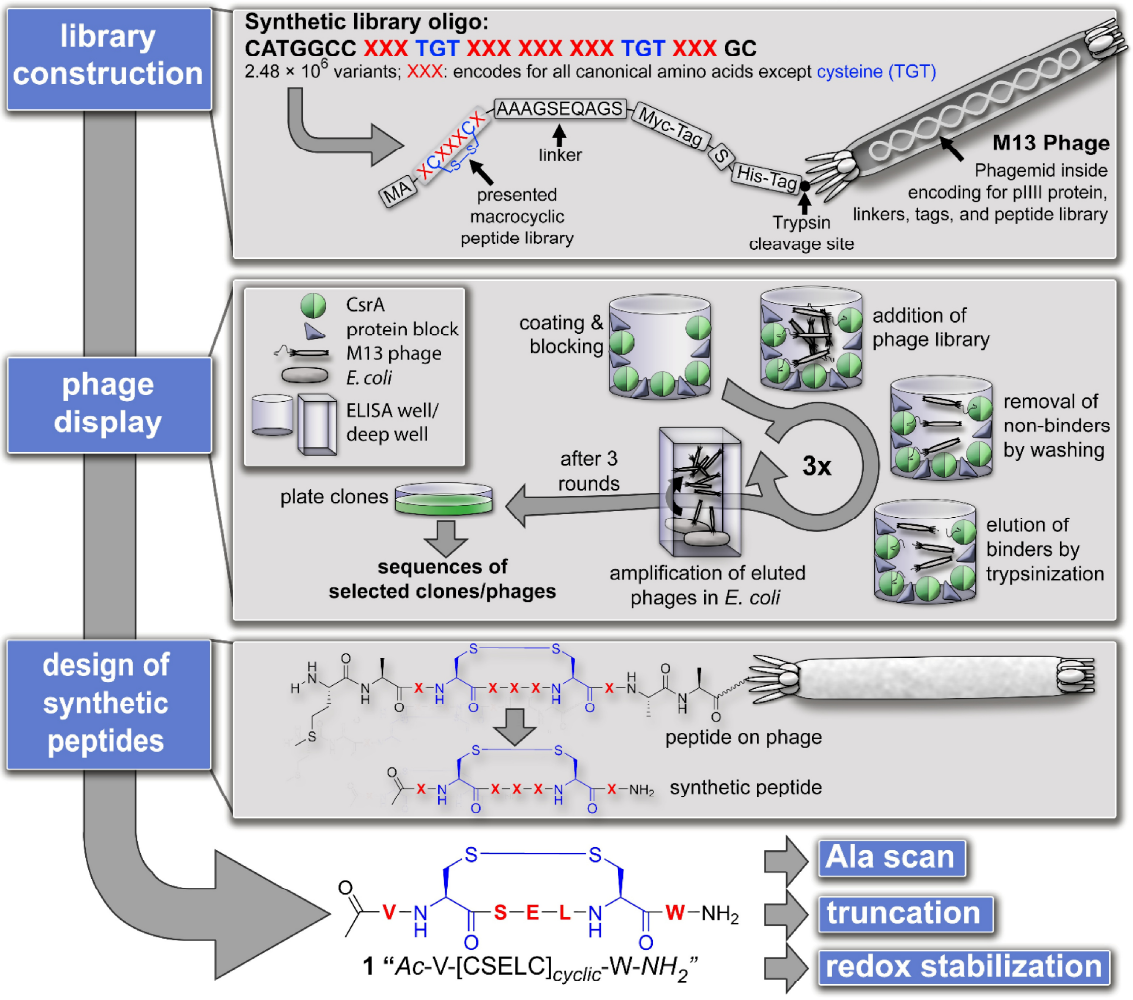

Scheme 1. Selection process from library design to peptide hit identification. Library construction: An oligomer was constructed to code for the subsequent peptide library. After cloning and packaging in M13 phage, genotype and phenotype are coupled by presenting the encoded peptide including tags and linkers simultaneously. Phage display: The peptide phage library was used in the panning process, in which the enrichment of potential CsrA binders is achieved. Sequences of the bound peptides were identified by sequencing the coding phage gene. Design of synthetic peptides: Representation of a phage from panning to which a general library peptide including peptide backbone is linked, compared to the synthesized peptides. Here, *N*-terminal acetylation and *C*-terminal amidation simulate the peptide backbone. Furthermore: A representation of the selected peptide **1** is given, which was characterized in more detail as a "Hit" in the context of this paper.

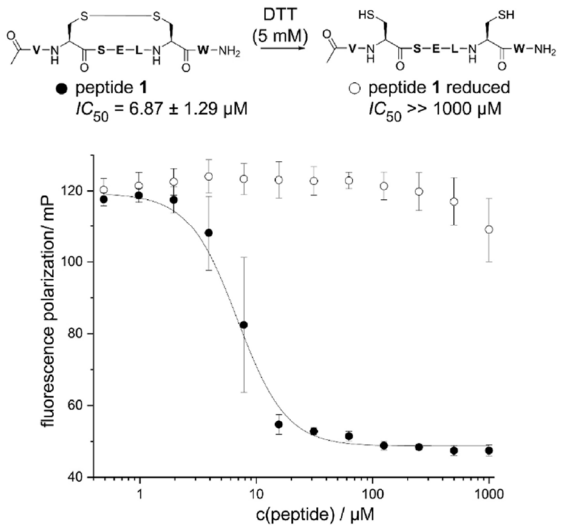

Figure 2. Displacement of RNAflc from CsrA_biot_His_6 with peptide **1** and its reduced derivative measured via fluorescence polarization. Data shown are from two independent experiments measured in duplicate and were fitted to a sigmoidal logistic, Levenberg Marquardt inhibition model (solid line). The results of peptide **1** (filled circles) as well as peptide **1** in the presence of 5 mM DTT in the assay are shown (open circles).

Table 1. Peptides **1**-**4b** with corresponding IC_{50} values obtained from the fluorescence polarization assay and their activity relative to peptide **1**.

Entry	Sequence[a]	IC_{50} / µM[b] *Y. pseudotuberculosis*	Relative activity[c]
1	*Ac*-V-[CSELC]$_{cyclic}$-W-*NH*$_2$	6.9 ± 1.3	1
2a	***H***-V-[CSELC]$_{cyclic}$-W-*NH*$_2$	27.6 ± 4.0	4.0
2b	*Ac*-V-[CSELC]$_{cyclic}$-W-***OH***	17.4 ± 2.0	2.5
3a	*Ac*-V**A**SEL**A**W-*NH*$_2$	>>1000	--
3b	*Ac*-**A**-[CSELC]$_{cyclic}$-W-*NH*$_2$	114 ± 8	16.5
3c	*Ac*-V-[C**A**ELC]$_{cyclic}$-W-*NH*$_2$	>1000	--
3d	*Ac*-V-[CS**A**LC]$_{cyclic}$-W-*NH*$_2$	22.8 ± 0.7	3.3
3e	*Ac*-V-[CSE**A**C]$_{cyclic}$-W-*NH*$_2$	57.9 ± 2.1	8.4
3f	*Ac*-V-[CSELC]$_{cyclic}$-**A**-*NH*$_2$	>500	--
4a	*Ac*- **–** -[CSELC]$_{cyclic}$-W-*NH*$_2$	128 ± 4	18.6
4b	*Ac*-V-[CSELC]$_{cyclic}$- **–** -*NH*$_2$	>>1000	--

[a] Differences relative to peptide **1** are shown in bold or as "–" for deletions. Each peptide is disulfide-cyclized (except **3a**) over the cysteines. [b] Standard error of the sigmoidal curve fit is given (two independent experiments, measured in duplicates). [c] Relative activity for a peptide **x** is given as the ratio IC_{50}(peptide **x**)/IC_{50}(peptide **1**).

To investigate the importance of the *N*-terminal acetylation as well as the *C*-terminal amide, peptides **2a** and **2b** were synthesized, respectively. We observed slightly increased IC_{50} values (27.6 ± 4.0 µM and 17.4 ± 2.0 µM, respectively) indicating that both modifications contribute to the overall affinity of peptide **1**.

To identify possible interaction hotspots, an alanine scan of peptide **1** was performed. As expected, activity was abolished when both cysteines were replaced by alanine (**3a**) corroborating our earlier findings when using DTT to linearize peptide **1** (Figure 1). Similarly, when Ser3 (**3c**) or Trp7 (**3f**) were changed to alanine, dramatic losses of activity were observed. Therefore, the interactions mediated by the serine and tryptophane sidechains are essential hotspots for high affinity. Furthermore, the Ala-scan allowed us to conclude that substitution of residues Val1 (**3b**), Glu4 (**3d**) or Leu5 (**3e**) has a less pronounced effect on activity, showing IC_{50} values of 114 ± 8 µM, 22.8 ± 0.7 µM, and 57.9 ± 2.1 µM, respectively. In the case of the Glu4Ala mutation, this result was surprising. CsrA is an RNA-binding protein possessing a positively charged surface area due to an abundance of lysine and arginine residues. Hence, the presence of the carboxylic acid function in peptide **1** hinted at a potential salt bridge as an important contribution to affinity. If the proposed ionic interaction between Glu4 and the basic amino acid sidechains of CsrA was optimally positioned, a dramatic loss of affinity would have been expected for compound **3d**. As this was not the case, this position should be investigated in more detail in future optimization efforts.

Two truncated versions were tested for inhibitory activity to check whether further reduction in size is possible. A version without Val1 (**4a**) had an IC_{50} of 128 ± 4 µM, which is comparable to the value obtained for the Val1Ala mutant, **3b** (114 ± 8 µM). If tryptophan is omitted (**4b**), the activity in the measured concentration range is completely lost and in line with our findings with the Trp7Ala mutant (**3f**). Hence, we conclude that the complete seven amino acid sequence is required for high activity.

In a final step, we sought to protect peptide **1** from reductive linearization, which we consider essential for achieving intracellular activity. To this end, we made use of the "triazole bridge" approach[29] and replaced the cysteine residues with non-natural amino acids bearing alkyne and azide functions in their sidechain for facile click chemistry-based macrocyclization.[30] Notably, this strategy provides selective access to either a 1,4-disubstituted or 1,5-disubstituted bridging motif depending on whether copper(I)- or ruthenium(II)-catalyzed azide-alkyne cycloaddition is applied (abbreviated CuAAC or RuAAC, respectively). By this means, a number of different triazole-bridged peptides were generated (Table 2). The linear precursor peptides were synthesized using commercially available building blocks Fmoc-protected propargylglycine (Fmoc-Pra-OH) and Fmoc-protected azidoalanine (Fmoc-Aza-OH) or Fmoc-protected azidohomoalanine (Fmoc-Aha-OH). In-solution CuAAC macrocyclization of the unprotected peptides in separate reactions delivered three 1,4-disubstituted 1,2,3-triazole variants (**5a**-**5c**), which were characterized by LC-MS, HRMS and NMR (Supporting Information) and tested in the fluorescence polarization assay (Table 2). **5a**, originating from an azidoalanine-bearing precursor, showed an IC_{50} of 35.3 ± 0.6 µM, which correlates to a moderate 5-fold reduction in potency compared to the disulfide counterpart **1**. Installing an elongated macrocyclization motif by using azidohomoalanine instead (**5c**) leads to a further drop in activity (76.0 ± 3.3 µM). Changing the orientation of the triazole ring by switching positions of the propargylglycine and azidoalanine residues (**5b**) resulted in an IC_{50} of 92.8 ± 4.0 µM.

Table 2. Peptide **1** and triazole-bridged variants **5a**-**6c** with corresponding IC_{50} values obtained for *Yersinia* and *E. coli* CsrA from a fluorescence polarization assay and their activity in relative to peptide **1**.

Entry	Sequence	IC_{50} / μM[a] *Y. pseudotuberculosis* (IC_{50} / μM[a] *E. coli*)	Rel. activity[b]
1	*Ac*-V-[CSELC]$_{cyclic}$-W-NH_2	6.9 ± 1.3 (182 ± 67)	1 (1)
5a	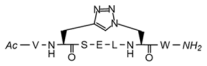	35.3 ± 0.6 (4.9 ± 0.9)	5.1 (0.027)
5b	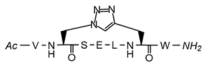	92.8 ± 4.0 (6.8 ± 1.5)	13.5 (0.037)
5c	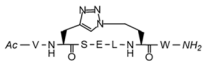	76.0 ± 3.3 (3.4 ± 0.6)	11.1 (0.019)
6a	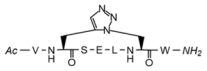	178 ± 12 (48.1 ± 16.0)	25.9 (0.26)
6b	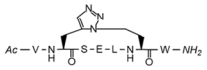	337 ± 34 (51.6 ± 27.1)	49.1 (0.28)
6c	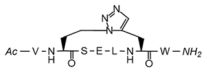	309 ± 15 (83.4 ± 47.1)	45.0 (0.46)

[a] Standard error of the sigmoidal curve fit is given (two independent experiments, measured in duplicate). [b] Relative activity for peptide **1** is set to 1. Values for other peptides relative to peptide **1** (*Y. pseudotuberculosis* CsrA).

Previous work on a 14-amino acid, backbone cyclic protease inhibitor peptide SFTI-1, demonstrated the utility of 1,5-disubstituted bridging motifs, which are installed via RuAAC in solution or on resin.[29,31] In the case of our current CsrA-RNA-interaction inhibitor **1**, this strategy was surprisingly not beneficial. Macrocyclic peptide **6a** achieved only an IC_{50} of 178 ± 12 μM. If the azidoalanine in position 2 was replaced by azidohomoalanine (**6b**), the IC_{50} value increased even further to 337 ± 34 μM. Finally, exchanging the positions of Aha and Pra (**6c**) did not show any significant difference in comparison to **6b** (IC_{50} = 309 ± 15 μM).

To demonstrate the potential for a broader anti-Gram-negative activity we tested peptide **1** as well as our triazole-stabilized derivatives against the *E. coli* homolog of CsrA (Table 2). Surprisingly, disulfide-cyclized inhibitor **1** showed a tremendously reduced activity (IC_{50} (*E. coli*) = 182 ± 67 μM), while the 1,4-disubstituted triazoles **5a**, **5b** and **5c** now outperformed the original peptide (IC_{50} (*E.coli*) = 4.9 ± 0.9 μM, 6.8 ± 1.5 μM, and 3.4 ± 0.6 μM). The 1,5-disubstituted congeners again showed reduced activity compared to their 1,4-counterparts, albeit still being more active than the disulfide compound **1**. Considering the high sequence identity between both proteins (95 %),[32] it is fair to assume that this finding provides evidence for the potential site of interaction of the macrocyclization motif for our inhibitor scaffold. The only differences in amino acid sequence between the *Y. pseudotuberculosis* and *E. coli* proteins are at distinct residues of the *C*-terminus, including Pro58Gln, Thr59Ser, and Thr60Ser, respectively (see sections regarding protein expression in the Supporting Information). This region is also close to the protein-RNA-interaction interface (Figure 3). Hence, we hypothesize that the inhibitor scaffold covers an area encompassing interactions to both sites (*C*-terminus and RNA-binding site). Unfortunately, attempts to co-crystallize the peptide with CsrA have not been successful to date. To gain access to structural information, we solved the structure of peptide **1** by NMR (PDB ID 7M7X, BMRB ID 30895, Figure 3a and Supporting Information). With this ligand structure ensemble in hand we performed a docking experiment based on a *Y. pseudotuberculosis* CsrA homology model derived from a protein-RNA complex determined by NMR.[33] The result of the docking experiment is shown in Figure 3b (see also Supporting Information). The binding pose of peptide **1** is in line with the SAR derived via the Ala-scan and truncation experiments. For example, the side chains of "hot spot" residues Ser3 and Trp7 form key contacts with Lys38 and Val40, while the other residues are primarily involved in backbone-based interactions (Figure 3c). Although this pose will need further validation in future studies, it provides a basis for explaining the observed differences between *Y. pseudotuberculosis* and *E. coli* CsrA. We hypothesize that the differences in activities seen for compounds in Table 2 are potentially resulting from the Pro58Gln exchange changing the *C*-terminal interaction site from a rather hydrophobic environment to a more polar one, which might favor the hydrogen acceptor functions of the triazole. Implementation of a 1,5-motif (**6a – 6c**), however, could result in steric clashes between the ligand and the protein target rendering them less effective in this scenario.

In summary, we have shown that the 1,4-disubstituted triazole bridging motif established in **5a** is a suitable disulfide replacement that is active against both *Y. pseudotuberculosis* and *E. coli* CsrA. In combination with our phage display-based screening methodology, we have provided a generic approach towards the identification, initial qualification, and subsequent redox-protection of short macrocyclic peptides as protein-RNA-interaction inhibitors. The phage display methodology proved to be a rapid approach towards identification of the first macrocyclic peptide able to disrupt the CsrA-RNA interaction. The starting scaffold peptide **1** was thoroughly characterized by fluorescence polarization-based functional activity tests as well as MST-based protein binding assay. Exchanging the disulfide bond against a redox stable 1,2,3-triazole bridge gave us active non-natural derivatives suitable for cell-based assays. Contrary to previous studies, we have observed that in the current system the synthetically easier accessible 1,4-disubstituted 1,2,3-triazole was the superior disulfide mimic showing an IC_{50} value in the 2-digit range. Based on NMR-based solution structure determination of the native peptide sequence and docking experiments structure-guided optimization can now be attempted. This novel scaffold serves as a suitable starting point for the generation of high potency CsrA inhibitors, also because it is probably applicable against CsrA from further bacterial species.

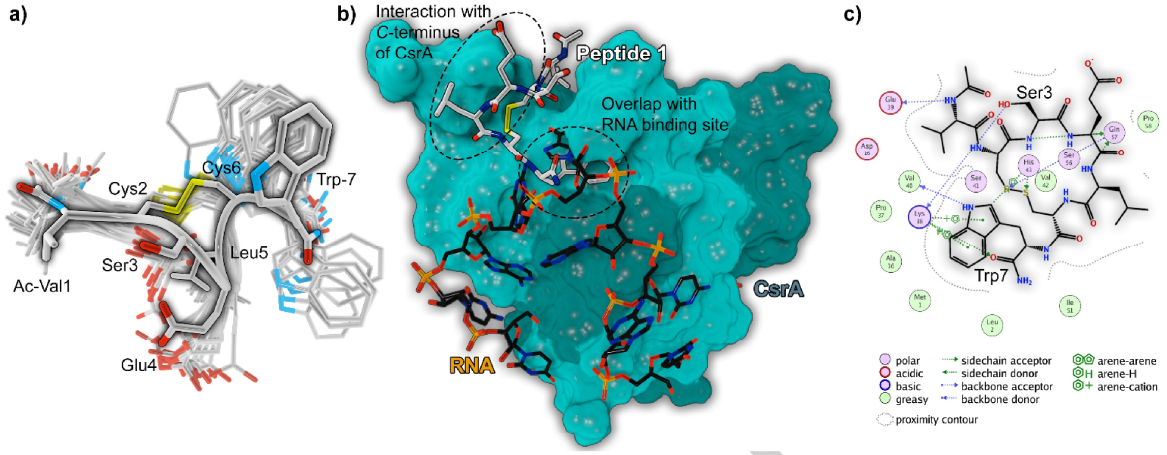

Figure 3. *In silico* analysis of the peptide-CsrA interaction. a) Overlay of 20 NMR-derived solution structures of peptide **1** (PDB ID 7M7X, BMRB ID 30895) showing the peptide backbone as a tube and highlighting conformer 1 (entry 1 in pdb) for clarity. b) Depiction of docking-derived interaction hypothesis highlighting key interaction sites. Carbons of peptide **1** are shown in white and RNA carbons in black. Surface of the two CsrA chains shown in light cyan and dark cyan. c) 2D interaction profile of binding hypothesis for peptide **1**. "Hot spot" residues identified via Ala-scan (Ser3 and Trp7) are indicated.

Acknowledgements

This work is supported by the Deutsche Forschungsgemeinschaft (DFG) through "RESIST - Resolving Infection Susceptibility" cluster of excellence (EXC 2155). Work in DJCs lab on cyclic peptides is supported by the Australian Research Council (CE200100012). We thank Prof. Dr. Tony Romeo for sending us the plasmid for *E. coli* CsrA expression.

Keywords: competitive inhibition • CsrA inhibition • disulfide bridges • disulfide mimetics • peptides • peptide library • phage display • triazole bridges

[1] a) M. Jemal, T. Deress, T. Belachew, Y. Adem, *Int. J. Microbiol.* **2020**, *2020*, 8893266; b) H. Inoue, R. Minghui, *Bull. World Health Organ.* **2017**, *95*, 242; c) Z. Kmietowicz, *BMJ* **2017**, *358*, j4339.
[2] S. Vasoo, J. N. Barreto, P. K. Tosh, *Mayo Clin. Proc.* **2015**, *90*, 395–403.
[3] Y. Irie, M. Starkey, A. N. Edwards, D. J. Wozniak, T. Romeo, M. R. Parsek, *Mol. Microbiol.* **2010**, *78*, 158–172.
[4] a) A. M. Nuss, A. K. Heroven, P. Dersch, *Trends Microbiol.* **2017**, *25*, 19–34; b) F. M. Barnard, M. F. Loughlin, H. P. Fainberg, M. P. Messenger, D. W. Ussery, P. Williams, P. J. Jenks, *Mol. Microbiol.* **2004**, *51*, 15–32.
[5] A. H. Potts, C. A. Vakulskas, A. Pannuri, H. Yakhnin, P. Babitzke, T. Romeo, *Nat. Commun.* **2017**, *8*, 1596.
[6] E. R. Morris, G. Hall, C. Li, S. Heeb, R. V. Kulkarni, L. Lovelock, H. Silistre, M. Messina, M. Cámara, J. Emsley et al., *Structure* **2013**, *21*, 1659–1671.
[7] C. K. Maurer, M. Fruth, M. Empting, O. Avrutina, J. Hoßmann, S. Nadmid, J. Gorges, J. Herrmann, U. Kazmaier, P. Dersch et al., *Future Med. Chem.* **2016**, *8*, 931–947.
[8] G. Sharma, S. Sharma, P. Sharma, D. Chandola, S. Dang, S. Gupta, R. Gabrani, *J. Appl. Microbiol.* **2016**, *121*, 309–319.
[9] J. Timmermans, L. van Melderen, *Cell. Mol. Life Sci.* **2010**, *67*, 2897–2908.
[10] a) E. van Assche, S. van Puyvelde, J. Vanderleyden, H. P. Steenackers, *Front. Microbiol.* **2015**, *6*, 1–16; b) N. A. Sabnis, H. Yang, T. Romeo, *J. Biol. Chem.* **1995**, *270*, 29096–29104.
[11] H. Yakhnin, C. S. Baker, I. Berezin, M. A. Evangelista, A. Rassin, T. Romeo, P. Babitzke, *J. Bacteriol.* **2011**, *193*, 6162–6170.
[12] B. L. Wei, A.-M. Brun-Zinkernagel, J. W. Simecka, B. M. Prüß, P. Babitzke, T. Romeo, *Mol. Microbiol.* **2001**, *40*, 245–256.
[13] M. Y. Liu, G. Gui, B. Wei, *J. Biol. Chem.* **1997**, *272*, 17502–17510.
[14] a) Y. Tan, Z.-Y. Liu, Z. Liu, H.-J. Zheng, F.-L. Li, *Mol. Omics* **2015**, *11*, 1434–1442; b) A. Matin, J. E. Schultz, *J. Mol. Biol.* **1991**, *218*, 129–140.
[15] D. W. Jackson, K. Suzuki, L. Oakford, J. W. Simecka, M. E. Hart, T. Romeo, *J. Bacteriol.* **2002**, *184*, 290–301.
[16] A. K. Dubey, C. S. Baker, K. Suzuki, A. D. Jones, P. Pandit, T. Romeo, P. Babitzke, *J. Bacteriol.* **2003**, *185*, 4450–4460.
[17] A. K. Dubey, C. S. Baker, T. Romeo, P. Babitzke, *RNA* **2005**, *11*, 1579–1587.
[18] X. Ren, R. Zeng, M. Tortorella, J. Wang, C. Wang, *Sci. Rep.* **2017**, *7*, 14934.
[19] a) G. B. Santos, A. Ganesan, F. S. Emery, *ChemMedChem* **2016**, *11*, 2245–2251; b) C. A. Lipinski, *Adv. Drug Deliv. Rev.* **2016**, *101*, 34–41.
[20] B. C. Doak, B. Over, F. Giordanetto, J. Kihlberg, *Chem. Biol.* **2014**, *21*, 1115–1142.
[21] A. Capecchi, M. Awale, D. Probst, J.-L. Reymond, *Mol. Inf.* **2019**, *38*, e1900016.
[22] V. Jakob, S. Helmsing, M. Hust, M. Empting in *Genotype Phenotype Coupling*, Springer US, New York, NY, **2020**, pp. 95–113.
[23] S. Dübel (Ed.) *Handbook of therapeutic antibodies*, Wiley-VCH, Weinheim, **2007**.
[24] C. G. Ullman, L. Frigotto, R. N. Cooley, *Brief. Funct. Genom.* **2011**, *10*, 125–134.
[25] a) A. Frenzel, T. Schirrmann, M. Hust, *MAbs* **2016**, *8*, 1177–1194; b) S. Dübel, O. Stoevesandt, M. J. Taussig, M. Hust, *Trends Biotechnol.* **2010**, *28*, 333–339.
[26] J. Kügler, J. Zantow, T. Meyer, M. Hust, *Viruses* **2013**, *5*, 2531–2545.

[27] V. Baeriswyl, C. Heinis, *Protein Eng. Des. Sel.* **2013**, *26*, 81–89.
[28] N. B. Adey, A. H. Mataragnon, J. E. Rider, J. Carter, B. K. Kay, *Gene* **1995**, *156*, 27–31.
[29] M. Empting, O. Avrutina, R. Meusinger, S. Fabritz, M. Reinwarth, M. Biesalski, S. Voigt, G. Buntkowsky, H. Kolmar, *Angew. Chem. Int. Ed.* **2011**, *50*, 5207–5211.
[30] a) X. Jiang, X. Hao, L. Jing, G. Wu, D. Kang, X. Liu, P. Zhan, *Expert Opin. Drug Discov.* **2019**, *14*, 779–789; b) M. Roice, I. Johannsen, M. Meldal, *QSAR Comb. Sci.* **2004**, *23*, 662–673; c) G. Appendino, S. Bacchiega, A. Minassi, M. G. Cascio, L. De Petrocellis, V. Di Marzo, *Angew. Chem.* **2007**, *119*, 9472–9475.
[31] A. M. White, S. J. de Veer, G. Wu, P. J. Harvey, K. Yap, G. J. King, J. E. Swedberg, C. K. Wang, R. H. P. Law, T. Durek et al., *Angew. Chem. Int. Ed.* **2020**, *59*, 11273–11277.
[32] A. K. Heroven, K. Böhme, P. Dersch, *RNA Biol* **2012**, *9*, 379–391.
[33] O. Duss, E. Michel, N. Diarra dit Konté, M. Schubert, F. H.-T. Allain, *Nucleic Acids Res.* **2014**, *42*, 5332–5346.

4 Final Discussion

The aim of this thesis was to generate new inhibitors that can prevent protein-nucleic acid interactions by displacing the nucleic acid and binding to the protein. On the one hand for the viral LANA-DNA interaction, which is responsible for the latent persistence of KSHV, on the other hand for the bacterial CsrA-RNA interaction, which is highly conserved in human pathogens such as *Yersinia*, *Pseudomonas* and *E. coli*. Thus, LANA and CsrA represent promising targets for the development of anti-KSHV drugs or agents that are applicable against a broad range of bacterial pathogens.

In general, it is often difficult to inhibit protein-nucleic acid interactions. This may be due to the size of the nucleic acids, which are very large in contrast to fragment-sized or small molecules. The corresponding binding pocket of the protein in which the nucleic acid is located may also be too large for a relatively small inhibitor. Therefore, solutions have to be found in the form of other approaches, such as a peptide-based approach.

In the first part (**Chapter A**, **B** and **C**), a fluorescence polarization assay (FP assay) for LANA was established after successful optimization of LANA protein expression. The first LANA-DNA-interaction inhibitors using fragment-based approach and hits from an in-house library were evaluated using this expressed protein and the established assay. Highly potent inhibitors against LANA emerged.

In the second part (**Chapter D**) a phage display procedure was established. The starting point was a self-designed peptide library encoding very small macrocyclic peptides. In the course of phage display panning, optimization steps were performed. Using the library, potential binders could theoretically be found for any target.

In the third part (**Chapter E**), a highly potent peptide-based CsrA-RNA inhibitor was successfully found. This hit was evaluated by biological assays and further structure-activity relationship (SAR) insights were obtained by different methods. By means of disulfide bridge replacement, a potent redox-stable inhibitor against CsrA was achieved.

All three parts will be discussed in the following.

4.1 Protein-DNA Interactions

In the first part of this work, the LANA protein was expressed as an initial step. For this purpose, an oligomerization-deficient KSHV LANA(1008-1146) mutant was used. The use of a *C*-terminal domain (CTD) of the LANA wild type (wt) results in higher homo oligomers. Moreover, with the CTD wt, quantitative precipitation of LANA and DNA occurs upon interaction with DNA, which also means poor solubility.[17] However, highly soluble LANA dimers were required for the experiments, in which form they would also bind to an LBS. The oligomerization-deficient mutant allowed this to be achieved with several point mutations. Hellert *et al*. were already able to establish a method to express this LANA mutant,[121] but this expression is extremely labor intensive, time consuming, and unreliable. Reasons are a complex medium (autoinduction), cell disruption by sonification (heating and time consuming) and an on-column refolding step. Because in this expression process, the LANA protein is mainly located in the inclusion bodies of *E. coli*, LANA would have to be denatured first and renatured on the column. With our method, these three steps could be significantly simplified. The main culture (conventional medium) was directly inoculated with a cryoculture without preculture usage. Expression generated sufficient solubilized protein outside the inclusion bodies. Other benefits included cell disruption with just one passage through a microfluidizer and simple Ni-affinity purification without a refolding step. Yields up to 2.5 mg per litre of culture could be achieved. Other oligomerization-deficient LANA constructs like LANA(996-1149) and LANA(1017-1149) for crystallization study trials were also successfully expressed using our method. The purified proteins were used in several assays to evaluate different compounds in assays.

Many potential fragment-sized molecules were synthesized by our former group member Philine Kirsch in the context of fragment-based drug discovery (FBDD)[41] up to the discovery of a new lead structure.[122] In addition, screening of an in-house library[123] has been performed.

Since this part of the work has happened hand in hand with the development of the FP assay, the following section will provide an overview of Philine Kirsch's fragment-based approach. In the fragment-based approach, 720 fragment-sized compounds had to be analyzed by Surface Plasmon Resonance Spectroscopy (SPR) as a biophysical assay and Thermal Shift Assay (TSA) to detect compound-protein binding. This resulted in 20 binders, which were evaluated as potential inhibitors in a fluorescence-based competition assay to investigate functional LANA-DNA interaction inhibition. This FP assay thus served as an SAR driver at each optimization step and supported that fragment-growing with finding a growth vector was successful. In

addition, an orthogonal LANA-DNA interaction inhibition assay (electrophoretic mobility shift assay, EMSA) was performed with LBS1 and 2 and 1 + 2 in combination. The assay gave three hits with increased potency and good physiochemical properties (fragment-like, best of the three: 17 ± 1 µM), although no X-ray structure was present. Co-crystallization of the fragments with LANA would be essential for structure-based optimization and interaction hotspots, but this has not yet been successful. However, saturation-transfer difference NMR (STD-NMR) and molecular docking offered a successful alternative for inhibitor-target interaction and to find out the putative binding mode (different compounds had different binding sites). Target binding was confirmed by microscale thermophoresis (MST) assay.

Our fluorescence-based competition assay for LANA was derived from an established method for CsrA developed by Maurer *et al*..[19] This assay was successfully transferred to the oligomerization-deficient LANA mutant. However, all parameters (such as DMSO tolerance and concentration of protein and the labeled ligand) were again precisely varied and checked. In addition, the LBS single strands had to be hybridized beforehand. The three LBS 1, 2 and 3 were used individually as smaller fluorescein-labeled DNA pieces for competition experiments with the synthesized compounds. The fragments showed similar activity against LBS 1, 2 and 3 in the FP assay, which may indicate that LANA can be displaced from all three binding sites, if the full TR unit would be present.

In an additional validation step, a Z-factor[124] of > 0.9 was achieved indicating suitable reproducibility. This statistical parameter of assay robustness can be seen as a measure for high throughput capability. After confirming that this established assay was high-throughput capable, screening of an in-house library with 670 drug-like compounds could be performed. However, the assay could not be transferred to the LANA CTD wt because, as already mentioned, this construct tends to oligomerize and precipitate together with DNA, which was not the case with the highly soluble mutant. The FP assay had thus proven to be a reliable tool to rapidly screen the synthesized fragments and those of the in-house library. To test compounds with wt protein, EMSA was performed in collaboration with the group of Thomas Schulz (Saskia Stein, Hannover Medical School, MHH). According to EMSA, the lead structure developed by Philine Kirsch was also active against wt LANA (LBS2: 8 ± 1 µM and wt LBS1: 60 ± 4 µM).

As mentioned earlier, it is not easy to displace relatively large DNA from the target with small molecules. However, this is exactly the case with the LANA-DNA interaction. However, only a small single LBS was displaced in the assay, while within the cellular environment actually

the entire viral DNA has to be displaced from binding to three LANA homo dimers. Considering this complex scenario, further optimization of the generated compounds will be necessary. It is promising that such a small inhibitor already shows decent activity in the *in vitro* assays (also against wt LANA). The binding pocket is large, flat and poorly defined. In conclusion, LANA is difficult to target but not undruggable for such small molecules as is often described.[125]

A viable alternative could be a peptide-based approach, which, with their larger molecular scaffolds, are more suited for macromolecule-macromolecule-interaction inhibition. Such a peptide could be identified by exploiting the phage display technology against LANA in the future. Importantly for peptides, whose size is beyond Lipinski space, mammalian (eukaryotic) cells are easier to permeate than those of e.g. Gram-negative bacteria.[126]

Another possibility to obtain larger compounds is the so-called compound merging or linking. Different compounds that already successfully inhibit LANA-DNA interaction are combined with each other. Especially since it is assumed that different compounds (in-house-library screening hits) bind to different sites of LANA.[123] Such a procedure could increase the inhibition potency.

Another way to defeat the latent persistence of KSHV might be the PROTAC (proteolysis targeting chimeras) approach.[127] Currently, PROTAC-based LANA degraders are being developed in our group. Such a degrader consists of two linked moieties, one part which binds to LANA (inhibitor) and one part which binds to E3 ligase (E3 ligand).[128] Upon binding, ubiquitylation of LANA and, hence, proteolytic degradation in the proteasome is induced by the PROTAC agent.

4.2 Phage Display

Besides fragment-based drug discovery, the peptide-based approach could be another method with high potential to address protein-nucleic acid interactions. Peptides are typically large compared to fragments and are thus better suited to displace nucleic acids from the target with a relatively large binding pocket. This chapter should not be specifically assigned to protein-DNA or protein-RNA interactions. This method can be used for any target and, furthermore, only potential binding to a target without nucleic acid competition is captured. However, the method has been optimized for the protein CsrA.

As described in **Chapter D**, a phage display procedure was established to quickly and easily obtain potential binders against any target. This method was based on $2.48 \cdot 10^6$ different heptapeptide variants (**Figure 9**) encoded by a self-designed library oligomer. This library first had to be cloned into a phagemid. Classical restriction cloning and subsequent ligation failed. However, a self-designed method for cloning very small peptide libraries proved succesful.[106] This outstanding method circumvented cumbersome inefficient restriction enzymatic steps and classical error-prone ligations using Hot Fusion cloning.[129] Here, the library oligomer was amplified via PCR and phagemid was linearized restriction-free via PCR (instead of with restriction enzymes). After Hot Fusion reaction with exonuclease and polymerase, transformation into *E. coli* was performed. Then, up to 50 % more positive clones were obtained with ligation compared to the variant with restriction enzymes and ligase. The great advantage of Hot Fusion cloning was that no purification steps were required. In classical restriction cloning, the PCR product of the library would first have to be purified at 60 bp, which is critical for most PCR cleanup kits. The purified product would be only 30 bp after restriction and would have to be separated and purified on an agarose gel from fragments that are 18 and 11 bp long. This turned out to be impossible in this form and a way out could have been native polyacrylamide gel electrophoresis (native PAGE), which would have taken a lot of time and expertise. Hot Fusion cloning eliminated these steps completely.

After transformation of the cloned library into *E. coli*, it was packed into M13 phages. Here it turned out to be necessary to combine several transformations in order to achieve a higher library diversity. A high diversity of approximately $1 \cdot 10^6$ was successfully achieved by pooling six transformations. A mapping of the complete library would probably not have been possible even with more transformations, because certain sequences could already be lost in the cloning process.

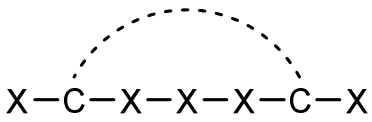

Figure 9: Schematic representation of the heptapeptide from the Phage Library containing two cysteines at fixed positions with a potential to build a macrocycle. X encodes for any amino acid except cysteine

The cloned library, which was packaged in M13 phages, could then be used in the actual phage display cycle - the so-called panning - for the selection of potential target binders. The exact procedure was described in **Chapter E** and in **Section 1.5**. Because the peptide library has two firmly positioned cysteines, they form a disulfide bridge under oxidative conditions. The

peptide thus formed a macrocycle, which was explicitly desired. Small macrocyclic peptides are quite a common form for peptides related to phage display, especially bicyclic peptides have been described in literature.[130] In addition, macrocyclic peptides have a higher potential for oral availability than linear ones.[131] After three rounds of panning, the genes of the binding peptides were successfully identified by sequencing. During panning, there were several points where optimization was possible. For example, the wells were coated with different target concentrations, the number of automated wash cycles before phage elution with trypsin was varied, and the Tween-20 content in the buffer was changed.

This panning procedure, which can be used universally for any target, was performed with *Yersinia* CsrA (biotinylated and His-tagged construct CsrA-biot-His_6) and also optimized for it.

The most significant effect was achieved by varying the number of wash cycles using a plate washer to remove non-binding phages. The fewer wash cycles, the more plausible peptide sequences came out after sequencing. The more wash cycles, the more non-specific binders were present (for exact criteria see **Section 4.3**). One reason for this could be that the binding/affinity of the presented peptides to the immobilized CsrA was relatively weak. The initial many wash cycles were taken from a protocol optimized for selection of stronger binding scFvs instead of peptides.[113] With many wash cycles, there was an increased probability that potential binders were also eliminated. Variation of target amount and Tween-20 had not yielded significant differences, so we decided to use an established amount, which was also described in the scFv protocol.[113]

One problem that could not be solved so far was that after sequencing, there were always quite a few clones that contained the “empty” phagemid pHAL30, i.e. phages that did not present any peptide during panning. This problem occurred already during phage packaging, where phages preferentially proliferated when there was no library insert present. One reason might be that they were not eliminated by the few washing cycles. The problem did not occur with more frequent washing. With this compromise - fewer wash cycles, a lot of empty vector but a few potential binders - CsrA binders were successfully obtained.

Of course, there would have been many more points where optimization during panning would have been possible, e.g. variation of incubation times, other buffers and intensity of the plate washer wash jet. This would mean additional effort and was not necessary in our case.

4.3 Protein-RNA Interactions

In the third and more exploratory part of this thesis, the peptide-based approach was applied to inhibit the protein-RNA interaction between CsrA and a short RNA segment. The established phage display discussed in **Chapter 4.2**, optimized for CsrA, was applied with *Yersinia* CsrA (biotinylated and His-tagged construct CsrA-biot-His_6). This means that the library was screened against immobilized CsrA.

After three rounds of panning and sequencing of 32 clones, we established criteria to facilitate preselection of potential binders. Intact sequences and avoidance of high tryptophan content (more than two tryptophans) were important as this implies non-specific binding. The presence of glutamic acid with its carboxyl group was advantageous for binding to the positively charged surface of CsrA, which has a high proportion of basic amino acids. Under these criteria, a first hit emerged which could be a potential CsrA binder.

Resynthesis by solid phase peptide synthesis (SPPS) including *N*-terminal acetylation, *C*-terminal amidation and macrocyclization through a disulfide bridge was performed. Reasons for this were the mimicking of the peptide backbone at *C*- and *N*-termini, in which the phage presented the peptide during panning. The synthesized hit **P1** is shown in **Table 1**. In the next step, the peptide hit **P1** was competitively screened for inhibitory activity against labeled RNA using FP assay according to Maurer *et al*.[19] on CsrA. This was a complete success as the RNA was displaced with an IC_{50} of 6.89 ± 1.29 µM. The orthogonal MST assay yielded a K_d of 10.5 ± 1.4 µM, providing evidence for direct, specific peptide-CsrA interaction. Our result is quite comparable to the best CsrA inhibitors to date, the natural products MM14 (4 ± 1 µM) and TubulysinAr-672 (11 ± 1 µM).[19] However, our peptide is much more synthetically accessible.

The goal was now to characterize this hit in more detail. The disulfide bridge was essential, because reduction to the two thiols (and thus linearization of the peptide) by addition of 5 mM DTT in the assay resulted in no activity. Thus, peptide binding to CsrA was strongly structure dependent. To further investigate this dependence, peptide derivatives were prepared by Fmoc-SPPS and examined by FP assay to obtain closer SAR insights. Omitting *N*-terminal acetylation or *C*-terminal amidation resulted in slightly higher IC_{50} values. For this reason, we left these residues on the peptide, as the peptide backbone is also better represented, as it was in the panning. To find out which amino acids were responsible for the activity/binding to CsrA, we performed an alanine scan. This had revealed that Ser3 and Trp7 were important interaction

hotspots to maintain activity against CsrA. As expected, linearization by substitution of cysteines with alanines showed no more activity. This confirmed the result of linearization by DTT and that the macrocycle was essential for inhibition. Val1, Glu4, and Leu5 were no hotspots or had only a minor impact on activity if replaced by alanine. The presence of glutamic acid was actually thought to be a criterion for good potential binders. CsrA has a positively polarized surface with many basic lysine and arginine residues. A strong salt bridge could be built by the carboxyl group. Since the loss of activity did not occur here, it is worthwhile to look at this residue in more detail in the future. It was also shown that it was not readily possible to truncate the peptide further; when Val1 or Trp7 were omitted, the activity losses were comparable to those from the Ala-scan (V→A/W→A). All seven amino acids were therefore required.

The disulfide bond in the peptide could be very easily incorporated synthetically, but there is a problem in certain physiological environments: reductive conditions prevail inside a cell. If such a macrocyclic peptide enters the cytoplasm, the peptide would be linearized by reduction, which would cause its effectiveness to disappear. As strategy to mitigate this problem, the triazole-bridge approach was investigated. Instead of cysteines, unnatural amino acids with alkyne and azide functions were incorporated. Using click chemistry, macrocyclization was then performed.[132–134] These disulfide mimetics were divided into two groups: 1,4-disubstituted 1,2,3-triazoles, which were synthesized by copper-catalyzed azide-alkyne 1,3-dipolar cycloaddition (CuAAC), and 1,5-disubstituted 1,2,3-triazoles, which were achieved by ruthenium-catalyzed azide-alkyne 1,3-dipolar cycloaddition (RuAAC). In total, there were six variants, all of which were tested/validated via the FP assay. Three variants of a 1,4-version were synthesized by our group. The best variant (**P2**) achieved an IC_{50} of 35.3 ± 0.6 µM, which was only 5-fold worse than the original peptide hit. Elongation of the cycle with a methyl group decreased the activity. Likewise, when changing the orientation of the triazole ring (**P3**), the activity became worse (IC_{50}: 92.8 ± 4.0 µM).

In cooperation with the group of David Craik (Thomas Durek, Andrew White, Queensland, Australia), three variants of a 1,5-version were synthesized. In the assay, these all showed lower activity (the best 178 ± 12 µM) than the 1,4-versions. This seemed unusual as it has been described in the literature that 1,5-versions have the better activity as these are more flexible and less rigid linkers. These observations were made in a different system using a 14 amino acid long protease inhibitor SFTI-1.[135–136] In the context of CsrA inhibitors, apparently our 1,4-versions can better adopt the active conformation from the peptide hit than the 1,5-versions.

Moreover, **P2** and **P3** had been shown to be active against *E. coli* CsrA. The remarkable 1-digit µM IC_{50}'s of 4.93 ± 0.89 and 6.80 ± 1.50 µM respectively are even comparable to peptide hit **P1** against *Yersinia* CsrA. **Table 1** gives an overview of **P1**, **P2** and **P3** with structures and activities. We thus showed that at least two forms of disulfide mimetics are also active against CsrA of at least one other bacterial species. Thus, these peptide-compounds have the potential to be broad-spectrum anti-infective agents. Nevertheless, it would be important to check the activity against CsrA/RsmA from additional bacterial species.

Table 1: Comparison of the small macrocyclic hepta peptides as CsrA-RNA interaction inhibitors.

Peptide	Structure	MW / g/mol	FP Assay IC_{50} (*Yersinia* CsrA) / µM	FP Assay IC_{50} (*E. coli* CsrA) / µM
P1	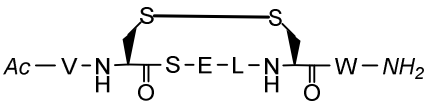	878.03	6.87 ± 1.29 K_D(MST): 10.5 ± 1.4	182 ± 67.
P2	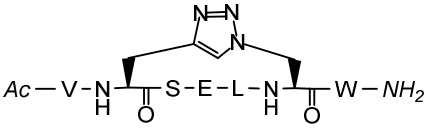	881.95	35.3 ± 0.6	4.93 ± 0.89
P3	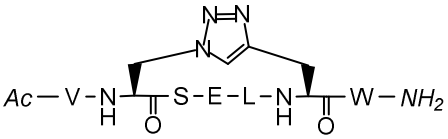	881.95	92.8 ± 4.0	6.80 ± 1.50

This part of the thesis led to a rather early and promising success. The original peptide hit **P1** and the relatively simple disulfide bridge exchange in the 1,4-disubstututed 1,2,3-triazoles (**P2**, **P3**) are a good starting point for further optimization. Moreover, the peptides are a very good starting point to generate further optimized highly potent drug-like CsrA-RNA inhibitors.

Upon panning, other peptides emerged after sequencing that may also be of interest and should be explored further in future studies.

The binding selectivity against a specific target (here: CsrA - but from different species) still needs to be checked using other nucleic acid binding proteins such as e.g. LANA. If the binding selectivity is not given, side effects should be checked.

As far as the molecular size (given in **Table 1**) of the peptides **P1**, **P2** and **P3** is concerned, the Lipinski space for oral bioavailability is slightly exceeded with a mass of about 880 Da. Hence, these peptides reside in the extended Lipinski space (500 - 1000 Da).[126,131,137] However, oral bioavailability may still be present for compounds of this size. A few examples from literature are Desmopressin[131] (1069 Da) for treatment of haemophilia A and the HIV protease inhibitor Ritonavir[137] (721 Da). Furthermore, oral bioavailability is not always needed for all indications.

5 Conclusion and Outlook

In this dissertation, the two poorly studied protein targets, both modulators of infectious diseases, LANA and CsrA were investigated. LANA as a viral target binds DNA and CsrA as a bacterial target binds RNA. In both cases a protein-nucleic acid interaction should be inhibited. An FP assay was established for LANA and the expression of LANA was optimized. Phage display as an important tool for finding suitable inhibitors was established and applied for CsrA.

Indeed, an FP assay was established, which acted as an excellent SAR driver for both targets. Expression/purification of the oligomerization-deficient LANA mutant was performed using a simplified method. A universally applicable phage display procedure for each target was established. With this, a first peptide-based inhibitor was identified, which interfered with the CsrA-RNA interaction in the 1-digit µM range. Two redox-stable disulfide mimetics for *E. coli* CsrA yielded similar activity. These peptides are good starting points for therapeutic agents, as they have the potential to be broad-spectrum active against other CsrA-harbouring species. This encourages further pursuit of the peptide-based approach for CsrA. A transfer of the peptide-based approach to LANA is still pending.

The FP assay was an excellent tool to test functional compounds in a cell-free setup. A next big step regarding the LANA project would be to test the cellular efficacy of the compounds or to generate cellular efficacy to inhibit the latent persistence of KSHV. In cooperation, a cell-based virus infection assay is planned for this purpose. A cell-based assay is also planned inhouse as well as in cooperation for CsrA.

For LANA and CsrA project it would be worth to solve co-crystal structures. This has been attempted but has not been successful to date. LANA in complex with one of the best synthesized inhibitors, CsrA together with the most active peptide hits. This would allow the actual binding mode to be elucidated. If this won't be successful for CsrA together with peptide, STD-NMR could also be helpful, as it was with LANA.

In the case of phage display, there is still the possibility of expanding the structural space. For this, the peptides presented by the phages could be chemically modified on cysteine residues providing new and non-natural macrocyclization motifs. Such "combinatorial chemical libraries"[119] are quite common, but require a high amount of elaboration.

Another variant to generate CsrA binders by phage display would be a panning against all-D-CsrA, which will be synthesized in collaboration. This would then enable to perform mirror

phage display, in which the identified peptide sequences would actually correspond to D-amino acid-based peptide hits against the natural (all-L) target. These may have better pharmacological properties than their corresponding L-peptides.[138]

6 References

1. Eigen M.: Selforganization of matter and the evolution of biological macromolecules. *Sci. Nat.* **1971,** 58, 465–523.
2. Young G.; Hundt N.; Cole D.; Fineberg A.; Andrecka J.; Tyler A., et al.: Quantitative mass imaging of single biological macromolecules. *Science* **2018,** 360, 423–427.
3. Cosic I.: Macromolecular Bioactivity: Is It Resonant Interaction Between Macromolecules?-Theory and Applications. *IEEE Trans. Biomed. Eng.* **1994,** 41, 1101–1114.
4. Gonzalez M. W.; Kann M. G.: Chapter 4: Protein interactions and disease. *PLOS Comput. Biol.* **2012,** 8, e1002819.
5. Sultana A.; Lee J. E.: Measuring protein-protein and protein-nucleic Acid interactions by biolayer interferometry. *Curr. Protoc. Protein Sci.* **2015,** 79, 19.25.1-19.25.26.
6. Ramakrishnan V.; White S. W.: Ribosomal protein structures: insights into the architecture, machinery and evolution of the ribosome. *Trends Biochem. Sci.* **1998,** 23, 208-212.
7. Moras D.: Arninoacyl-tRNA synthetases. *Curr. Opin. Struct. Biol.* **1992,** 2, 138–142.
8. Varani G.; Nagai K.: RNA Recognition by RNP Proteins During RNA Processing. *Annu. Rev. Biophys. Biomol. Struct.* **1998,** 27, 407–445.
9. MacCallum R. M.; Martin A. C. R.; Thornton J. M.: Antibody-antigen Interactions: Contact Analysis and Binding Site Topography. *J. Mol. Biol.* **1996,** 262, 732–745.
10. Tsai C. S.: *Biomacromolecules: Introduction to structure, function and informatics.:* John Wiley & Sons, Ltd, **2007**.
11. Rößler P.; Mathieu D.; Gossert A. D.: Enabling NMR Studies of High Molecular Weight Systems Without the Need for Deuteration: The XL-ALSOFAST Experiment with Delayed Decoupling. *Angew. Chem.* **2020,** 59, 19329–19337.
12. Lee S.; Blundell T. L.: BIPA: a database for protein-nucleic acid interaction in 3D structures. *Bioinformatics* **2009,** 25, 1559–1560.
13. Cerný J.; Hobza P.: Non-covalent interactions in biomacromolecules. *Phys. Chem. Chem. Phys.* **2007,** 9, 5291–5303.
14. Harrison S. C.: A structural taxonomy of DNA-binding domains. *Nature* **1991,** 353, 715–719.

15. Jones S.; Daley D. T. A.; Luscombe N. M.; Berman H. M.; Thornton J. M.: Protein-RNA interactions: a structural analysis. *Nucleic Acids Res.* **2001,** 29, 943–954.
16. Jones S.; van Heyningen P.; Berman H. M.; Thornton J. M.: Protein-DNA Interactions: A Structural Analysis. *J. Mol. Biol.* **1999,** 287, 877–896.
17. Hellert J.; Krausze J.; Schulz T. F.; Lührs T.: Crystallization, room-temperature X-ray diffraction and preliminary analysis of Kaposi's sarcoma herpesvirus LANA bound to DNA. *Acta Crystallogr. F* **2014,** 70, 1570–1574.
18. Jonas K.; Edwards A. N.; Simm R.; Romeo T.; Römling U.; Melefors O.: The RNA binding protein CsrA controls cyclic di-GMP metabolism by directly regulating the expression of GGDEF proteins. *Mol. Microbiol.* **2008,** 70, 236–257.
19. Maurer C. K.; Fruth M.; Empting M.; Avrutina O.; Hoßmann J.; Nadmid S., et al.: Discovery of the first small-molecule CsrA-RNA interaction inhibitors using biophysical screening technologies. *Future Med. Chem.* **2016,** 8, 931–947.
20. Singh R. K.; Lamplugh Z. L.; Lang F.; Yuan Y.; Lieberman P.; You J.; Robertson E. S.: KSHV-encoded LANA protects the cellular replication machinery from hypoxia induced degradation. *PLOS Pathog.* **2019,** 15, e1008025.
21. Grinde B.: Herpesviruses: latency and reactivation - viral strategies and host response. *J. Oral. Microbiol.* **2013,** 5, doi:10.3402/jom.v5i0.22766.
22. Davison A. J.: "Overview of classification." Human Herpesviruses: Biology, Therapy, and Immunoprophylaxis **2007,** 3–9.
23. Jordan M. C.; Jordan G. W.; Stevens J. G.; Miller G.: Latent Herpesviruses of Humans. *Ann. Intern. Med.* **1984,** 100, 866–880.
24. Mocroft A.; Youle M.; Gazzard B.; Morcinek J.; Halai R.; Phillips A. N.: Anti-herpesvirus treatment and risk of Kaposi's sarcoma in HIV infection. Royal Free/Chelsea and Westminster Hospitals Collaborative Group. *AIDS* **1996,** 10, 1101–1105.
25. Zuckerman A. J.; Banatvala J. E.; Schoub B. D.; Griffiths P. D.; Mortimer P.; Mahy W. J.: *Principles and Practice of Clinical Virology.* Chichester, UK: John Wiley & Sons, Ltd, **2009**.
26. Uldrick T. S.; Whitby D.: Update on KSHV epidemiology, Kaposi Sarcoma pathogenesis, and treatment of Kaposi Sarcoma. *Cancer Lett.* **2011,** 305, 150–162.
27. Mesri E. A.; Cesarman E.; Boshoff C.: Kaposi's sarcoma and its associated herpesvirus. *Nat. Rev. Cancer* **2010,** 10, 707–719.
28. Schulz T. F.; Cesarman E.: Editorial overview: Viruses and cancer: How tumor viruses affect the cellular genome. *Curr. Opin. Virol.* **2017,** 26, vi–vii.

29. Kaposi M.: Idiopathisches multiples Pigmentsarkom der Haut. *Arch. f. Dermat.* **1872,** 4, 265–273.
30. Mallery S. R.; Pei P.; Landwehr D. J.; Clark C. M.; Bradburn J. E.; Ness G. M.; Robertson F. M.: Implications for oxidative and nitrative stress in the pathogenesis of AIDS-related Kaposi's sarcoma. *Carcinogenesis* **2004,** 25, 597–603.
31. Pyakurel P.; Pak F.; Mwakigonja A. R.; Kaaya E.; Biberfeld P.: KSHV/HHV-8 and HIV infection in Kaposi's sarcoma development. *Infect. Agents Cancer* **2007,** 2, doi:10.1186/1750-9378-2-4.
32. Cesarman E.; Damania B.; Krown S. E.; Martin J.; Bower M.; Whitby D.: Kaposi sarcoma. *Nat. Rev. Dis. Primers* **2019,** 5, doi:10.1038/s41572-019-0060-9.
33. Schulz T. F.: The pleiotropic effects of Kaposi's sarcoma herpesvirus. *J. Pathol.* **2006,** 208, 187–198.
34. Jakob L.; Metzler G.; Chen K.-M.; Garbe C.: Non-AIDS associated Kaposi's sarcoma: clinical features and treatment outcome. *PloS one* **2011,** 6, e18397.
35. Dittmer D.; Lagunoff M.; Renne R.; Staskus K.; Haase A.; Ganem D.: A Cluster of Latently Expressed Genes in Kaposi's Sarcoma-Associated Herpesvirus. *J. Virol.* **1998,** 72, 8309–8315.
36. Yan L.; Majerciak V.; Zheng Z.-M.; Lan K.: Towards Better Understanding of KSHV Life Cycle: from Transcription and Posttranscriptional Regulations to Pathogenesis. *Virol. Sin.* **2019,** 34, 135–161.
37. Ballestas M. E.; Chatis P. A.; Kaye K. M.: Efficient persistence of extrachromosomal KSHV DNA mediated by latency- associated nuclear antigen. *Science* **1999,** 284, 641–644.
38. Rainbow L.; Platt G. M.; Simpson G. R.; Sarid R.; Gao S. J.; Stoiber H., et al.: The 222- to 234-kilodalton latent nuclear protein (LNA) of Kaposi's sarcoma-associated herpesvirus (human herpesvirus 8) is encoded by orf73 and is a component of the latency-associated nuclear antigen. *J. Virol.* **1997,** 71, 5915–5921.
39. Verma S. C.; Lan K.; Robertson E.: Structure and function of latency-associated nuclear antigen. *Curr. Top. Microbiol. Immunol.* **2007,** 312, 101–136.
40. Hellert J.; Weidner-Glunde M.; Krausze J.; Lünsdorf H.; Ritter C.; Schulz T. F.; Lührs T.: The 3D structure of Kaposi sarcoma herpesvirus LANA C-terminal domain bound to DNA. *Proc. Natl. Acad. Sci. U.S.A.* **2015,** 112, 6694–6699.
41. Kirsch P.; Jakob V.; Oberhausen K.; Stein S. C.; Cucarro I.; Schulz T. F.; Empting M.: Fragment-Based Discovery of a Qualified Hit Targeting the Latency-Associated Nuclear

Antigen of the Oncogenic Kaposi's Sarcoma-Associated Herpesvirus/Human Herpesvirus 8. *J. Med. Chem.* **2019,** 62, 3924–3939.

42. Juillard F.; Tan M.; Li S.; Kaye K. M.: Kaposi's Sarcoma Herpesvirus Genome Persistence. *Front. Microbiol.* **2016,** 7, doi:10.3389/fmicb.2016.01149.
43. Uppal T.; Banerjee S.; Sun Z.; Verma S. C.; Robertson E. S.: KSHV LANA--the master regulator of KSHV latency. *Viruses* **2014,** 6, 4961–4998.
44. Hu J.; Garber A. C.; Renne R.: The latency-associated nuclear antigen of Kaposi's sarcoma-associated herpesvirus supports latent DNA replication in dividing cells. *J. Virol.* **2002,** 76, 11677–11687.
45. Ballestas M. E.; Kaye K. M.: The latency-associated nuclear antigen, a multifunctional protein central to Kaposi's sarcoma-associated herpesvirus latency. *Future Microbiol.* **2011,** 6, 1399–1413.
46. Rawlins D. R.; Milman G.; Hayward S. D.; Hayward G. S.: Sequence-specific DNA binding of the Epstein-Barr virus nuclear antigen (EBNA-1) to clustered sites in the plasmid maintenance region. *Cell* **1985,** 42, 859–868.
47. Hegde R. S.: The papillomavirus E2 proteins: structure, function, and biology. *Annu. Rev. Biophys. Biomol. Struct.* **2002,** 31, 343–360.
48. Liu, M. U. Y. A., Yang, H.; Wanner B.: The Product of the Pleiotropic Escherichia coli Gene csrA Modulates Glycogen Biosynthesis via Effects on mRNA Stability. *J. Bacteriol.* **1995,** 177, 2663–2672.
49. Liu M. Y.; Gui G.; Wei B.; Preston J. F.; Oakford L.; Yüksel U., et al.: The RNA molecule CsrB binds to the global regulatory protein CsrA and antagonizes its activity in Escherichia coli. *J. Biol. Chem.* **1997,** 272, 17502–17510.
50. Irie Y.; Starkey M.; Edwards A. N.; Wozniak D. J.; Romeo T.; Parsek M. R.: Pseudomonas aeruginosa biofilm matrix polysaccharide Psl is regulated transcriptionally by RpoS and post-transcriptionally by RsmA. *Mol. Microbiol.* **2010,** 78, 158–172.
51. Romeo T.: Global regulation by the small RNA-binding protein CsrA and the non-coding RNA molecule CsrB. *Mol. Microbiol.* **1998,** 29, 1321–1330.
52. Dubey A. K.; Baker C. S.; Suzuki K.; Jones A. D.; Pandit P.; Romeo T.; Babitzke P.: CsrA regulates translation of the Escherichia coli carbon starvation gene, cstA, by blocking ribosome access to the cstA transcript. *J. Bacteriol.* **2003,** 185, 4450–4460.
53. Dubey A. K.; Baker C. S.; Romeo T.; Babitzke P.: RNA sequence and secondary structure participate in high-affinity CsrA-RNA interaction. *RNA* **2005,** 11, 1579–1587.

54. Heeb S.; Kuehne S. A.; Bycroft M.; Crivii S.; Allen M. D.; Haas D., et al.: Functional analysis of the post-transcriptional regulator RsmA reveals a novel RNA-binding site. *J. Mol. Biol.* **2006,** 355, 1026–1036.
55. Schubert M.; Lapouge K.; Duss O.; Oberstrass F. C.; Jelesarov I.; Haas D.; Allain F. H.-T.: Molecular basis of messenger RNA recognition by the specific bacterial repressing clamp RsmA/CsrA. *Nat. Struct. Mol. Biol.* **2007,** 14, 807–813.
56. Heroven A. K.; Böhme K.; Dersch P.: The Csr/Rsm system of Yersinia and related pathogens: a post-transcriptional strategy for managing virulence. *RNA Biol.* **2012,** 9, 379–391.
57. White D.; Hart A. E.; Romeo T.: Phylogenetic distribution of the global regulatory gene csrA among eubacteria. *Gene* **1996,** 182, 221–223.
58. Gutiérrez P.; Li Y.; Osborne M. J.; Pomerantseva E.; Liu Q.; Gehring K.: Solution structure of the carbon storage regulator protein CsrA from Escherichia coli. *J. Bacteriol.* **2005,** 187, 3496–3501.
59. Mercante J.; Suzuki K.; Cheng X.; Babitzke P.; Romeo T.: Comprehensive Alanine-scanning Mutagenesis of Escherichia coli CsrA Defines Two Subdomains of Critical Functional Importance. *J. Biol. Chem.* **2006,** 281, 31832–31842.
60. Mulcahy H.; O'Callaghan J.; O'Grady E. P.; Maciá M. D.; Borrell N.; Gómez C., et al.: Pseudomonas aeruginosa RsmA plays an important role during murine infection by influencing colonization, virulence, persistence, and pulmonary inflammation. *Infect. Immun.* **2008,** 76, 632–638.
61. Barnard F. M.; Loughlin M. F.; Fainberg H. P.; Messenger M. P.; Ussery D. W.; Williams P.; Jenks P. J.: Global regulation of virulence and the stress response by CsrA in the highly adapted human gastric pathogen Helicobacter pylori. *Mol. Microbiol.* **2004,** 51, 15–32.
62. Sabnis N. A.; Yang H.; Romeo T.: Pleiotropic regulation of central carbohydrate metabolism in Escherichia coli via the gene csrA. *J. Biol. Chem.* **1995,** 270, 29096–29104.
63. Sobrero P. M.; Valverde C.: Comparative Genomics and Evolutionary Analysis of RNA-Binding Proteins of the CsrA Family in the Genus Pseudomonas. *Front. Mol. Biosci.* **2020,** 7, doi:10.3389/fmolb.2020.00127.
64. Yakhnin H.; Pandit P.; Petty T. J.; Baker C. S.; Romeo T.; Babitzke P.: CsrA of Bacillus subtilis regulates translation initiation of the gene encoding the flagellin protein (hag) by blocking ribosome binding. *Mol. Microbiol.* **2007,** 64, 1605–1620.

65. Heurlier K.; Williams F.; Heeb S.; Dormond C.; Pessi G.; Singer D., et al.: Positive control of swarming, rhamnolipid synthesis, and lipase production by the posttranscriptional RsmA/RsmZ system in Pseudomonas aeruginosa PAO1. *J. Bacteriol.* **2004,** 186, 2936–2945.
66. Wei B. L.; Brun-Zinkernagel A.-M.; Simecka J. W.; Prüß B. M.; Babitzke P.; Romeo T.: Positive regulation of motility and flhDC expression by the RNAbinding protein CsrA of Escherichia coli. *Mol. Microbiol.* **2001,** 40, 245-256.
67. Fahrner K. A.; Berg H. C.: Mutations That Stimulate flhDC Expression in Escherichia coli K-12. *J. Bacteriol.* **2015,** 197, 3087–3096.
68. Ottemann K. M.; Miller J. F.: Roles for motility in bacterial-host interactions. *Mol. Microbiol.* **1997,** 24, 1109–1117.
69. Pourciau C.; Lai Y.-J.; Gorelik M.; Babitzke P.; Romeo T.: Diverse Mechanisms and Circuitry for Global Regulation by the RNA-Binding Protein CsrA. *Front. Microbiol.* **2020,** 11, doi:10.3389/fmicb.2020.601352.
70. Baker C. S.; Morozov I.; Suzuki K.; Romeo T.; Babitzke P.: CsrA regulates glycogen biosynthesis by preventing translation of glgC in Escherichia coli. *Mol. Microbiol.* **2002,** 44, 1599–1610.
71. Preiss J.; Romeo T.: Molecular Biology and Regulatory Aspects of Glycogen Biosynthesis in Bacteria: Progress in Nucleic Acid Research and Molecular Biology, 299–329.
72. Romeo, T., Gong, M. I. N.; Liu, M. U. Y. A.: Identification and Molecular Characterization of csrA , a Pleiotropic Gene from Escherichia coli That Affects Glycogen Biosynthesis , Gluconeogenesis , Cell Size , and Surface Properties. *J. Bacteriol.* **1993,** 175, 4744-4755.
73. Kleinermanns K.; Dorfmüller T.; Bergmann L.; Schaefer C.: *Gase, Nanosysteme, Flüssigkeiten.* Berlin: de Gruyter, **2006**.
74. Perrin F.: Polarisation de la lumière de fluorescence. Vie moyenne des molécules dans l'etat excité. *J. Phys. Radium* **1926,** 7, 390–401.
75. Laurence D. J. R.: A Study of the Adsorption of Dyes on Bovine Serum Albumin by the Method of Polarization of Fluorescence. *Biochem. J.* **1952,** 51, 168–180.
76. Bolger R.; Wiese T. E.; Ervin K.; Nestich S.; Checovich W.: Rapid Screening of Environmental Chemicals for Estrogen Receptor Binding Capacity. *Environ. Health Perspect.* **1998,** 106, 551–557.

77. Knight S. M. G.; Umezawa N.; Lee H.-S.; Gellman S. H.; Kay B. K.: A fluorescence polarization assay for the identification of inhibitors of the p53-DM2 protein-protein interaction. *Anal. Biochem.* **2002,** 300, 230–236.
78. Wu; P.; Brasseur M.; Schindler U.: A High-Throughput STAT Binding Assay Using Fluorescence Polarization. *Anal. Biochem.* **1997,** 249, 26–36.
79. James R. Lundblad, Megan Laurance, and Richard H. Goodman: Fluorescence Polarization Analysis of Protein-DNA and Protein-Protein Interactions. *Mol. Endo.* **1996,** 10, 607–612.
80. Nikolovska-Coleska Z.; Wang R.; Fang X.; Pan H.; Tomita Y.; Li P., et al.: Development and optimization of a binding assay for the XIAP BIR3 domain using fluorescence polarization. *Anal. Biochem.* **2004,** 332, 261–273.
81. Penniston J. T.: Fluorescence Polarization Measurement of Binding of Fluorescein to Albumin. *Exp. Eye Res.* **1982,** 35, 435–443.
82. Lea W. A.; Simeonov A.: Fluorescence polarization assays in small molecule screening. *Expert Opin. Drug Discov.* **2011,** 6, 17–32.
83. Jameson D. M.; Croney J. C.: Fluorescence polarization: past, present and future. *Comb. Chem. High Throughput Screen.* **2003,** 6, 167–173.
84. Weber G.: Polarization of the Fluorescence of Macromolecules. *Biochem.* **1952,** 51, 145–155.
85. Weigert F.: Über die spezifische Wirkung der polarisierten Strahlung. *Ann. Phys.* **1920,** 24, 681–725.
86. Huang X.: Fluorescence polarization competition assay: the range of resolvable inhibitor potency is limited by the affinity of the fluorescent ligand. *J. Biomol. Screen.* **2003,** 8, 34–38.
87. Roehrl M. H. A.; Wang J. Y.; Wagner G.: A general framework for development and data analysis of competitive high-throughput screens for small-molecule inhibitors of protein-protein interactions by fluorescence polarization. *Biochemistry* **2004,** 43, 16056–16066.
88. Kim J.; Felts S.; Llauger L.; He H.; Huezo H.; Rosen N.; Chiosis G.: Development of a fluorescence polarization assay for the molecular chaperone Hsp90. *J. Biomol. Screen.* **2004,** 9, 375–381.
89. Takahashi T. T.; Austin R. J.; Roberts R. W.: mRNA display: ligand discovery, interaction analysis and beyond. *Trends Biochem. Sci.* **2003,** 28, 159–165.
90. Hanes J.; Plückthun A.: In vitro selection and evolution of functional proteins by using ribosome display. *Proc. Natl. Acad. Sci.* **1997,** 94, 4937–4942.

91. Odegrip R.; Coomber D.; Eldrigde B.; Hederer R.; Kuhlman P. A.; Ullman C., et al.: CIS display: In vitro selection of peptides from libraries of protein–DNA complexes. *Proc. Natl. Acad. Sci. U.S.A.* **2004,** 101, 2806–2810.
92. Ullman C. G.; Frigotto L.; Cooley R. N.: In vitro methods for peptide display and their applications. *Brief. Funct. Genom.* **2011,** 10, 125–134.
93. Colwill K.; Gräslund S.: A roadmap to generate renewable protein binders to the human proteome. *Nat. Methods* **2011,** 8, 551–558.
94. Wu C.-H.; Liu I.-J.; Lu R.-M.; Wu H.-C.: Advancement and applications of peptide phage display technology in biomedical science. *J. Biomed. Sci.* **2016,** 23, doi:10.1186/s12929-016-0223-x.
95. Hammers C. M.; Stanley J. R.: Antibody phage display: technique and applications. *J. Investig. Dermatol.* **2014,** 134, 1–5.
96. Smith G. P.: Filamentous fusion phage: novel expression vectors that display cloned antigens on the virion surface. *Science* **1985,** 228, 1315–1317.
97. Barderas R.; Benito-Peña E.: The 2018 Nobel Prize in Chemistry: phage display of peptides and antibodies. *Anal. Bioanal. Chem.* **2019,** 411, 2475–2479.
98. Kügler J.; Zantow J.; Meyer T.; Hust M.: Oligopeptide m13 phage display in pathogen research. *Viruses* **2013,** 5, 2531–2545.
99. Danner S.; Belasco J. G.: T7 phage display: A novel genetic selection system for cloning RNA-binding proteins from cDNA libraries. *Proc. Natl. Acad. Sci. U.S.A.* **2001,** 98, 12954–12959.
100. Beghetto E.; Gargano N.: Antigen discovery using whole-genome phage display libraries. *Methods Mol. Biol.* **2013,** 1061, 79–95.
101. Løset G. Å.; Roos N.; Bogen B.; Sandlie I.: Expanding the versatility of phage display II: improved affinity selection of folded domains on protein VII and IX of the filamentous phage. *PloS one* **2011,** 6, e17433.
102. Hust M.; Dübel S.: Phage display vectors for the in vitro generation of human antibody fragments. *Methods Mol. Biol.* **2005,** 295, 71–96.
103. Christen P.; Jaussi R.; Benoit R.: Gentechnik. In Christen P.; Jaussi R.; Benoit R. (eds): Biochemie und Molekularbiologie. Eine Einführung in 40 Lerneinheiten. Berlin, Heidelberg: Springer Spektrum, **2016,** 501–517.
104. Cwirla S. E.; Peters E. A.; Barrett R. W.; Dower W. J.: Peptides on phage: a vast library of peptides for identifying ligands. *Proc. Natl. Acad. Sci.* **1990,** 87, 6378–6382.

105. Hust M.; Toleikis L.; Dbel S.: Selection Strategies II: Antibody Phage Display. In Dübel S. (ed): Handbook of therapeutic antibodies. Weinheim: Wiley-VCH, **2007,** 45–68.

106. Jakob V.; Helmsing S.; Hust M.; Empting M.: Restriction-Free Construction of a Phage-Presented Very Short Macrocyclic Peptide Library. *Methods Mol. Biol.* **2020,** 2070, 95–113.

107. Smith G. P.; Scott J. K.: Libraries of Peptides and Proteins Displayed on Filamentous Phage. *Methods Enzymol.* **1993,** 217, 228–257.

108. Qi H.; Lu H.; Qiu H.-J.; Petrenko V.; Liu A.: Phagemid vectors for phage display: properties, characteristics and construction. *J. Mol. Biol.* **2012,** 417, 129–143.

109. Kügler J.; Wilke S.; Meier D.; Tomszak F.; Frenzel A.; Schirrmann T., et al.: Generation and analysis of the improved human HAL9/10 antibody phage display libraries. *BMC Biotechnol.* **2015,** 15, doi:10.1186/s12896-015-0125-0.

110. Parmley S. F.; Smith G. P.: Antibody-selectable filamentous fd phage vectors: affinity purification of target genes. *Gene* **1988,** 73, 305–318.

111. Meyer T.; Schirrmann T.; Frenzel A.; Miethe S.; Stratmann-Selke J.; Gerlach G. F., et al.: Identification of immunogenic proteins and generation of antibodies against Salmonella Typhimurium using phage display. *BMC Biotechnol.* **2012,** 12, doi:10.1186/1472-6750-12-29.

112. Viera J.; Messing J.: Production of Single-Stranded Plasmid DNA. In Wu R.; Grossman L.; Moldave K. (eds): Recombinant DNA Methodology. Burlington: Elsevier Science, **2014,** 225–233.

113. Russo G.; Meier D.; Helmsing S.; Wenzel E.; Oberle F.; Frenzel A.; Hust M.: Parallelized Antibody Selection in Microtiter Plates. *Methods Mol. Biol.* **2018,** 1701, 273–284.

114. Rebollo I. R.; Angelini A.; Heinis C.: Phage display libraries of differently sized bicyclic peptides. *Med. Chem. Commun.* **2013,** 4, 145–150.

115. Dübel S. (ed): *Handbook of therapeutic antibodies.* Weinheim: Wiley-VCH **2007**.

116. Bird R. E.; Hardman K. D.; Jacobson J. W.; Johnson S.; Kaufman B. M.; Lee S.-M., et al.: Single-Chain Antigen-Binding Proteins. *Science* **1988,** 242, 423–426.

117. Bird R. E.; Walker B. W.: Single chain antibody variable regions. *Trends Biotechnol.* **1991,** 9, 132–137.

118. Molek P.; Strukelj B.; Bratkovic T.: Peptide phage display as a tool for drug discovery: targeting membrane receptors. *Molecules* **2011,** 16, 857–887.

119. Heinis C.; Rutherford T.; Freund S.; Winter G.: Phage-encoded combinatorial chemical libraries based on bicyclic peptides. *Nat. Chem. Biol.* **2009,** 5, 502–507.

120. Baeriswyl V.; Heinis C.: Phage selection of cyclic peptide antagonists with increased stability toward intestinal proteases. *Protein Eng. Des. Sel.* **2013,** 26, 81–89.

121. Hellert J.; Weidner-Glunde M.; Krausze J.; Richter U.; Adler H.; Fedorov R., et al.: A structural basis for BRD2/4-mediated host chromatin interaction and oligomer assembly of Kaposi sarcoma-associated herpesvirus and murine gammaherpesvirus LANA proteins. *PLOS Pathog.* **2013,** 9, e1003640.

122. Kirsch P.; Stein S. C.; Berwanger A.; Rinkes J.; Jakob V.; Schulz T. F.; Empting M.: Hit-to-lead optimization of a latency-associated nuclear antigen inhibitor against Kaposi's sarcoma-associated herpesvirus infections. *Eur. J. Med. Chem.* **2020,** 202, doi:10.1016/j.ejmech.2020.112525.

123. Kirsch P.; Jakob V.; Elgaher W. A. M.; Walt C.; Oberhausen K.; Schulz T. F.; Empting M.: Discovery of Novel Latency-Associated Nuclear Antigen Inhibitors as Antiviral Agents Against Kaposi's Sarcoma-Associated Herpesvirus. *ACS Chem. Biol.* **2020,** 15, 388–395.

124. Zhang J.-H.; Chung T. D. Y.; Oldenburg K. R.: A Simple Statistical Parameter for Use in Evaluation and Validation of High Throughput Screening Assays. *J. Biomol. Screen.* **1999,** 4, 67–73.

125. Valkov E.; Sharpe T.; Marsh M.; Greive S.; Hyvönen M.: Targeting protein-protein interactions and fragment-based drug discovery. *Top. Curr. Chem.* **2012,** 317, 145–179.

126. Lipinski C. A.: Rule of five in 2015 and beyond: Target and ligand structural limitations, ligand chemistry structure and drug discovery project decisions. *Adv. Drug Deliv. Rev.* **2016,** 101, 34–41.

127. Pei H.; Peng Y.; Zhao Q.; Chen Y.: Small molecule PROTACs: an emerging technology for targeted therapy in drug discovery. *RSC Adv.* **2019,** 9, 16967–16976.

128. Konstantinidou M.; Li J.; Zhang B.; Wang Z.; Shaabani S.; Brake F. ter, et al.: PROTACs- a game-changing technology. *Expert Opin. Drug Discov.* **2019,** 14, 1255–1268.

129. Fu C.; Donovan W. P.; Shikapwashya-Hasser O.; Ye X.; Cole R. H.: Hot Fusion: an efficient method to clone multiple DNA fragments as well as inverted repeats without ligase. *PloS one* **2014,** 9, e115318.

130. Diderich P.; Heinis C.: Phage selection of bicyclic peptides binding Her2. *Tetrahedron* **2014,** 70, 7733–7739.

131. Santos G. B.; Ganesan A.; Emery F. S.: Oral Administration of Peptide-Based Drugs: Beyond Lipinski's Rule. *ChemMedChem* **2016,** 11, 2245–2251.

132. Appendino G.; Bacchiega S.; Minassi A.; Cascio M. G.; De Petrocellis L.; Di Marzo V.: The 1,2,3-Triazole Ring as a Peptido- and Olefinomimetic Element: Discovery of Click Vanilloids and Cannabinoids. *Angew. Chem.* **2007,** 119, 9472–9475.

133. Jiang X.; Hao X.; Jing L.; Wu G.; Kang D.; Liu X.; Zhan P.: Recent applications of click chemistry in drug discovery. *Expert Opin. Drug Discov.* **2019,** 14, 779–789.

134. Roice M.; Johannsen I.; Meldal M.: High Capacity Poly(ethylene glycol) Based Amino Polymers for Peptide and Organic Synthesis. *QSAR Comb. Sci.* **2004,** 23, 662–673.

135. Empting M.; Avrutina O.; Meusinger R.; Fabritz S.; Reinwarth M.; Biesalski M., et al.: "Triazole bridge": disulfide-bond replacement by ruthenium-catalyzed formation of 1,5-disubstituted 1,2,3-triazoles. *Angew. Chem. Int. Ed.* **2011,** 50, 5207–5211.

136. White A. M.; Veer S. J. de; Wu G.; Harvey P. J.; Yap K.; King G. J., et al.: Application and Structural Analysis of Triazole-Bridged Disulfide Mimetics in Cyclic Peptides. *Angew. Chem. Int. Ed.* **2020,** 59, 11273–11277.

137. Doak B. C.; Over B.; Giordanetto F.; Kihlberg J.: Oral druggable space beyond the rule of 5: insights from drugs and clinical candidates. *Chem. Biol.* **2014,** 21, 1115–1142.

138. Liu M.; Li X.; Xie Z.; Xie C.; Zhan C.; Hu X., et al.: D-Peptides as Recognition Molecules and Therapeutic Agents. *Chem. Rec.* **2016,** 16, 1772–1786.

139. Krieger E.; Koraimann G.; Vriend G.: Increasing the precision of comparative models with YASARA NOVA--a self-parameterizing force field. *Proteins* **2002,** 47, 393–402.

7 Appendix

7.1 Supporting Information Chapter A

SUPPORTING INFORMATION

Fragment-based discovery of a qualified hit targeting the Latency-associated Nuclear Antigen of the oncogenic Kaposi's Sarcoma-associated Herpesvirus/Human Herpesvirus 8

Philine Kirsch†[1,2,3], Valentin Jakob[1,2], Kevin Oberhausen[1,2], Saskia C. Stein[3,4], Ivano Cucarro[1,2], Thomas F. Schulz[3,4], Martin Empting[1,2,3*]

[1]Helmholtz-Institute for Pharmaceutical Research Saarland (HIPS)-Helmholtz Centre for Infection Research (HZI), Department of Drug Design and Optimization (DDOP), Campus E8.1, 66123 Saarbrücken, Germany

[2]Department of Pharmacy, Saarland University, Campus E8.1, 66123 Saarbrücken, Germany

[3]German Centre for Infection Research (DZIF), Partner Site Hannover-Braunschweig, Saarbrücken, Germany

[4]Institute of Virology, Hannover Medical School, Carl-Neuberg-Strasse 1, 30625 Hannover, Germany

Contents

1. Materials and Methods

1.1. Chemistry

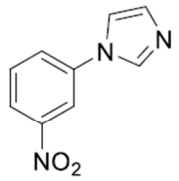

1-(3-nitrophenyl)-1*H*-imidazole

1-(3-nitrophenyl)-1*H*-imidazole (3): 3 was prepared according to general procedure I using 3-bromo–nitrobenzene (150 mg, 0.74 mmol), K_2CO_3 (122 mg, 0.89 mmol), CuCl (7.0 mg, 0.04 mmol), 1*H*-imidazole (73 mg, 0.89 mmol) and DMF (5 mL). Additionally, *N*1,*N*2-dimethylethane-1,2-diamine (13 mg, 0.08 mmol) was added and the reaction mixture was heated up to 150 °C in a crimp vial. The obtained crude was purified by column chromatography (PE:EE 1:9) to yield the title compound (45 mg, 0.23 mmol, 31 %) ^{1}H NMR (300 MHz, DMSO-d_6) δ ppm 7.32 (m, J = 8.75 Hz, 2 H) 7.75 (m, J = 8.75 Hz, 2 H) 7.84 - 7.96 (m, 1 H) 8.23 (t, J = 1.72 Hz, 1 H) 9.70 (t, J = 1.35 Hz, 1 H); ^{13}C NMR (75 MHz, DMSO-d_6) δ ppm 119.72, 120.43, 120.59, 121.03, 123.40, 134.25, 139.41, 140.05.

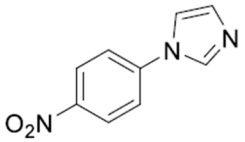

1-(4-nitrophenyl)-1*H*-imidazole

1-(4-nitrophenyl)-1*H*-imidazole (4): 4 was prepared according to general procedure I using 4-iodo–nitrobenzene (150 mg, 0.60 mmol), K_2CO_3 (99 mg, 0.72 mmol), CuCl (7.0 mg, 0.06 mmol), 1*H*-imidazole (73 mg, 0.89 mmol) and DMF (5 mL). Additionally, *N*1,*N*2-dimethylethane-1,2-diamine (19 mg, 0.12 mmol) was added. The obtained crude was purified by column chromatography (PE:EE 1:9) to yield the title compound (60 mg, 0.31 mmol, 52%) ^{1}H NMR (300 MHz, DMSO-d_6) δ ppm 7.18 (s, 1 H) 7.86 - 8.02 (m, 3 H) 8.24 - 8.45 (m, 2 H) 8.50 (s, 1 H); ^{13}C NMR (75 MHz, DMSO-d_6) δ ppm 117.86, 120.37, 125.50, 130.78, 136.03, 141.67, 145.27.

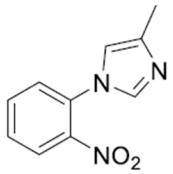

4-methyl-1-(2-nitrophenyl)-1*H*-imidazole

4-methyl-1-(2-nitrophenyl)-1*H*-imidazole (5): 5 was prepared according to general procedure I using 2-Iod–nitrobenzene (400 mg, 1.60 mmol), K_2CO_3 (263 mg, 1.90 mmol), CuI (40 mg, 0.16 mmol), 4-methyl-1*H*-imidazole (156 mg, 1.90 mmol) and DMF (12 mL). The obtained crude was purified by column chromatography (PE:EE 1:9) to yield the title compound (168 mg, 0.83 mmol, 52 %) MS (ESI^+) *m/z* 204 (M+H).

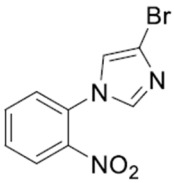

4-bromo-1-(2-nitrophenyl)-1*H*-imidazole

4-bromo-1-(2-nitrophenyl)-1*H*-imidazole (6): 6 was prepared according to general procedure I using 2-Iod–nitrobenzene (120 mg, 0.48 mmol), K_2CO_3 (79 mg, 0.57 mmol), CuI (12 mg, 0.05 mmol), 4-bromo-1*H*-imidazole (84 mg, 0.57 mmol) and DMF (4 mL). The obtained crude was purified by column chromatography (PE:EE 1:1) to yield the title compound (50 mg, 0.18 mmol, 38 %). MS (ESI^+) *m/z* 268, 270 (M+H).

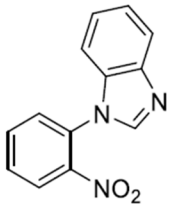

1-(2-nitrophenyl)-1*H*-benzo[*d*]imidazole

1-(2-nitrophenyl)-1*H*-benzo[*d*]imidazole (7): 7 was prepared according to general procedure I using 2-Iod–nitrobenzene (100 mg, 0.40 mmol), K_2CO_3 (66 mg, 0.48 mmol), CuI (7.5 mg, 0.04 mmol), 1*H*-benzimidazole (56 mg, 0.48 mmol) and DMF (3 mL). The obtained crude was purified by column chromatography (PE:EE 1:1) to yield the title compound (80 mg, 0.33 mmol, 82 %). MS (ESI^+) *m/z* 240 (M+H).

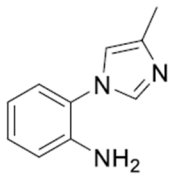

2-(4-methyl-1*H*-imidazol-1-yl)aniline

2-(4-methyl-1*H*-imidazol-1-yl)aniline (11): 11 was prepared to the general procedure II using 4-methyl-1-(2-nitrophenyl)-1*H*-imidazole **5** (100 mg, 0.49 mmol), $SnCl_2$ (553 mg, 2.46 mmol) and ethanol (10 mL). The obtained crude was purified by flash column chromatography (gradient elution, DCM:MeOH 95:5 - 90:10) to yield the target compound (53 mg, 0.30 mmol, 61%). ^{1}H NMR (300 MHz, $CDCl_3$) δ ppm 2.32 (s, 3 H) 3.70 (br. s., 2 H) 6.72 - 6.95 (m, 3 H) 7.10 (dd, *J* = 7.68, 1.26 Hz, 1 H) 7.17 - 7.26 (m, 1 H) 7.56 (br. s., 1 H); ^{13}C NMR (75 MHz, $CDCl_3$) δ ppm 15.66, 116.30, 118.55, 123.67, 125.44, 127.06, 129.58, 141.86, 142.87.

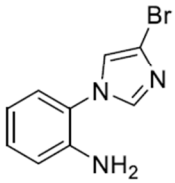

2-(4-bromo-1*H*-imidazol-1-yl)aniline

2-(4-bromo-1*H*-imidazol-1-yl)aniline (12): 12 was prepared to the general procedure II using 4-bromo-1-(2-nitrophenyl)-1*H*-imidazole **6** (50 mg, 0.19 mmol), $SnCl_2$ (209 mg, 0.93 mmol) and ethanol (7 mL). The obtained crude was purified by prep. HPLC (revered-phase, mobile phase consisting of acetonitrile containing 0.05% FA (v/v) and water containing 0.05% FA (v/v); 5:95 - 90:10) to yield the target compound (15 mg, 0.06 mmol, 31%). ^{1}H NMR (300 MHz, $CDCl_3$) δ ppm 3.73 (br. s., 2 H) 6.75 - 6.91 (m, 2 H) 7.05 - 7.16 (m, 2 H) 7.18 - 7.33 (m, 1 H) 7.52 (d, *J* = 1.49 Hz, 1 H); ^{13}C NMR (75 MHz, $CDCl_3$) δ ppm 116.19, 116.55, 118.66, 119.32, 122.49, 127.04 , 130.31, 137.37, 141.79.

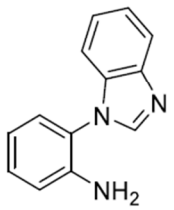

2-(1*H*-benzo[*d*]imidazol-1-yl)aniline

2-(1*H*-benzo[*d*]imidazol-1-yl)aniline (13): 13 was prepared to the general procedure II using 4-methyl-1-(2-nitrophenyl)-1*H*-imidazole **7** (80 mg, 0.33 mmol), $SnCl_2$ (350 mg, 1.56 mmol) and ethanol (10 mL). The obtained crude was purified by flash column chromatography (gradient elution, DCM:MeOH 98:2 - 9:1) to yield the target compound (32 mg, 0.15 mmol, 45 %). ^{1}H NMR (300 MHz, $CDCl^3$) δ ppm 3.65 (br. s., 2 H) 6.83 - 6.96 (m, 2 H) 7.19 (dd, *J* = 7.82, 1.49 Hz, 1 H) 7.23 - 7.39 (m, 4 H) 7.84 - 7.94 (m, 1 H) 7.97 - 8.05 (m, 1 H); ^{13}C NMR (75 MHz, $CDCl_3$) δ ppm 110.79, 116.54, 118.73, 120.50, 121.16, 122.72, 123.60, 128.18, 130.24, 133.88, 142.71, 143.23, 143.51.

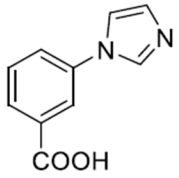

3-(1*H*-imidazol-1-yl)benzoic acid

3-(1*H*-imidazol-1-yl)benzoic acid (17): 17 was prepared according to general procedure III using 3-bromo–benzoic acid, *N*1,*N*2-dimethylethane-1,2-diamine, K_2CO_3, CuCl, 1*H*-imidazole and DMF. ^{1}H NMR (500 MHz, DMSO-d_6) δ ppm 7.13 (br. s., 1 H) 7.65 (d, *J* = 6.56 Hz, 1 H) 7.84 (br. s., 1 H) 7.91 (br. s., 2 H) 8.10 (br. s., 1 H) 8.34 (br. s., 1 H); ^{13}C NMR (126 MHz, DMSO-d_6) δ ppm 118.18, 120.78, 124.62, 127.57, 130.14, 130.25, 135.77, 137.15, 166.64.

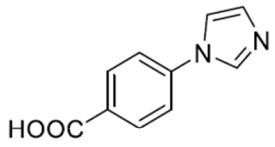

4-(1*H*-imidazol-1-yl)benzoic acid

4-(1*H*-imidazol-1-yl)benzoic acid (18): 18 was prepared according to general procedure III using 4-bromo–benzoic acid, *N*1,*N*2-dimethylethane-1,2-diamine, K_2CO_3, CuCl, 1*H*-imidazole and DMF. ^{1}H NMR (500 MHz, DMSO-d_6) δ ppm 7.15 (br. s., 1 H) 7.81 (br. s., 2 H) 7.87 (br. s., 1 H) 8.05 (br. s., 2 H) 8.40 (br. s., 1 H); ^{13}C NMR (126 MHz, DMSO-d_6) δ ppm 117.66, 119.63, 130.22, 130.92, 135.55, 139.91, 166.42.

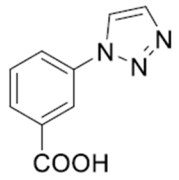

3-(1*H*-1,2,3-triazol-1-yl)benzoic acid

3-(1*H*-1,2,3-triazol-1-yl)benzoic acid (27): 27 was synthesized according to procedure IV using 3-azidobenzoic acid and ethynyltrimethylsilane as starting material.^{1}H NMR (500 MHz, DMSO-d_6) δ ppm 7.74 (d, *J* = 6.26 Hz, 1 H) 8.04 (s, 1 H) 8.01 (s, 1 H) 8.18 (br. s., 1 H) 8.42 (br. s., 1 H) 8.97 (br. s., 1 H) 13.43 (br. s., 1 H); ^{13}C NMR (126 MHz, DMSO-d_6) δ ppm 120.52, 123.45, 124.22, 129.16, 130.39, 134.68, 136.86, 166.39.

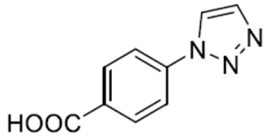

4-(1*H*-1,2,3-triazol-1-yl)benzoic acid

4-(1*H*-1,2,3-triazol-1-yl)benzoic acid (28): 28 was synthesized according to procedure IV using 4-azidobenzoic acid and ethynyltrimethylsilane as starting material. ^{1}H NMR (500 MHz, DMSO-d_6) δ ppm 8.03 (br. s., 1 H) 8.07 (br. s., 2 H) 8.14 (br. s., 2 H) 8.96 (br. s., 1 H); ^{13}C NMR (126 MHz, DMSO-d_6) δ ppm 119.86, 123.43, 131.09, 134.81, 139.54, 166.48.

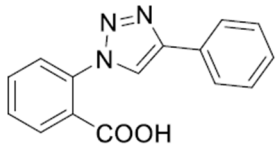

2-(4-phenyl-1*H*-1,2,3-triazol-1-yl)benzoic acid

2-(4-phenyl-1*H*-1,2,3-triazol-1-yl)benzoic acid (29): 29 was synthesized according to procedure V using 2-azidobenzoic acid **21** and ethynyl benzene as starting material. ^{1}H NMR (300 MHz, DMSO-d_6) δ ppm 7.28 - 7.41 (m, 1 H) 7.44 - 7.54 (m, 2 H) 7.64 - 7.85 (m, 3 H) 7.88 - 8.01 (m, 3 H) 9.00 (s, 1 H); ^{13}C NMR (75 MHz, DMSO-d_6) δ ppm 123.00, 125.20, 126.48, 128.04, 128.81, 128.96, 130.01, 130.44, 130.49, 132.42, 135.32, 146.33, 166.50.

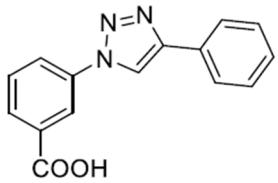

3-(4-phenyl-1*H*-1,2,3-triazol-1-yl)benzoic acid

3-(4-phenyl-1*H*-1,2,3-triazol-1-yl)benzoic acid (30): 30 was synthesized according to procedure V using 3-azidobenzoic acid **22** and ethynyl benzene as starting material. ^{1}H NMR (500 MHz, DMSO-d_6) δ ppm 4.62 (s, 2 H) 5.35 (br. s., 1 H) 7.73 (t, J = 7.86 Hz, 1 H) 8.02 (d, J = 7.78 Hz, 1 H) 8.16 (dd, J = 8.09, 1.37 Hz, 1 H) 8.41 (s, 1 H) 8.81 (s, 1 H) 13.42 (br. s., 1 H); ^{13}C NMR (75 MHz, DMSO-d_6) δ ppm 115.45, 124.36, 126. 31, 128.67, 129.21, 129.99, 131.42 131.98, 139.46, 146.56, 166.57.

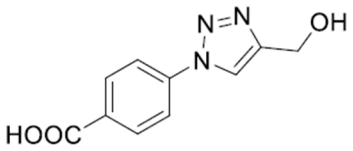

4-(4-(hydroxymethyl)-1*H*-1,2,3-triazol-1-yl)benzoic acid

4-(4-(hydroxymethyl)-1*H*-1,2,3-triazol-1-yl)benzoic acid (32): 32 was synthesized according to procedure V using 4-azidobenzoic acid and propargyl alcohol as starting material. ^{1}H NMR (300 MHz, DMSO-d_6) δ ppm 4.63 (s., 2 H) 5.37 (s., 1 H) 7.97 - 8.26 (m, 4 H) 8.80 (s, 1 H) 13.19 (br. s., 1 H); ^{13}C NMR (75 MHz, DMSO-d_6) δ ppm 55.39, 120.14, 121.59, 131.59, 140.14, 149.98, 158.70, 166.87.

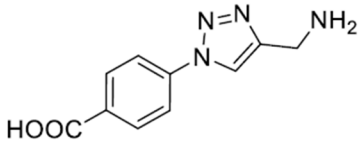

4-(4-(aminomethyl)-1*H*-1,2,3-triazol-1-yl)benzoic acid

4-(4-(aminomethyl)-1*H*-1,2,3-triazol-1-yl)benzoic acid (33): 33 was synthesized according to procedure V using 4-azidobenzoic acid and propargyl amine as starting material. ^{1}H NMR (500 MHz, DMSO-d_6) δ ppm 2.13 (s, 2 H) 5.61 (d, J = 8.54 Hz, 2 H) 5.90 (d, J = 8.55 Hz, 2 H) 6.34 (s, 1 H); ^{13}C NMR (126 MHz, DMSO-d_6) δ ppm 31.73, 118.59, 121.53, 129.20, 137.31, 138.39, 166.93.

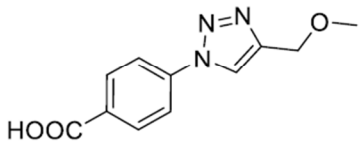

4-(4-(methoxymethyl)-1*H*-1,2,3-triazol-1-yl)benzoic acid

4-(4-(methoxymethyl)-1*H*-1,2,3-triazol-1-yl)benzoic acid (34): 34 was synthesized according to procedure V using 4-azidobenzoic acid and methyl propargyl ether as starting material. ^{1}H NMR (500 MHz, DMSO-d_6) δ ppm 3.32 (s, 3 H) 4.55 (s, 2 H) 8.06 (m, J = 7.78 Hz, 2 H) 8.13 (m, J = 8.24 Hz, 2 H) 8.84 - 9.02 (m, 1 H); ^{13}C NMR (126 MHz, DMSO-d_6) δ ppm 57.56, 64.85, 119.87, 122.38, 131.25, 139.58, 145.37, 166.39.

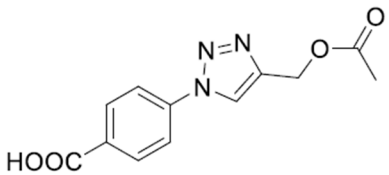

4-(4-(acetoxymethyl)-1*H*-1,2,3-triazol-1-yl)benzoic acid

4-(4-(acetoxymethyl)-1*H*-1,2,3-triazol-1-yl)benzoic acid (35): 35 was synthesized according to procedure V using 4-azidobenzoic acid and propargyl acetate as starting material. ^{1}H NMR (300 MHz, DMSO-d_6) δ ppm 2.07 (s, 3 H) 5.22 (s, 2 H) 7.98 - 8.09 (m, 2 H) 8.09 - 8.21 (m, 2 H) 8.97 (s, 1 H); ^{13}C NMR (75 MHz, DMSO-d_6) δ ppm 20.58, 56.83, 119.88, 123.03, 130.84, 131.05, 139.35, 143.47, 166.37, 170.07.

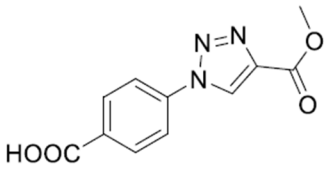

4-(4-(methoxycarbonyl)-1*H*-1,2,3-triazol-1-yl)benzoic acid

4-(4-(methoxycarbonyl)-1*H*-1,2,3-triazol-1-yl)benzoic acid (36): 36 was synthesized according to procedure V using 4-azidobenzoic acid and methyl propiolate as starting material. ^{1}H NMR (500 MHz, DMSO-d_6) δ ppm 3.91 (s., 3 H) 8.16 (br. s., 4 H) 9.65 (s., 1 H); ^{13}C NMR (126 MHz, DMSO-d_6) δ ppm 52.10, 120.43, 127.59, 131.05, 139.00, 139.78, 160.48, 166.44.

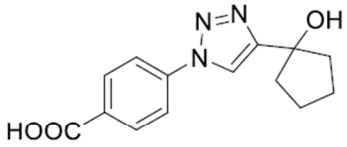

4-(4-(1-hydroxycyclopentyl)-1*H*-1,2,3-triazol-1-yl)benzoic acid

4-(4-(1-hydroxycyclopentyl)-1*H*-1,2,3-triazol-1-yl)benzoic acid (37): 37 was synthesized according to procedure V using 4-azidobenzoic acid and 1-ethynylcyclopentan-1-ol as starting material. ^{1}H NMR (500 MHz, DMSO-d_6) δ ppm 1.72 (s., 2 H) 1.86 (s., 2 H) 1.91 (d, J = 13.28 Hz, 2 H) 2.04 (s., 2 H) 5.18 (br. s., 1 H) 8.08 (s, 2 H) 8.11 (s, 2 H) 8.72 (s., 1 H) 13.27 (br. s., 1 H); ^{13}C NMR (126 MHz, DMSO-d_6) δ ppm 23.31, 40.61, 77.35, 119.58, 131.11, 139.74, 155.99, 166.47.

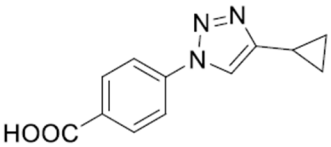

4-(4-cyclopropyl-1*H*-1,2,3-triazol-1-yl)benzoic acid

4-(4-cyclopropyl-1*H*-1,2,3-triazol-1-yl)benzoic acid (38): 38 was synthesized according to procedure V using 4-azidobenzoic acid and ethynyl cyclopropane as starting material. ^{1}H NMR (500 MHz, DMSO-d_6) δ ppm 0.81 (br. s., 2 H) 0.98 (br. s., 2 H) 1.97 - 2.12 (m, 1 H) 8.00 (s., 2 H) 8.11 (s., 2 H) 8.66 (s., 1 H) 13.18 (br. s., 1 H); ^{13}C NMR (126 MHz, DMSO-d_6) δ ppm 6.52, 7.83, 119.01, 119.22, 119.42, 130.28, 131.09, 131.25, 139.66, 150.70, 166.46.

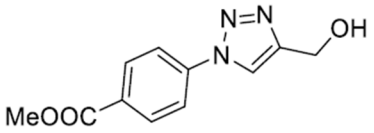

methyl 4-(4-(hydroxymethyl)-1*H*-1,2,3-triazol-1-yl)benzoate

methyl 4-(4-(hydroxymethyl)-1*H*-1,2,3-triazol-1-yl)benzoate (39): 39 was synthesized according to procedure V using methyl 4-azidobenzoate **25** and propargyl alcohol as starting material. ^{1}H NMR (500 MHz, DMSO-d_6) δ ppm 3.89 (s, 3 H) 4.62 (s, 2 H) 5.39 (br. s., 1 H) 8.05 - 8.23 (m, 4 H) 8.83 (s, 1 H); ^{13}C NMR (126 MHz, DMSO-d_6) δ ppm 52.44, 54.92, 119.76, 121.15, 129.18, 131.01, 139.94, 149.58, 165.38.

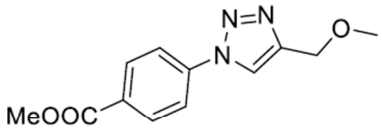

methyl 4-(4-(methoxymethyl)-1*H*-1,2,3-triazol-1-yl)benzoate

methyl 4-(4-(methoxymethyl)-1*H*-1,2,3-triazol-1-yl)benzoate (40): 40 was synthesized according to procedure V using methyl 4-azidobenzoate **25** and methyl propargyl ether as starting material. ^{1}H NMR (500 MHz, DMSO-d_6) δ ppm 3.32 (s, 3 H) 3.33 (s, 3 H) 4.56 (s, 2 H) 8.08 - 8.12 (m, 2 H) 8.14 - 8.18 (m, 2 H) 8.96 (s, 1 H); ^{13}C NMR (126 MHz, DMSO-d_6) δ ppm 52.25, 57.32, 64.62, 119.70, 122.19, 129.13, 130.82, 139.64, 145.19, 165.17.

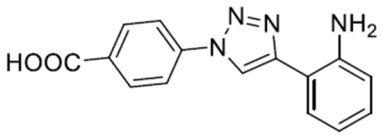

4-(4-(2-aminophenyl)-1*H*-1,2,3-triazol-1-yl)benzoic acid

4-(4-(2-aminophenyl)-1*H*-1,2,3-triazol-1-yl)benzoic acid (41): 41 was synthesized according to procedure V using 4-azidobenzoic acid and 2-ethynyl aniline as starting material. ^{1}H NMR (500 MHz, DMSO-d_6) δ ppm 6.64 (t, J = 7.02 Hz, 1 H) 6.81 (d, J = 7.78 Hz, 1 H) 7.09 (t, J = 7.40 Hz, 1 H) 7.61 (d, J = 7.63 Hz, 1 H) 8.08 - 8.31 (m, 5 H) 9.31 (s, 1 H); ^{13}C NMR (126 MHz, DMSO-d_6) δ ppm 112.15, 116.01, 119.92, 127.97, 129.05, 131.20, 139.53, 145.86, 148.34, 166.55.

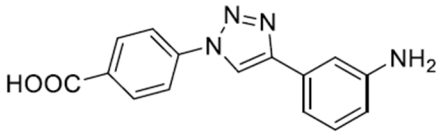

4-(4-(3-aminophenyl)-1*H*-1,2,3-triazol-1-yl)benzoic acid

4-(4-(3-aminophenyl)-1*H*-1,2,3-triazol-1-yl)benzoic acid (42): 42 was synthesized according to procedure V using 4-azidobenzoic acid and 3-ethynyl aniline as starting material. ^{1}H NMR (500 MHz, DMSO-d_6) δ ppm 5.28 (br. s., 2 H) 6.58 (s., 1 H) 7.04 (s., 1 H) 7.08 - 7.16 (m, 1 H) 7.21 (s., 1 H) 8.15 (s, 2 H) 8.11 (s, 2 H) 9.27 (s., 1 H); ^{13}C NMR (126 MHz, DMSO-d_6) δ ppm 59.78, 110.58, 113.25, 114.07, 119.21, 119.66, 129.50, 130.47, 131.16, 139.46, 148.32, 149.19, 154.19, 166.87.

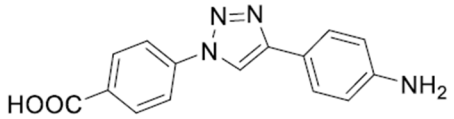

4-(4-(4-aminophenyl)-1*H*-1,2,3-triazol-1-yl)benzoic acid

4-(4-(4-aminophenyl)-1*H*-1,2,3-triazol-1-yl)benzoic acid (43): 43 was synthesized according to procedure V using 4-azidobenzoic acid and 4-ethynyl aniline as starting material. ^{1}H NMR (500 MHz, DMSO-d_6) δ ppm 6.70 (d, J = 8.24 Hz, 2 H) 7.63 (d, J = 8.39 Hz, 2 H) 8.04 - 8.10 (m, 2 H) 8.14 - 8.17 (m, 2 H) 9.14 (s, 1 H); ^{13}C NMR (126 MHz, DMSO-d_6) δ ppm 114.52, 117.32, 119.42, 119.64, 126.46, 130.30, 131.12, 139.69, 148.52, 166.44.

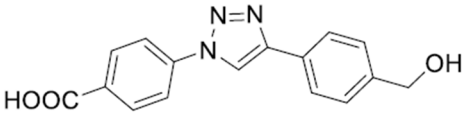

4-(4-(4-(hydroxymethyl)phenyl)-1*H*-1,2,3-triazol-1-yl)benzoic acid

4-(4-(4-(hydroxymethyl)phenyl)-1*H*-1,2,3-triazol-1-yl)benzoic acid (44): 44 was synthesized according to procedure V using 4-azidobenzoic acid and (4-ethynylphenyl) methanol as starting material. ^{1}H NMR (500 MHz, DMSO-d_6) δ ppm 4.55 (d, J = 3.51 Hz, 2 H) 5.26 (br. s., 1 H) 7.45 (m, J = 8.09 Hz, 2 H) 7.92 (m, J = 8.09 Hz, 2 H) 8.08 (d, J = 7.32 Hz, 2 H) 8.16 (d, J = 8.39 Hz, 2 H) 9.40 (s, 1 H) ^{13}C NMR (126 MHz, DMSO-d_6) δ ppm 62.63, 119.55, 125.16, 127.01, 131.07, 142.88, 147.58, 147.88, 159.71, 168.68.

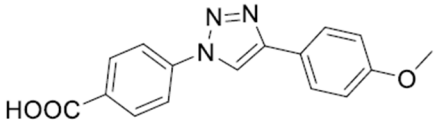

4-(4-(4-methoxyphenyl)-1*H*-1,2,3-triazol-1-yl)benzoic acid

4-(4-(4-methoxyphenyl)-1*H*-1,2,3-triazol-1-yl)benzoic acid (45): 45 was synthesized according to procedure V using 4-azidobenzoic acid and 1-ethynyl-4-methoxybenzene as starting material. ^{1}H NMR (500 MHz, DMSO-d_6) δ ppm 3.81 (s., 3 H) 7.08 (s., 2 H) 7.88 (s., 2 H) 8.10 (s., 2 H) 8.17 (s., 2 H) 9.33 (s., 1 H) 13.21 (br. s., 1 H); ^{13}C NMR (126 MHz, DMSO-d_6) δ ppm 55.23, 114.49, 118.68, 119.58, 126.79, 131.16, 139.58, 139.85, 147.55, 159.45, 166.58.

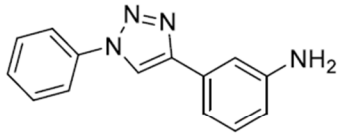

3-(1-phenyl-1*H*-1,2,3-triazol-4-yl)aniline

3-(1-phenyl-1*H*-1,2,3-triazol-4-yl)aniline (46): 46 was synthesized according to procedure V using azidobenzene **20** and 3-ethynyl aniline as starting material. ^{1}H NMR (500 MHz, DMSO-d_6) δ ppm 5.24 (br. s., 2 H) 6.50 - 6.65 (m, 1 H) 6.98 - 7.07 (m, 1 H) 7.07 - 7.17 (m, 1 H) 7.22 (t, J = 1.83 Hz, 1 H) 7.43 - 7.53 (m, 1 H) 7.58 - 7.79 (m, 2 H) 7.88 - 8.09 (m, 2 H) 9.15 (s, 1 H); ^{13}C NMR (126 MHz, DMSO-d_6) δ ppm 113.87, 114.07, 119.21, 119.66, 120.54, 128.57, 130.20, 131.16, 139.34, 148.35, 149.57.

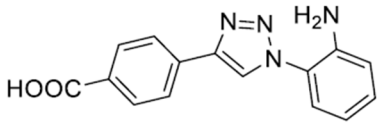

4-(1-(2-aminophenyl)-1*H*-1,2,3-triazol-4-yl)benzoic acid

4-(1-(2-aminophenyl)-1*H*-1,2,3-triazol-4-yl)benzoic acid (47): 47 was synthesized according to procedure V using 2-azido aniline **19** and 4-ethynyl benzoic acid as starting material. ^{1}H NMR (500 MHz, DMSO-d_6) δ ppm 5.48 (br. s., 2 H) 6.71 (t, J = 7.48 Hz, 1 H) 6.95 (d, J = 8.24 Hz, 1 H) 7.18 - 7.41 (m, 2 H) 7.94 - 8.17 (m, 4 H) 8.93 - 9.11 (m, 1 H) 12.99 (br. s., 1 H); ^{13}C NMR (126 MHz, DMSO-d_6) δ ppm 116.05, 116.69, 121.81, 123.73, 125.30, 125.66, 130.03, 130.24, 134.71, 142.64, 145.48, 167.06.

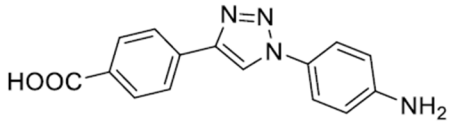

4-(1-(4-aminophenyl)-1*H*-1,2,3-triazol-4-yl)benzoic acid

4-(1-(4-aminophenyl)-1*H*-1,2,3-triazol-4-yl)benzoic acid (48): 48 was synthesized according to procedure V using 4-azido aniline and 4-ethynyl benzoic acid as starting material. ^{1}H NMR (500 MHz, DMSO-d_6) δ ppm 5.54 (br. s., 2 H) 6.72 (m, *J* = 8.54 Hz, 2 H) 7.54 (m, *J* = 8.70 Hz, 2 H) 8.04 (s, 4 H) 9.15 (s, 1 H); ^{13}C NMR (126 MHz, DMSO-d_6) δ ppm 113.81, 120.26, 121.60, 125.13, 125.76, 130.07, 134.68, 145.85, 149.57, 167.10.

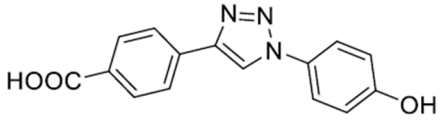

4-(1-(4-hydroxyphenyl)-1*H*-1,2,3-triazol-4-yl)benzoic acid

4-(1-(4-hydroxyphenyl)-1*H*-1,2,3-triazol-4-yl)benzoic acid (49): 49 was synthesized according to procedure V using 4-azido phenol **23** and 4-ethynyl benzoic acid as starting material. ^{1}H NMR (500 MHz, DMSO-d_6) δ ppm 6.97 (m, *J* = 8.85 Hz, 2 H) 7.72 (m, *J* = 8.70 Hz, 2 H) 8.05 (s., 4 H) 9.25 (s, 1 H); ^{13}C NMR (126 MHz, DMSO-d_6) δ ppm 116.10, 120.61, 121.96, 125.32, 128.66, 134.38, 146.13, 157.94.

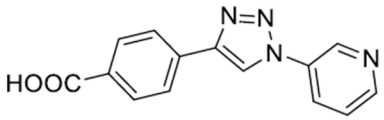

4-(1-(pyridin-3-yl)-1*H*-1,2,3-triazol-4-yl)benzoic acid

4-(1-(pyridin-3-yl)-1*H*-1,2,3-triazol-4-yl)benzoic acid (50): 50 was synthesized according to procedure V using 3-azido pyridine **24** and 4-ethynyl benzoic acid as starting material. ^{1}H NMR (500 MHz, DMSO-d_6) δ ppm 7.59 - 7.80 (m, 1 H) 8.07 (br. s., 4 H) 8.40 (d, *J* = 8.24 Hz, 1 H) 8.75 (br. s., 1 H) 9.22 (br. s., 1 H) 9.53 (s, 1 H); ^{13}C NMR (126 MHz, DMSO-d_6) δ ppm 121.17, 124.81, 125.38, 127.99, 130.24, 134.03, 141.35, 146.68, 149.94, 167.35.

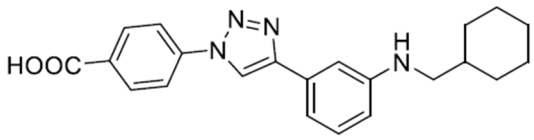

4-(4-(3-((cyclohexylmethyl)amino)phenyl)-1*H*-1,2,3-triazol-1-yl)benzoic acid

4-(4-(3-((cyclohexylmethyl)amino)phenyl)-1*H*-1,2,3-triazol-1-yl)benzoic acid (52): 52 was synthesized according to procedure VI using 4-(4-(3-aminophenyl)-1*H*-1,2,3-triazol-1-yl)benzoic acid **42** (30 mg, 0.11 mmol), cesium carbonate (107 mg, 0.33 mmol) and (bromomethyl) cyclohexane (39 mg, 0.22 mmol, 2 eq.) in DMF (5 mL). Yield: 22 mg (0.06 mmol, 54 %) ^{1}H NMR (500 MHz, $CDCl_3$) δ ppm 1.04 - 1.19 (m, 2 H) 1.20 - 1.40 (m, 4 H) 1.73 (d, *J* = 12.21 Hz, 1 H) 1.76 - 1.87 (m, 4 H) 3.81 (br. s., 1 H) 4.19 (d, *J* = 6.26 Hz, 2 H) 6.72 (dt, *J* = 7.32, 1.83 Hz, 1 H) 7.17 - 7.27 (m, 2 H) 7.36 (s, 1 H) 7.91 (d, *J* = 8.55 Hz, 2 H) 8.22 (s, 1 H) 8.24 (d, *J* = 8.54 Hz, 2 H); ^{13}C NMR (126 MHz, $CDCl_3$) δ ppm 25.69, 26.35, 29.76, 37.24, 70.51, 112.36, 115.36, 116.17, 117.27, 119.81, 129.92, 130.59, 130.81, 131.32, 140.04, 147.00, 148.90, 165.51.

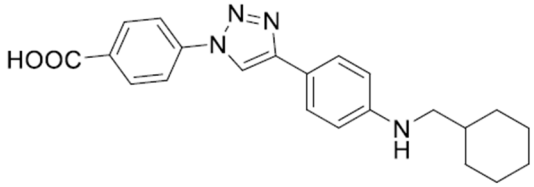

4-(4-(4-((cyclohexylmethyl)amino)phenyl)-1*H*-1,2,3-triazol-1-yl)benzoic acid

4-(4-(4-((cyclohexylmethyl)amino)phenyl)-1*H*-1,2,3-triazol-1-yl)benzoic acid (53): 53 was synthesized according to procedure VI using 4-(4-(4-aminophenyl)-1*H*-1,2,3-triazol-1-yl) benzoic acid **43** (30 mg, 0.11 mmol), cesium carbonate (107 mg, 0.33 mmol, 3 eq.) and (bromomethyl) cyclohexane (39 mg, 0.22 mmol, 2 eq.) in DMF (5 mL). Yield: 15 mg (0.04 mmol, 36 %) ^{1}H NMR (500 MHz, $CDCl_3$) δ ppm 1.10 (d, *J* = 11.90 Hz, 2 H) 1.23 - 1.37 (m, 4 H) 1.72 (d, *J* = 12.21 Hz, 1 H) 1.77 - 1.81 (m, 2 H) 1.86 (d, *J* = 11.90 Hz, 2 H) 3.83 (br. s., 1 H) 4.18 (d, *J* = 6.10 Hz, 2 H) 6.78 (m, *J* = 8.39 Hz, 2 H) 7.72 (m, *J* = 8.39 Hz, 2 H) 7.87 - 7.92 (m, 2 H) 8.12 (s, 1 H) 8.22 (d, *J* = 8.55 Hz, 2 H); ^{13}C NMR (126 MHz, $CDCl_3$) δ ppm 25.42, 26.08, 29.50, 36.98, 53.16, 70.21, 115.00, 119.43, 126.90, 131.01, 139.88, 146.67, 148.87, 165.29.

2. Biology

2.1. Expression and purification of a His-tagged oligomerization-deficient mutant of the KSHV LANA *C*-terminal DNA binding domain (DBD; aa1008-1146)

For the expression of the previous described[1] His-tagged oligomerization-deficient mutant of the KSHV LANA *C*-terminal DBD (aa1008-1146) we used the pETRO1.01 vector.

BL21 (DE3) was transformed (chemical transformation) with the plasmid pETRO1.01- LANA 1008-1146 olig-mut. An expression culture of LB-medium (Lennox) containing 100 µg/mL ampicillin was grown over night at 37 °C (200 rpm) to an OD_{600} of 3.0 was reached. Cells were harvested by centrifugation (6200 rpm, 4 °C, 20 min) and the supernatant was removed. The cells were resuspended in lysis buffer (100 mM NaH_2PO_4, 10 mM Tris-Cl, 2 mM DTT, pH 8.0) followed by cell distribution with a Microfluidizer® (Microfluides, Benchtop High-Pressure Homogenizer 25 mL) with one cycle. After removal of cellular debris by centrifugation (19000 rpm, 1 h, 4 °C) the lysate was filtered through a 0.22 µM filter. His-tagged LANA target protein was purified by Ni-NTA affinity chromatography using ÄKTAxpress (GE Healthcare). A HisTrap HP 1 mL column (GE Healthcare) was equilibrated with lysis buffer until the UV signal was stable. The lysate was applied to the column at 1 mL/min, washed with a linear washing gradient (2.5 mL/min) starting from 100% lysis buffer to 100% wash buffer (100 mM NaH_2PO_4, 10 mM Tris-Cl, 2 mM DTT, 500 mM imidazole, pH 8.0). Subsequently the target protein was eluted (2.5 mL/min) with elution buffer (100 mM NaH_2PO_4, 10 mM Tris-Cl, 2 mM DTT, 1000 mM imidazole, pH 5.8). The buffer in the protein containing fractions was exchanged to storage buffer (20 mM Bis-Tris-Cl, 300 mM NaCl, 2 mM DTT, pH 6,5) using a PD10 column (GE Healthcare) and concentrated via centrifugal filtration using Vivaspin 20 columns (MWCO 10,000 Da, Sartorius).

2.2. Expression and purification of a GST-tagged KSHV LANA *C*-terminal domain (CTD; aa934-1162)

The expression and purification of the GST-tagged KSHV LANA C-terminal domain (CTD; aa934-1162) was described previously and the protocol was adopted.[2]

2.3. SPR-based Screening

In total 720 library compounds were tested in SPR-based screening using constant concentrations of 500 µM of each compound. Compounds which showed a response higher than 9 RU were selected from the first screening which resulted in 52 compounds.

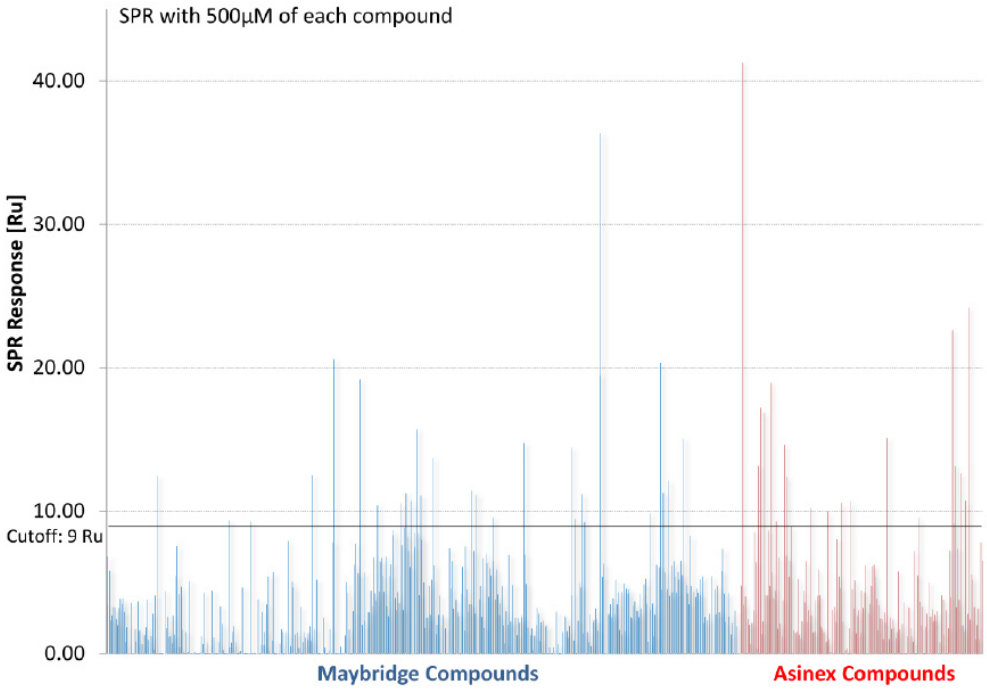

Figure S1: Results of SPR based screening of compounds from the Maybridge library (blue) and compounds from the Asinex library (red).

2.4. DSF-based Screening

The 52 compounds identified by SPR screening were tested in DSF with a constant concentration of 500 µM. Compounds showing $T_M > + 0.5$ °C and $T_M < -1$ °C were selected for further investigations (20 compounds).

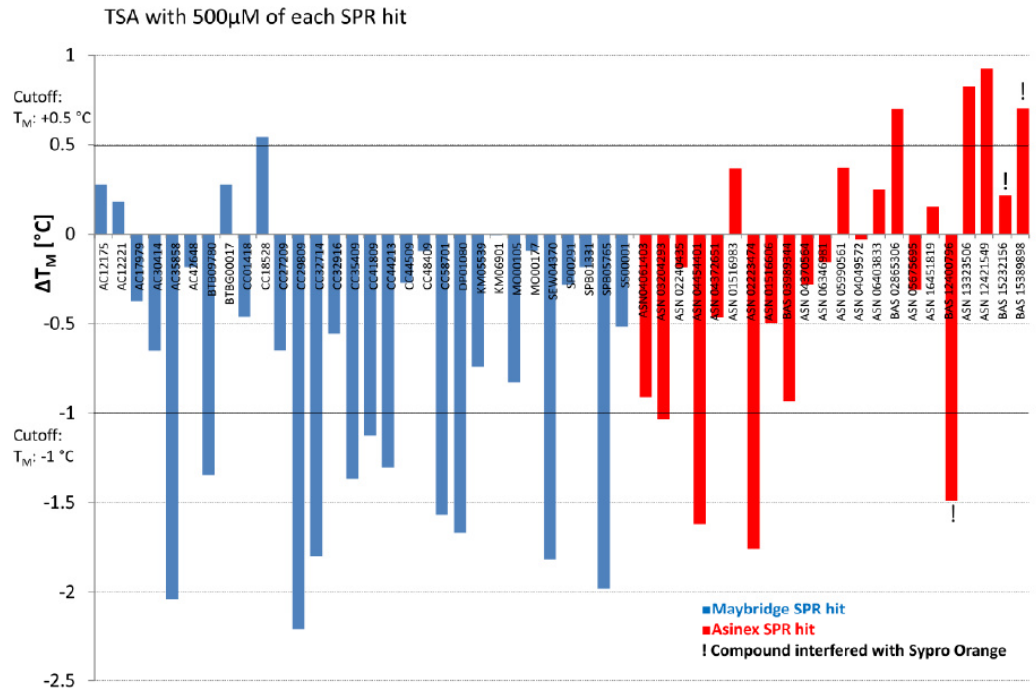

Figure S2: Results of DSF based screening of 52 positive compounds from previous SPR screening. Compounds from Maybridge library are displayed in blue and from Asinex in red.

2.5. Fluorescence Polarization Assay

2.5.1. DNA Hybridisation:

DNA oligonucleotide stocks were always prepared freshly. DNA hybridisation was done by mixing the corresponding sense and antisense oligonucleotides in a ratio of 1:1, heating the mixture at 95 °C for 12 minutes and cooling slowly to room temperature again. The sequences of all used sense and antisense oligonucleotides are listed in table S1. All oligomers were obtained from Sigma Aldrich in HPLC purity and were used as received. Fluorescein was used as fluorescence label.

Table S1: DNA sense and antisense oligonucleotides for FP assay.

DNA	Base sequence
LBS1_sense	5'-TCCCGCCCGGGCATGGGGCC
LBS1_sense_flc	5'-TCCCGCCCGGGCATGGGGCC_flc
LBS1_antisense	5'-GGCCCCATGCCCGGGCGGGA
LBS2_sense	5'-CGCCGCCGGGGCCTGCGGCG
LBS2_sense_flc	5'-CGCCGCCGGGGCCTGCGGCG _flc
LBS2_antisense	5'_CGCCGCAGGCCCCGGCGGCG
LBS3_sense	5'-CCGCGCCGGGCCCTGAGGCG
LBS3_sense_flc	5'-CCGCGCCGGGCCCTGAGGCG_flc
LBS3_antisense	5'-CGCCTCAGGGCCCGGCGCGG

2.5.2. FP-Assay Optimization Studies

To determine the optimal concentrations of protein and DNA for this experiment different concentration dependent experiments were performed (Figure S3, **A**). Three different protein concentrations (400 nM, 266 nM and 134 nM final) were tested with fixed concentration of LBS2_flc (15 nM final) and increasing concentrations of LBS2. Best results were observed using a final concentration of 400 nM. Furthermore, different concentrations of labelled LBS2 (5 nM, 10 nM and 15 nM final of LBS2_flc) were tested with a constant protein concentration of 400 nM (Figure S3; **B**). Based on these experiments we chose a final concentration of 10 nM DNA_flc in subsequent assays.

Assay robustness was measured by testing control run plates (Figure S3; **C**). A high control (HC) plate contained 192 samples with LANA (400 nM), LBS2_flc (10 nM) and DMSO (5% [v/v]) in FP assay buffer while a low control (LC) plate contained the same samples without LANA. A high dynamic range, low coefficients of variations (CVs) and a Z' factor of 0.925 indicated that the assay was robust and suitable for measuring the inhibitory efficiency of our compounds.

DMSO tolerance was measured by incubating various concentrations of DMSO (0-10 % [v/v] final), a fixed concentration of LBS2_flc (10 nM final) and different concentrations of LANA (0 nM, 150 nM, 400 nM) (Figure S3; **D**). Accordingly, a final concentration of 5% DMSO was chosen for the assay.

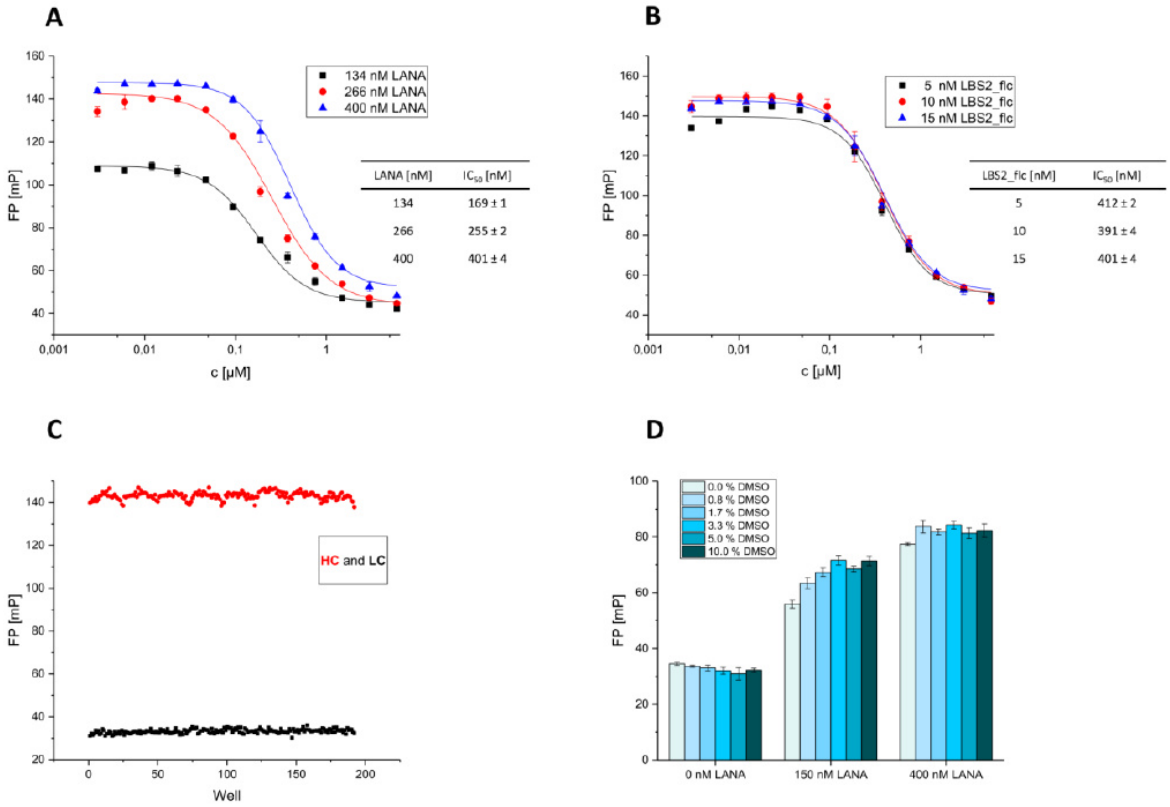

Figure S3: **A**: Dose-dependent experiments using different LANA concentrations. **B**: Dose-dependent experiments using different DNA concentrations. **C**: Determination of assay robustness, HC (red) and LC (black). **D**: DMSO tolerance measurement for different LANA and DMSO concentrations.

2.5.3. Dose-dependent Studies with LBS1, 2 and 3

We performed dose dependent experiments using LBS2 as the fluorescent probe and used varying concentrations of unlabeled LBS1, LBS2 and LBS3.

A

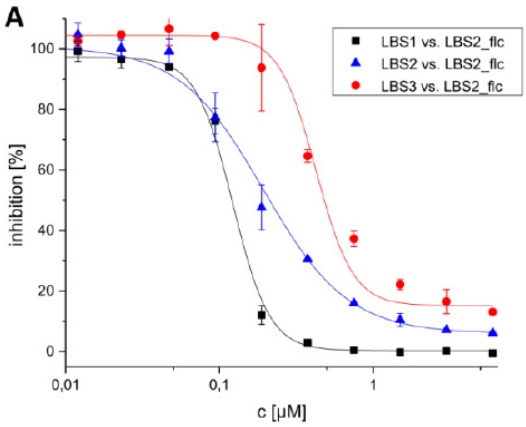

B

DNA	IC_{50} [nM]
LBS1 vs. LBS2_flc	122 ± 1
LBS2 vs. LBS2_flc	193 ± 3
LBS3 vs. LBS2_flc	425 ± 28

C LBS1: 5'-TCCCGCCCGGGCATGGGGCC-3'

LBS2: 5'-CGCCGCCGGGGCCTGCGGCG-3'

LBS3: 5'-CCGCGCCGGGCCCTGAGGCG-3'

Figure S4: **A**: Dose-dependent studies with LBS1, 2 and 3 as a representative example for FP-based competition experiments. Representative curves of one independent experiment are shown with normalized data points (inhibition from 0 - 100%) representing averaged FP values of duplicates ± standard deviation. **B**: IC_{50} values [nM] calculated using a four-parameter dose-response model. **C**: Sequences of LBS1, 2 and 3 oligonucleotides as used in this experiment.

2.5.4. Dose dependent Studies of Compounds 37, 41 - 43, 47 and 50

We carried out dose–dependent competition studies with our compounds. Representative curves showing the results obtained with compounds 37, 41 - 43, 47 and 50 are shown in figure 5, which based on normalized data points (% inhibition from 0 - 100%) representing averaged FP values of duplicates ± standard deviation. Curves were fit to a four-parameter dose response model using OriginLab (2016) to calculate IC_{50} values. Compounds were tested in dose dependent experiments starting at 1 mM or 500 µM depending on solubility. LBS2_flc was used as fluorescent probe.

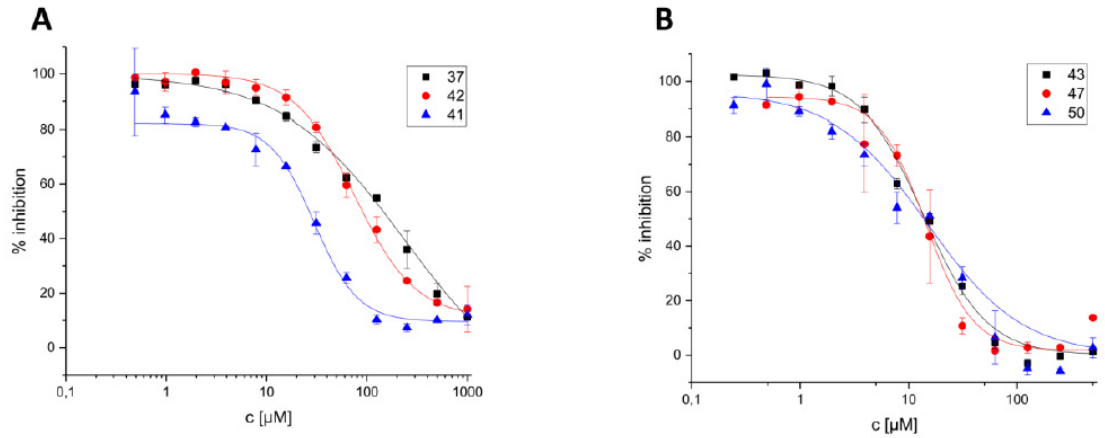

Figure S5: **A**: Dose-dependent experiments for compounds 37, 41 and 42 in FP-based competition experiments. **B**: Dose-dependent experiments for compounds 43, 47 and 50 in FP-based competition experiments.

2.6. Calculation of LogP and Ligand Efficiency (LE)

Calculation of LogP values (clogP) was done using ACD/Percepta version 2012 (Build 2203, 29 jan. 2013), ACD/Labs with the LogPGALAS model.

LE of compounds 37, 41 - 43, 47 and 50 was calculated based on their IC_{50} obtained using LBS2:

$$LE = 1.4 * \frac{pIC50}{NAH}$$

pIC_{50} = -log (IC_{50} [M])

NAH = number of heavy atoms

2.7. Electrophoretic Mobility Shift Assay (EMSA)

Table S2: sense and antisense oligonucleotides used for EMSA.

DNA	Base sequence
LBS1_sense	5'-TCCCGCCCGGGCATGGGGCC
LBS1_antisense	5'-GGCCCCATGCCCGGGCGGGA
LBS1+2_sense	5´-GGGGACGCCGCCGGGGCCTGCGGCGCCTCCCGCCCGGGCATGGGGCC
LBS1+2_antisense	5´-GGCCCCATGCCCGGGCGGGAGGCGCCGCAGGCCCCGGCGGCGTCCCC
Competitor_sense	5'-GAGGCGGCGCGCGGGGACGCCGCCGGGGCCTGCGGCGCCTCCCGCCCGGGCATGGGGCC
Competitor_antisense	5'-GGCCCCATGCCCGGGCGGGAGGCGCCGCAGGCCCCGGCGGCGTCCCCGCGCGCCGCCTC

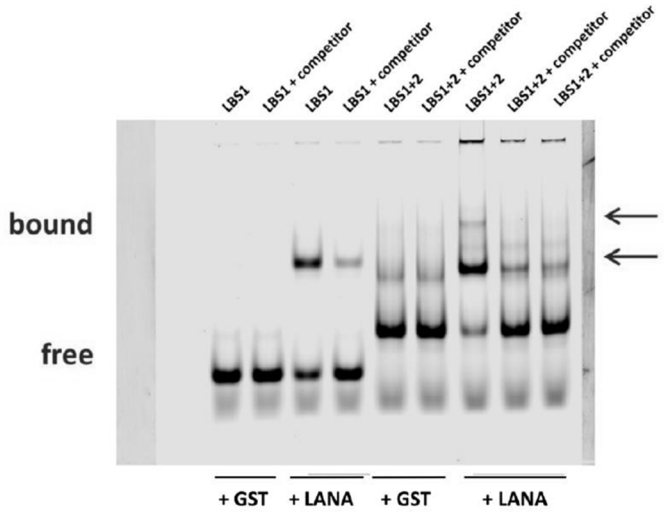

Figure S6: Gel of EMSA experiment using LBS1 and LBS1+2 as probes at 20 nM, non DNA-binding protein GST as control at 200 nM, LANA DBD mutant at 200 nM and competitor at 200 nM.

2.7.1. EMSA Experiments for Compounds 37, 41, 42, 43, 47, and 50

Calculation for normalized data for top bands:

(X - GST+DMSO+LBS top band) / (GST+DMSO+LBS bottom band) * 100 [%] (equation 1)

Calculation for normalized data for bottom bands:

(X - LANA+LBS+DMSO bottom band) / (GST+DMSO+LBS bottom band - LANA+LBS+DMSO bottom band) * 100 [%] (equation 2)

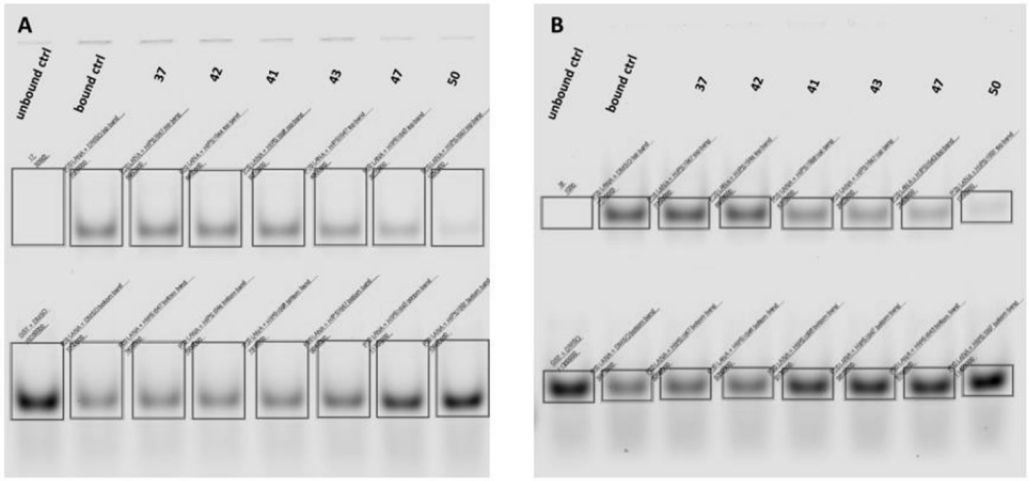

Figure S7: Two independent EMSA experiments using LBS1 as probes. Unbound control: GST+LBS1, bound control: DMSO+LANA+LBS1 and compound+LANA+LBS1 (**37**, **41**, **42**, **43**, **47**, and **50**). **A**: Gel 1 and **B**: Gel 2. Fixed concentrations of DNA probes of 20 nM, LANA DBD mutant and GST of 200 nM and each compounds of 500 µM were used.

Table S3: Intensities of top bands of the two independent EMSA experiments using LBS1 (Fig. S7).

Top Band	Intensities Gel 1	Intensities Gel 2	Normalized Gel 1* [%]	Normalized Gel 2* [%]	Mean [%]	Standard deviation [%]
LANA +LBS1+DMSO	7082303	7273467	43,49	64,60	54,04	10,6
LANA+LBS1+37	6949745	7250647	42,67	64,40	53,53	10,9
LANA+LBS1+42	6477320	6993989	39,76	62,12	50,94	11,2
LANA+LBS1+41	6320920	4309422	38,79	38,27	38,53	0,3
LANA+LBS1+43	4798905	3824099	29,41	33,96	31,68	2,3
LANA+LBS1+47	3220508	2636996	19,67	23,41	21,54	1,9
LANA+LBS1+50	1278539	1252071	7,69	11,11	9,40	1,7
GST+DMSO+LBS1	30900	1060	0,0	0,0	0,0	0,0

*equation 1

Table S4: Intensities of bottom bands of the two independent EMSA experiments using LBS1(Fig. S7).

Bottom Band	Intensities Gel 1	Intensities Gel 2	Normalized Gel 1* [%]	Normalized Gel 2* [%]	Mean [%]	Standard deviation [%]
LANA +LBS1+DMSO	7700812	5974719	0,00	0,00	54,04	10,6
LANA+LBS1+37	7869608	6387713	1,98	7,82	53,53	10,9
LANA+LBS1+42	7496542	6327240	-2,40	6,67	50,94	11,2
LANA+LBS1+41	7866835	9132550	1,95	59,77	38,53	0,3
LANA+LBS1+43	9040171	9815636	15,73	72,70	31,68	2,3
LANA+LBS1+47	11677697	9789259	46,72	72,20	21,54	1,9
LANA+LBS1+50	13583109	11350337	69,10	101,75	9,40	1,7
GST+DMSO+LBS1	16213805	11257853	100,00	100,00	100,00	0,00

*equation 2

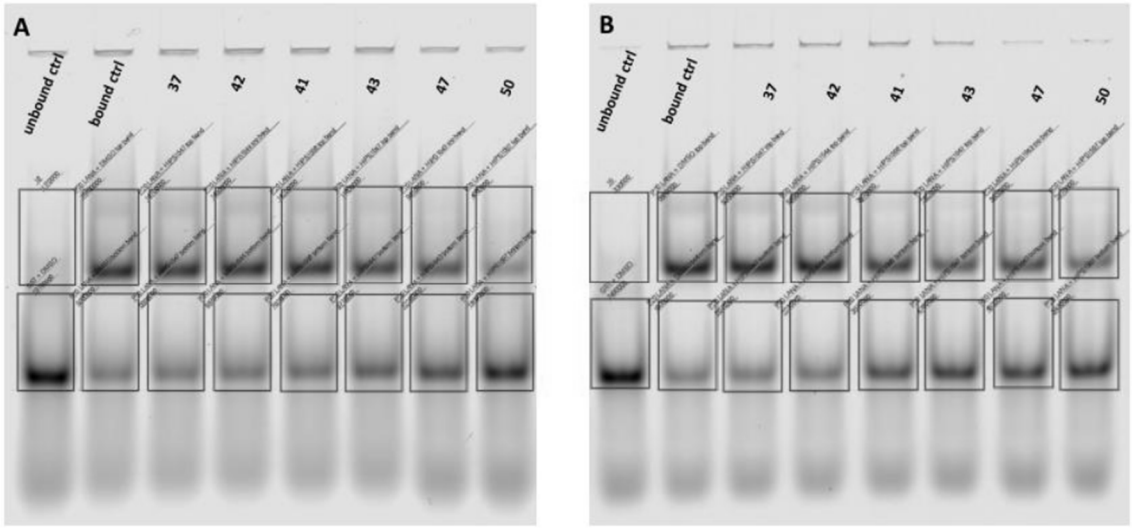

Figure S8: Two independent EMSA experiments using LBS1+2 as probes. Unbound control: GST+LBS1+2, bound control: DMSO+LANA+LBS1+2 and compound+LANA+LBS1+2 (**37**, **41**, **42**, **43**, **47**, and **50**). **A**: Gel 1 and **B**: Gel 2. Fixed concentrations of DNA probes of 20 nM, LANA DBD mutant and GST of 200 nM and each compounds of 500 µM were used.

Table S5: Intensities of top bands of two independent EMSA experiments using LBS1+2 (Fig. S8).

Top Band	Intensities Gel 1	Intensities Gel 2	Normalized Gel 1* [%]	Normalized Gel 2* [%]	Mean [%]	Standard deviation [%]
LANA +LBS1+DMSO	15403664	5878857	61,01	74,08	67,55	6,5
LANA+LBS1+37	14680225	5352544	57,88	67,06	62,47	4,6
LANA+LBS1+42	14875512	5587054	58,73	70,19	64,46	5,7
LANA+LBS1+41	14194824	3974357	55,78	48,66	52,22	3,6
LANA+LBS1+43	11770175	2918459	45,28	34,56	39,92	5,4
LANA+LBS1+47	9410393	3529022	35,07	42,71	38,89	3,8
LANA+LBS1+50	4083551	2174762	12,01	24,63	18,32	6,3
GST+DMSO+LBS1	1310000	330000	0,00	0,00	0,00	0,00

*equation 1

Table S6: Intensities of bottom bands of two independent EMSA experiments using LBS1+2 (Fig. S8).

Bottom Band	Intensities Gel 1	Intensities Gel 2	Normalized Gel 1* [%]	Normalized Gel 2* [%]	Mean [%]	Standard deviation [%]
LANA +LBS1+DMSO	6346736	1904508	0,00	0,00	0,00	0,0
LANA+LBS1+37	6394300	2067054	0,28	2,91	1,60	1,3
LANA+LBS1+42	6870768	2228421	3,13	5,80	4,46	1,3
LANA+LBS1+41	7621028	3512216	7,61	28,78	18,19	10,6
LANA+LBS1+43	9772169	4781537	20,45	51,51	35,98	15,5
LANA+LBS1+47	12194399	4622428	34,90	48,66	41,78	6,9
LANA+LBS1+50	17995263	5431572	69,53	63,15	66,34	3,2
GST+DMSO+LBS1	23100000	7490000	100,00	100,00	100,00	0,0

*equation 2

2.7.2. Dose-dependent EMSA Experiments with Compound 50.

We carried out dose-dependent competition studies with compound 50. EMSA gels showing the results obtained with varying concentrations of compound **50** and LANA DBD mutant are shown in figure S9. Similar experiments were performed using wild-type C-terminal LANA (Fig. S10). Dose-dependent curves which based on normalized data points (% band intensity of top bands from 0 - 100%) representing averaged FP values of duplicates ± standard deviation. Curves were fit to a four-parameter dose response model using OriginLab (2016) to calculate IC_{50} values. Compounds were tested in dose dependent experiments starting at 2 mM. LBS1 was used as probe.

Calculation for normalized data for top bands:

(X + GST+DMSO+LBS1 top band) / (LANA+DMSO+LBS1 top band + GST+DMSO+LBS1 top band) *100 [%] (equation 3)

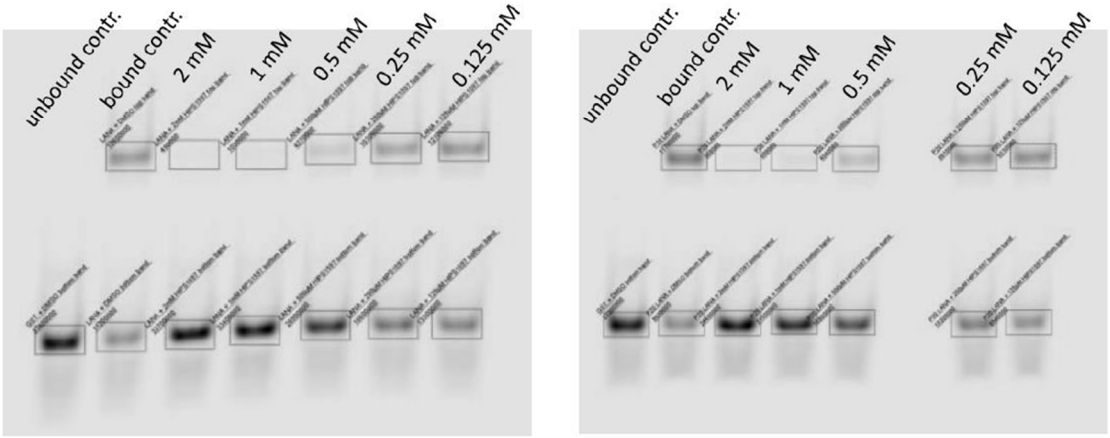

Figure S9: Two independent EMSA experiments using LBS1 as probes. Unbound control: GST+LBS1, bound control: DMSO+LANA+LBS1 and compound **50**+LANA+LBS1. **A**: Gel 1 and **B**: Gel 2. Fixed concentrations of DNA probes of 20 nM, LANA DBD mutant and GST of 200 nM were used. Compound **50** was used at 2 mM, 1mM, 500 µM, 250 µM and 125 µM.

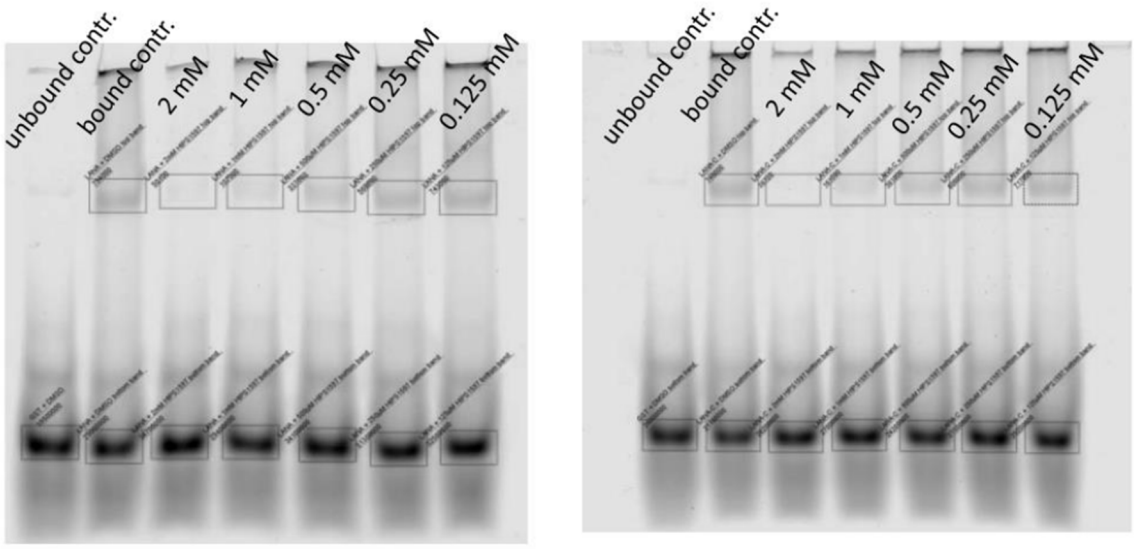

Figure S10: Two independent EMSA experiments using LBS1 as probes. Unbound control: GST+LBS1, bound control: DMSO+wild-type LANA+LBS1 and compound **50**+wild-type LANA+LBS1. **A**: Gel 1 and **B**: Gel 2. Fixed concentrations of DNA probes of 20 nM, wild-type C-terminal LANA and GST of 200 nM were used. Compound **50** was used at 2 mM, 1mM, 500 µM, 250 µM and 125 µM.

Table S7: Intensities of top bands of two independent EMSA experiments using LBS1 and LANA mutant and varying concentrations of compound **50** (see Gel Fig. S9).

Top Band	Intensities Gel 1	Intensities Gel 2	Normalized Gel 1* [%]	Normalized Gel 2* [%]	Mean [%]	Standard deviation [%]
LANA +LBS1+DMSO	12600282	11705533	100,00	100,00	100,00	0,0
LANA+LBS1+ 50(2 mM)	490249	367666	7,49	6,09	6,79	0,7
LANA+LBS1+ 50(1 mM)	1027522	699015	11,59	8,84	10,21	1,4
LANA+LBS1+50(0.5 mM)	4270214	4041334	36,37	36,52	36,44	0,1
LANA+LBS1+50(0.25 mM)	10263509	8810879	82,15	76,02	79,09	3,1
LANA+LBS1+50(0.125 mM)	12146712	9232463	96,54	79,52	88,03	8,5
GST+DMSO+LBS1	490249	367666	0,00	0,00	0,00	0,00

*equation 3

Table S8: Intensities of top bands of two independent EMSA experiments using LBS1 and LANA wild-type and varying concentrations of compound **50** (see Gels Fig. S10).

Top Band	Intensities Gel 1	Intensities Gel 2	Normalized Gel 1* [%]	Normalized Gel 2* [%]	Mean [%]	Standard deviation [%]
LANA +LBS1+DMSO	746156	754214	100,00	100,00	100,00	0,0
LANA+LBS1+ 50(2 mM)	36663	50134	9,37	12,47	10,92	1,5
LANA+LBS1+ 50(1 mM)	160620	106993	25,20	19,53	22,37	2,8
LANA+LBS1+50(0.5 mM)	360528	337027	50,74	48,13	49,44	1,3
LANA+LBS1+50(0.25 mM)	607872	568304	82,34	76,89	79,61	2,7
LANA+LBS1+50(0.125 mM)	717155	743068	96,30	98,61	97,45	1,2
GST+DMSO+LBS1	36663	50134	0,00	0,00	0,00	0,00

*equation 3

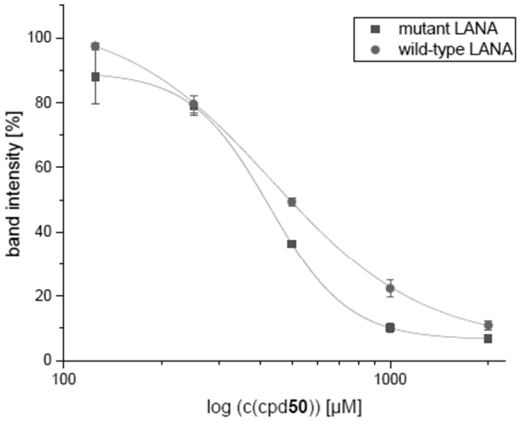

Figure S11: Dose-dependent EMSA experiments with compound **50**. LBS1 as probes and LANA DBD mutant (black) or LANA CTD wild-type (red) as target protein was used. IC_{50} (LANA DBD mutant) 426 ± 2 µM, IC_{50} (LANA CTD wild-type) 435 ± 6 µM.

2.8. Saturation-Transfer Difference NMR (STD-NMR)

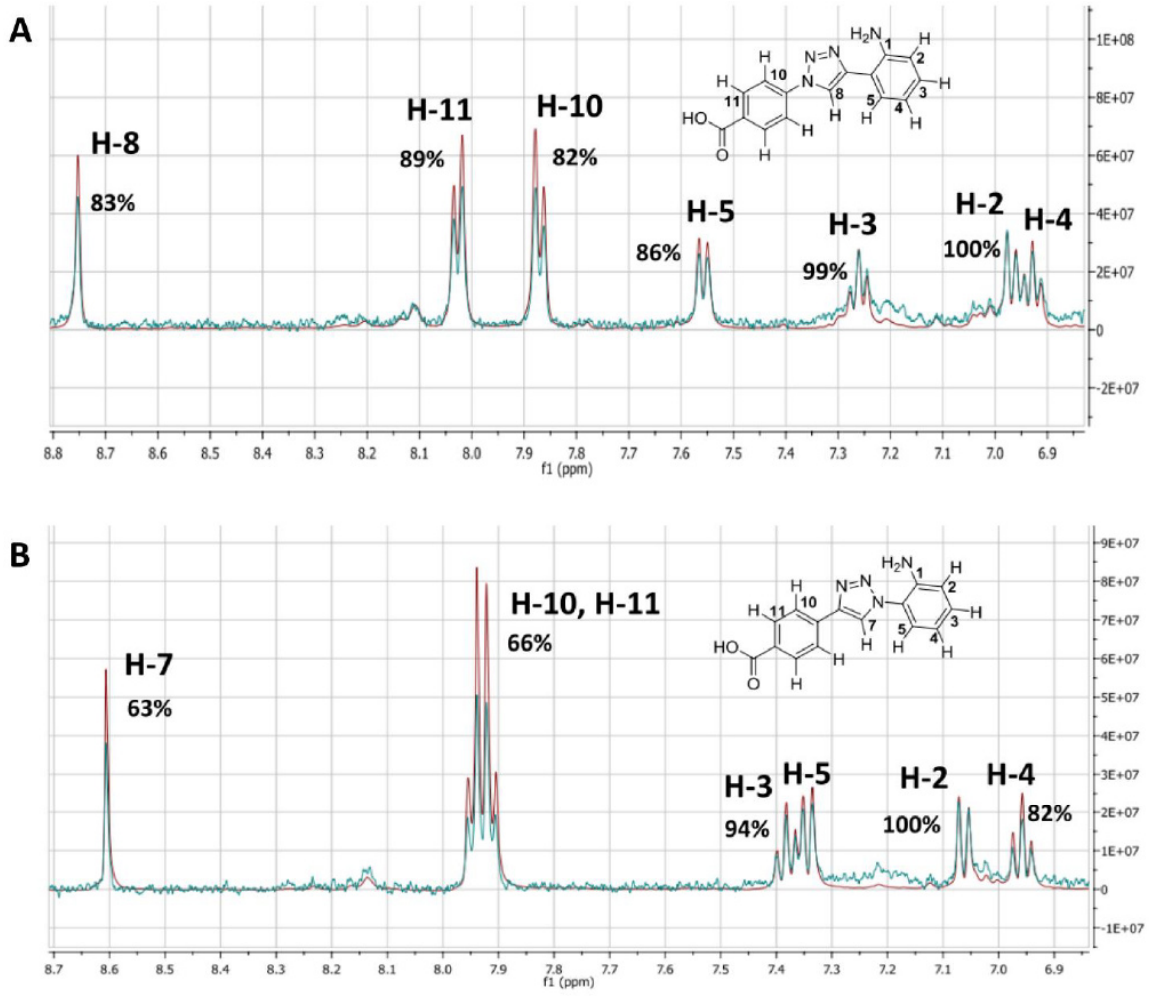

Figure S12: STD-NMR of **A**: compound **41** and **B**: compound **47** in complex with LANA DBD. The reference spectra are displaced in red (STD-off) and STD difference spectra (STD-on) in blue. Overlaid spectra were normalized to the signals which showed the strongest enhancement (**A**: H-2, H-4; **B**: H-2).

2.9. Molecular Docking

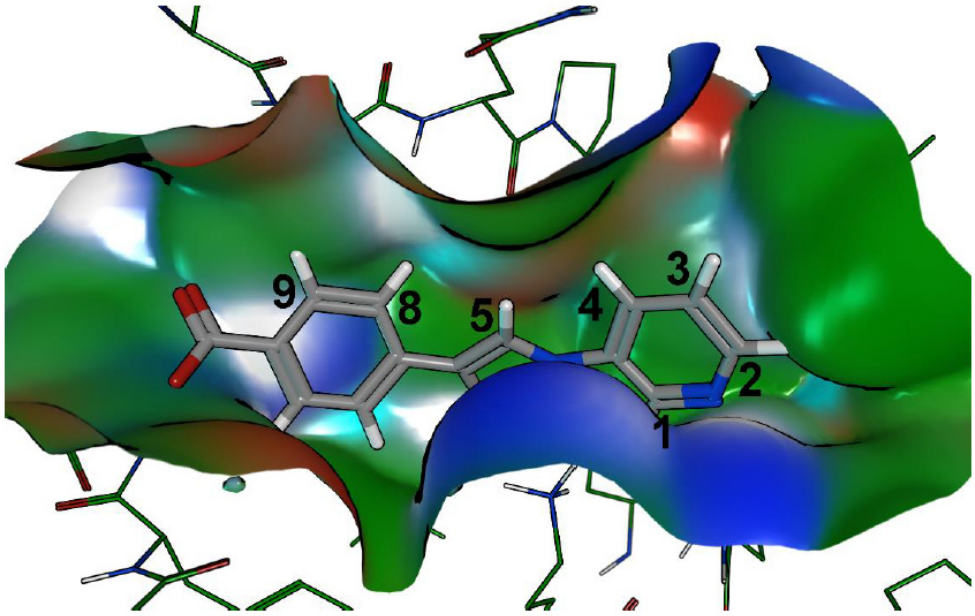

Figure S13: Docking pose of compound **50**. Surface indicates van der Waals radius of LANA residues. Protons at positions 1, 2 and one 8/9 pair are in close proximity to the protein, while protons 3, 4, 5, and the other 8/9 pair are exposed

2.10. Additional information to Hit 1 and alternative Hits 1a and 1b

Table S9: Additional information to Hit 1, 1a, 1b.

	Chemical Formula:	Molecular Weight [g/mol]	Response [RU] (SPR @ 500 µM)	T_M [°C] (DSF @ 500 µM)
Hit 1	$C_9H_9N_3$	159,19	15.69 ± 9.3	-1.80 ± 1.41
Hit 1a	$C_5H_7N_3$	109,13	12.66 ± 2.1	-1.36 ± 1.5
Hit 1b	$C_{10}H_{11}NO_2$	177,20	14.73 ± 1.9	-1.55 ± 0.83

3. High Resolution Mass Spectrometry (HRMS)

HRMS were measured on a Thermo Scientific Q Exactive Focus (Germany) equipped with DIONEX ultimate 3000 UHPLC^{+} focused. For gradient eluation, an EC 150/2 NUCLEODUR C18 Pyramid (3 µm) column (Machery-Nagel, Germany) was used with a mobile phase consisting of acetonitrile containing 0.1% formic acid (FA; v/v; eluent A) and water containing 0.1% FA (v/v; eluent B). Eluation method was used with a total run time of 7.5 min and gradient conditions 10% A to 90% A. Mass spectrometry was used in positive or negative mode using electrospray ionisation (ESI). Measured (upper spectrum) and calculated (lower spectrum) HRMS spectra of each final synthesized compound were depicted below.

1-(2-nitrophenyl)-1*H*-imidazole (2)

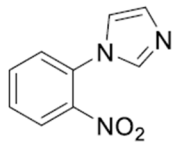

1-(2-nitrophenyl)-1*H*-imidazole

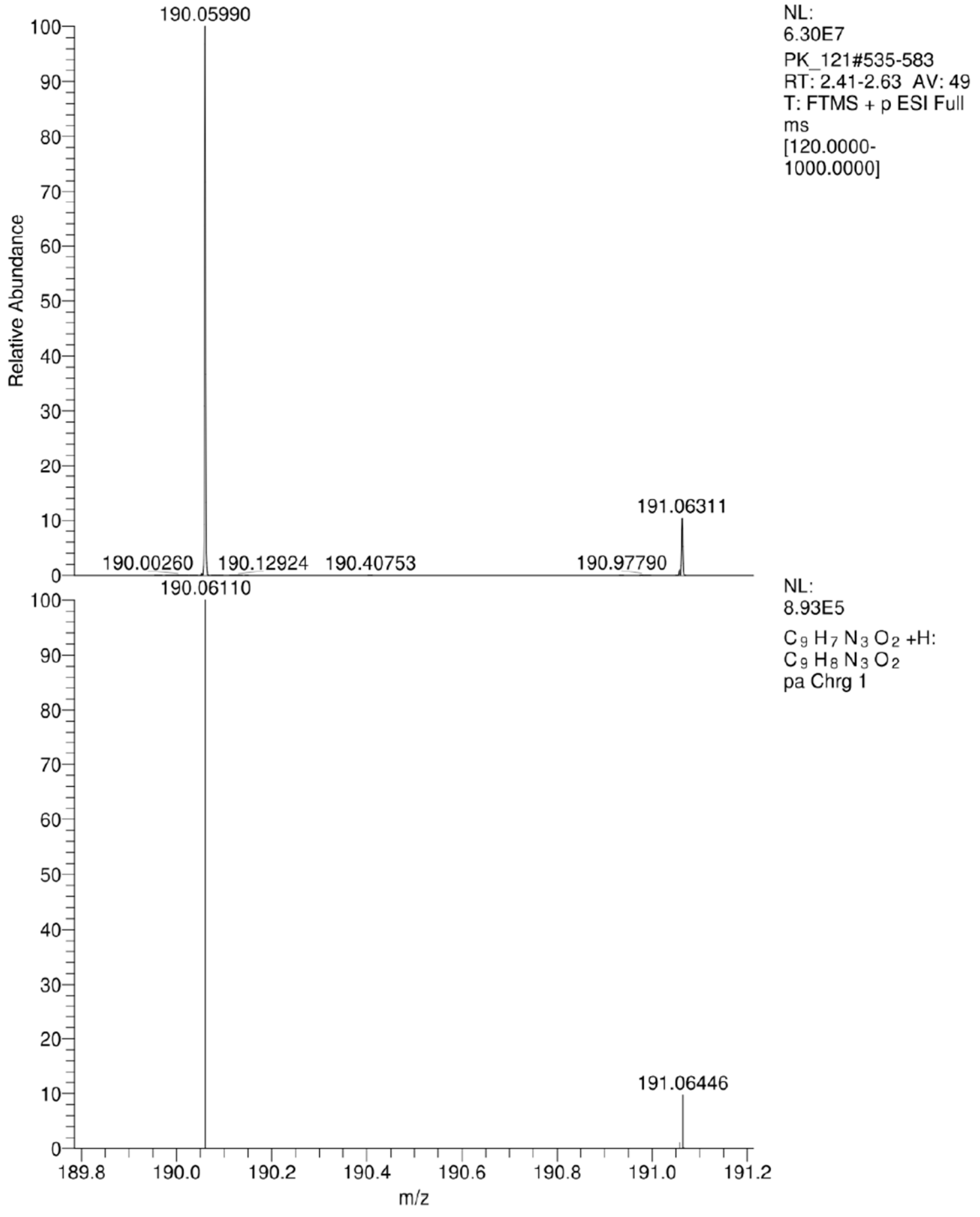

S31

1-(3-nitrophenyl)-1*H*-imidazole (3)

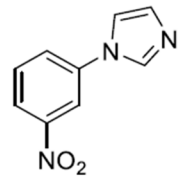

1-(3-nitrophenyl)-1*H*-imidazole

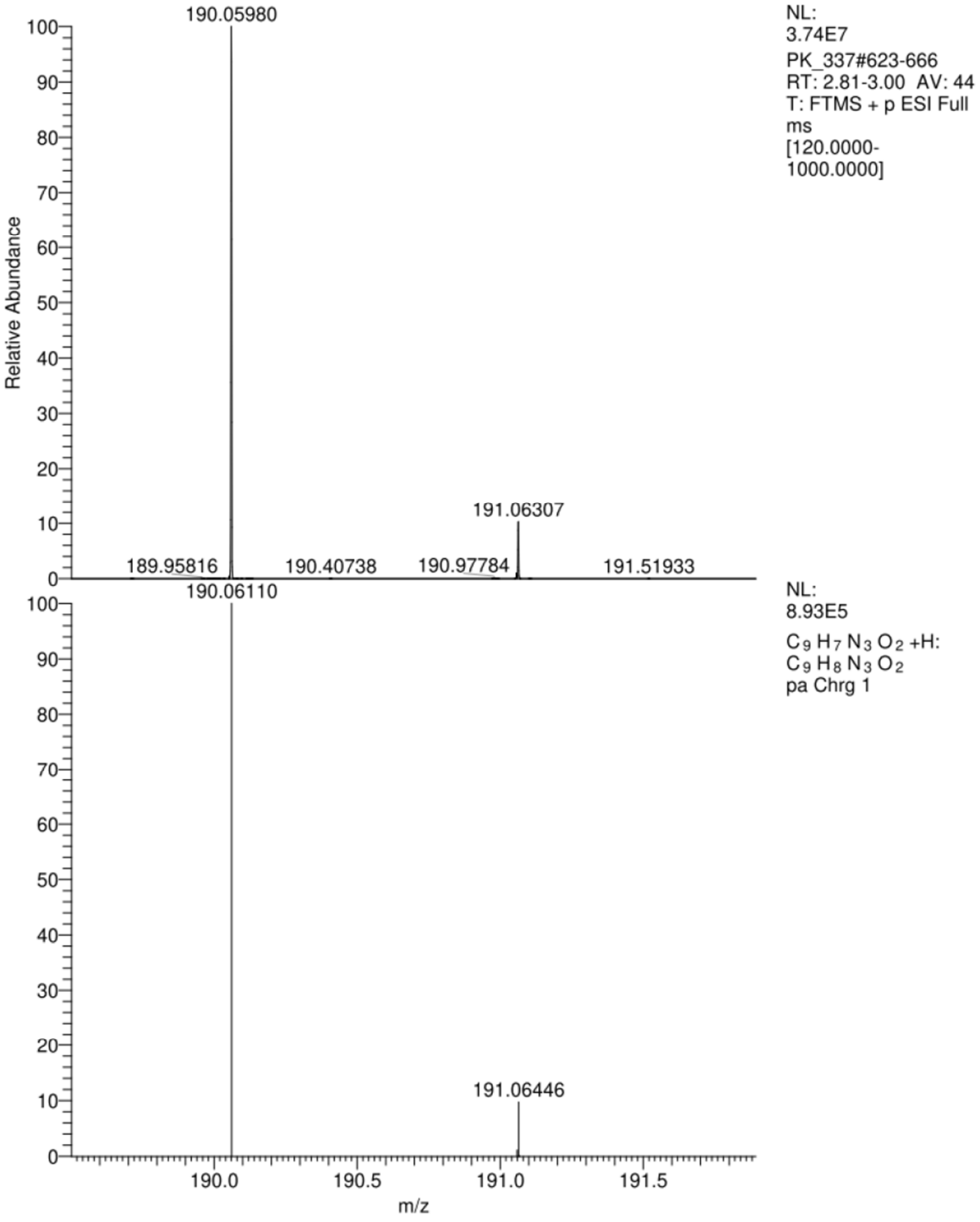

S32

1-(4-nitrophenyl)-1*H*-imidazole (4)

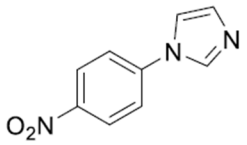

1-(4-nitrophenyl)-1*H*-imidazole

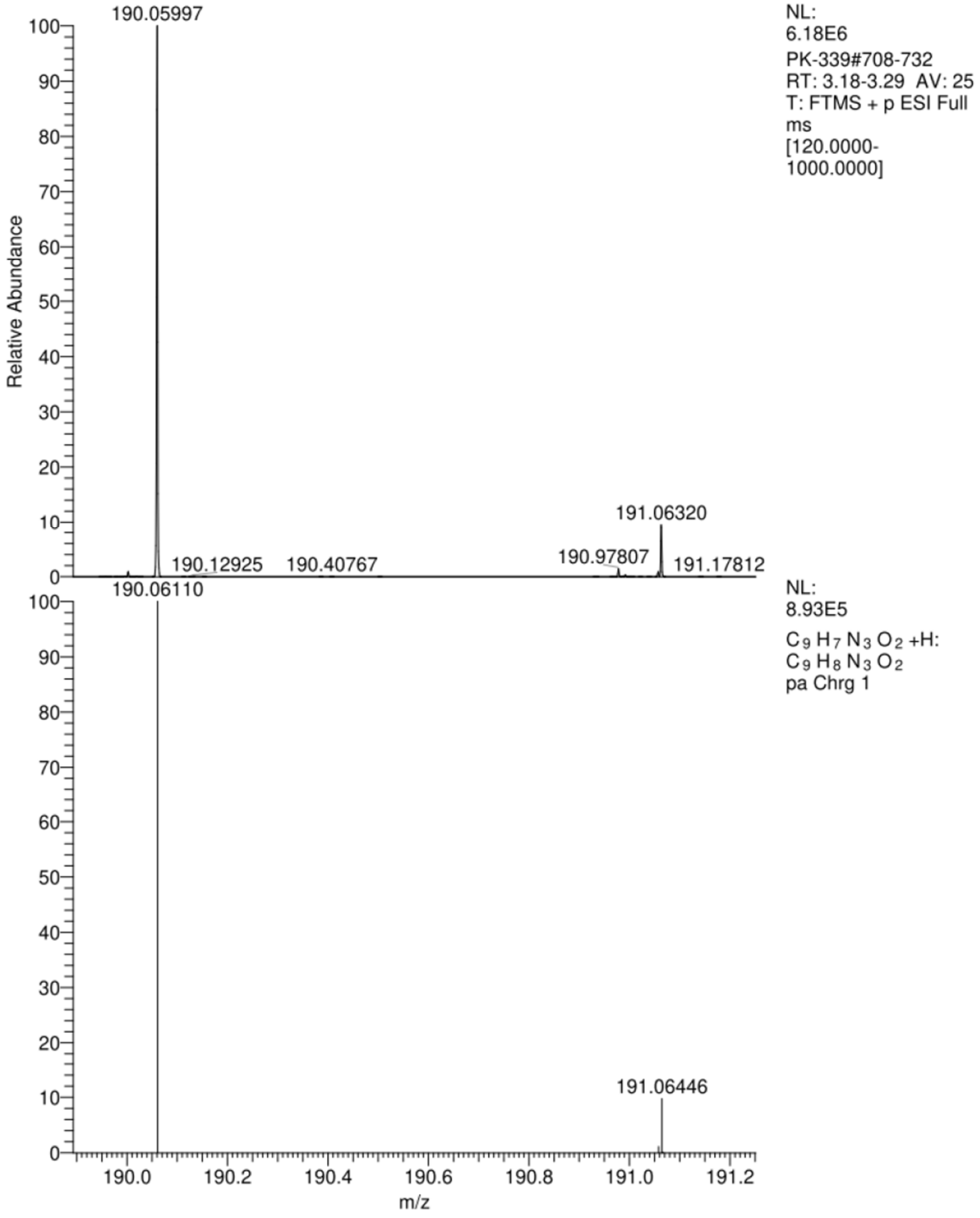

2-(1*H*-imidazol-1-yl)aniline (1)

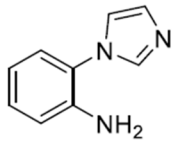

2-(1*H*-imidazol-1-yl)aniline

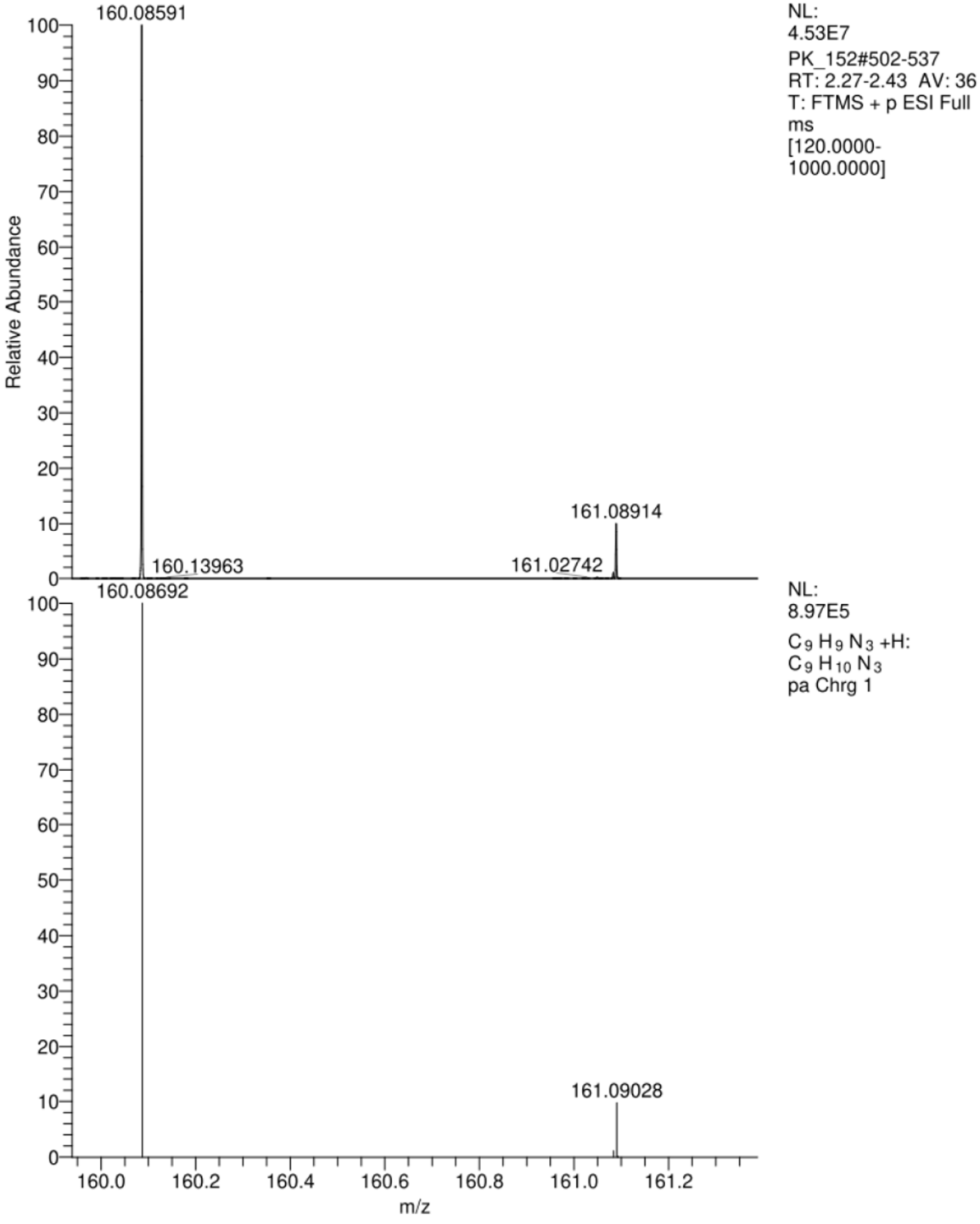

2-(4-methyl-1*H*-imidazol-1-yl)aniline (11)

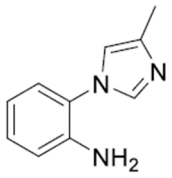

2-(4-methyl-1*H*-imidazol-1-yl)aniline

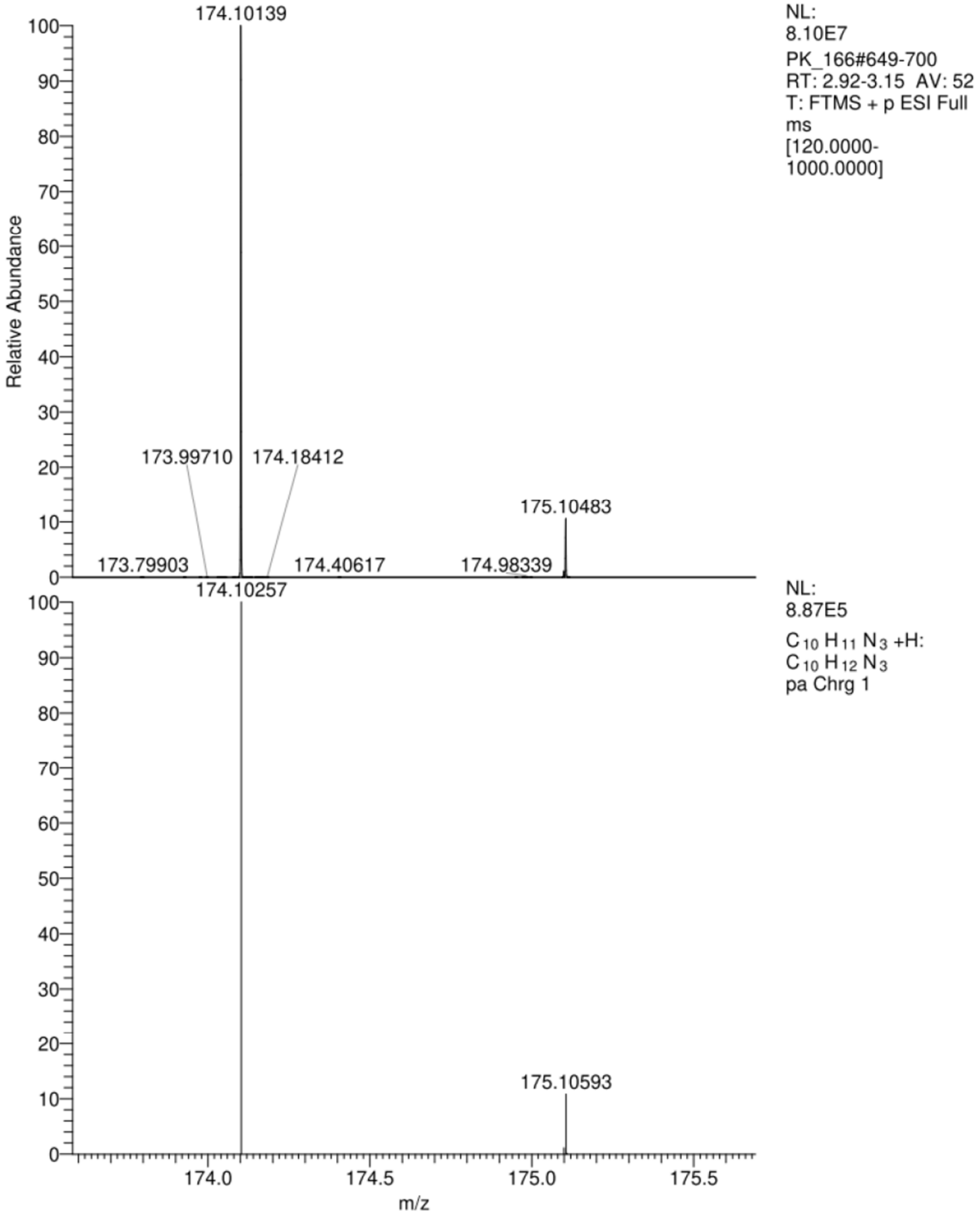

S35

2-(4-bromo-1*H*-imidazol-1-yl)aniline (12)

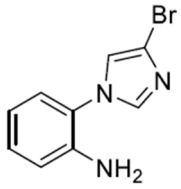

2-(4-bromo-1*H*-imidazol-1-yl)aniline

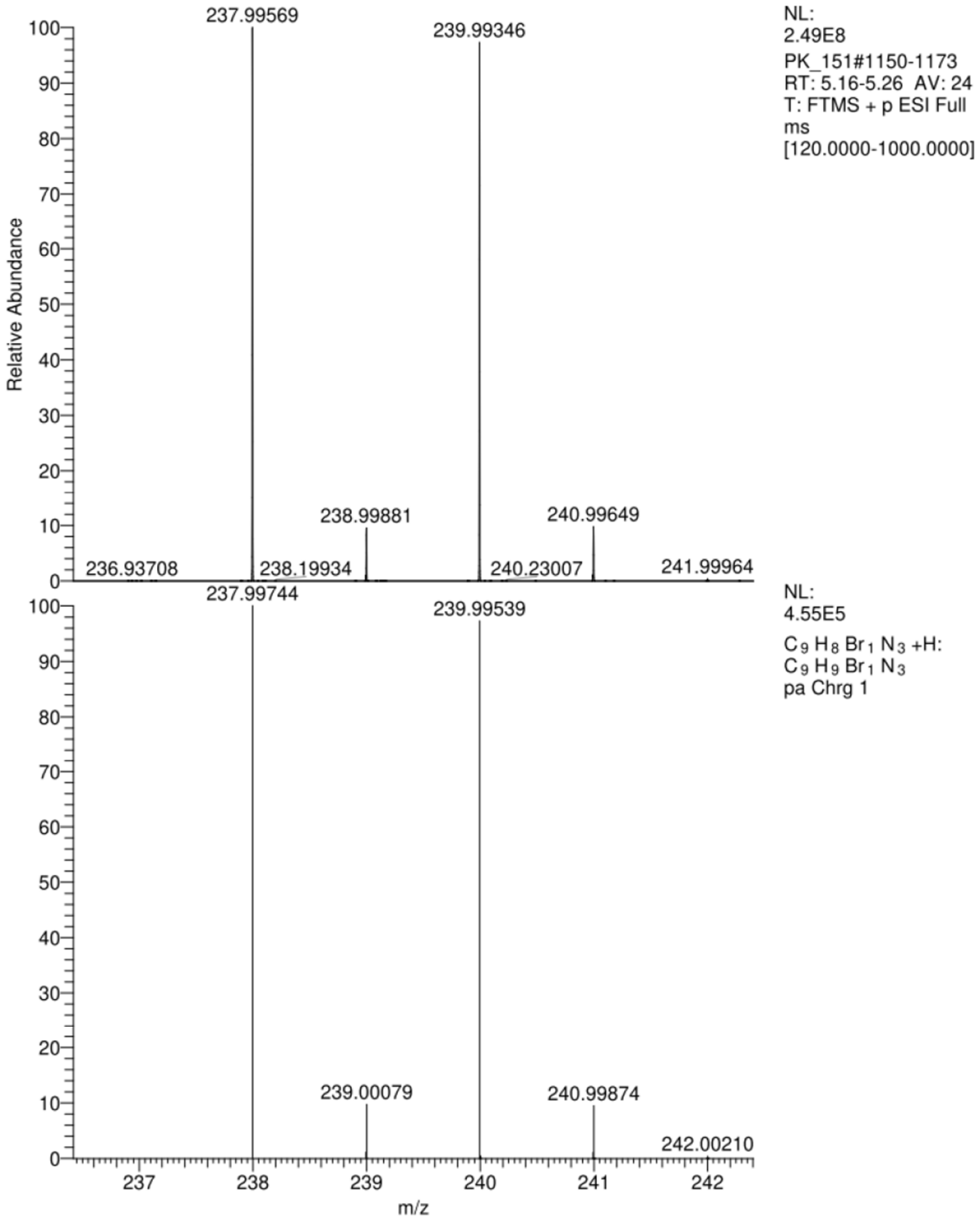

S36

2-(1*H*-benzo[*d*]imidazol-1-yl)aniline (13)

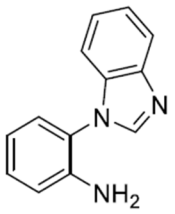

2-(1*H*-benzo[*d*]imidazol-1-yl)aniline

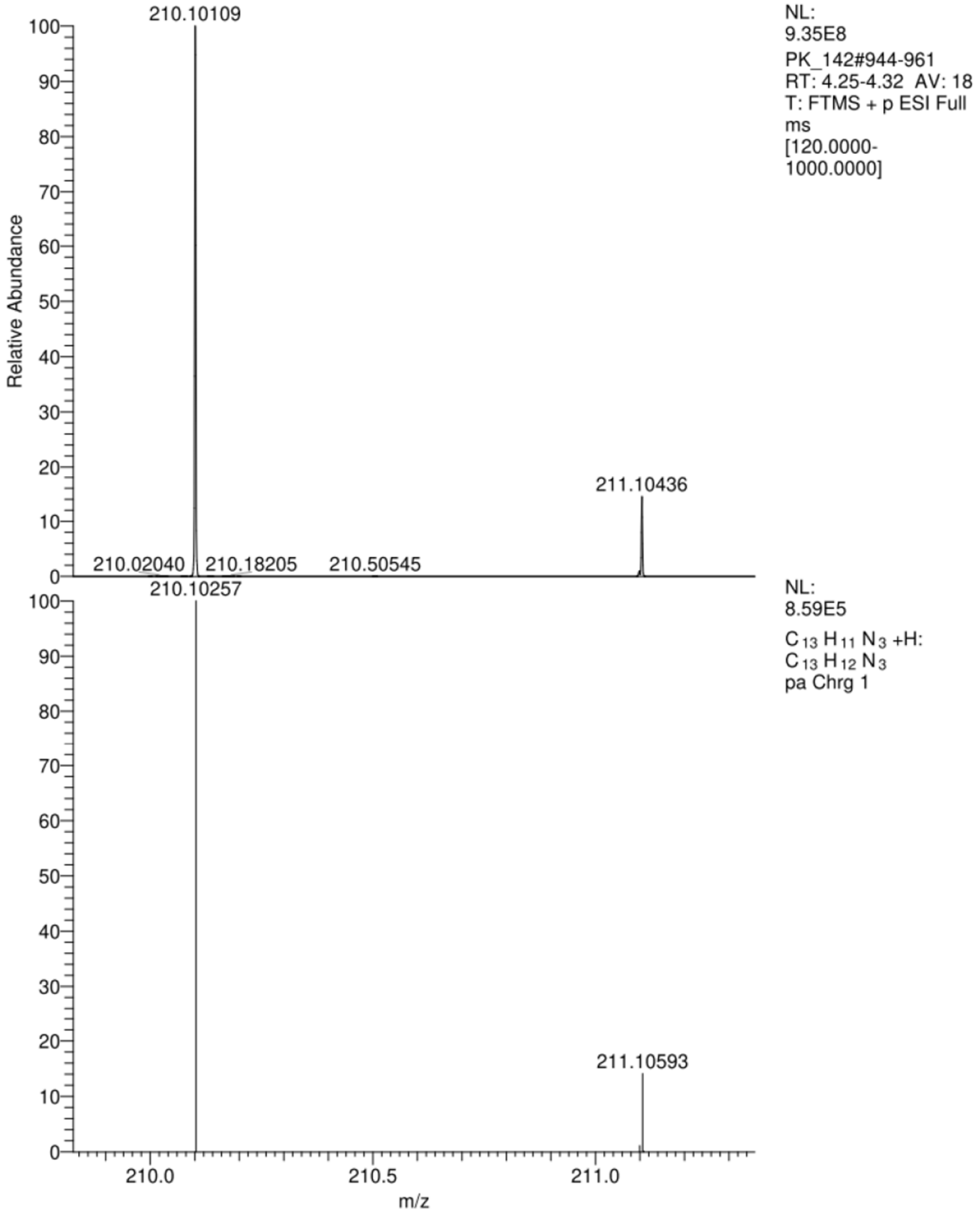

S37

_N_-(2-(1_H_-Imidazol-1-yl)phenyl)acetamide (8)

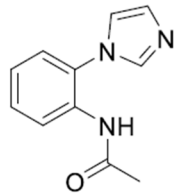

_N_-(2-(1_H_-imidazol-1-yl)phenyl)acetamide

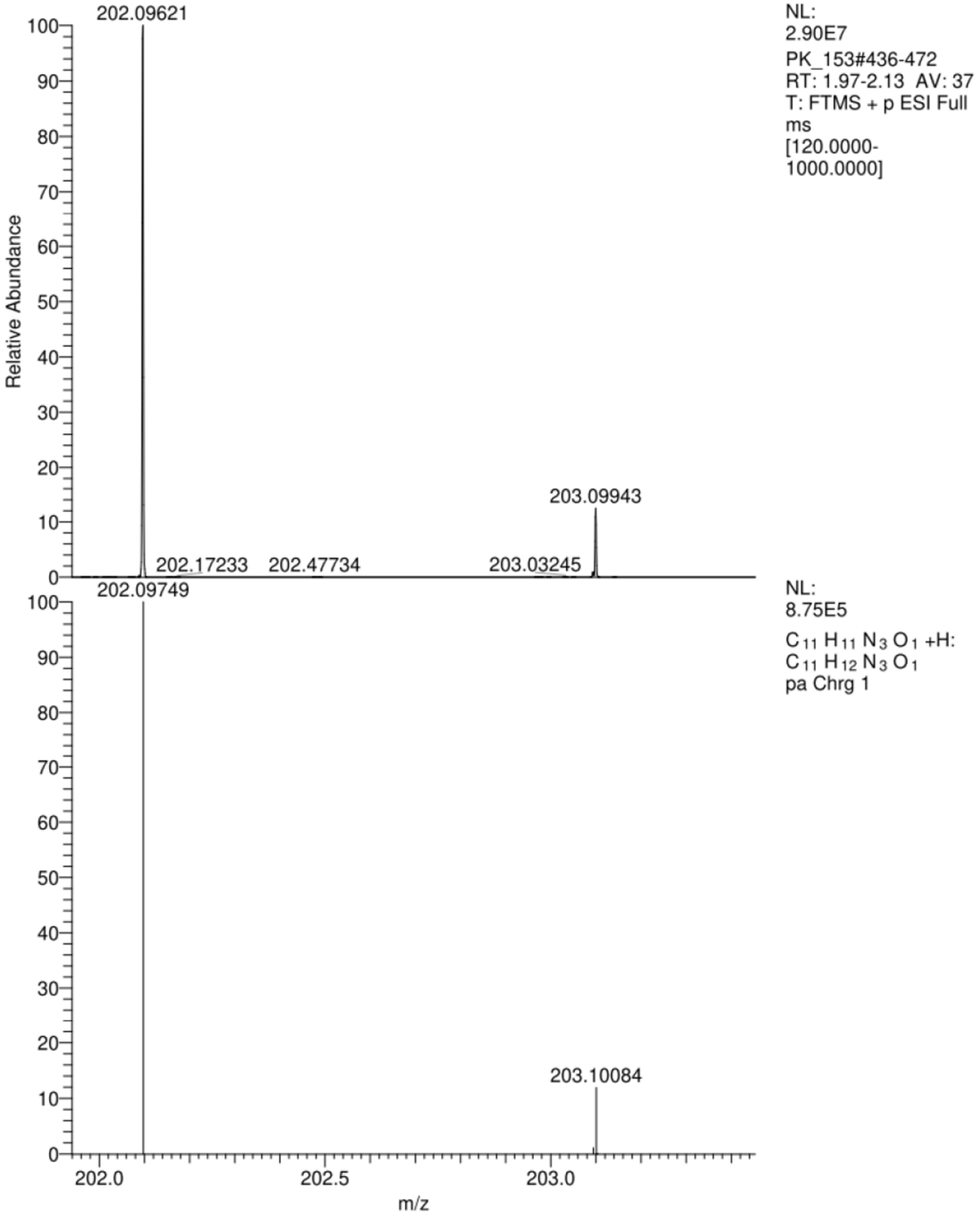

2-(1*H*-Imidazol-1-yl)phenol (15)

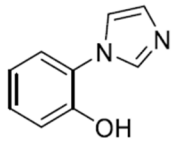

2-(1*H*-imidazol-1-yl)phenol

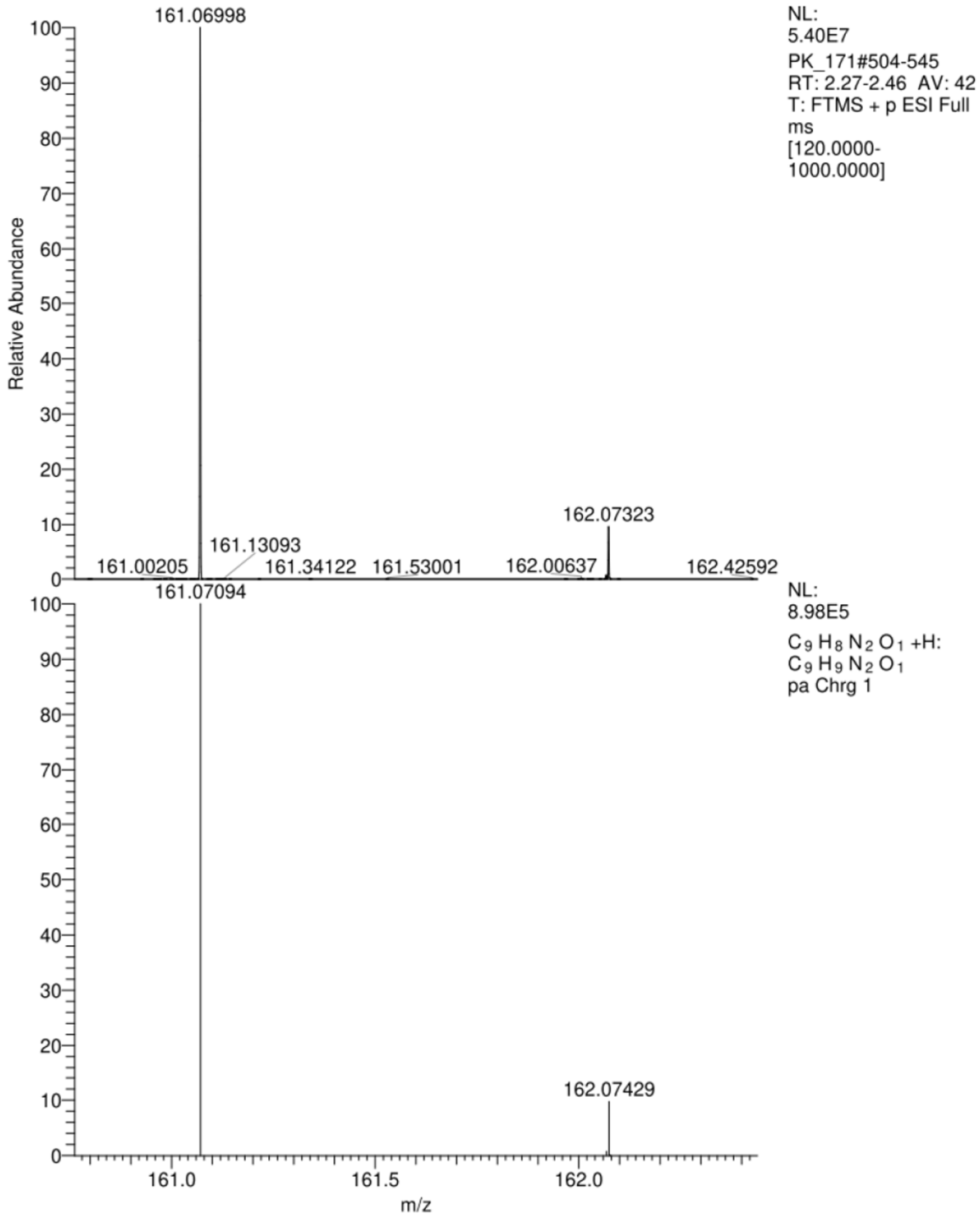

2-(1*H*-imidazol-1-yl)benzoic acid (16)

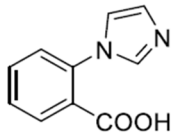

2-(1*H*-imidazol-1-yl)benzoic acid

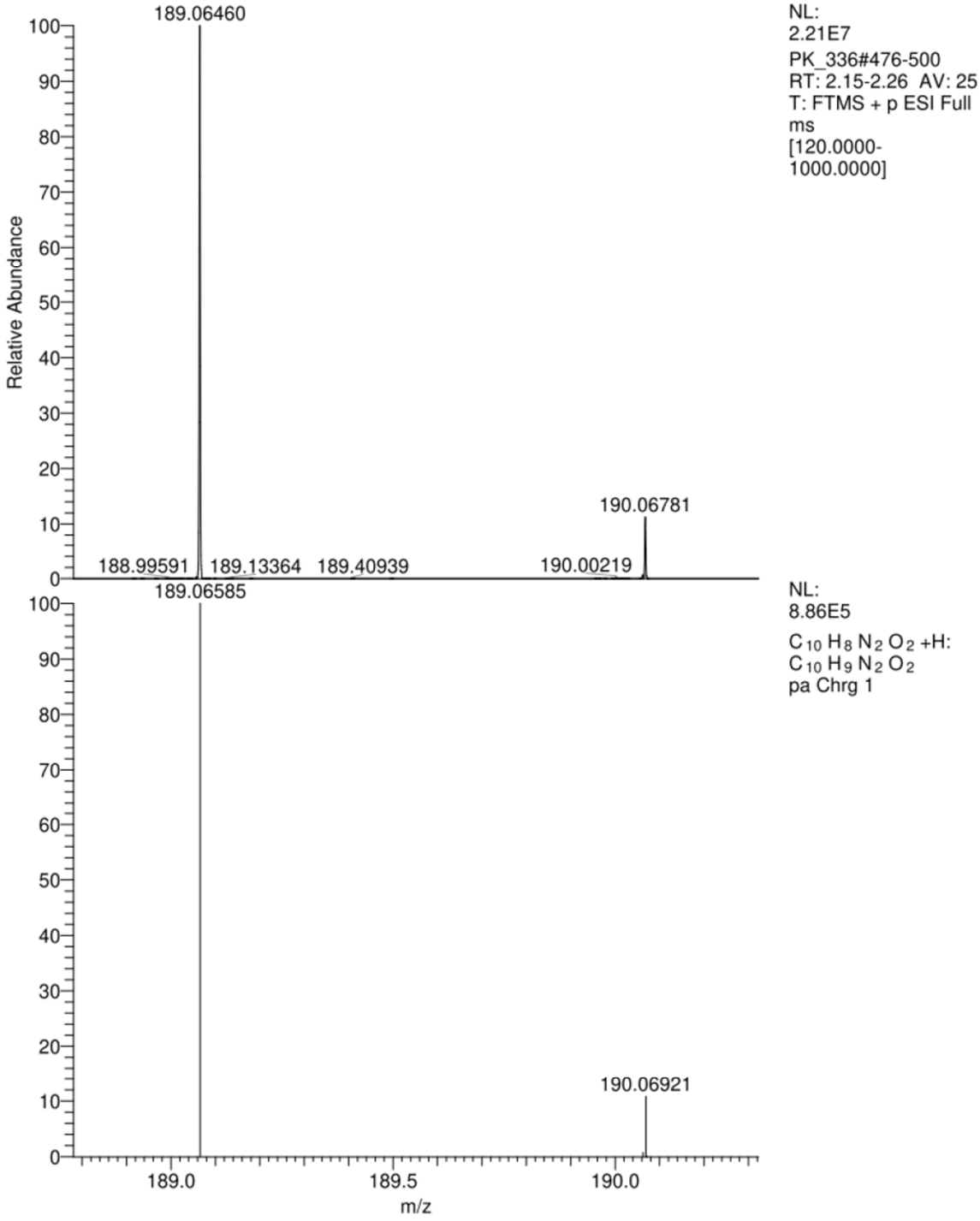

3-(1*H*-imidazol-1-yl)benzoic acid (17)

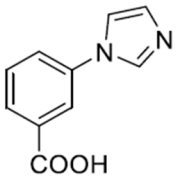

3-(1*H*-imidazol-1-yl)benzoic acid

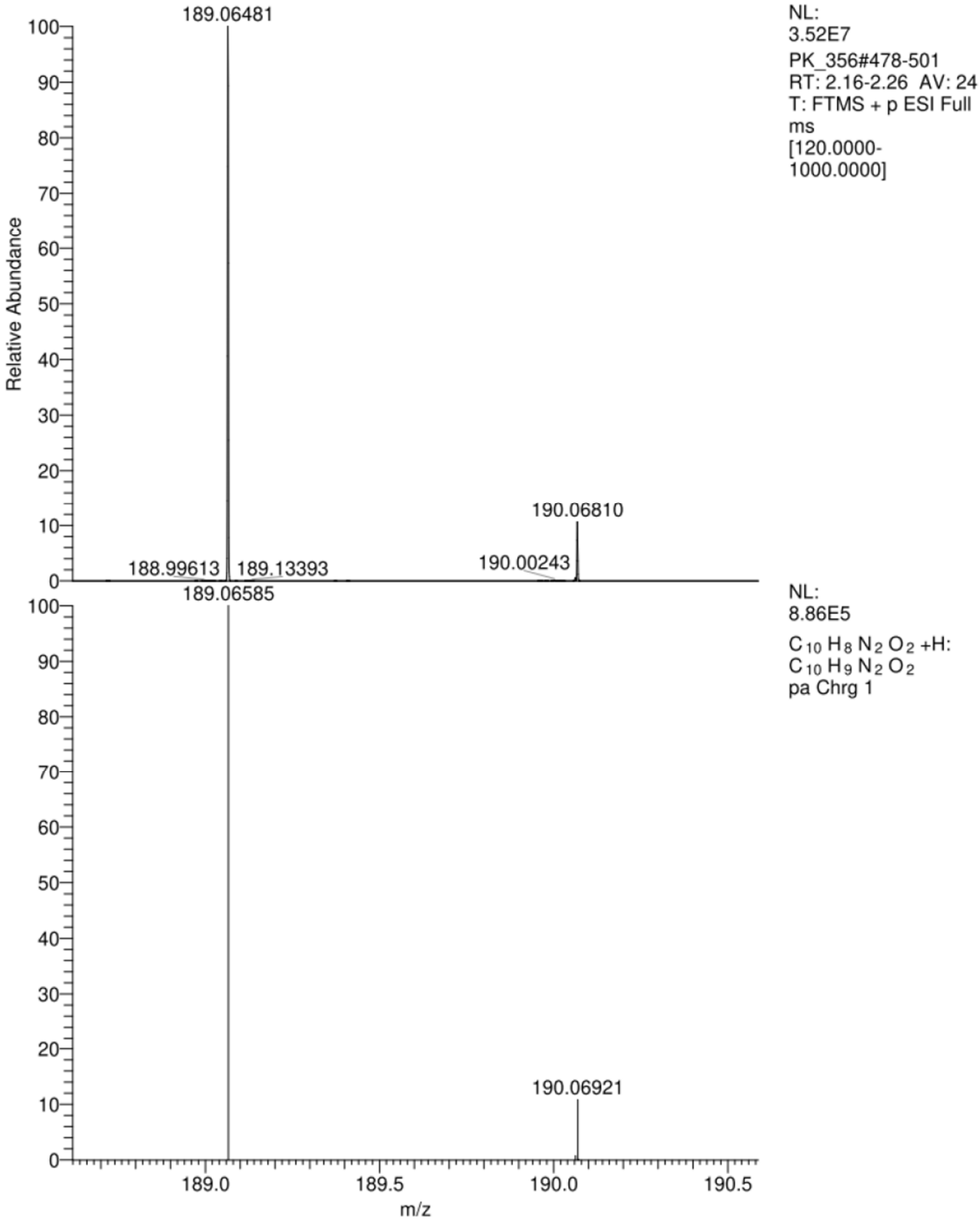

4-(1*H*-imidazol-1-yl)benzoic acid (18)

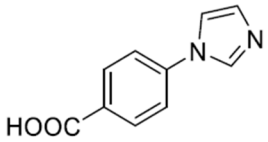

4-(1*H*-imidazol-1-yl)benzoic acid

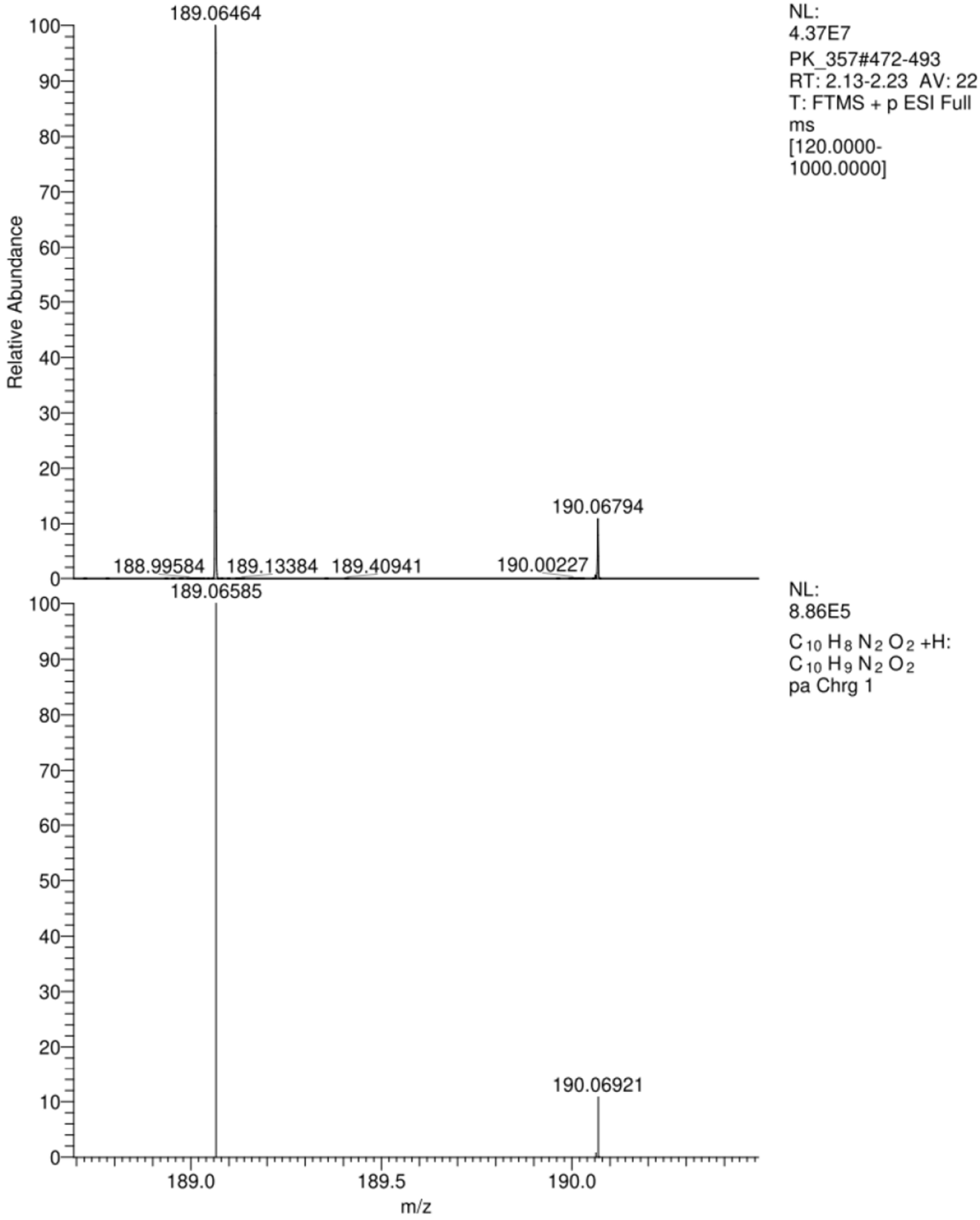

2-(1*H*-1,2,3-triazol-1-yl)benzoic acid (26)

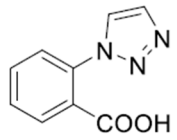

2-(1*H*-1,2,3-triazol-1-yl)benzoic acid

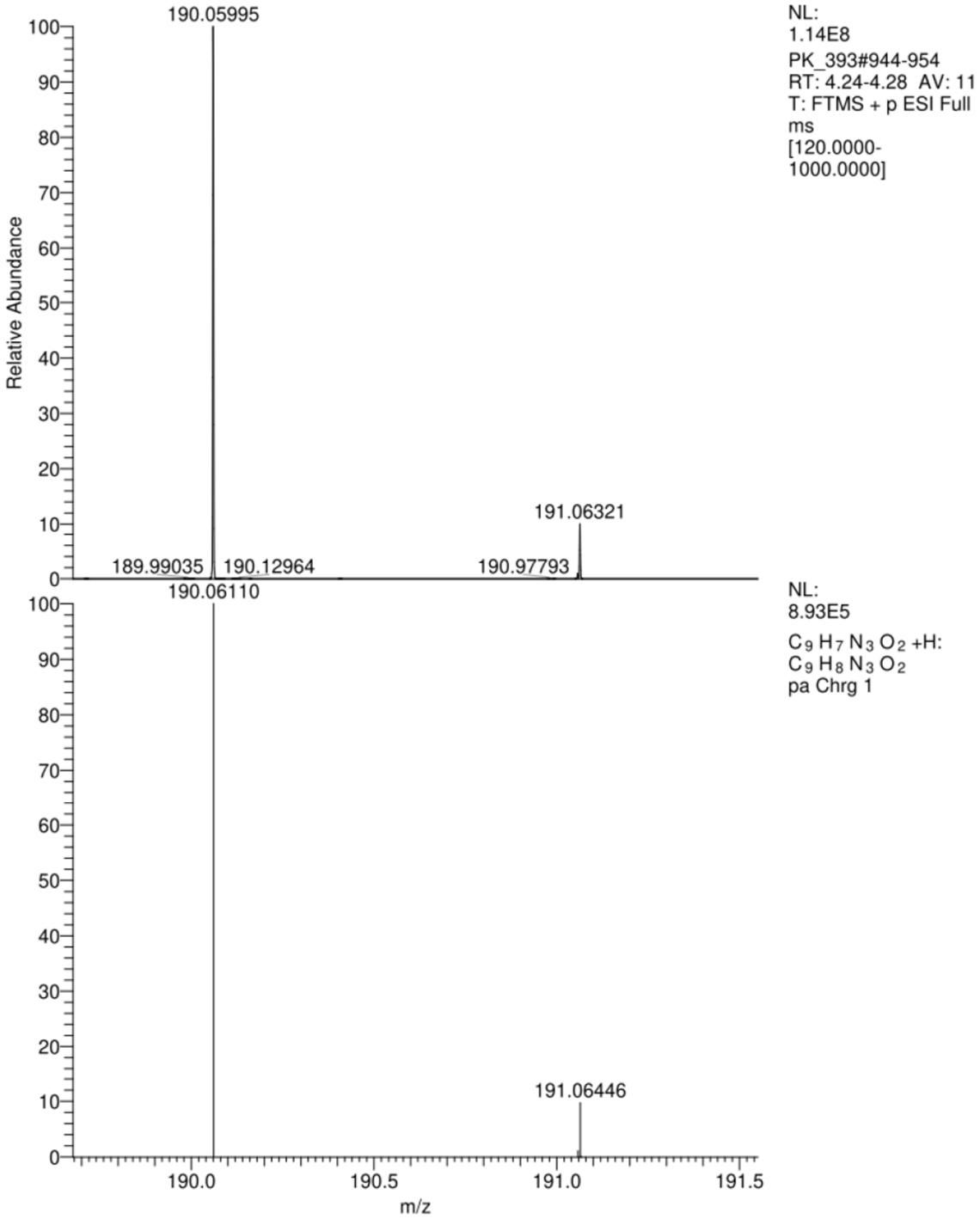

S43

3-(1*H*-1,2,3-triazol-1-yl)benzoic acid (27)

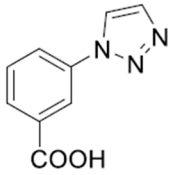

3-(1*H*-1,2,3-triazol-1-yl)benzoic acid

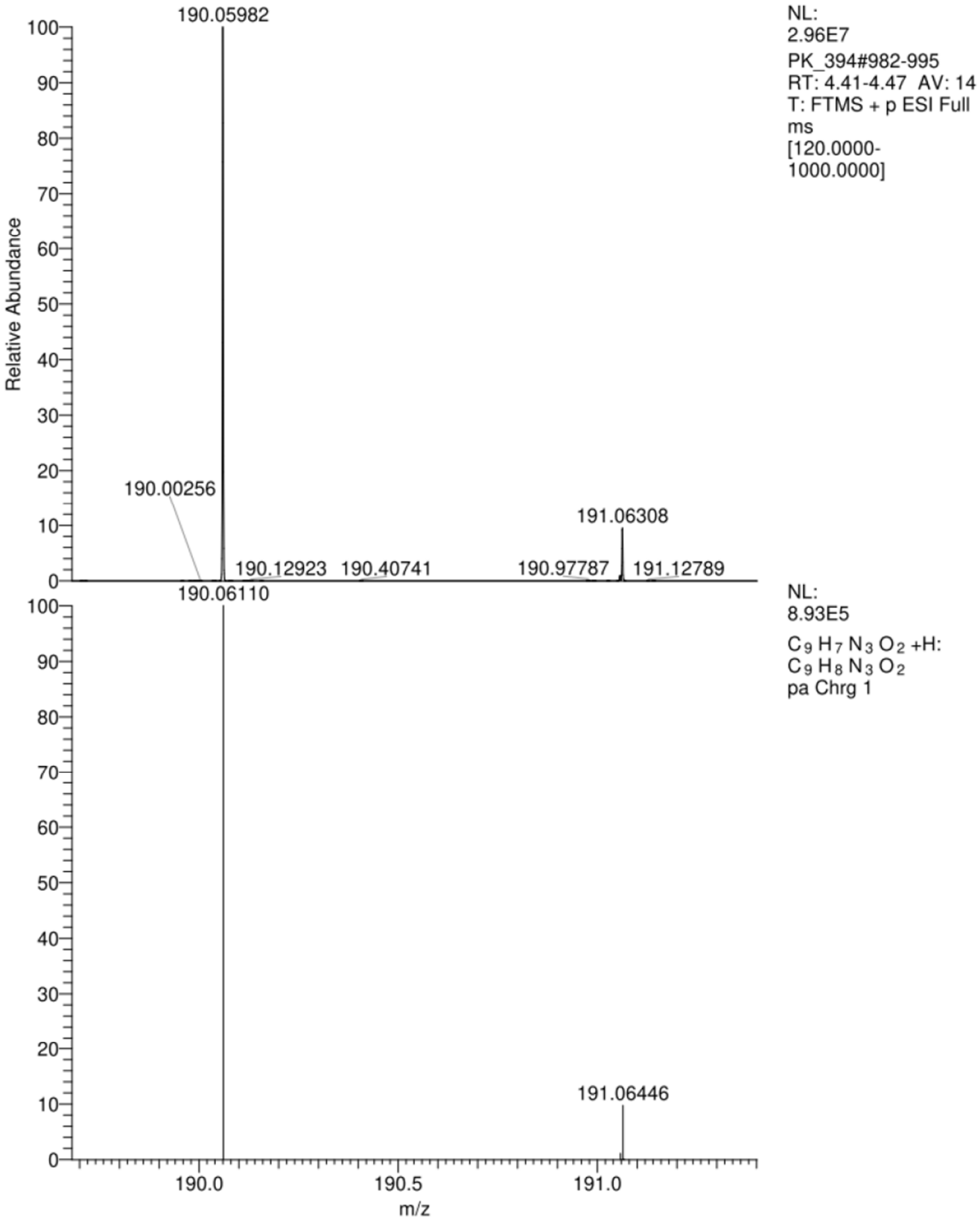

S44

4-(1*H*-1,2,3-triazol-1-yl)benzoic acid (28)

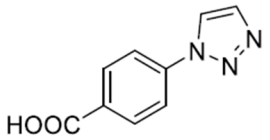

4-(1*H*-1,2,3-triazol-1-yl)benzoic acid

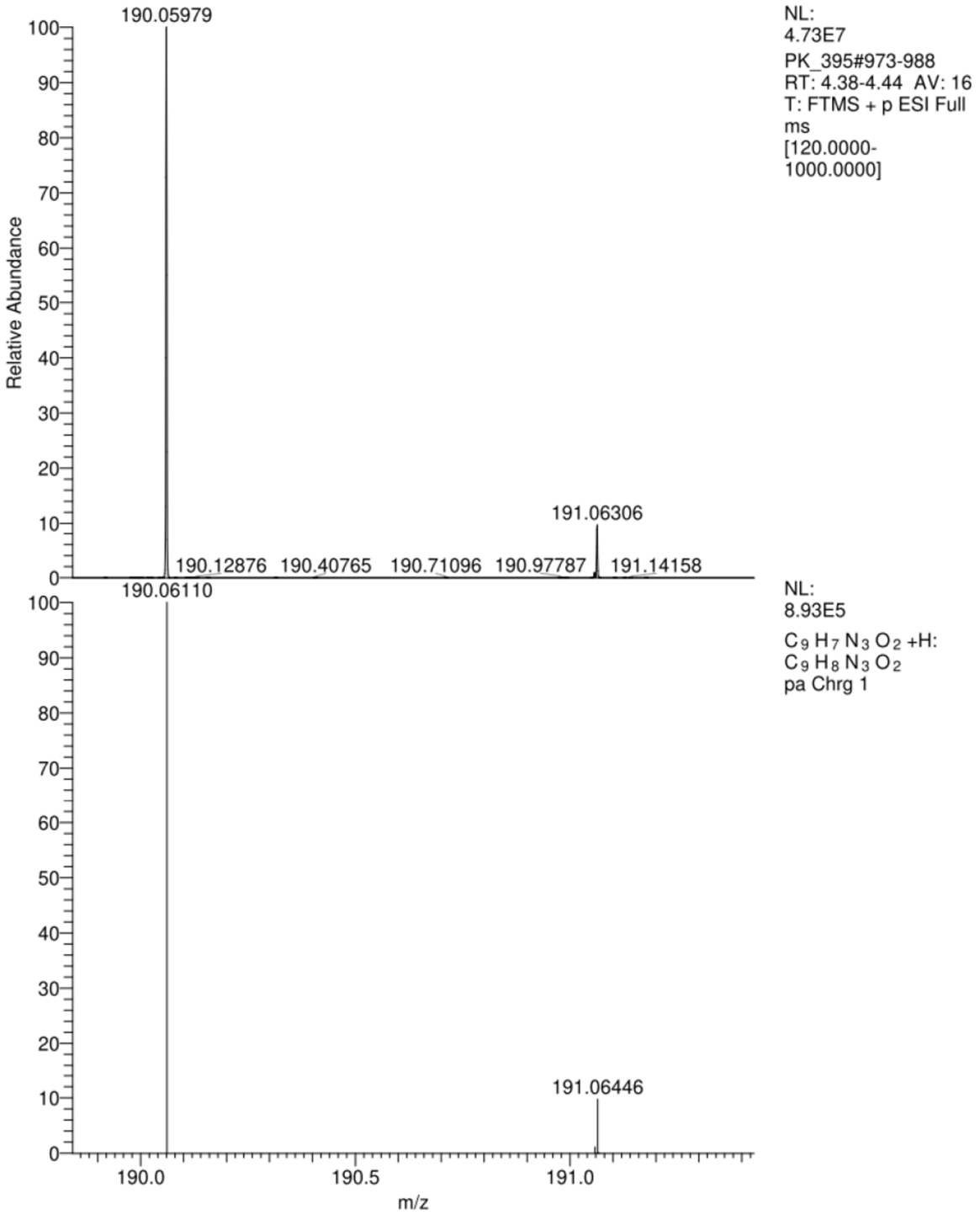

2-(4-phenyl-1*H*-1,2,3-triazol-1-yl)benzoic acid (29)

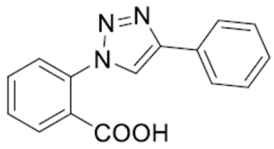

2-(4-phenyl-1*H*-1,2,3-triazol-1-yl)benzoic acid

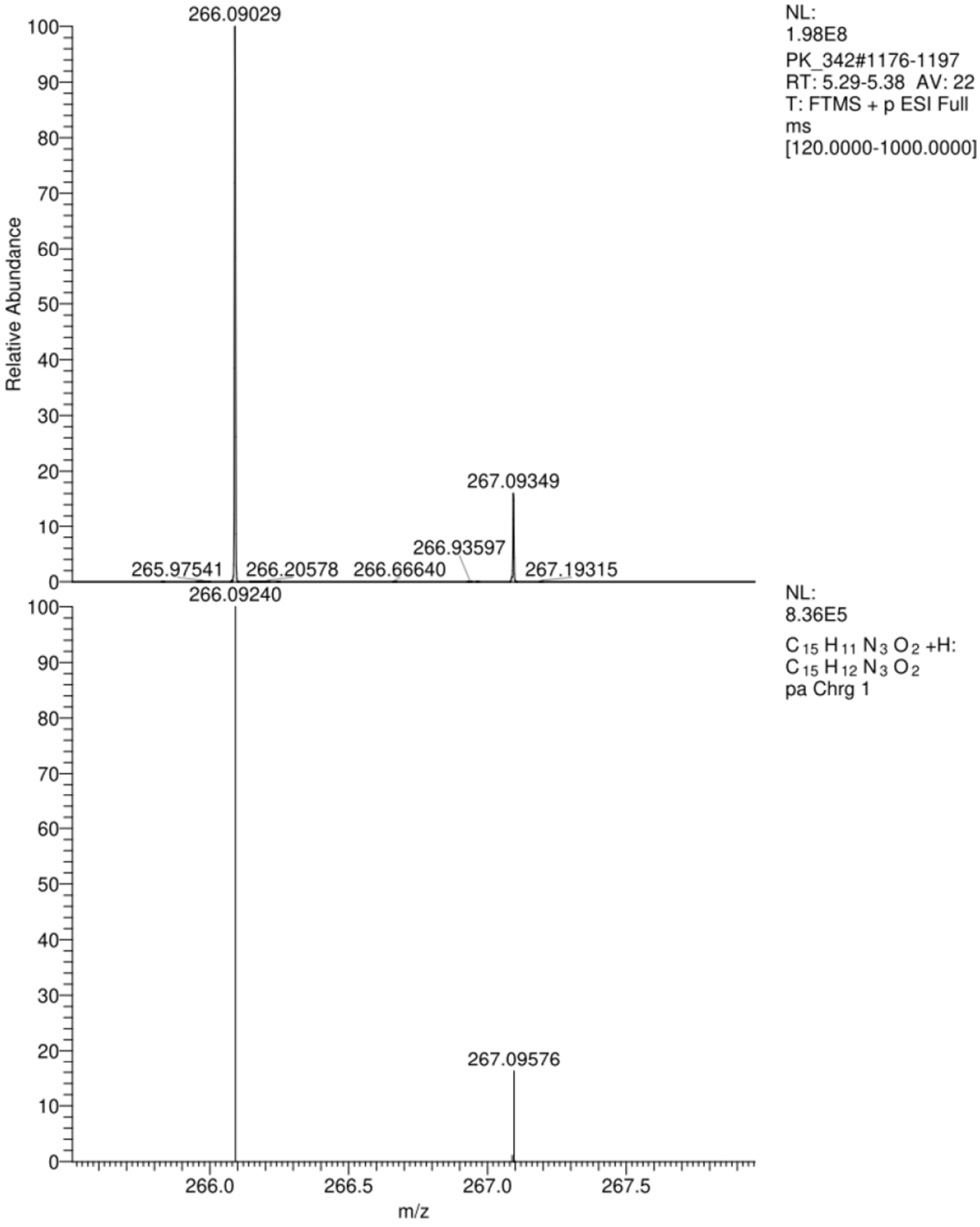

3-(4-phenyl-1*H*-1,2,3-triazol-1-yl)benzoic acid (30)

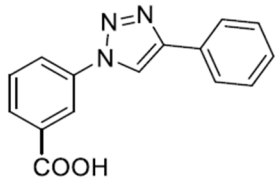

3-(4-phenyl-1*H*-1,2,3-triazol-1-yl)benzoic acid

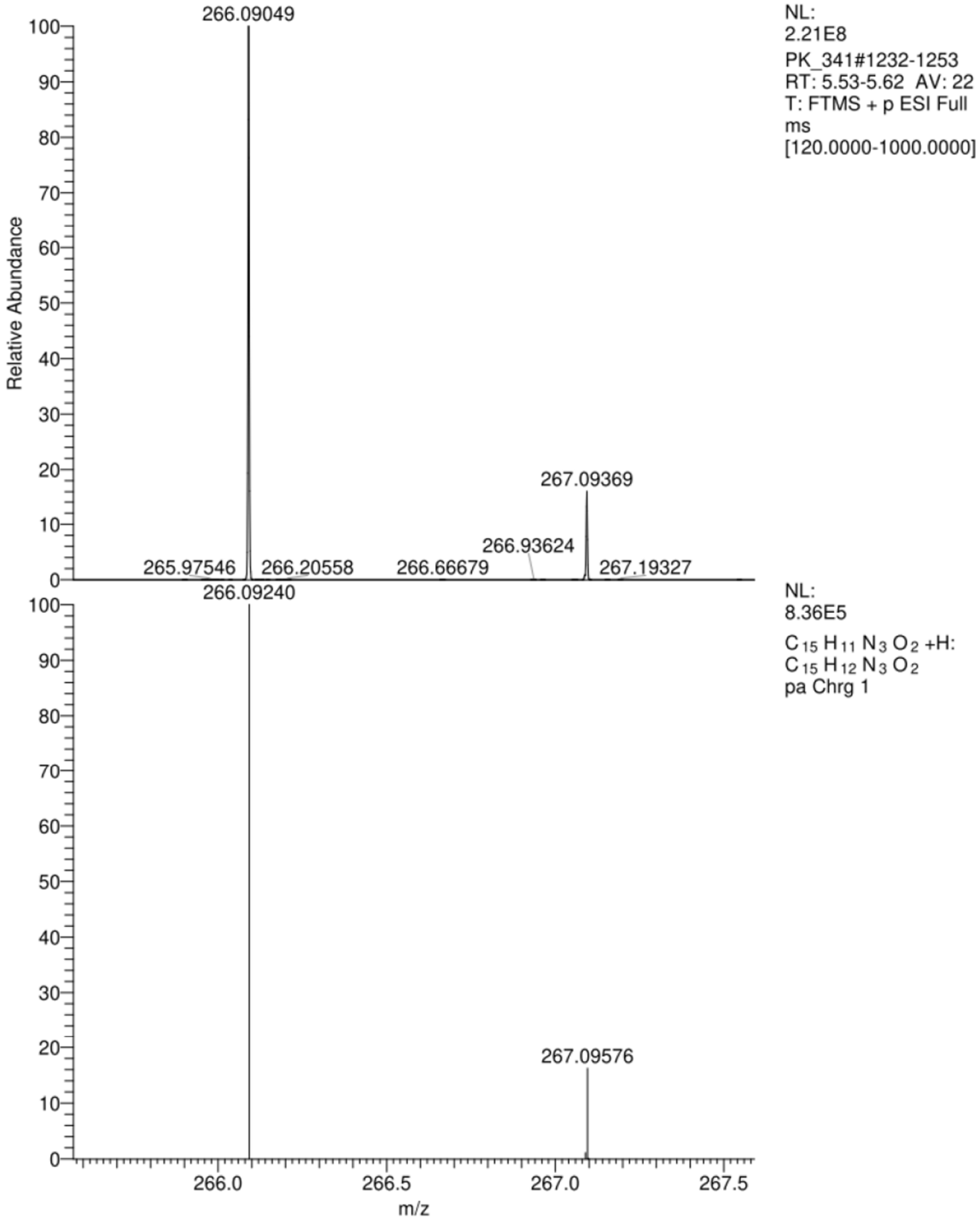

4-(4-phenyl-1*H*-1,2,3-triazol-1-yl)benzoic acid (31)

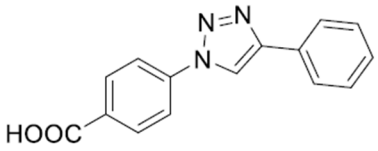

4-(4-phenyl-1*H*-1,2,3-triazol-1-yl)benzoic acid

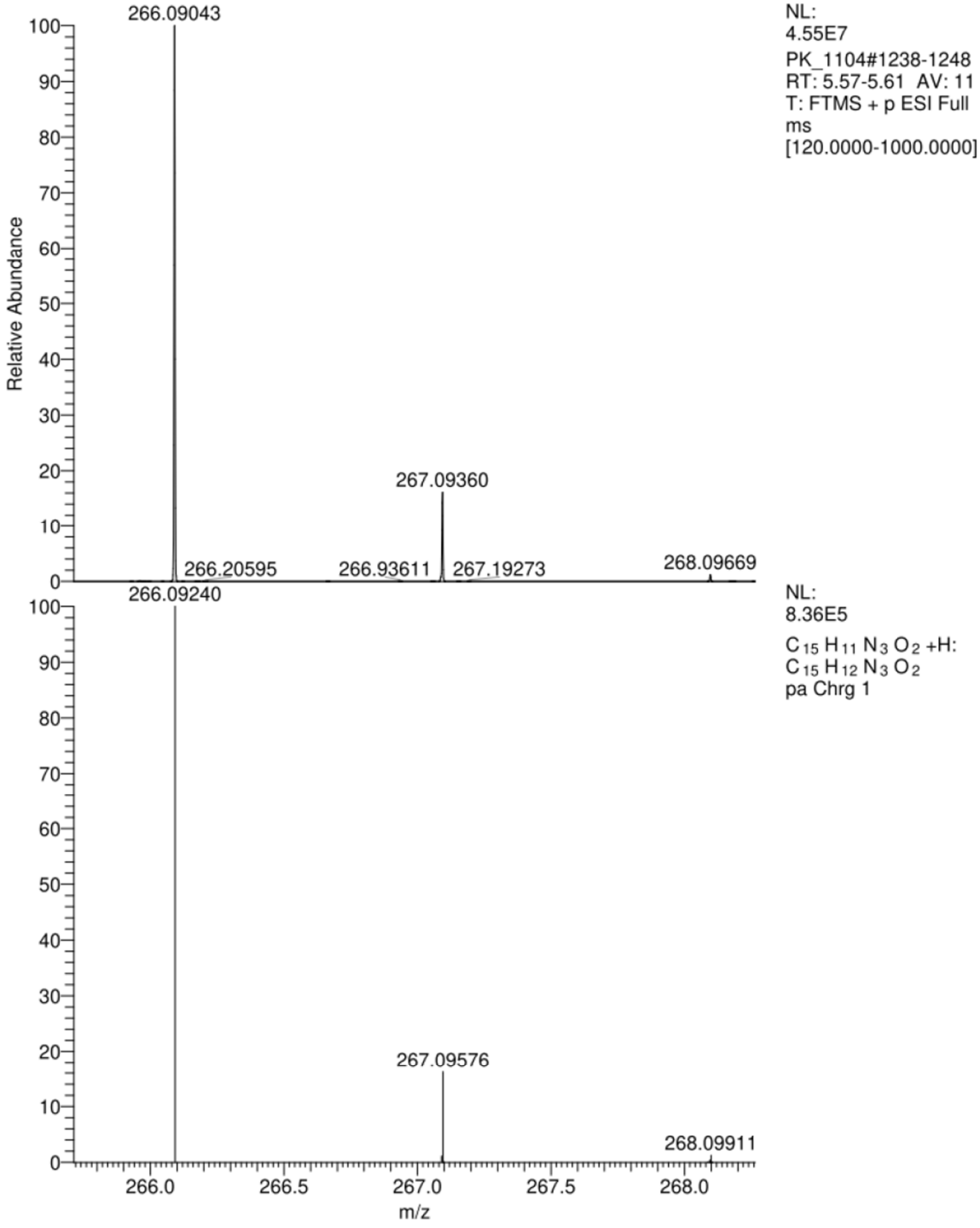

4-(4-(hydroxymethyl)-1*H*-1,2,3-triazol-1-yl)benzoic acid (32)

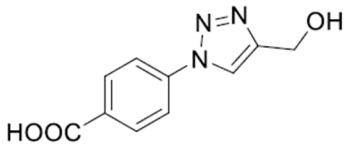

4-(4-(hydroxymethyl)-1*H*-1,2,3-triazol-1-yl)benzoic acid

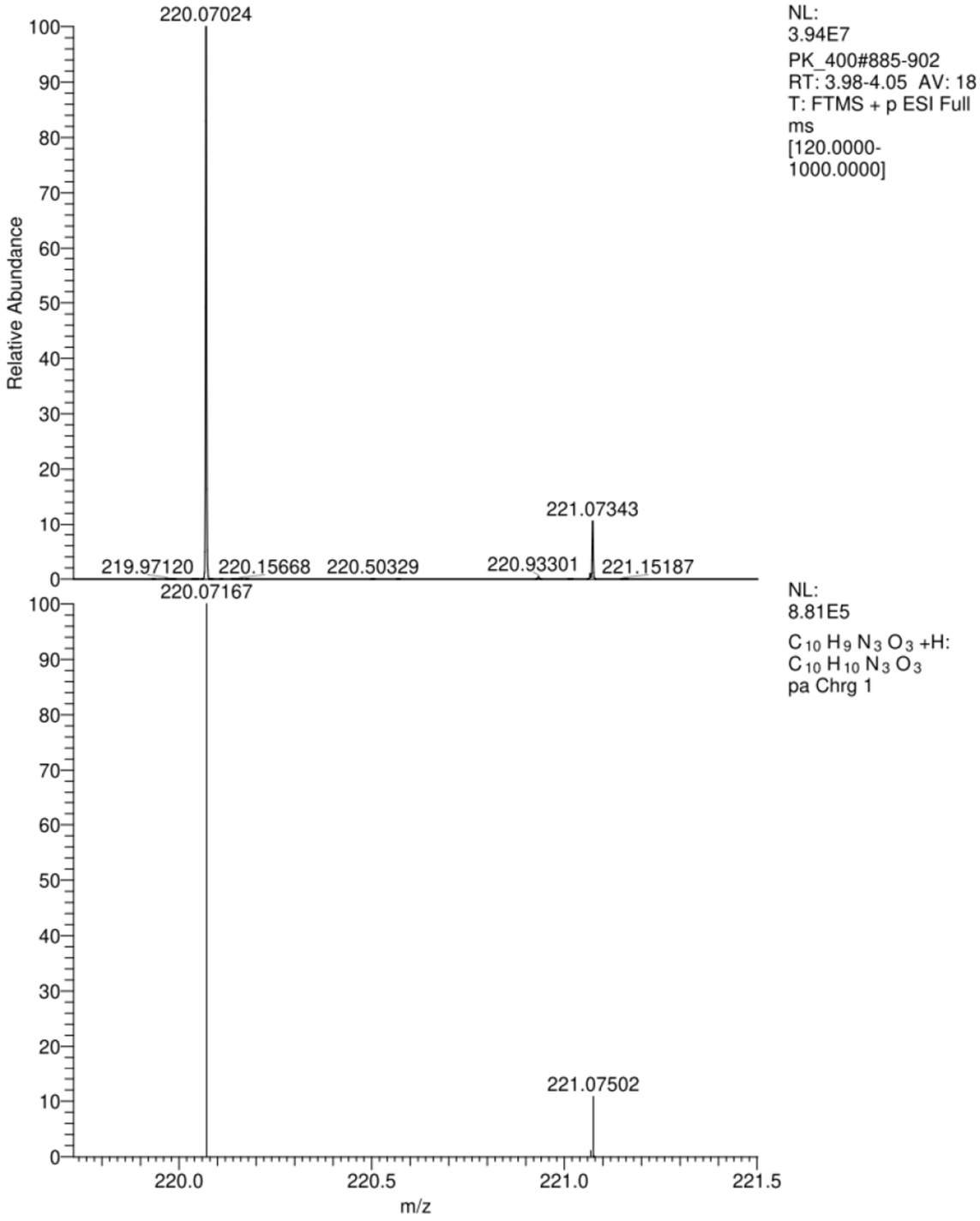

4-(4-(aminomethyl)-1*H*-1,2,3-triazol-1-yl)benzoic acid (33)

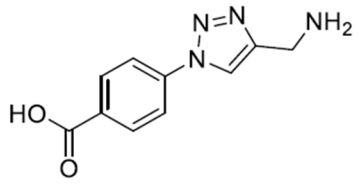

4-(4-(aminomethyl)-1*H*-1,2,3-triazol-1-yl)benzoic acid

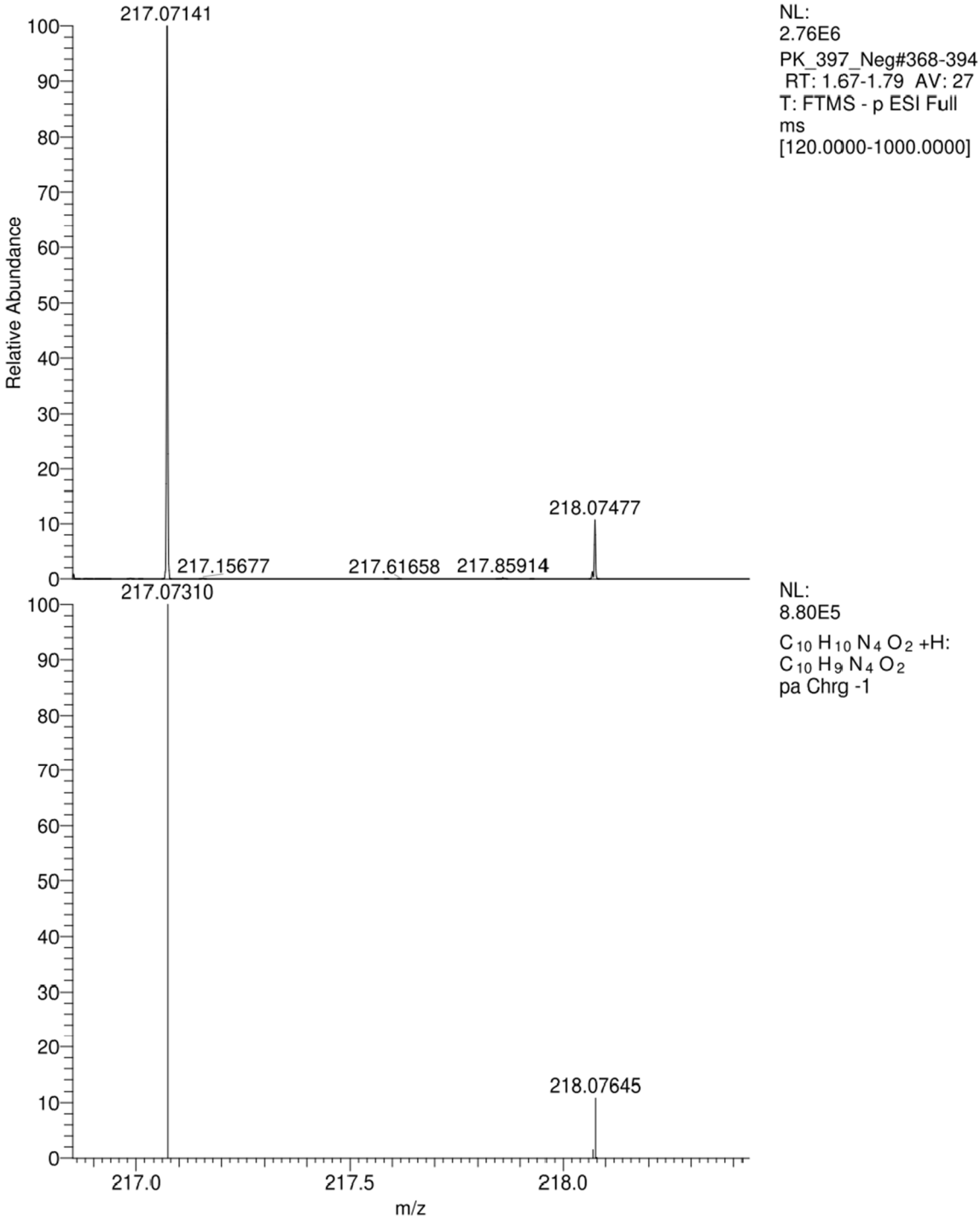

S50

4-(4-(methoxymethyl)-1*H*-1,2,3-triazol-1-yl)benzoic acid (34)

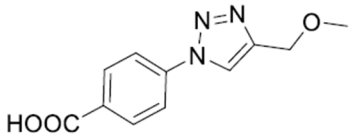

4-(4-(methoxymethyl)-1*H*-1,2,3-triazol-1-yl)benzoic acid

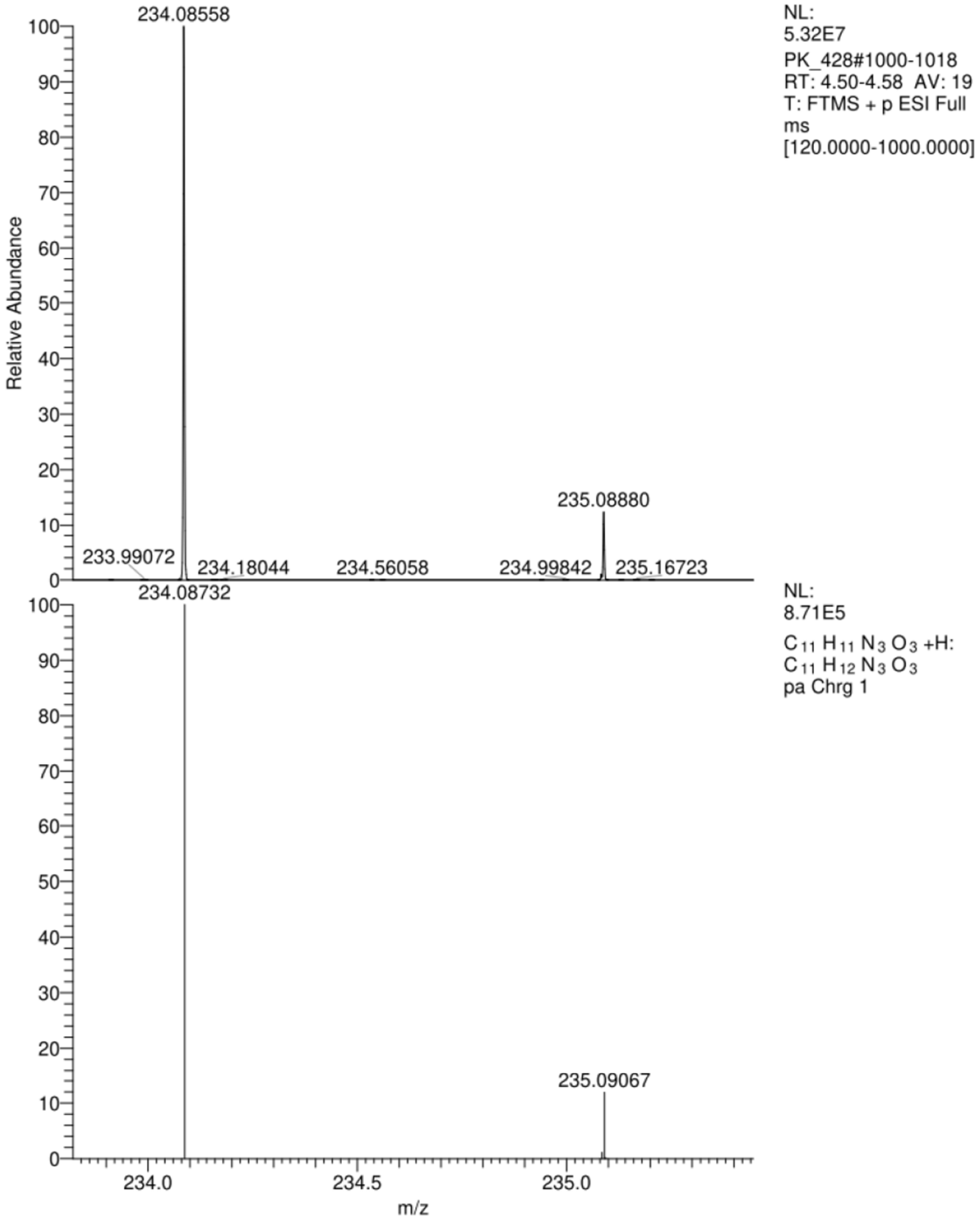

S51

4-(4-(acetoxymethyl)-1*H*-1,2,3-triazol-1-yl)benzoic acid (35)

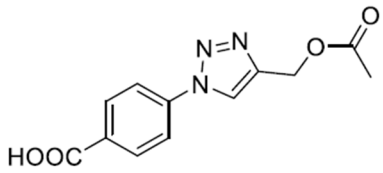

4-(4-(acetoxymethyl)-1*H*-1,2,3-triazol-1-yl)benzoic acid

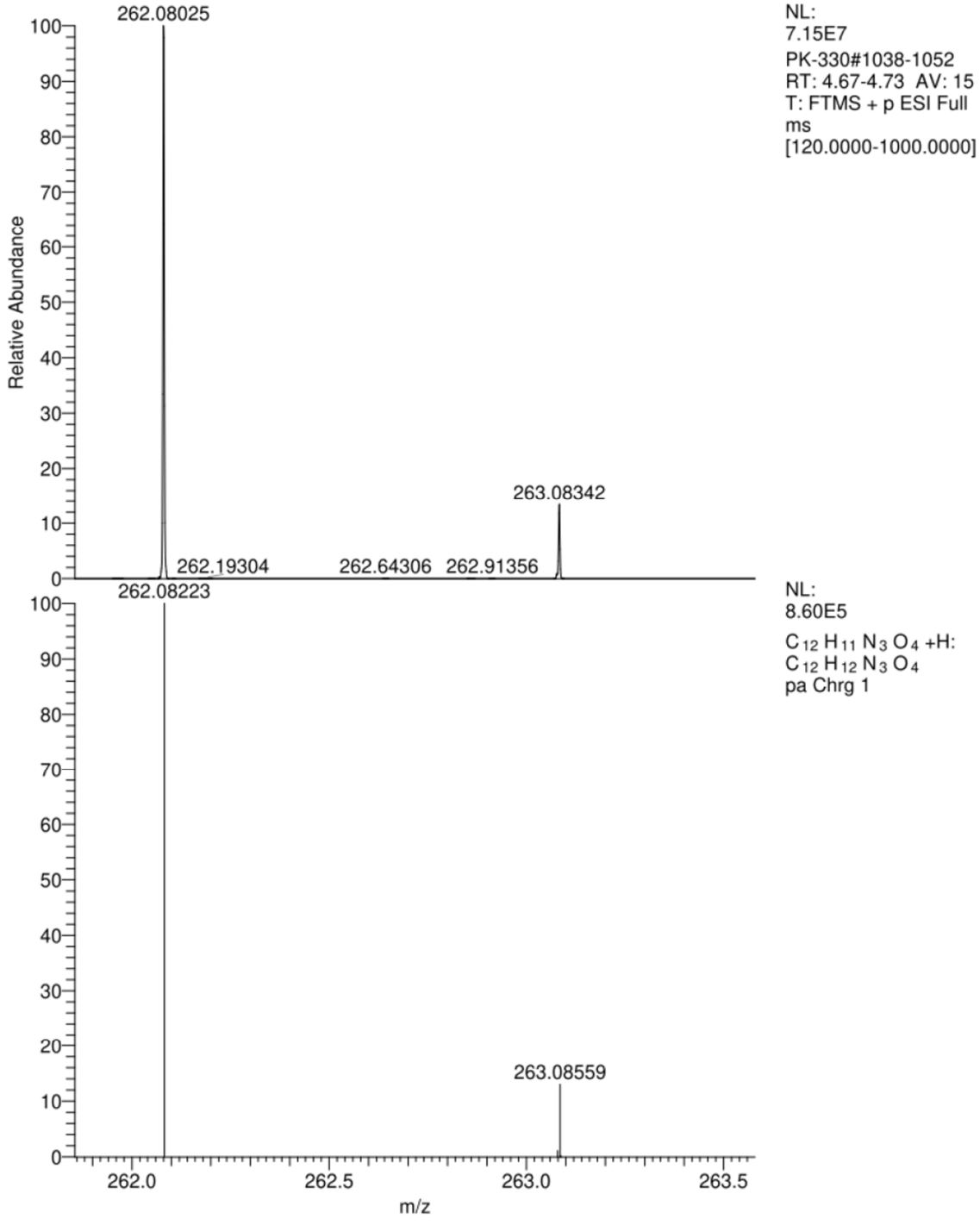

4-(4-(methoxycarbonyl)-1*H*-1,2,3-triazol-1-yl)benzoic acid (36)

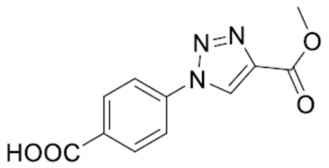

4-(4-(methoxycarbonyl)-1*H*-1,2,3-triazol-1-yl)benzoic acid

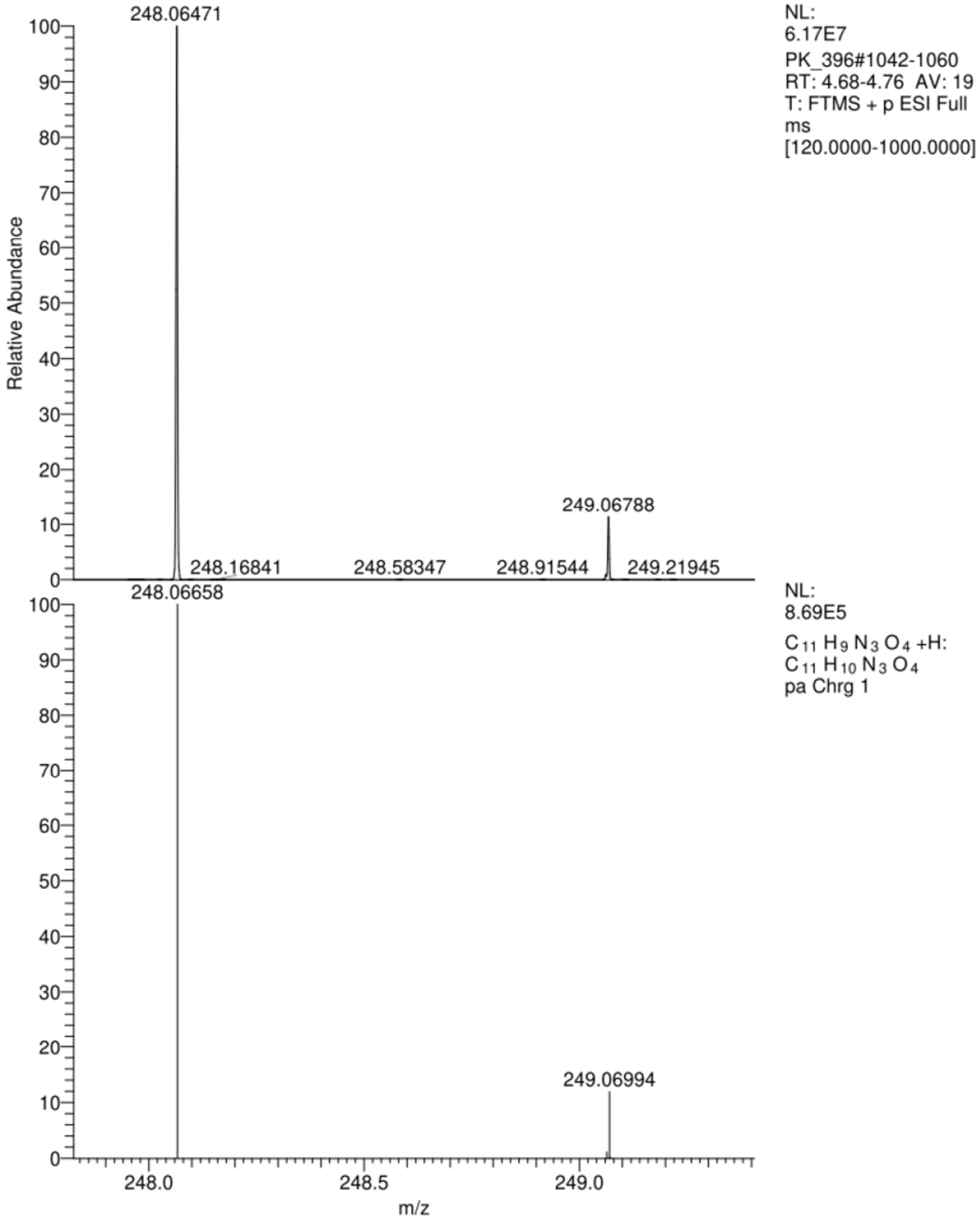

4-(4-(1-hydroxycyclopentyl)-1*H*-1,2,3-triazol-1-yl)benzoic acid (37)

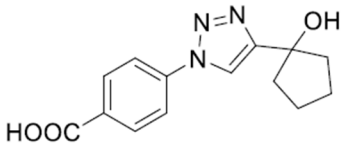

4-(4-(1-hydroxycyclopentyl)-1*H*-1,2,3-triazol-1-yl)benzoic acid

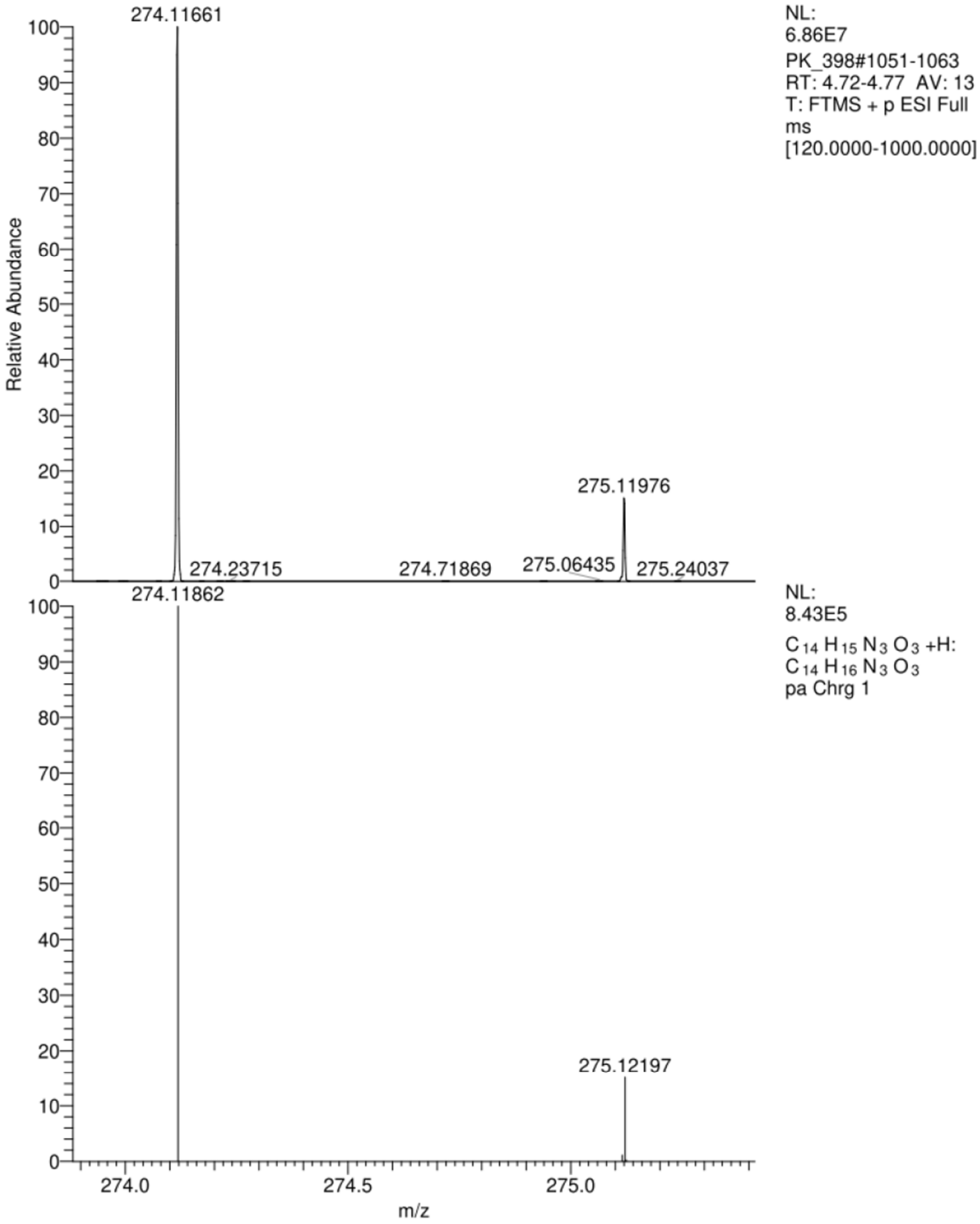

4-(4-cyclopropyl-1*H*-1,2,3-triazol-1-yl)benzoic acid (38)

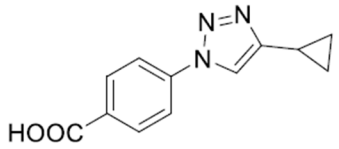

4-(4-cyclopropyl-1*H*-1,2,3-triazol-1-yl)benzoic acid

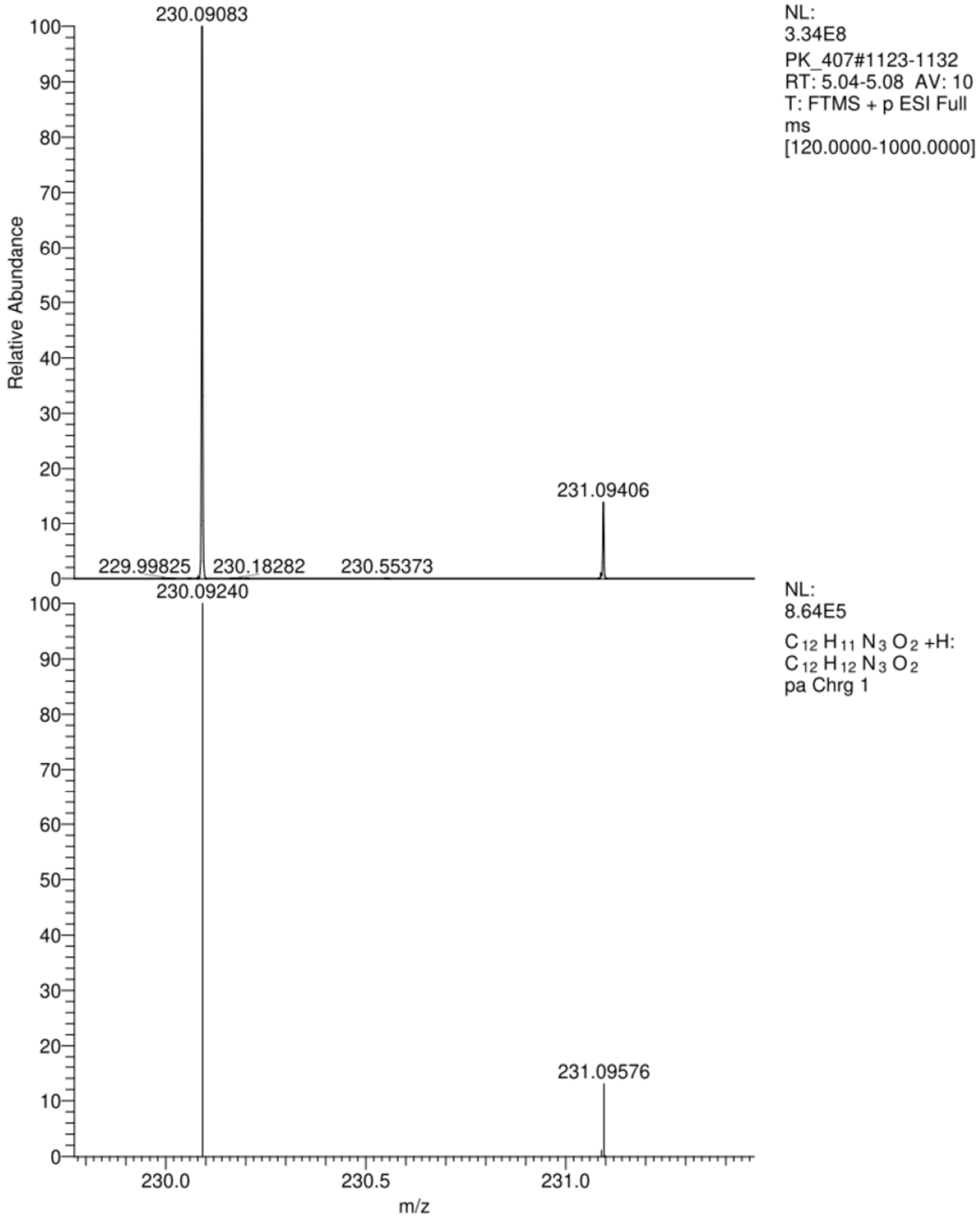

S55

methyl 4-(4-(hydroxymethyl)-1*H*-1,2,3-triazol-1-yl)benzoate (39)

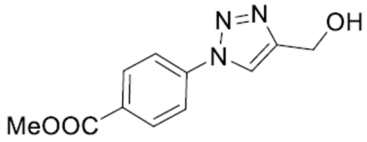

methyl 4-(4-(hydroxymethyl)-1*H*-1,2,3-triazol-1-yl)benzoate

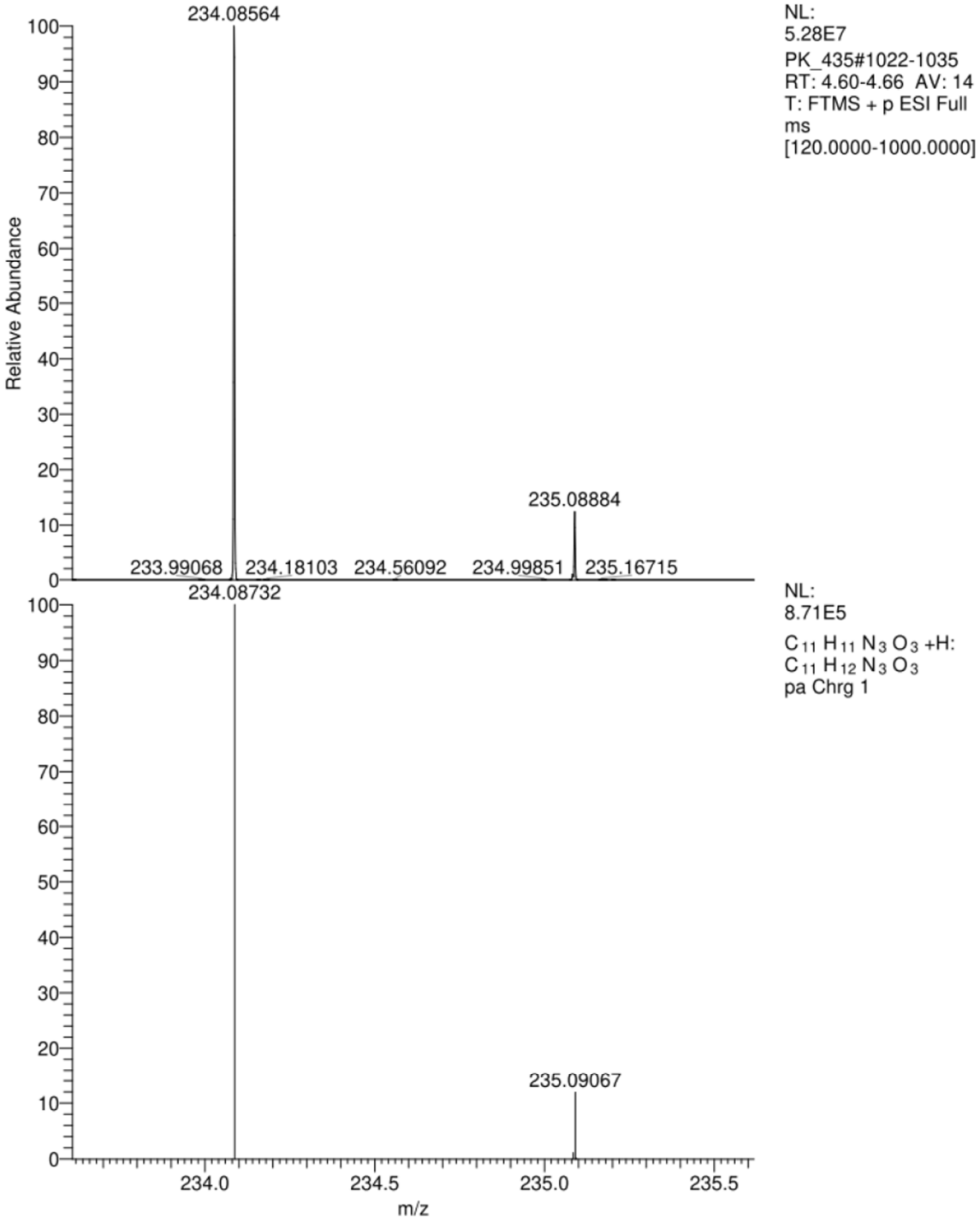

methyl 4-(4-(methoxymethyl)-1H-1,2,3-triazol-1-yl)benzoate (40)

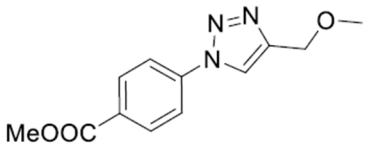

methyl 4-(4-(methoxymethyl)-1*H*-1,2,3-triazol-1-yl)benzoate

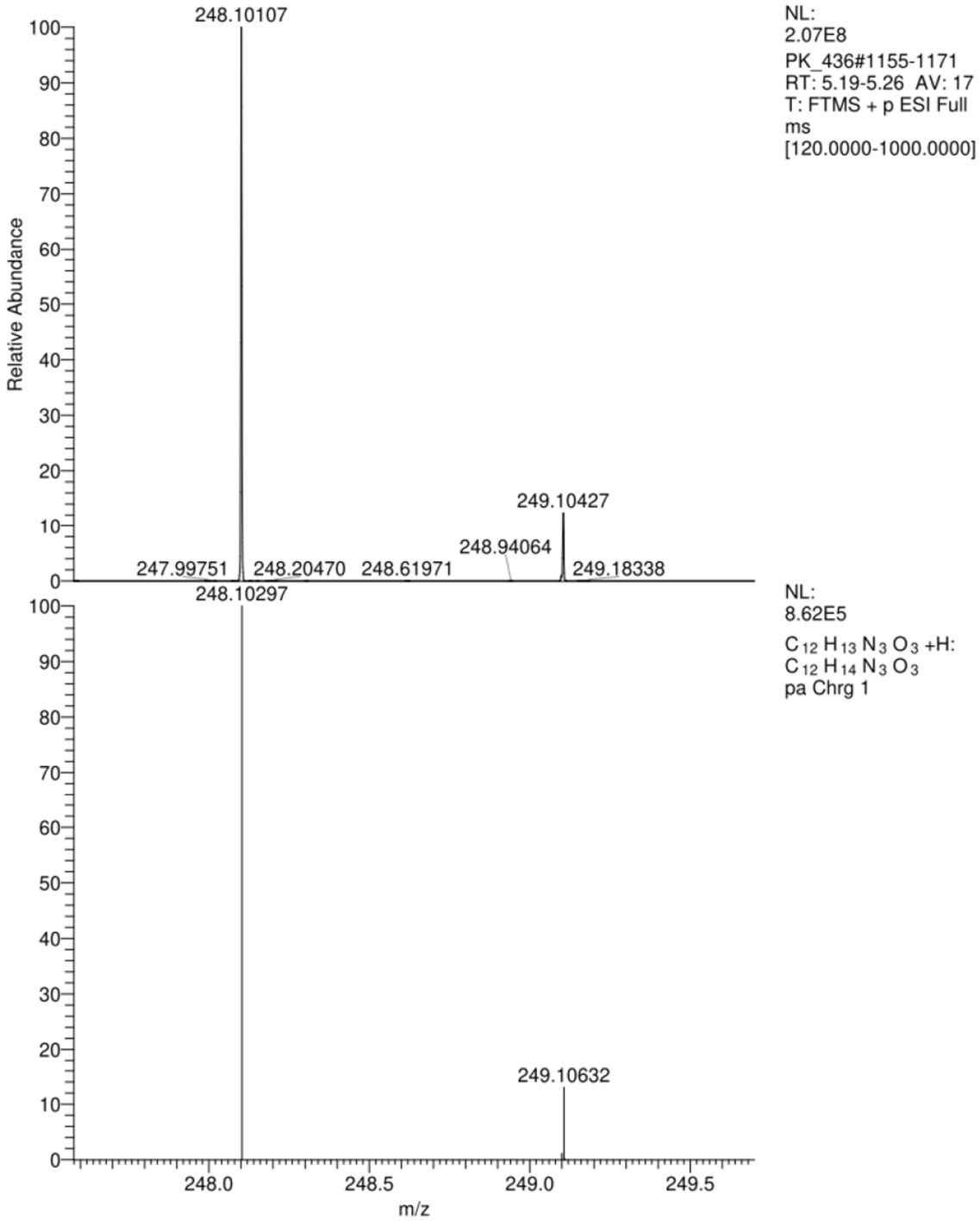

4-(4-(2-aminophenyl)-1*H*-1,2,3-triazol-1-yl)benzoic acid (41)

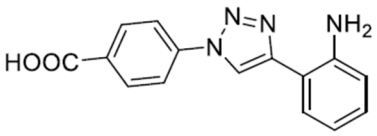

4-(4-(2-aminophenyl)-1*H*-1,2,3-triazol-1-yl)benzoic acid

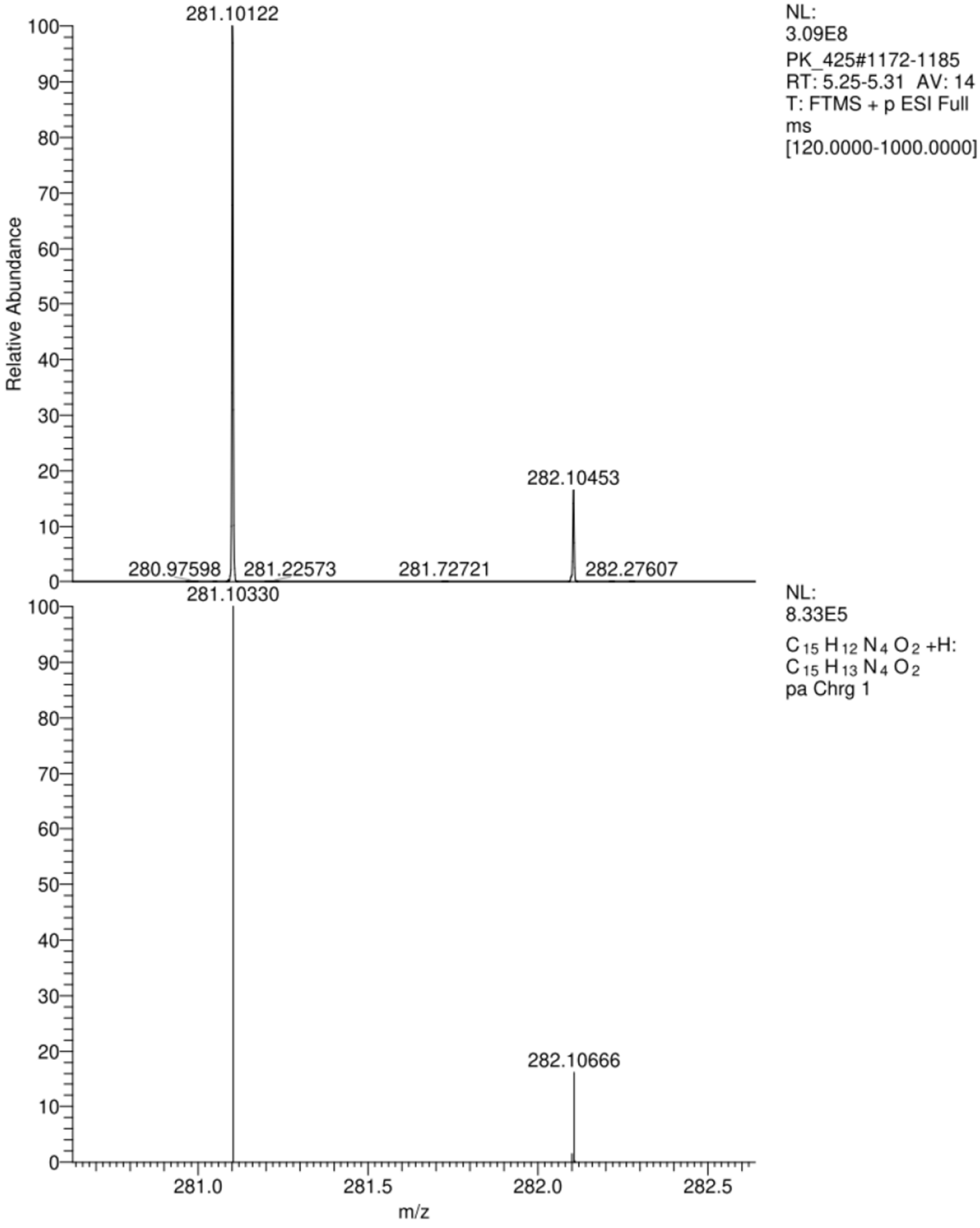

4-(4-(3-aminophenyl)-1*H*-1,2,3-triazol-1-yl)benzoic acid (42)

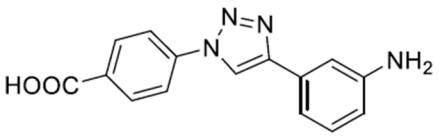

4-(4-(3-aminophenyl)-1*H*-1,2,3-triazol-1-yl)benzoic acid

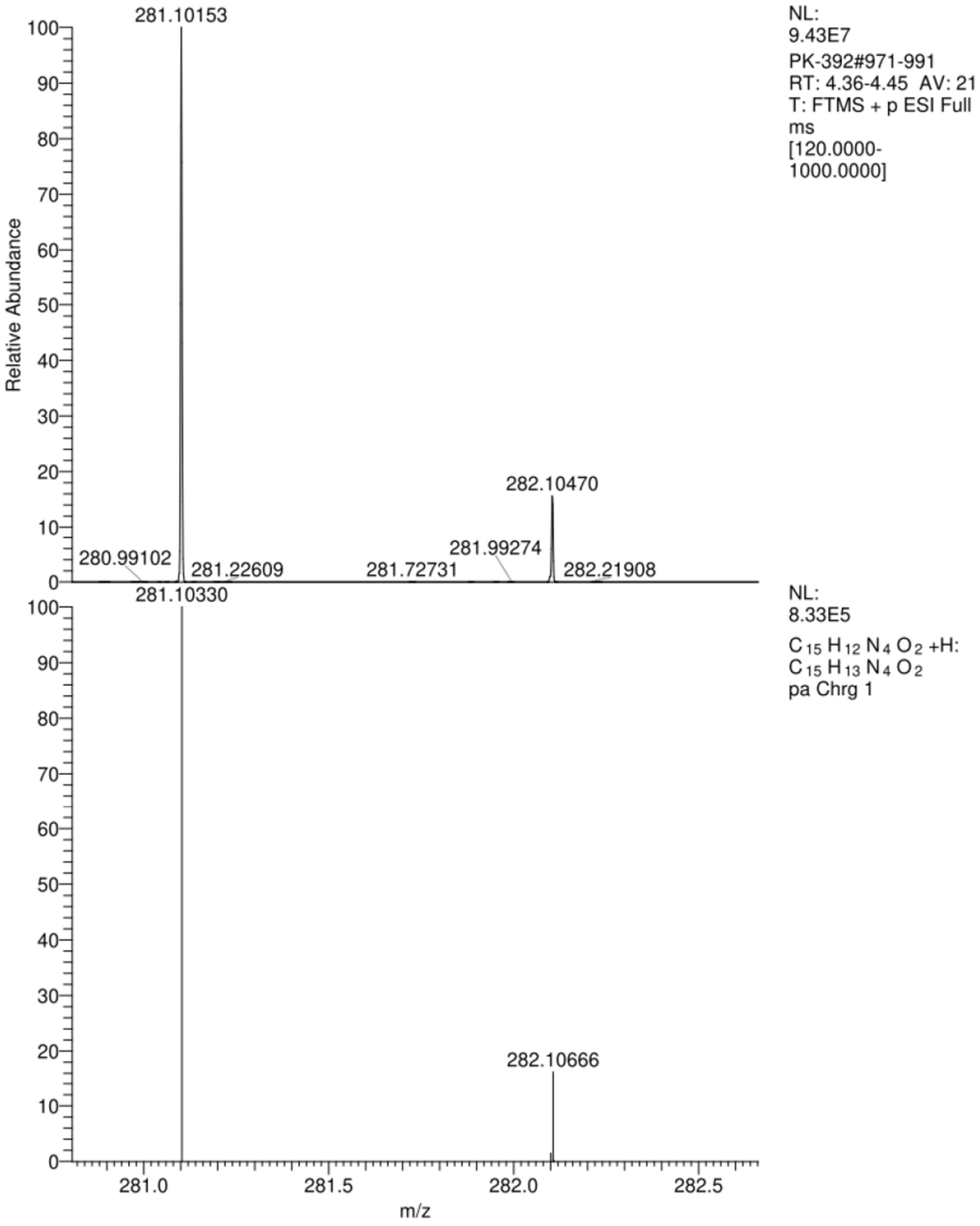

S59

4-(4-(4-aminophenyl)-1*H*-1,2,3-triazol-1-yl)benzoic acid (43)

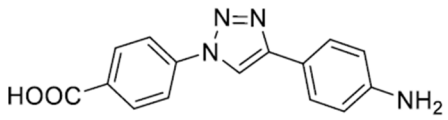

4-(4-(4-aminophenyl)-1*H*-1,2,3-triazol-1-yl)benzoic acid

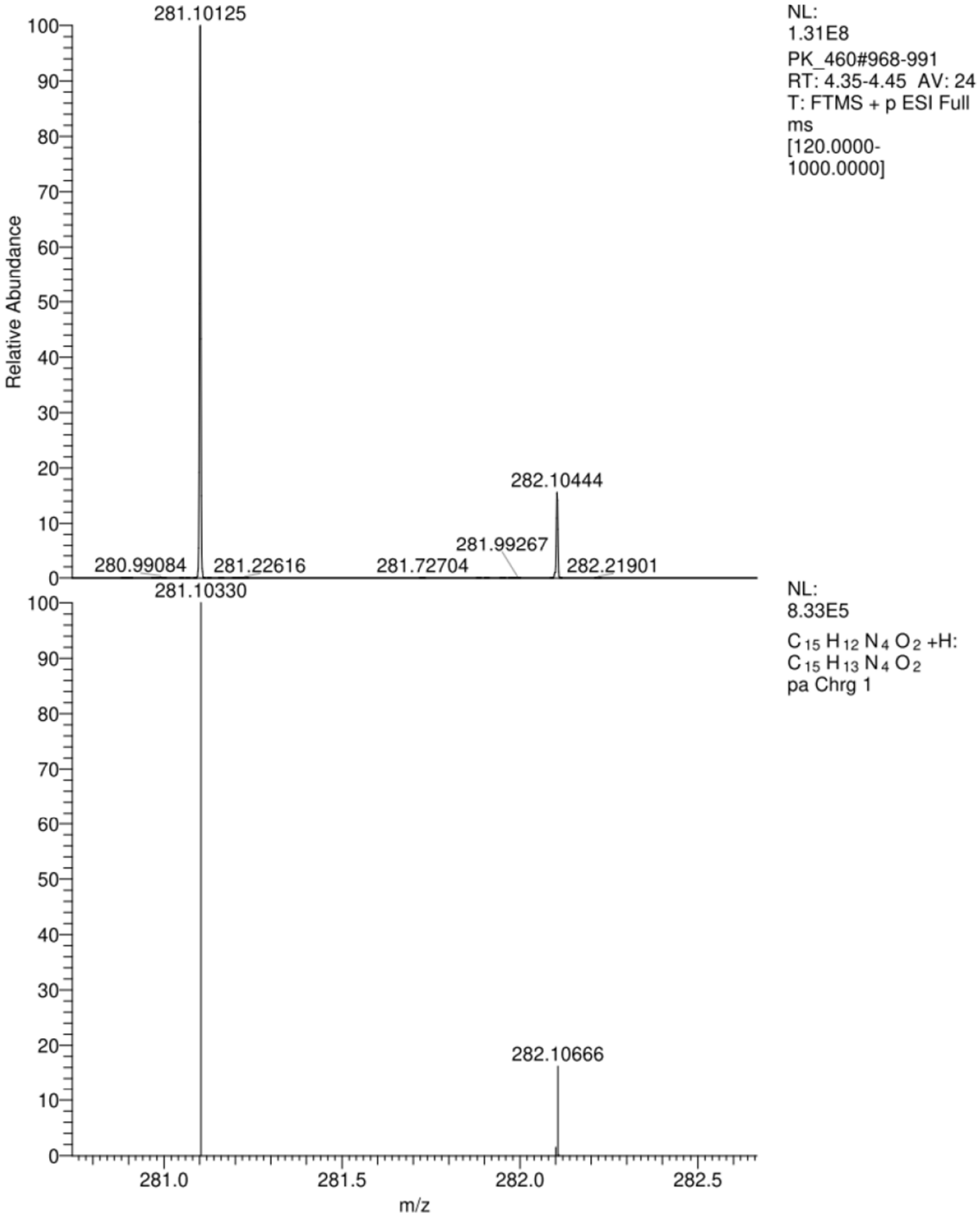

4-(4-(4-(hydroxymethyl)phenyl)-1*H*-1,2,3-triazol-1-yl)benzoic acid (44)

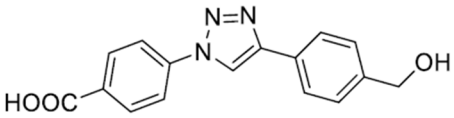

4-(4-(4-(hydroxymethyl)phenyl)-1*H*-1,2,3-triazol-1-yl)benzoic acid

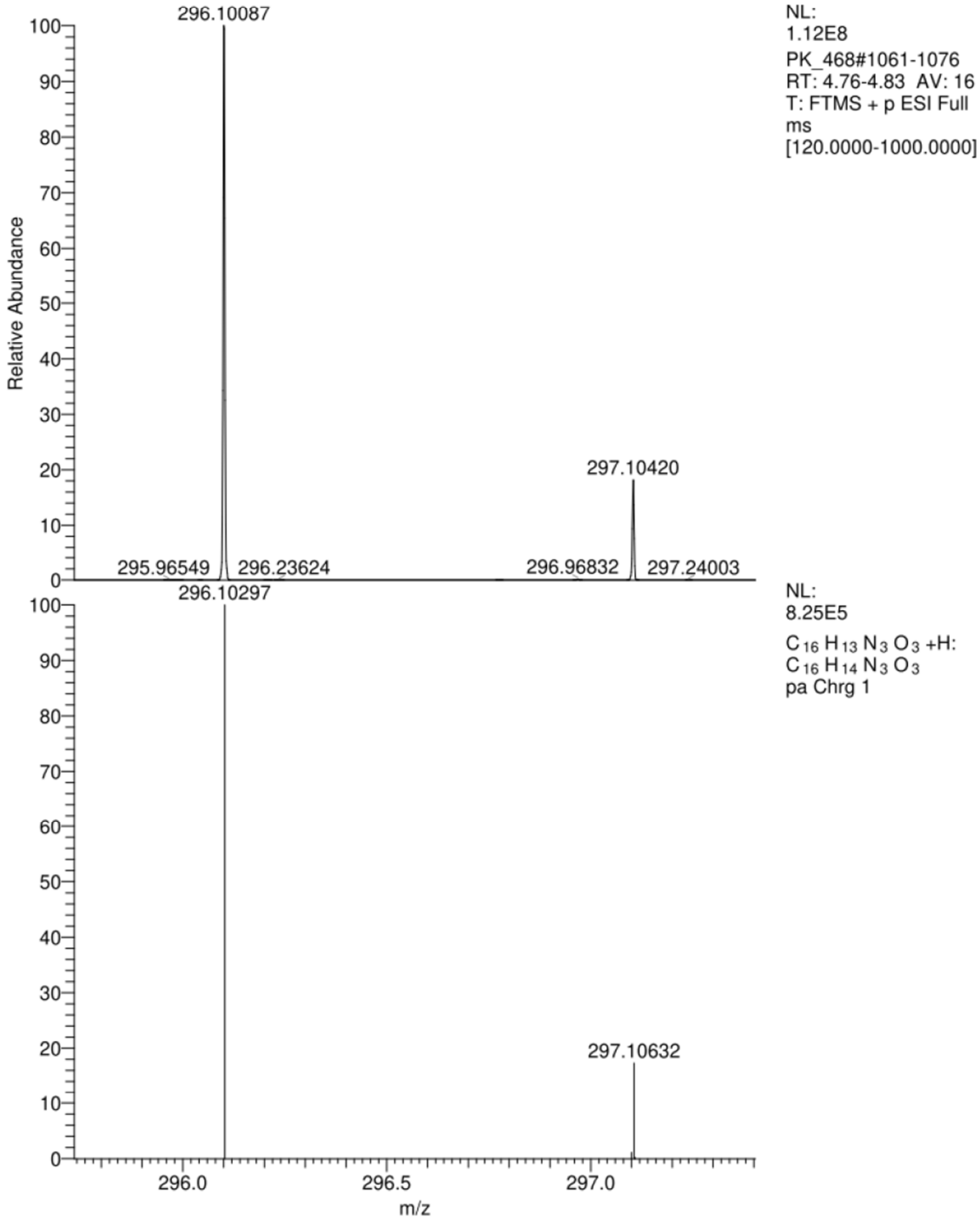

S61

4-(4-(4-methoxyphenyl)-1*H*-1,2,3-triazol-1-yl)benzoic acid (45):

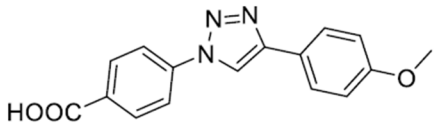

4-(4-(4-methoxyphenyl)-1*H*-1,2,3-triazol-1-yl)benzoic acid

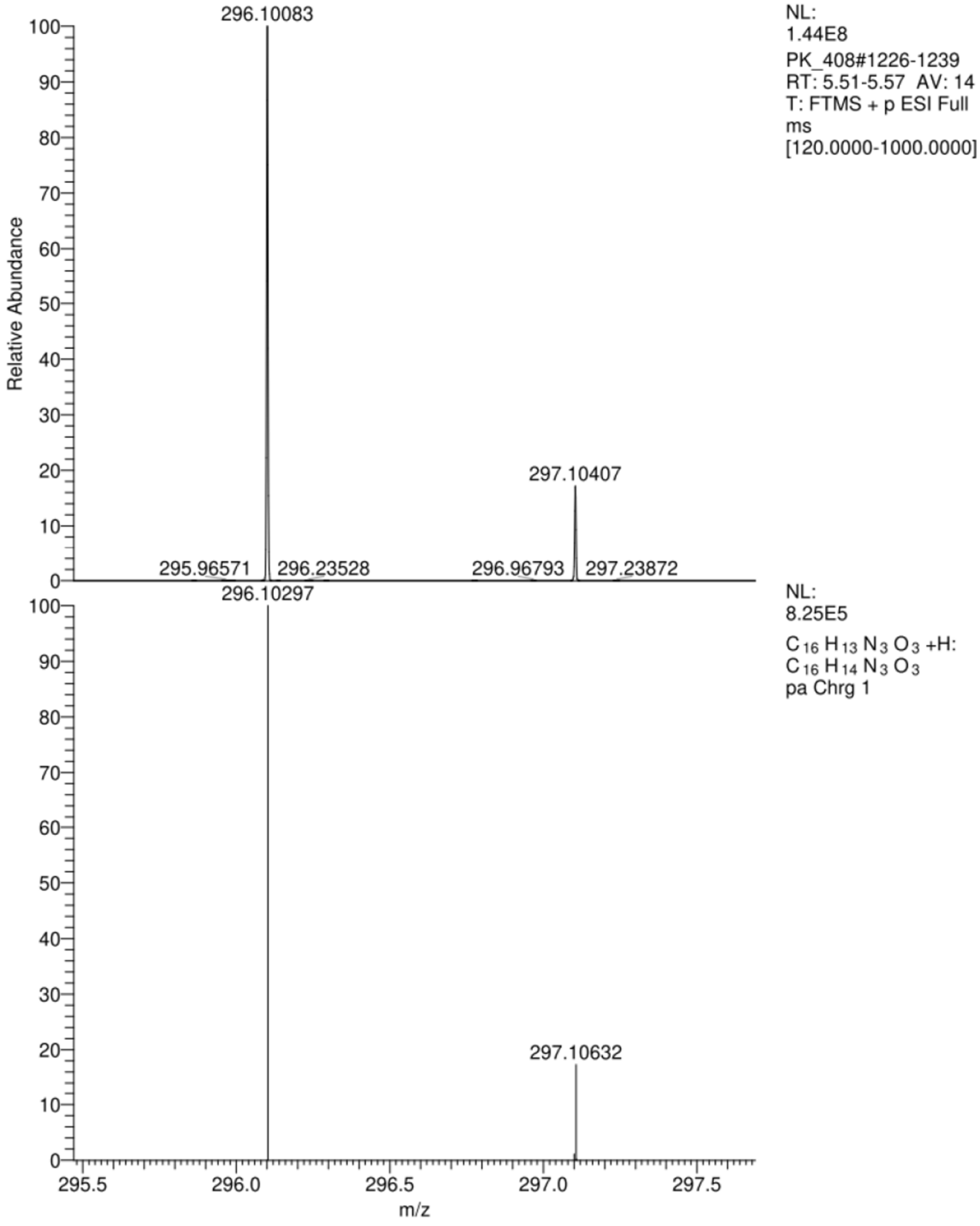

3-(1-phenyl-1*H*-1,2,3-triazol-4-yl)aniline (46)

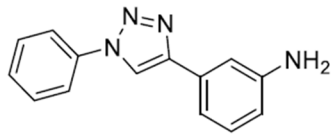

3-(1-phenyl-1*H*-1,2,3-triazol-4-yl)aniline

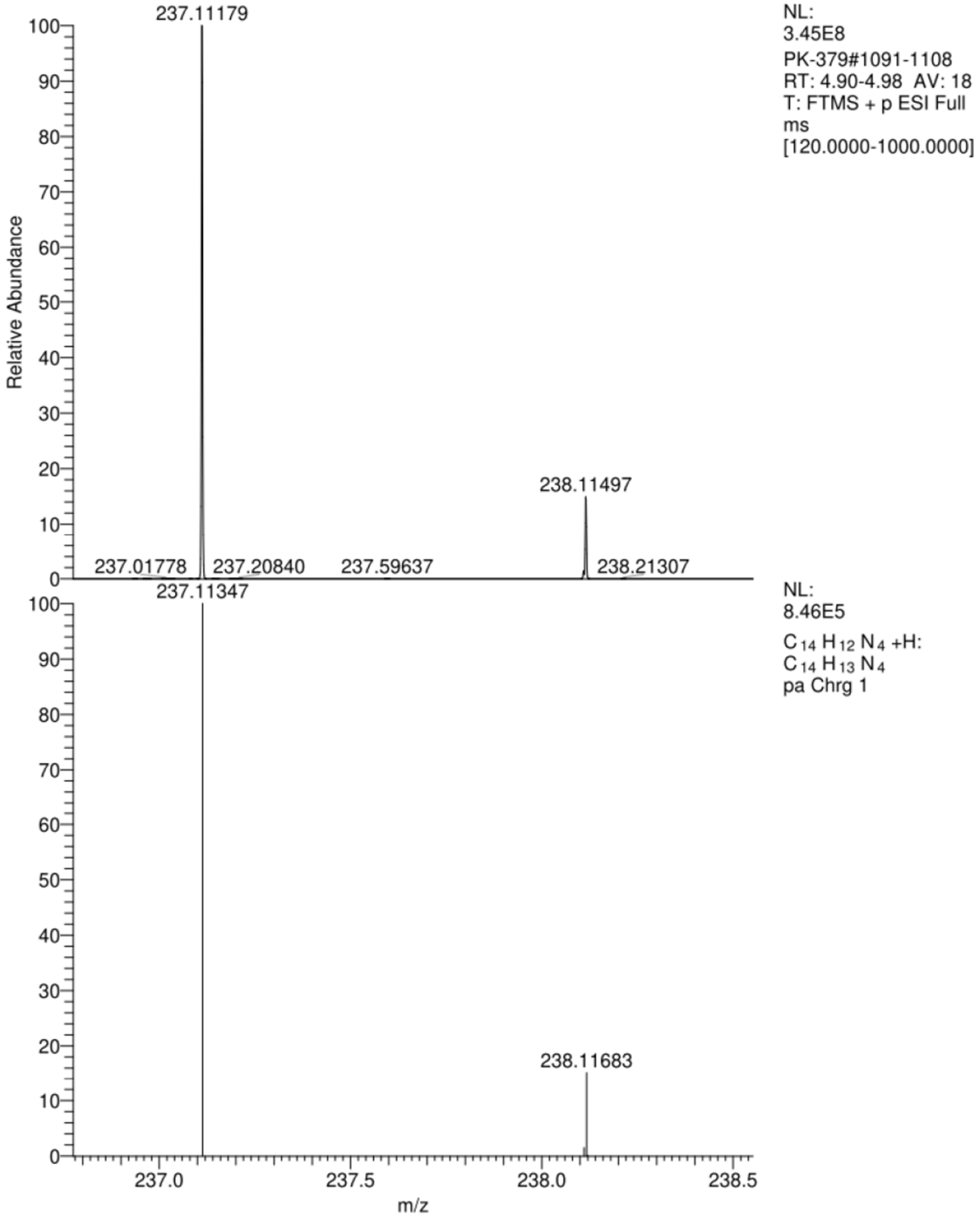

S63

4-(1-(2-aminophenyl)-1*H*-1,2,3-triazol-4-yl)benzoic acid (47)

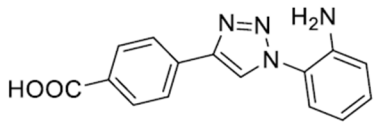

4-(1-(2-aminophenyl)-1*H*-1,2,3-triazol-4-yl)benzoic acid

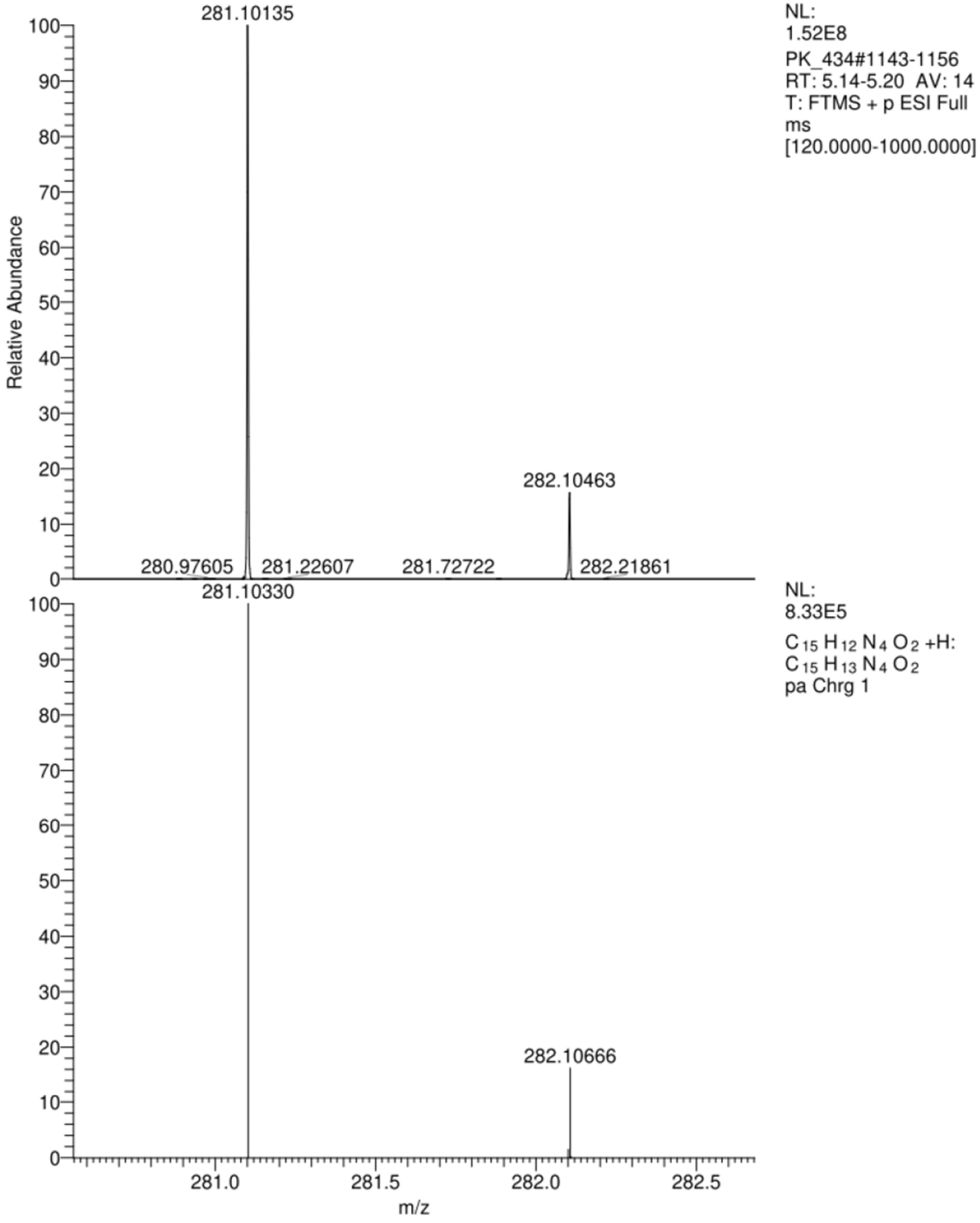

4-(1-(4-aminophenyl)-1*H*-1,2,3-triazol-4-yl)benzoic acid (48)

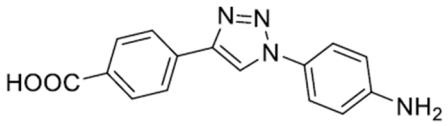

4-(1-(4-aminophenyl)-1*H*-1,2,3-triazol-4-yl)benzoic acid

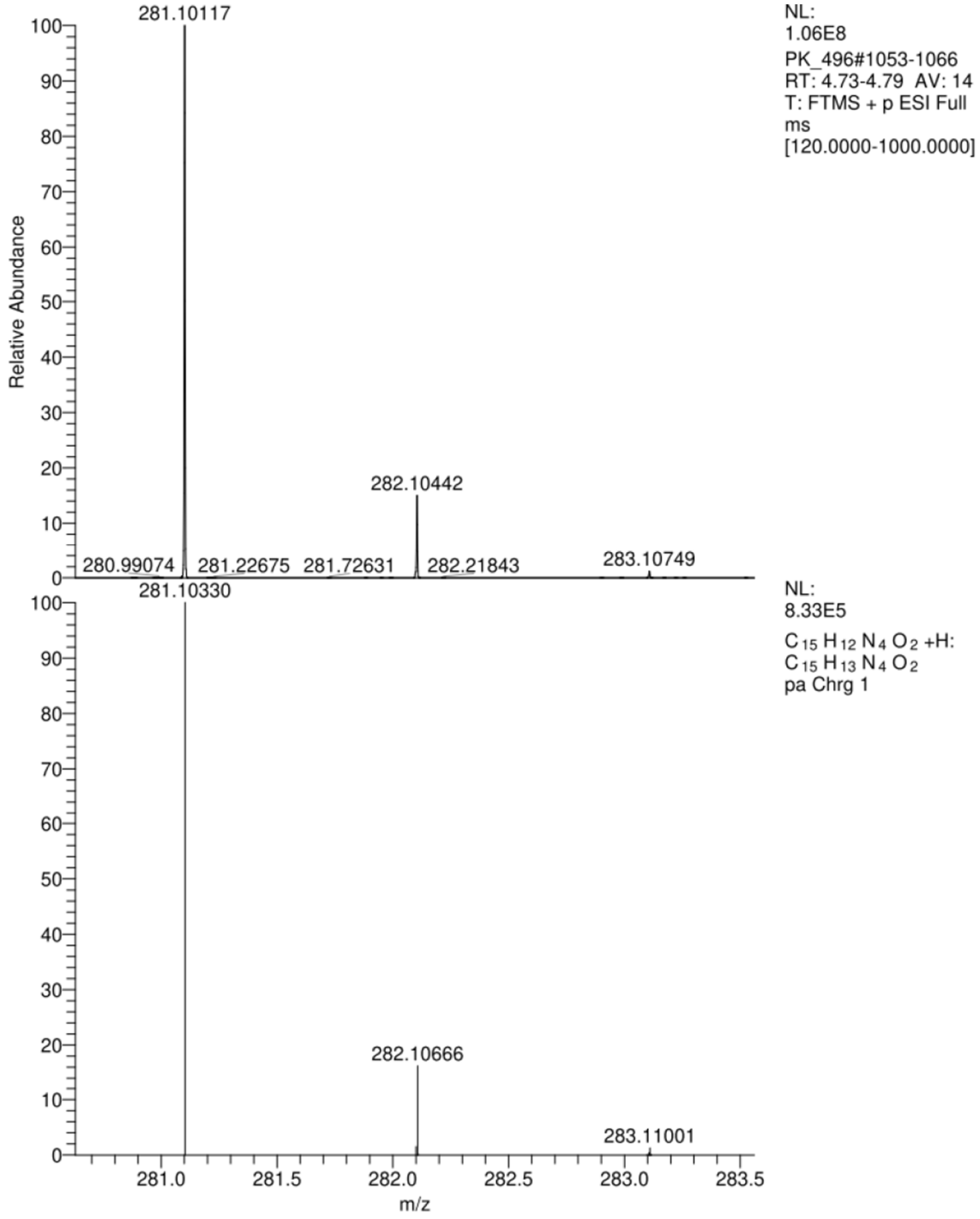

S65

4-(1-(4-hydroxyphenyl)-1*H*-1,2,3-triazol-4-yl)benzoic acid (49)

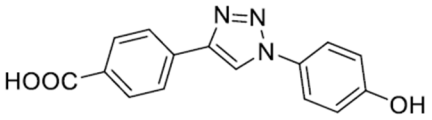

4-(1-(4-hydroxyphenyl)-1*H*-1,2,3-triazol-4-yl)benzoic acid

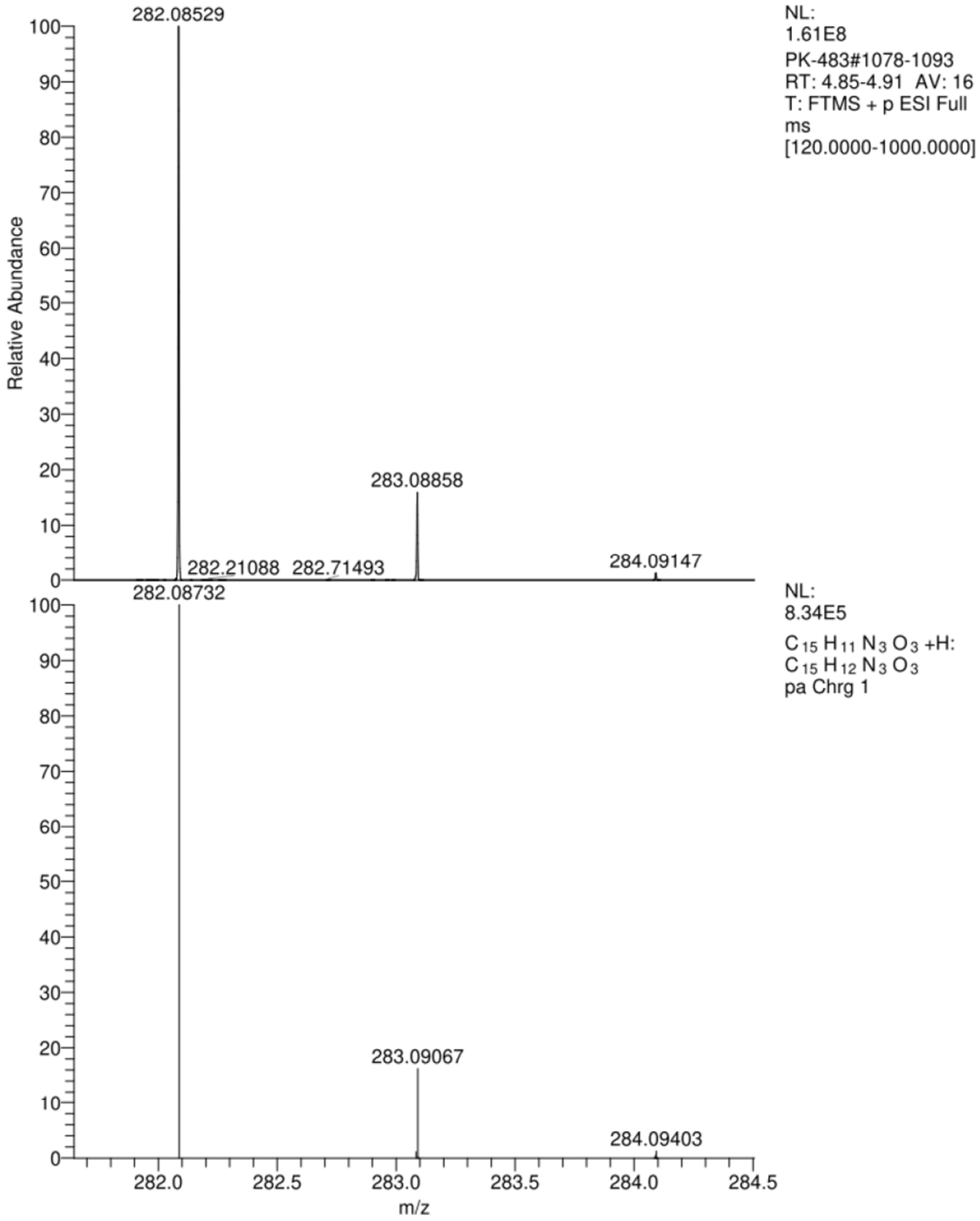

4-(1-(pyridin-3-yl)-1*H*-1,2,3-triazol-4-yl)benzoic acid (50)

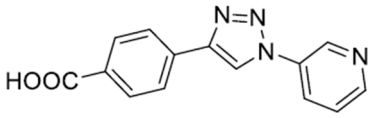

4-(1-(pyridin-3-yl)-1*H*-1,2,3-triazol-4-yl)benzoic acid

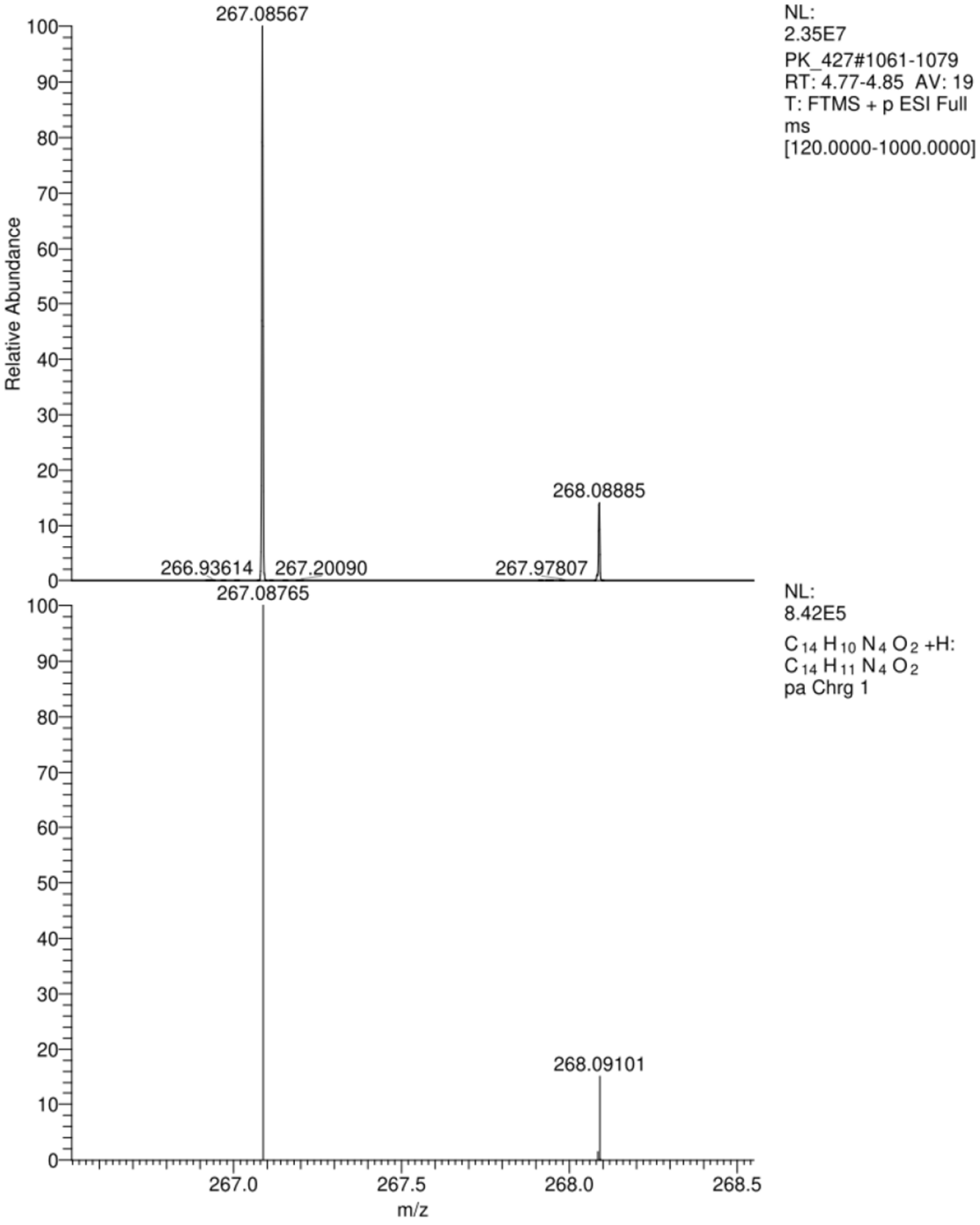

4-(4-(2-((cyclohexylmethyl)amino)phenyl)-1*H*-1,2,3-triazol-1-yl)benzoic acid (51)

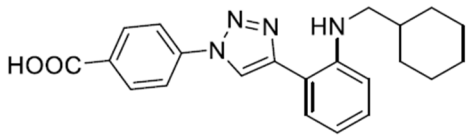

4-(4-(2-((cyclohexylmethyl)amino)phenyl)-1*H*-1,2,3-triazol-1-yl)benzoic acid

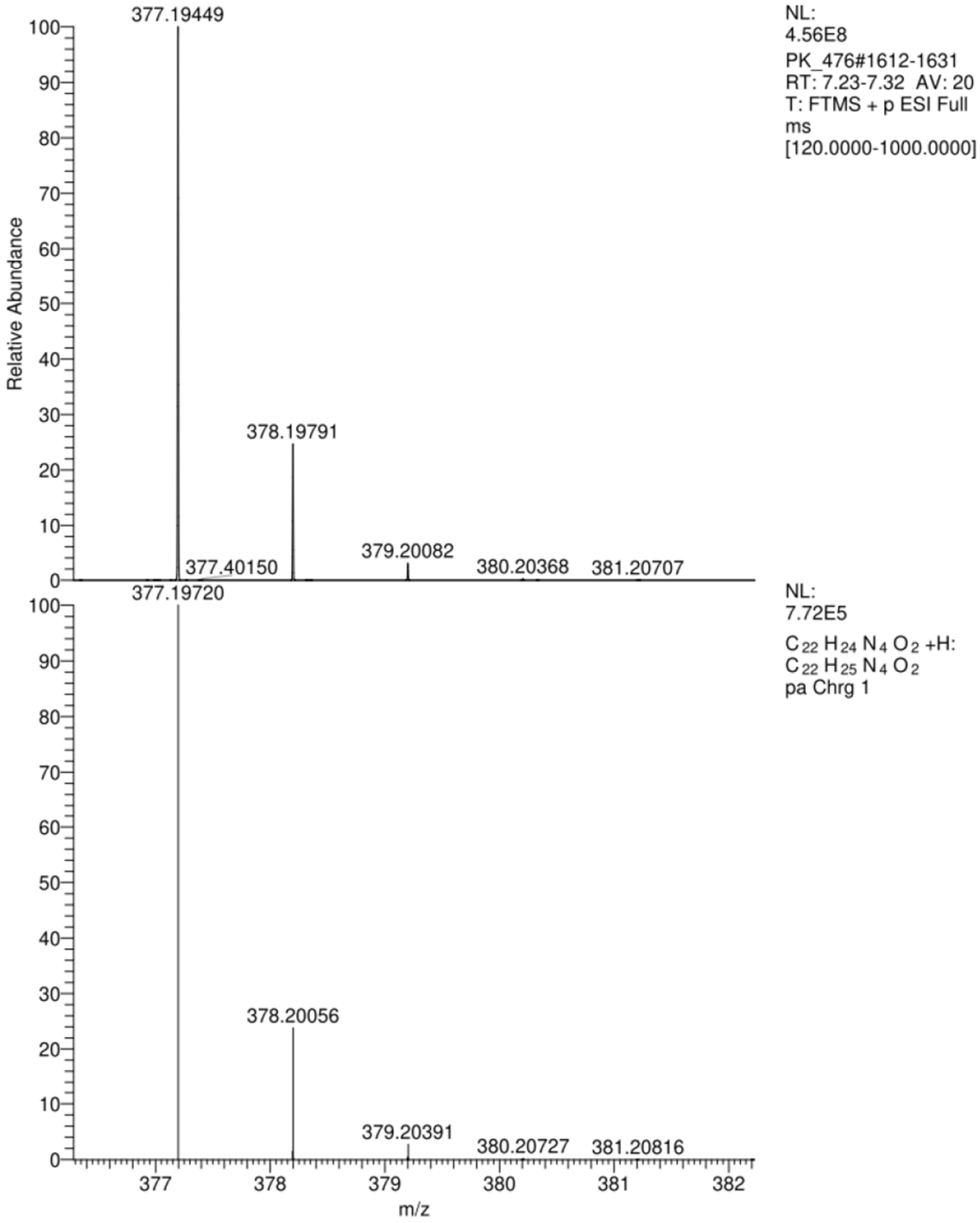

4-(4-(3-((cyclohexylmethyl)amino)phenyl)-1*H*-1,2,3-triazol-1-yl)benzoic acid (52)

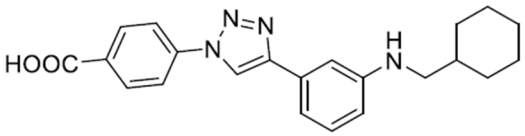

4-(4-(3-((cyclohexylmethyl)amino)phenyl)-1*H*-1,2,3-triazol-1-yl)benzoic acid

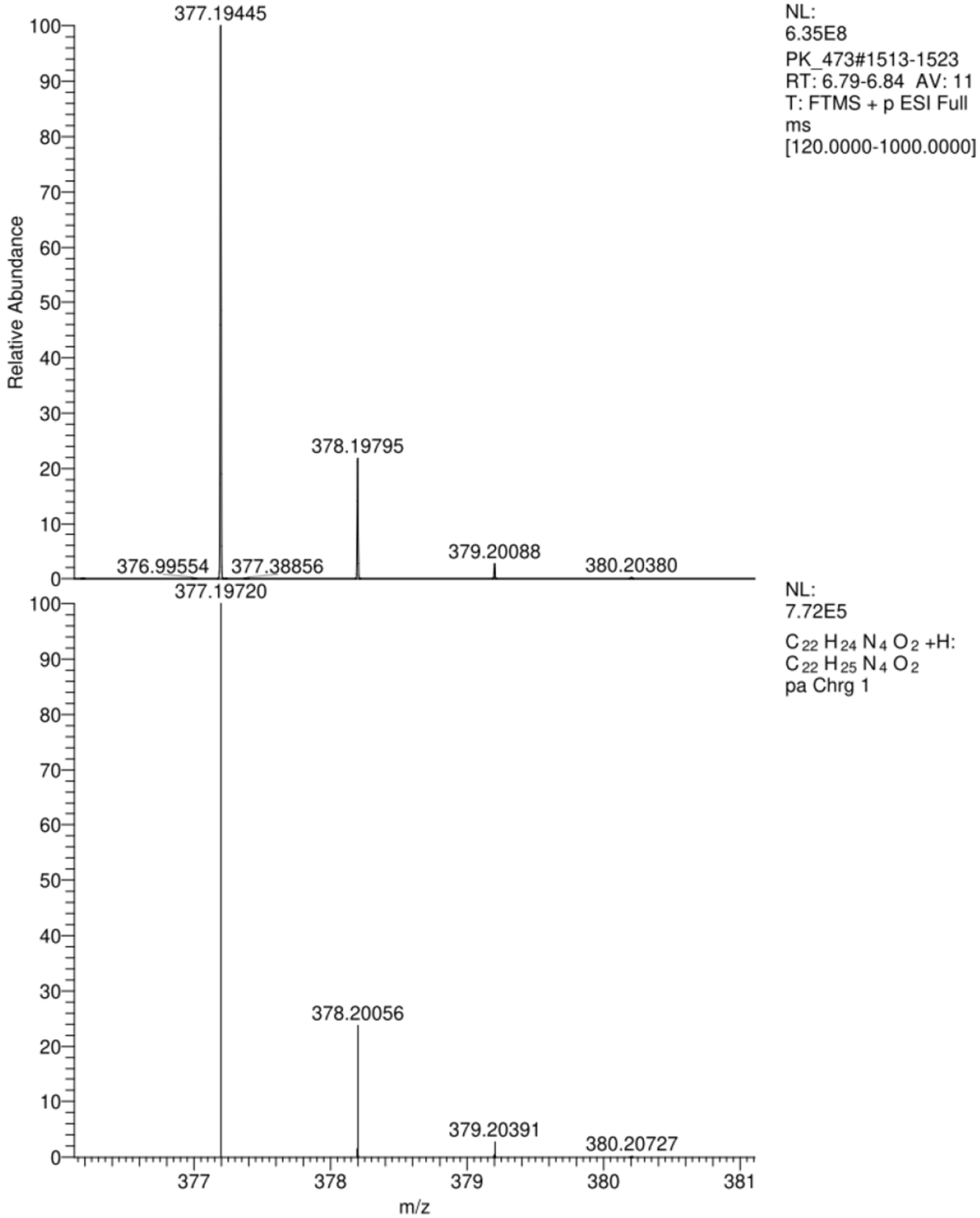

4-(4-(4-((cyclohexylmethyl)amino)phenyl)-1*H*-1,2,3-triazol-1-yl)benzoic acid (53)

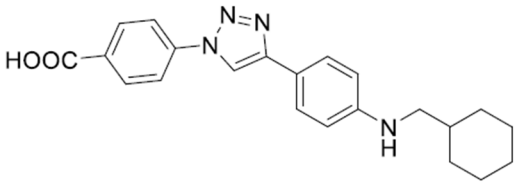

4-(4-(4-((cyclohexylmethyl)amino)phenyl)-1*H*-1,2,3-triazol-1-yl)benzoic acid

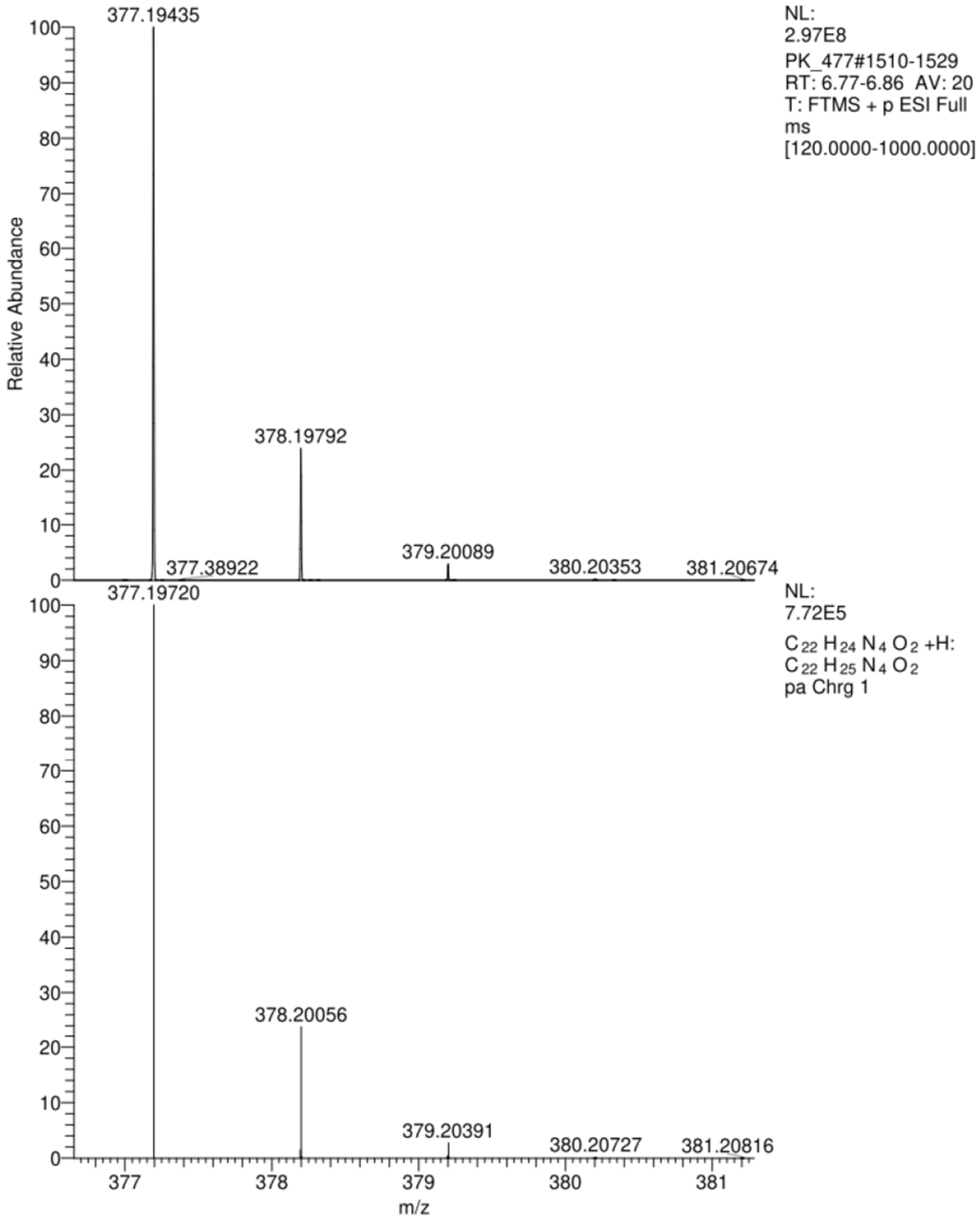

4-(4-(3-((2-Morpholinoethyl)amino)phenyl)-1*H*-1,2,3-triazol-1-yl)benzoic acid (54)

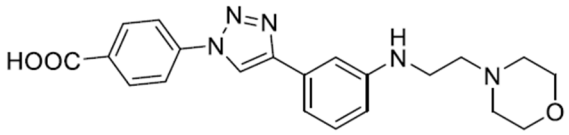

4-(4-(3-((2-morpholinoethyl)amino)phenyl)-1*H*-1,2,3-triazol-1-yl)benzoic acid

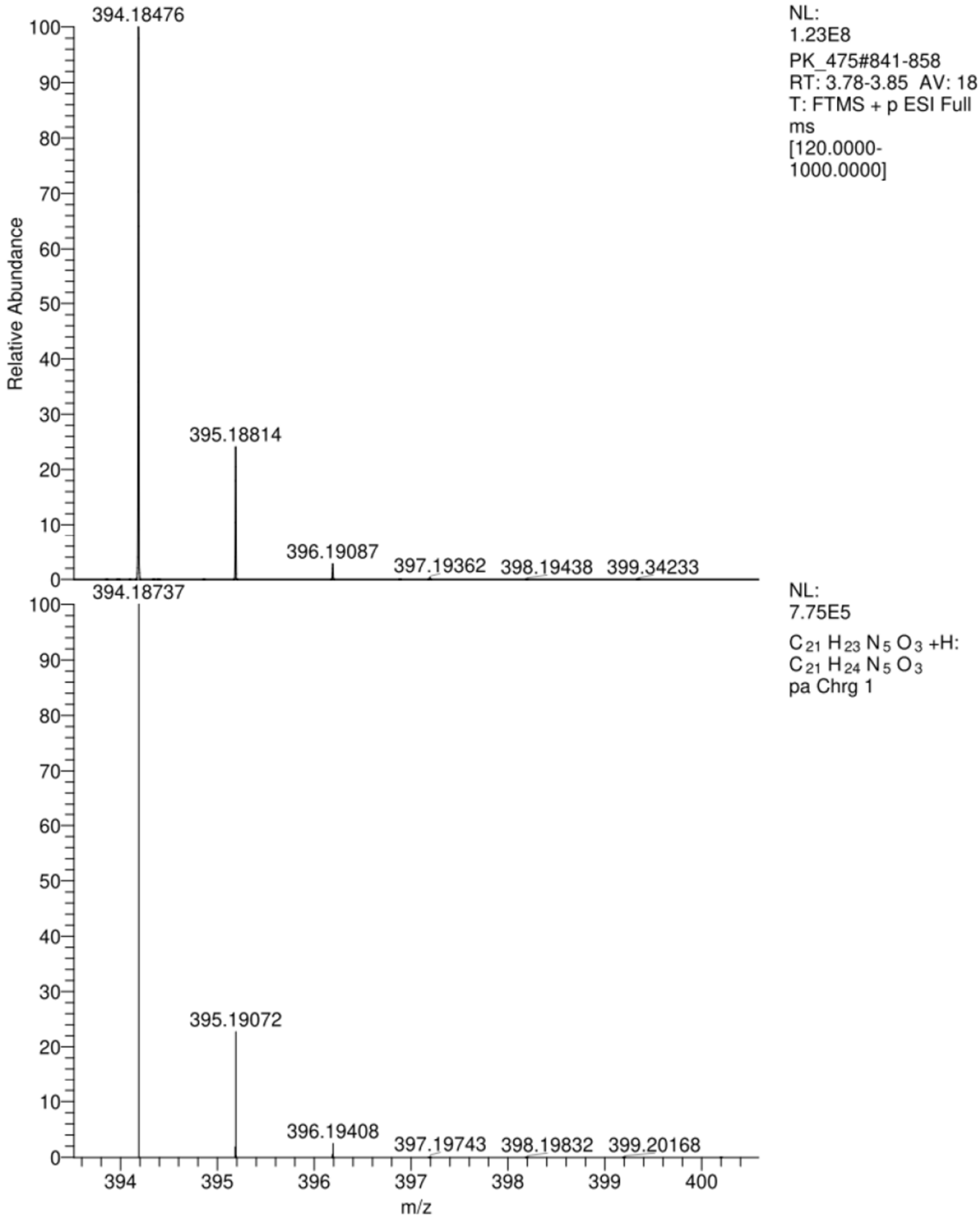

4-(4-(3-(Phenethylamino)phenyl)-1*H*-1,2,3-triazol-1-yl)benzoic acid (55)

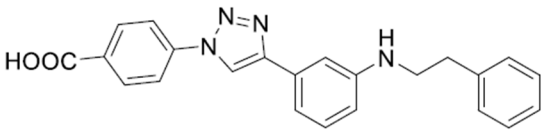

4-(4-(3-(phenethylamino)phenyl)-1*H*-1,2,3-triazol-1-yl)benzoic acid

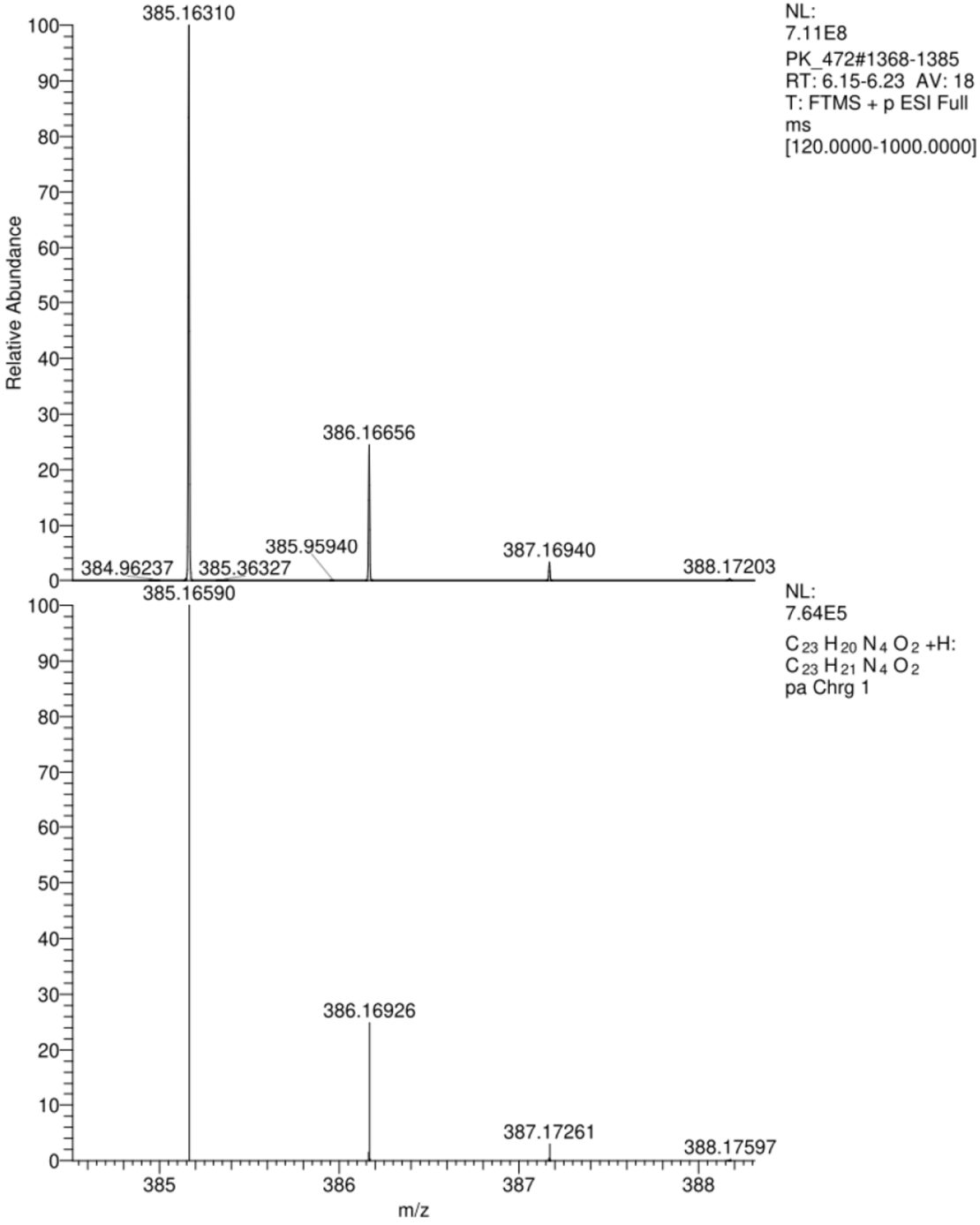

References

(1) Hellert, J.; Weidner-Glunde, M.; Krausze, J.; Lünsdorf, H.; Ritter, C.; Schulz, T. F.; Lührs, T. *The 3D structure of kaposi sarcoma herpesvirus LANA C-terminal domain bound to DNA*. *Proc. Natl. Acad. Sci. U. S. A.*, **2015,** *112*, 6694–6699.

(2) Hellert, J.; Weidner-Glunde, M.; Krausze, J.; Richter, U.; Adler, H.; Fedorov, R.; Pietrek, M.; Rückert, J.; Ritter, C.; Schulz, T. F.; Lührs, T. *A structural basis for BRD2/4-mediated host chromatin interaction and oligomer assembly of kaposi sarcoma-associated herpesvirus and murine gammaherpesvirus LANA proteins*. *PLoS Pathog.*, **2013,** *9*, e1003640.

7.2 Supporting Information Chapter B

Supporting Information

Discovery of Novel Latency-Associated Nuclear Antigen Inhibitors as Antiviral Agents Against Kaposi´s Sarcoma-associated Herpesvirus

Philine Kirsch,[⊥,†,‡,§] Valentin Jakob,[⊥,†,‡,§] Walid A. M. Elgaher,[†] Christine Walt,[†] Kevin Oberhausen,[†] Thomas F. Schulz[§,∥] and Martin Empting*[,†,‡,§]

[†]Department of Drug Design and Optimization (DDOP), Helmholtz-Institute for Pharmaceutical Research Saarland (HIPS) - Helmholtz Centre for Infection Research (HZI), Campus E8.1, 66123 Saarbrücken, Germany.

[‡]Department of Pharmacy, Saarland University, Campus E8.1, 66123 Saarbrücken, Germany.

[§]German Centre for Infection Research (DZIF), Partner Site Hannover-Braunschweig, 66123 Saarbrücken, Germany.

[∥]Institute of Virology, Hannover Medical School, Carl-Neuberg-Strasse 1, 30625 Hannover, Germany.

Table of Contents

1 Screening Results

1.1 FP-based Spot Test Screening @ 100 µM

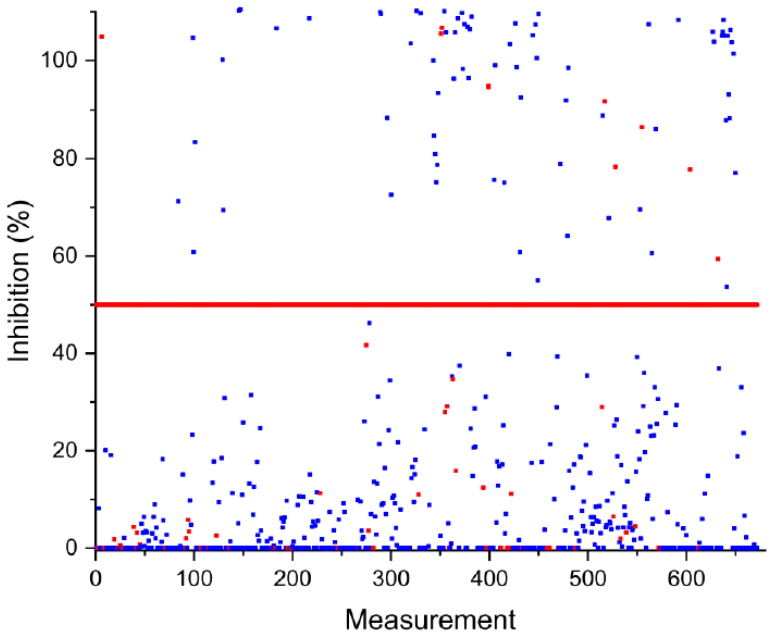

Figure S1: Results of spot test FP-based assay. Compounds were tested at 100 µM and threshold was set to 50% inhibition. Primary screening resulted in 86 hits with 12.8% hit rate.

1.2 Results of dose-dependent FP-based competition screening

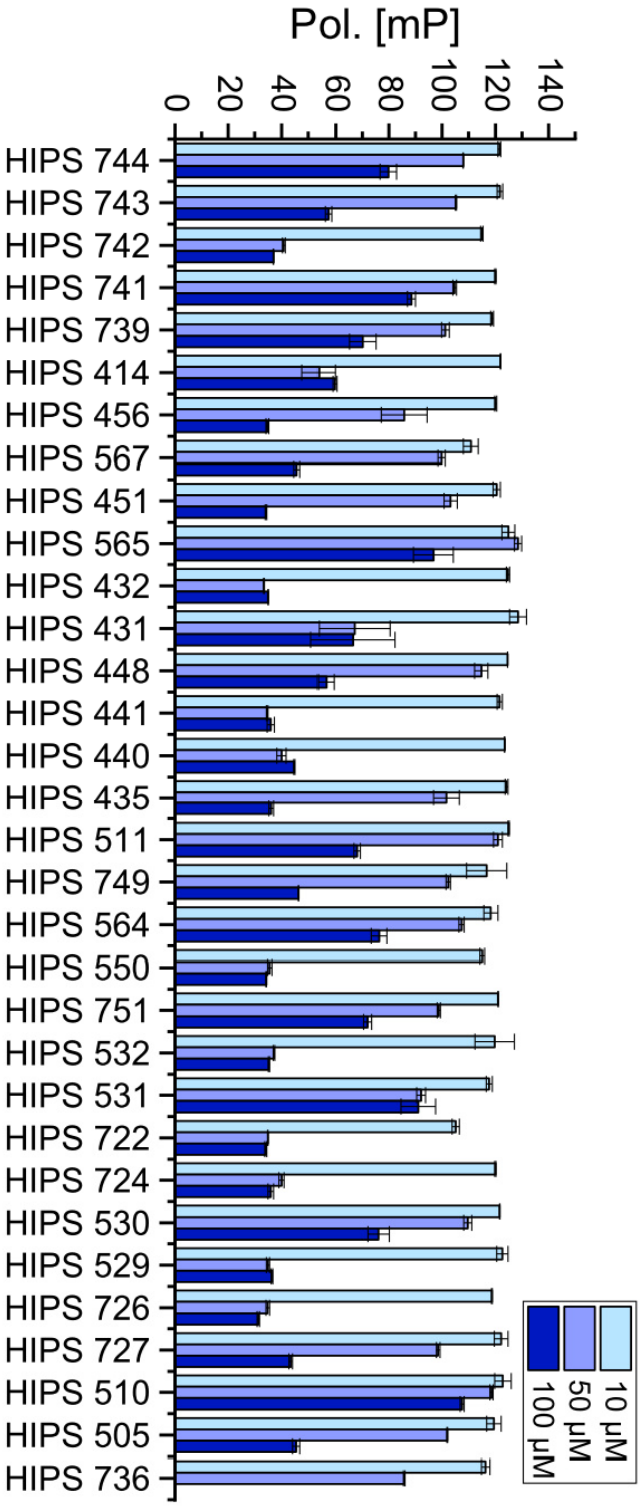

Figure S2: Results of dose-dependent FP-based screening (Class I, Part 1).

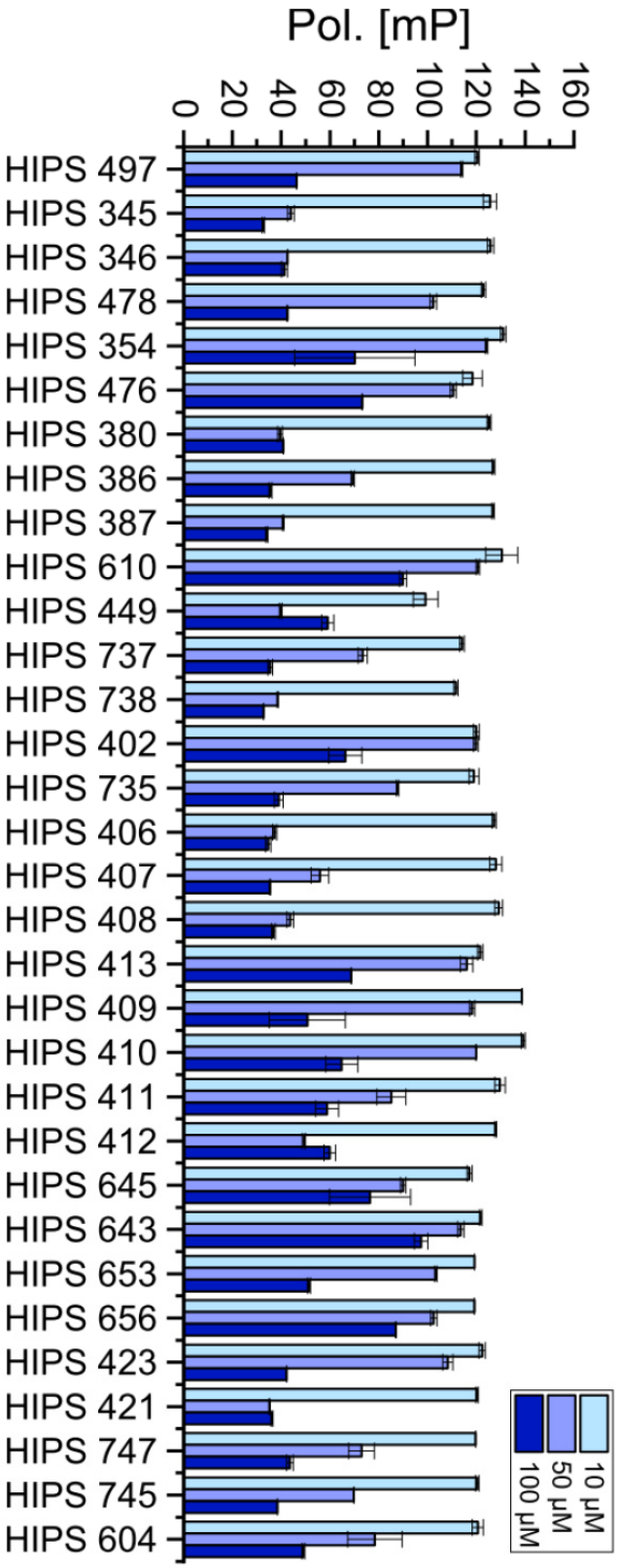

Figure S3: Results of dose-dependent FP-based screening (Class I, Part 2).

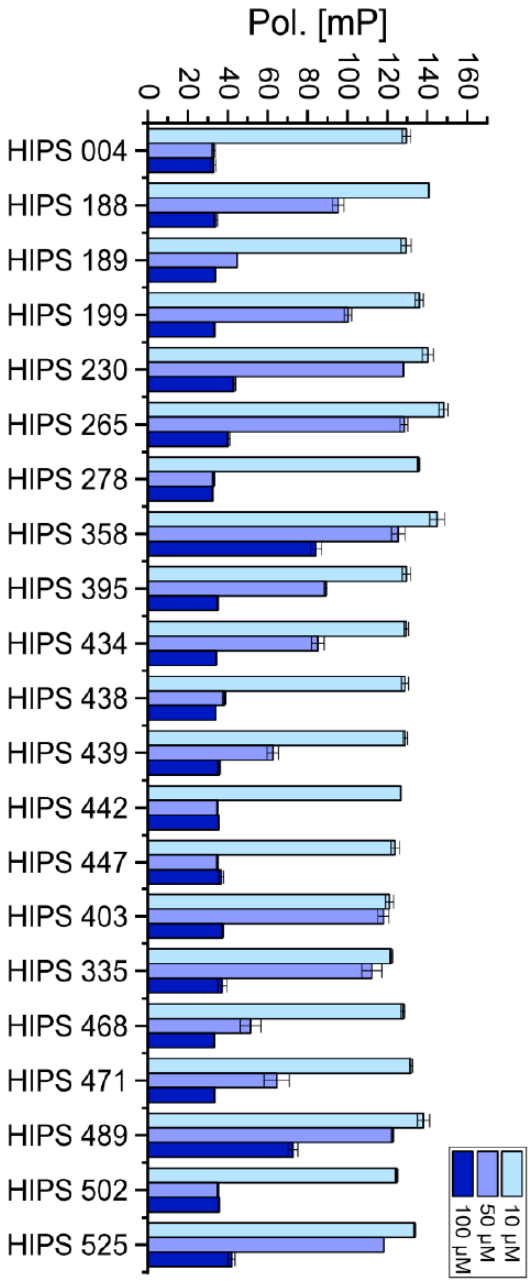

Figure S4: Results of dose-dependent FP-based screening (Class II).

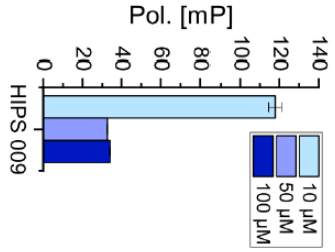

Figure S5: Results of dose-dependent FP-based screening (Class III).

2 Compound Characterization

2.1 FP-based IC_{50} determination for hit compounds 1–9.

The curves are showing the obtained results for hit compounds **1–9** in the FP-based competition assay using LBS2 as fluorescent probe and His-tagged oligomerization-deficient LANA DBD (aa1008−1146). *(1)* Compounds were tested in duplicates and in two independent experiments. Curves were based on obtained FP values of duplicates ± standard deviation. Finally, curves were fit to a four-parameter dose-response model using OriginPro 2018 to calculate IC_{50} values.

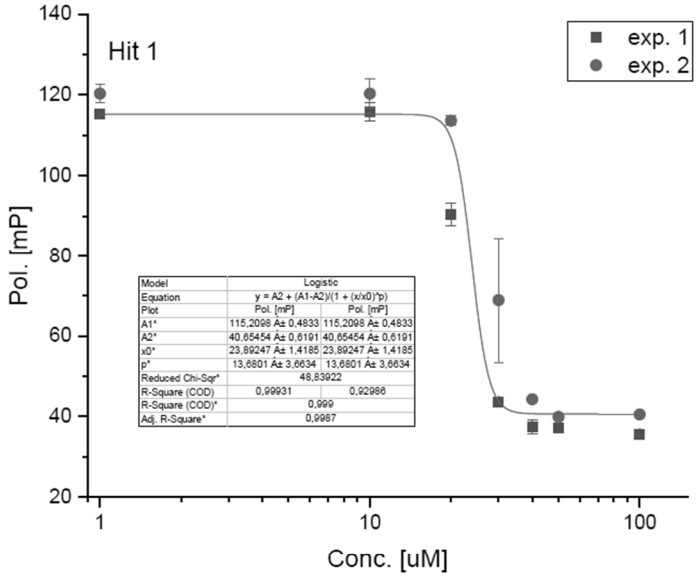

Figure S6: Results of dose-dependent FP-assay for Hit **1**.

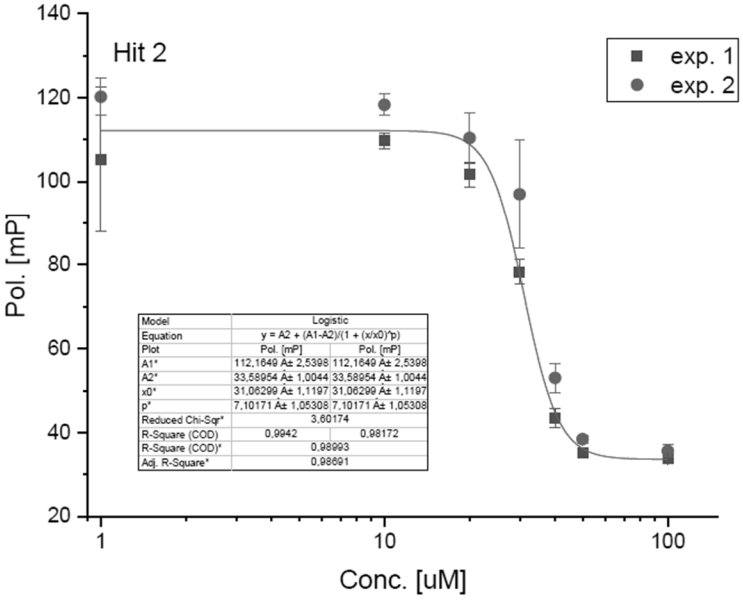

Figure S7: Results of dose-dependent FP-assay for Hit **2**.

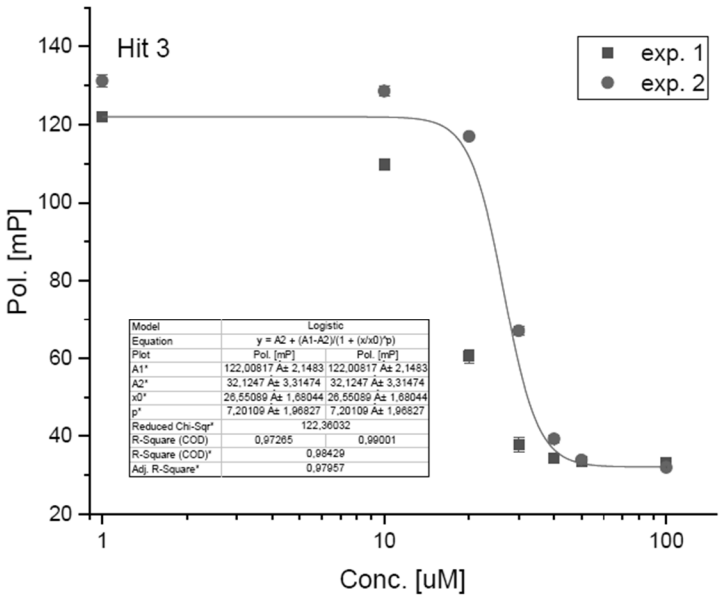

Figure S8: Results of dose-dependent FP-assay for Hit **3**.

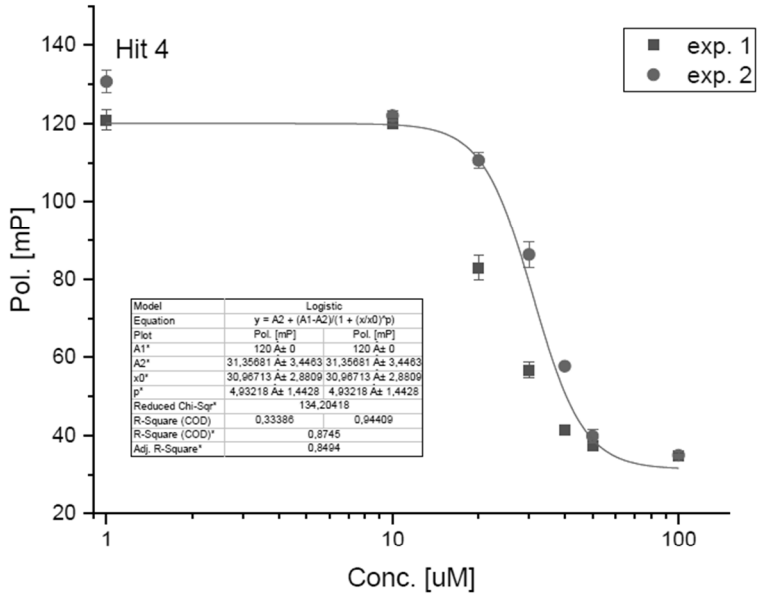

Figure S9: Results of dose-dependent FP-assay for Hit **4**.

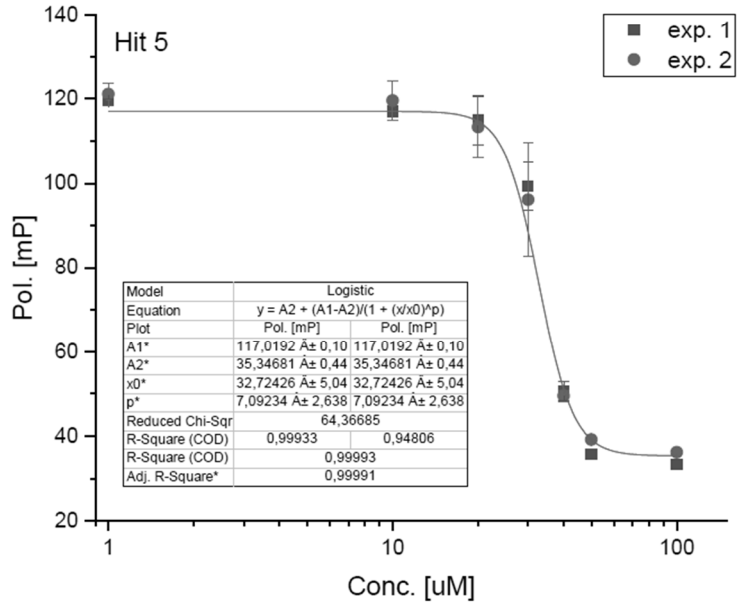

Figure S10: Results of dose-dependent FP-assay for Hit **5**.

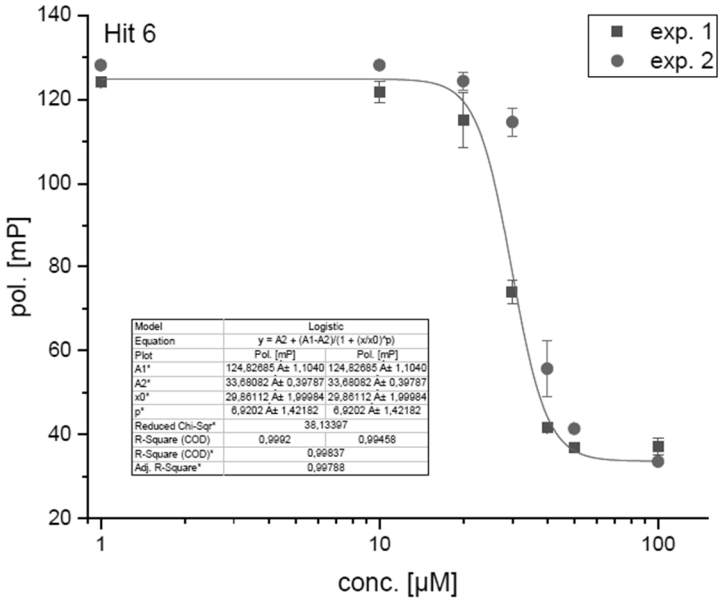

Figure S11: Results of dose-dependent FP-assay for Hit **6**.

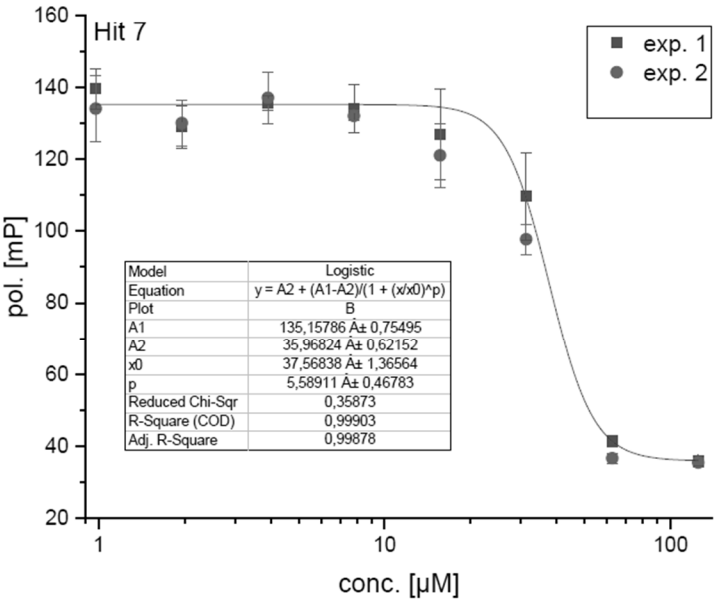

Figure S12: Results of dose-dependent FP-assay for Hit **7**.

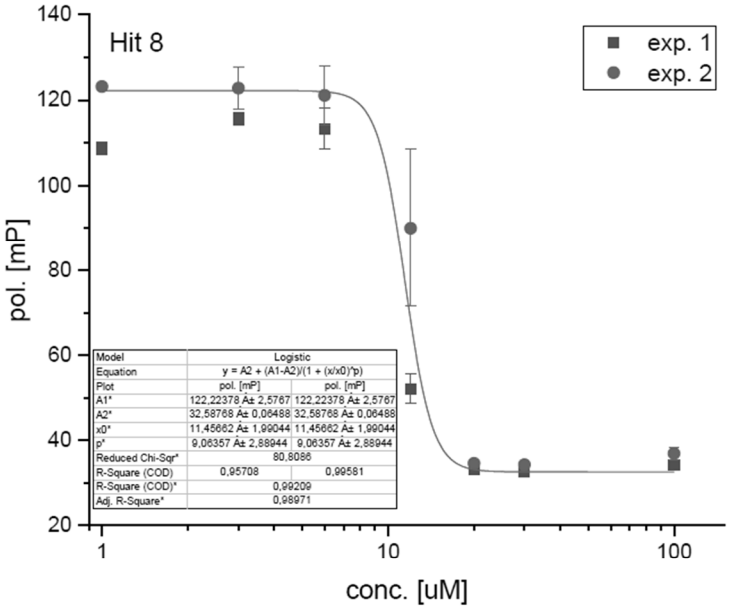

Figure S13: Results of dose-dependent FP-assay for Hit **8**.

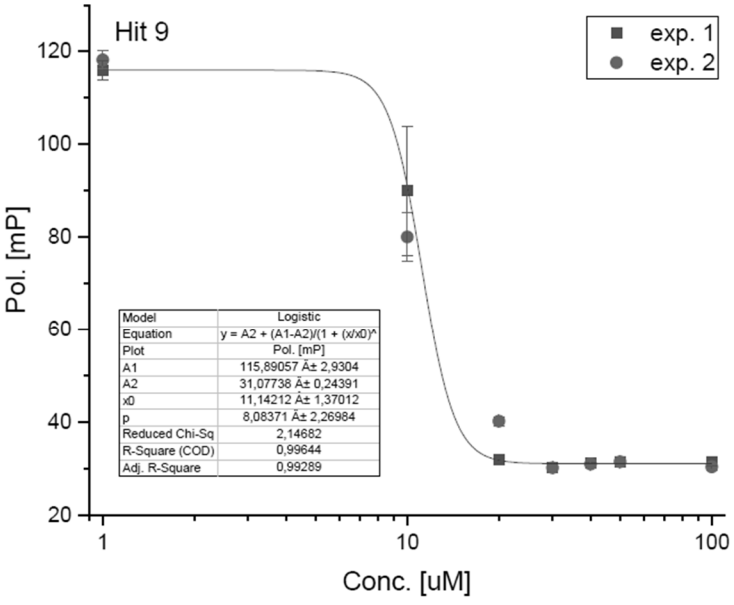

Figure S14: Results of dose-dependent FP-assay for Hit **9**.

2.2 Surface Plasmon Resonance (SPR) Studies

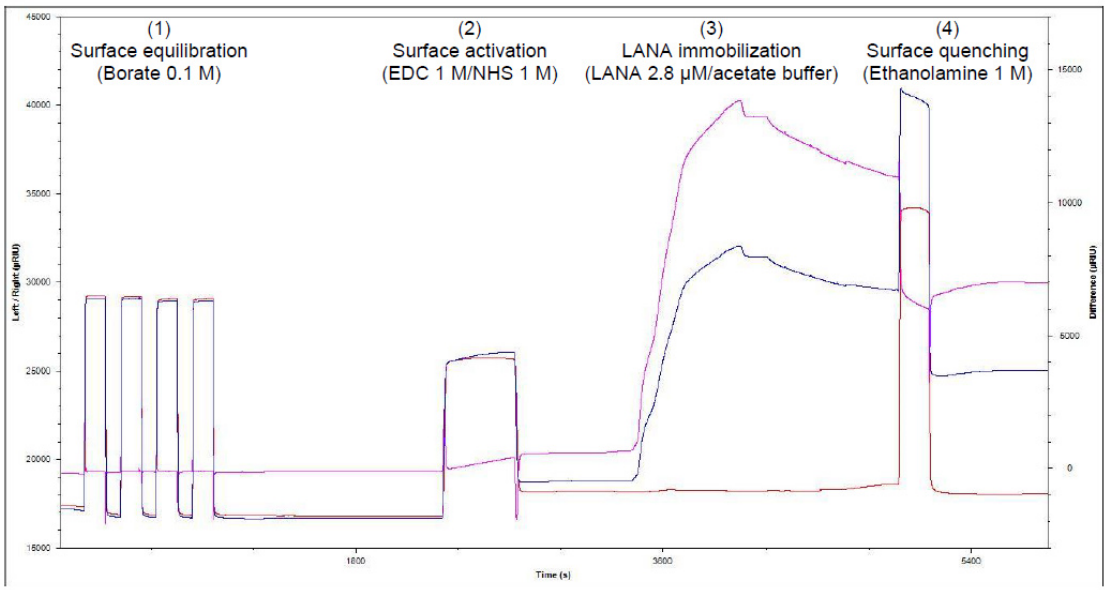

Figure S15: Sensorgram of the immobilization procedure for LANA (1008-1147) DBD mutant on CMD500M sensor chip: (1) Four injections of cleaning solution, (2) activation solution, (3) LANA 1008-1147, and (4) quenching solution. The blue, red, and magenta curves represent the left (active) channel, right (reference) channel, and the difference, respectively.

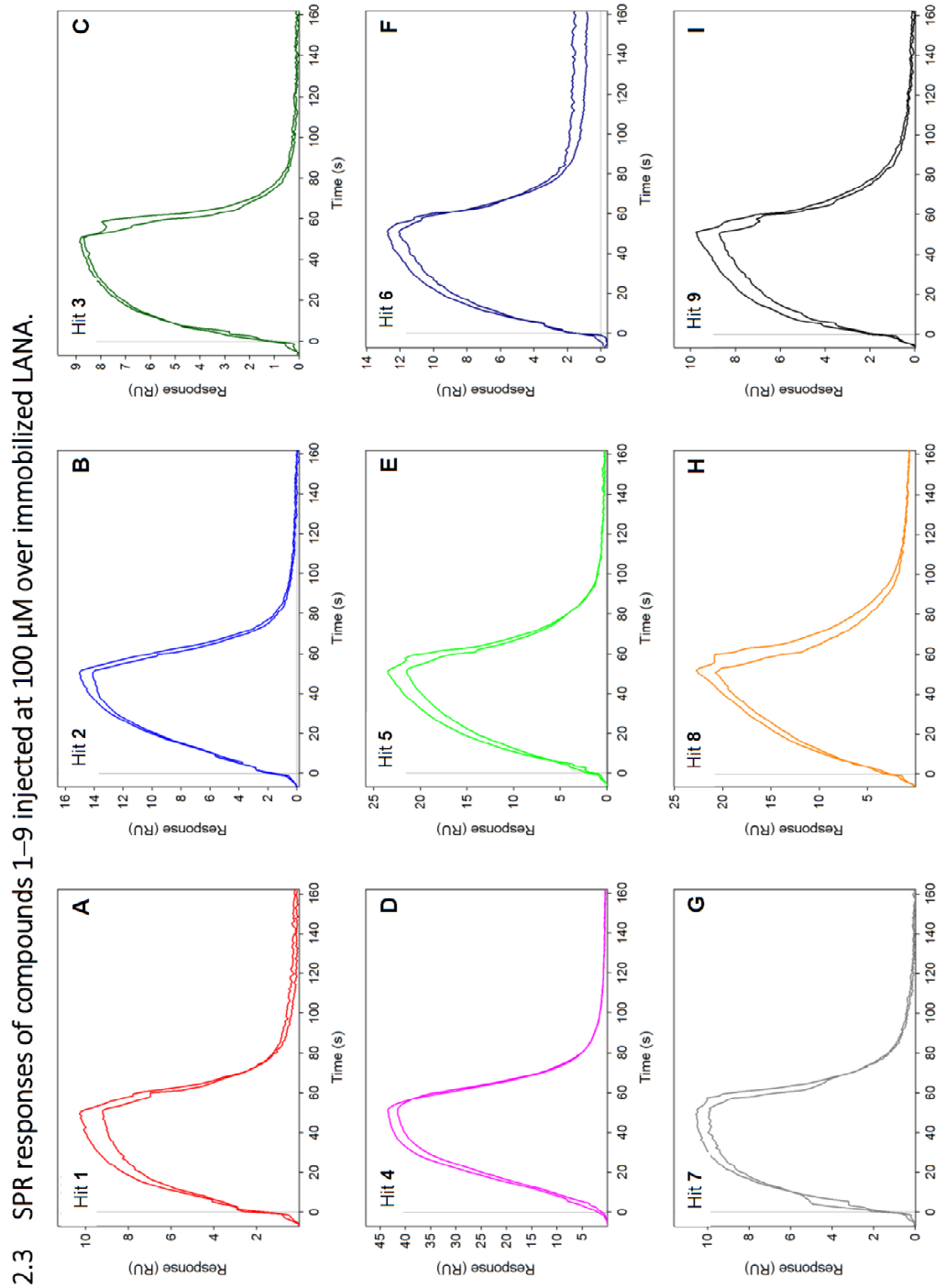

Figure S16: A-I) Sensorgrams overlay showing the SPR responses of hit compounds **1–9** injected over an immobilized LANA DBD mutant (Association phase: 60 s and dissociation phase: 120 s). Compounds were tested in two independent experiments at 100 µM final concentration.

S12

Table S1: SPR response values (RU) of the tested compounds at 100 µM injected over an immobilized LANA DBD mutant.

Compound	Response (RU)		
	Experiment 1	Experiment 2	Mean ± standard deviation
1	8.8	10.2	9.5 ± 0.7
2	13.8	15.0	14.4 ± 0.6
3	8.5	8.7	8.6 ± 0.1
4	43.1	41.5	42.3 ± 0.8
5	21.0	23.3	22.1 ± 1.2
6	11.6	12.7	12.2 ± 0.6
7	9.6	10.6	10.1 ± 0.5
8	20.1	22.2	21.2 ± 1.1
9	8.4	9.7	9.1 ± 0.7

2.4 Determination of equilibrium dissociation constant (K_D) for compounds 1, 6 and 9.

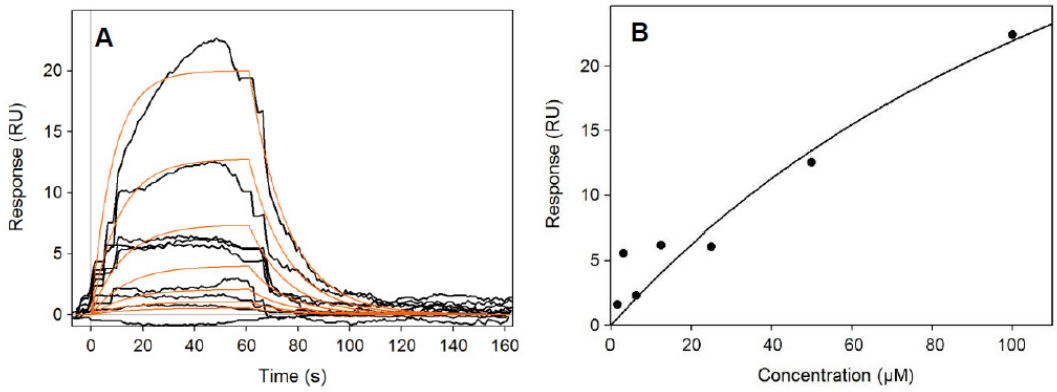

Figure S17: (A) Sensorgrams overlay (black) of **1** at concentrations of 1.6–100.0 μM running over an immobilized LANA DBD mutant. Global fitting of the association and dissociation curves (red); (B) Langmuir binding isotherm (K_D value: 131 ± 9 μM).

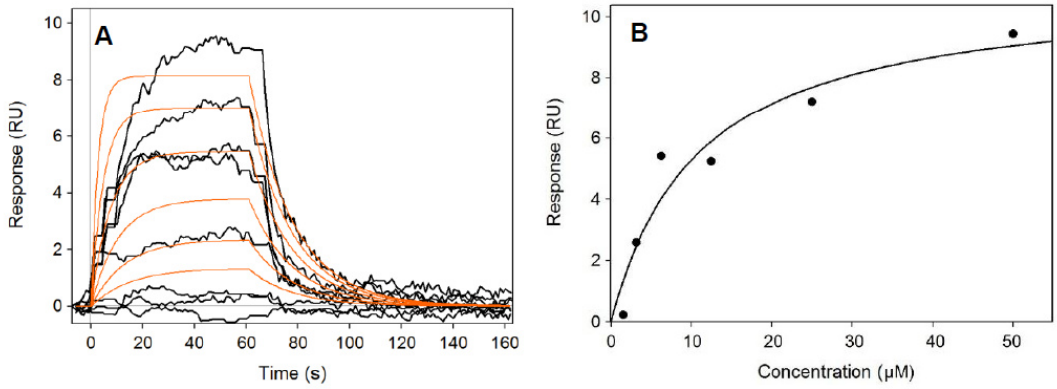

Figure S18: (A) Sensorgrams overlay (black) of **6** at concentrations of 1.6–50.0 μM running over an immobilized LANA DBD mutant. Global fitting of the association and dissociation curves (red); (B) Langmuir binding isotherm (K_D value: 10 ± 1 μM).

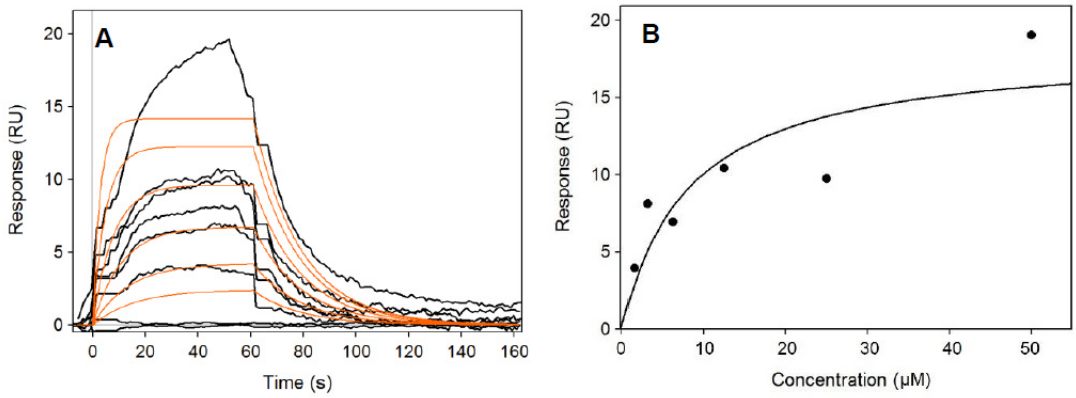

Figure S19: (A) Sensorgrams overlay (black) of **9** at concentrations of 1.6–50.0 μM running over an immobilized LANA DBD mutant. Global fitting of the association and dissociation curves (red); (B) Langmuir binding isotherm (K_D value: 9 ± 1 μM).

Table S2: The kinetic parameters of compounds **1**, **6** and **9** binding to LANA.

Compound	R_{max} (RU)	k_{on} ($M^{-1}s^{-1}$)	k_{off} (s^{-1})	K_D (μM)	Res sd
1	46 ± 2	$5.2 \pm 0.3 \times 10^2$	0.068 ± 0.002	131.0 ± 9.0	1.5
6	10 ± 1	$6.0 \pm 0.2 \times 10^3$	0.059 ± 0.001	9.9 ± 0.4	0.8
9	17 ± 1	$6.0 \pm 0.3 \times 10^3$	0.055 ± 0.002	9.3 ± 0.4	1.7

R_{max}: maximum analyte binding capacity; k_{on}: association rate constant; k_{off}: dissociation rate constant; K_D: equilibrium dissociation constant; Res sd: residual standard deviation.

2.5 STD-MNR Spectra for compounds 1, 6 and Inhibitor I

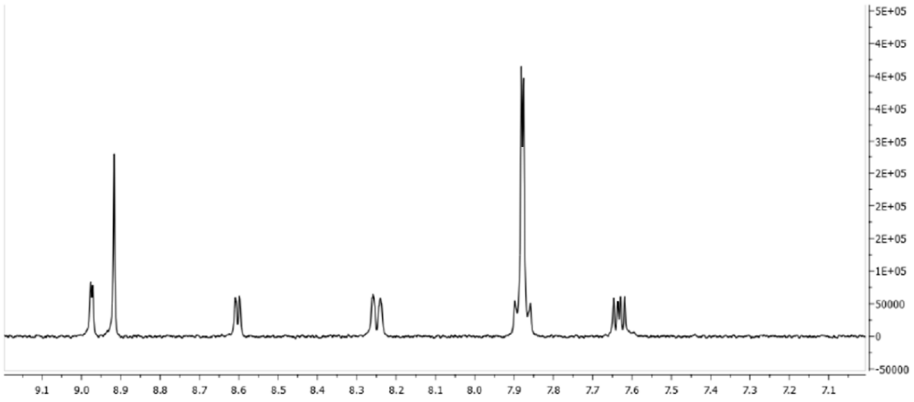

Figure S20: Off resonance NMR spectrum of Inhibitor **I** at a concentration of 250 µM.

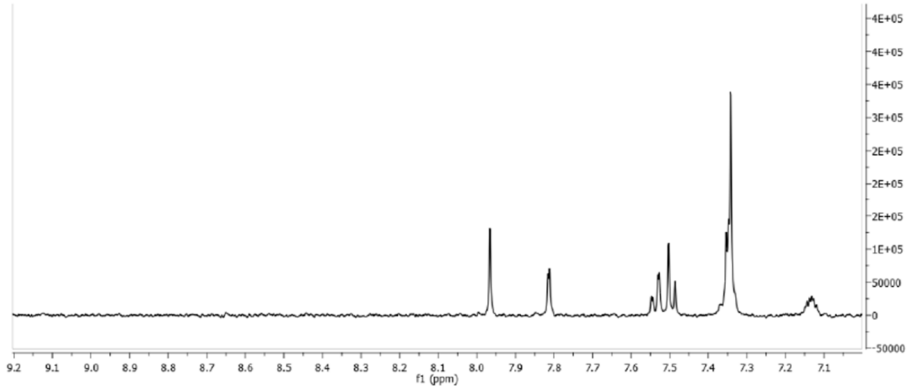

Figure S21: Off resonance NMR spectrum of Hit **1** at a concentration of 250 µM.

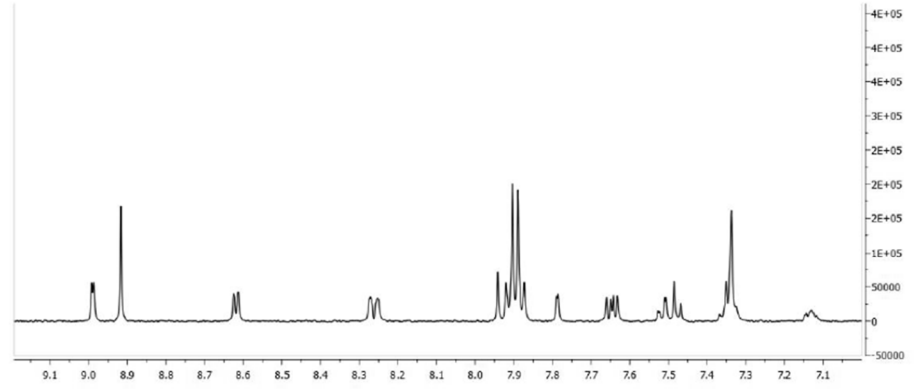

Figure S22: Off resonance NMR spectrum of Inhibitor **I** mixed with Hit **1**, each at a concentration of 250 µM.

S16

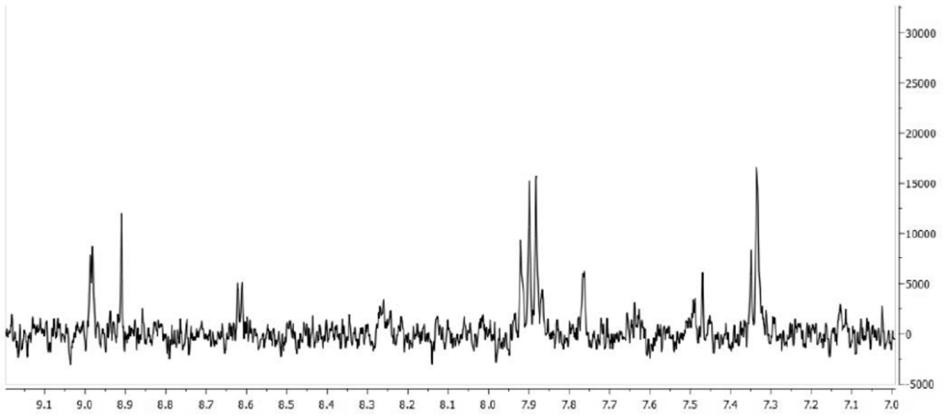

Figure S23: STD-NMR spectrum of Inhibitor **I** (final concentration of 500 µM) mixed with Hit **1** (final concentration of 250 µM).

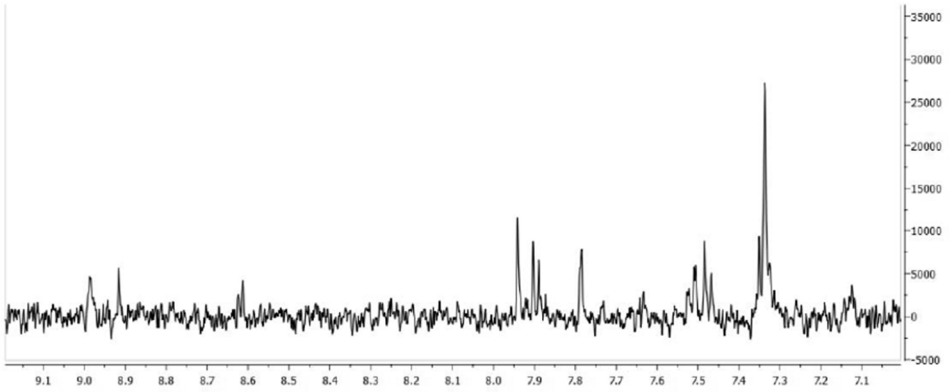

Figure S24: STD-NMR spectrum of Inhibitor **I** (final concentration of 250 µM) mixed with Hit **1** (final concentration of 250 µM).

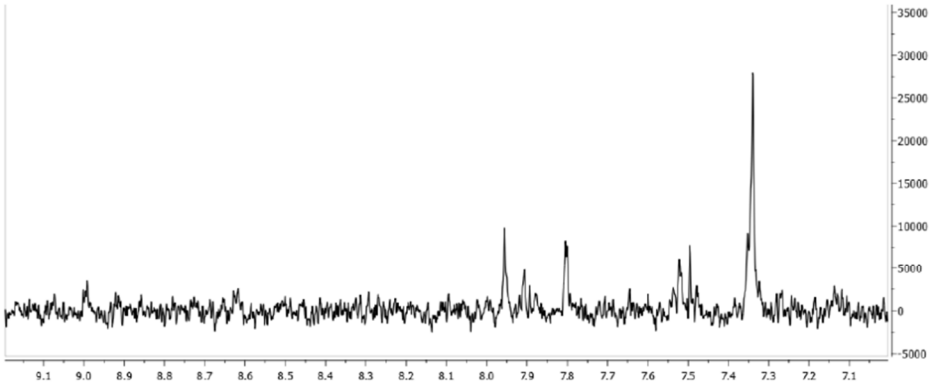

Figure S25: STD-NMR spectrum of Inhibitor **I** (final concentration of 125 µM) mixed with Hit **1** (final concentration of 250 µM).

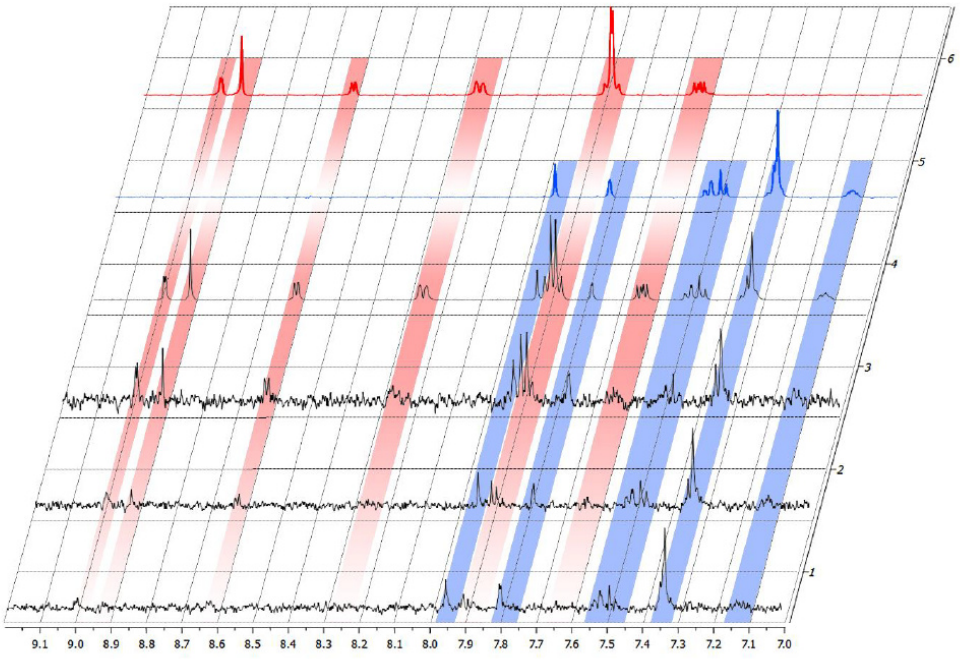

Figure S26: STD-NMR competition experiments with inhibitor **I** and hit **1** in complex with LANA DBD mutant. The respective protons of each compound are highlighted with a corresponding color, Inhibitor **I** in red and Hit **1** in blue; Spectrum 6 (red): off resonance spectrum of Inhibitor **I** with final concentration of 250 µM; Spectrum 5 (blue): off resonance spectrum of hit **1** with final concentration of 250 µM; Spectrum 4: off resonance spectrum of Inhibitor **I** mixed with hit **1**, each with a final concentration of 250 µM; Spectrum 3: STD spectrum of Inhibitor **I** mixed with hit **1**, inhibitor **I** with a final concentration of 500 µM and hit **1** with a final concentration of 250 µM; Spectrum 2: STD spectrum of Inhibitor **I** mixed with hit **1**, each with a final concentration of 250 µM; Spectrum 1: STD spectrum of Inhibitor **I** mixed with hit **1**, inhibitor **I** with a final concentration of 125 µM and hit **1** with a final concentration of 250 µM.

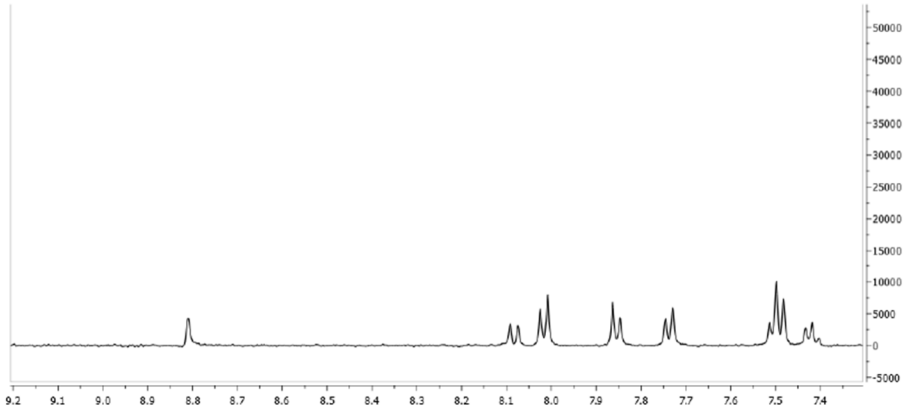

Figure S27: Off resonance NMR spectrum of Hit **6** at a concentration of 250 µM.

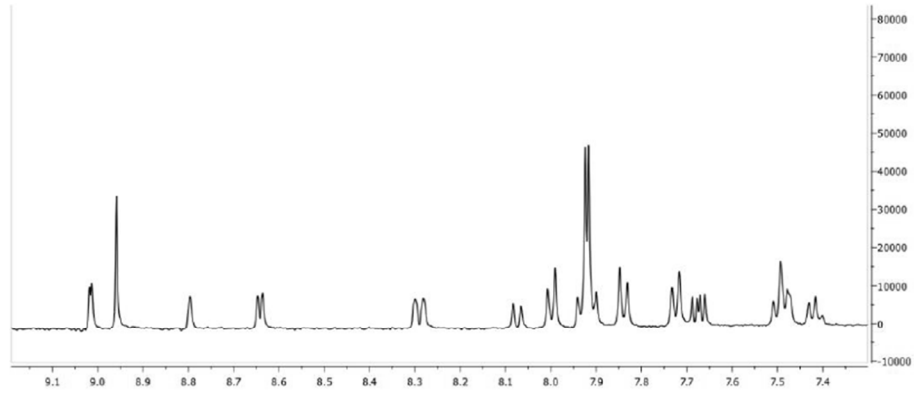

Figure S28: Off resonance NMR spectrum of Inhibitor **I** mixed with Hit **6**, each at a concentration of 250 µM.

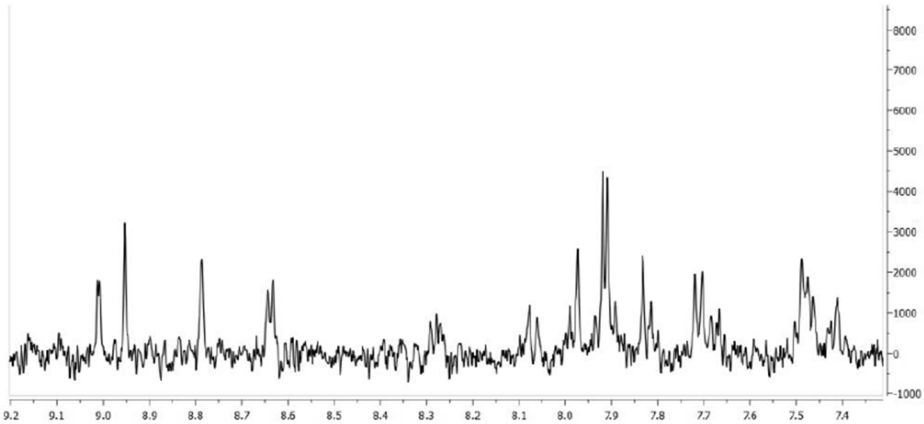

Figure S29: STD-NMR spectrum of Inhibitor **I** (final concentration of 500 µM) mixed with Hit **6** (final concentration of 250 µM).

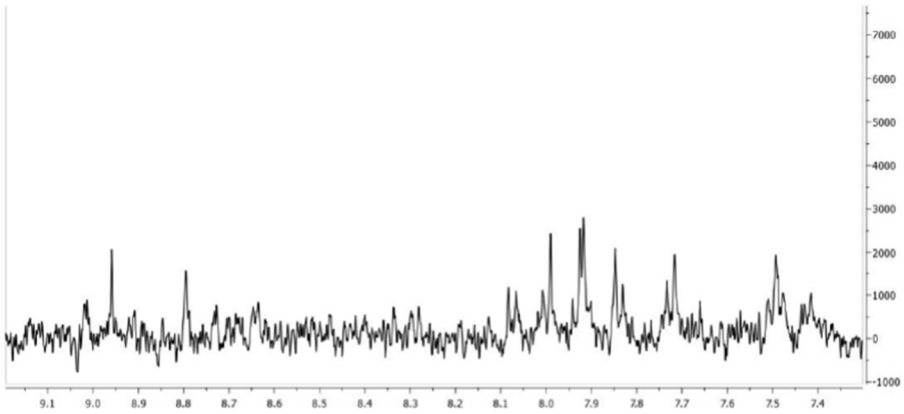

Figure S29: STD-NMR spectrum of Inhibitor **I** (final concentration of 250 µM) mixed with Hit **6** (final concentration of 250 µM).

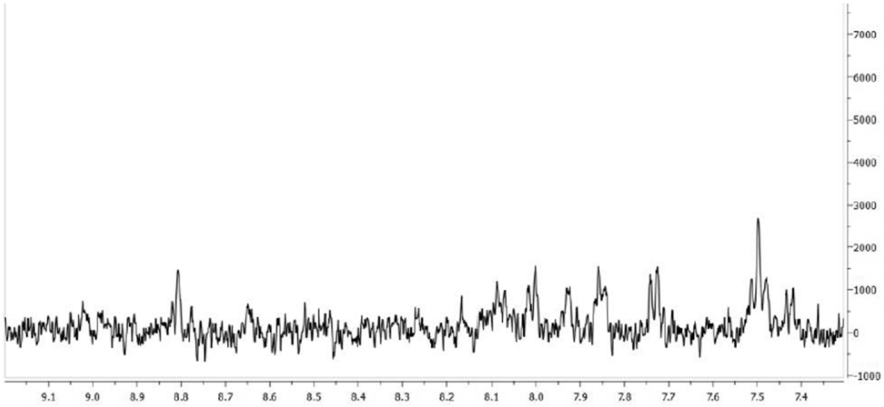

Figure S30: STD-NMR spectrum of Inhibitor **I** (final concentration of 125 µM) mixed with Hit **6** (final concentration of 250 µM).

2.6 Cytotoxicity data for compounds 1, 6 and 9.

Compounds were tested in two independent experiments at a final concentration of 100 µM.

Table S3: Cytotoxicity Assay – HepG2 cells

Compound	Concentration [µM]	HepG2 Relative viability after 48 h [%]	
		Experiment 1	Experiment 2
1	100	84.91	144.76
6	100	155.94	138.43
9	100	27.35	14.59

Table S4: Cytotoxicity Assay – Hek293 cells

Compound	Concentration [µM]	Hek293 Relative viability after 48 h [%]	
		Experiment 1	Experiment 2
1	100	41.66	45.56
6	100	82.55	87.18
9	100	11.15	2.34

3 References

1. Kirsch, P., Jakob, V., Oberhausen, K., Stein, S. C., Cucarro, I., Schulz, T. F., and Empting, M. (2019) Fragment-Based Discovery of a Qualified Hit Targeting the Latency-Associated Nuclear Antigen of the Oncogenic Kaposi's Sarcoma-Associated Herpesvirus/Human Herpesvirus 8, *Journal of medicinal chemistry 62,* 3924–3939.

7.3 Supporting Information Chapter C

Supporting Information

Hit-to-Lead Optimization of a Potent Latency-associated Nuclear Antigen Inhibitor against Kaposi's Sarcoma-associated Herpesvirus Infections

Philine Kirsch,[1,2,3] Saskia C. Stein,[3,4] Aylin Berwanger,[1,2,3] Julia Rinkes,[1,2,3] Valentin Jakob,[1,2,3] Thomas F. Schulz[3,4] and Martin Empting*[,1,2,3]

[1]Department of Drug Design and Optimization (DDOP), Helmholtz-Institute for Pharmaceutical Research Saarland (HIPS) - Helmholtz Centre for Infection Research (HZI), Campus E8.1, 66123 Saarbrücken, Germany.

[2]Department of Pharmacy, Saarland University, Campus E8.1, 66123 Saarbrücken, Germany.

[3]German Centre for Infection Research (DZIF), Partner Site Hannover-Braunschweig, 66123 Saarbrücken, Germany.

[4]Institute of Virology, Hannover Medical School, Carl-Neuberg-Strasse 1, 30625 Hannover, Germany.

Table of Contents

1 Materials and Methods

1.1 Chemistry

3-azidopyridine (2): The azide was synthesized according to **GP1** using pyridin-3-amine **1** (376 mg, 4 mmol), sodium nitrite (1.7 eq., 469 mg, 6.8 mmol), sodium azide (1.7 eq., 442 mg, 6.8 mmol), EtOAc (8 mL), 6 M HCl (5 mL). The crude product (245 mg, 2 mmol, 50%) was used as obtained in the next step without further purifications. R_f = 0.37 (PE/EtOAc 7:3)

4-(1-(pyridin-3-yl)-1*H*-1,2,3-triazol-4-yl)benzoic acid (3): The triazole was synthesized according to **GP3** using 4-ethynylbenzoic acid and 3-azidopyridine **2** as described previously.[1]

3-(1-(pyridin-3-yl)-1*H*-1,2,3-triazol-4-yl)benzoic acid (4): The triazole was synthesized according to **GP3** using 3-ethynylbenzoic acid (92 mg, 0.64 mmol) and 3-azidopyridine **2** (1.3 eq., 100 mg, 0.83 mmol) as starting materials. The crude was obtained as a white solid (110 mg, 0.41 mmol, 64%). Purification was done using prep. HPLC. ^{1}H NMR (500 MHz, DMSO-d_6) δ ppm 7.66 (br. s., 1 H) 7.68 - 7.79 (m, 1 H) 7.88 - 8.06 (m, 1 H) 8.19 (d, *J*=7.63 Hz, 1 H) 8.41 (d, *J*=8.24 Hz, 1 H) 8.53 (s., 1 H) 8.76 (s., 1 H) 9.25 (s., 1 H) 9.55 (s, 1 H) 13.23 (br. s., 1 H); ^{13}C NMR (126 MHz, DMSO-d_6) δ ppm 120.56, 124.96, 127.82, 129.40, 141.24, 146.80, 149.81, 167.30

methyl 4-(1-(pyridin-3-yl)-1*H*-1,2,3-triazol-4-yl)benzoate (5): The triazole was synthesized according to **GP3** using methyl 4-ethynylbenzoate (103 mg, 0.64 mmol) and 3-azidopyridine **2** (1.3 eq., 100 mg, 0.83 mmol) as starting materials. The crude was obtained as a yellow solid (117 mg, 0.41 mmol, 49%). Purification was done using prep. HPLC. ^{1}H NMR (500 MHz, DMSO-d_6) δ ppm 3.89 (s, 3 H) 7.71 (dd, *J*=8.32, 4.81 Hz, 1 H) 8.01 - 8.18 (m, 4 H) 8.30 - 8.46 (m, 1 H) 8.74 (d, *J*=4.12 Hz, 1 H) 9.21 (br. s., 1 H) 9.56 (s, 1 H); ^{13}C NMR (126 MHz, DMSO-d_6) δ ppm 52.24, 121.36, 124.72, 125.49, 127.99, 129.18, 130.08, 134.52, 141.33, 146.47, 149.95, 165.89

ethyl 4-(1-(pyridin-3-yl)-1*H*-1,2,3-triazol-4-yl)benzoate (6): 4-(1-(pyridin-3-yl)-1*H*-1,2,3-triazol-4-yl) benzoic acid **3** (40 mg, 0.15 mmol) was dissolved in thionyl chloride (1 mL) and a few drops of DMF. The mixture was heated to 60 °C for 1 h. After cooling to room temperature, the solvent was removed under reduced pressure. Subsequently, ice-cold ethanol (5 mL) containing a few drips DIPEA was added slowly at 0 °C and the mixture was stirred at room temperature overnight. The solvent was removed under reduced pressure and EtOAc and sat. aq. $NaHCO_3$ solution were added. The mixture was extracted with EtOAc (3x), the combined organic layers were dried over sodium sulfate and concentrated under reduced pressure to obtain the crude. The purification was done using automated flash chromatography (DCM/MeOH 1:0 → 9:1). **6** was obtained as white powder (23 mg, 0.08 mmol, 53%). ^{1}H NMR (500 MHz, DMSO-d6) δ ppm 1.35 (t, *J*=7.10 Hz, 3 H) 4.35 (q, *J*=7.17 Hz, 2 H) 7.71 (dd, *J*=8.32, 4.81 Hz, 1 H) 8.10 (s, 4 H) 8.36 - 8.47 (m, 1 H) 8.74 (dd, *J*=4.73, 1.53 Hz, 1 H) 9.21 (d, *J*=2.44 Hz, 1 H) 9.56 (s, 1 H); ^{13}C NMR (126 MHz, DMSO-d_6) δ ppm 14.67, 61.32, 121.81, 125.16, 125.93, 128.47, 129.93, 130.49, 133.69, 134.92, 141.81, 146.95, 150.41, 165.85

4-(1-(pyridin-3-yl)-1*H*-1,2,3-triazol-4-yl)benzamide (7): 4-(1-(pyridin-3-yl)-1*H*-1,2,3-triazol-4-yl) benzoic acid **3** (40 mg, 0.15 mmol) was dissolved in thionyl chloride (1 mL) and a few drops of DMF. The mixture was heated to 60 °C for 1 h. After cooling to room temperature, the solvent was removed under reduced pressure. Subsequently, ice-cold aqueous ammonium hydroxide (5 mL) was added slowly at 0 °C and the mixture was stirred at room temperature overnight. DCM and water were added. The mixture was extracted with DCM (3x), the combined organic layers were dried over sodium sulfate and concentrated under reduced pressure to obtain the crude. The purification was done using automated flash chromatography (DCM/MeOH 1:0 → 8:2). **7** was obtained as white powder (10 mg, 0.04 mmol, 27%). ^{1}H NMR (500 MHz, DMSO-d_6) δ ppm 7.44 (br. s., 1 H) 7.72 (dd, *J*=8.01, 4.35 Hz, 1 H) 8.02 (s, 4 H) 8.39 (d, *J*=8.09 Hz, 1 H) 8.76 (br. s., 1 H) 9.23 (br. s., 1 H) 9.50 (s, 1 H); ^{13}C NMR (126 MHz, DMSO-d_6) δ ppm 120.86, 125.05, 127.93, 128.34, 132.59, 133.93, 141.31, 146.83, 149.87, 167.36

methyl 2-chloro-4-(1-(pyridin-3-yl)-1*H*-1,2,3-triazol-4-yl)benzoate (8): The triazole was synthesized according to **GP3** using methyl 2-chloro-4-ethynylbenzoate (62 mg, 0.32 mmol) and 3-azidopyridine **2** (1.3 eq., 50 mg, 0.41mmol) as starting materials. Purification was done using flash chromatography (DCM:MeOH 1:0 → 9:1) and **8** was obtained as a white solid (81 mg, 0.26 mmol, 81%). ^{1}H NMR (500 MHz, DMSO-d_6) δ ppm 3.89 (s, 3 H) 7.72 (ddd, *J*=8.28, 4.77, 0.69 Hz, 1 H) 8.00 (d, *J*=8.09 Hz, 1 H) 8.02 - 8.07 (m, 1 H) 8.12 (d, *J*=1.53 Hz, 1 H) 8.38 (ddd, *J*=8.28, 2.63, 1.45 Hz, 1 H) 8.75 (dd, *J*=4.73, 1.37 Hz, 1 H) 9.19 (d, *J*=2.59 Hz, 1 H) 9.61 (s, 1 H); ^{13}C NMR (126 MHz, DMSO-d_6) δ ppm 52.59, 121.91, 123.82, 124.72, 127.09, 128.00, 128.97, 132.26, 132.93, 133.13, 134.66, 141.31, 145.18, 150.04, 165.01

2-chloro-4-(1-(pyridin-3-yl)-1*H*-1,2,3-triazol-4-yl)benzoic acid (9): The synthesis was done according to **GP5** using methyl 2-chloro-4-(1-(pyridin-3-yl)-1*H*-1,2,3-triazol-4-yl)benzoate **8** (10 mg, 0.03 mmol) at 80°C for 1 h. **9** was obtained as a white solid (5 mg, 0.02 mmol, 66%). ^{1}H NMR (500 MHz, DMSO-d_6) δ ppm 7.72 (dd, *J*=8.32, 4.81 Hz, 1 H) 7.88 - 8.03 (m, 2 H) 8.09 (d, *J*=1.37 Hz, 1 H) 8.38 (ddd, *J*=8.28, 2.63, 1.45 Hz, 1 H) 8.75 (dd, *J*=4.65, 1.30 Hz, 1 H) 9.19 (d, *J*=2.44 Hz, 1 H) 9.59 (s, 1 H) 13.53 (br. s., 1 H); ^{13}C NMR (126 MHz, DMSO-d_6) δ ppm 122.18, 124.19, 125.20, 127.45, 128.47, 132.49, 133.63, 140.89, 141.79, 145.82, 150.48, 166.72

(4-(1-(pyridin-3-yl)-1*H*-1,2,3-triazol-4-yl)phenyl)methanol (10): The triazole was synthesized according to **GP3** using (4-ethynylphenyl)methanol (300 mg, 2.27 mmol) and 3-azidopyridine **2** (1.2 eq., 326 mg, 2.72 mmol) as starting materials. The crude was obtained as a yellow solid (466 mg, 1.86 mmol, 82%). Purification was done using prep. HPLC. ^{1}H NMR (500 MHz, DMSO-d_6) δ ppm 4.55 (d, *J*=5.65 Hz, 2 H) 5.26 (t, *J*=5.72 Hz, 1 H) 7.46 (m, *J*=8.24 Hz, 2 H) 7.70 (dd, *J*=8.24, 4.73 Hz, 1 H) 7.90 (m, *J*=8.09 Hz, 2 H) 8.36 - 8.42 (m, 1 H) 8.72 (dd, *J*=4.73, 1.22 Hz, 1 H) 9.20 (d, *J*=2.44 Hz, 1 H) 9.36 (s, 1 H); ^{13}C NMR (126 MHz, DMSO-d_6) δ ppm 62.62, 119.74, 124.66, 125.16, 127.04, 127.83, 128.40, 133.32, 141.21, 142.88, 147.58, 149.72

4-(1-(pyridin-3-yl)-1*H*-1,2,3-triazol-4-yl)aniline (11): The triazole was synthesized according to **GP3** using 4-ethynylaniline (75 mg, 0.64 mmol) and 3-azidopyridine **2** (1.3 eq., 100 mg, 0.83 mmol) as starting materials. After full conversion (LCMS control) the mixture was basified with sat. aq. $NaHCO_3$ solution and the product was precipitated. The crude was obtained as a brown solid (91 mg, 0.38 mmol, 60%). Purification was done using prep. HPLC. ^{1}H NMR (500 MHz, DMSO-d_6) δ ppm 5.35 (s, 2 H) 6.62 - 6.69 (m, 2 H) 7.56 - 7.62 (m, 2 H) 7.68 (dd, *J*=8.09, 4.58 Hz, 1 H) 8.32 - 8.38 (m, 1 H) 8.72 (br.

s., 1 H) 9.09 (s, 1 H) 9.20 (br. s., 1 H); ^{13}C NMR (126 MHz, DMSO-d_6) δ 113.95, 117.36, 117.43, 126.46, 127.50, 140.99, 148.62, 149.16, 149.43

***N*-(4-(1-(pyridin-3-yl)-1*H*-1,2,3-triazol-4-yl)phenyl)acetamide (12)**: 4-(1-(pyridin-3-yl)-1*H*-1,2,3-triazol-4-yl) aniline **11** (35 mg, 0.14 mmol) and triethylamine (2 eq., 0.28 mmol, 28 mg) were dissolved in a mixture of DCM (2 mL) and DMF (1 mL). Acetyl chloride (1.2 eq., 0.17 mmol, 13 mg) was added slowly at room temperature and the mixture was stirred for 16 h. TLC control indicated full conversion and the solvent was removed under reduced pressure to obtain the crude. Purification was done using automated flash chromatography (DCM/MeOH 1:0 → 9:1) to obtain **12** (5 mg, 0.02 mmol, 14%). ^{1}H NMR (500 MHz, DMSO-d_6) δ ppm 2.07 (s, 3 H) 7.61 - 7.78 (m, 3 H) 7.81 - 7.92 (m, 2 H) 8.32 - 8.41 (m, 1 H) 8.72 (dd, *J*=4.73, 1.22 Hz, 1 H) 9.19 (d, *J*=2.44 Hz, 1 H) 9.30 (s, 1 H) 10.10 (s, 1 H); ^{13}C NMR (126 MHz, DMSO-d_6) δ ppm 24.08, 119.29, 124.67, 125.88, 127.80, 133.34, 139.50, 141.19, 147.47, 149.72, 168.50

4-(1-(pyridin-3-yl)-1*H*-1,2,3-triazol-4-yl)benzonitrile (13): The triazole was synthesized according to **GP3** using 4-ethynylbenzonitrile (80 mg, 0.63 mmol) and 3-azidopyridine **2** (1.2 eq., 90 mg, 0.75 mmol) as starting materials. The crude was obtained as a yellow solid (100 mg, 0.40 mmol, 64%). Purification was done using prep. HPLC. ^{1}H NMR (500 MHz, DMSO-d_6) δ ppm 7.72 (dd, *J*=8.24, 4.73 Hz, 1 H) 8.01 (d, *J*=8.39 Hz, 2 H) 8.08 - 8.17 (m, 2 H) 8.35 - 8.44 (m, 1 H) 8.75 (d, *J*=4.27 Hz, 1 H) 9.19 (br. s., 1 H) 9.59 (s, 1 H); ^{13}C NMR (126 MHz, DMSO-d_6) δ ppm 110.67, 118.75, 121.84, 124.72, 125.93, 128.09, 133.16, 133.21, 134.48, 141.40, 145.93, 150.04

3-(azidomethyl)pyridine (15): To a solution of 3-(bromomethyl)pyridine **14** (200 mg, 1.17 mmol) in DMSO (5 mL), Et_3N (0.1 mL) and NaN_3 (1.1 eq., 84 mg, 1.29 mmol) were added. The mixture was stirred over night at room temperature, diluted with water and extracted with diethyl ether (3x). The combined organic layers were washed with brine, dried over $MgSO_4$ and concentrated under reduced pressure. The product was obtained as a colorless oil (123 mg, 0.92 mmol, 78%) and was used without further purification. R_f = 0.36 (PE/EtOAc 9:1)

4-(1-(pyridin-3-ylmethyl)-1*H*-1,2,3-triazol-4-yl)benzoic acid (16): The triazole was synthesized according to **GP3** using 4-ethynylbenzoic acid (50 mg, 0.31 mmol) and 3-(azidomethyl)pyridine **15** (1.3 eq., 53 mg, 0.40 mmol) as starting materials. The crude was obtained as a yellow solid (42 mg, 0.15 mmol, 51%). Purification was done using prep. HPLC. ^{1}H NMR (500 MHz, DMSO-d_6) δ ppm 5.88 (s, 2 H) 7.86 (br. s., 1 H) 7.94 - 7.99 (m, 3 H) 8.00 - 8.04 (m, 2 H) 8.27 (d, *J*=7.93 Hz, 1 H) 8.81 (s., 1 H) 8.85 (s, 1 H) 8.93 (s., 1 H); ^{13}C NMR (126 MHz, DMSO-d_6) δ ppm 49.95, 123.11, 125.14, 126.11, 130.02, 130.06, 133.89, 134.56, 142.03, 144.60, 144.82, 145.84, 166.96

3-azido-4-methylpyridine (18a): The azide was synthesized according to **GP1** using 4-methylpyridin-3-amine **17a** (150 mg, 1.4 mmol), sodium nitrite (1.7 eq., 165 mg, 2.4 mmol), sodium azide (1.7 eq. 155 mg, 2.4 mmol), EtOAc (4 mL), 6 M HCl (2.4 mL). The crude product (120 mg, 0.89 mmol, 64%) was used as obtained in the next step without further purifications. R_f = 0.35 (PE/EtOAc 7:3)

3-azido-4-chloropyridine (18b): The azide was synthesized according to **GP1** using 4-chloropyridin-3-amine **17b** (200 mg, 1.56 mmol), sodium nitrite (1.7 eq., 182 mg, 2.65 mmol), sodium azide (1.7 eq.,

172 mg, 2.65 mmol), EtOAc (8 mL), 6 M HCl (4.8 mL). The crude product (120 mg, 0.77 mmol, 50%) was used as obtained in the next step without further purifications. R_f = 0.71 (PE/EtOAc 7:3)

3-azido-4-phenylpyridine (18c): The azide was synthesized according to **GP1** using 4-phenylpyridin-3-amine **17c** (100 mg, 0.48 mmol), sodium nitrite (1.7 eq., 57 mg, 0.82 mmol), sodium azide (1.7 eq., 53 mg, 0.82 mmol), EtOAc (4 mL), 6 M HCl (2.4 mL). The crude product (92 mg, 0.47 mmol, 98%) was used as obtained in the next step without further purifications. R_f = 0.44 (PE/EtOAc 7:3)

3-azido-5-methylpyridine (18d): The azide was synthesized according to **GP1** using 5-methylpyridin-3-amine **17d** (150 mg, 1.4 mmol), sodium nitrite (1.7 eq., 165 mg, 2.4 mmol), sodium azide (1.7 eq. 155 mg, 2.4 mmol), EtOAc (4 mL), 6 M HCl (2.4 mL). The crude product (141 mg, 1.05 mmol, 75%) was used as obtained in the next step without further purifications. R_f = 0.35 (PE/EtOAc 7:3)

5-azidopicolinonitrile (18e): The azide was synthesized according to **GP1** using 5-aminopicolinonitrile **17e** (100 mg, 0.84 mmol), sodium nitrite (1.7 eq., 98 mg, 1.43 mmol), sodium azide (1.7 eq., 93 mg, 1.43 mmol), EtOAc (4 mL), 6 M HCl (1.2 mL). The crude product (107 mg, 0.74 mmol, 88%) was used as obtained in the next step without further purifications. R_f = 0.69 (PE/EtOAc 7:3)

5-azido-2-chloro-4-methylpyridine (18f): The azide was synthesized according to **GP1** using 6-chloro-4-methylpyridin-3-amine **17f** (200 mg, 1.41 mmol), sodium nitrite (1.7 eq., 165 mg, 2.40 mmol), sodium azide (1.7 eq., 155 mg, 2.40 mmol), EtOAc (8 mL), 6 M HCl (4.8 mL). The crude product (190 mg, 1.13 mmol, 80%) was used as obtained in the next step without further purifications. R_f = 0.82 (PE/EtOAc 7:3)

5-azido-*N*-methylpyridin-2-amine (18g): The azide was synthesized according to **GP1** using N^2-methylpyridine-2,5-diamine **17g** (200 mg, 1.62 mmol), sodium nitrite (1.7 eq., 2.75 mmol, 190 mg), sodium azide (1.7 eq., 2.75 mmol, 181 mg), EtOAc (13 mL), 6 M HCl (7 mL). The crude product (234 mg, 1.57 mmol, 97%) was used as obtained in the next step without further purifications. R_f = 0.46 (PE/EtOAc 7:3)

5-azido-*N*-isopropylpyridin-2-amine (18h): The azide was synthesized according to **GP1** using N^2-isopropylpyridine-2,5-diamine **17h** (300 mg, 1.98 mmol), sodium nitrite (1.7 eq., 3.36 mmol, 231 mg), sodium azide (1.7 eq., 3.36 mmol, 221 mg), EtOAc (10 mL), 6 M HCl (5 mL). The crude product (308 mg, 1.78 mmol, 90%) was used as obtained in the next step without further purifications. R_f = 0.75 (PE/EtOAc 7:3)

5-azido-*N*-phenylpyridin-2-amine (18i): The azide was synthesized according to **GP1** using N^2-phenylpyridine-2,5-diamine **17i** (200 mg, 1.08 mmol), sodium nitrite (1.7 eq., 1.84 mmol, 126 mg), sodium azide (1.7 eq., 1.84 mmol, 121 mg), EtOAc (6 mL), 6 M HCl (2.5 mL). The crude product (203 mg, 0.96 mmol, 89%) was used as obtained in the next step without further purifications. R_f = 0.78 (PE/EtOAc 7:3)

3-azido-5-fluoropyridine (18j): The azide was synthesized according to **GP1** using 5-fluoropyridin-3-amine (100 mg, 0.91 mmol) **17j** (100 mg, 0.91 mmol), sodium nitrite (1.7 eq., 1.54 mmol, 105 mg), sodium azide (1.7 eq., 1.84 mmol, 101 mg), EtOAc (3 mL), 6 M HCl (1.25 mL). The crude product (37 mg, 0.27 mmol, 30%) was used as obtained in the next step without further purifications. R_f = 0.54 (PE/EtOAc 7:3)

5-azido-2-methoxypyridine (18k): The azide was synthesized according to **GP1** using 6-methoxypyridin-3-amine **17k** (100 mg, 0.81 mmol), sodium nitrite (1.7 eq., 94 mg, 1.37 mmol), sodium azide (1.7 eq., 88 mg, 1.37 mmol), EtOAc (4 mL), 6 M HCl (2.4 mL). The crude product (110 mg, 0.73 mmol, 90%) was used as obtained in the next step without further purifications. R_f = 0.77 (PE/EtOAc 7:3)

5-azido-2-phenoxypyridine (18l): The azide was synthesized according to **GP1** using 6-phenoxypyridin-3-amine **17l** (180 mg, 0.97 mmol), sodium nitrite (1.7 eq., 1.14 mmol, 77 mg), sodium azide (1.7 eq., 1.14 mmol, 74 mg), EtOAc (3 mL), 6 M HCl (6 mL). The crude product (150 mg, 0.70 mmol, 72%) was used as obtained in the next step without further purifications. R_f = 0.85 (PE/EtOAc 6:4)

1-azido-4-phenoxybenzene (18m): The azide was synthesized according to **GP1** using 4-phenoxyaniline **17m** (100 mg, 0.54 mmol), sodium nitrite (1.7 eq., 0.91 mmol, 61 mg), sodium azide (1.7 eq., 1.82 mmol, 58 mg), EtOAc (4 mL), 6 M HCl (7 mL). The crude product (90 mg, 0.45 mmol, 83%) was used as obtained in the next step without further purifications. R_f = 0.43 (PE/EtOAc 7:3)

3-(4-azidophenoxy) pyridine (18n): The azide was synthesized according to **GP1** using 4-(pyridin-3-yloxy) aniline **17n** (200 mg, 1.07 mmol), sodium nitrite (1.7 eq., 1.82 mmol, 125 mg), sodium azide (1.7 eq., 1.82 mmol, 118 mg), EtOAc (5 mL), 6 M HCl (10 mL). The crude product (190 mg, 0.89 mmol, 83%) was used as obtained in the next step without further purifications. R_f = 0.35 (PE/EtOAc 7:3)

4-(1-(4-methylpyridin-3-yl)-1*H*-1,2,3-triazol-4-yl)benzoic acid (19a): The triazole was synthesized according to **GP3** using 4-ethynylbenzoic acid (118 mg, 0.81mmol) and 3-azido-4-methylpyridine **18a** (1.3 eq., 141 mg, 1.05 mmol) as starting materials. The crude was obtained as a white solid (45 mg, 0.16 mmol, 20%). Purification was done using prep. HPLC. ^{1}H NMR (500 MHz, DMSO-d_6) δ ppm 2.32 (s, 3 H) 7.60 (d, *J*=5.04 Hz, 1 H) 8.07 (s, 5 H) 8.66 (d, *J*=4.73 Hz, 1 H) 8.73 (s, 1 H) 9.20 (s, 1 H) 13.04 (br. s., 1 H); ^{13}C NMR (126 MHz, DMSO-d_6) δ ppm 17.05, 124.45, 125.32, 126.25, 130.13, 130.26, 134.27, 142.44, 145.87, 145.97, 150.53, 166.96

4-(1-(4-chloropyridin-3-yl)-1*H*-1,2,3-triazol-4-yl)benzoic acid (19b): The triazole was synthesized according to **GP3** using 4-ethynylbenzoic acid (83 mg, 0.56 mmol) and 3-azido-4-chloropyridine **18b** (1.3 eq., 114 mg, 0.74 mmol) as starting materials. The crude was obtained as a yellow solid (40 mg, 0.13 mmol, 23%). Purification was done using prep. HPLC. ^{1}H NMR (500 MHz, DMSO-d_6) δ ppm 7.97 (dd, *J*=4.96, 4.20 Hz, 1 H) 8.02 - 8.18 (m, 4 H) 8.71 - 8.89 (m, 1 H) 8.98 (br. s., 1 H) 9.27 (d, *J*=3.97 Hz, 1 H) 13.11 (br. s., 1 H); ^{13}C NMR (126 MHz, DMSO-d_6) δ ppm 124.96, 125.39, 125.51, 130.17, 131.55, 133.82, 138.59, 145.98, 148.18, 152.25, 167.01

4-(1-(4-phenylpyridin-3-yl)-1*H*-1,2,3-triazol-4-yl)benzoic acid (19c): The triazole was synthesized according to **GP3** using 4-ethynylbenzoic acid (53 mg, 0.36 mmol) and 3-azido-4-phenylpyridine **18c** (1.3 eq., 92 mg, 0.47 mmol) as starting materials. The crude was obtained as a white solid (30 mg, 0.09 mmol, 25%). Purification was done using prep. HPLC. ^{1}H NMR (500 MHz, DMSO-d_6) δ ppm 7.17 - 7.25 (m, 2 H) 7.31 - 7.40 (m, 3 H) 7.74 (d, *J*=5.04 Hz, 1 H) 7.89 - 7.96 (m, 2 H) 7.98 - 8.04 (m, 2 H) 8.88 (d, *J*=5.19 Hz, 1 H) 8.90 (s, 1 H) 8.93 (s, 1 H); ^{13}C NMR (126 MHz, DMSO-d_6) δ ppm 125.05, 125.17, 125.21, 128.02, 128.83, 129.13, 130.12, 131.18, 134.01, 134.55, 144.74, 145.79, 147.47, 151.54, 166.98

4-(1-(5-methylpyridin-3-yl)-1*H*-1,2,3-triazol-4-yl)benzoic acid (19d): The triazole was synthesized according to **GP3** using 4-ethynylbenzoic acid (100 mg, 0.68 mmol) and 3-azido-5-methylpyridine **18d** (1.3 eq., 120 mg, 0.89 mmol) as starting materials. The crude was obtained as a yellow solid (103 mg, 0.36 mmol, 53%). Purification was done using prep. HPLC. ^{1}H NMR (500 MHz, DMSO-d_6) δ ppm 2.46 (s, 3 H) 8.00 - 8.13 (m, 4 H) 8.25 (s, 1 H) 8.59 (s, 1 H) 9.01 (s., 1 H) 9.51 (s, 1 H) 13.04 (br. s., 1 H); ^{13}C NMR (126 MHz, DMSO-d_6) δ ppm 17.74, 121.11, 125.32, 128.06, 130.18, 130.41, 132.92, 134.09, 134.59, 138.41, 146.58, 150.25, 166.96

4-(1-(6-cyanopyridin-3-yl)-1*H*-1,2,3-triazol-4-yl)benzoic acid (19e): The triazole was synthesized according to **GP3** using 4-ethynylbenzoic acid (125 mg,0.86 mmol) and 5-azidopicolinonitrile **18e** (1.3 eq., 161mg, 1.11 mmol) as starting materials. The crude was obtained as a yellow solid (113 mg, 0.39 mmol, 45%). Purification was done using prep. HPLC. ^{1}H NMR (500 MHz, DMSO-d_6) δ ppm 8.07 (d, *J*=7.48 Hz, 4 H) 8.38 (d, *J*=8.55 Hz, 1 H) 8.66 (dd, *J*=8.47, 2.52 Hz, 1 H) 9.42 (d, *J*=2.44 Hz, 1 H) 9.67 (s, 1 H); ^{13}C NMR (126 MHz, DMSO-d_6) δ ppm 115.35, 117.02, 121.28, 125.35, 128.55, 130.30, 131.83, 135.25, 142.55, 147.00, 166.96

4-(1-(6-chloro-4-methylpyridin-3-yl)-1*H*-1,2,3-triazol-4-yl)benzoic acid (19f): The triazole was synthesized according to **GP3** using 4-ethynylbenzoic acid (78 mg, 0.53 mmol) and 5-azido-2-chloro-4-methylpyridine **18f** (1.3 eq., 116 mg, 0.69 mmol) as starting materials. The crude was obtained as a white yellow solid (128 mg, 0.41 mmol, 77%). Purification was done using prep. HPLC. ^{1}H NMR (500 MHz, DMSO-d_6) δ ppm 2.33 (s, 3 H) 7.81 (s, 1 H) 8.07 (s, 4 H) 8.63 (s, 1 H) 9.20 (s, 1 H); ^{13}C NMR (126 MHz, DMSO-d_6) δ ppm 17.21, 124.56, 125.38, 126.34, 130.18, 130.34, 132.94, 134.15, 145.98, 146.15, 146.55, 150.87, 166.98

4-(1-(6-(methylamino)pyridin-3-yl)-1*H*-1,2,3-triazol-4-yl)benzoic acid (19g): The triazole was synthesized according to **GP3** using 4-ethynylbenzoic acid (60 mg, 0.41mmol) and 5-azido-*N*-methylpyridin-2-amine **18g** (1.2 eq., 73 mg, 0.49 mmol) as starting materials. The crude was obtained as a white solid (70 mg, 0.24 mmol, 59%). Purification was done using prep. HPLC. ^{1}H NMR (500 MHz, DMSO-d_6) δ ppm 2.84 (d, *J*=4.73 Hz, 3 H) 6.64 (d, *J*=9.00 Hz, 1 H) 7.05 (d, *J*=4.73 Hz, 1 H) 7.89 (dd, *J*=8.93, 2.67 Hz, 1 H) 8.00 - 8.14 (m, 4 H) 8.49 (d, *J*=2.59 Hz, 1 H) 9.21 (s, 1 H) 13.01 (br. s., 1 H); ^{13}C NMR (126 MHz, DMSO-d_6) δ ppm 28.03, 108.01, 120.84, 123.47, 125.21, 130.12, 130.15, 134.57, 140.28, 146.01, 159.45, 167.01

4-(1-(6-(isopropylamino)pyridin-3-yl)-1*H*-1,2,3-triazol-4-yl)benzoic acid (19h): The triazole was synthesized according to **GP3** using 4-ethynylbenzoic acid (60 mg, 0.41 mmol) and 5-azido-*N*-isopropylpyridin-2-amine **18h** (1.2 eq., 87 mg, 0.49 mmol) as starting materials. The crude was obtained as a white solid (93 mg, 0.29 mmol, 70%). Purification was done using prep. HPLC. ^{1}H NMR (500 MHz, DMSO-d_6) δ ppm 1.17 (s, 3 H) 1.19 (s, 3 H) 4.06 (dq, *J*=13.35, 6.59 Hz, 1 H) 6.62 (d, *J*=9.00 Hz, 1 H) 6.94 (d, *J*=7.48 Hz, 1 H) 7.85 (dd, *J*=9.00, 2.75 Hz, 1 H) 7.96 - 8.17 (m, 4 H) 8.45 (d, *J*=2.59 Hz, 1 H) 9.18 (s, 1 H); ^{13}C NMR (126 MHz, DMSO-d_6) δ ppm 22.50, 41.86, 108.53, 120.81, 123.23, 125.16, 130.09, 130.17, 134.42, 140.32, 146.01, 158.27, 167.07

4-(1-(6-(phenylamino)pyridin-3-yl)-1*H*-1,2,3-triazol-4-yl)benzoic acid (19i): The triazole was synthesized according to **GP3** using 4-ethynylbenzoic acid (60 mg, 0.41 mmol) and 5-azido-*N*-phenylpyridin-2-amine **18i** (1.2eq., 104 mg, 0.49 mmol) as starting materials. The crude was obtained as a white solid (132 mg, 0.37 mmol, 90%). Purification was done using prep. HPLC. ^{1}H NMR (500 MHz, DMSO-d_6) δ ppm 6.96 (s, 1 H) 7.04 (d, *J*=8.85 Hz, 1 H) 7.32 (t, *J*=7.71 Hz, 2 H) 7.72 (d, *J*=8.24 Hz, 2 H) 8.06 (s, 4 H) 8.10 (dd, *J*=8.93, 2.67 Hz, 1 H) 8.68 (d, *J*=2.59 Hz, 1 H) 9.31 (s, 1 H) 9.48 (s, 1 H); ^{13}C NMR (126 MHz, DMSO-d_6) δ ppm 111.04, 118.52, 120.86, 121.31, 125.25, 125.49, 128.78, 130.15, 130.49, 134.38, 139.59, 140.94, 146.21, 155.89, 167.04

4-(1-(5-fluoropyridin-3-yl)-1*H*-1,2,3-triazol-4-yl)benzoic acid (19j): The triazole was synthesized according to **GP3** using 4-ethynylbenzoic acid (40 mg, 0.27 mmol) and 3-azido-5-fluoropyridine **18j** (1.1 eq., 41 mg, 0.30 mmol) as starting materials. The crude was obtained as a white solid (31 mg, 0.11 mmol, 40%). Purification was done using prep. HPLC. ^{1}H NMR (500 MHz, DMSO-d_6) δ ppm 7.97 - 8.11 (m, 4 H) 8.46 (dt, *J*=9.50, 2.35 Hz, 1 H) 8.79 (d, *J*=2.59 Hz, 1 H) 9.14 (s, 1 H) 9.55 (s, 1 H); ^{13}C NMR (126 MHz, DMSO-d_6) δ ppm 116.06, 125.67, 130.62, 137.90, 138.53, 138.78, 143.33, 155.08, 169.50

4-(1-(6-methoxypyridin-3-yl)-1*H*-1,2,3-triazol-4-yl)benzoic acid (19k): The triazole was synthesized according to **GP3** using 4-ethynylbenzoic acid (90 mg, 0.62 mmol) and 5-azido-2-methoxypyridine **18k** (1.3 eq., 120 mg, 0.81 mmol) as starting materials. The crude was obtained as a white solid (101 mg, 0.34 mmol, 55%). Purification was done using prep. HPLC. ^{1}H NMR (500 MHz, DMSO-d_6) δ ppm 3.95 (s, 3 H) 7.11 (dd, *J*=8.93, 0.53 Hz, 1 H) 7.97 - 8.11 (m, 4 H) 8.27 (dd, *J*=8.93, 2.82 Hz, 1 H) 8.69 - 8.81 (m, 1 H) 9.36 (s, 1 H); ^{13}C NMR (126 MHz, DMSO-d_6) δ ppm 53.89, 111.50, 121.16, 125.16, 128.26, 130.10, 132.30, 139.03, 163.44

4-(1-(6-phenoxypyridin-3-yl)-1*H*-1,2,3-triazol-4-yl)benzoic acid (19l): The triazole was synthesized according to **GP3** using 4-ethynylbenzoic acid (85 mg, 0.58 mmol) and 5-azido-2-phenoxypyridine **18l** (1.2 eq., 150 mg, 0.70 mmol) as starting materials. The crude was obtained as a white solid (160 mg, 0.45 mmol, 77%). Purification was done using prep. HPLC. ^{1}H NMR (500 MHz, DMSO-d_6) δ ppm 7.18 - 7.24 (m, 2 H) 7.24 - 7.30 (m, 1 H) 7.32 (d, *J*=8.85 Hz, 1 H) 7.44 - 7.53 (m, 2 H) 8.05 (q, *J*=8.39 Hz, 4 H) 8.42 (dd, *J*=8.85, 2.75 Hz, 1 H) 8.72 (d, *J*=2.75 Hz, 1 H) 9.40 (s, 1 H); ^{13}C NMR (126 MHz, DMSO-d_6) δ ppm 112.36, 121.25, 121.43, 125.13, 125.25, 129.54, 129.95, 130.18, 133.05, 133.76, 139.48, 146.62, 153.55, 162.88, 167.29

4-(1-(4-phenoxyphenyl)-1*H*-1,2,3-triazol-4-yl)benzoic acid (19m): The triazole was synthesized according to **GP3** using 4-ethynylbenzoic acid (25 mg, 0.17 mmol) and 1-azido-4-phenoxybenzene **18m**

(1.2 eq., 42 mg, 0.2 mmol) as starting materials. The crude was obtained as a white solid (32 mg, 0.09 mmol, 53%). Purification was done using prep. HPLC. ^{1}H NMR (500 MHz, DMSO-d_6) δ ppm 7.13 (dd, *J*=8.62, 0.99 Hz, 2 H) 7.20 - 7.27 (m, 3 H) 7.46 (dd, *J*=8.55, 7.48 Hz, 2 H) 7.96 (d, *J*=9.00 Hz, 2 H) 8.06 (s, 4 H) 9.40 (s, 1 H); ^{13}C NMR (126 MHz, DMSO-d_6) δ ppm 119.23, 119.38, 120.88, 122.17, 124.22, 125.27, 130.14, 130.32, 131.97, 134.36, 146.37, 156.01, 157.11, 166.98

4-(1-(4-(pyridin-3-yloxy)phenyl)-1*H*-1,2,3-triazol-4-yl)benzoic acid (19n): The triazole was synthesized according to **GP3** using 4-ethynylbenzoic acid (25 mg, 0.17 mmol) and 3-(4-azidophenoxy)pyridine **18n** (1.2 eq., 42 mg, 0.20 mmol) as starting materials. The crude was obtained as a white solid (42 mg, 0.12 mmol, 70%). Purification was done using prep. HPLC. ^{1}H NMR (500 MHz, DMSO-d_6) δ ppm 7.33 - 7.40 (m, 2 H) 7.58 - 7.63 (m, 1 H) 7.70 - 7.76 (m, 1 H) 7.98 - 8.04 (m, 2 H) 8.07 (s, 4 H) 8.51 (br. s., 1 H) 8.59 (br. s., 1 H) 9.45 (s, 1 H); ^{13}C NMR (126 MHz, DMSO-d_6) δ ppm 119.91, 120.97, 122.30, 125.34, 125.66, 128.02, 130.20, 130.27, 132.74, 134.38, 140.04, 143.88, 146.45, 156.15, 167.05

4-(1-(6-hydroxypyridin-3-yl)-1*H*-1,2,3-triazol-4-yl)benzoic acid (19o): 4-(1-(6-methoxypyridin-3-yl)-1*H*-1,2,3-triazol-4-yl)benzoic acid **19k** (20 mg, 0.07 mmol) was dissolved in 48% HBr aq. solution (1 mL) and was stirred at 80 °C for 12 h. After cooling to room temperature, water was added and the product precipitated. The solids were collected, washed with water, and dried under vacuum to obtain the crude product (17 mg, 0.06 mmol, 86%). The product was purified using prep. HPLC. ^{1}H NMR (500 MHz, DMSO-d_6) δ ppm 6.59 (d, *J*=9.61 Hz, 1 H) 7.99 (d, *J*=3.05 Hz, 1 H) 8.00 - 8.04 (m, 2 H) 8.04 - 8.08 (m, 2 H) 8.12 (d, *J*=2.75 Hz, 1 H) 9.21 (s, 1 H), 12.59 (br. s, 1 H); ^{13}C NMR (126 MHz, DMSO-d_6) δ ppm 121.39, 125.20, 130.17, 134.38, 135.14, 146.01, 161.76, 166.98

4-azido-3-methylpyridine (21): The azide was synthesized according to **GP1** using 3-methylpyridin-4-amine **20** (150 mg, 1.4 mmol), sodium nitrite (1.7 eq., 165 mg, 2.4 mmol), sodium azide (1.7 eq. 155 mg, 2.4 mmol), EtOAc (4 mL), 6 M HCl (2.4 mL). The crude product (51 mg, 0.38 mmol, 4%) was used as obtained in the next step without further purifications. R_f = 0.31 (PE/EtOAc 7:3)

4-(1-(3-methylpyridin-4-yl)-1*H*-1,2,3-triazol-4-yl)benzoic acid (22): The triazole was synthesized according to **GP3** using 4-ethynylbenzoic acid (40 mg, 0.27 mmol) and 4-azido-3-methylpyridine **21** (1.3 eq., 51 mg, 0.35 mmol) as starting materials. Purification was done using flash chromatography (DCM:MeOH 1:0 → 9:1) and **22** was obtained as a white solid (56 mg, 0.20 mmol, 77%). ^{1}H NMR (500 MHz, DMSO-d$_6$) δ ppm 2.32 (s, 3 H) 7.60 (d, *J*=5.04 Hz, 1 H) 8.07 (s, 5 H) 8.66 (d, *J*=5.04 Hz, 1 H) 8.73 (s, 1 H) 9.20 (s, 1 H) 13.07 (br. s., 1 H); ^{13}C NMR (126 MHz, DMSO-d$_6$) δ ppm 17.05, 124.43, 125.32, 126.25, 130.13, 130.41, 133.36, 134.22, 142.45, 145.89, 145.98, 150.54, 167.00

2-(5-amino-4-methylpyridin-2-yl)phenol (24a): The coupling was done according to **GP4** using 6-bromo-4-methylpyridin-3-amine **23** (130 mg, 0.69 mmol), (2-hydroxyphenyl)boronic acid (1.2 eq., 113 mg, 0.83 mmol), sodium carbonate (3 eq., 218 mg, 2.08 mmol,) and tetrakis (triphenylphosphine) palladium (0.1 eq., 78 mg, 0.07 mmol) in 1,4-dioxan:water (1:1, 6 mL). **24b** was obtained as yellow solid (103 mg, 0.52 mmol, 75%). MS (ESI+) m/z 201 (M + H).

(4'-amino-3'-methyl-[1,1'-biphenyl]-3-yl)methanol (24b): The coupling was done according to **GP4** using 6-bromo-4-methylpyridin-3-amine **23** (100 mg, 0.53 mmol), (3-(hydroxymethyl)phenyl)boronic acid (1.2 eq., 97 mg, 0.64 mmol), sodium carbonate (3 eq., 167 mg, 1.59 mmol,) and tetrakis (triphenylphosphine) palladium (0.1 eq., 57 mg, 0.05 mmol) in 1,4-dioxan:water (1:1, 6 mL). **24a** was obtained as yellow-broun solid (70 mg, 0.33 mmol, 62%). MS (ESI+) m/z 215 (M + H).

2-(5-azido-4-methylpyridin-2-yl)phenol (25a): The azide was synthesized according to **GP1** using 2-(5-amino-4-methylpyridin-2-yl)phenol **25a** (56 mg, 0.27 mmol), sodium nitrite (1.7 eq., 0.46 mmol, 32 mg), sodium azide (1.7 eq., 0.46 mmol, 30 mg), EtOAc (2 mL), 6 M HCl (4 mL). The crude product (58 mg, 0.25 mmol, 99%) was used as obtained in the next step without further purifications. R_f = 0.75 (PE/EtOAc 0:1)

(3-(5-azido-4-methylpyridin-2-yl)phenyl)methanol (25b): The azide was synthesized according to **GP1** using (4'-amino-3'-methyl-[1,1'-biphenyl]-3-yl)methanol **24a** (70 mg, 0.33 mmol), sodium nitrite (1.7 eq., 0.55 mmol, 38 mg), sodium azide (1.7 eq., 0.55 mmol, 33 mg), EtOAc (3 mL) and 6 M HCl (5 mL). The crude product (77 mg, 0.32 mmol, 98%) was used as obtained in the next step without further purifications. R_f = 0.80 (PE/EtOAc 0:1)

4-(1-(6-(2-hydroxyphenyl)-4-methylpyridin-3-yl)-1*H*-1,2,3-triazol-4-yl)benzoic acid (26a): The triazole was synthesized according to **GP3** using 4-ethynylbenzoic acid (32 mg, 0.22 mmol) and 2-(5-azido-4-methylpyridin-2-yl)phenol **25a** (1 eq., 50 mg, 0.22 mmol) as starting materials. The crude was obtained as a white solid (30 mg, 0.08 mmol, 36%). Purification was done using prep. HPLC. ^{1}H NMR (500 MHz, DMSO-d_6) δ ppm 2.43 (s, 3 H) 6.95 - 7.01 (m, 2 H) 7.37 (td, *J*=7.71, 1.53 Hz, 1 H) 8.06 (s, 1 H) 8.08 (s, 4 H) 8.11 (dd, *J*=8.39, 1.53 Hz, 1 H) 8.42 (s, 1 H) 8.84 (s, 1 H) 9.25 (s, 1 H) 13.22 (br. s, 1 H); ^{13}C NMR (126 MHz, DMSO-d_6) δ ppm 17.81, 118.03, 119.01, 119.33, 122.78, 124.54, 125.39, 128.05, 130.24, 131.72, 132.07, 143.28, 144.60, 146.06, 157.48, 158.82, 167.15

4-(1-(6-(3-(hydroxymethyl)phenyl)-4-methylpyridin-3-yl)-1*H*-1,2,3-triazol-4-yl)benzoic acid (26b): The triazole was synthesized according to **GP3** using 4-ethynylbenzoic acid (36 mg, 0.26 mmol) and (3-(5-azido-4-methylpyridin-2-yl)phenyl)methanol **25a** (1.0 eq., 60 mg, 0.26 mmol) as starting materials. The crude was obtained as a white solid (50 mg, 0.13 mmol, 50%). Purification was done using prep. HPLC. ^{1}H NMR (500 MHz, DMSO-d_6) δ ppm 2.40 (s, 3 H) 4.62 (br. s., 2 H) 5.34 (br. s., 1 H) 7.45 (d, *J*=7.63 Hz, 1 H) 7.51 (t, *J*=7.63 Hz, 1 H) 8.03 - 8.06 (m, 1 H) 8.06 - 8.11 (m, 4 H) 8.16 (s, 1 H) 8.19 (s, 1 H) 8.81 (s, 1 H) 9.24 (s, 1 H) 13.07 (br. s., 1 H); ^{13}C NMR (126 MHz, DMSO-d_6) δ ppm 17.49, 62.90, 122.55, 124.52, 125.00, 125.33, 125.42, 127.91, 128.79, 130.24, 130.31, 130.39, 132.29, 134.34, 137.32, 143.38, 145.83, 145.97, 157.02, 167.10

(3-(5-aminopyridin-3-yl)phenyl)methanol (29a): The coupling was done according to **GP4** using 5-bromopyridin-3-amine **27** (120 mg, 0.69 mmol), (3-(hydroxymethyl)phenyl)boronic acid (1.2 eq., 125 mg, 0.83 mmol), sodium carbonate (3 eq., 218 mg, 2.08 mmol,) and tetrakis (triphenylphosphine) palladium (0.1 eq., 78 mg, 0.07 mmol) in 1,4-dioxan:water (1:1, 6 mL). **29a** was obtained as yellow solid (96 mg, 0.48 mmol, 69%). MS (ESI+) m/z 201 (M + H).

4-chloro-5-phenylpyridin-3-amine (29b): The coupling was done according to **GP4** using 5-bromo-4-chloropyridin-3-amine **28** (150 mg, 0.72 mmol), phenylboronic acid (1.2 eq., 104 mg, 0.86 mmol), sodium carbonate (3 eq., 227 mg, 2.17 mmol,) and tetrakis (triphenylphosphine) palladium (0.1 eq., 78 mg, 0.07 mmol) in 1,4-dioxan:water (1:1, 7 mL). **29b** was obtained as yellow oil (30 mg, 0.15 mmol, 21%). MS (ESI+) m/z 205 (M + H).

(3-(5-azidopyridin-3-yl)phenyl)methanol (30a): The azide was synthesized according to **GP1** using (3-(5-aminopyridin-3-yl)phenyl)methanol **29a** (60 mg, 0.30 mmol), sodium nitrite (1.7 eq., 0.51 mmol, 36 mg), sodium azide (1.7 eq., 0.51 mmol, 34 mg), EtOAc (2 mL) and 6 M HCl (4 mL). The crude product (58 mg, 0.26 mmol, 86%) was used as obtained in the next step without further purifications. R_f = 0.79 (PE/EtOAc 0:1)

3-azido-4-chloro-5-phenylpyridine (30b): The azide was synthesized according to **GP1** using 4-chloro-5-phenylpyridin-3-amine **29b** (30 mg, 0.15 mmol sodium nitrite (1.7 eq., 0.25 mmol, 17 mg), sodium azide (1.7 eq., 0.25 mmol, 14 mg), EtOAc (1 mL), 6 M HCl (3 mL). The crude product (30 mg, 0.13 mmol, 86%) was used as obtained in the next step without further purifications. R_f = 0.9 (PE/EtOAc 0:1)

4-(1-(5-(3-(hydroxymethyl)phenyl)pyridin-3-yl)-1*H*-1,2,3-triazol-4-yl)benzoic acid (31a): The triazole was synthesized according to **GP3** using 4-ethynylbenzoic acid (30 mg, 0.20 mmol) and (3-(5-azidopyridin-3-yl)phenyl)methanol **30a** (1.2 eq., 54 mg, 0.24 mmol) as starting materials. The crude was obtained as a white solid (31 mg, 0.08 mmol, 40%). Purification was done using prep. HPLC. ^{1}H NMR (500 MHz, DMSO-d_6) δ ppm 4.63 (s, 2 H) 5.35 (br. s., 1 H) 7.47 (d, *J*=7.63 Hz, 1 H) 7.54 (t, *J*=7.63 Hz, 1 H) 7.77 (d, *J*=7.78 Hz, 1 H) 7.83 (s, 1 H) 8.01 - 8.23 (m, 4 H) 8.64 (t, *J*=2.14 Hz, 1 H) 9.05 (br. s., 1 H) 9.22 (br. s., 1 H) 9.65 (s, 1 H); ^{13}C NMR (126 MHz, DMSO-d_6) δ ppm 62.77, 121.43, 125.27, 125.33, 125.47, 125.64, 127.05, 129.13, 130.25, 130.64, 133.43, 134.04, 135.45, 136.67, 139.89, 143.78, 146.66, 147.68, 167.05

4-(1-(4-chloro-5-phenylpyridin-3-yl)-1*H*-1,2,3-triazol-4-yl)benzoic acid (31b): The triazole was synthesized according to **GP3** using 4-ethynylbenzoic acid (22 mg, 0.15 mmol) and 3-azido-4-chloro-5-phenylpyridine **30b** (1.0 eq., 35 mg, 0.15 mmol) as starting materials. The crude was obtained as a white solid (43 mg, 0.11 mmol, 76%). Purification was done using prep. HPLC. ^{1}H NMR (500 MHz, DMSO-d_6) δ ppm 7.53 - 7.62 (m, 5 H) 8.07 (s, 4 H) 8.85 (s, 1 H) 8.98 (s, 1 H) 9.29 (s, 1 H) 13.13 (br. s., 1 H); ^{13}C NMR (126 MHz, DMSO-d_6) δ ppm 125.21, 125.38, 128.77, 129.08, 129.62, 130.22, 131.96, 134.08, 136.85, 137.48, 145.98, 147.09, 152.41, 167.04

3-azido-5-bromopyridine (33a): The azide was synthesized according to **GP1** using 5-bromopyridin-3-amine **32a** (150 mg, 0.87 mmol), sodium nitrite (1.7 eq., 101 mg, 1.47 mmol), sodium azide (1.7 eq., 96 mg, 1.47 mmol), EtOAc (4 mL), 6 M HCl (2.4 mL). The crude product (60 mg, 0.3 mmol, 34%) was used as obtained in the next step without further purifications. R_f = 0.75 (PE/EtOAc 7:3)

5-azido-2-chloro-4-methylpyridine (33b): The azide was synthesized according to **GP1** using 6-chloro-4-methylpyridin-3-amine **32b** (200 mg, 1.41 mmol), sodium nitrite (1.7 eq., 165 mg, 2.40 mmol), sodium azide (1.7 eq., 155 mg, 2.40 mmol), EtOAc (8 mL), 6 M HCl (4.8 mL). The crude

product (190 mg, 1.13 mmol, 80%) was used as obtained in the next step without further purifications. R_f = 0.82 (PE/EtOAc 7:3)

methyl 4-(1-(5-bromopyridin-3-yl)-1*H*-1,2,3-triazol-4-yl)benzoate (34a): The triazole was synthesized according to **GP3** using methyl 4-ethynylbenzoate (200 mg, 1.25 mmol) and 3-azido-5-bromopyridine **33a** (1.2 eq. 298 mg, 1.5 mmol) as starting materials. **34a** was obtained as a yellow solid (238 mg, 0.79 mmol, 63%) and was used as obtained without further purification. MS (ESI+) m/z 360 (M + H).

methyl 4-(1-(6-chloro-4-methylpyridin-3-yl)-1H-1,2,3-triazol-4-yl)benzoate (34b): The triazole was synthesized according to **GP3** using methyl 4-ethynylbenzoate (230 mg,2.0 mmol) and 5-azido-2-chloro-4-methylpyridine **33b** (1.2 eq., 400 mg, 2.4 mmol) as starting materials. The mixture was acidified with 1 M HCl, extracted with EtOAc (2x) and the combined organic layers were dried over sodium sulfate and concentrated under reduced pressure to obtain the crude (525 mg, 1.6 mmol, 80%). **34b** was used as obtained without further purification. MS (ESI+) m/z 329 (M + H).

methyl 4-(1-(5-phenylpyridin-3-yl)-1H-1,2,3-triazol-4-yl)benzoate (35a): The coupling was done according to **GP4** using methyl 4-(1-(5-bromopyridin-3-yl)-1*H*-1,2,3-triazol-4-yl)benzoate **34a** (30 mg, 0.08 mmol) and phenylboronic acid (1.2 eq., 12 mg, 0.10 mmol). **35a** was obtained as yellow-brown solid (21 mg, 0.06 mmol, 75%). MS (ESI+) m/z 357 (M + H).

methyl 4-(1-(5-(2-methoxyphenyl)pyridin-3-yl)-1*H*-1,2,3-triazol-4-yl)benzoate (35b): The coupling was done according to **GP4** using methyl 4-(1-(5-bromopyridin-3-yl)-1*H*-1,2,3-triazol-4-yl)benzoate **34a** (40 mg, 0.11 mmol) and (2-methoxyphenyl)boronic acid (1.5 eq., 25 mg, 0.16 mmol). **35b** was obtained as a brown solid (25 mg, 0.06 mmol, 54%). MS (ESI+) m/z 387 (M + H). NMR ABE181

methyl 4-(1-(5-(3-methoxyphenyl)pyridin-3-yl)-1*H*-1,2,3-triazol-4-yl)benzoate (35c): The coupling was done according to **GP4** using methyl 4-(1-(5-bromopyridin-3-yl)-1*H*-1,2,3-triazol-4-yl)benzoate **34a** (30 mg, 0.08 mmol) and (3-methoxyphenyl)boronic acid (1.2 eq., 15 mg, 0.10 mmol). **35c** was obtained as a yellow-brown solid (29 mg, 0.07 mmol, 87%). MS (ESI+) m/z 387 (M + H).

methyl 4-(1-(5-(4-methoxyphenyl)pyridin-3-yl)-1*H*-1,2,3-triazol-4-yl)benzoate (35d): The coupling was done according to **GP4** using methyl 4-(1-(5-bromopyridin-3-yl)-1*H*-1,2,3-triazol-4-yl)benzoate **34a** (30 mg, 0.08 mmol) and (4-methoxyphenyl)boronic acid (1.2 eq., 15 mg, 0.10 mmol). **35d** was obtained as a brown solid (26 mg, 0.07 mmol, 87%). MS (ESI+) m/z 373 (M + H).

methyl 4-(1-(5-(3-hydroxyphenyl)pyridin-3-yl)-1*H*-1,2,3-triazol-4-yl)benzoate (35e): The coupling was done according to **GP4** using methyl 4-(1-(5-bromopyridin-3-yl)-1*H*-1,2,3-triazol-4-yl)benzoate **34a** (40 mg, 0.11 mmol) and (3-hydroxyphenyl) boronic acid (1.2 eq., 18 mg,0.13 mmol). **35e** was obtained as yellow-brown solid (15 mg, 0.04 mmol, 36 %). MS (ESI+) m/z 373 (M + H).

methyl 4-(1-(5-(3,4-dimethylphenyl)pyridin-3-yl)-1*H*-1,2,3-triazol-4-yl)benzoate (35f): The coupling was done according to **GP4** using methyl 4-(1-(5-bromopyridin-3-yl)-1*H*-1,2,3-triazol-4-yl)benzoate **34a** (40 mg, 0.11 mmol) and (3,4-dimethylphenyl) boronic acid (1.2 eq., 19 mg,0.13 mmol). **35f** was obtained as yellow-brown solid (25 mg, 0.06 mmol, 60%). MS (ESI+) m/z 385 (M + H).

methyl 4-(1-(5-(3,4-difluorophenyl)pyridin-3-yl)-1*H*-1,2,3-triazol-4-yl)benzoate (35g): The coupling was done according to **GP4** using methyl 4-(1-(5-bromopyridin-3-yl)-1*H*-1,2,3-triazol-4-yl)benzoate **34a** (40 mg, 0.11 mmol) and (3,4-difluorophenyl)boronic acid (1.2 eq., 21 mg, 0.13 mmol). **35g** was obtained as yellow-brown solid (41 mg, 0.10 mmol, 90%). MS (ESI+) m/z 393 (M + H).

methyl 4-(1-(5-(4-(hydroxymethyl)phenyl)pyridin-3-yl)-1*H*-1,2,3-triazol-4-yl)benzoate (35h): The coupling was done according to **GP4** using methyl 4-(1-(5-bromopyridin-3-yl)-1*H*-1,2,3-triazol-4-yl)benzoate **34a** (40 mg, 0.11mmol) and (4-(hydroxymethyl)phenyl)boronic acid (1.2 eq., 20 mg, 0.13 mmol). **35h** was obtained as a yellow solid (15 mg, 0.04 mmol, 36%). MS (ESI+) m/z 387 (M + H).

methyl 4-(1-(5-(3-fluoro-5-methoxyphenyl)pyridin-3-yl)-1*H*-1,2,3-triazol-4-yl)benzoate (35i): The coupling was done according to **GP4** using methyl 4-(1-(5-bromopyridin-3-yl)-1*H*-1,2,3-triazol-4-yl)benzoate **34a** (40 mg, 0.11mmol) and (3-fluoro-5-methoxyphenyl) boronic acid (1.2 eq., 22 mg, 0.13 mmol). **35h** was obtained as a yellow-brown solid (8 mg, 0.02 mmol, 20%). MS (ESI+) m/z 405 (M + H).

methyl 4-(1-(5-(furan-3-yl)pyridin-3-yl)-1*H*-1,2,3-triazol-4-yl)benzoate (35j): The coupling was done according to **GP4** using methyl 4-(1-(5-bromopyridin-3-yl)-1*H*-1,2,3-triazol-4-yl)benzoate **34a** (40 mg, 0.11 mmol) and furan-3-yl boronic acid (1.2 eq., 15 mg, 0.13 mmol). **35j** was obtained as a yellow solid (28 mg, 0.08 mmol, 73%). MS (ESI+) m/z 347 (M + H).

methyl 4-(1-(4-methyl-6-phenylpyridin-3-yl)-1*H*-1,2,3-triazol-4-yl)benzoate (35k): The coupling was done according to **GP4** using methyl 4-(1-(6-chloro-4-methylpyridin-3-yl)-1*H*-1,2,3-triazol-4-yl)benzoate **34b** (40 mg, 0.12 mmol) and phenylboronic acid (1.2 eq., 18 mg, 0.14 mmol). **35k** was obtained as yellow-brown solid (38 mg, 0.10 mmol, 83%). MS (ESI+) m/z 371 (M + H).

methyl 4-(1-(6-(4-chlorophenyl)-4-methylpyridin-3-yl)-1*H*-1,2,3-triazol-4-yl)benzoate (35l): The coupling was done according to **GP4** using methyl 4-(1-(6-chloro-4-methylpyridin-3-yl)-1*H*-1,2,3-triazol-4-yl)benzoate **34b** (40 mg, 0.12 mmol) and (4-chlorophenyl)boronic acid (1.2 eq., 23 mg, 0.14 mmol). **35l** was obtained as brown solid (22 mg, 0.05 mmol, 41%). MS (ESI+) m/z 405 (M + H).

4-(1-(5-phenylpyridin-3-yl)-1*H*-1,2,3-triazol-4-yl)benzoic acid (36a): The synthesis was done according to **GP5** using methyl 4-(1-(5-phenylpyridin-3-yl)-1*H*-1,2,3-triazol-4-yl)benzoate **35a** (20 mg, 0.06 mmol). The crude was obtained as a white solid (13 mg, 0.04 mmol, 66%). Purification was done using prep. HPLC.^{1}H NMR (500 MHz, DMSO-d_6) δ ppm 7.49 - 7.54 (m, 1 H) 7.56 - 7.61 (m, 2 H) 7.84 - 7.95 (m, 2 H) 8.02 - 8.16 (m, 4 H) 8.65 (t, *J*=2.21 Hz, 1 H) 9.07 (d, *J*=1.98 Hz, 1 H) 9.22 (d, *J*=2.29

Hz, 1 H) 9.64 (s, 1 H);^{13}C NMR (126 MHz, DMSO-d_6) δ ppm 121.41, 125.29, 125.57, 127.30, 128.97, 129.30, 130.22, 133.38, 133.97, 135.68, 136.49, 139.93, 146.65, 147.70, 167.01

4-(1-(5-(2-methoxyphenyl)pyridin-3-yl)-1*H*-1,2,3-triazol-4-yl)benzoic acid (36b): The synthesis was done according to **GP5** using methyl 4-(1-(5-(2-methoxyphenyl)pyridin-3-yl)-1H-1,2,3-triazol-4-yl)benzoate **35b** (25 mg, 0.06 mmol). The crude was obtained as a white solid (21 mg, 0.05 mmol, 83%). Purification was done using prep. HPLC.^{1}H NMR (500 MHz, DMSO-d_6) δ ppm 3.84 (s, 3 H) 7.14 (d, *J*=0.92 Hz, 1 H) 7.23 (d, *J*=7.78 Hz, 1 H) 7.46 - 7.51 (m, 1 H) 7.53 (dd, *J*=7.48, 1.68 Hz, 1 H) 8.08 (d, *J*=2.14 Hz, 4 H) 8.48 (t, *J*=2.14 Hz, 1 H) 8.85 (d, *J*=1.83 Hz, 1 H) 9.16 (d, *J*=2.44 Hz, 1 H) 9.59 (s, 1 H); ^{13}C NMR (126 MHz, DMSO-d_6) δ ppm 55.75, 111.96, 121.10, 121.33, 124.81, 125.32, 128.00, 130.20, 130.54, 130.70, 132.87, 134.68, 139.40, 146.66, 149.86, 156.32, 167.01

4-(1-(5-(3-methoxyphenyl)pyridin-3-yl)-1*H*-1,2,3-triazol-4-yl)benzoic acid (36c): The synthesis was done according to **GP5** using methyl 4-(1-(5-(3-methoxyphenyl)pyridin-3-yl)-1H-1,2,3-triazol-4-yl)benzoate **35c** (25 mg, 0.06 mmol). The crude was obtained as a white solid (18 mg, 0.05 mmol, 83%). Purification was done using prep. HPLC.^{1}H NMR (500 MHz, DMSO-d_6) δ ppm 3.87 (s, 3 H) 7.01 - 7.16 (m, 1 H) 7.34 - 7.55 (m, 3 H) 8.02 - 8.15 (m, 4 H) 8.64 (t, *J*=2.21 Hz, 1 H) 9.08 (d, *J*=1.98 Hz, 1 H) 9.22 (d, *J*=2.44 Hz, 1 H) 9.64 (s, 1 H); ^{13}C NMR (126 MHz, DMSO-d_6) δ ppm 55.37, 112.81, 114.60, 119.53, 121.51, 125.34, 125.76, 130.25, 130.44, 133.36, 134.11, 136.38, 137.11, 140.10, 146.61, 147.85, 159.99, 166.98

4-(1-(5-(3-hydroxyphenyl)pyridin-3-yl)-1*H*-1,2,3-triazol-4-yl)benzoic acid (36e): The synthesis was done according to **GP5** using methyl 4-(1-(5-(3-hydroxyphenyl)pyridin-3-yl)-1*H*-1,2,3-triazol-4-yl)benzoate **35e** (15 mg,0.04 mmol). Purification was done using prep. HPLC. **36e** was obtained as a white solid (6 mg, 0.02 mmol, 50%). ^{1}H NMR (500 MHz, DMSO-d_6) δ ppm 6.82 - 6.97 (m, 1 H) 7.28 (br. s., 1 H) 7.30 (d, *J*=7.78 Hz, 1 H) 7.37 (t, *J*=7.78 Hz, 1 H) 7.99 - 8.15 (m, 4 H) 8.59 (t, *J*=2.14 Hz, 1 H) 8.99 (d, *J*=1.83 Hz, 1 H) 9.21 (d, *J*=2.44 Hz, 1 H) 9.65 (s, 1 H); ^{13}C NMR (126 MHz, DMSO-d_6) δ ppm 114.11, 116.00, 118.03, 121.41, 125.34, 125.50, 130.29, 130.49, 133.43, 136.72, 137.09, 139.91, 146.79, 147.63, 158.22, 167.22

4-(1-(5-(4-methoxyphenyl)pyridin-3-yl)-1*H*-1,2,3-triazol-4-yl)benzoic acid (36d): The synthesis was done according to **GP5** using methyl 4-(1-(5-(4-methoxyphenyl)pyridin-3-yl)-1*H*-1,2,3-triazol-4-yl)benzoate **35d** (25 mg, 0.06 mmol). The crude was obtained as a white solid (14 mg, 0.04 mmol, 66%). Purification was done using prep. HPLC. ^{1}H NMR (500 MHz, DMSO-d_6) δ ppm 3.84 (s, 3 H) 7.13 (m, *J*=8.85 Hz, 2 H) 7.87 (m, *J*=8.85 Hz, 2 H) 8.09 (d, *J*=3.51 Hz, 4 H) 8.59 (s, 1 H) 9.03 (d, *J*=1.98 Hz, 1 H) 9.15 (d, *J*=2.29 Hz, 1 H) 9.63 (s, 1 H); ^{13}C NMR (126 MHz, DMSO-d_6) δ ppm 55.36, 114.75, 121.42, 124.85, 125.32, 127.83, 128.53, 130.23, 133.37, 134.09, 136.16, 139.16, 146.60, 147.26, 160.03, 166.99

4-(1-(5-(3,4-dimethylphenyl)pyridin-3-yl)-1*H*-1,2,3-triazol-4-yl)benzoic acid (36f): The synthesis was done according to **GP5** using methyl 4-(1-(5-(3,4-dimethylphenyl)pyridin-3-yl)-1*H*-1,2,3-triazol-4-yl)benzoate **35f** (25 mg, 0.06 mmol). Purification was done using prep. HPLC. **36f** was obtained as a white solid (7 mg, 0.02 mmol, 33%). ^{1}H NMR (500 MHz, DMSO-d_6) δ ppm 2.30 (s, 3 H) 2.34 (s, 3 H) 7.33 (d, *J*=7.93 Hz, 1 H) 7.63 (dd, *J*=7.78, 1.83 Hz, 1 H) 7.70 (s, 1 H) 8.01 - 8.10 (m, 4 H) 8.60 (t, *J*=2.21 Hz, 1 H) 9.04 (d, *J*=1.98 Hz, 1 H) 9.17 (d, *J*=2.29 Hz, 1 H) 9.62 (s, 1 H); ^{13}C NMR (126 MHz,

DMSO-d_6) δ ppm 19.26, 19.59, 121.39, 124.59, 125.17, 125.31, 128.21, 130.27, 130.45, 133.08, 133.47, 136.58, 137.43, 137.46, 139.59, 146.80, 147.53, 167.20

4-(1-(5-(3,4-difluorophenyl)pyridin-3-yl)-1*H*-1,2,3-triazol-4-yl)benzoic acid (36g): The synthesis was done according to **GP5** using methyl 4-(1-(5-(3,4-difluorophenyl)pyridin-3-yl)-1*H*-1,2,3-triazol-4-yl)benzoate **35g** (40 mg, 0.10 mmol). Purification was done using prep. HPLC. **36g** was obtained as a white solid (12 mg, 0.03 mmol, 31%). ^{1}H NMR (500 MHz, DMSO-d_6) δ ppm 7.67 (dt, *J*=10.57, 8.60 Hz, 1 H) 7.78 - 7.85 (m, 1 H) 8.04 - 8.10 (m, 5 H) 8.69 (t, *J*=2.21 Hz, 1 H) 9.10 (d, *J*=1.98 Hz, 1 H) 9.24 (d, *J*=2.29 Hz, 1 H) 9.61 (s, 1 H); ^{13}C NMR (126 MHz, DMSO-d_6) δ ppm 113.00, 116.56, 116.71, 118.33, 118.47, 121.34, 124.43, 125.24, 125.80, 130.20, 133.32, 134.34, 140.38, 146.72, 147.71, 149.04, 167.06

4-(1-(5-(4-(hydroxymethyl)phenyl)pyridin-3-yl)-1*H*-1,2,3-triazol-4-yl)benzoic acid (36h): The synthesis was done according to **GP5** using methyl 4-(1-(5-(4-(hydroxymethyl)phenyl)pyridin-3-yl)-1H-1,2,3-triazol-4-yl)benzoate **35h** (15 mg, 0.04 mmol). Purification was done using prep. HPLC. **36h** was obtained as a white solid (7 mg, 0.02 mol, 50%).^{1}H NMR (500 MHz, DMSO-d_6) δ ppm 4.59 (s, 2 H) 5.32 (br. s., 1 H) 7.51 (m, *J*=8.39 Hz, 2 H) 7.88 (m, *J*=8.24 Hz, 2 H) 7.99 - 8.10 (m, 4 H) 8.64 (t, *J*=2.21 Hz, 1 H) 9.07 (d, *J*=1.83 Hz, 1 H) 9.20 (d, *J*=2.29 Hz, 1 H) 9.61 (s, 1 H); ^{13}C NMR (126 MHz, DMSO-d_6) δ ppm 62.54, 118.26, 125.14, 125.37, 127.07, 127.30, 130.21, 133.51, 134.00, 136.47, 139.79, 140.13, 143.60, 145.22, 147.61, 168.22

4-(1-(5-(3-fluoro-5-methoxyphenyl)pyridin-3-yl)-1*H*-1,2,3-triazol-4-yl)benzoic acid (36i): The synthesis was done according to **GP5** using methyl 4-(1-(5-(3-fluoro-5-methoxyphenyl)pyridin-3-yl)-1*H*-1,2,3-triazol-4-yl)benzoate **35i** (5 mg, 0.01 mmol). Purification was done using prep. HPLC. **36i** was obtained as a white solid (3 mg, 0.007 mmol, 70%).^{1}H NMR (500 MHz, DMSO-d_6) δ ppm 3.89 (s, 3 H) 6.99 (dt, *J*=10.95, 2.23 Hz, 1 H) 7.35 (t, *J*=1.75 Hz, 1 H) 7.40 (dt, *J*=9.69, 1.87 Hz, 1 H) 8.01 - 8.13 (m, 4 H) 8.68 (t, *J*=2.21 Hz, 1 H) 9.11 (d, *J*=1.98 Hz, 1 H) 9.25 (d, *J*=2.44 Hz, 1 H) 9.62 (s, 1 H); ^{13}C NMR (126 MHz, DMSO-d_6) δ ppm 56.43, 102.31, 102.51, 106.66, 106.84, 109.91, 118.56, 121.80, 125.63, 126.36, 130.62, 133.80, 135.60, 138.83, 141.05, 147.23, 148.29, 161.79, 167.57

4-(1-(5-(furan-3-yl)pyridin-3-yl)-1*H*-1,2,3-triazol-4-yl)benzoic acid (36j): The synthesis was done according to **GP5** using methyl 4-(1-(5-(furan-3-yl)pyridin-3-yl)-1*H*-1,2,3-triazol-4-yl)benzoate **34a** (20 mg, 0.06 mmol). Purification was done using prep. HPLC. **36j** was obtained as a white solid (4 mg, 0.01 mmol, 16%). ^{1}H NMR (500 MHz, DMSO-d_6) δ ppm 2.54 (s, 4 H) 7.23 (s, 1 H) 7.88 (s, 1 H) 8.02 - 8.10 (m, 5 H) 8.51 (s, 1 H) 8.62 (s, 1 H) 9.08 (s, 1 H) 9.06 (s, 1 H) 9.54 (s, 1 H); ^{13}C NMR (126 MHz, DMSO-d_6) δ 108.67, 117.70, 121.39, 121.92, 124.28, 125.43, 128.93, 130.30, 131.53, 131.61, 139.45, 141.30, 145.10, 146.86, 167.14

4-(1-(4-methyl-6-phenylpyridin-3-yl)-1*H*-1,2,3-triazol-4-yl)benzoic acid (36k): The synthesis was done according to **GP5** using methyl 4-(1-(4-methyl-6-phenylpyridin-3-yl)-1*H*-1,2,3-triazol-4-yl)benzoate **35k** (20 mg, 0.05 mmol). Purification was done using prep. HPLC. **36k** was obtained as a white solid (7 mg, 0.02 mmol, 40%). ^{1}H NMR (500 MHz, DMSO-d_6) δ ppm 2.40 (s, 3 H) 7.48 - 7.53 (m, 1 H) 7.54 - 7.58 (m, 2 H) 8.07 (s, 4 H) 8.18 (s, 1 H) 8.81 (s, 1 H) 9.22 (s, 1 H); ^{13}C NMR (126 MHz, DMSO-d_6) δ ppm 17.91, 123.03, 124.82, 125.74, 127.37, 129.40, 130.23, 130.59, 132.74, 137.95, 143.77, 146.26, 157.32, 167.58

4-(1-(6-(4-chlorophenyl)-4-methylpyridin-3-yl)-1*H*-1,2,3-triazol-4-yl)benzoic acid (36l): The synthesis was done according to **GP5** using methyl 4-(1-(6-(4-chlorophenyl)-4-methylpyridin-3-yl)-1*H*-1,2,3-triazol-4-yl)benzoate **35l** (22 mg, 0.05 mmol). The mixture was extracted with DCM and 1 M HCl and after purification using prep HPLC a white solid (5 mg, 0.01 mmol, 20%) was obtained. ^{1}H NMR (500 MHz, DMSO-d_6) δ ppm 2.41 (s, 3 H) 7.63 (d, *J*=8.70 Hz, 2 H) 8.08 (s, 4 H) 8.23 (d, *J*=8.70 Hz, 2 H) 8.25 (s, 1 H) 8.83 (s, 1 H) 9.23 (s, 1 H); ^{13}C NMR (126 MHz, DMSO-d_6) δ ppm 17.56, 122.75, 124.46, 125.40, 128.76, 129.08, 130.23, 132.53, 134.76, 136.36, 143.58, 145.93, 146.06, 155.64, 167.17

4-methyl-6-phenoxypyridin-3-amine (38a): The aryl ether was synthesized according to **GP6** using 6-bromo-4-methylpyridin-3-amine **37** (100 mg, 0.53 mmol), phenol (1.2 eq., 0.60 mmol, 70 mg), cesium carbonate (3 eq., 1.61 mmol, 523 mg) and CuI (0.1 eq., 0.05 mmol, 9 mg) in DMF (3 mL). The product was purified using automated flash chromatography (DCM/MeOH 1:0 → 9:1). Yield: (30 mg, 0.15 mmol, 28%) MS (ESI+) m/z 201 (M + H).

6-(2-fluorophenoxy)-4-methylpyridin-3-amine (38b): The aryl ether was synthesized according to **GP6** using 6-bromo-4-methylpyridin-3-amine **37** (100 mg, 0.53 mmol), 2-fluorophenol (1.2 eq., 0.64 mmol, 72 mg), cesium carbonate (3 eq., 1.61 mmol, 523 mg) and CuI (0.1 eq., 0.05 mmol, 9 mg) in DMF (3 mL). The product (102 mg, 0.47 mmol, 88%) was used as obtained without further purifications. MS (ESI+) m/z 219 (M + H).

6-(3-fluorophenoxy)-4-methylpyridin-3-amine (38c): The aryl ether was synthesized according to **GP6** using 6-bromo-4-methylpyridin-3-amine **37** (100 mg, 0.53 mmol), 3-fluorophenol (1.2 eq., 0.64 mmol, 72 mg), cesium carbonate (3 eq., 1.61 mmol, 523 mg) and CuI (0.1 eq., 0.05 mmol, 9 mg) in DMF (3 mL). The product (85 mg, 0.39 mmol, 73%) was used as obtained without further purifications. MS (ESI+) m/z 219 (M + H).

6-(4-fluorophenoxy)-4-methylpyridin-3-amine (38d): The aryl ether was synthesized according to **GP6** using 6-bromo-4-methylpyridin-3-amine **37** (100 mg, 0.53 mmol), 4-fluorophenol (1.2 eq., 0.64 mmol, 72 mg), cesium carbonate (3 eq., 1.61 mmol, 523 mg) and CuI (0.1 eq., 0.05 mmol, 9 mg) in DMF (3 mL). The product (109 mg, 0.50 mmol, 94%) was used as obtained without further purifications. MS (ESI+) m/z 219 (M + H).

4-methyl-6-(phenylthio)pyridin-3-amine (38e): The arylether was synthesized according to **GP6** using 6-bromo-4-methylpyridin-3-amine **37** (100 mg, 0.53 mmol), benzenethiol (1.2 eq., 0.64 mmol, 70 mg), cesium carbonate (3 eq., 1.61 mmol, 523 mg) and CuI (0.1 eq., 0.05 mmol, 9 mg) in DMF (3 mL). The crude product was purified using automated flash chromatography (DCM/MeOH 1:0 → 9:1). Yield: (54 mg, 0.25 mmol, 47%) MS (ESI+) m/z 217 (M + H).

5-azido-4-methyl-2-phenoxypyridine (39a): The azide was synthesized according to **GP1** using 4-methyl-6-phenoxypyridin-3-amine **38a** (30 mg, 0.15 mmol), sodium nitrite (1.7 eq., 0.25 mmol, 17 mg), sodium azide (1.7 eq., 0.25 mmol, 14 mg), EtOAc (1 mL), 6 M HCl (3 mL). The crude product (29 mg, 0.13 mmol, 86%) was used as obtained in the next step without further purifications. R_f = 0.79 (PE/EtOAc 0:1)

5-azido-2-(2-fluorophenoxy)-4-methylpyridine (39b): The azide was synthesized according to **GP1** using 6-(2-fluorophenoxy)-4-methylpyridin-3-amine **38b** (102 mg, 0.47 mmol), sodium nitrite (1.7 eq., 0.80 mmol, 55 mg), sodium azide (1.7 eq., 0.80 mmol, 52 mg), EtOAc (2.5 mL), and 6 M HCl (5 mL). The crude product (107 mg, 0.44 mmol, 93%) was used as obtained in the next step without further purifications. R_f = 0.84 (PE/EtOAc 7:3)

5-azido-2-(3-fluorophenoxy)-4-methylpyridine (39c): The azide was synthesized according to **GP1** using 6-(3-fluorophenoxy)-4-methylpyridin-3-amine **38c** (85 mg, 0.39 mmol), sodium nitrite (1.7 eq., 0.66 mmol, 46 mg), sodium azide (1.7 eq., 0.66 mmol, 43 mg), EtOAc (2.5 mL), 6 M HCl (5 mL). The crude product (95 mg, 0.39 mmol, 99%) was used as obtained in the next step without further purifications. R_f = 0.84 (PE/EtOAc 7:3)

5-azido-2-(4-fluorophenoxy)-4-methylpyridine (39d): The azide was synthesized according to **GP1** using 6-(4-fluorophenoxy)-4-methylpyridin-3-amine **38d** (109 mg, 0.50 mmol), sodium nitrite (1.7 eq., 0.85 mmol, 59 mg), sodium azide (1.7 eq., 0.85 mmol, 55 mg), EtOAc (2.5 mL), 6 M HCl (5 mL). The crude product (120 mg, 0.49 mmol, 98%) was used as obtained in the next step without further purifications. R_f = 0.84 (PE/EtOAc 7:3)

5-azido-4-methyl-2-(phenylthio) pyridine (39e): The azide was synthesized according to **GP1** using 4-methyl-6-(phenylthio) pyridin-3-amine **38e** (54 mg, 0.25 mmol), sodium nitrite (1.7 eq., 0.42 mmol, 30 mg), sodium azide (1.7 eq., 0.42 mmol, 23 mg), EtOAc (2 mL), 6 M HCl (4 mL). The crude product (41 mg, 0.17 mmol, 70%) was used as obtained in the next step without further purifications. R_f = 0.81 (PE/EtOAc 0:1)

4-(1-(4-methyl-6-phenoxypyridin-3-yl)-1*H*-1,2,3-triazol-4-yl)benzoic acid (40a): The triazole was synthesized according to **GP3** using 4-ethynylbenzoic acid (15 mg, 0.11 mmol) and 5-azido-4-methyl-2-phenoxypyridine **39a** (1.2 eq., 29 mg,0.13 mmol) as starting materials. 1 M HCl was added and the mixture was extracted with EtOAc (3x), the combined organic layers were dried over sodium sulfate and concentrated under reduced pressure to obtain the crude. Purification was done using flash chromatography (PE:EtOAc 1:0 → 1:0). **40a** was obtained as a white solid (21 mg, 0.05 mmol, 45%). ^{1}H NMR (500 MHz, DMSO-d_6) δ ppm 2.27 (s, 3 H) 7.19 - 7.23 (m, 2 H) 7.24 (s, 1 H) 7.25 - 7.29 (m, 1 H) 7.44 - 7.50 (m, 2 H) 7.99 - 8.13 (m, 5 H) 8.32 (s, 1 H) 9.12 (s, 1 H); ^{13}C NMR (126 MHz, DMSO-d_6) δ ppm 17.28, 112.78, 121.54, 124.75, 125.13, 125.35, 129.57, 129.92, 130.19, 130.29, 134.35, 144.21, 145.83, 147.15, 153.43, 163.58, 167.05

4-(1-(6-(2-fluorophenoxy)-4-methylpyridin-3-yl)-1*H*-1,2,3-triazol-4-yl)benzoic acid (40b): The triazole was synthesized according to **GP3** using 4-ethynylbenzoic acid (65 mg, 0.45 mmol) and 5-azido-2-(2-fluorophenoxy)-4-methylpyridine **39b** (1.2 eq., 129 mg, 0.53 mmol) as starting materials. The crude was obtained as a white solid (140 mg, 0.36 mmol, 80%). Purification was done using prep. HPLC. ^{1}H NMR (500 MHz, DMSO-d_6) δ ppm 2.29 (s, 3 H) 7.27 - 7.31 (m, 1 H) 7.31 - 7.36 (m, 1 H) 7.37 (s, 1 H) 7.38 - 7.44 (m, 2 H) 8.05 (s, 5 H) 8.30 (s, 1 H) 9.13 (s, 1 H) 13.06 (br. s., 1 H); ^{13}C NMR (126 MHz, DMSO-d_6) δ ppm 17.26, 112.04, 116.81, 116.95, 124.37, 124.75, 125.30, 125.37, 125.40, 126.97, 127.03, 129.87, 130.17, 130.44, 134.25, 140.01, 140.10, 144.04, 145.84, 147.49, 153.28, 155.24, 162.66, 167.05

4-(1-(6-(3-fluorophenoxy)-4-methylpyridin-3-yl)-1H-1,2,3-triazol-4-yl)benzoic acid (40c): The triazole was synthesized according to **GP3** using 4-ethynylbenzoic acid (65 mg, 0.45 mmol) and 5-azido-2-(3-fluorophenoxy)-4-methylpyridine **39c** (1.2 eq., 129 mg, 0.53 mmol) as starting materials. The crude was obtained as a white solid (160 mg, 0.41 mmol, 93%). Purification was done using prep. HPLC. ^{1}H NMR (500 MHz, DMSO-d_6) δ ppm 2.29 (s, 3 H) 7.08 (dd, *J*=8.01, 1.75 Hz, 1 H) 7.10 - 7.15 (m, 1 H) 7.18 (dt, *J*=10.15, 2.33 Hz, 1 H) 7.30 (s, 1 H) 7.50 (td, *J*=8.24, 6.87 Hz, 1 H) 8.06 (s, 4 H) 8.35 (s, 1 H) 9.12 (s, 1 H); ^{13}C NMR (126 MHz, DMSO-d_6) δ ppm 17.29, 109.27, 109.46, 111.92, 112.09, 113.04, 117.66, 117.69, 124.69, 125.31, 129.89, 130.17, 131.04, 131.12, 134.23, 144.19, 145.86, 147.34, 154.48, 154.57, 161.65, 163.04, 163.60, 167.06

4-(1-(6-(4-fluorophenoxy)-4-methylpyridin-3-yl)-1*H*-1,2,3-triazol-4-yl)benzoic acid (40d): The triazole was synthesized according to **GP3** using 4-ethynylbenzoic acid (65 mg, 0.45 mmol) and 5-azido-2-(4-fluorophenoxy)-4-methylpyridine **39d** (1.2 eq., 129 mg, 0.53 mmol) as starting materials. The crude was obtained as a white solid (155 mg, 0.39 mmol, 86%). Purification was done using prep. HPLC. ^{1}H NMR (500 MHz, DMSO-d_6) δ ppm 2.27 (s, 3 H) 7.25 (s, 1 H) 7.26 - 7.32 (m, 4 H) 8.06 (s, 4 H) 8.32 (s, 1 H) 9.11 (s, 1 H) 13.08 (br. s., 1 H); ^{13}C NMR (126 MHz, DMSO-d_6) δ ppm 17.25, 112.61, 116.32, 116.51, 123.44, 124.70, 125.31, 129.59, 130.17, 130.40, 134.28, 144.10, 145.84, 147.17, 149.37, 158.28, 160.19, 163.57, 167.06

4-(1-(4-methyl-6-(phenylthio)pyridin-3-yl)-1*H*-1,2,3-triazol-4-yl)benzoic acid (40e): The triazole was synthesized according to **GP3** using 4-ethynylbenzoic acid (19 mg, 0.13 mmol) and 5-azido-4-methyl-2-(phenylthio)pyridine **39e** (1.2 eq., 40 mg, 0.16 mmol) as starting materials. The crude was obtained as a white solid (25 mg, 0.06 mmol, 46%). Purification was done using prep. HPLC. ^{1}H NMR (500 MHz, DMSO-d_6) δ ppm 2.18 (s, 3 H) 7.18 (s, 1 H) 7.44 - 7.60 (m, 3 H) 7.61 - 7.77 (m, 2 H) 7.95 - 8.14 (m, 4 H) 8.56 (s, 1 H) 9.13 (s, 1 H) 13.09 (br. s., 1 H); ^{13}C NMR (126 MHz, DMSO-d_6) δ ppm 17.22, 122.67, 124.51, 125.33, 129.41, 129.71, 130.03, 130.17, 130.82, 134.22, 134.91, 143.68, 145.86, 145.90, 161.32, 167.04

4-azidoisoquinoline (42): The azide was synthesized according to **GP1** using isoquinolin-4-amine **41** (150 mg, 1 mmol), sodium nitrite (1.7 eq., 122 mg, 1.7 mmol), sodium azide (1.7 eq. 115 mg, 1.7 mmol), EtOAc (4 mL), 6 M HCl (2.4 mL). The crude product (143 mg, 0.84 mmol, 84%) was used as obtained in the next step without further purifications. R_f = 0.63 (PE/EtOAc 7:3)

4-(1-(isoquinolin-4-yl)-1*H*-1,2,3-triazol-4-yl)benzoic acid (43): The triazole was synthesized according to **GP3** using 4-ethynylbenzoic acid (95 mg, 0.65 mmol) and 4-azidoisoquinoline **42** (1.3 eq., 143 mg, 0.84 mmol) as starting materials. The crude was obtained as a yellow solid (183 mg, 0.58 mmol, 90%). Purification was done using prep. HPLC. ^{1}H NMR (500 MHz, DMSO-d_6) δ ppm 7.80 - 7.86 (m, 1 H) 7.89 (ddd, *J*=8.09, 7.02, 1.07 Hz, 1 H) 7.92 - 7.99 (m, 1 H) 8.06 - 8.11 (m, 2 H) 8.11 - 8.19 (m, 2 H) 8.39 (d, *J*=8.24 Hz, 1 H) 8.86 (s, 1 H) 9.38 (s, 1 H) 9.60 (s, 1 H) 13.06 (br. s., 1 H); ^{13}C NMR (126 MHz, DMSO-d_6) δ ppm 121.42, 125.32, 125.43, 128.26, 128.45, 128.51, 128.85, 130.00, 130.15, 130.31, 132.83, 134.28, 139.26, 146.00, 154.60, 166.98

3-azidoquinoline (45): The azide was synthesized according to **GP1** using quinolin-3-amine **44** (100 mg, 0.69 mmol), sodium nitrite (1.7 eq., 81 mg, 1.63 mmol), sodium azide (1.7 eq., 77 mg, 1.63

mmol), EtOAc (3.5 mL), 6 M HCl (2.0 mL). The crude product (107 mg, 0.63 mmol, 91%) was used as obtained in the next step without further purifications. R_f = 0.73 (PE/EtOAc 7:3)

4-(1-(quinolin-3-yl)-1*H*-1,2,3-triazol-4-yl)benzoic acid (46): The triazole was synthesized according to **GP3** using 4-ethynylbenzoic acid (60 mg, 0.41 mmol) and 3-azidoquinoline **45** (1.2 eq., 83 mg, 0.49 mmol) as starting materials. The crude was obtained as a white solid (70 mg, 0.22 mmol, 54%). Purification was done using prep. HPLC. ^{1}H NMR (500 MHz, DMSO-d_6) δ ppm 7.73 - 7.80 (m, 1 H) 7.90 (ddd, *J*=8.35, 6.98, 1.30 Hz, 1 H) 8.10 (s, 4 H) 8.18 (t, *J*=8.62 Hz, 2 H) 9.01 (d, *J*=2.29 Hz, 1 H) 9.53 (d, *J*=2.59 Hz, 1 H) 9.67 (s, 1 H); ^{13}C NMR (126 MHz, DMSO-d_6) δ ppm 121.33, 125.35, 126.02, 127.09, 128.24, 128.70, 128.99, 130.13, 130.22, 130.63, 134.01, 143.16, 146.69, 147.02, 167.07

6-methylisoquinolin-4-amine (48a): The amino isoquinolin was synthesized according to **GP2** using 4-bromo-6-methylisoquinoline **47a** (100 mg, 0.46 mmol), L-proline (0.1 eq., 0.05 mmol, 5 mg), sodium azide (1.3 eq., 0.60 mmol, 34 mg), sodium carbonate (1.3 eq., 0.60 mmol, 64 mg), sodium ascorbate (1.3 eq., 0.60 mmol, 119 mg), copper sulfate heptahydrate (1 eq., 0.46 mmol, 115 mg), DMF (4 mL) and water (2 mL). The crude product (70 mg, 0.44 mmol, 97%) was used as obtained in the next step without further purifications. MS (ESI+) m/z 159 (M + H).

7-chloroisoquinolin-4-amine (48b): The amino isoquinolin was synthesized according to **GP2** using 4-bromo-7-chloroisoquinoline **47b** (100 mg, 0.36 mmol), L-proline (0.1 eq., 0.04 mmol, 4 mg), sodium azide (1.3 eq., 0.46 mmol, 30 mg), sodium carbonate (1.3 eq., 0.49 mmol, 64 mg), sodium ascorbate (1.3 eq., 0.46 mmol, 92 mg), copper sulfate heptahydrate (1 eq., 0.36 mmol, 89 mg), DMF (4 mL) and water (2 mL). The crude product (56 mg, 0.31 mmol, 88%) was used as obtained in the next step without further purifications. MS (ESI+) m/z 179 (M + H).

methyl 4-aminoisoquinoline-7-carboxylate (48c): The amino isoquinolin was synthesized according to **GP2** using methyl 4-bromoisoquinoline-7-carboxylate **47c** (50 mg, 0.18 mmol), L-proline (0.1 eq., 0.02 mmol, 2 mg), sodium azide (1.3 eq., 0.24 mmol, 16 mg), sodium carbonate (1.3 eq., 0.24 mmol, 26 mg), sodium ascorbate (1.3 eq., 0.24 mmol, 48 mg), copper sulfate heptahydrate (1 eq., 0.18 mmol, 46 mg), DMF (2 mL) and water (1 mL). The crude product (33 mg, 0.16 mmol, 90%) was used as obtained in the next step without further purifications. MS (ESI+) m/z 203 (M + H).

4-azido-6-methylisoquinoline (49a): The azide was synthesized according to **GP1** using 6-methylisoquinolin-4-amine **48a** (70 mg, 0.44 mmol), sodium nitrite (1.7 eq., 0.75 mmol, 52 mg), sodium azide (1.7 eq., 0.75 mmol, 48 mg), EtOAc (2 mL), 6 M HCl (4 mL). The crude product (74 mg, 0.40 mmol, 91%) was used as obtained in the next step without further purifications. R_f = 0.33 (PE/EtOAc 7:3)

4-azido-7-chloroisoquinoline (49b): The azide was synthesized according to **GP1** using 7-chloroisoquinolin-4-amine **48b** (56 mg, 0.31 mmol), sodium nitrite (1.7 eq., 0.52 mmol, 36 mg), sodium azide (1.7 eq., 0.52 mmol, 34 mg), EtOAc (2.5 mL), 6 M HCl (5 mL). The crude product (57 mg, 0.28 mmol, 90%) was used as obtained in the next step without further purifications. R_f = 0.47 (PE/EtOAc 7:3)

methyl 4-azidoisoquinoline-7-carboxylate (49c): The azide was synthesized according to **GP1** using methyl 4-aminoisoquinoline-7-carboxylate **48c** (33 mg, 0.16 mmol), sodium nitrite (1.7 eq., 0.27 mmol, 19 mg), sodium azide (1.7 eq., 0.27 mmol, 17 mg), EtOAc (2 mL), 6 M HCl (4 mL). The crude product (25 mg, 0.11mmol, 68%) was used as obtained in the next step without further purifications. R_f = 0.36 (PE/EtOAc 7:3)

4-(1-(6-methylisoquinolin-4-yl)-1*H*-1,2,3-triazol-4-yl)benzoic acid (50a): The triazole was synthesized according to **GP3** using 4-ethynylbenzoic acid (28 mg, 0.19 mmol) and 4-azido-6-methylisoquinoline **49a** (1.2 eq., 42 mg, 0.23 mmol) as starting materials. The crude was obtained as a white solid (16 mg, 0.04 mmol, 21%). Purification was done using prep. HPLC. ^{1}H NMR (500 MHz, DMSO-d_6) δ ppm 2.54 (s, 3 H) 7.59 (s, 1 H) 7.73 (dd, *J*=8.47, 1.30 Hz, 1 H) 8.09 (m, *J*=8.55 Hz, 2 H) 8.14 (m, *J*=8.55 Hz, 2 H) 8.29 (d, *J*=8.39 Hz, 1 H) 8.79 (s, 1 H) 9.36 (s, 1 H) 9.52 (s, 1 H); ^{13}C NMR (126 MHz, DMSO-d_6) δ ppm 22.00, 119.99, 125.41, 125.50, 128.22, 130.25, 130.43, 131.07, 139.62, 143.54, 146.06, 154.22, 167.14

4-(1-(7-chloroisoquinolin-4-yl)-1*H*-1,2,3-triazol-4-yl)benzoic acid (50b): The triazole was synthesized according to **GP3** using 4-ethynylbenzoic acid (44 mg, 0.30 mmol) and 4-azido-7-chloroisoquinoline **49b** (1.2 eq., 73 mg, 0.36 mmol) as starting materials. The crude was obtained as a white solid (35 mg, 0.10 mmol, 33%). Purification was done using prep. HPLC. ^{1}H NMR (500 MHz, DMSO-d_6) δ ppm 7.92 - 7.99 (m, 2 H) 8.05 - 8.11 (m, 4 H) 8.56 (d, *J*=1.98 Hz, 1 H) 8.90 (s, 1 H) 9.37 (s, 1 H) 9.57 (s, 1 H); ^{13}C NMR (126 MHz, DMSO-d_6) δ ppm 124.37, 125.26, 125.43, 127.10, 128.50, 129.24, 130.22, 133.21, 133.32, 139.60, 146.23, 153.84, 167.21

4-(1-(7-(methoxycarbonyl)isoquinolin-4-yl)-1*H*-1,2,3-triazol-4-yl)benzoic acid (50c): The triazole was synthesized according to **GP3** using 4-ethynylbenzoic acid (23 mg, 0.16 mmol) and methyl 4-azidoisoquinoline-7-carboxylate **49c** (1.2 eq., 43 mg, 1.9 mmol) as starting materials. The crude was obtained as a white solid (15 mg, 0.04 mmol, 25%). Purification was done using prep. HPLC. ^{1}H NMR (500 MHz, DMSO-d_6) δ ppm 3.98 (s, 3 H) 8.00 (d, *J*=8.85 Hz, 1 H) 8.07 - 8.15 (m, 5 H) 8.38 (dd, *J*=8.93, 1.75 Hz, 1 H) 9.00 (s, 1 H) 9.09 (d, *J*=1.22 Hz, 1 H) 9.40 (s, 1 H) 9.81 (s, 1 H) 13.07 (br. s., 1 H); ^{13}C NMR (126 MHz, DMSO-d_6) δ ppm 52.75, 122.63, 125.32, 125.45, 127.88, 128.41, 129.46, 130.18, 130.87, 131.40, 132.00, 141.34, 146.13, 156.07, 165.34, 167.02

1.2 Fluorescence Polarization (FP) Assay

Representative curves of dose-dependent competition studies with compounds **19c**, **19n** ,**31b**, **26a-b** and **50a-b** were shown in Figure S1, which based on normalized data points (% polarization from 0 - 100%) representing averaged FP values of duplicates ± standard deviation. Curves were fit to a four-parameter dose response model using OriginLab (2019) to calculate IC_{50} values. Compounds were tested in two independent experiments using LBS1_flc, LBS2_flc and LBS3_flc, respectively, as fluorescent probe.

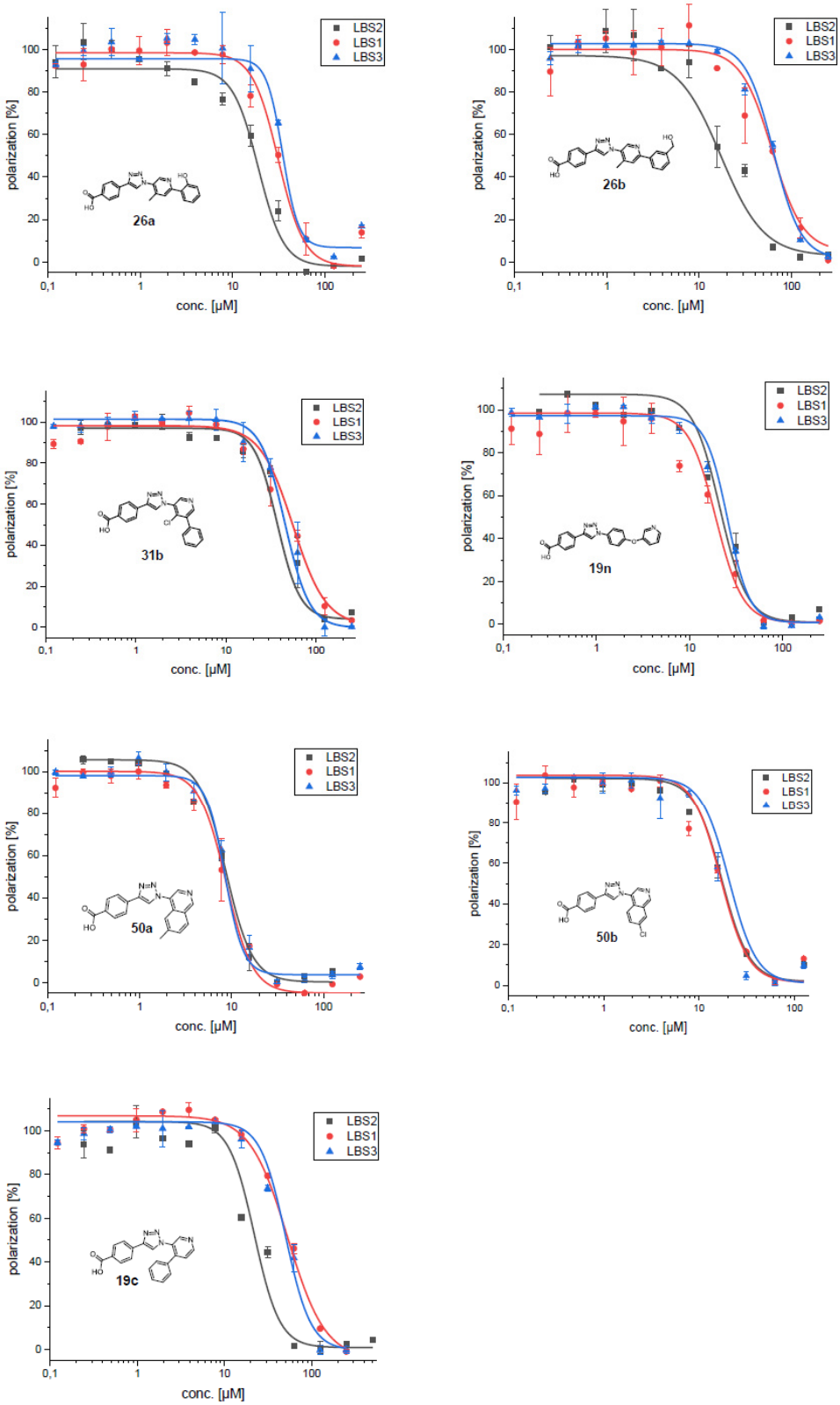

Figure S1: **A**: Representative curves of dose-dependent experiments for compounds **19c**, **31b**, **26a**-**b**, **19n** and **50a**-**b** in FP-based competition experiments using LANA DBD mutant (1008-1146) and fluorescence labeled LBS1, LBS2 and LBS3, respectively.

1.3 Electrophoretic Mobility Shift Assay (EMSA)

Gels of dose-dependent EMSA experiments of compounds **19c**, **31b**, **26a-b**, **19n** and **50a-b** are shown in Figure S2 and S3. Curves are shown with normalized data points (inhibition from 0 - 100%) representing intensities of LANA-DNA-complex bands. IC_{50} values were calculated using a four-parameter dose-response model (Figure S4)

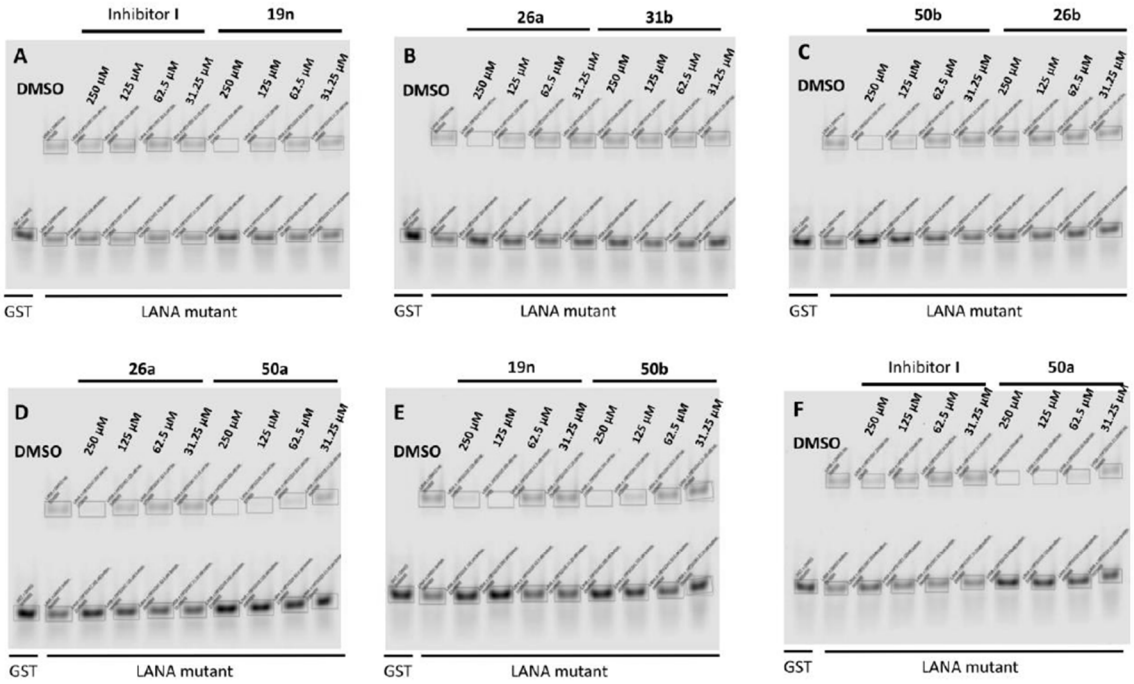

Figure S2: Gels of dose-dependent EMSA experiments using LANA DBD mutant and LBS1. (**A**) Inhibitor **I** and compound **19n**. (**B**) Compounds **26a** and **31b** (**C**) Compounds **50b** and **26b**. (**D**) Compounds **26a** and **50a**. (**E**) Compounds **19n** and **50b**. (**F**) Inhibitor **I** and **50a**.

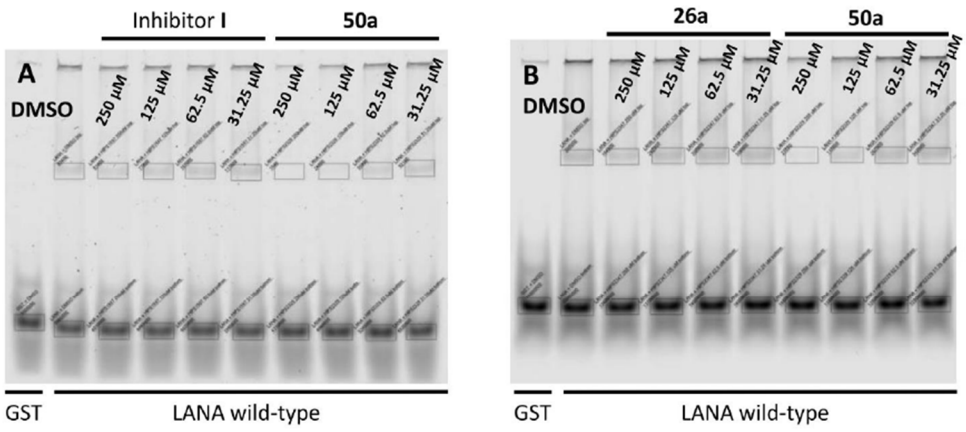

Figure S3: Gels of dose-dependent EMSA experiments. (**A**) Inhibitor **I** and **50a** using wild-type LANA CTD and LBS1. (**B**) Inhibitor **26a** and **50a** using wild-type LANA CTD and LBS1.

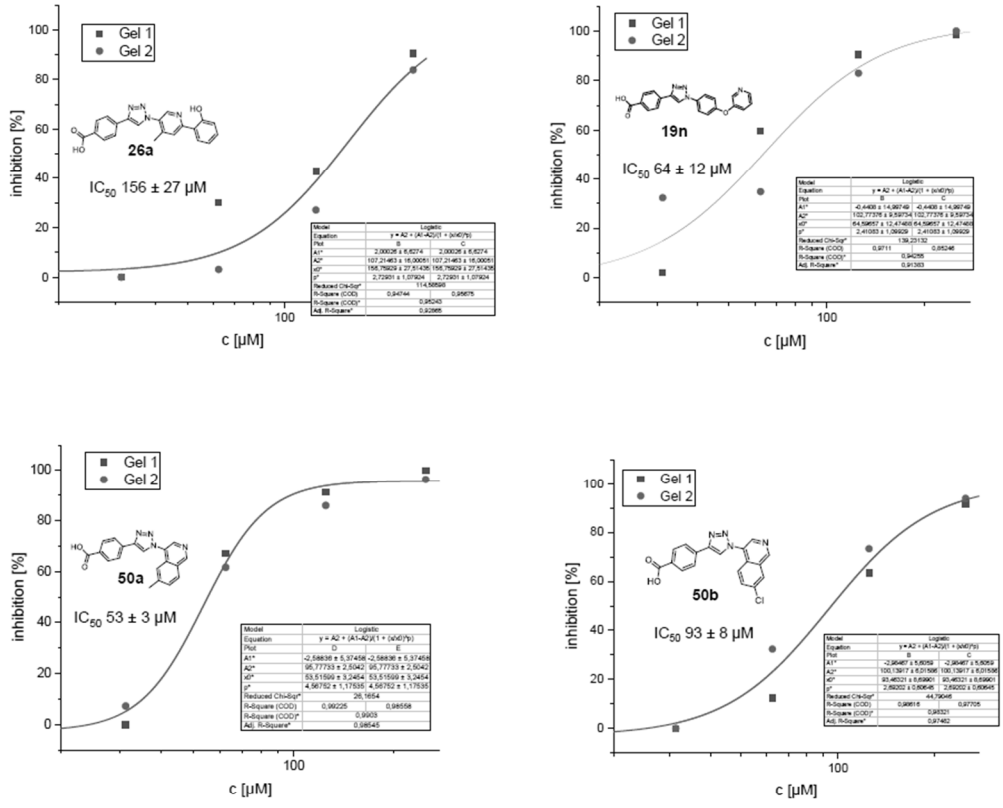

Figure S4: Dose-dependent EMSA experiments with compounds **26a**, **19n** and **50a-b**. Curve shows normalized data points (inhibition from 0 - 100%) representing averaged intensities of LANA-DNA-complex bands (upper bands) of duplicates ± standard deviation. IC_{50} value was calculated using a four-parameter dose-response model.

1.4 ^{1}H and ^{13}C NMR Spectra and High Resolution Mass Spectrometry (HRMS)

Representative ^{1}H and ^{13}C of each final compound were depicted in below. The high resolution masses of all final compounds were measured on a Thermo Scientific Q Exactive Focus (Germany) equipped with DIONEX ultimate 3000 UHPLC+ focused. For gradient elution, an EC 150/2 NUCLEODUR C18 Pyramid (3 µm) column (Machery-Nagel, Germany) was used with a mobile phase consisting of acetonitrile containing 0.1% formic acid (FA; [v/v]; eluent A) and water containing 0.1% FA ([v/v]; eluent B). Elution method was used with a total run time of 7.5 min and gradient conditions 10% A to 90% A. Mass spectrometry was used in positive or negative mode using electrospray ionization (ESI). Measured (upper spectrum) and calculated (lower spectrum) HRMS spectra of each final synthesized compound were depicted below.

3-(1-(pyridin-3-yl)-1*H*-1,2,3-triazol-4-yl)benzoic acid (4):

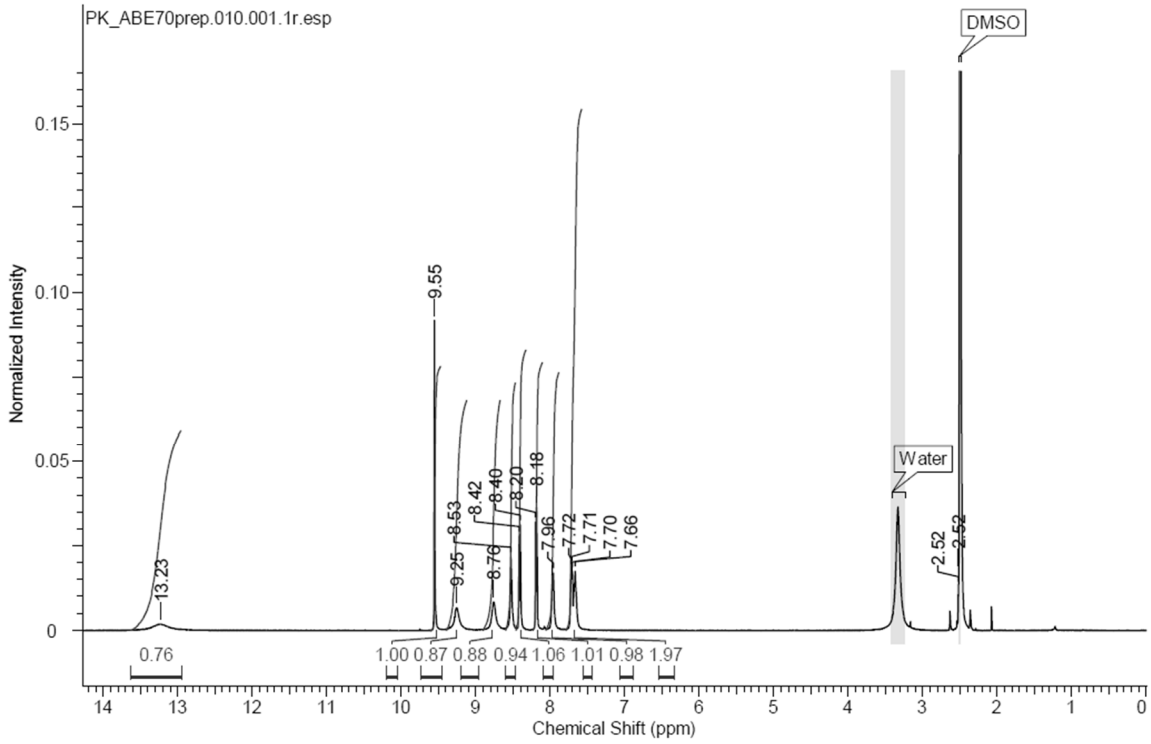

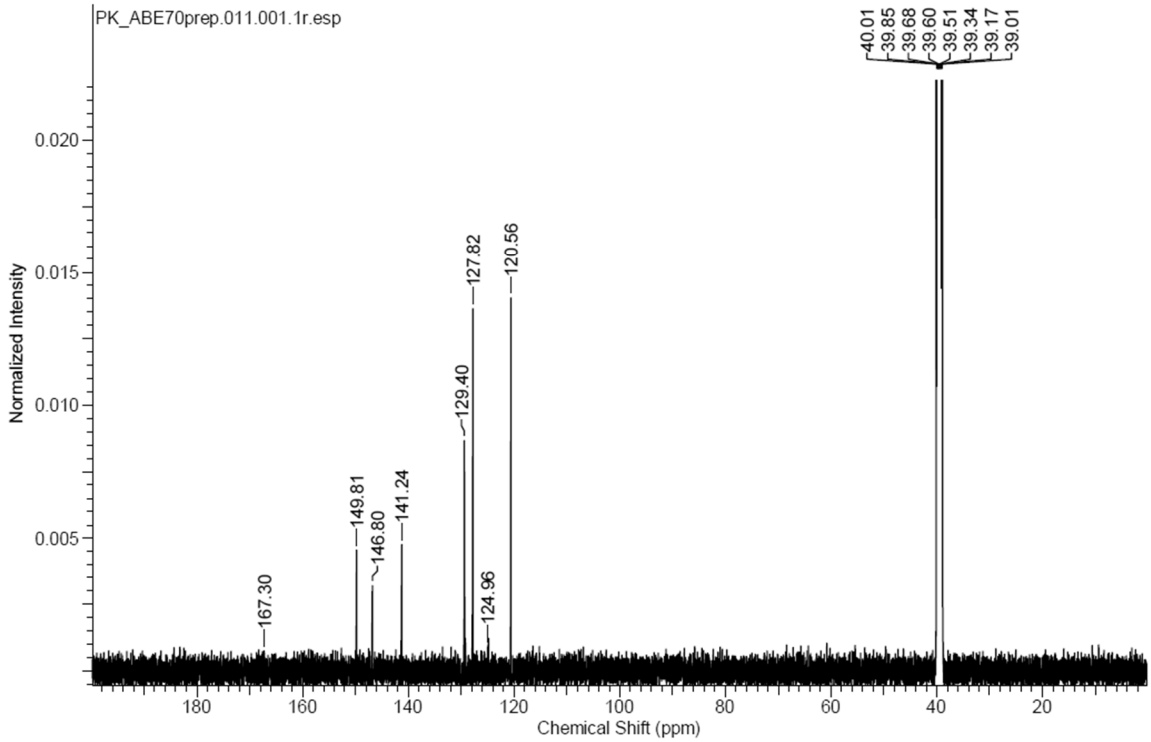

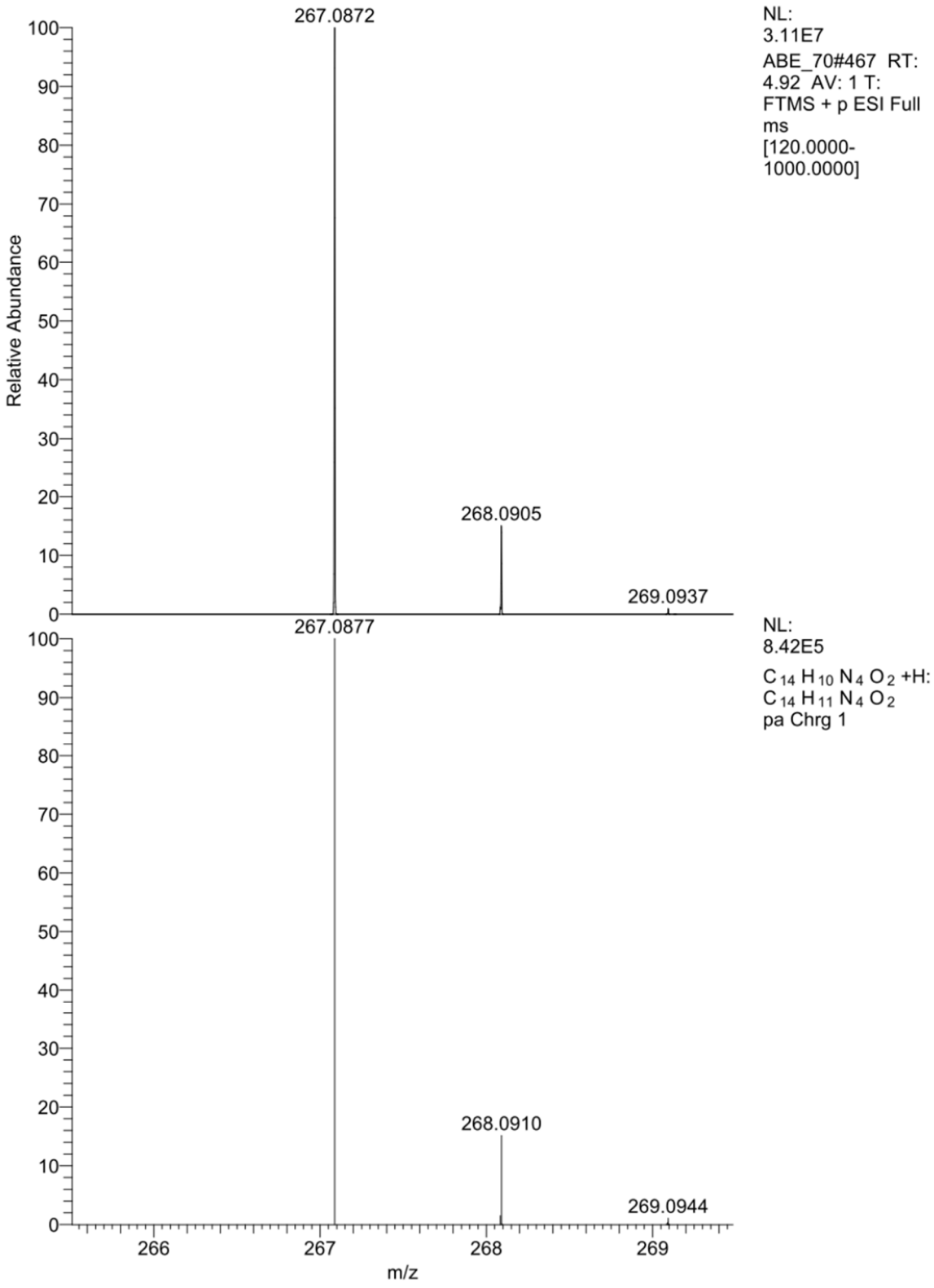
267.0872
NL:
3.11E7
ABE_70#467 RT:
4.92 AV: 1 T:
FTMS + p ESI Full
ms
[120.0000-
1000.0000]
268.0905
269.0937
Relative Abundance
267.0877
NL:
8.42E5
C14 H10 N4 O2 +H:
C14 H11 N4 O2
pa Chrg 1
268.0910
269.0944
m/z

methyl 4-(1-(pyridin-3-yl)-1*H*-1,2,3-triazol-4-yl)benzoate (5):

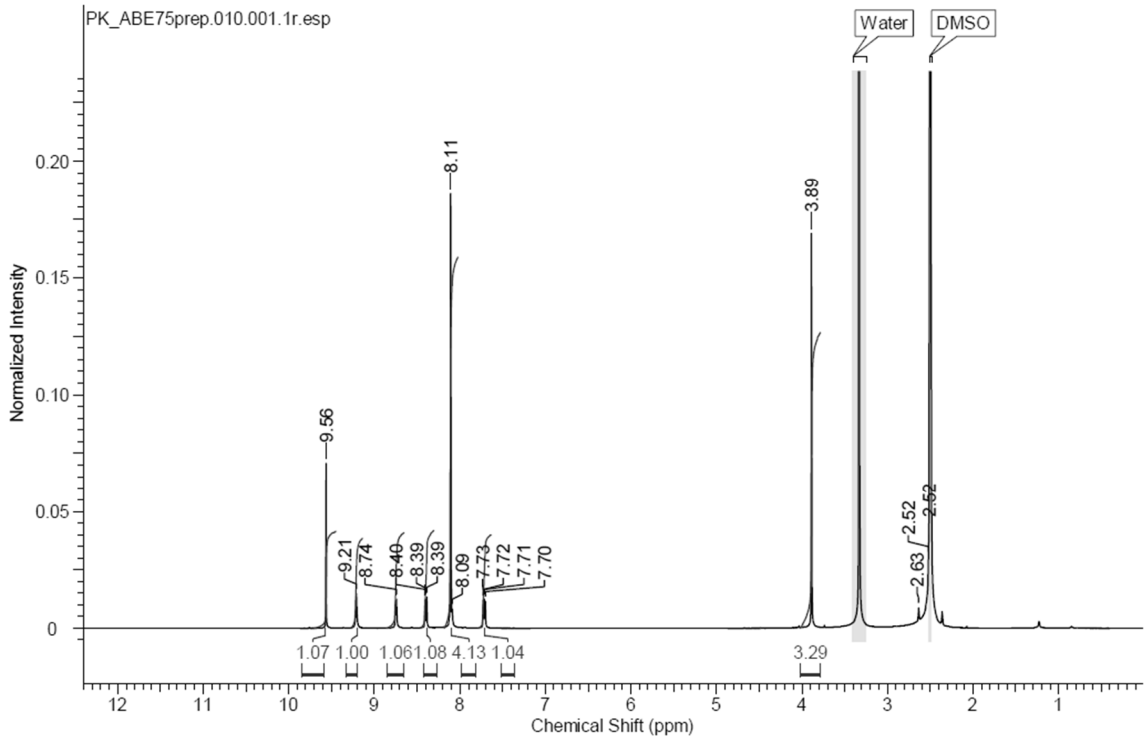

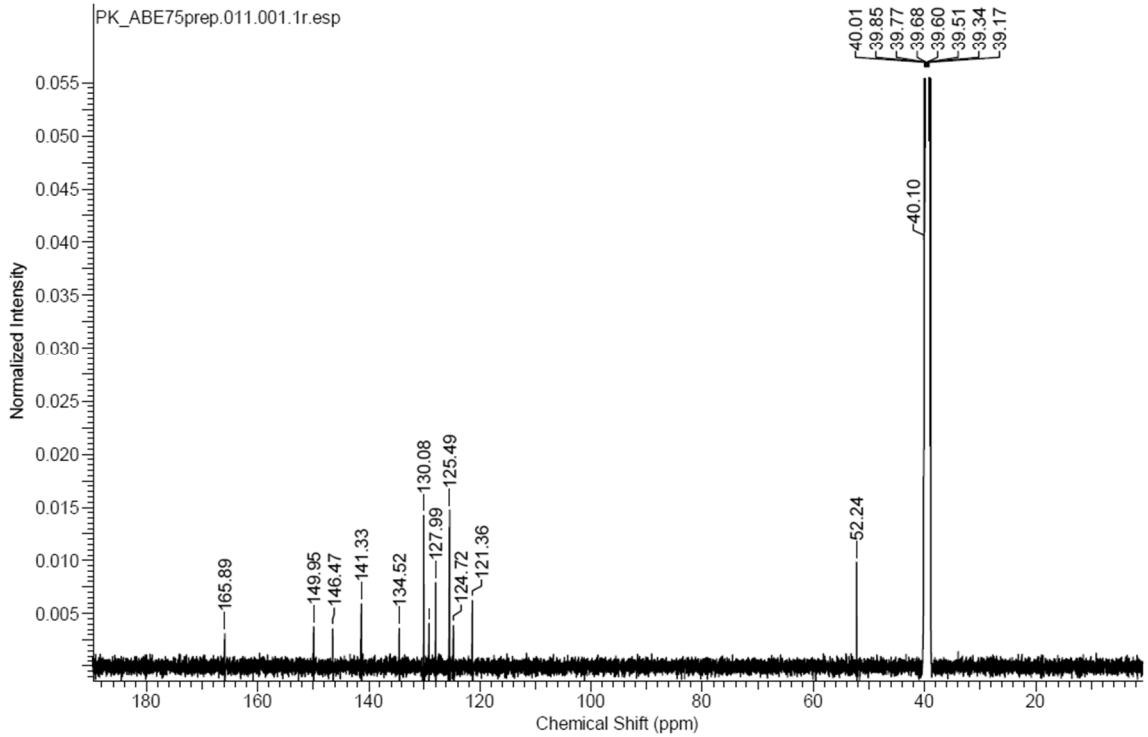

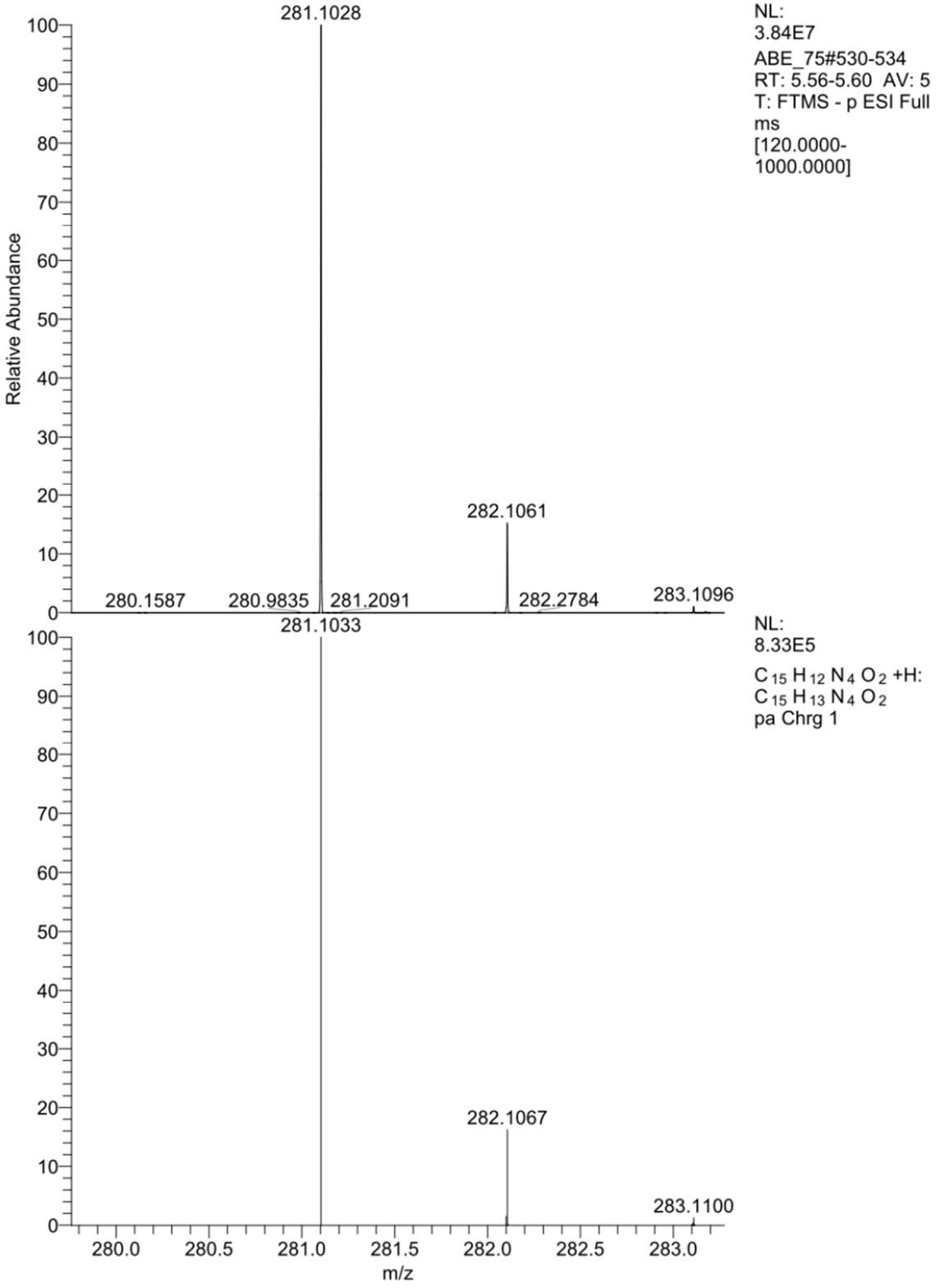
281.1028
NL:
3.84E7
ABE_75#530-534
RT: 5.56-5.60 AV: 5
T: FTMS - p ESI Full
ms
[120.0000-
1000.0000]
Relative Abundance
282.1061
280.1587
280.9835
281.2091
282.2784
283.1096
281.1033
NL:
8.33E5
C15 H12 N4 O2 +H:
C15 H13 N4 O2
pa Chrg 1
282.1067
283.1100
m/z

ethyl 4-(1-(pyridin-3-yl)-1*H*-1,2,3-triazol-4-yl)benzoate (6):

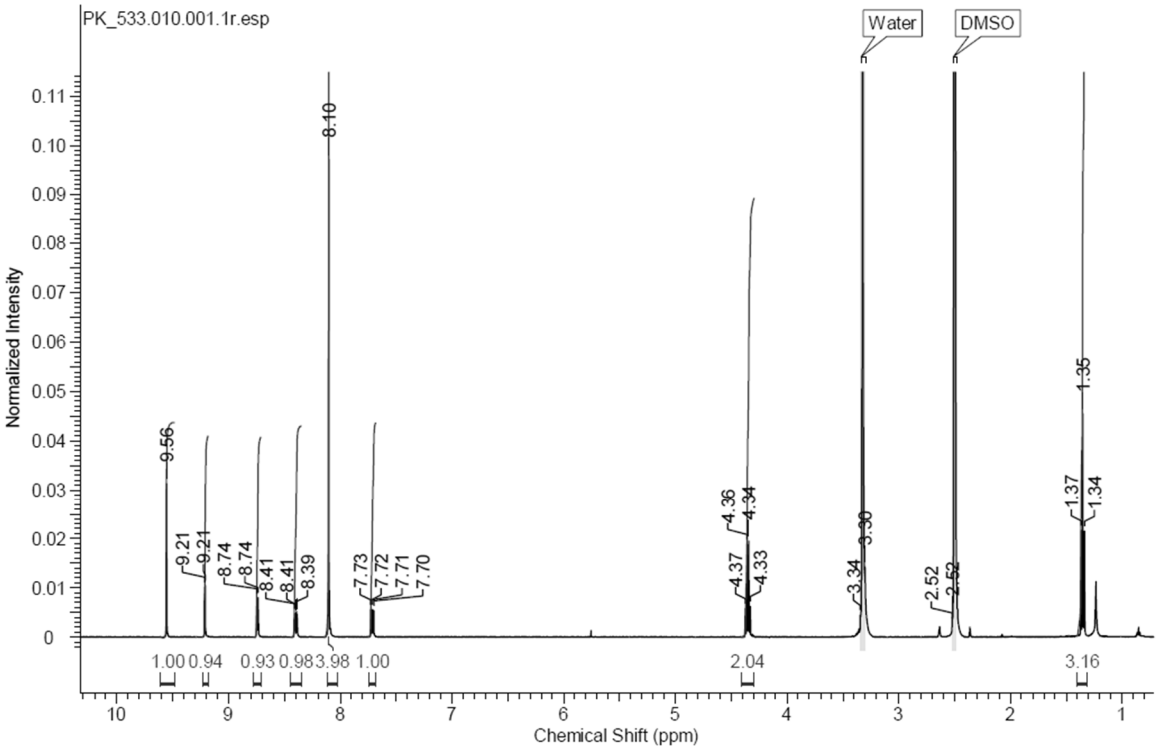

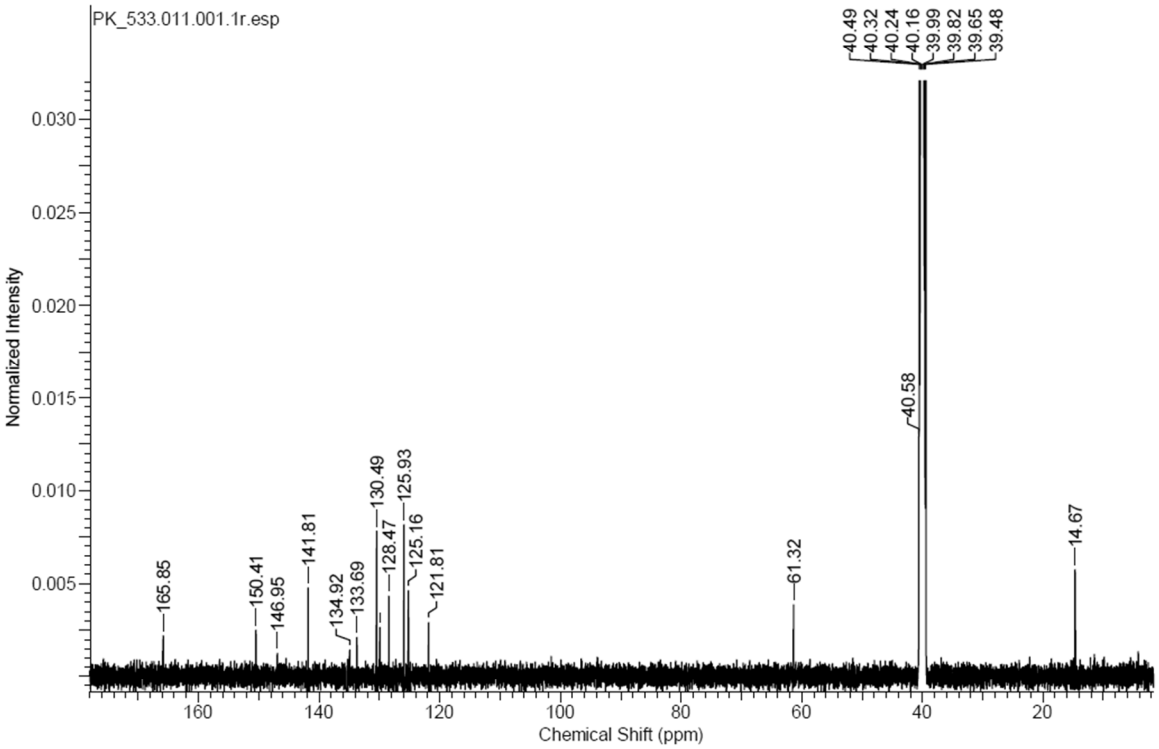

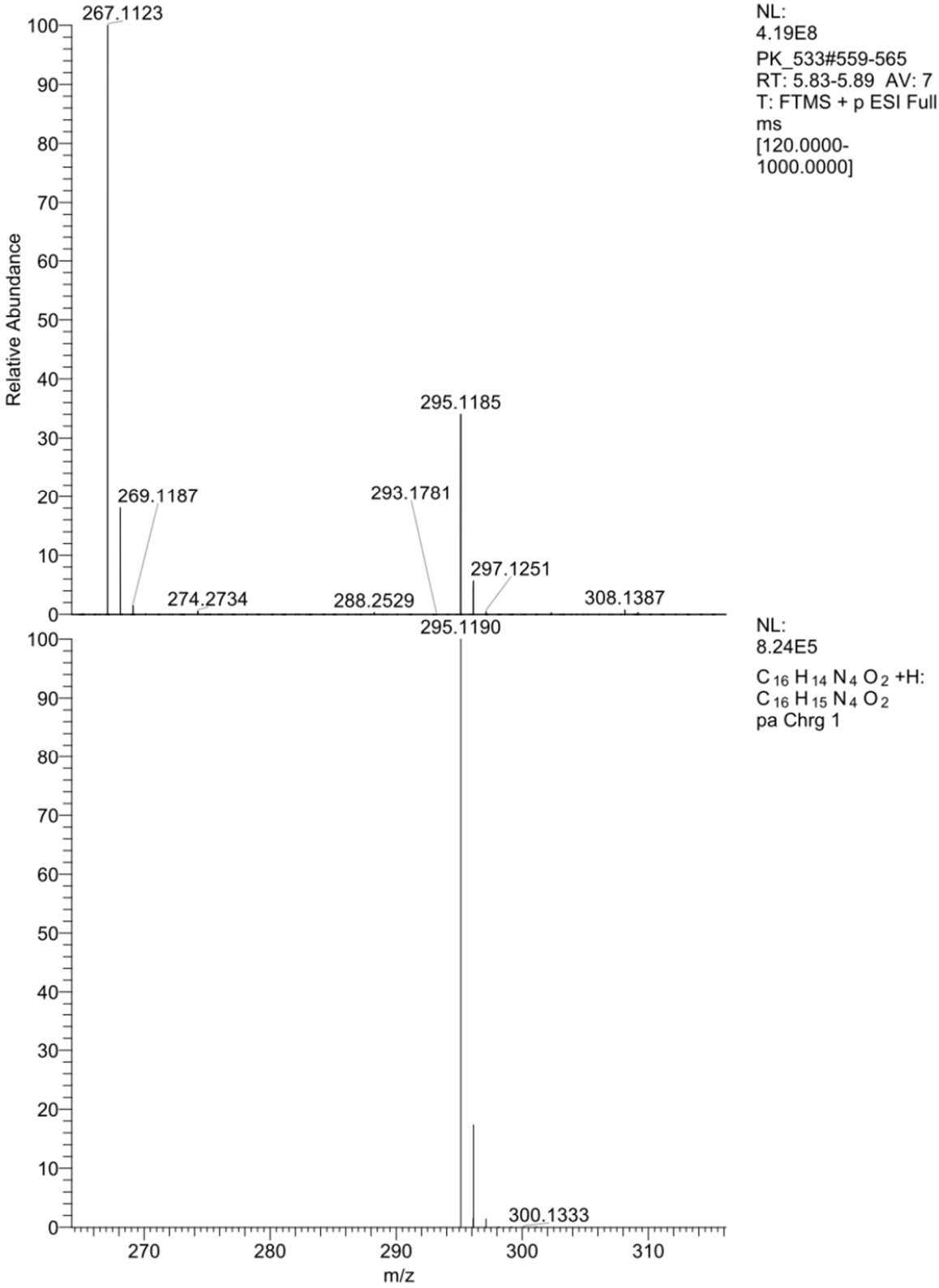
267.1123
NL:
4.19E8
PK_533#559-565
RT: 5.83-5.89 AV: 7
T: FTMS + p ESI Full
ms
[120.0000-
1000.0000]
Relative Abundance
295.1185
269.1187
293.1781
297.1251
274.2734
288.2529
308.1387
295.1190
NL:
8.24E5
C16 H14 N4 O2 +H:
C16 H15 N4 O2
pa Chrg 1
300.1333
m/z

4-(1-(pyridin-3-yl)-1*H*-1,2,3-triazol-4-yl)benzamide (7):

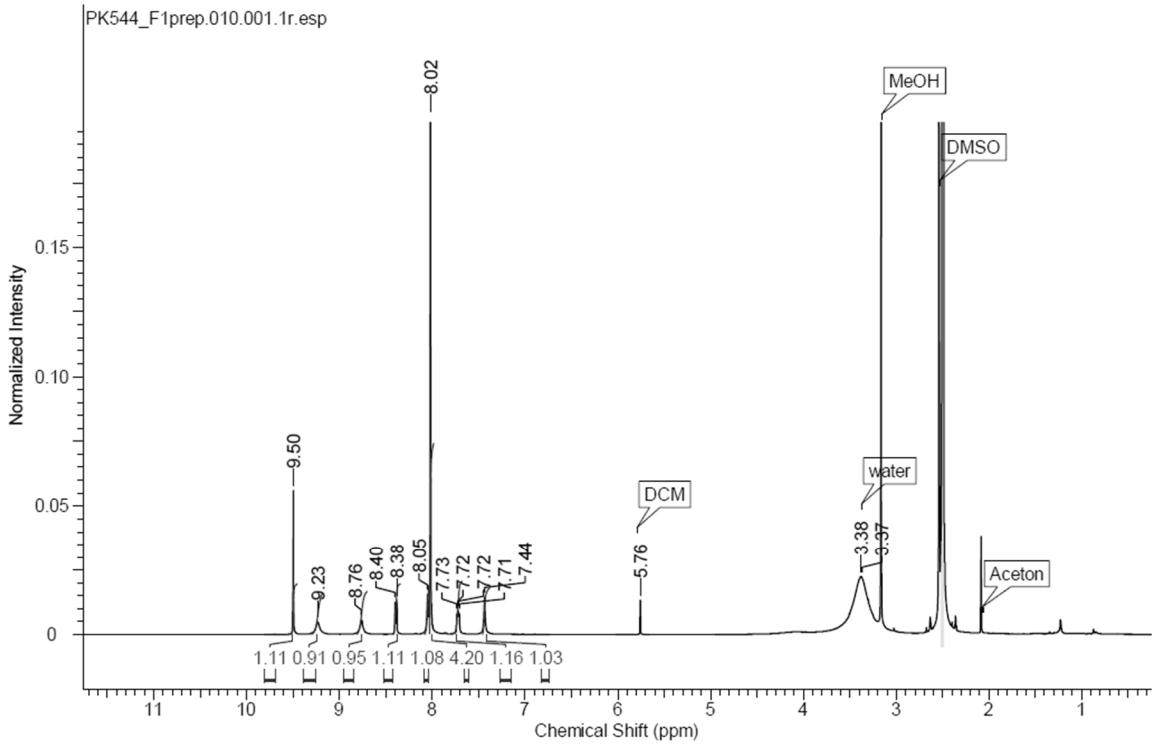

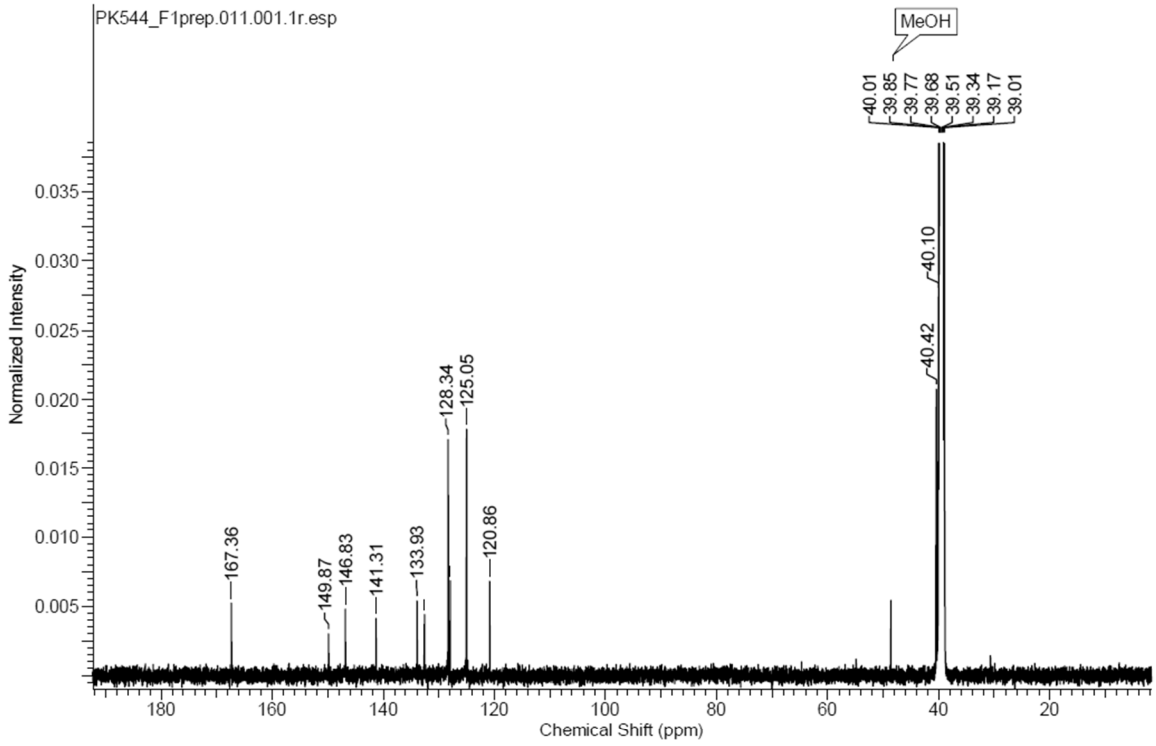

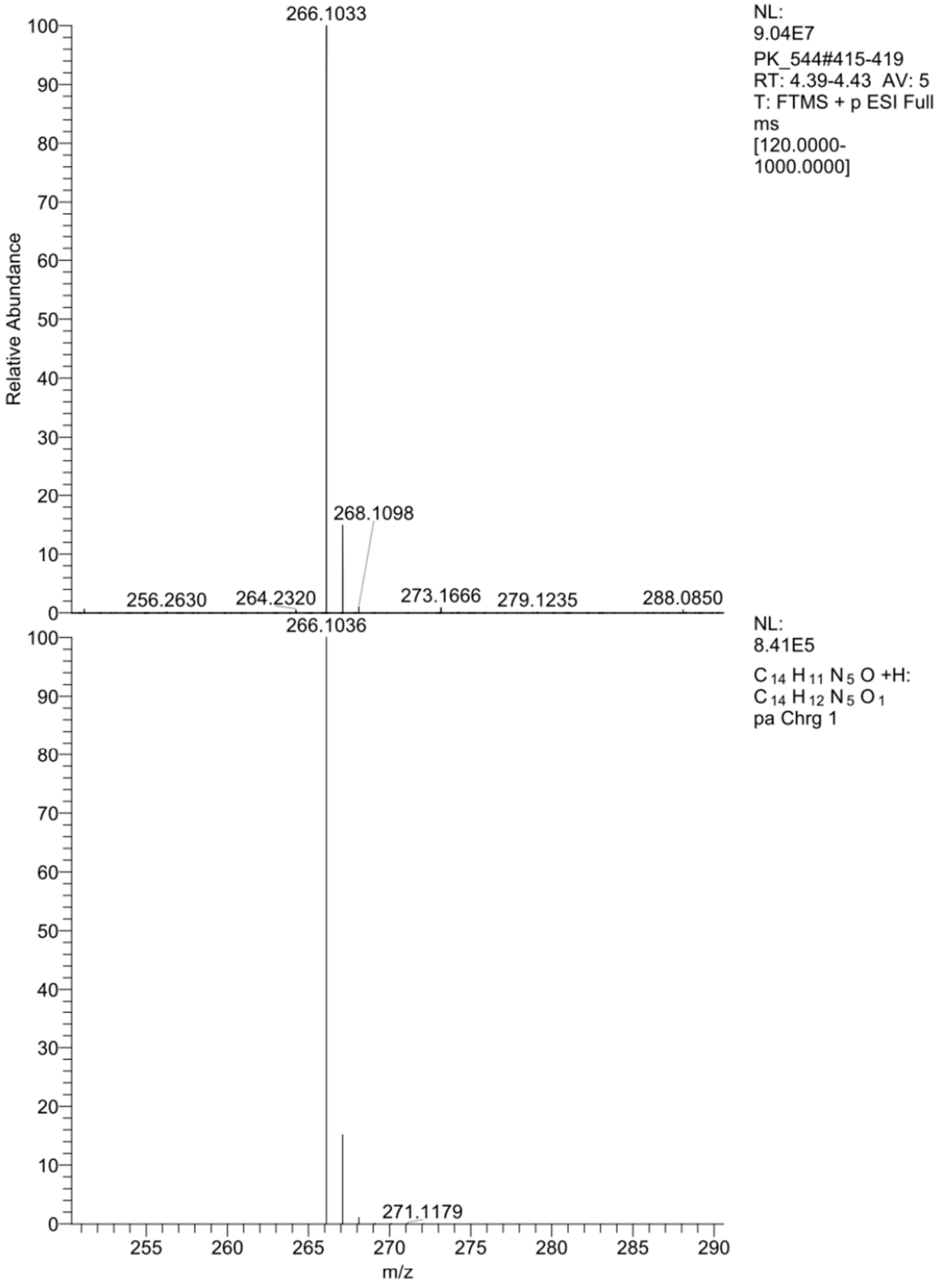
266.1033
NL:
9.04E7
PK_544#415-419
RT: 4.39-4.43 AV: 5
T: FTMS + p ESI Full
ms
[120.0000-
1000.0000]
Relative Abundance
268.1098
256.2630
264.2320
273.1666
279.1235
288.0850
266.1036
NL:
8.41E5
C 14 H 11 N 5 O +H:
C 14 H 12 N 5 O 1
pa Chrg 1
271.1179
m/z

2-chloro-4-(1-(pyridin-3-yl)-1*H*-1,2,3-triazol-4-yl)benzoic acid (9):

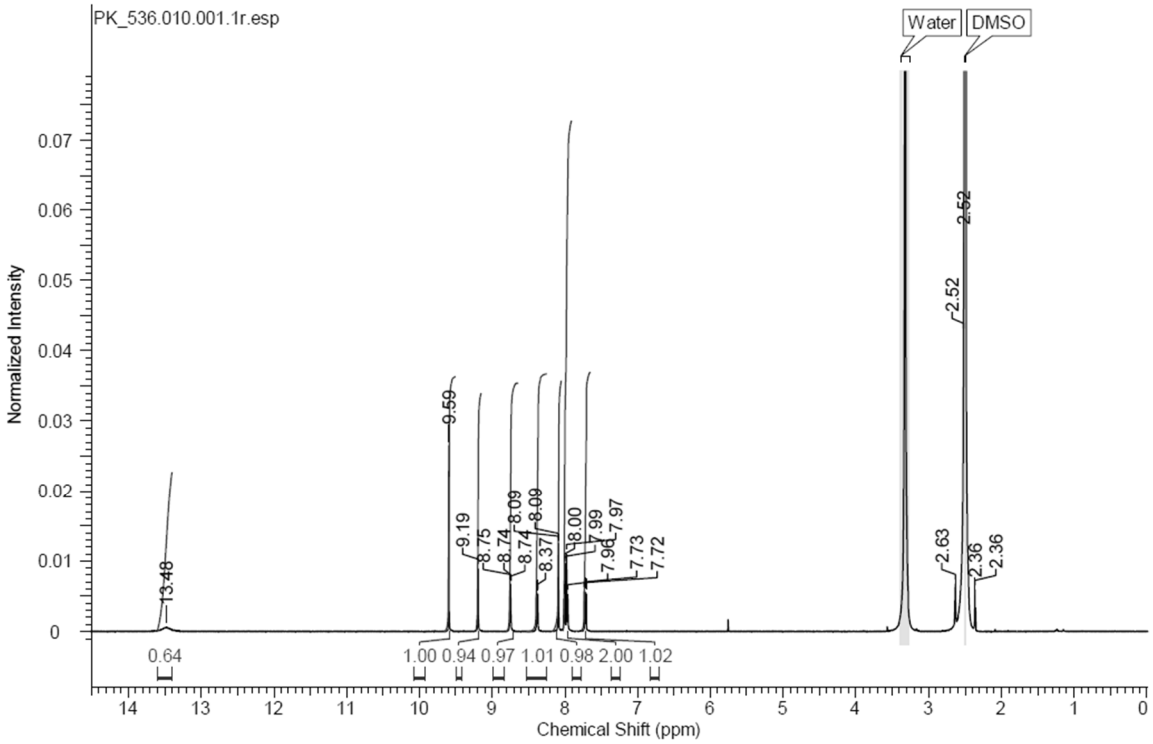

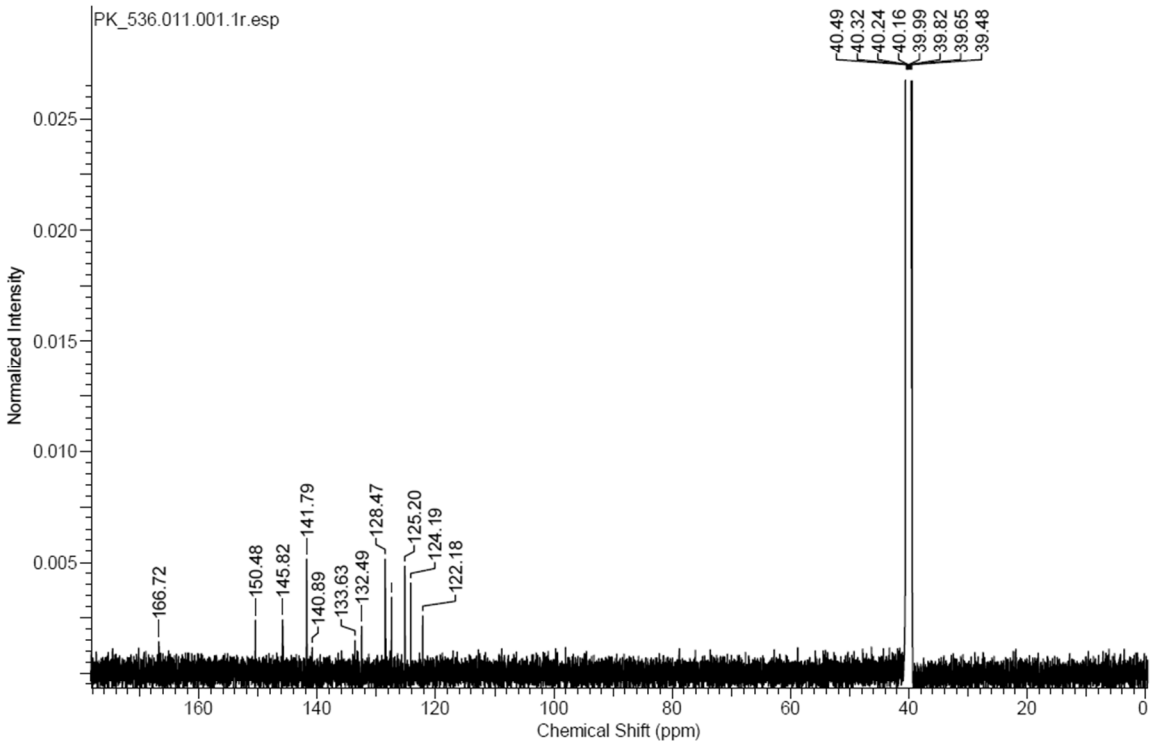

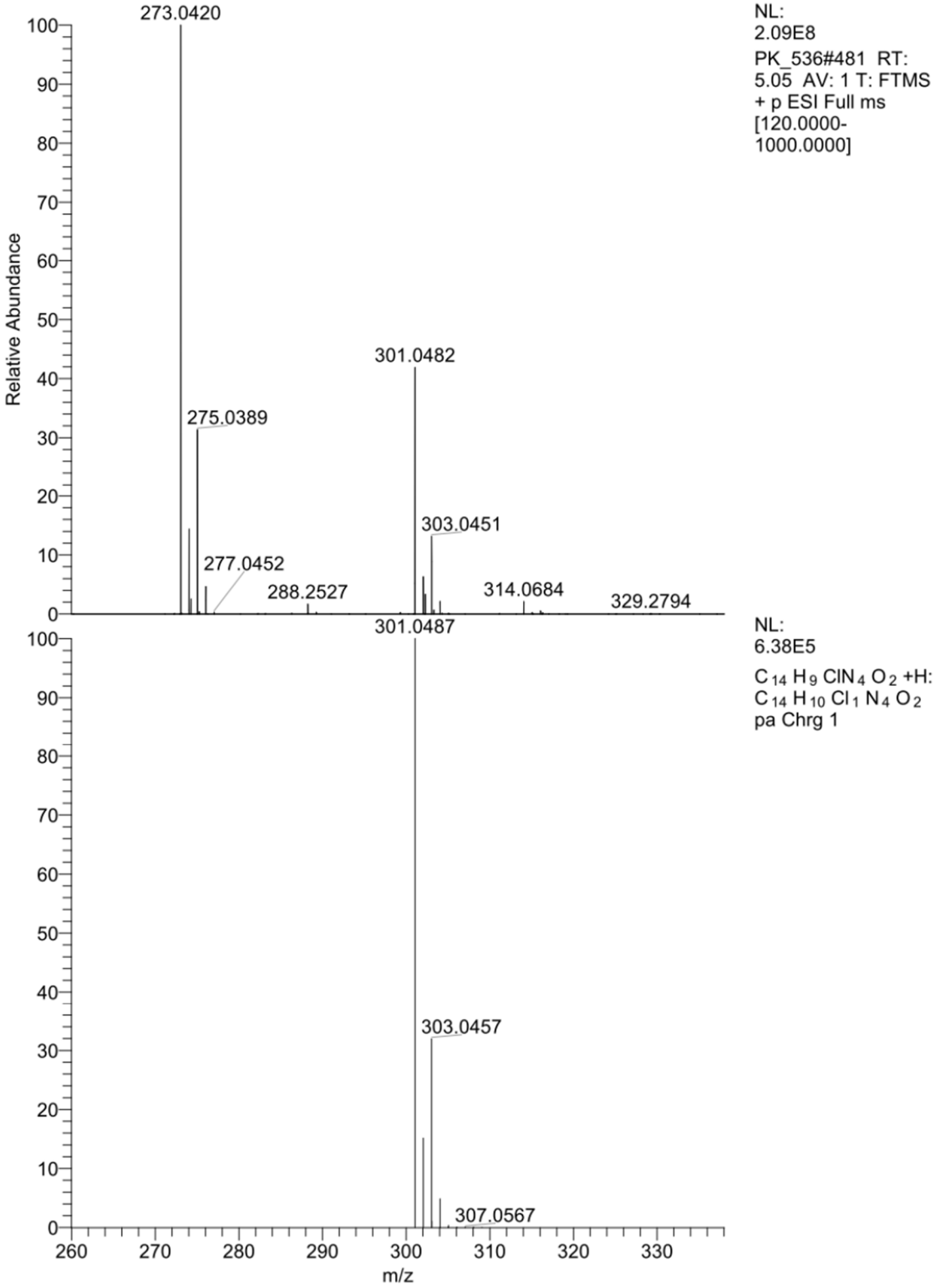
273.0420
NL:
2.09E8
PK_536#481 RT:
5.05 AV: 1 T: FTMS
+ p ESI Full ms
[120.0000-
1000.0000]
301.0482
275.0389
303.0451
277.0452
288.2527
314.0684
329.2794
Relative Abundance
301.0487
NL:
6.38E5
C14 H9 ClN4 O2 +H:
C14 H10 Cl1 N4 O2
pa Chrg 1
303.0457
307.0567
m/z

(4-(1-(pyridin-3-yl)-1*H*-1,2,3-triazol-4-yl)phenyl)methanol (10):

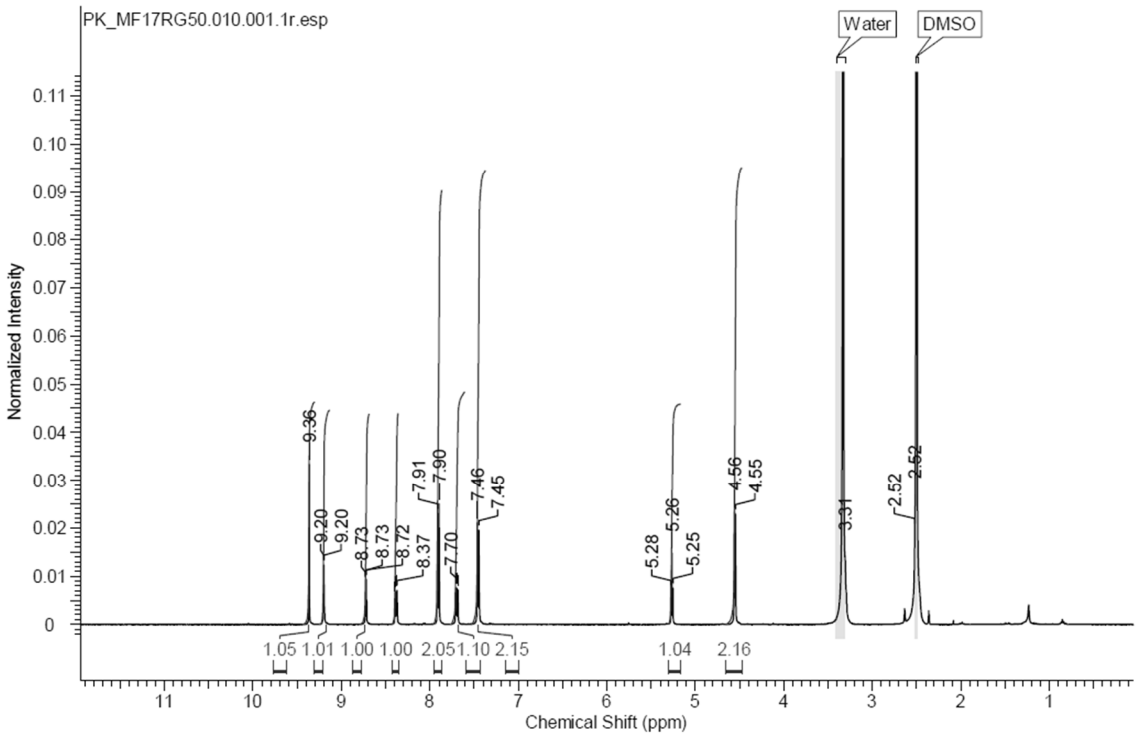

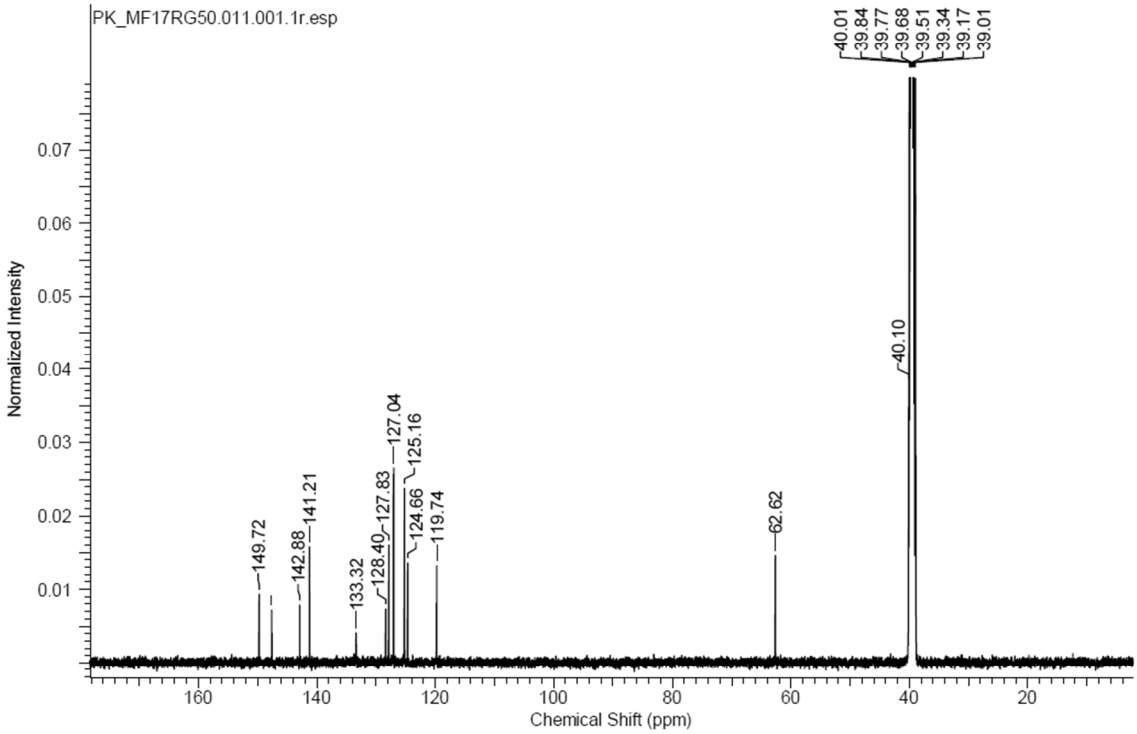

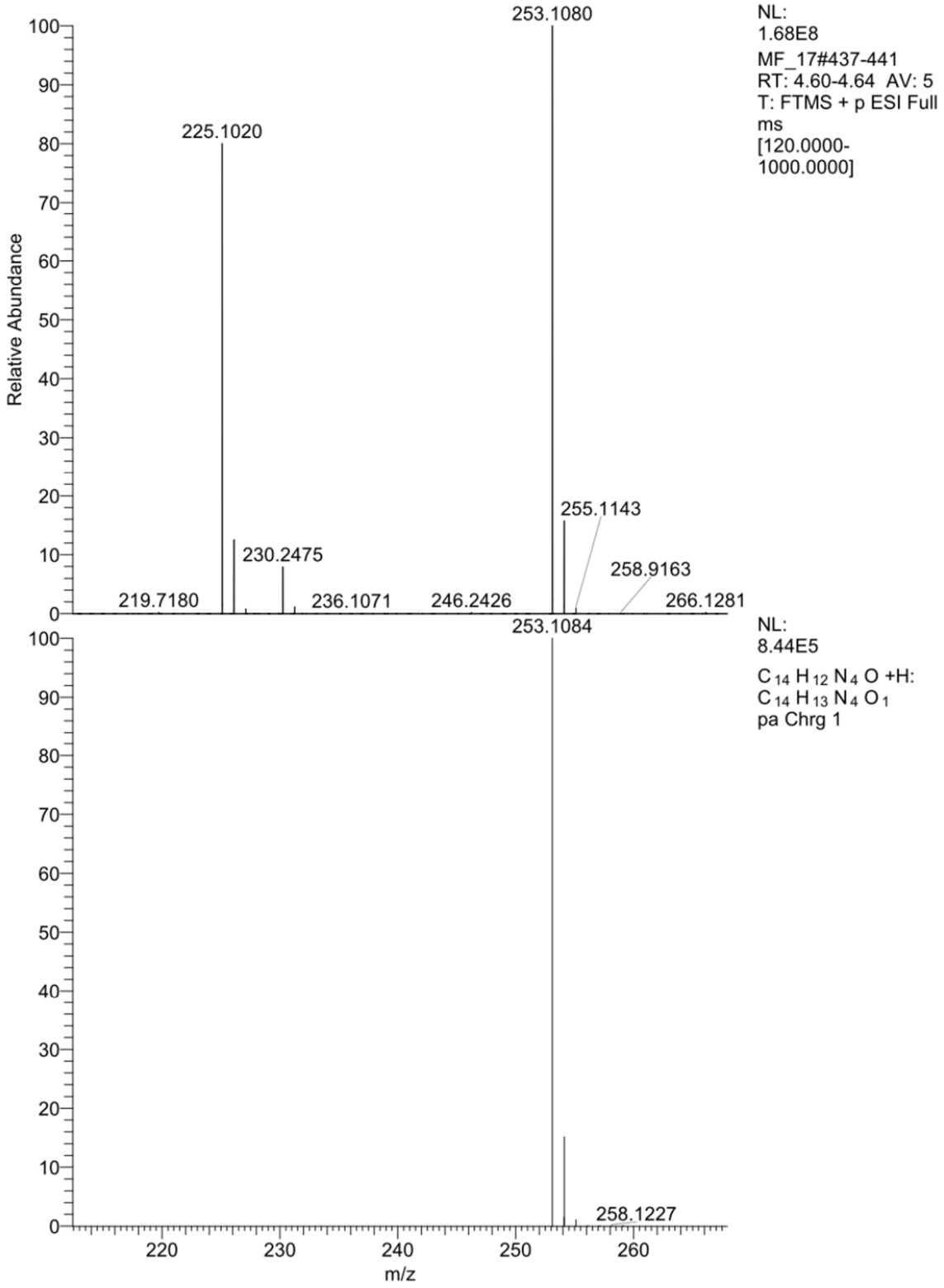
253.1080
NL:
1.68E8
MF_17#437-441
RT: 4.60-4.64 AV: 5
T: FTMS + p ESI Full
ms
[120.0000-
1000.0000]
225.1020
255.1143
230.2475
258.9163
219.7180
236.1071
246.2426
266.1281
Relative Abundance
253.1084
NL:
8.44E5
C 14 H 12 N 4 O +H:
C 14 H 13 N 4 O 1
pa Chrg 1
258.1227
m/z

4-(1-(pyridin-3-yl)-1*H*-1,2,3-triazol-4-yl)aniline (11):

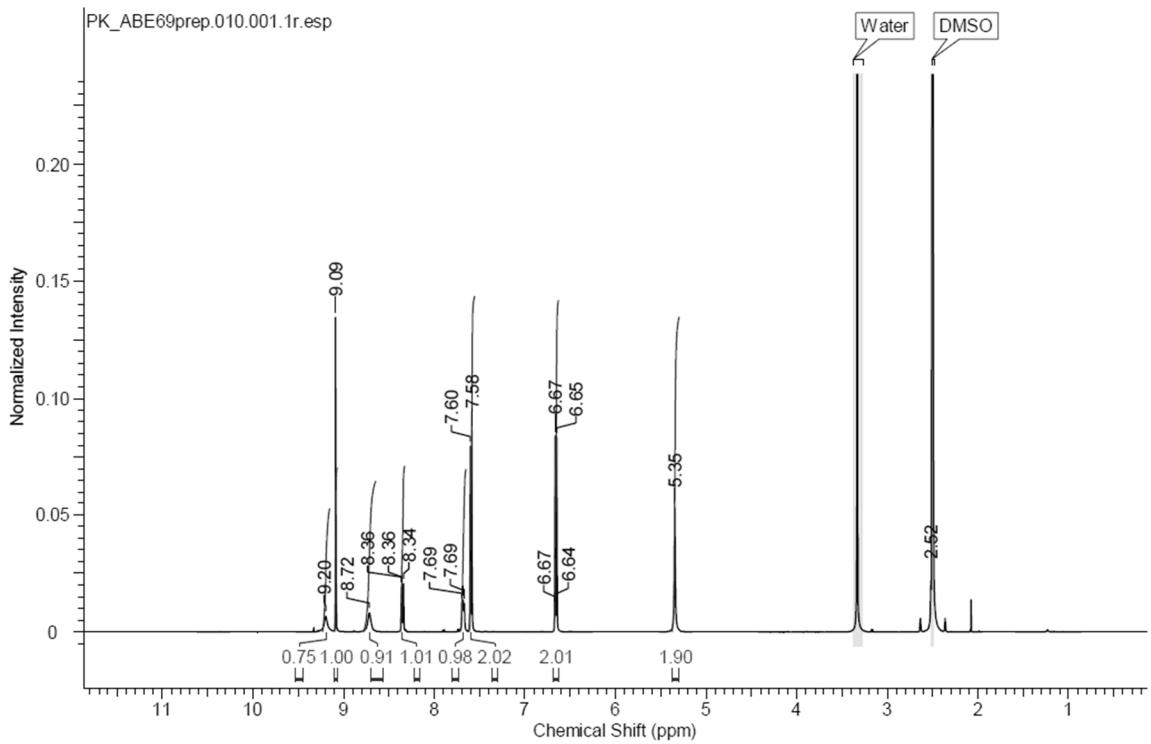

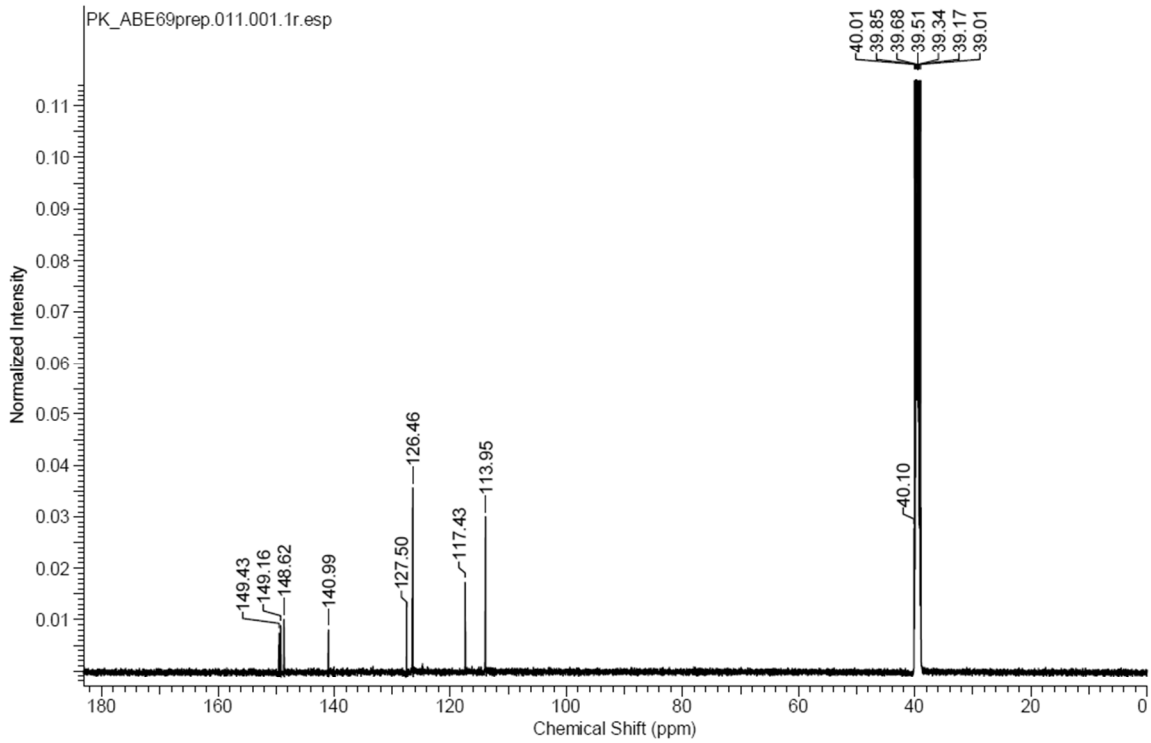

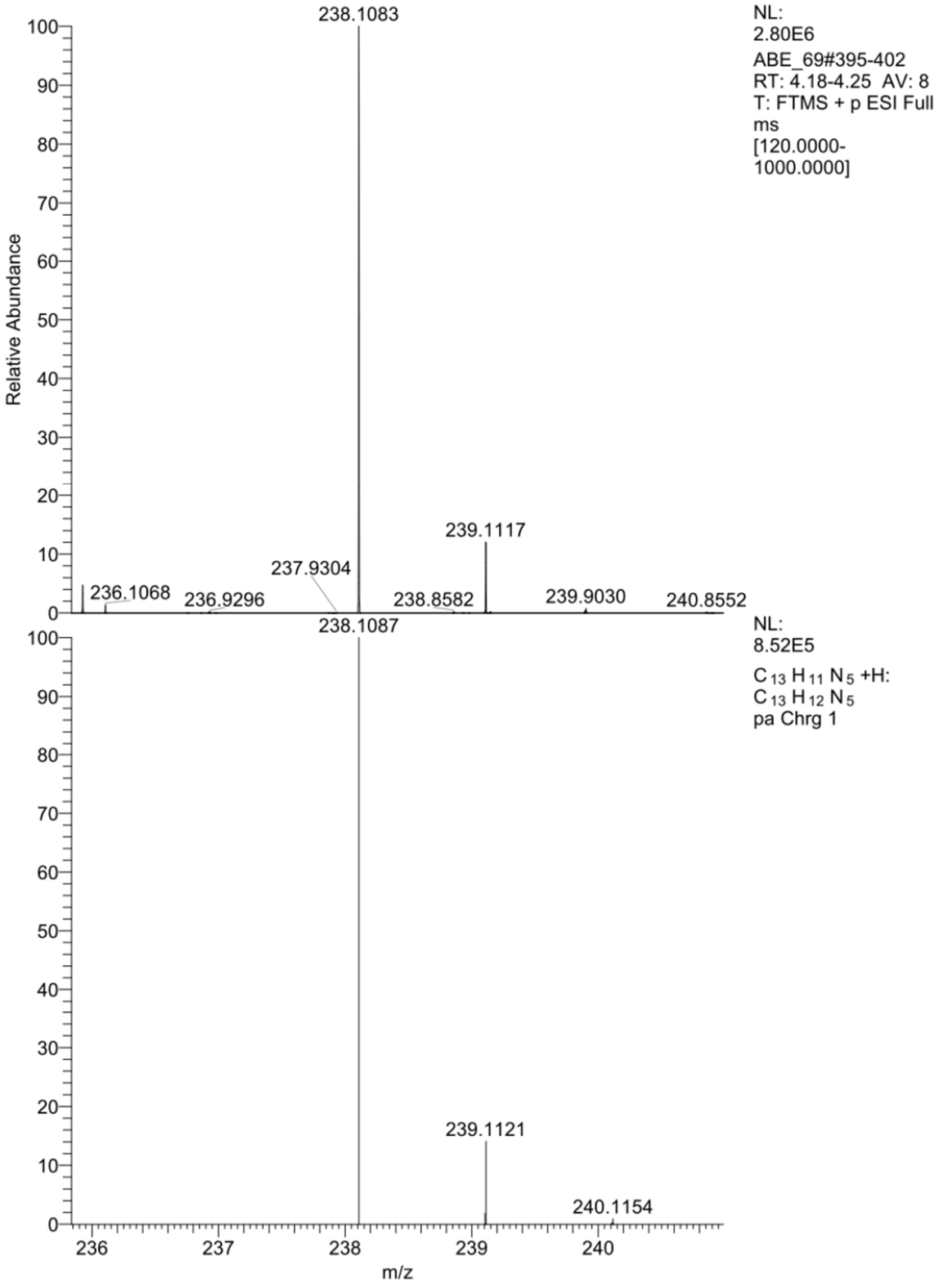
238.1083
NL:
2.80E6
ABE_69#395-402
RT: 4.18-4.25 AV: 8
T: FTMS + p ESI Full
ms
[120.0000-
1000.0000]
239.1117
237.9304
236.1068
236.9296
238.8582
239.9030
240.8552
238.1087
NL:
8.52E5
C13 H11 N5 +H:
C13 H12 N5
pa Chrg 1
239.1121
240.1154
Relative Abundance
m/z
100
90
80
70
60
50
40
30
20
10
0
236
237
238
239
240

***N*-(4-(1-(pyridin-3-yl)-1*H*-1,2,3-triazol-4-yl)phenyl)acetamide (12)**:

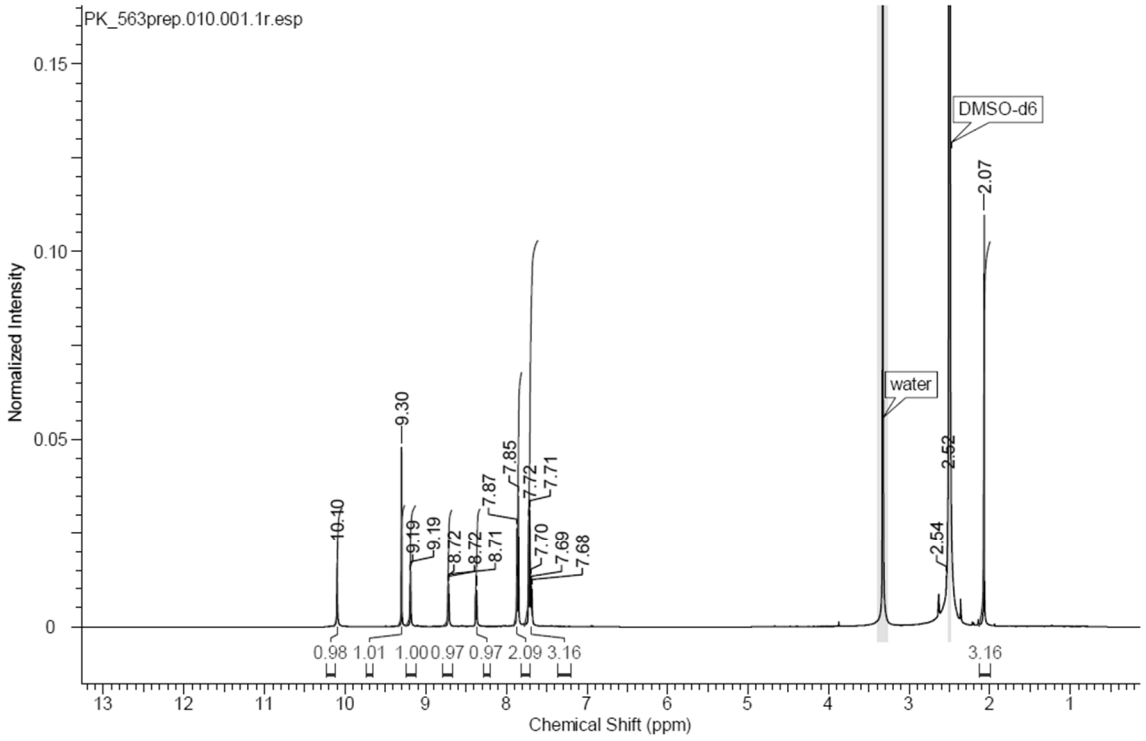

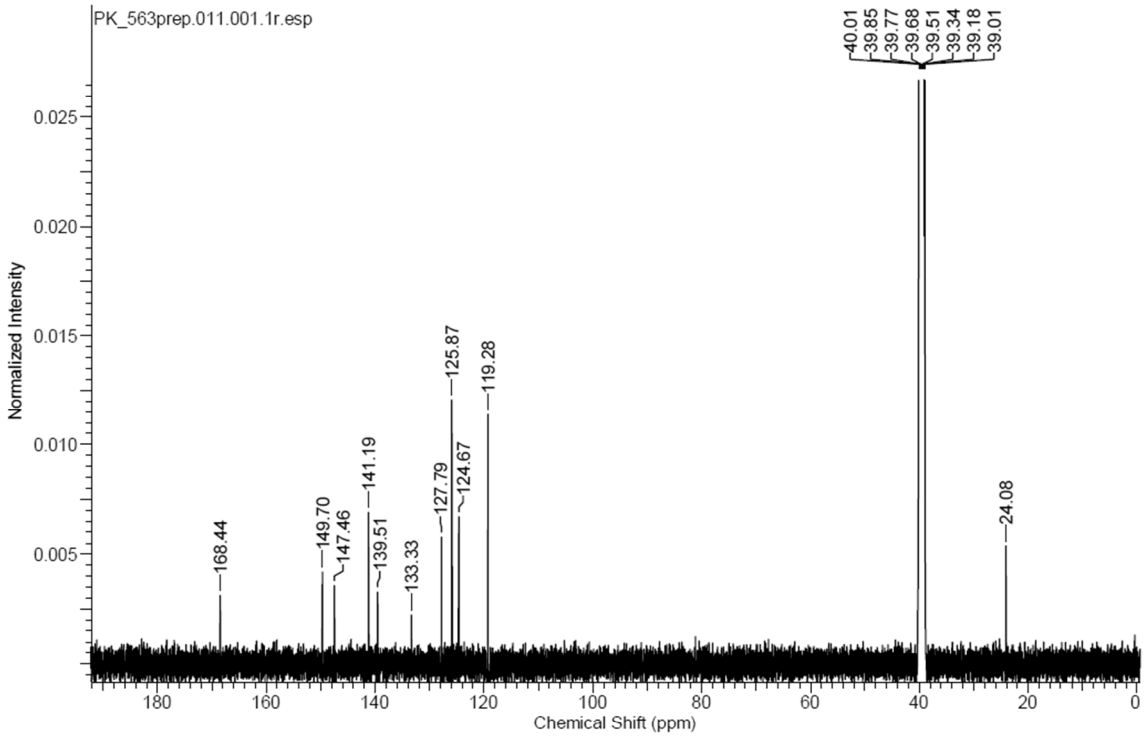

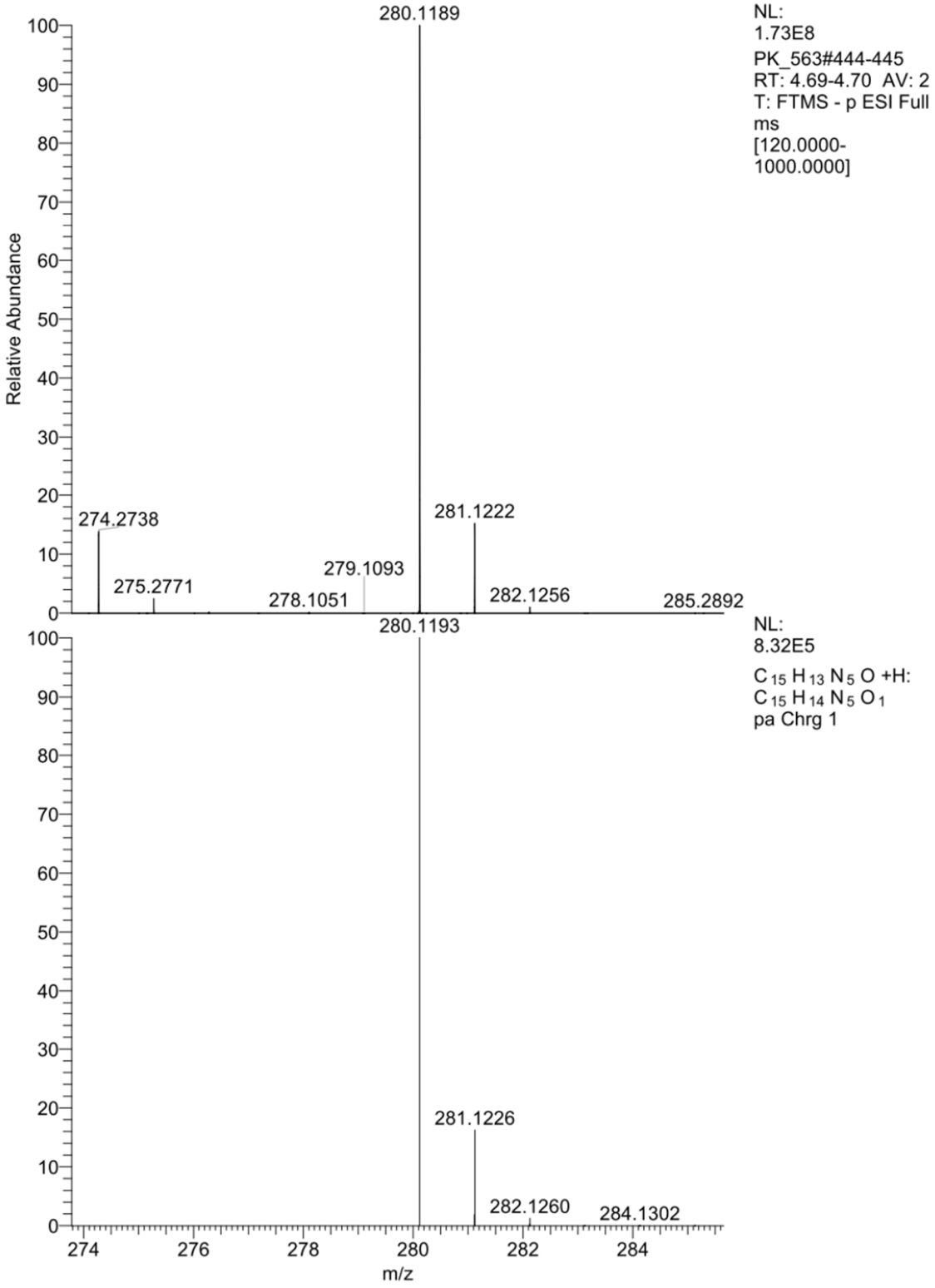
280.1189
NL:
1.73E8
PK_563#444-445
RT: 4.69-4.70 AV: 2
T: FTMS - p ESI Full
ms
[120.0000-
1000.0000]
Relative Abundance
274.2738
275.2771
278.1051
279.1093
281.1222
282.1256
285.2892
280.1193
NL:
8.32E5
C 15 H 13 N 5 O +H:
C 15 H 14 N 5 O 1
pa Chrg 1
281.1226
282.1260
284.1302
m/z

4-(1-(pyridin-3-yl)-1*H*-1,2,3-triazol-4-yl)benzonitrile (13):

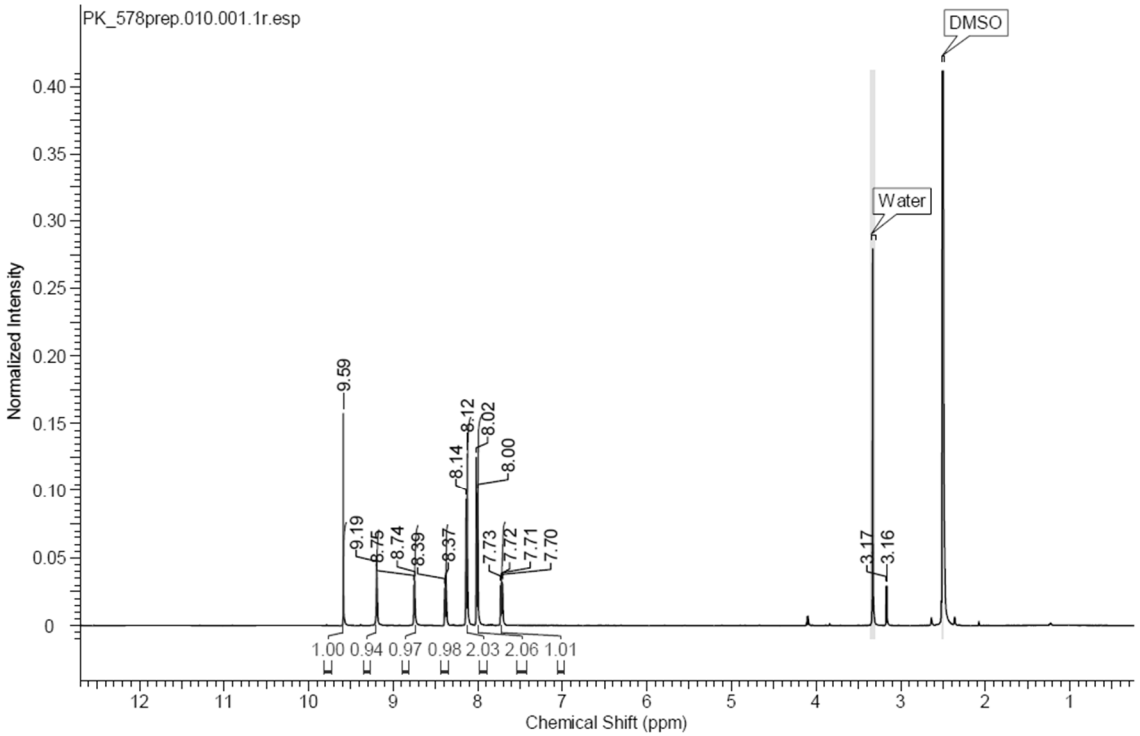

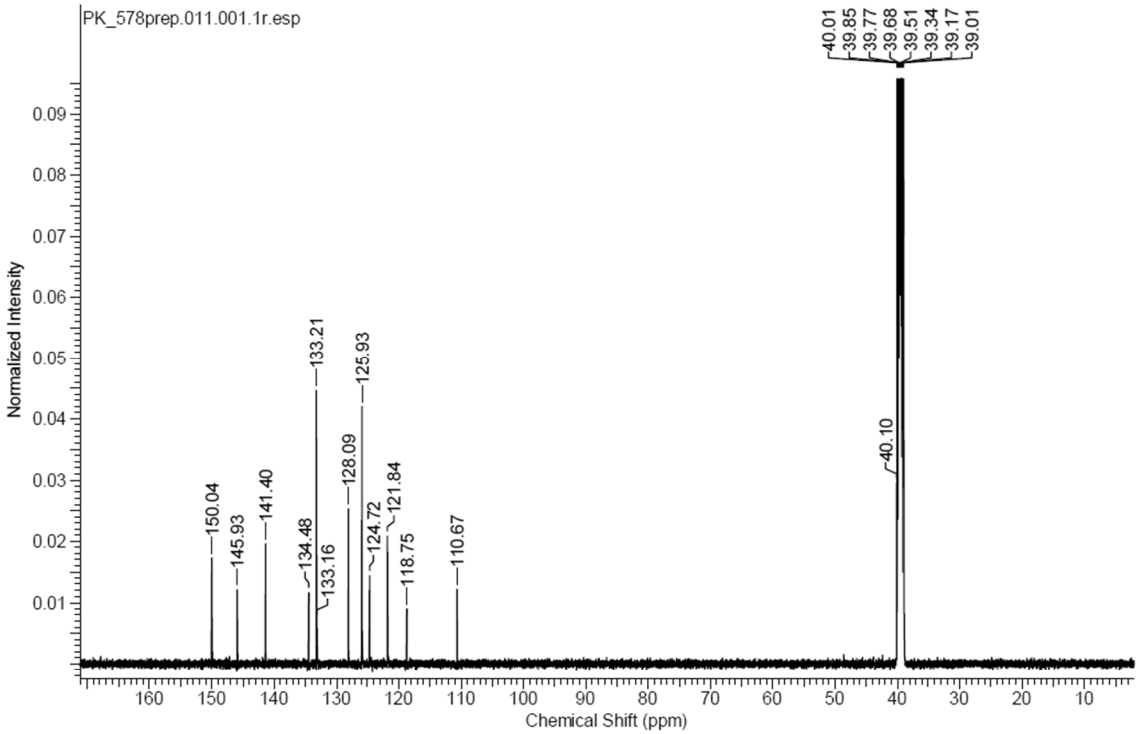

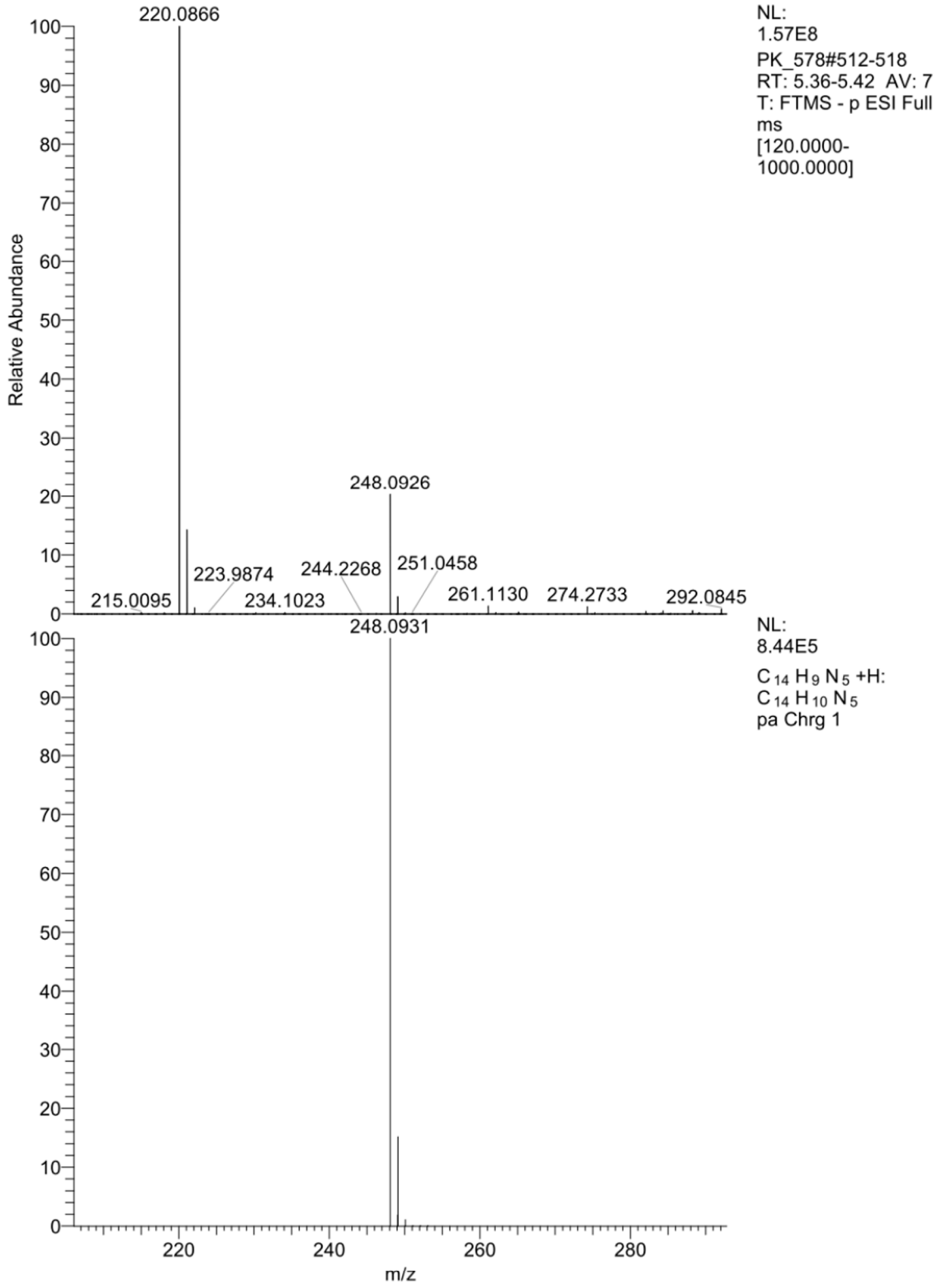
220.0866
NL:
1.57E8
PK_578#512-518
RT: 5.36-5.42 AV: 7
T: FTMS - p ESI Full
ms
[120.0000-
1000.0000]
Relative Abundance
248.0926
223.9874
244.2268
251.0458
215.0095
234.1023
261.1130
274.2733
292.0845
248.0931
NL:
8.44E5
C 14 H 9 N 5 +H:
C 14 H 10 N 5
pa Chrg 1
m/z

4-(1-(pyridin-3-ylmethyl)-1*H*-1,2,3-triazol-4-yl)benzoic acid (16):

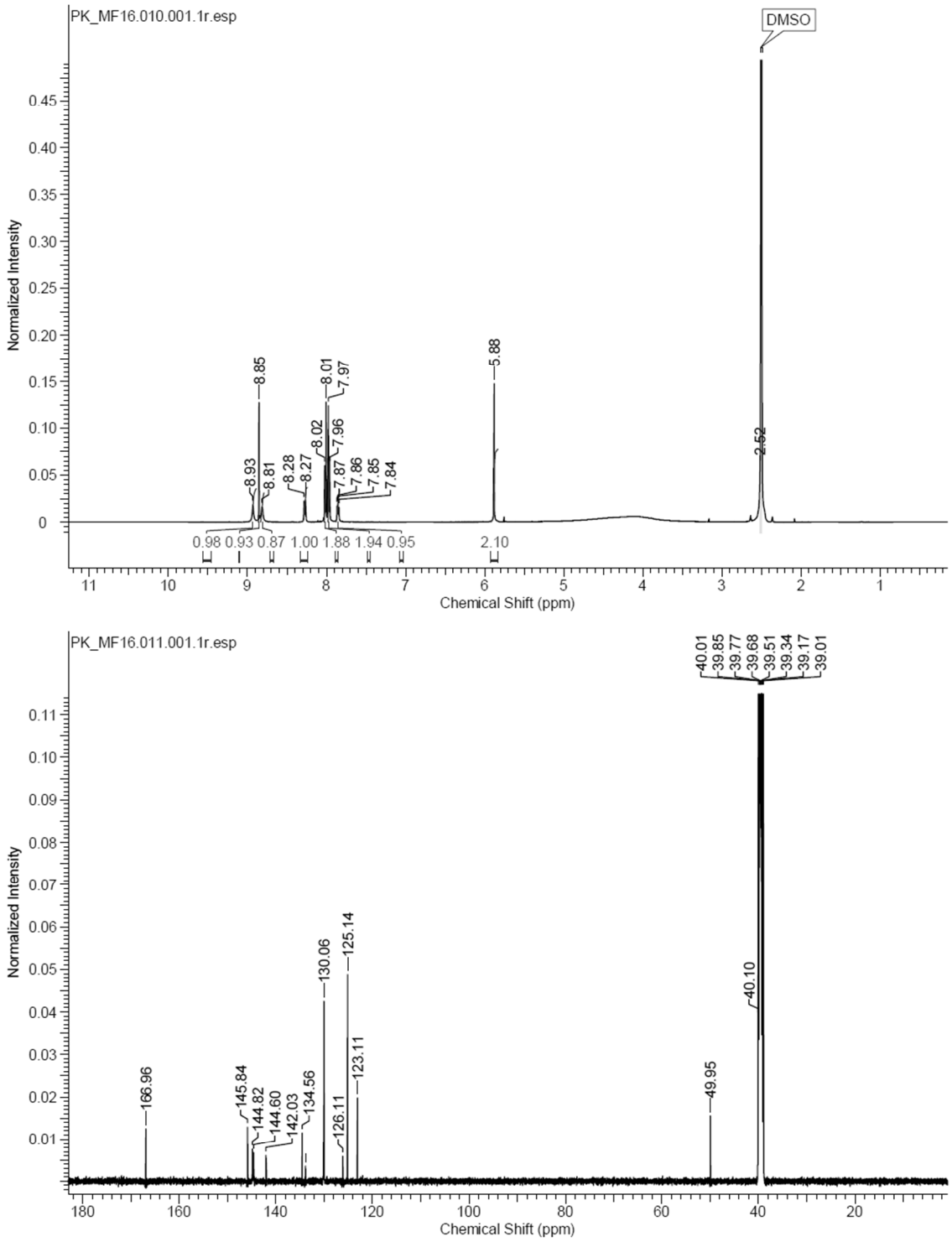

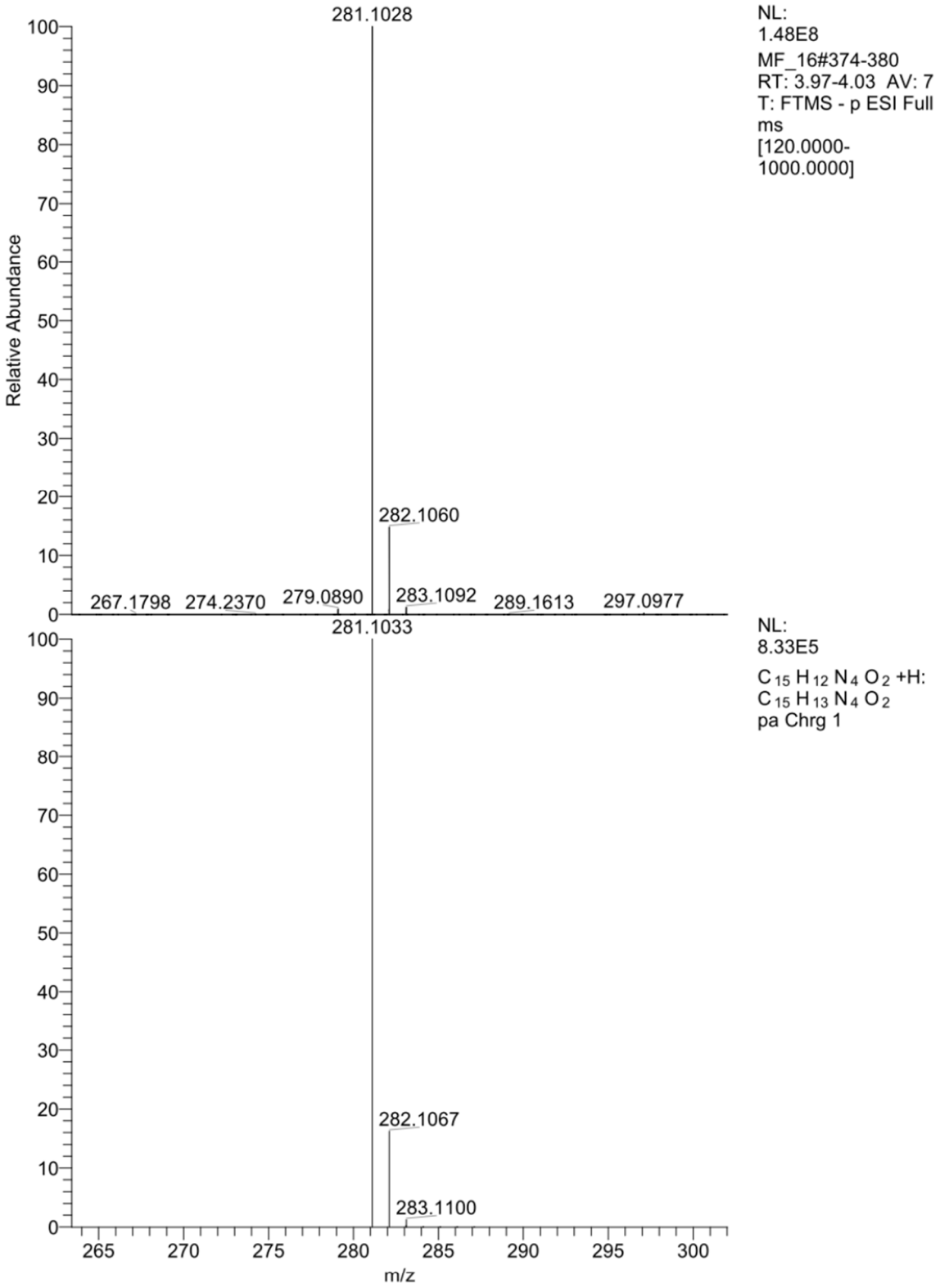
281.1028
NL:
1.48E8
MF_16#374-380
RT: 3.97-4.03 AV: 7
T: FTMS - p ESI Full
ms
[120.0000-
1000.0000]
282.1060
267.1798
274.2370
279.0890
283.1092
289.1613
297.0977
281.1033
NL:
8.33E5
C 15 H 12 N 4 O 2 +H:
C 15 H 13 N 4 O 2
pa Chrg 1
282.1067
283.1100
Relative Abundance
m/z

4-(1-(4-methylpyridin-3-yl)-1*H*-1,2,3-triazol-4-yl)benzoic acid (19a):

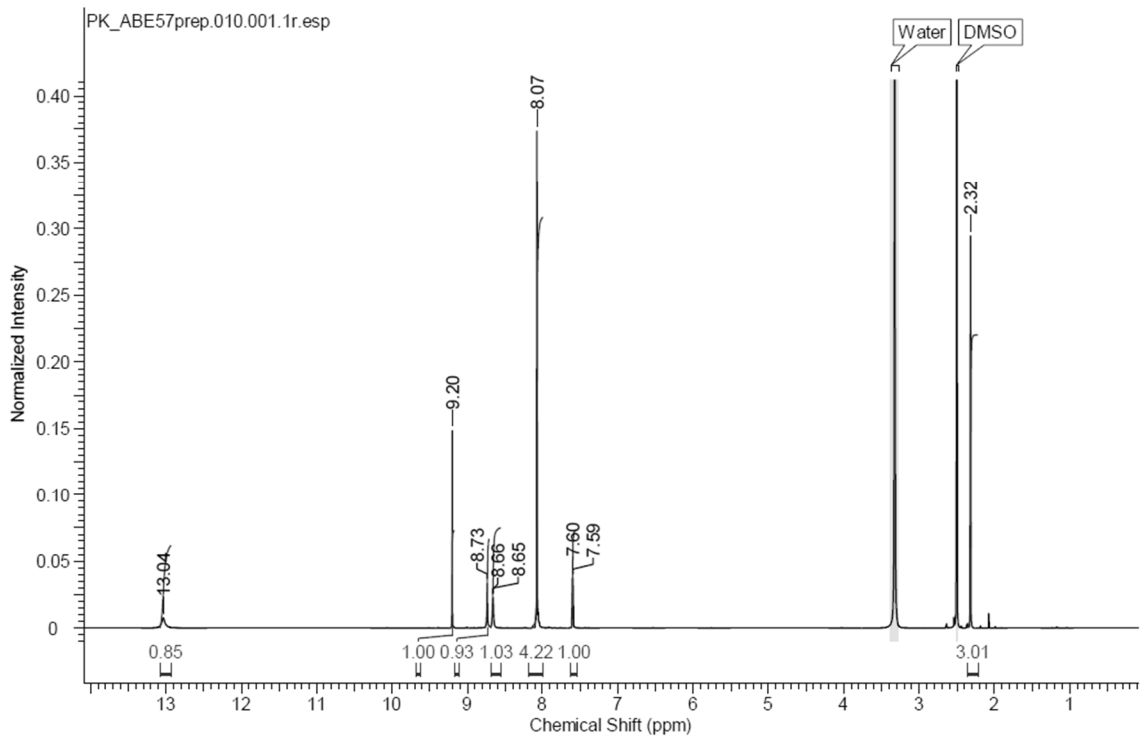

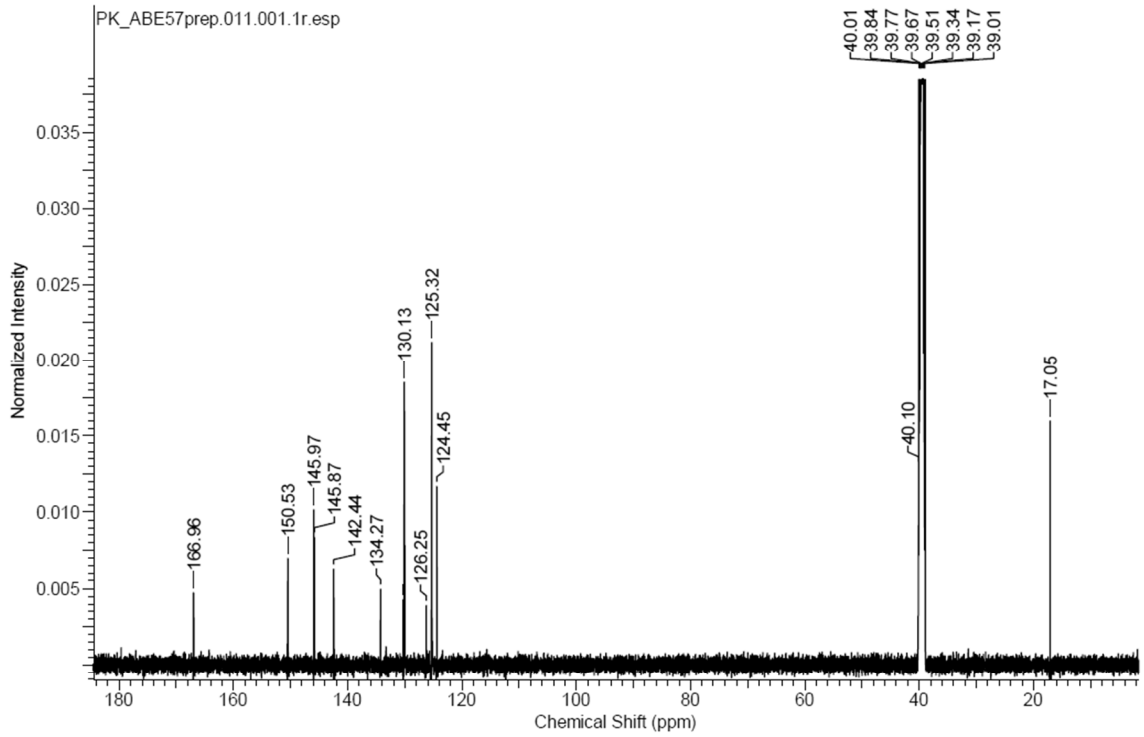

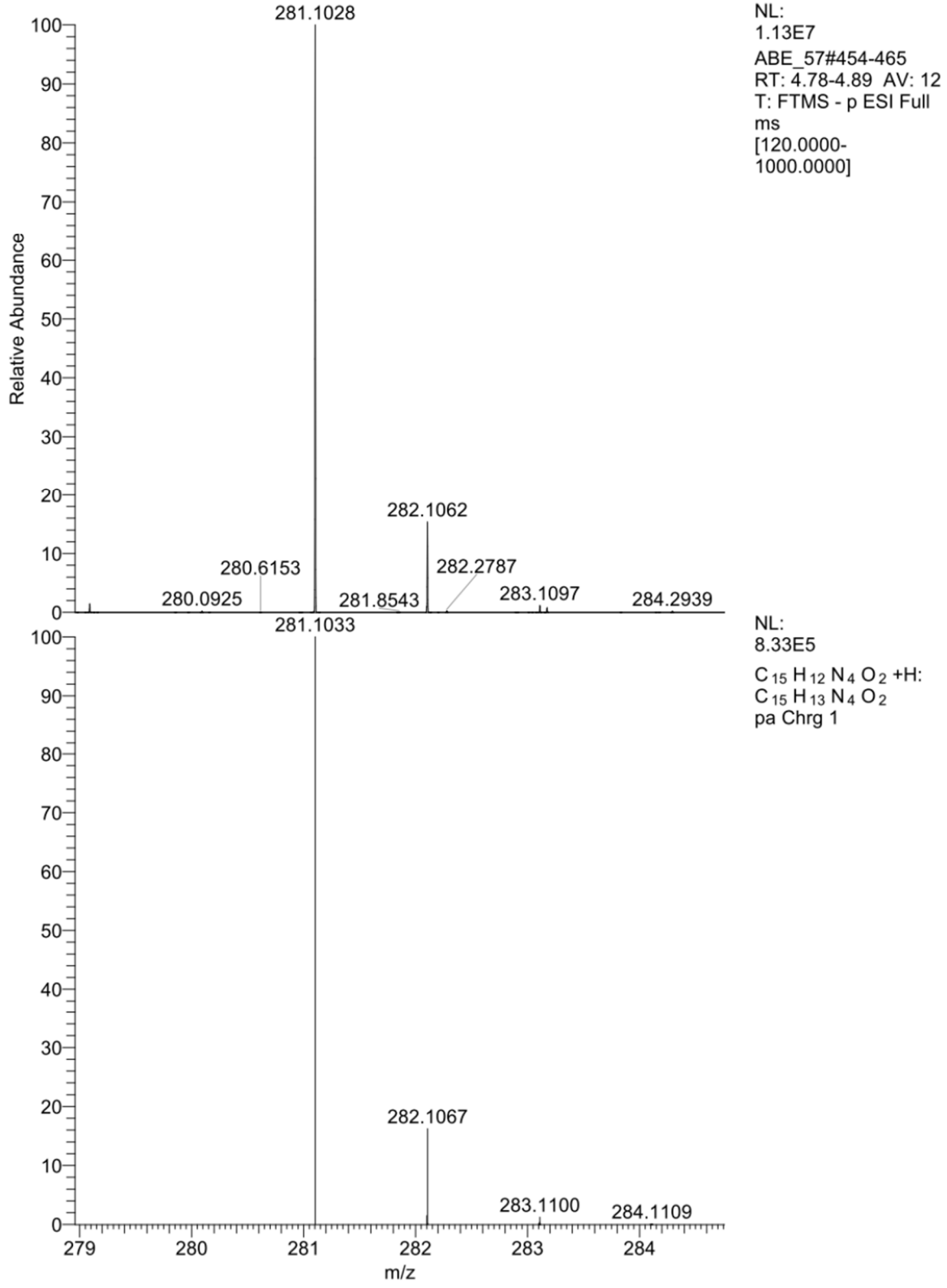
281.1028
NL:
1.13E7
ABE_57#454-465
RT: 4.78-4.89 AV: 12
T: FTMS - p ESI Full
ms
[120.0000-
1000.0000]
Relative Abundance
282.1062
280.6153
282.2787
280.0925
281.8543
283.1097
284.2939
281.1033
NL:
8.33E5
C15 H12 N4 O2 +H:
C15 H13 N4 O2
pa Chrg 1
282.1067
283.1100
284.1109
279
280
281
282
283
284
m/z

4-(1-(4-chloropyridin-3-yl)-1*H*-1,2,3-triazol-4-yl)benzoic acid (19b):

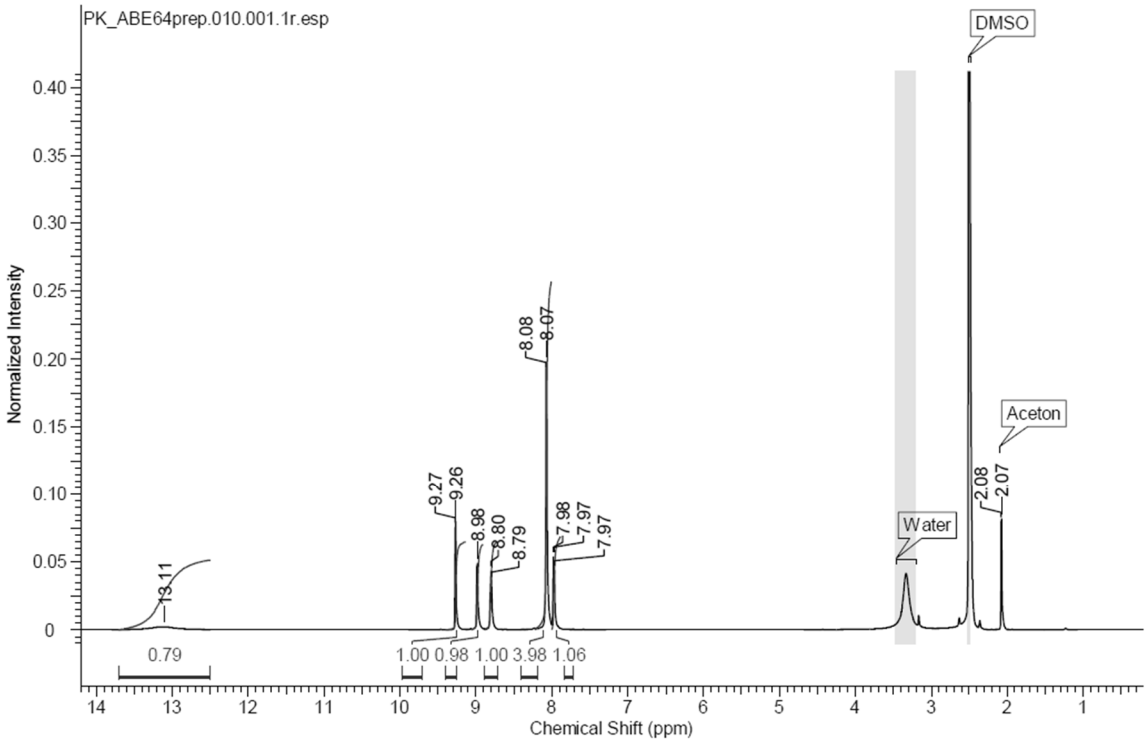

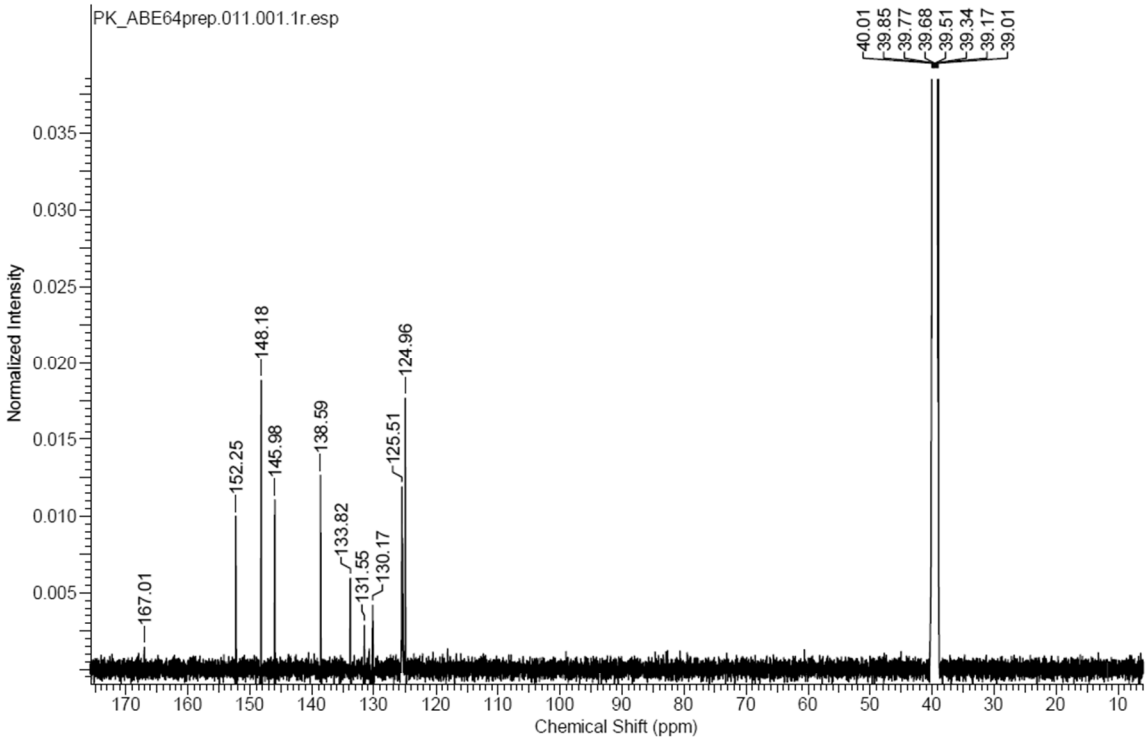

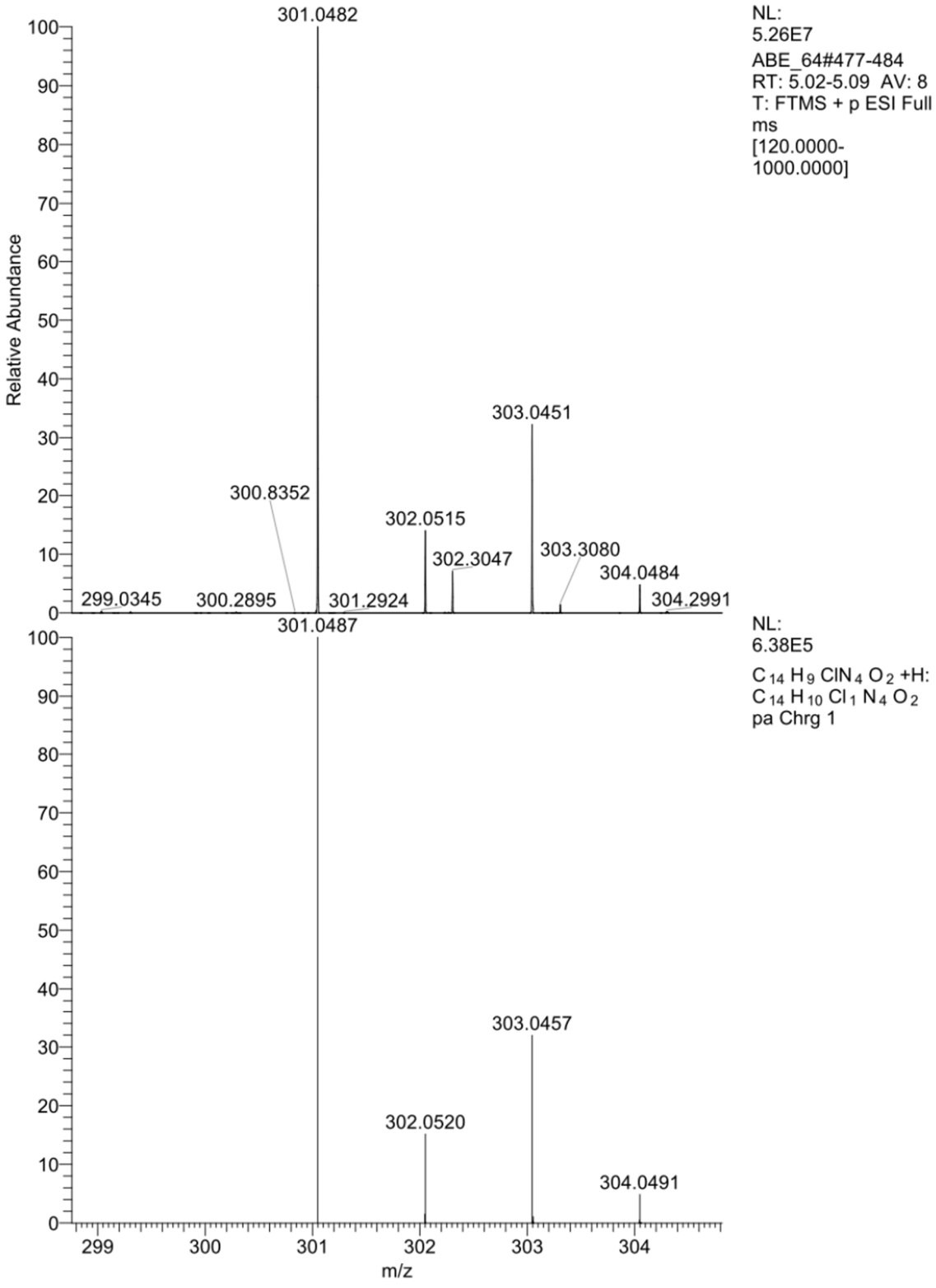
301.0482
NL:
5.26E7
ABE_64#477-484
RT: 5.02-5.09 AV: 8
T: FTMS + p ESI Full
ms
[120.0000-
1000.0000]
303.0451
300.8352
302.0515
303.3080
302.3047
304.0484
299.0345
300.2895
301.2924
304.2991
Relative Abundance
301.0487
NL:
6.38E5
C14 H9 ClN4 O2 +H:
C14 H10 Cl1 N4 O2
pa Chrg 1
303.0457
302.0520
304.0491
m/z

4-(1-(4-phenylpyridin-3-yl)-1*H*-1,2,3-triazol-4-yl)benzoic acid (19c):

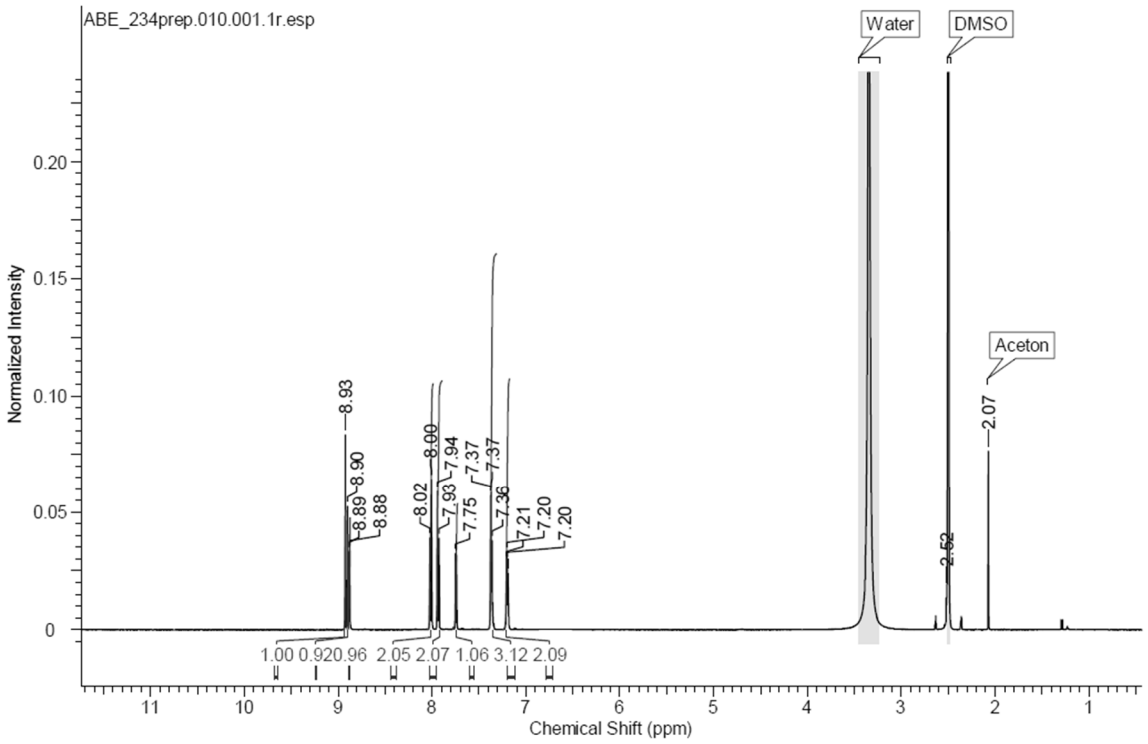

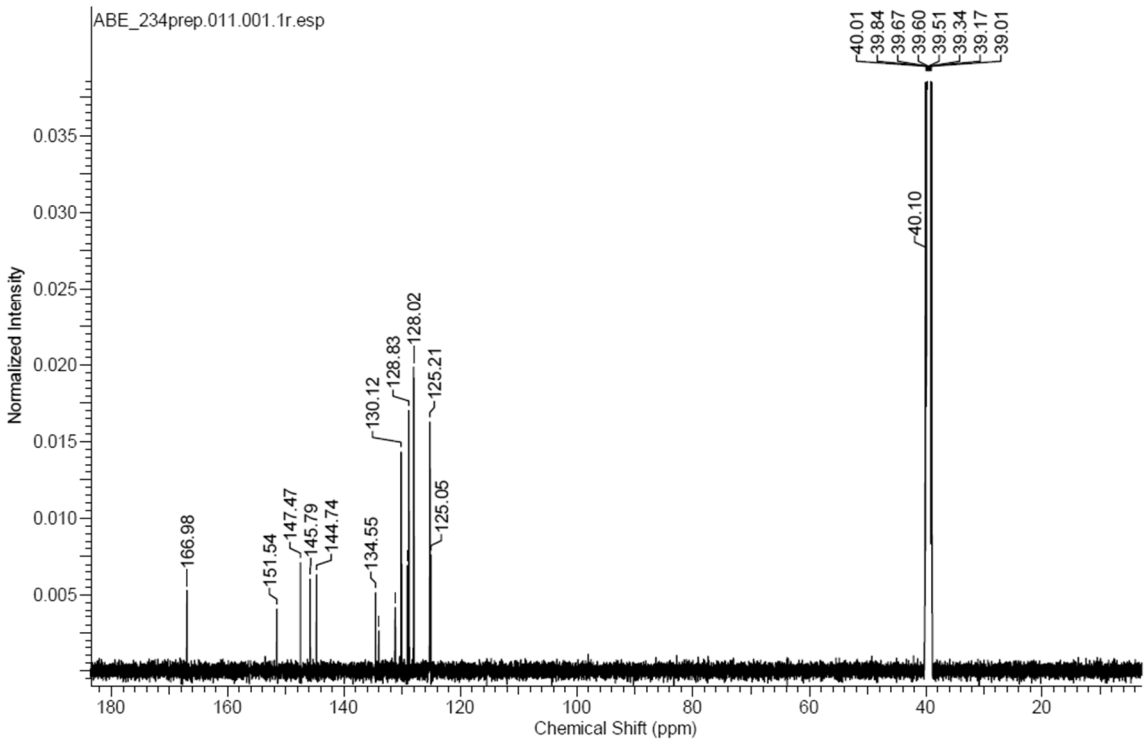

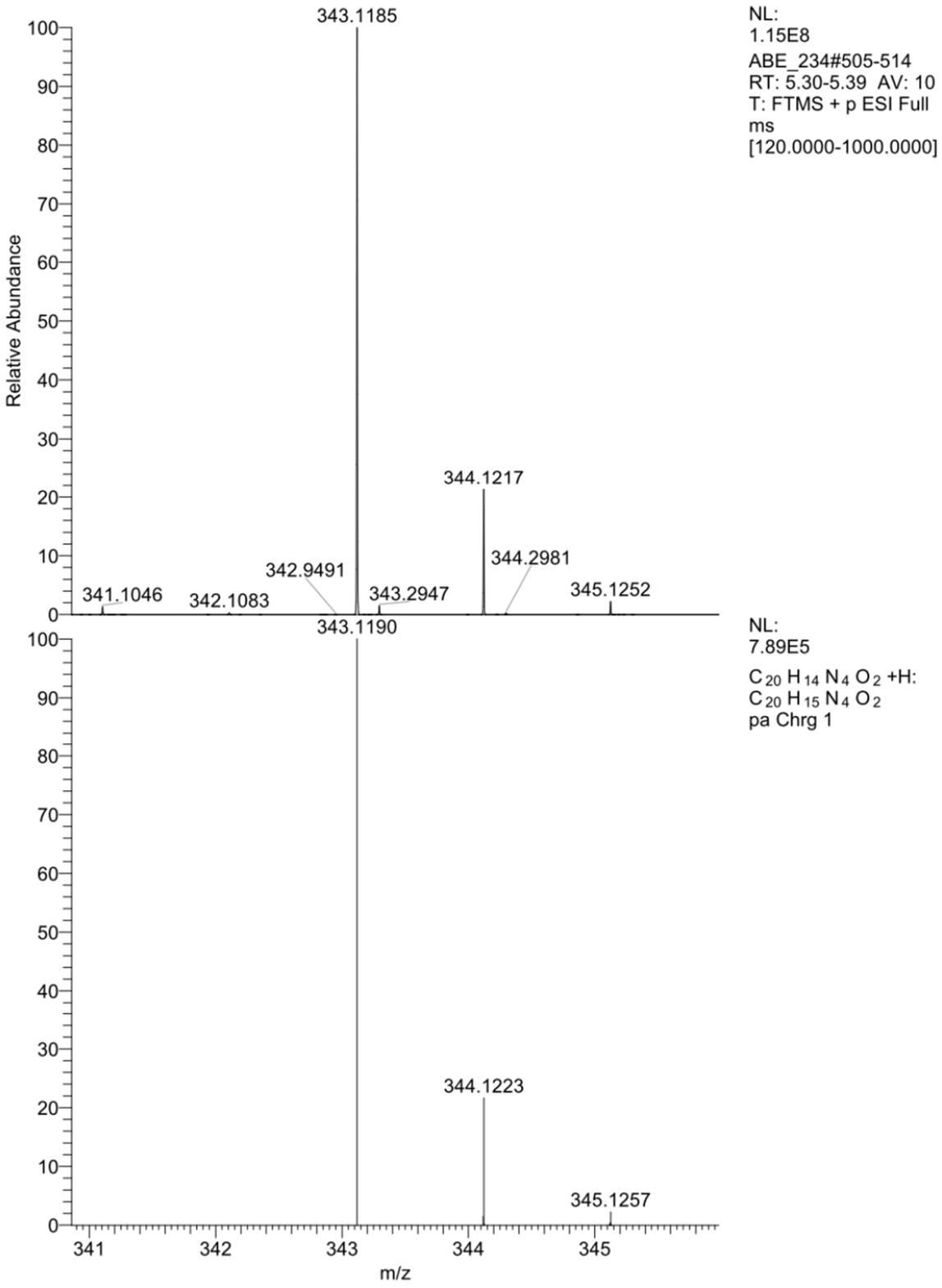
343.1185
NL:
1.15E8
ABE_234#505-514
RT: 5.30-5.39 AV: 10
T: FTMS + p ESI Full
ms
[120.0000-1000.0000]
344.1217
344.2981
342.9491
341.1046
342.1083
343.2947
345.1252
343.1190
NL:
7.89E5
C20 H14 N4 O2 +H:
C20 H15 N4 O2
pa Chrg 1
344.1223
345.1257
Relative Abundance
m/z
100
90
80
70
60
50
40
30
20
10
0
341
342
343
344
345

4-(1-(5-methylpyridin-3-yl)-1*H*-1,2,3-triazol-4-yl)benzoic acid (19d):

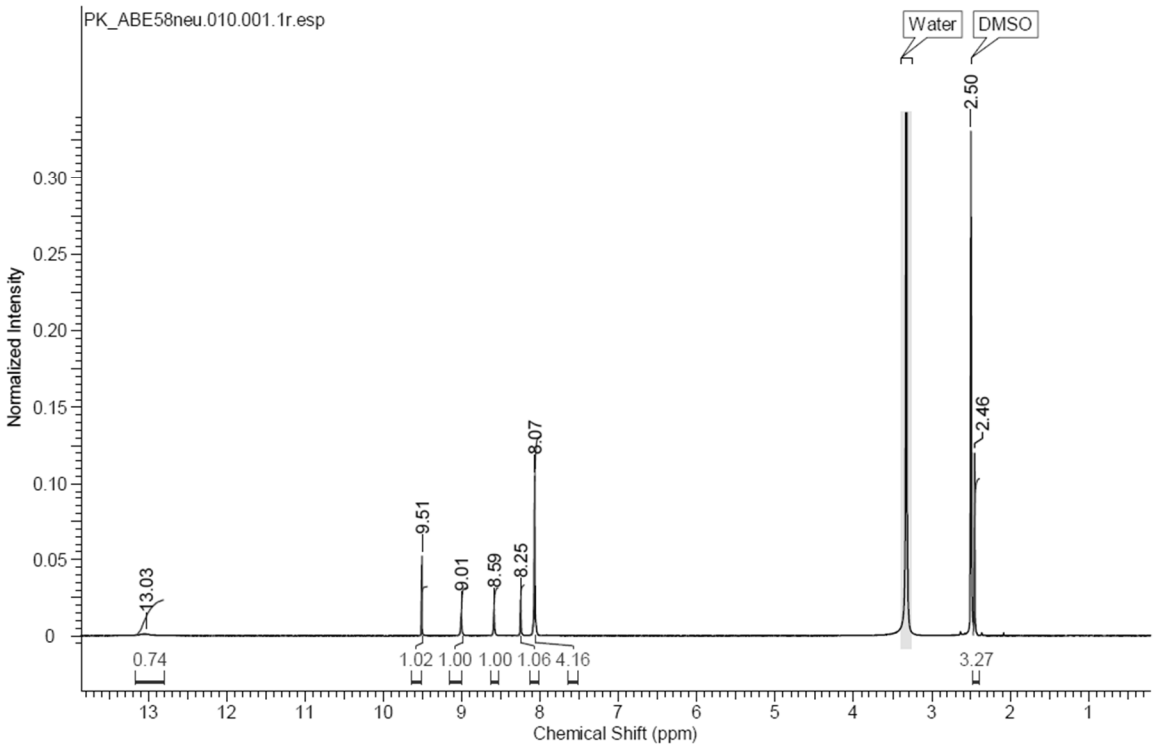

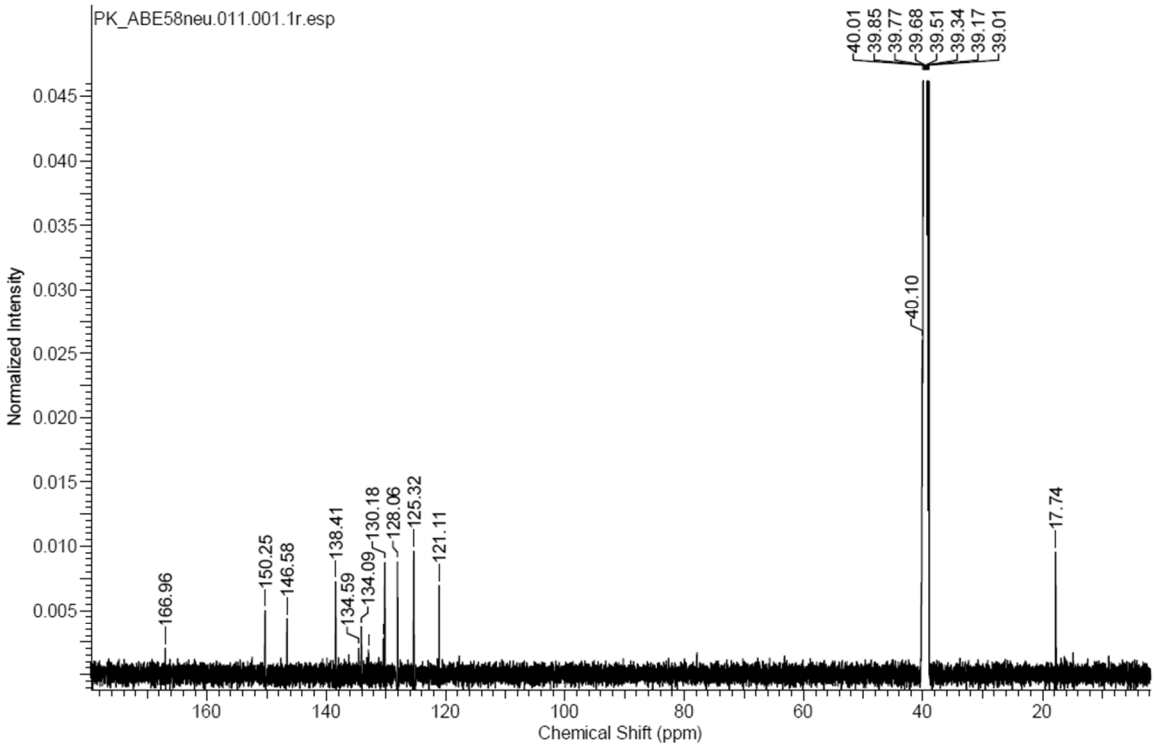

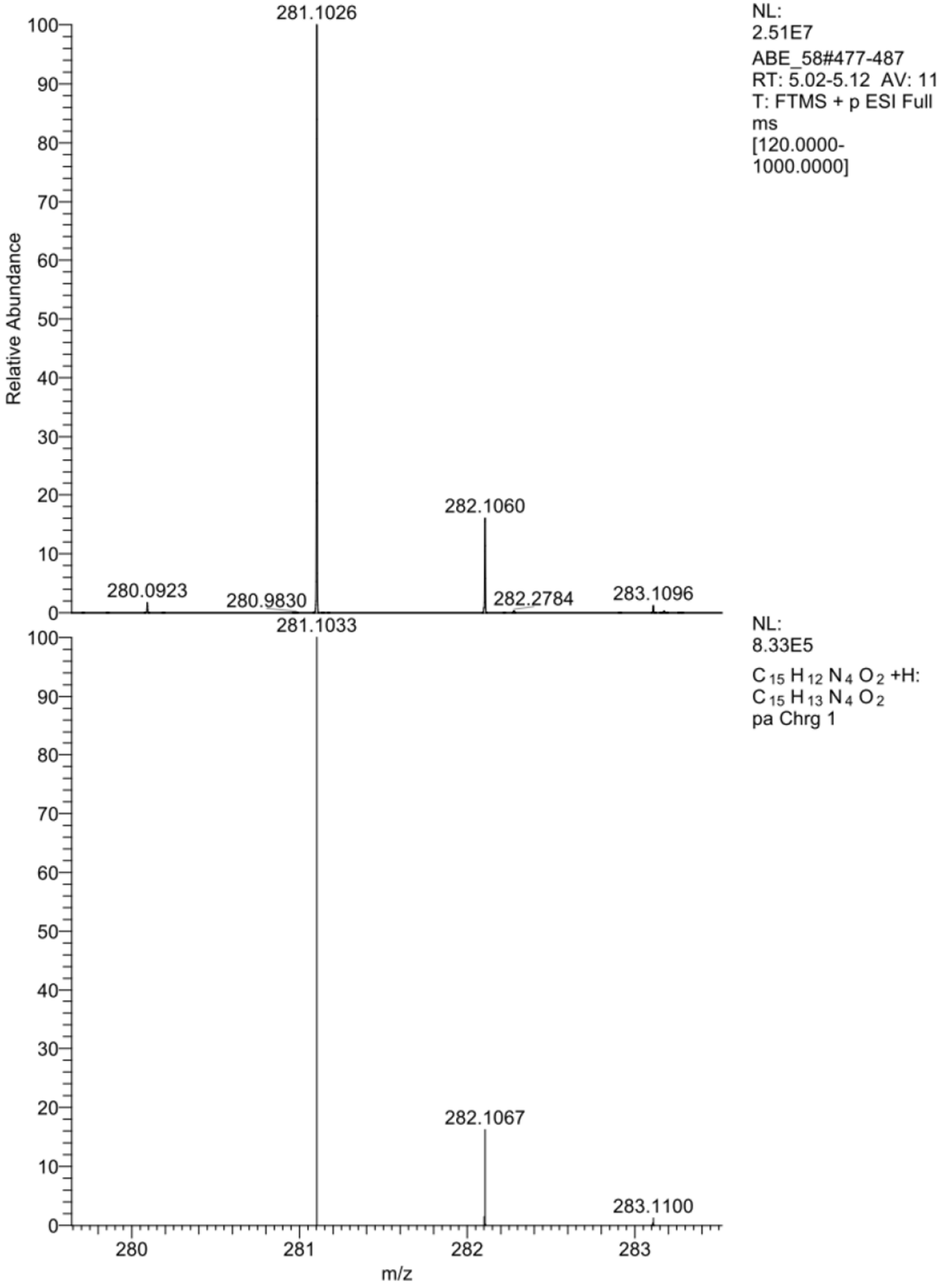
281.1026
NL:
2.51E7
ABE_58#477-487
RT: 5.02-5.12 AV: 11
T: FTMS + p ESI Full
ms
[120.0000-
1000.0000]
282.1060
280.0923
280.9830
282.2784
283.1096
Relative Abundance
281.1033
NL:
8.33E5
C15 H12 N4 O2 +H:
C15 H13 N4 O2
pa Chrg 1
282.1067
283.1100
m/z

4-(1-(6-cyanopyridin-3-yl)-1*H*-1,2,3-triazol-4-yl)benzoic acid (19e):

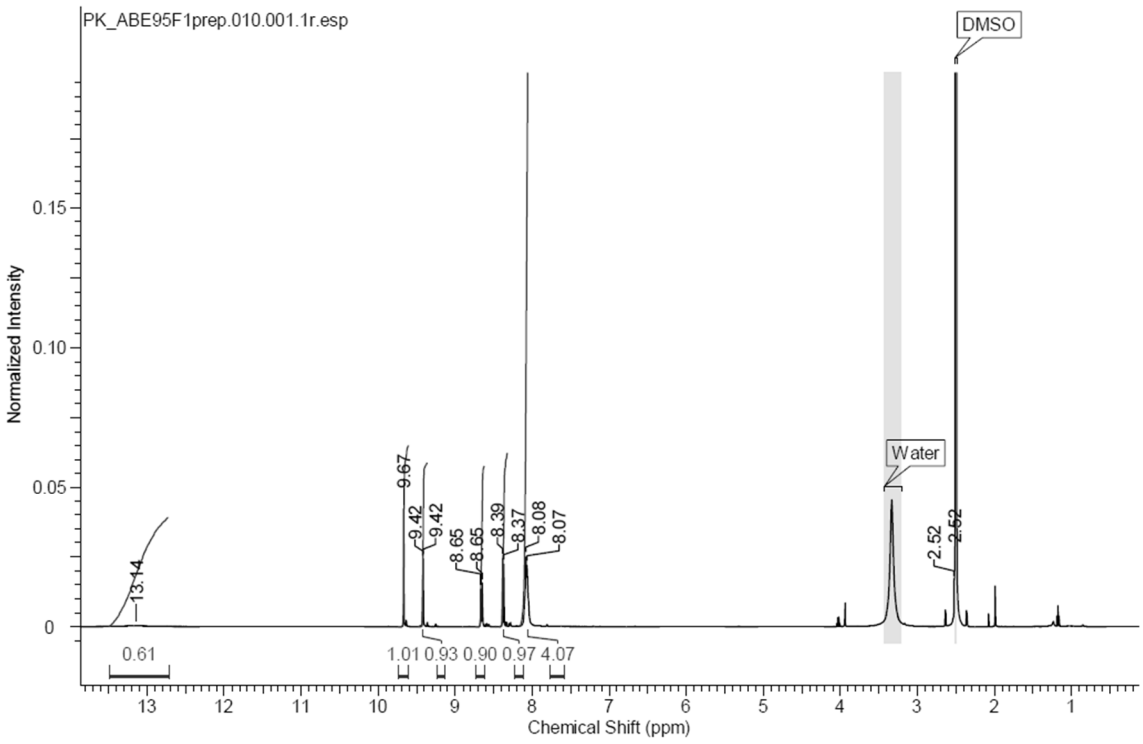

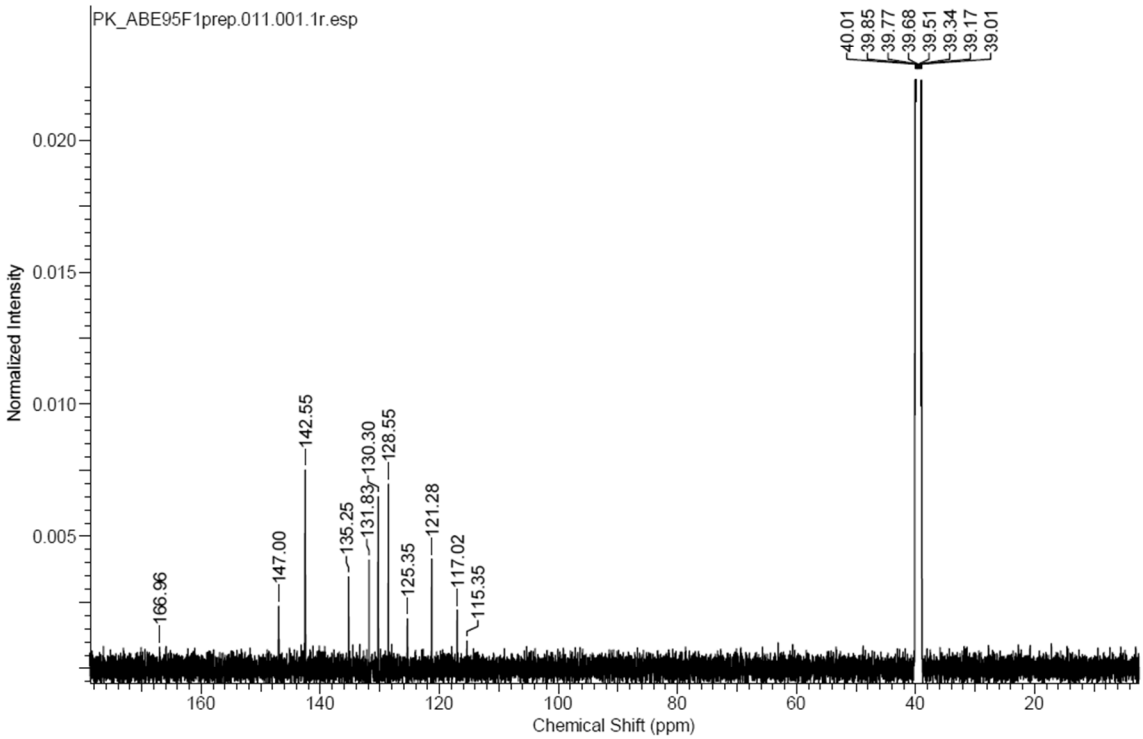

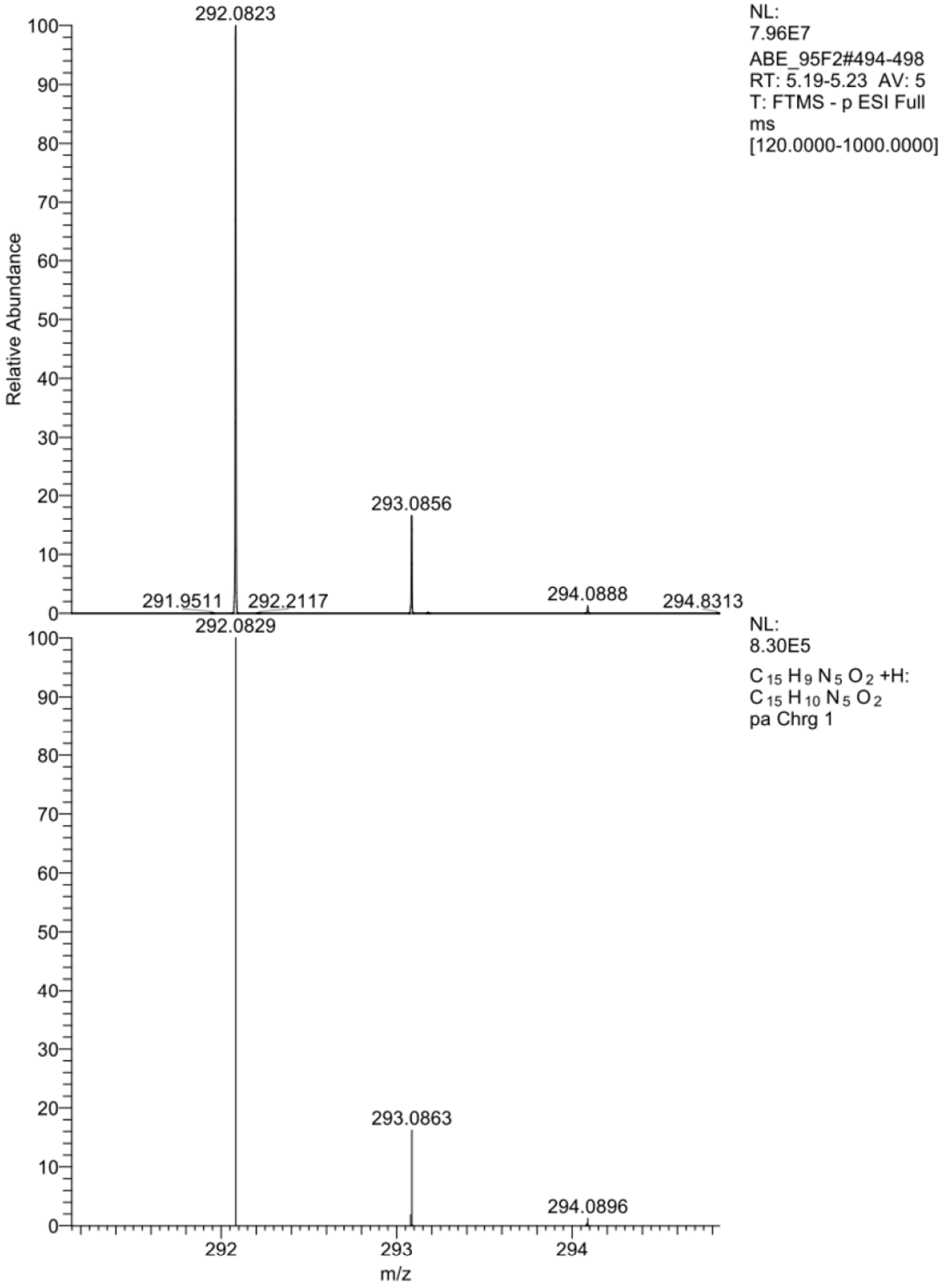
292.0823
NL:
7.96E7
ABE_95F2#494-498
RT: 5.19-5.23 AV: 5
T: FTMS - p ESI Full
ms
[120.0000-1000.0000]
Relative Abundance
293.0856
291.9511
292.2117
294.0888
294.8313
292.0829
NL:
8.30E5
C15 H9 N5 O2 +H:
C15 H10 N5 O2
pa Chrg 1
293.0863
294.0896
292
293
294
m/z

4-(1-(6-chloro-4-methylpyridin-3-yl)-1*H*-1,2,3-triazol-4-yl)benzoic acid (19f):

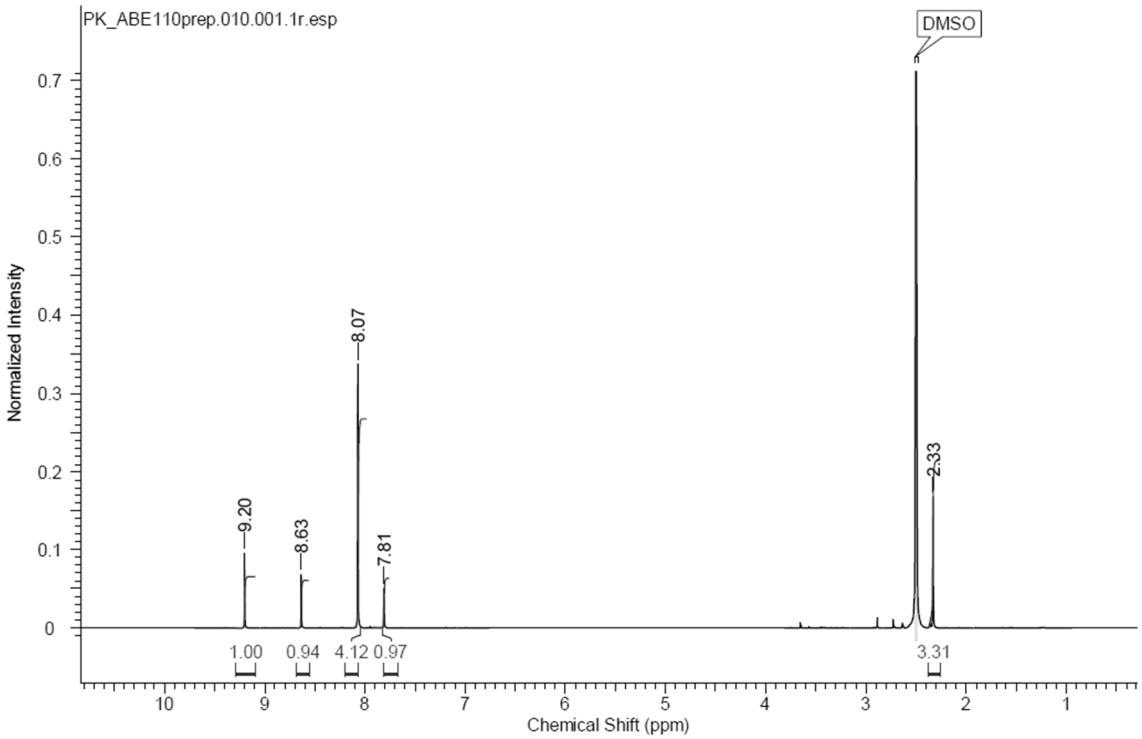

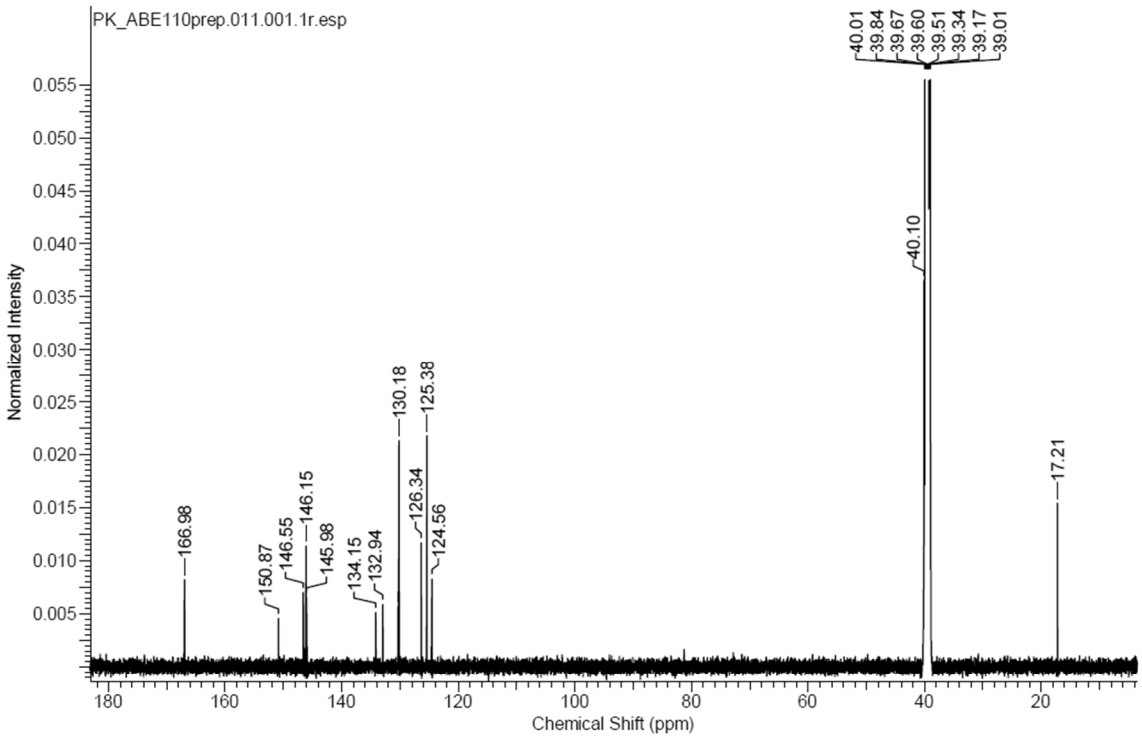

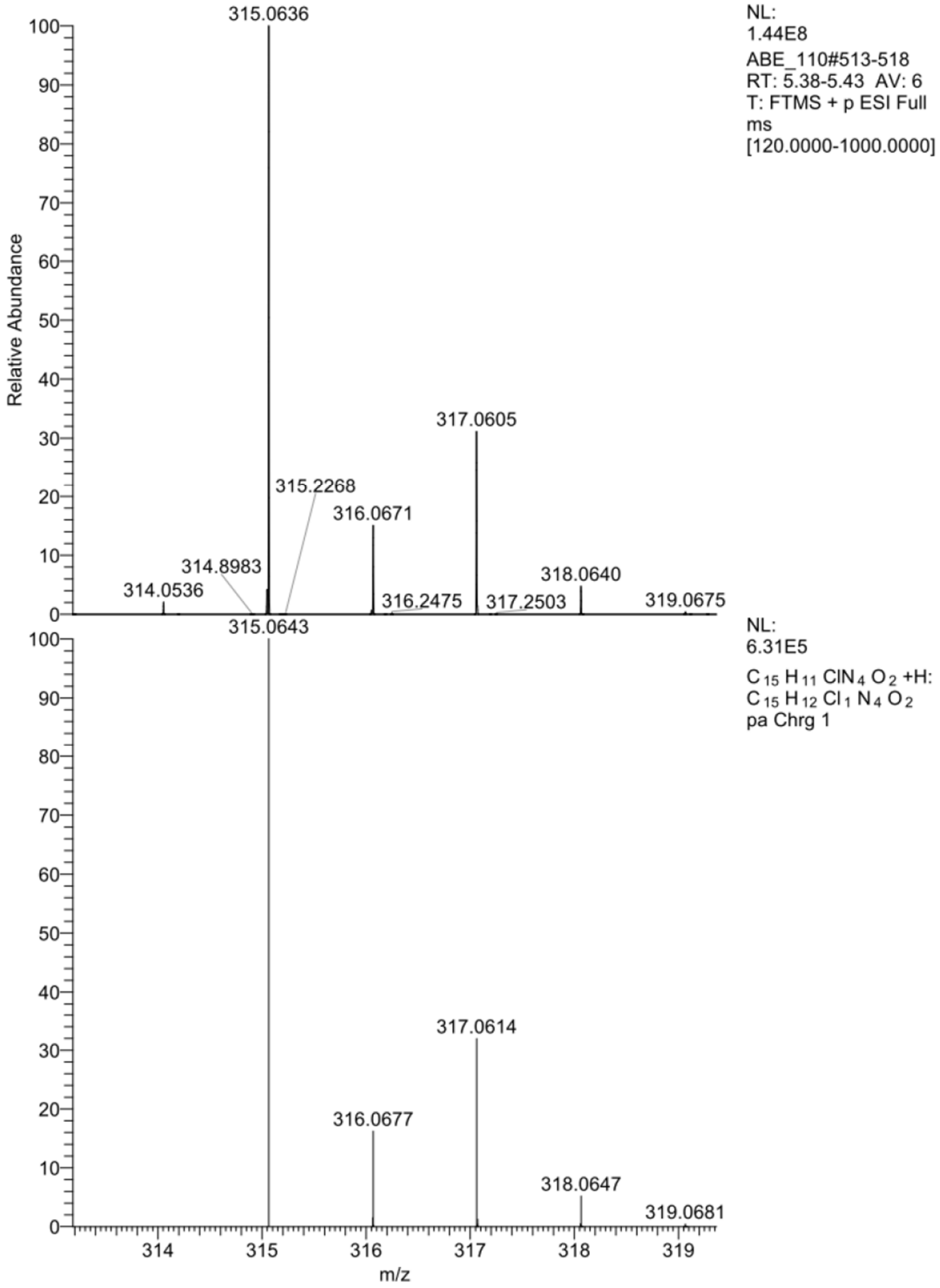
315.0636
NL:
1.44E8
ABE_110#513-518
RT: 5.38-5.43 AV: 6
T: FTMS + p ESI Full
ms
[120.0000-1000.0000]
317.0605
315.2268
316.0671
314.8983
314.0536
318.0640
316.2475
317.2503
319.0675
315.0643
NL:
6.31E5
C 15 H 11 ClN 4 O 2 +H:
C 15 H 12 Cl 1 N 4 O 2
pa Chrg 1
317.0614
316.0677
318.0647
319.0681
Relative Abundance
m/z
100
90
80
70
60
50
40
30
20
10
0
314
315
316
317
318
319

4-(1-(6-(methylamino)pyridin-3-yl)-1*H*-1,2,3-triazol-4-yl)benzoic acid (19g):

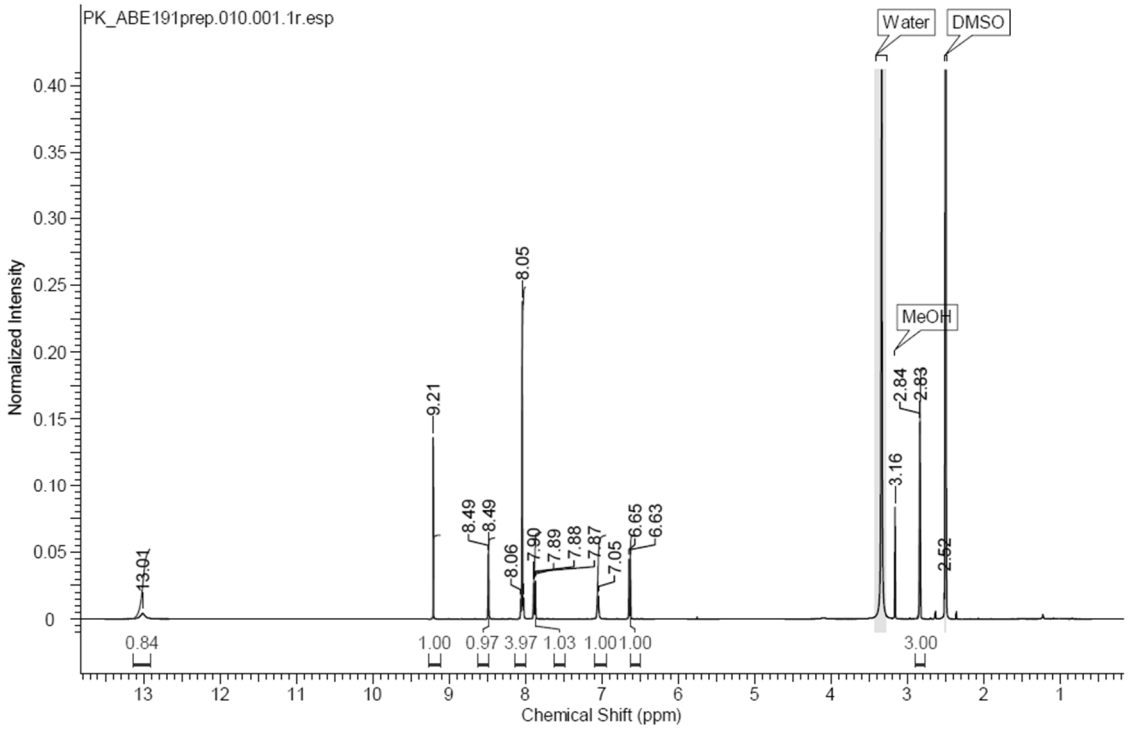

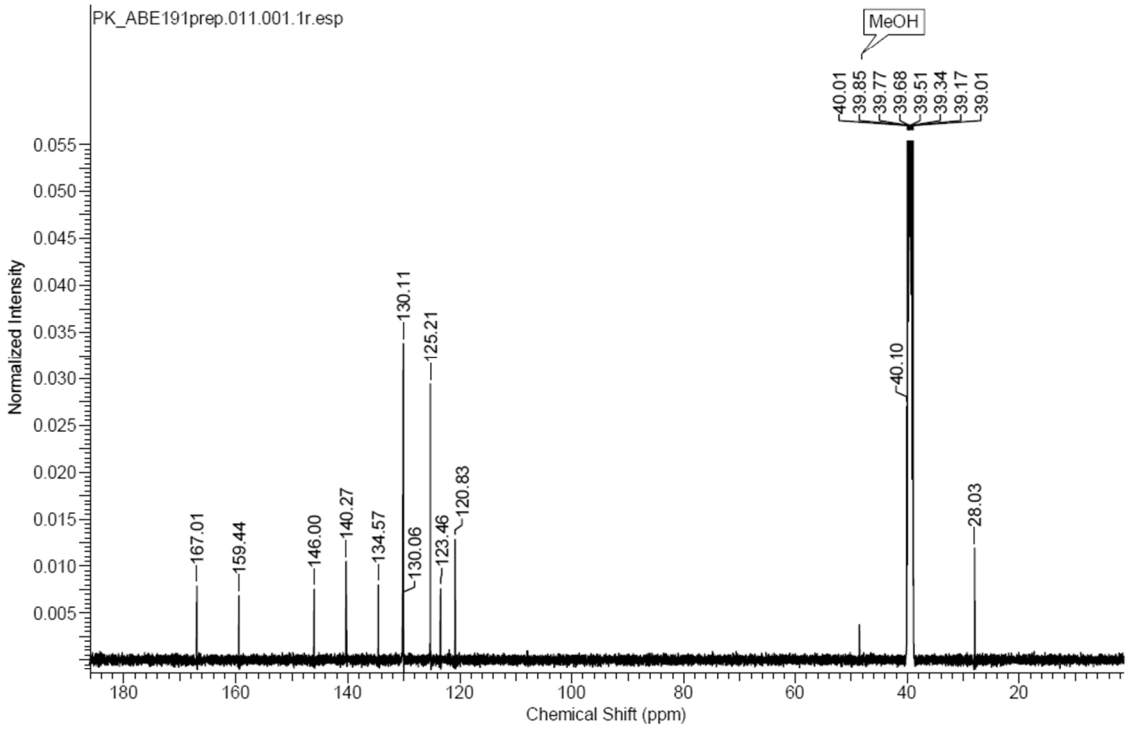

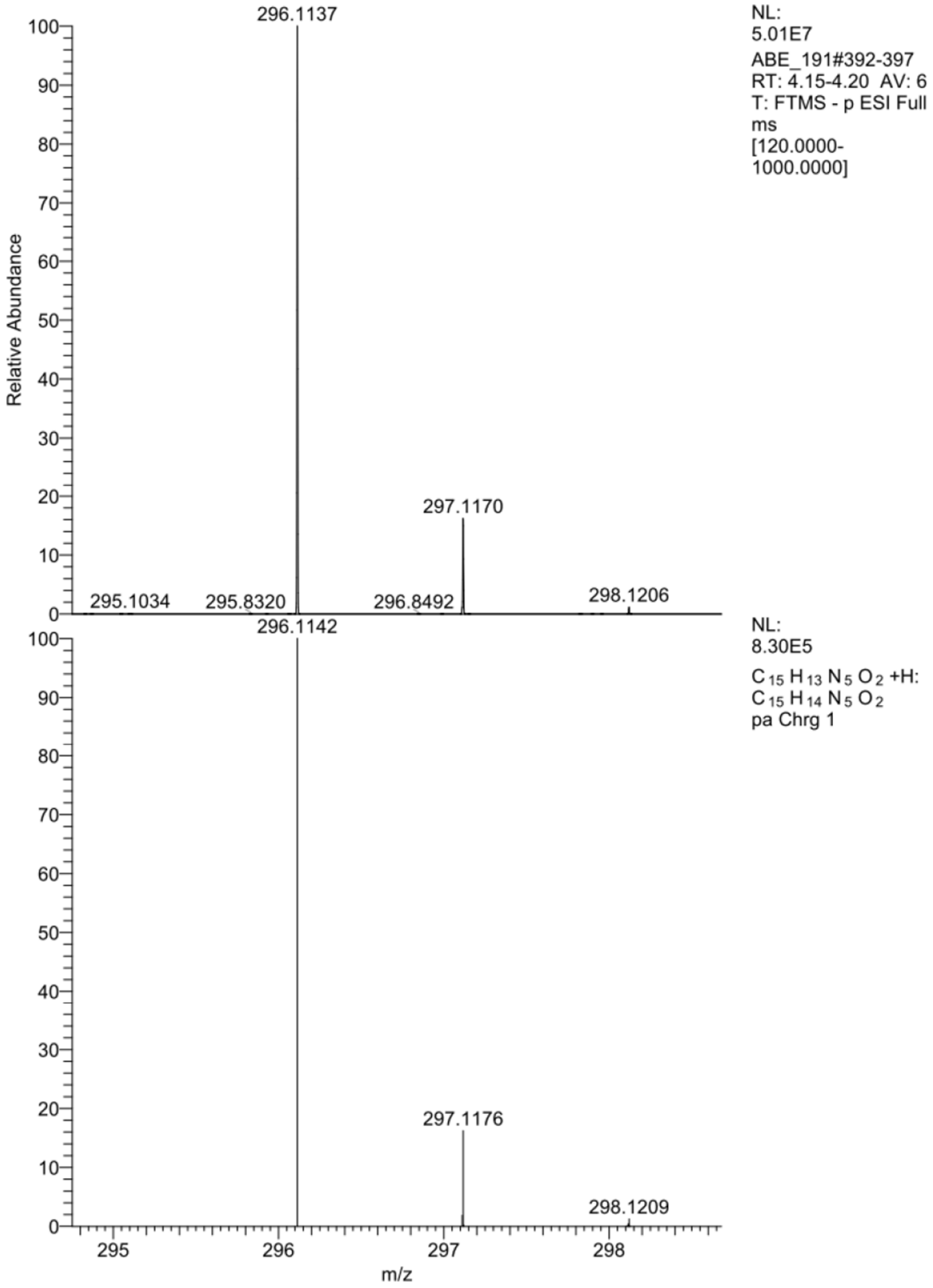
296.1137
NL:
5.01E7
ABE_191#392-397
RT: 4.15-4.20 AV: 6
T: FTMS - p ESI Full
ms
[120.0000-
1000.0000]
297.1170
295.1034
295.8320
296.8492
298.1206
Relative Abundance
296.1142
NL:
8.30E5
C15 H13 N5 O2 +H:
C15 H14 N5 O2
pa Chrg 1
297.1176
298.1209
295
296
297
298
m/z

4-(1-(6-(isopropylamino)pyridin-3-yl)-1*H*-1,2,3-triazol-4-yl)benzoic acid (19h):

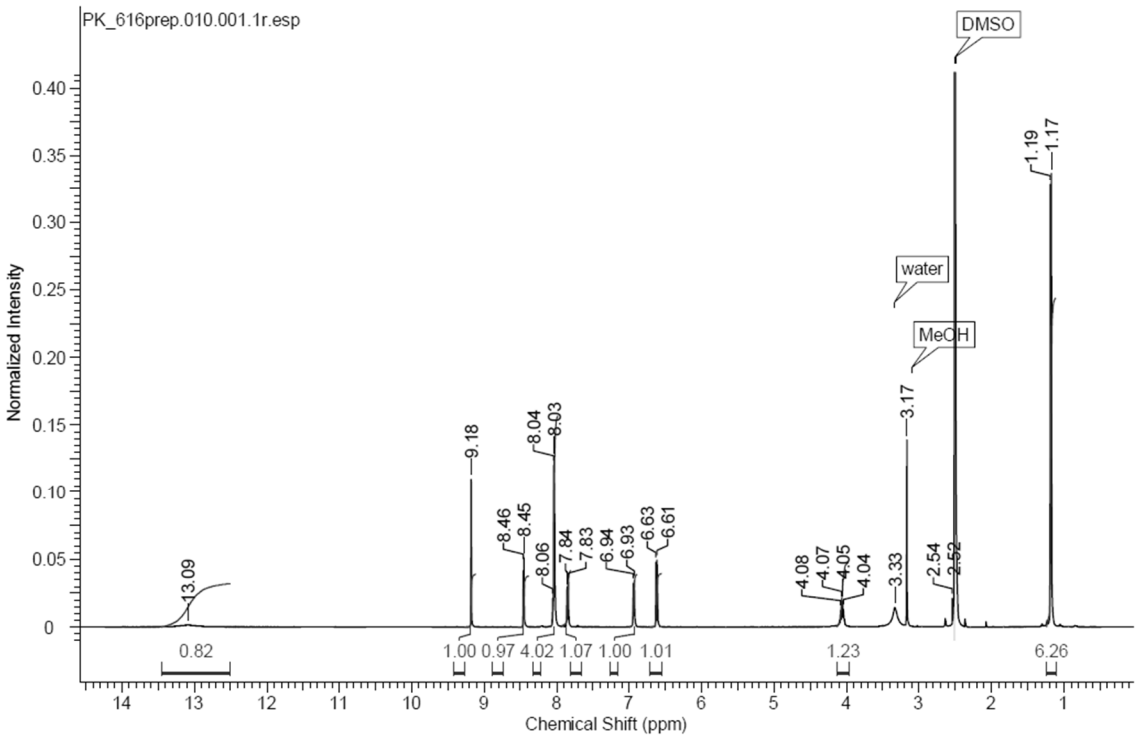

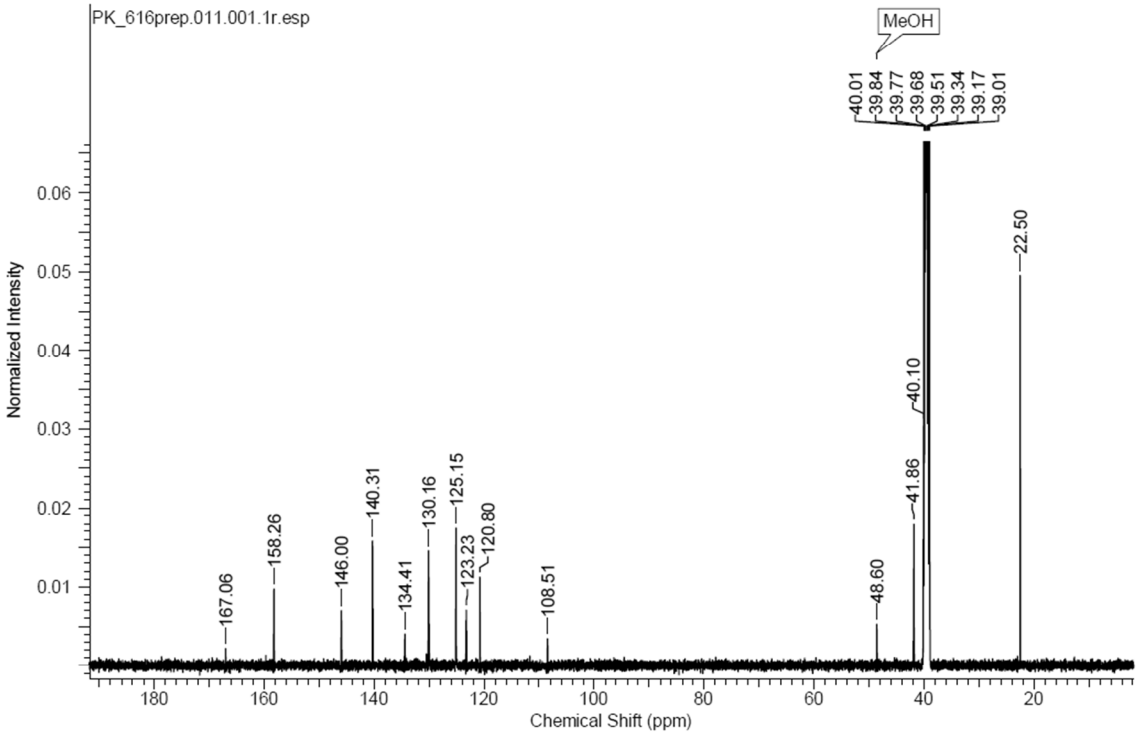

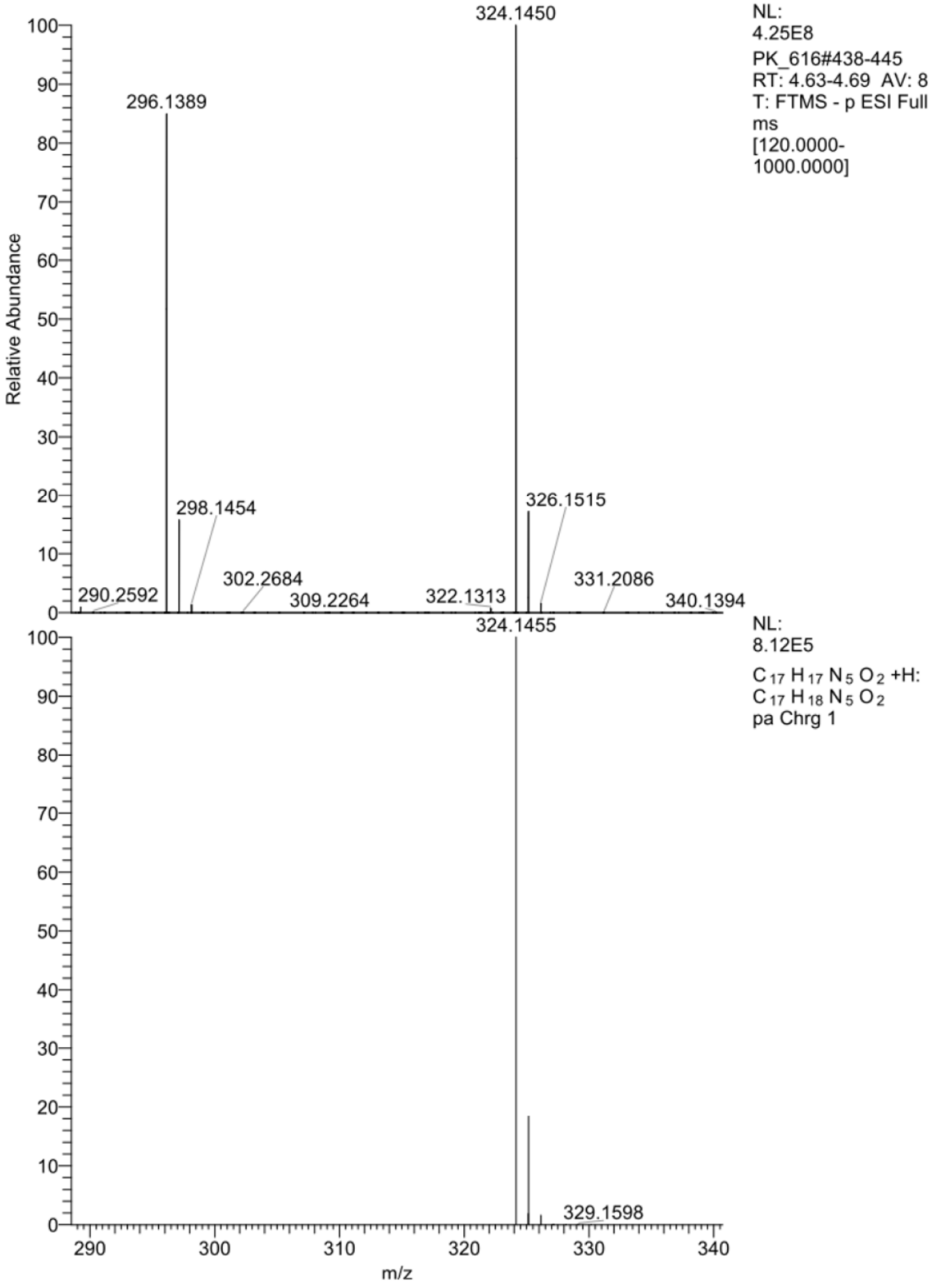
324.1450
NL:
4.25E8
PK_616#438-445
RT: 4.63-4.69 AV: 8
T: FTMS - p ESI Full
ms
[120.0000-
1000.0000]
296.1389
298.1454
326.1515
302.2684
331.2086
290.2592
309.2264
322.1313
340.1394
Relative Abundance
324.1455
NL:
8.12E5
C17 H17 N5 O2 +H:
C17 H18 N5 O2
pa Chrg 1
329.1598
m/z

4-(1-(6-(phenylamino)pyridin-3-yl)-1*H*-1,2,3-triazol-4-yl)benzoic acid (19i):

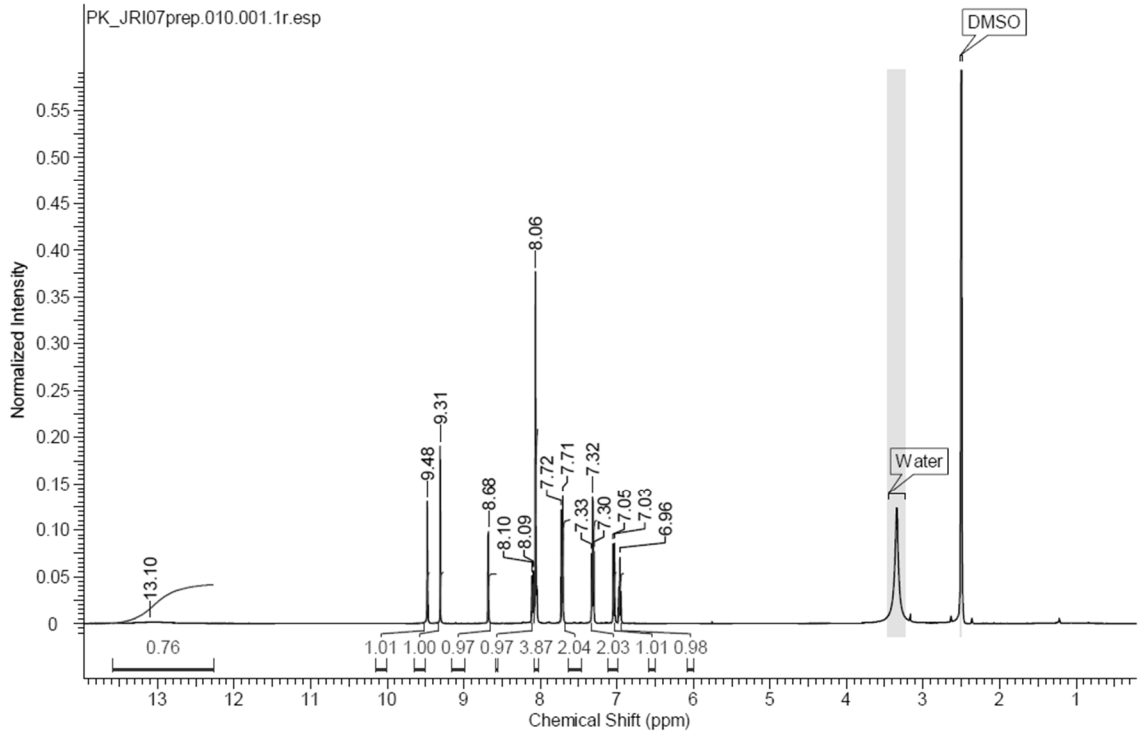

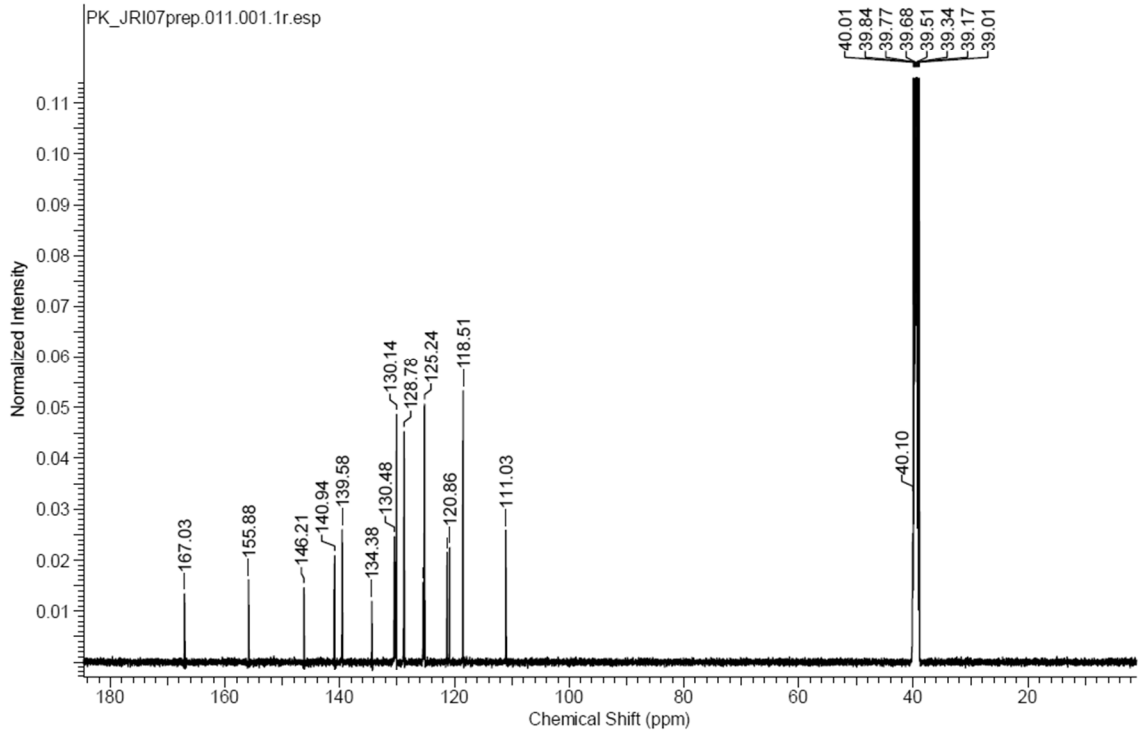

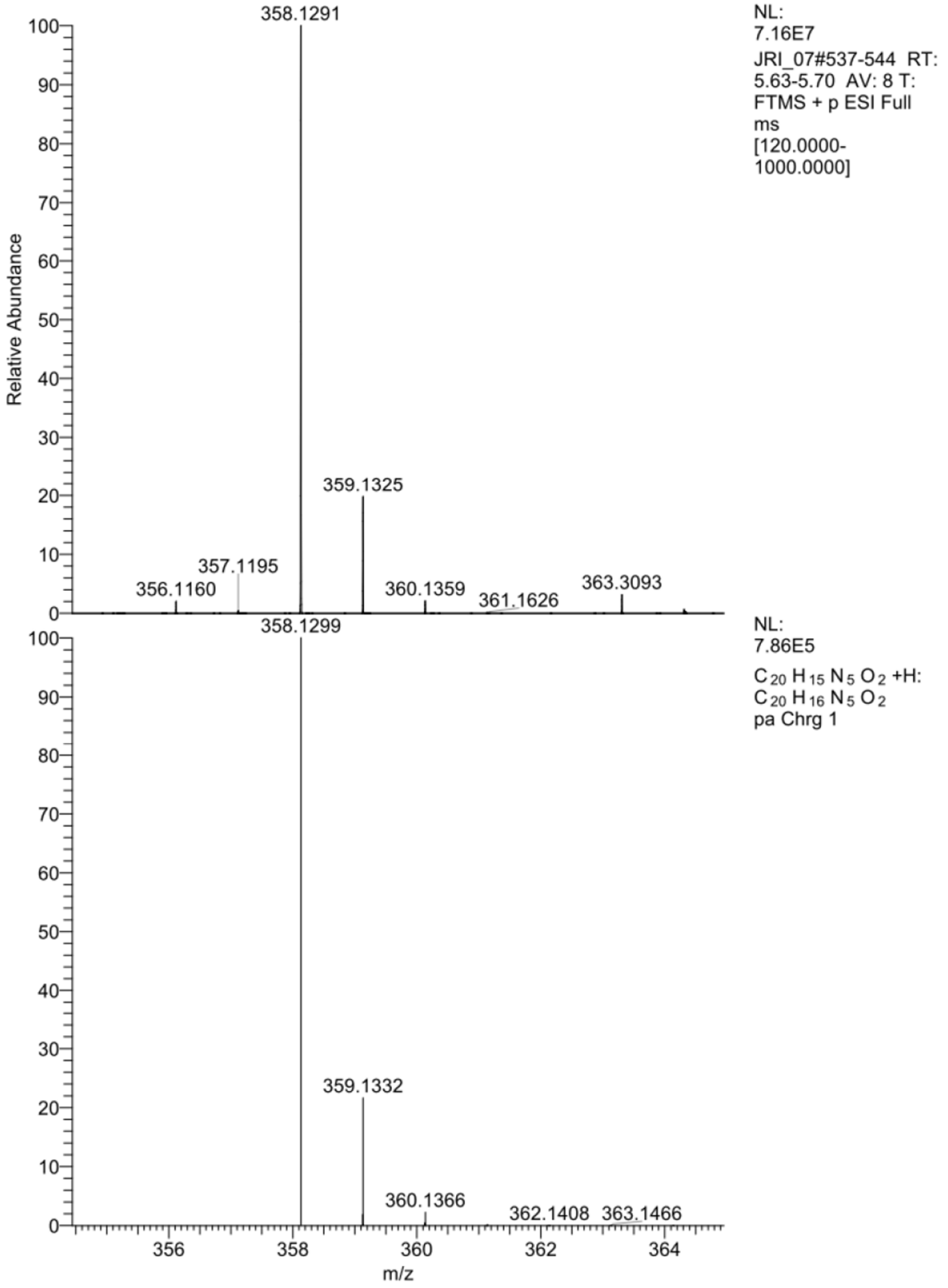
358.1291
NL:
7.16E7
JRI_07#537-544 RT:
5.63-5.70 AV: 8 T:
FTMS + p ESI Full
ms
[120.0000-
1000.0000]
359.1325
357.1195
356.1160
360.1359
361.1626
363.3093
Relative Abundance
358.1299
NL:
7.86E5
C20 H15 N5 O2 +H:
C20 H16 N5 O2
pa Chrg 1
359.1332
360.1366
362.1408
363.1466
356
358
360
362
364
m/z

4-(1-(5-fluoropyridin-3-yl)-1*H*-1,2,3-triazol-4-yl)benzoic acid (19j):

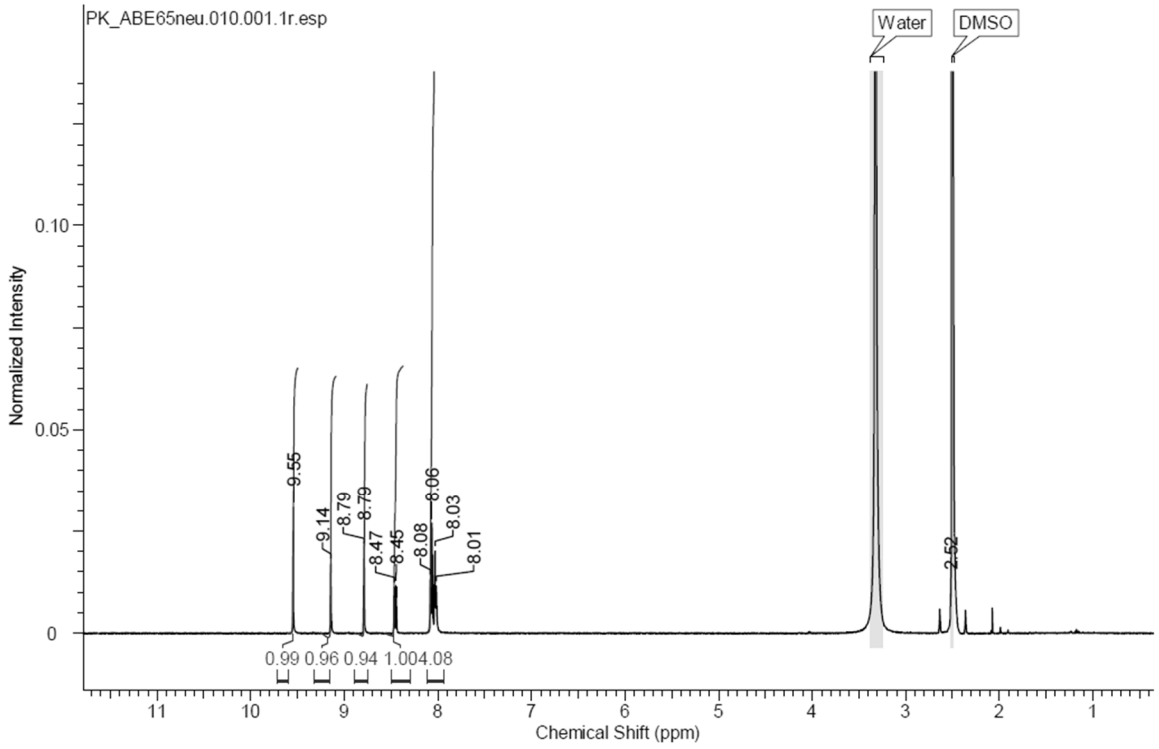

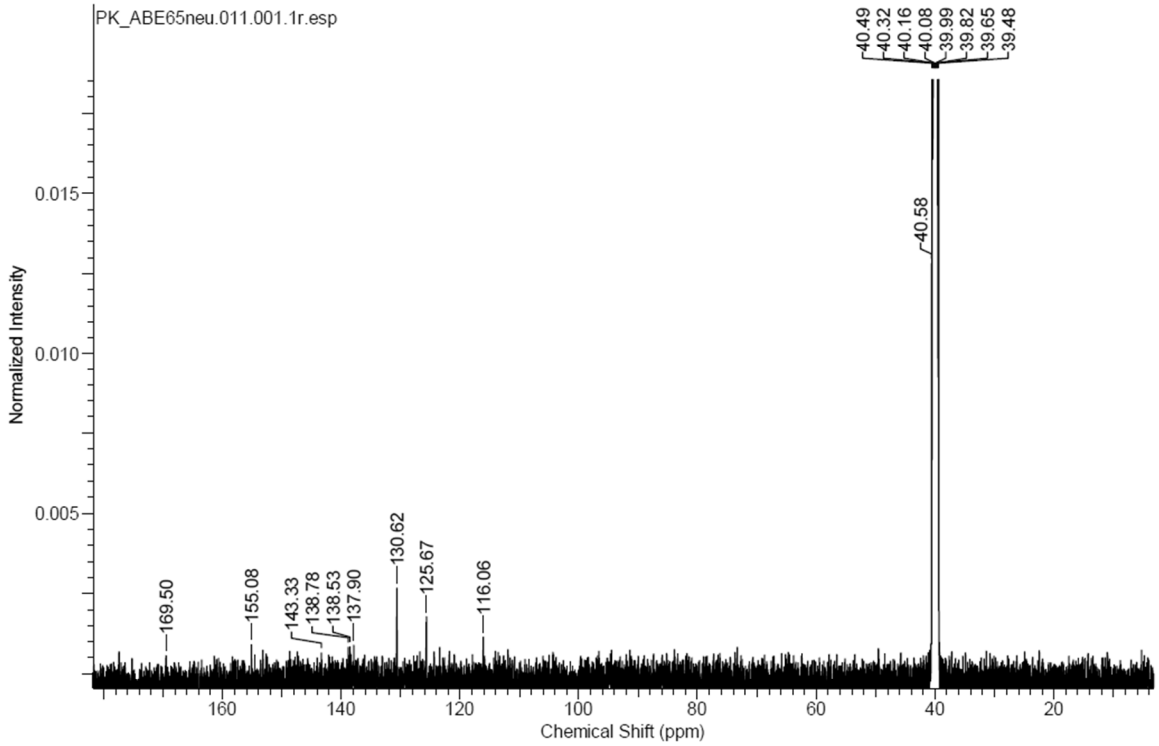

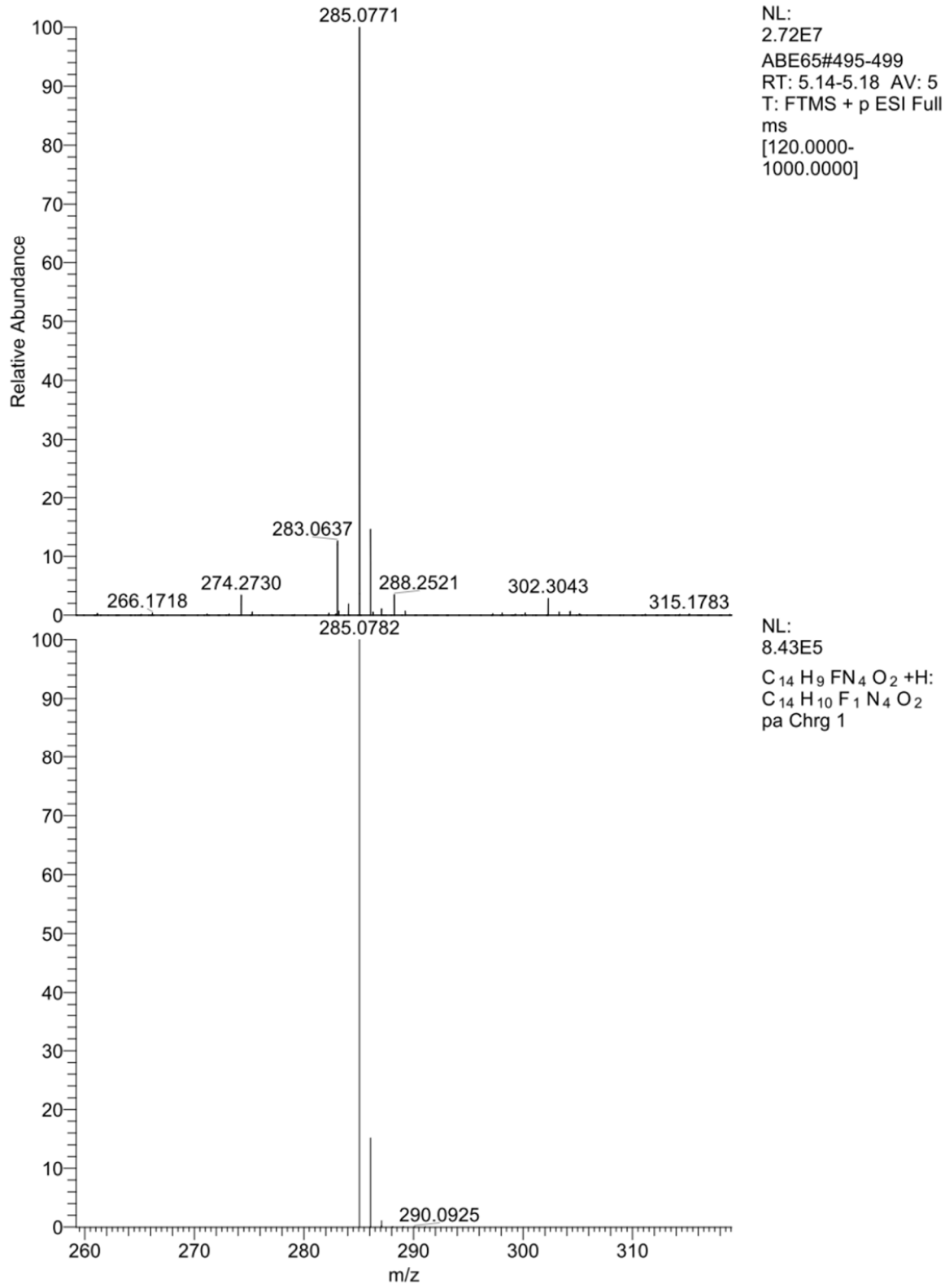
285.0771
NL:
2.72E7
ABE65#495-499
RT: 5.14-5.18 AV: 5
T: FTMS + p ESI Full
ms
[120.0000-
1000.0000]
Relative Abundance
283.0637
274.2730
288.2521
302.3043
266.1718
315.1783
285.0782
NL:
8.43E5
C14 H9 FN4 O2 +H:
C14 H10 F1 N4 O2
pa Chrg 1
290.0925
m/z

4-(1-(6-methoxypyridin-3-yl)-1*H*-1,2,3-triazol-4-yl)benzoic acid (19k):

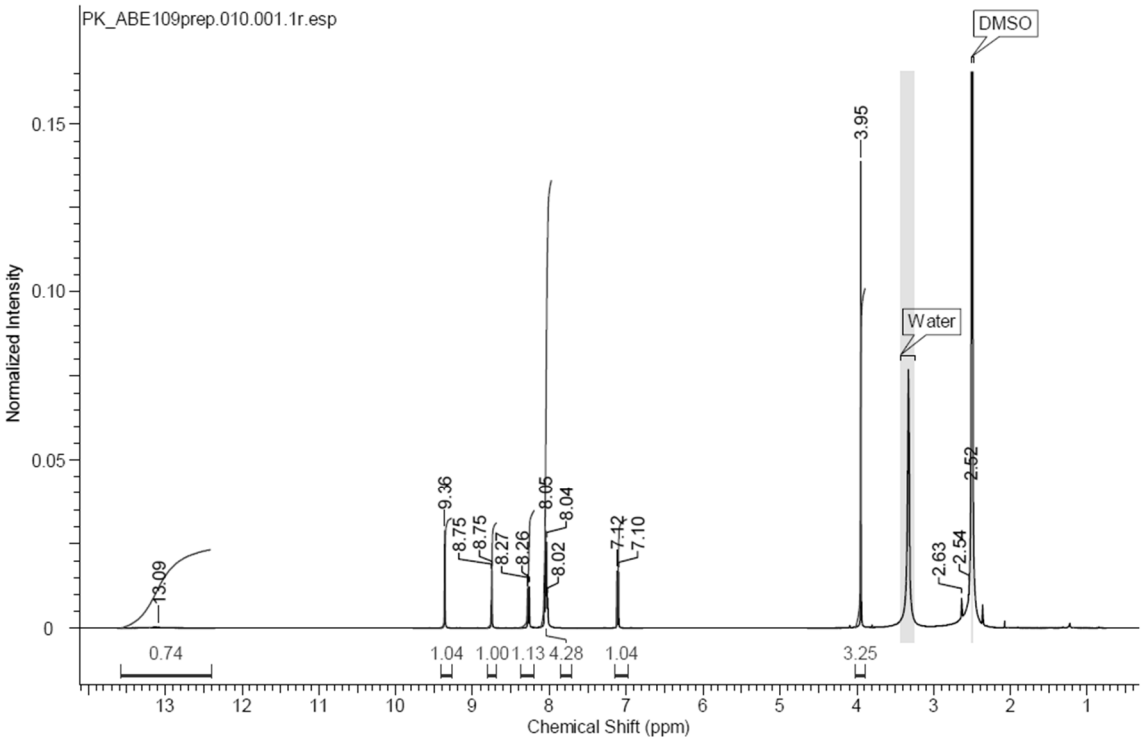

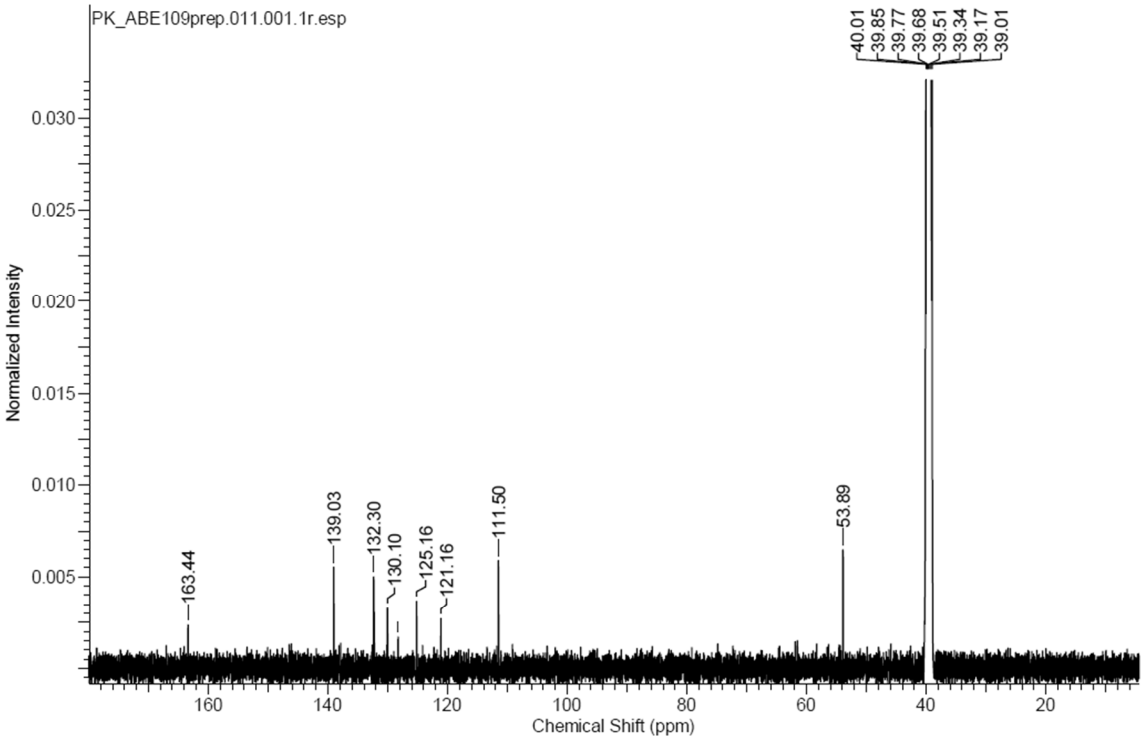

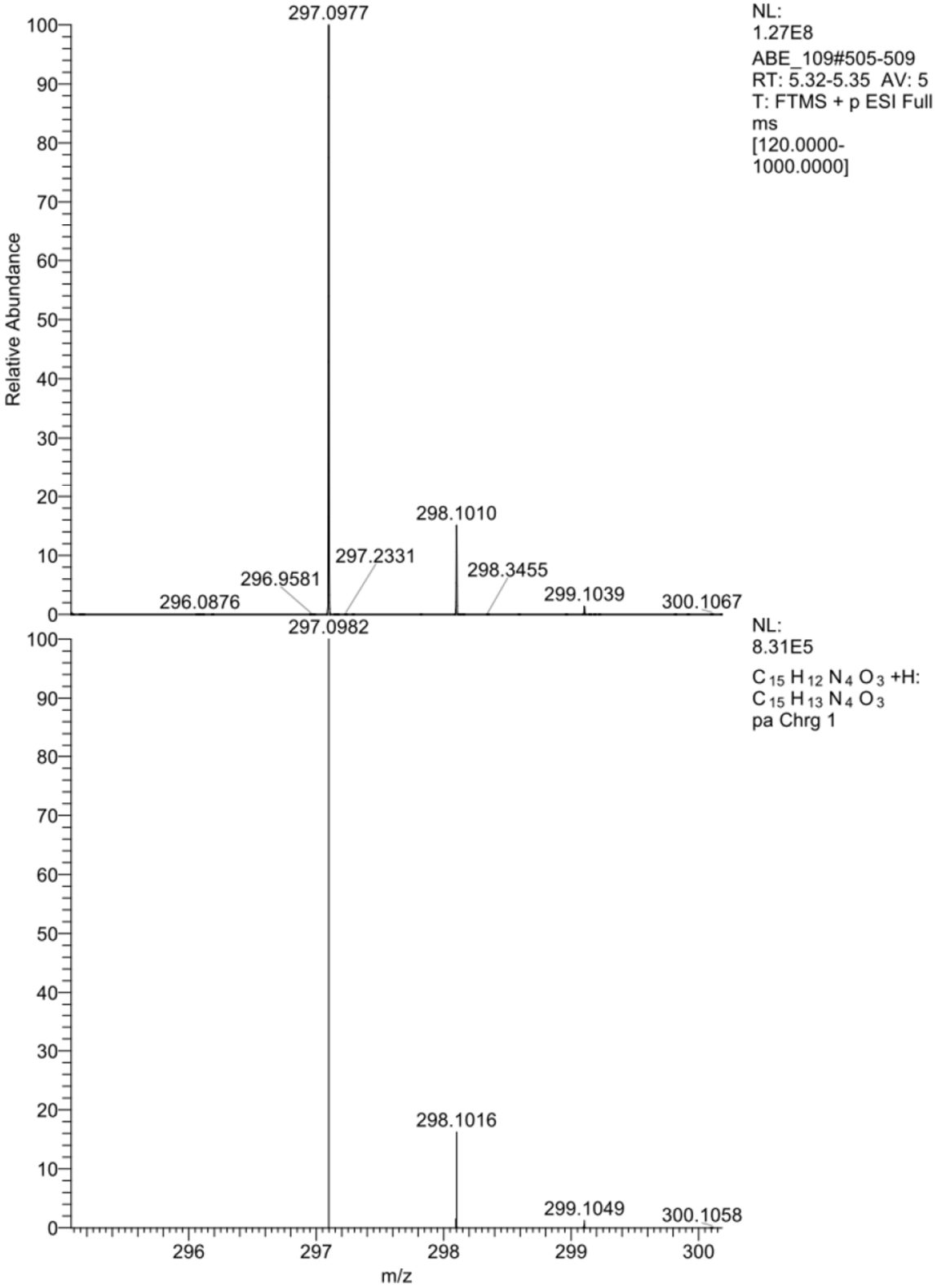
297.0977
NL:
1.27E8
ABE_109#505-509
RT: 5.32-5.35 AV: 5
T: FTMS + p ESI Full
ms
[120.0000-
1000.0000]
Relative Abundance
298.1010
297.2331
296.9581
298.3455
299.1039
296.0876
300.1067
297.0982
NL:
8.31E5
C15 H12 N4 O3 +H:
C15 H13 N4 O3
pa Chrg 1
298.1016
299.1049
300.1058
296
297
298
299
300
m/z

4-(1-(6-phenoxypyridin-3-yl)-1*H*-1,2,3-triazol-4-yl)benzoic acid (19l):

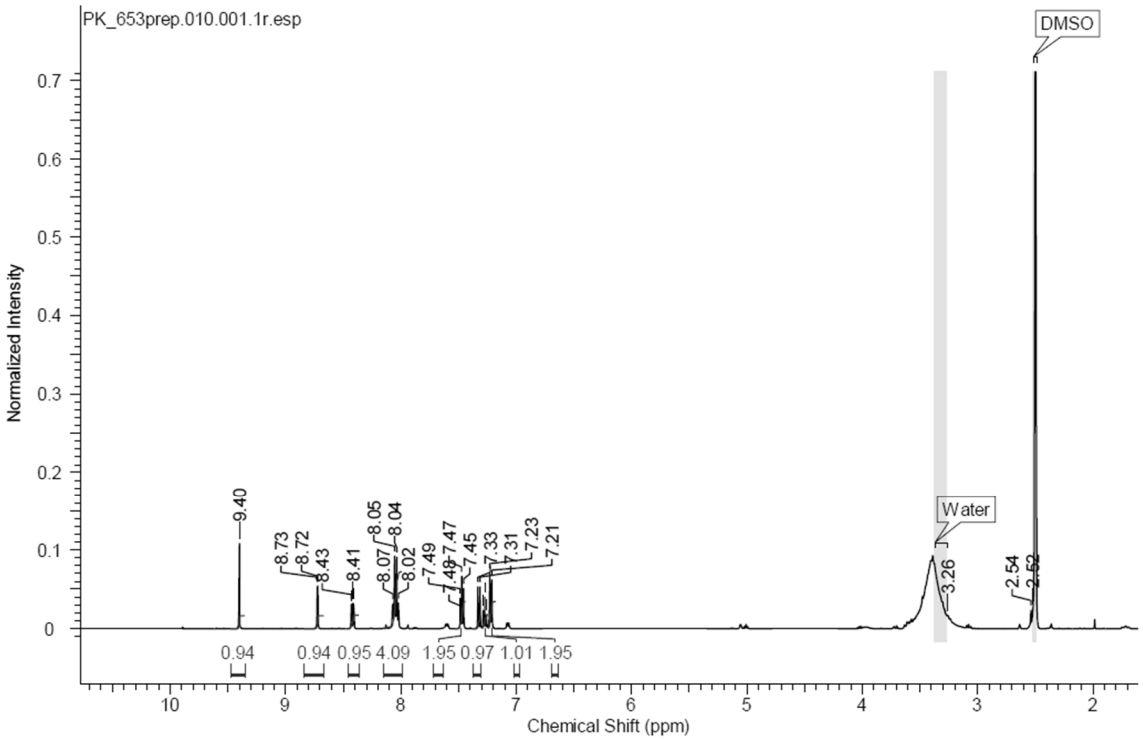

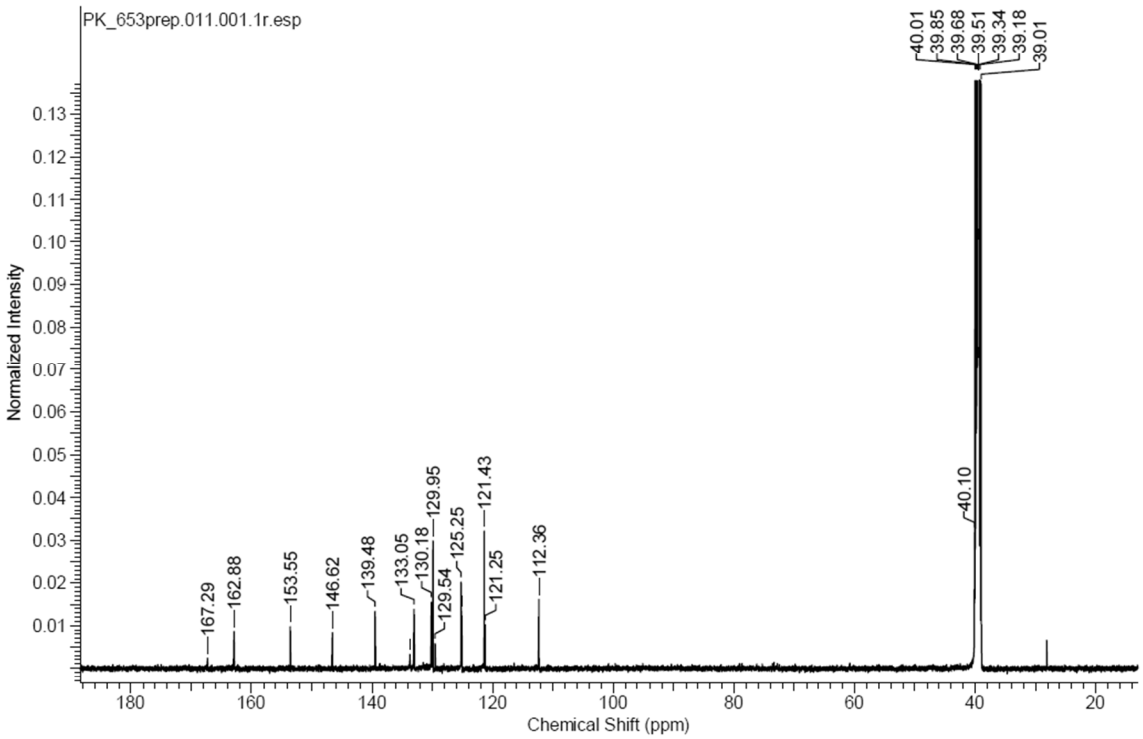

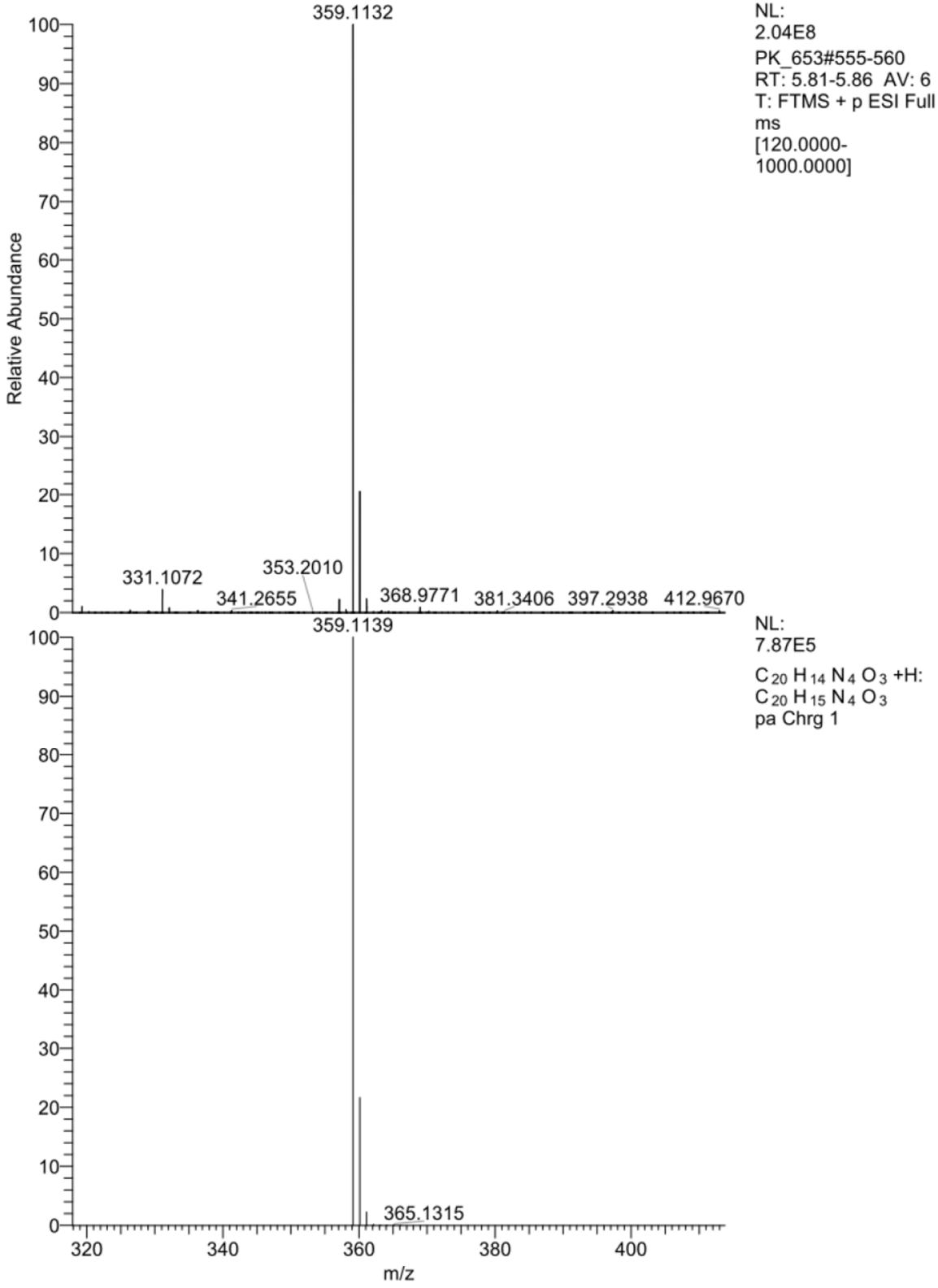
359.1132
NL:
2.04E8
PK_653#555-560
RT: 5.81-5.86 AV: 6
T: FTMS + p ESI Full
ms
[120.0000-
1000.0000]
Relative Abundance
331.1072
353.2010
341.2655
368.9771
381.3406
397.2938
412.9670
359.1139
NL:
7.87E5
C20 H14 N4 O3 +H:
C20 H15 N4 O3
pa Chrg 1
365.1315
m/z

4-(1-(4-phenoxyphenyl)-1*H*-1,2,3-triazol-4-yl)benzoic acid (19m):

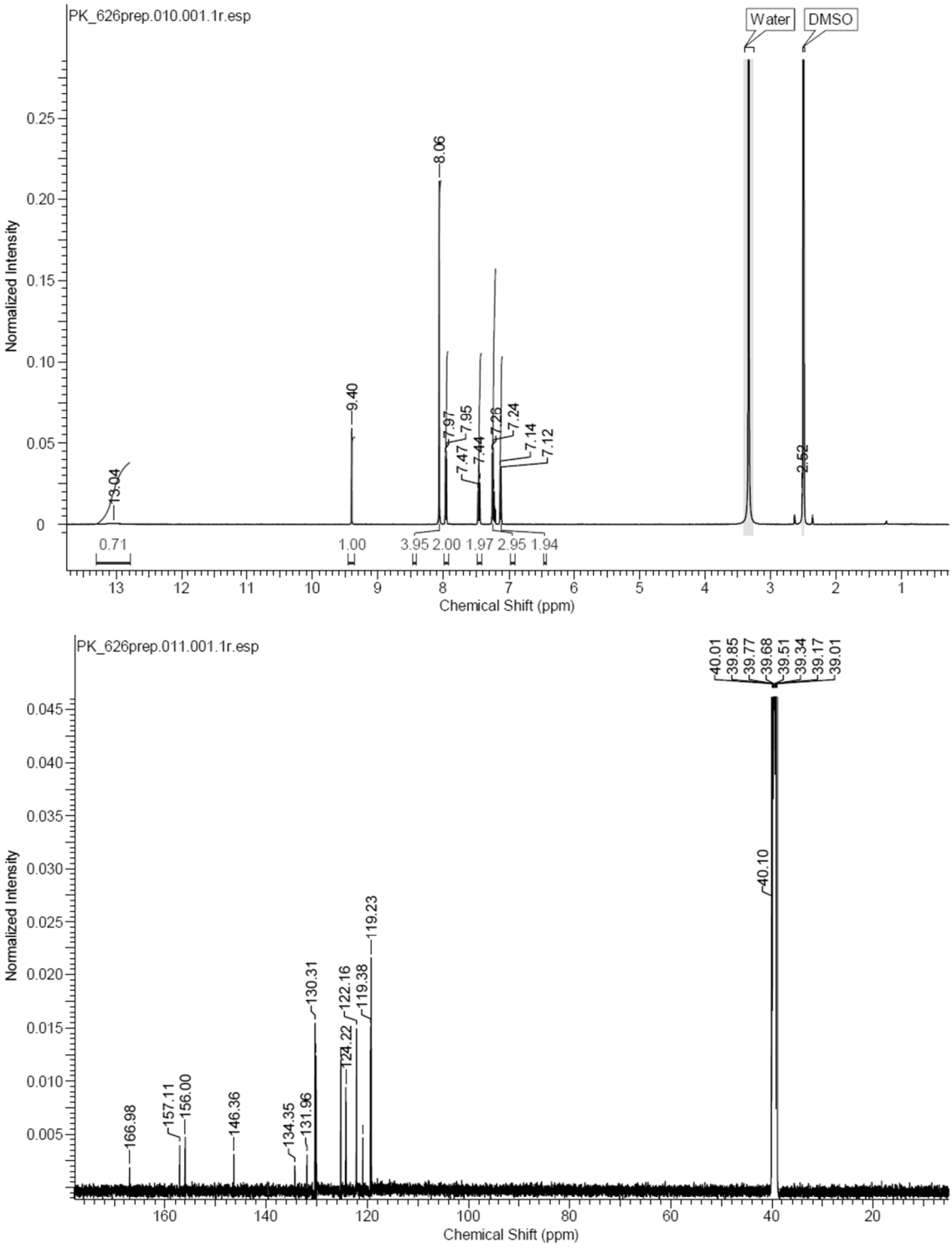

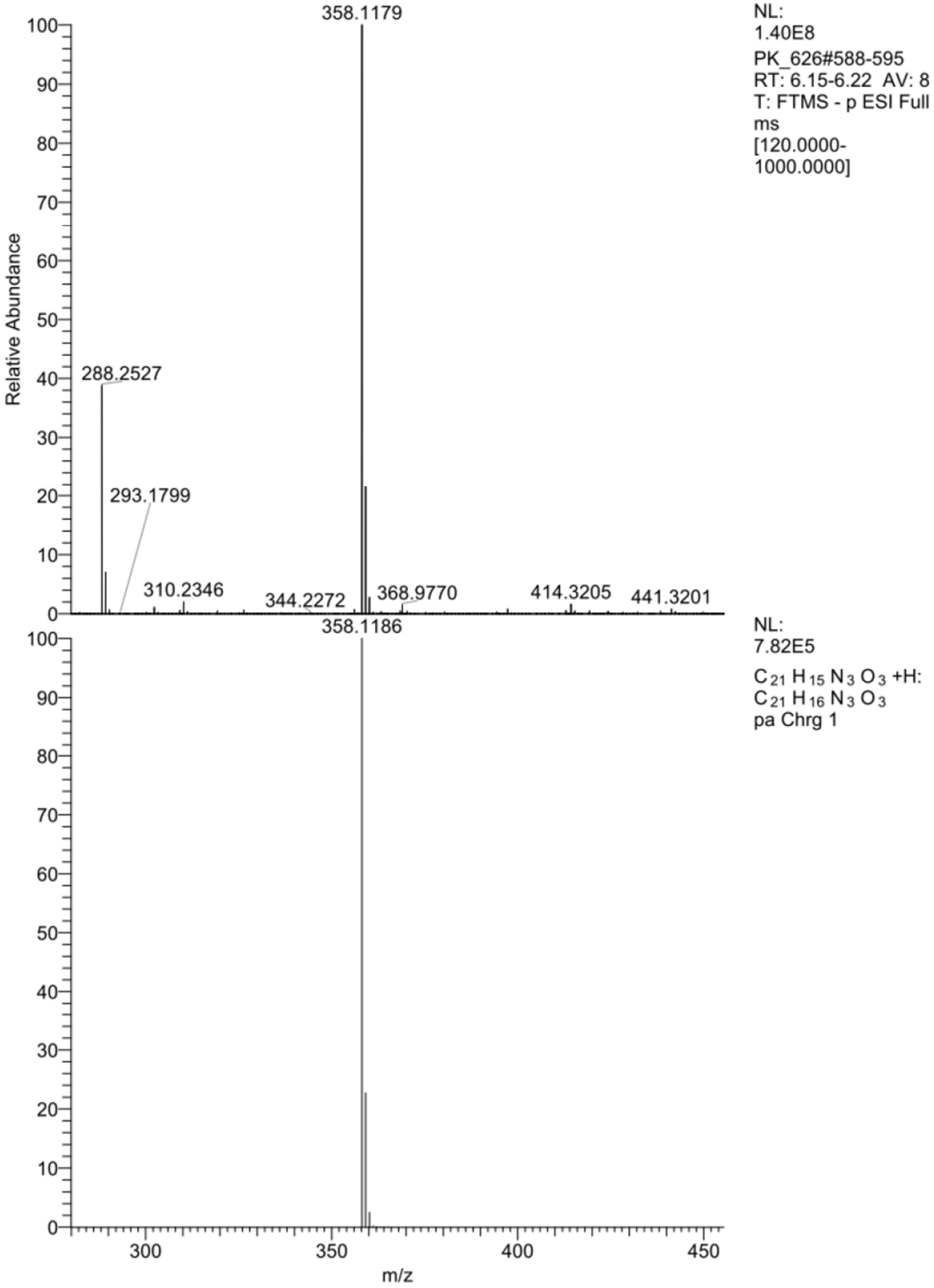
358.1179
NL:
1.40E8
PK_626#588-595
RT: 6.15-6.22 AV: 8
T: FTMS - p ESI Full
ms
[120.0000-
1000.0000]
Relative Abundance
288.2527
293.1799
310.2346
344.2272
368.9770
414.3205
441.3201
358.1186
NL:
7.82E5
C21 H15 N3 O3 +H:
C21 H16 N3 O3
pa Chrg 1
m/z

4-(1-(4-(pyridin-3-yloxy)phenyl)-1*H*-1,2,3-triazol-4-yl)benzoic acid (19n):

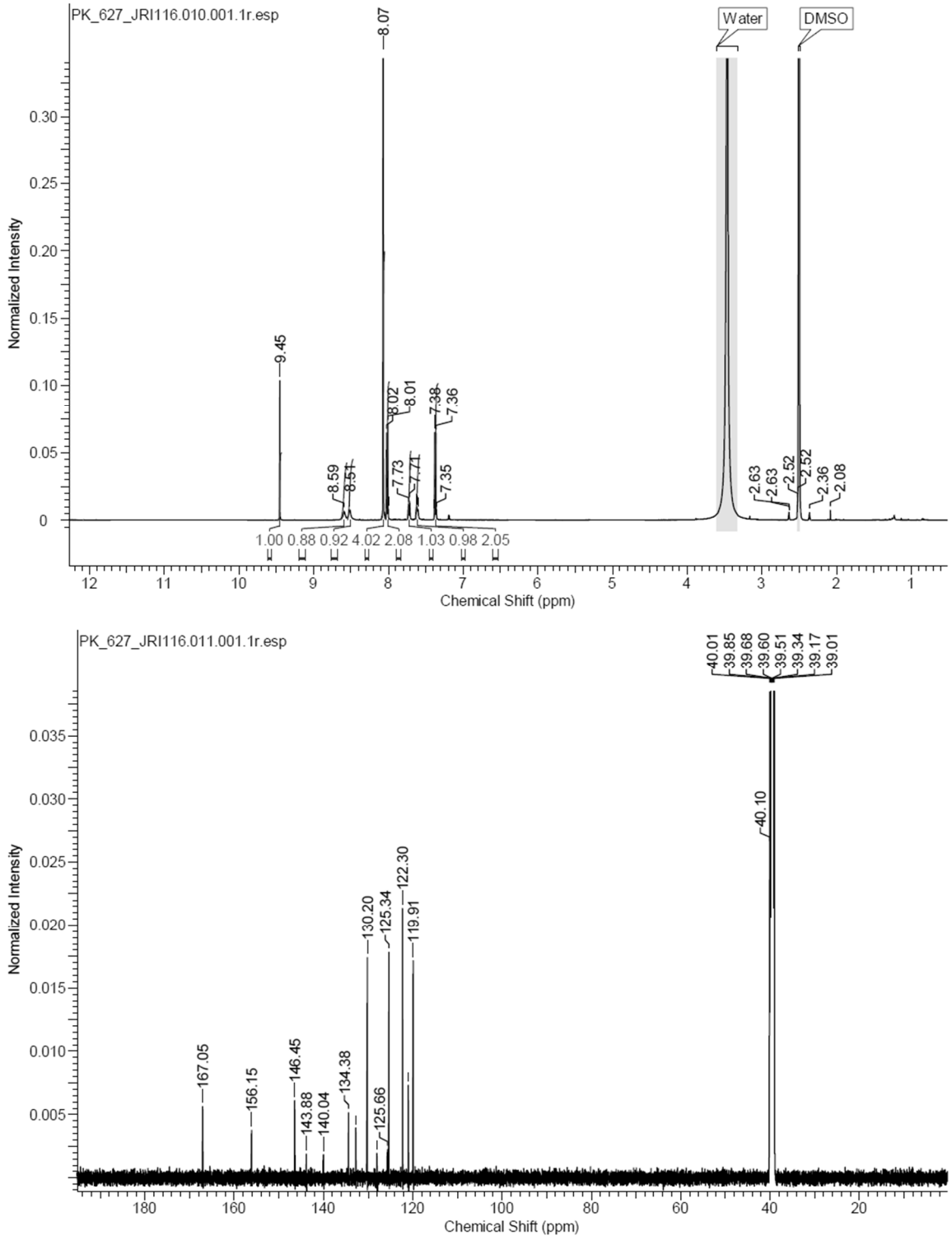

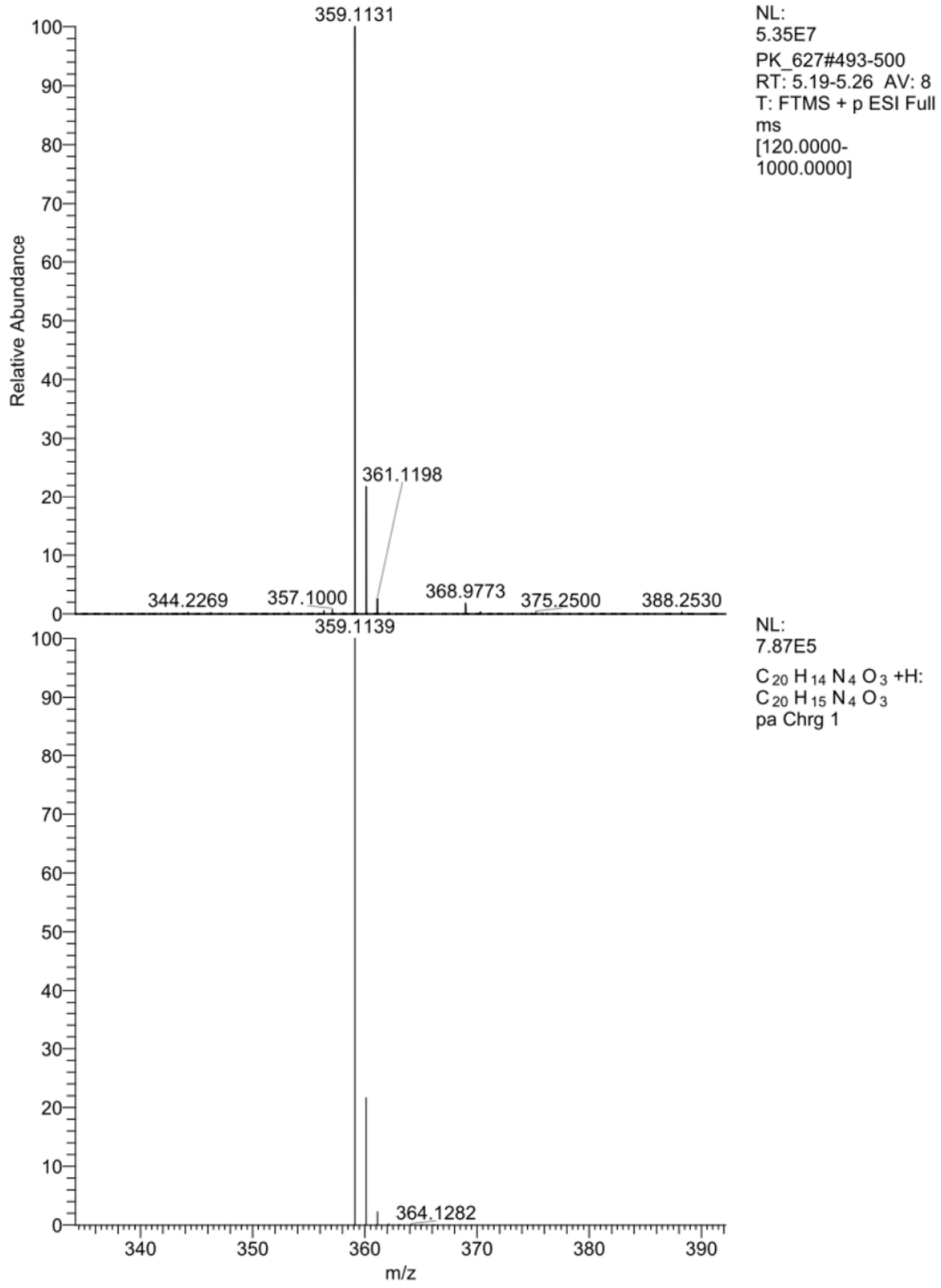
359.1131
NL:
5.35E7
PK_627#493-500
RT: 5.19-5.26 AV: 8
T: FTMS + p ESI Full
ms
[120.0000-
1000.0000]
Relative Abundance
361.1198
344.2269
357.1000
368.9773
375.2500
388.2530
359.1139
NL:
7.87E5
C20 H14 N4 O3 +H:
C20 H15 N4 O3
pa Chrg 1
364.1282
m/z

4-(1-(6-hydroxypyridin-3-yl)-1*H*-1,2,3-triazol-4-yl)benzoic acid (19o):

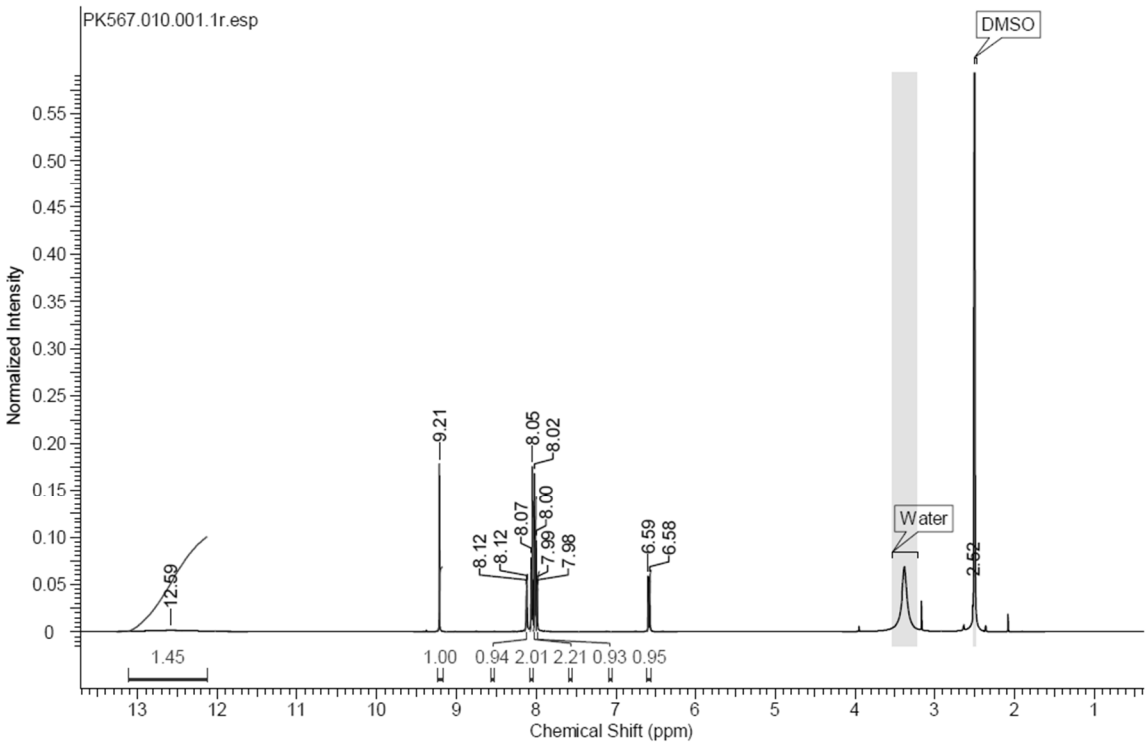

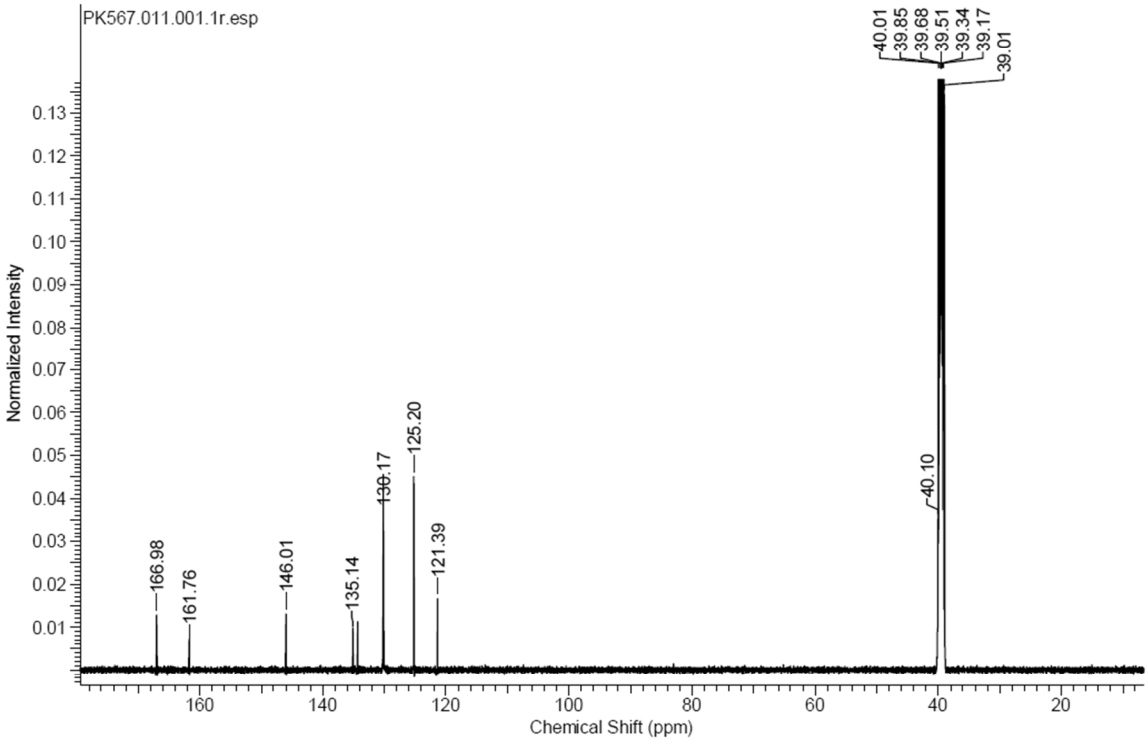

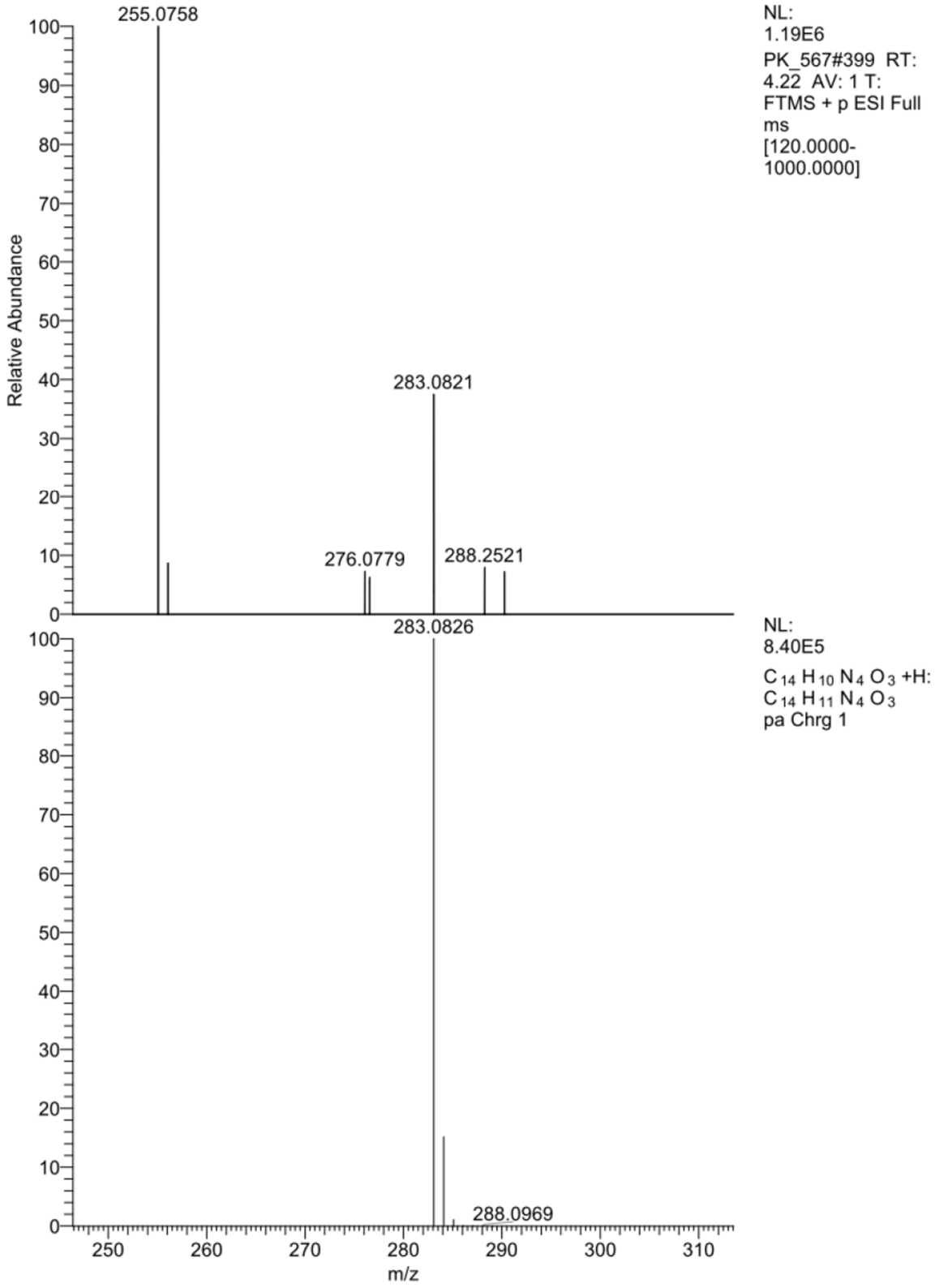
255.0758
283.0821
276.0779
288.2521
283.0826
288.0969
Relative Abundance
m/z
NL:
1.19E6
PK_567#399 RT:
4.22 AV: 1 T:
FTMS + p ESI Full
ms
[120.0000-
1000.0000]
NL:
8.40E5
C14 H10 N4 O3 +H:
C14 H11 N4 O3
pa Chrg 1

4-(1-(3-methylpyridin-4-yl)-1*H*-1,2,3-triazol-4-yl)benzoic acid (22):

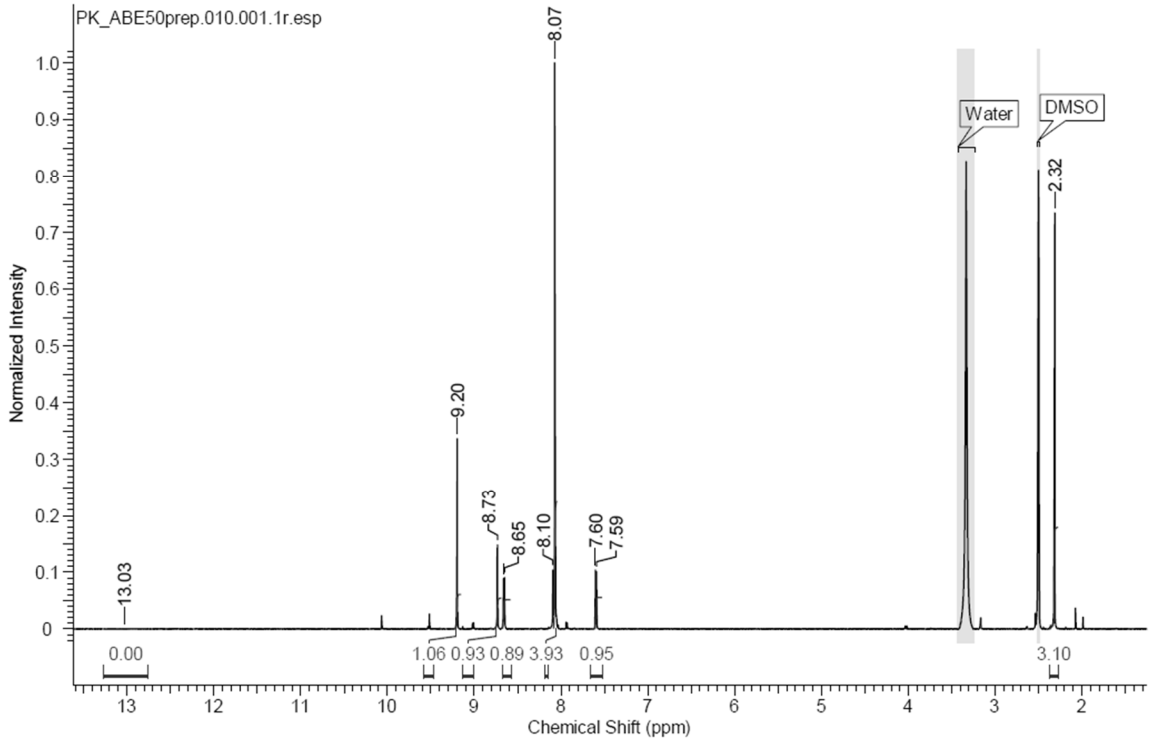

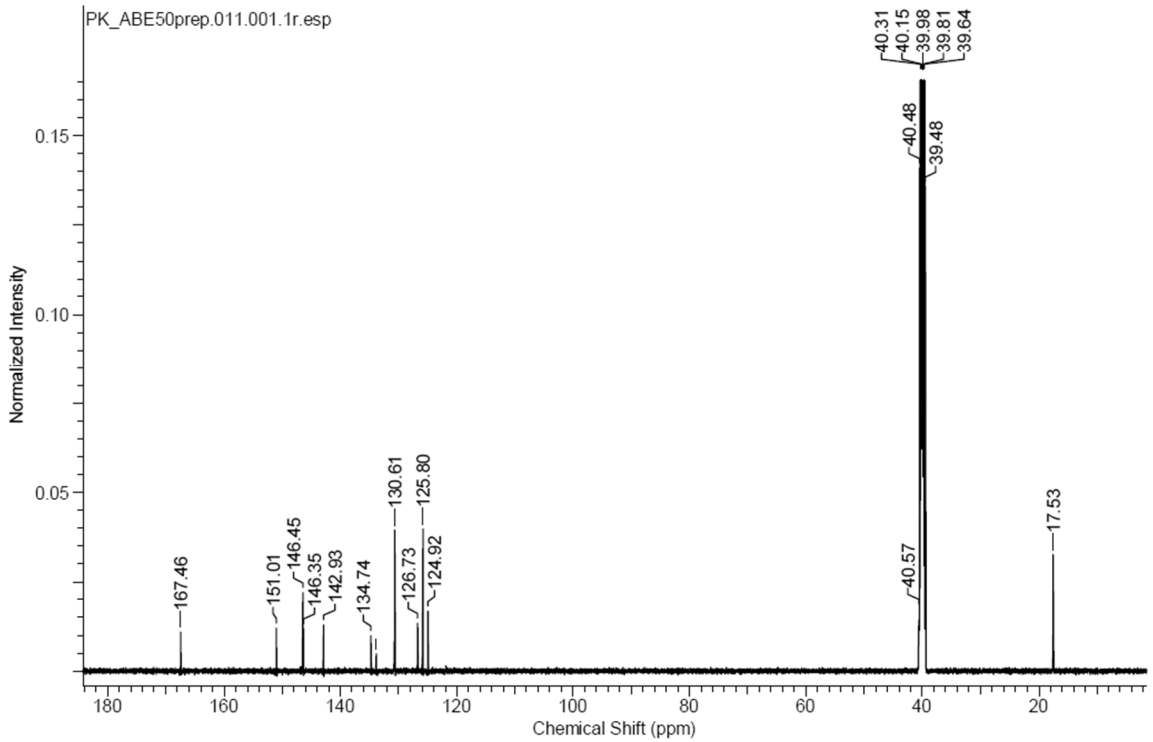

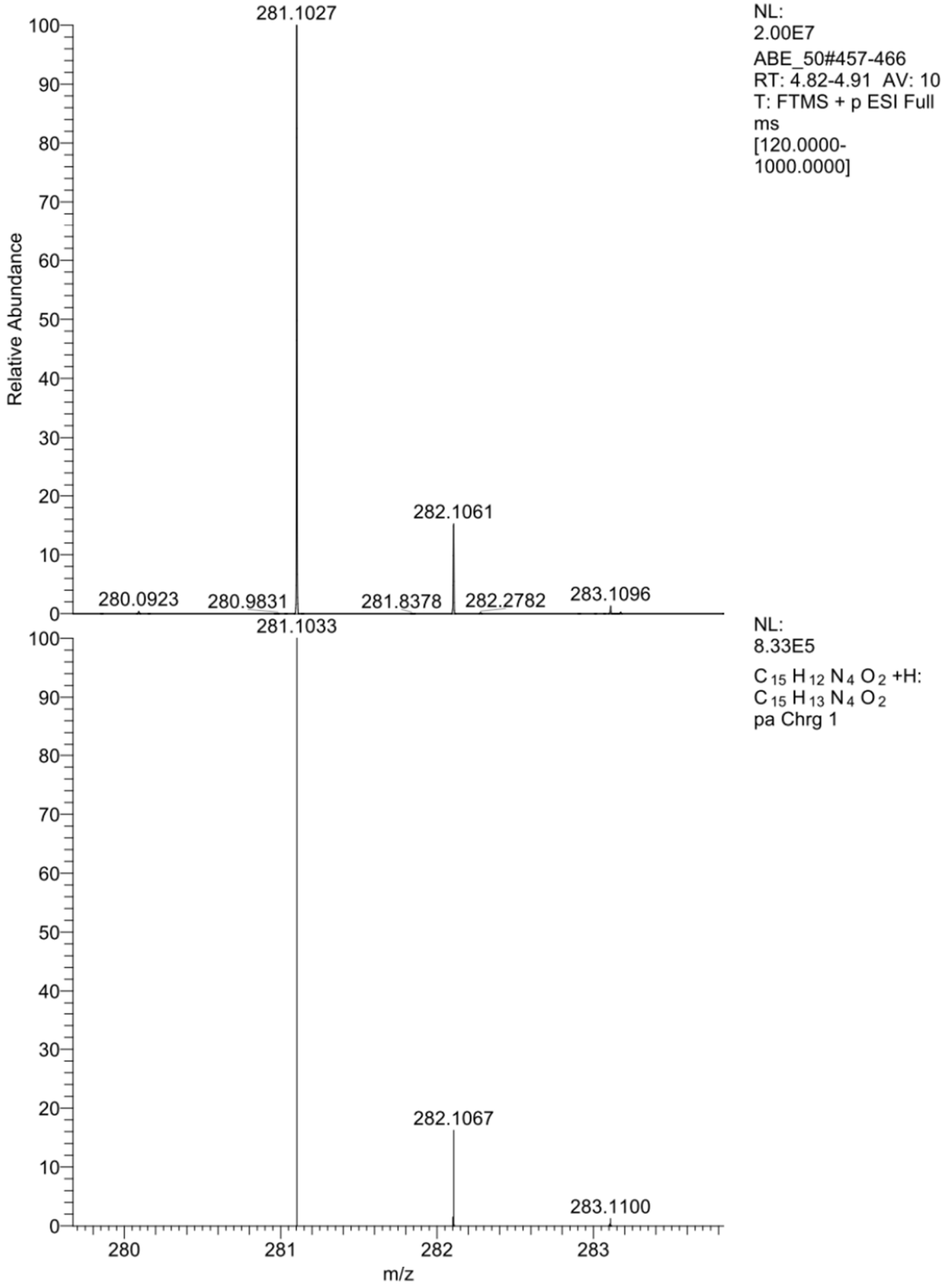
281.1027
NL:
2.00E7
ABE_50#457-466
RT: 4.82-4.91 AV: 10
T: FTMS + p ESI Full
ms
[120.0000-
1000.0000]
282.1061
280.0923
280.9831
281.8378
282.2782
283.1096
Relative Abundance
281.1033
NL:
8.33E5
C15 H12 N4 O2 +H:
C15 H13 N4 O2
pa Chrg 1
282.1067
283.1100
280
281
282
283
m/z

4-(1-(6-(2-hydroxyphenyl)-4-methylpyridin-3-yl)-1*H*-1,2,3-triazol-4-yl)benzoic acid (26a):

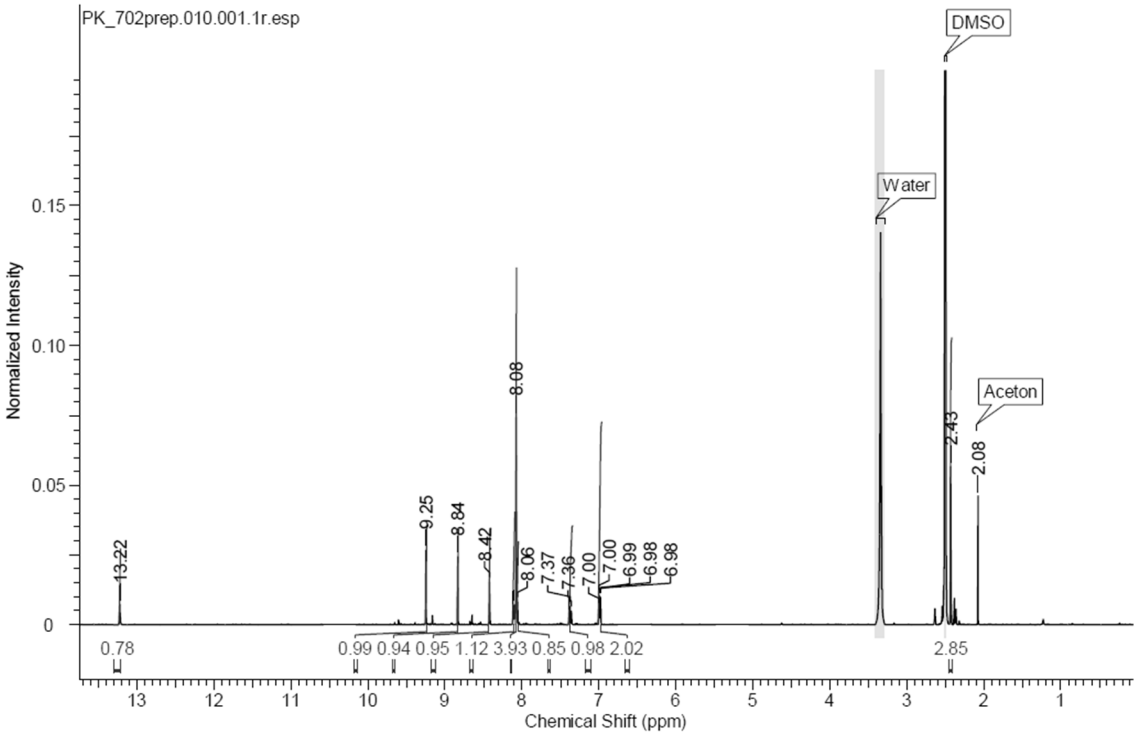

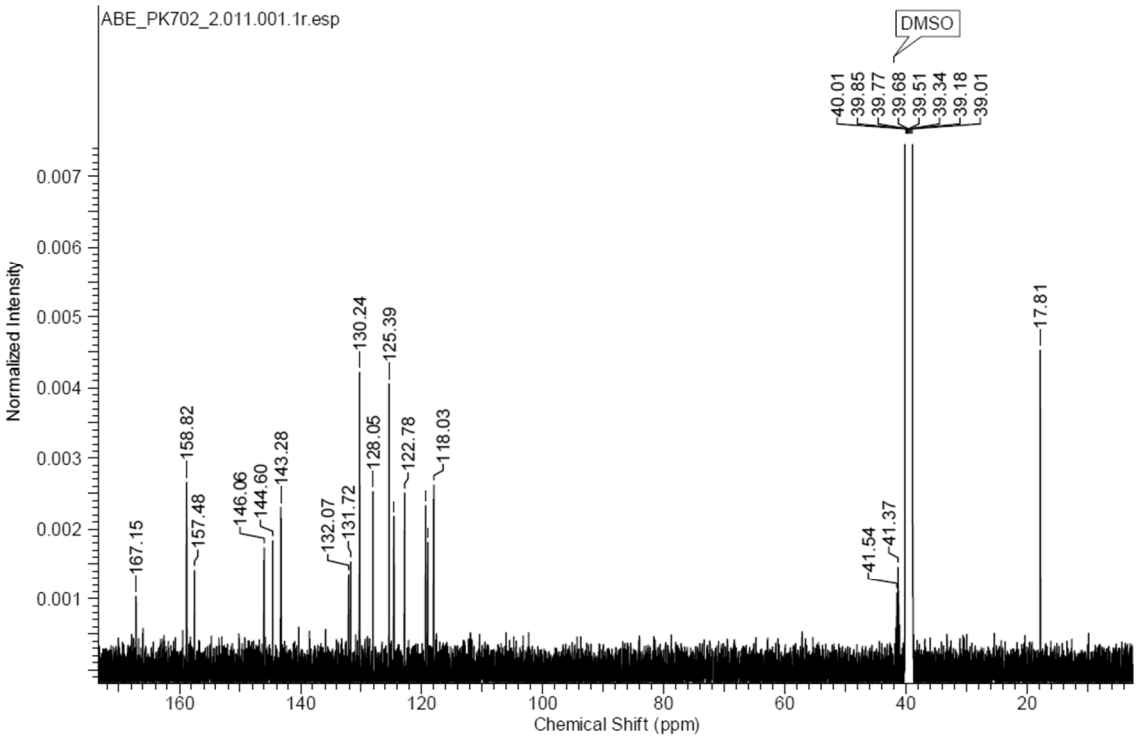

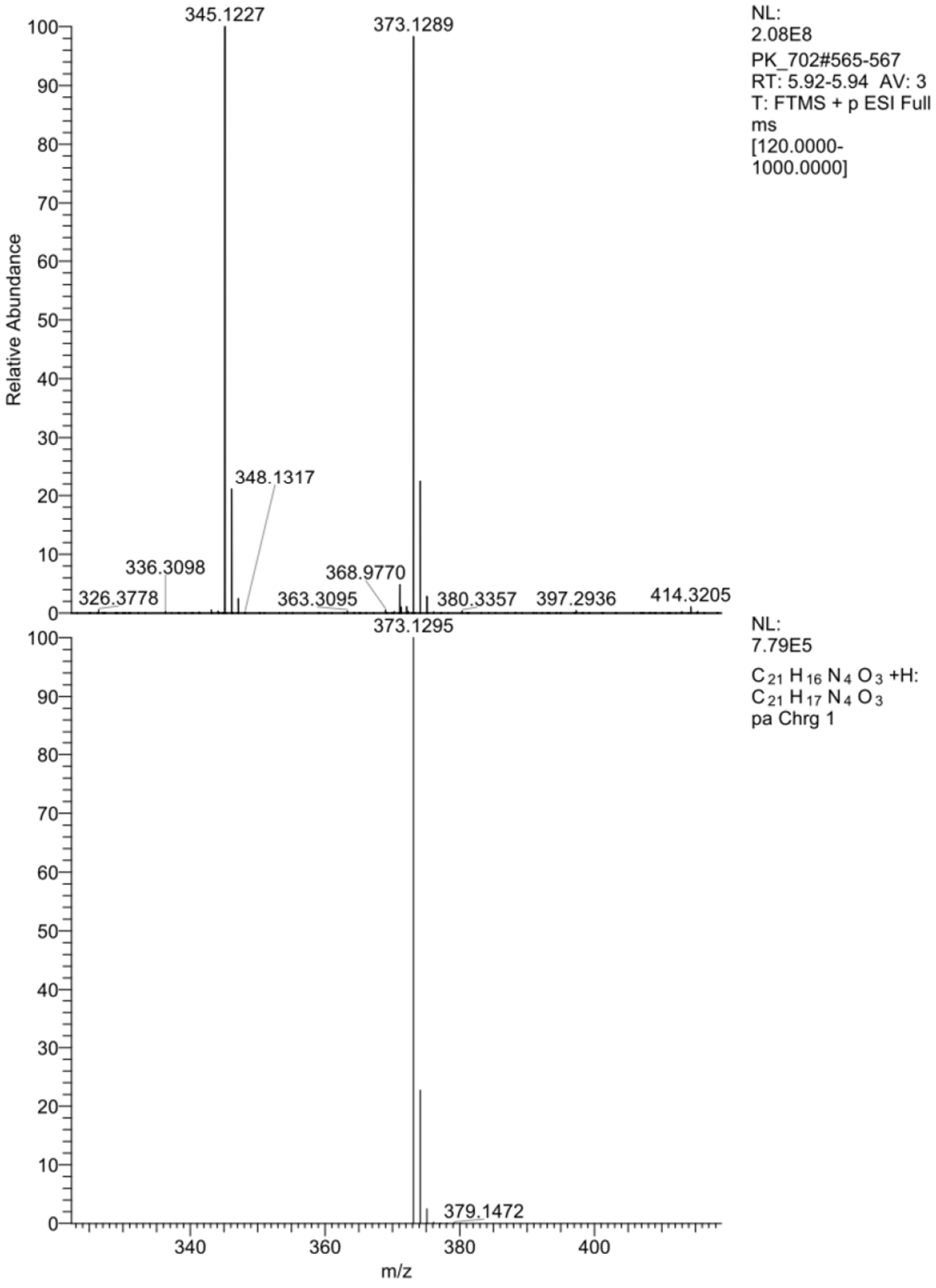
345.1227
373.1289
NL:
2.08E8
PK_702#565-567
RT: 5.92-5.94 AV: 3
T: FTMS + p ESI Full
ms
[120.0000-
1000.0000]
Relative Abundance
348.1317
336.3098
368.9770
326.3778
363.3095
380.3357
397.2936
414.3205
373.1295
NL:
7.79E5
C21 H16 N4 O3 +H:
C21 H17 N4 O3
pa Chrg 1
379.1472
340
360
380
400
m/z

4-(1-(6-(3-(hydroxymethyl)phenyl)-4-methylpyridin-3-yl)-1*H*-1,2,3-triazol-4-yl)benzoic acid (26b):

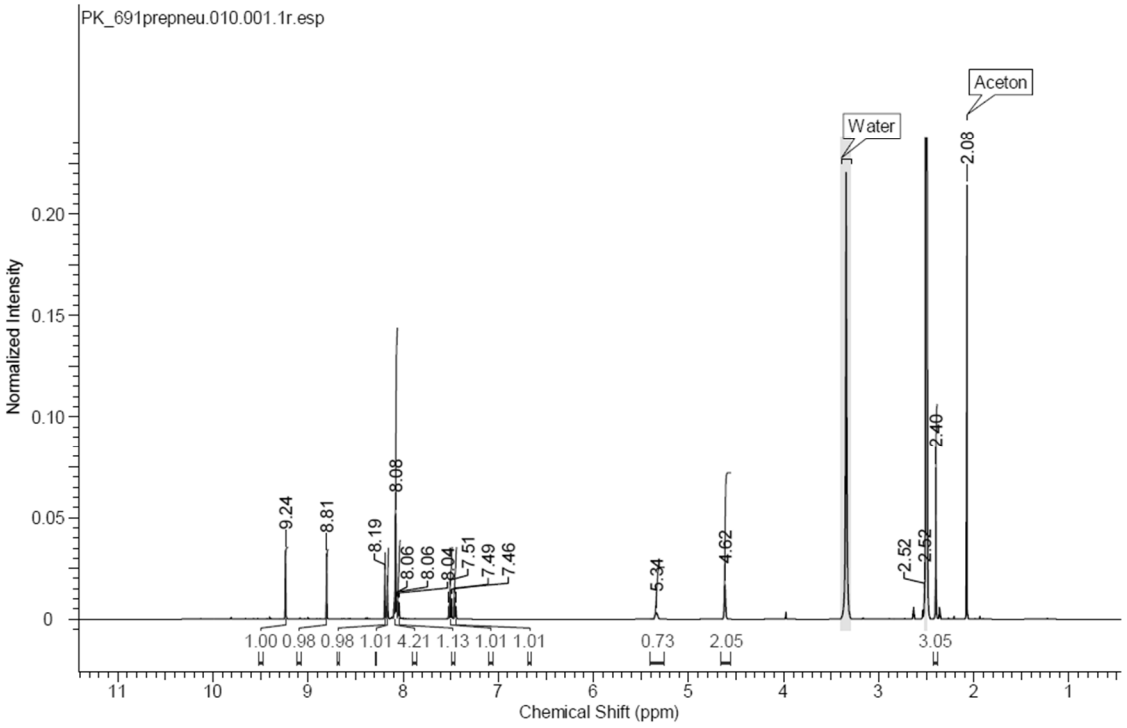

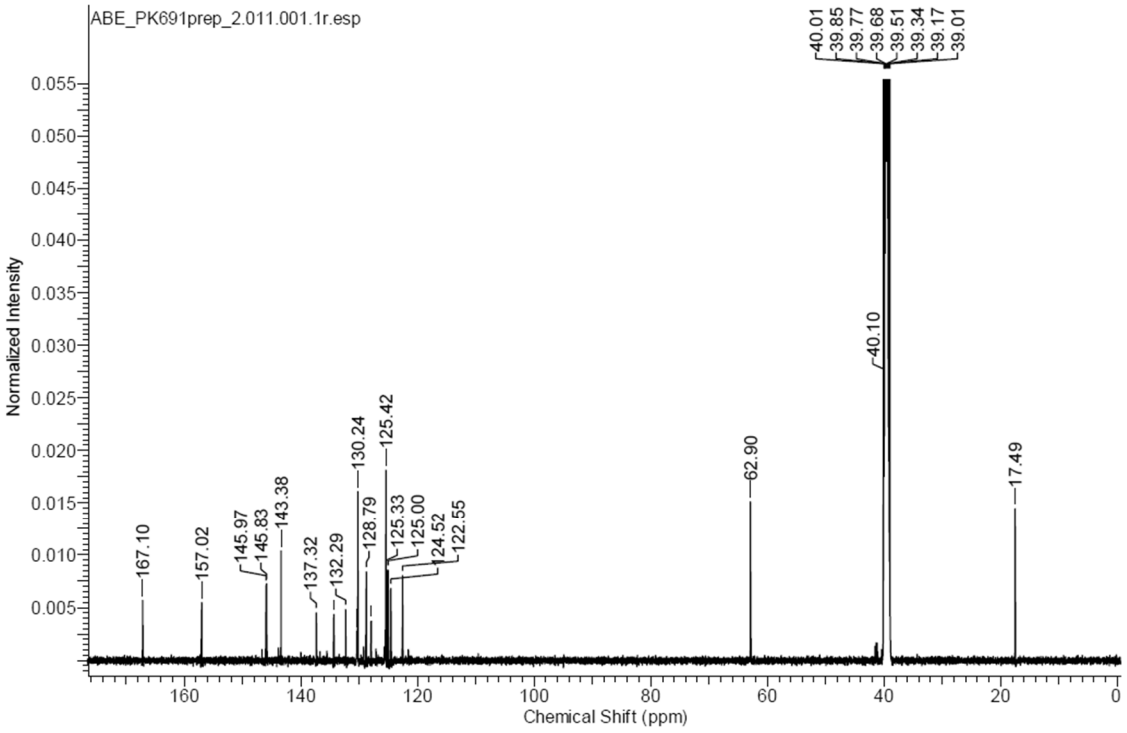

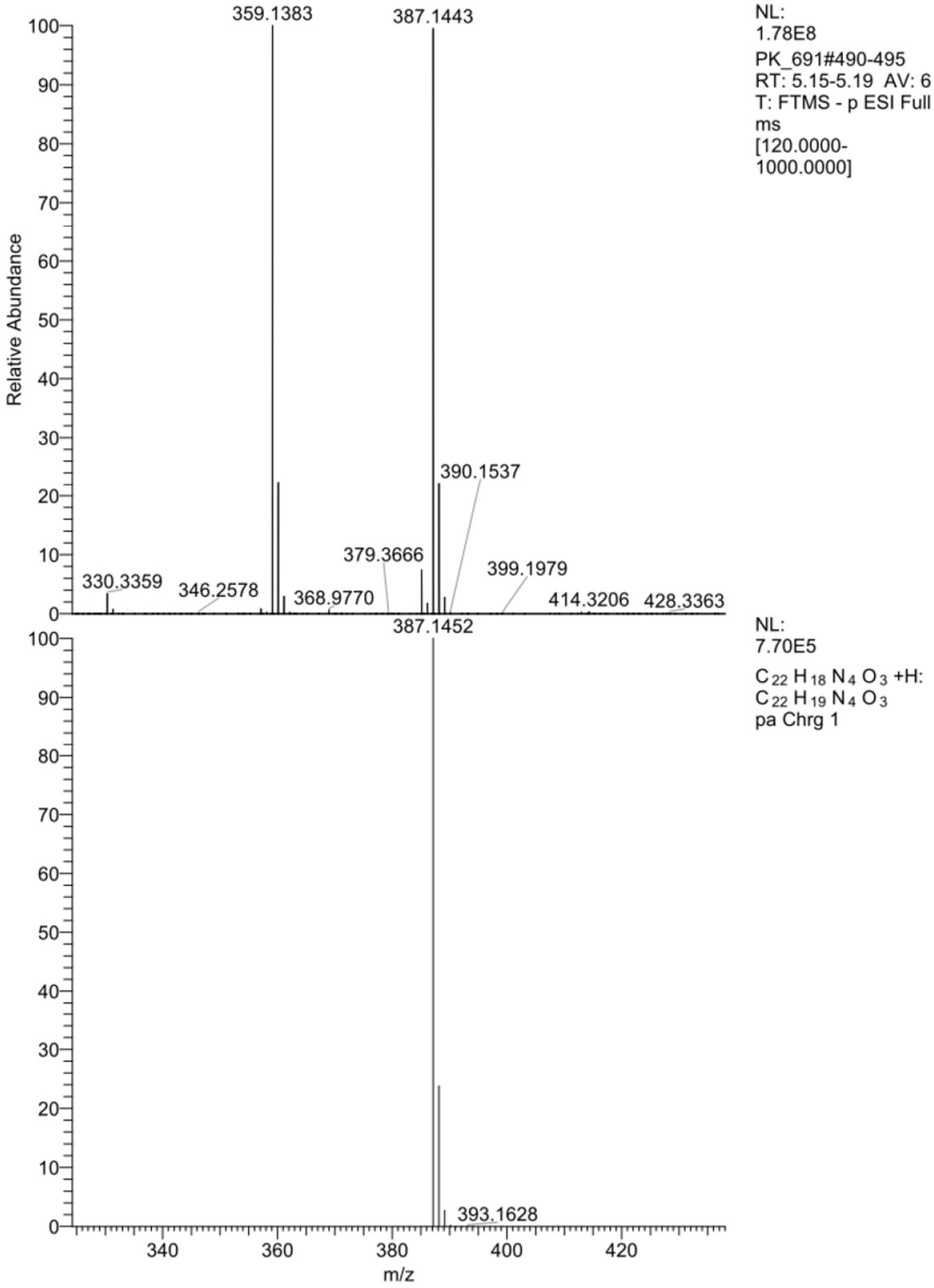
359.1383
387.1443
NL:
1.78E8
PK_691#490-495
RT: 5.15-5.19 AV: 6
T: FTMS - p ESI Full
ms
[120.0000-
1000.0000]
Relative Abundance
390.1537
379.3666
399.1979
330.3359
346.2578
368.9770
414.3206
428.3363
387.1452
NL:
7.70E5
C22 H18 N4 O3 +H:
C22 H19 N4 O3
pa Chrg 1
393.1628
m/z

4-(1-(5-(3-(hydroxymethyl)phenyl)pyridin-3-yl)-1*H*-1,2,3-triazol-4-yl)benzoic acid (31a):

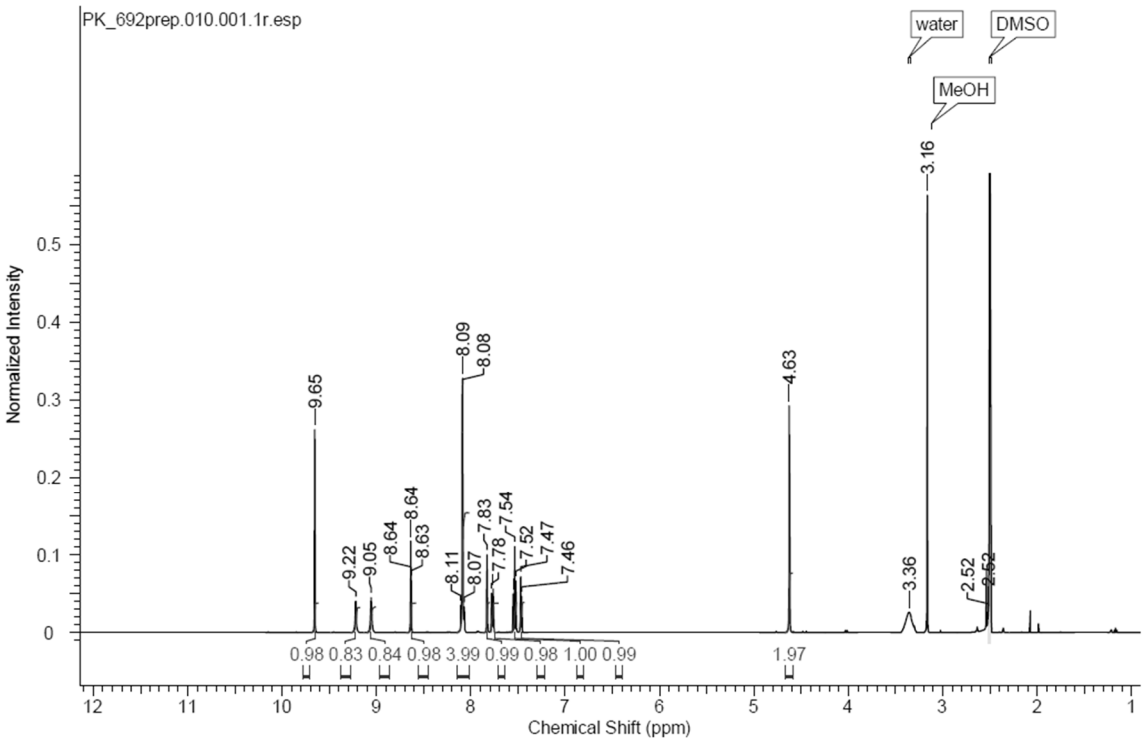

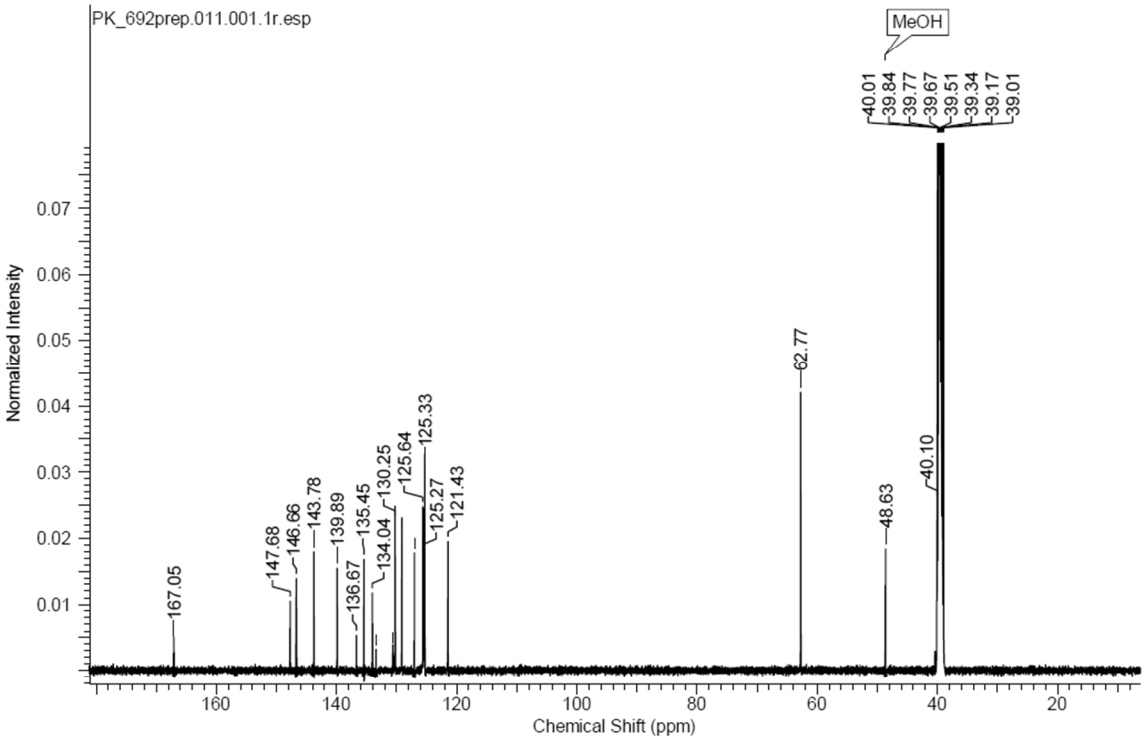

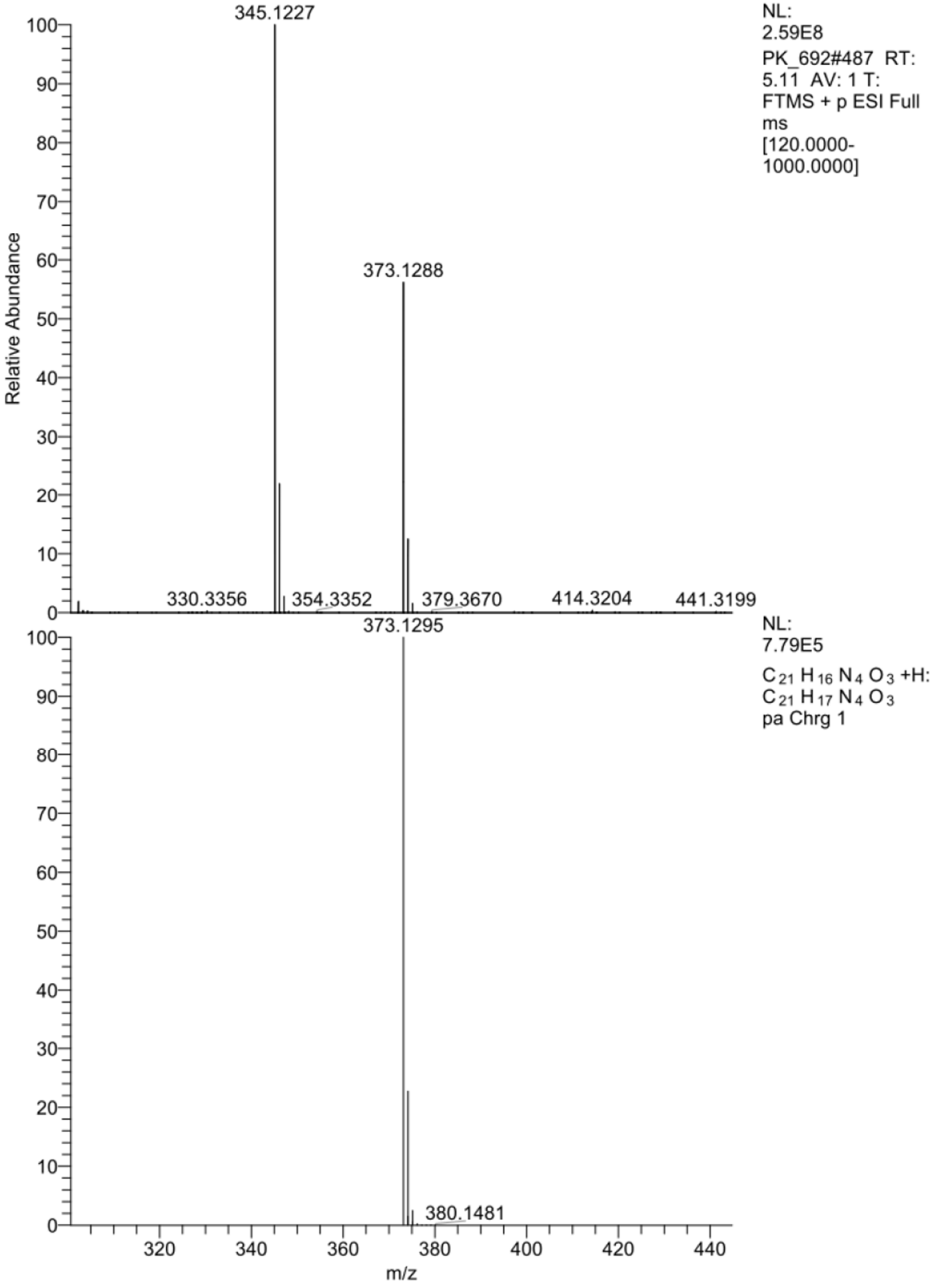
345.1227
NL:
2.59E8
PK_692#487 RT:
5.11 AV: 1 T:
FTMS + p ESI Full
ms
[120.0000-
1000.0000]
373.1288
Relative Abundance
330.3356
354.3352
379.3670
414.3204
441.3199
373.1295
NL:
7.79E5
C21 H16 N4 O3 +H:
C21 H17 N4 O3
pa Chrg 1
380.1481
m/z

4-(1-(4-chloro-5-phenylpyridin-3-yl)-1*H*-1,2,3-triazol-4-yl)benzoic acid (31b):

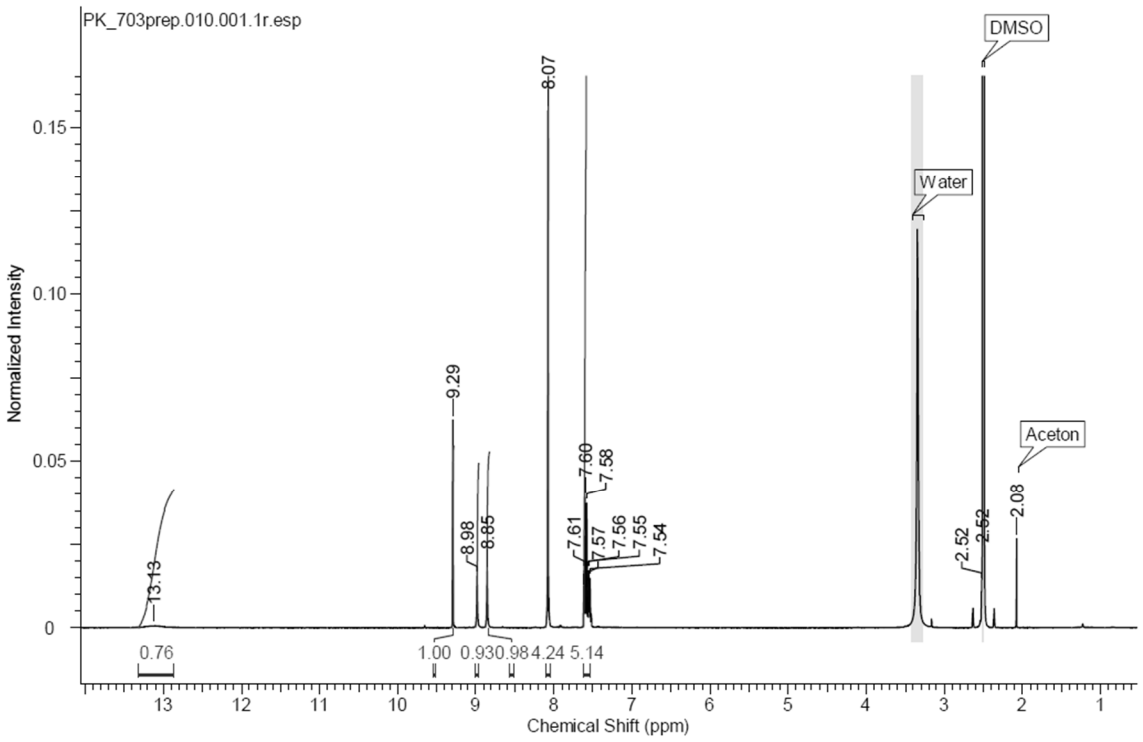

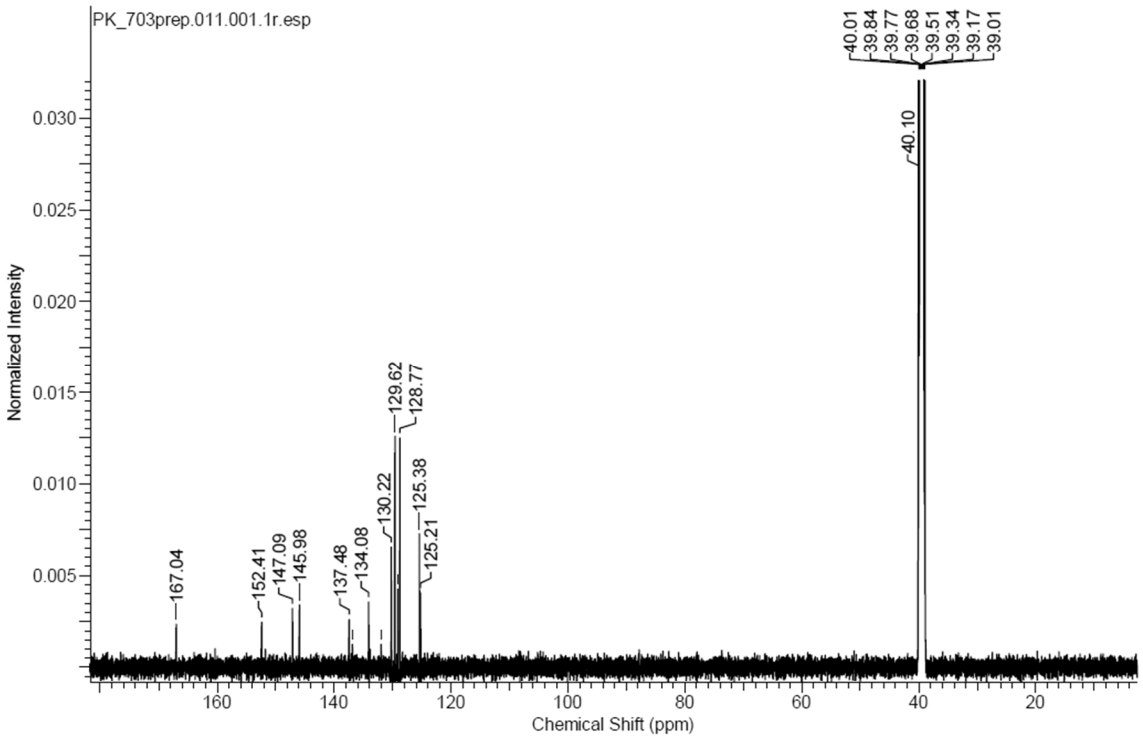

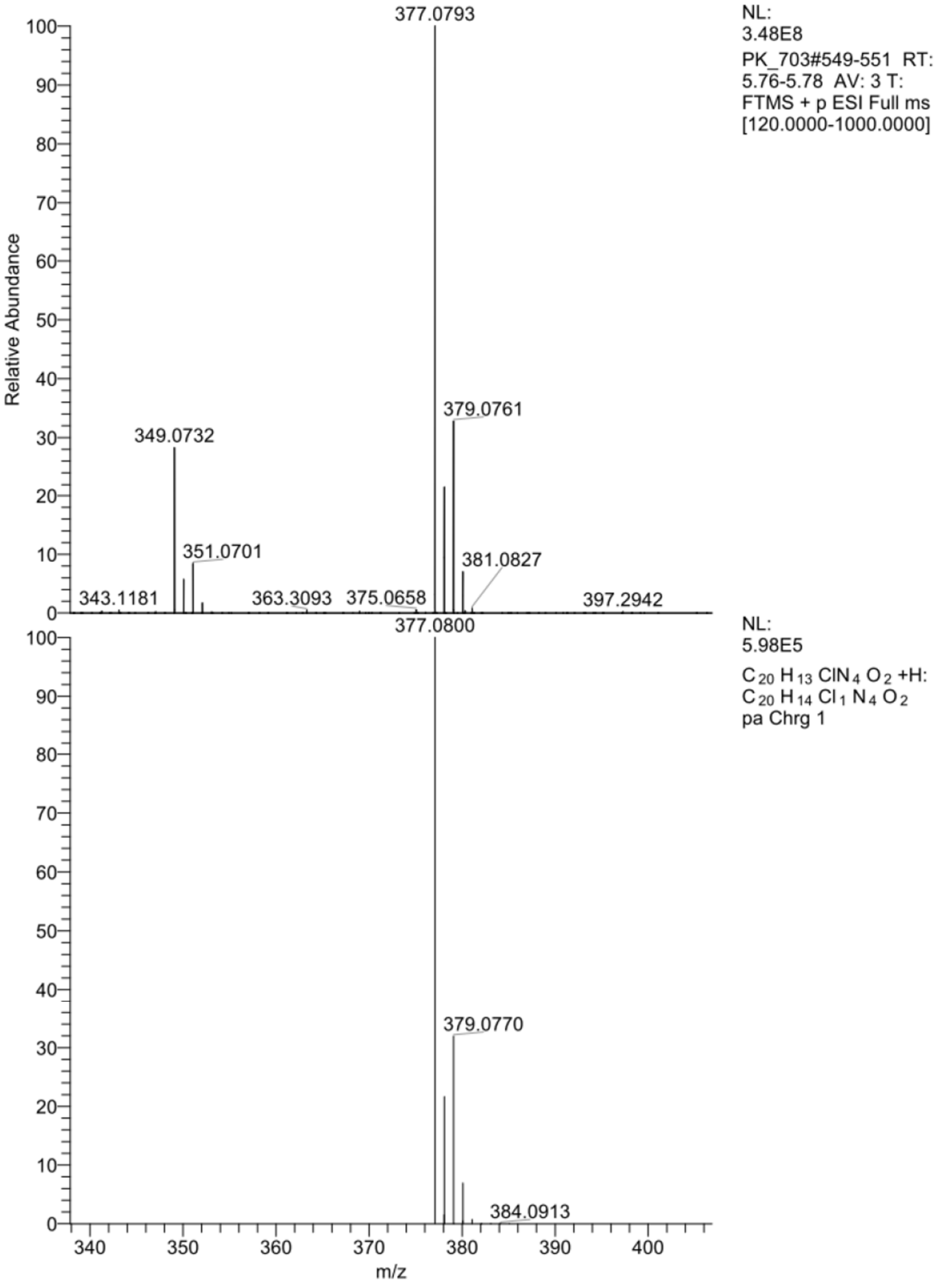
377.0793
NL:
3.48E8
PK_703#549-551 RT:
5.76-5.78 AV: 3 T:
FTMS + p ESI Full ms
[120.0000-1000.0000]
379.0761
349.0732
351.0701
381.0827
343.1181
363.3093
375.0658
397.2942
377.0800
NL:
5.98E5
C20 H13 ClN4 O2 +H:
C20 H14 Cl1 N4 O2
pa Chrg 1
379.0770
384.0913
Relative Abundance
m/z

4-(1-(5-phenylpyridin-3-yl)-1*H*-1,2,3-triazol-4-yl)benzoic acid (36a):

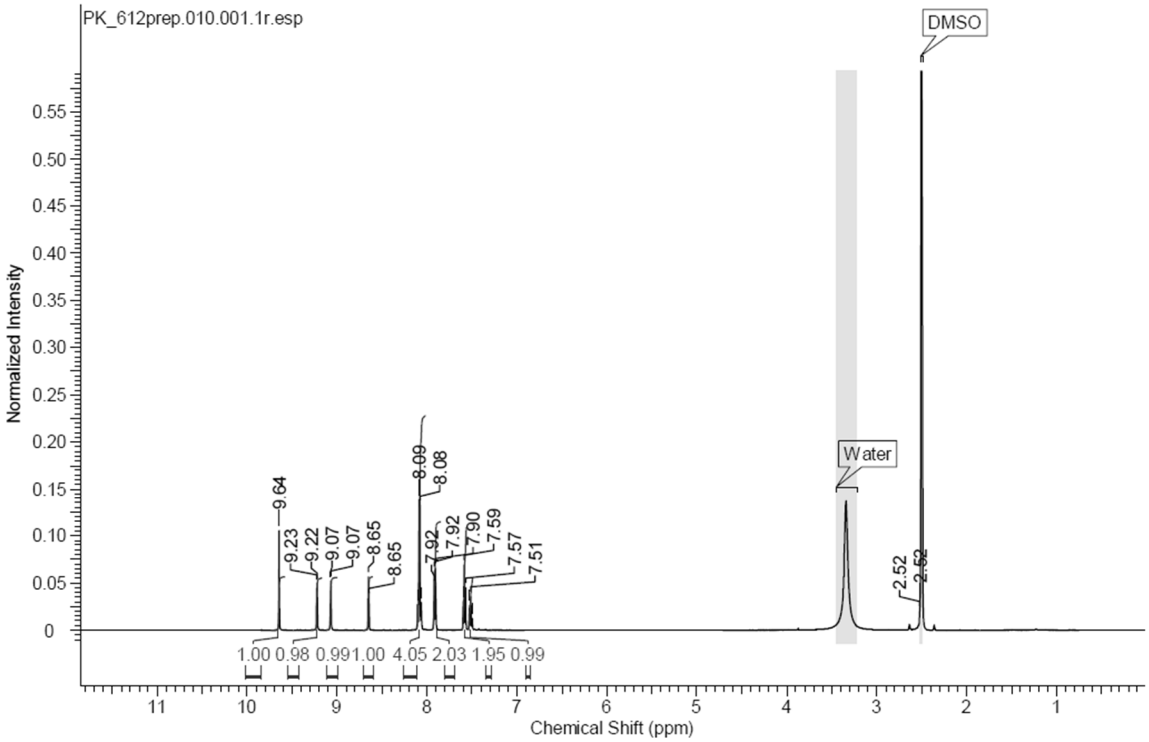

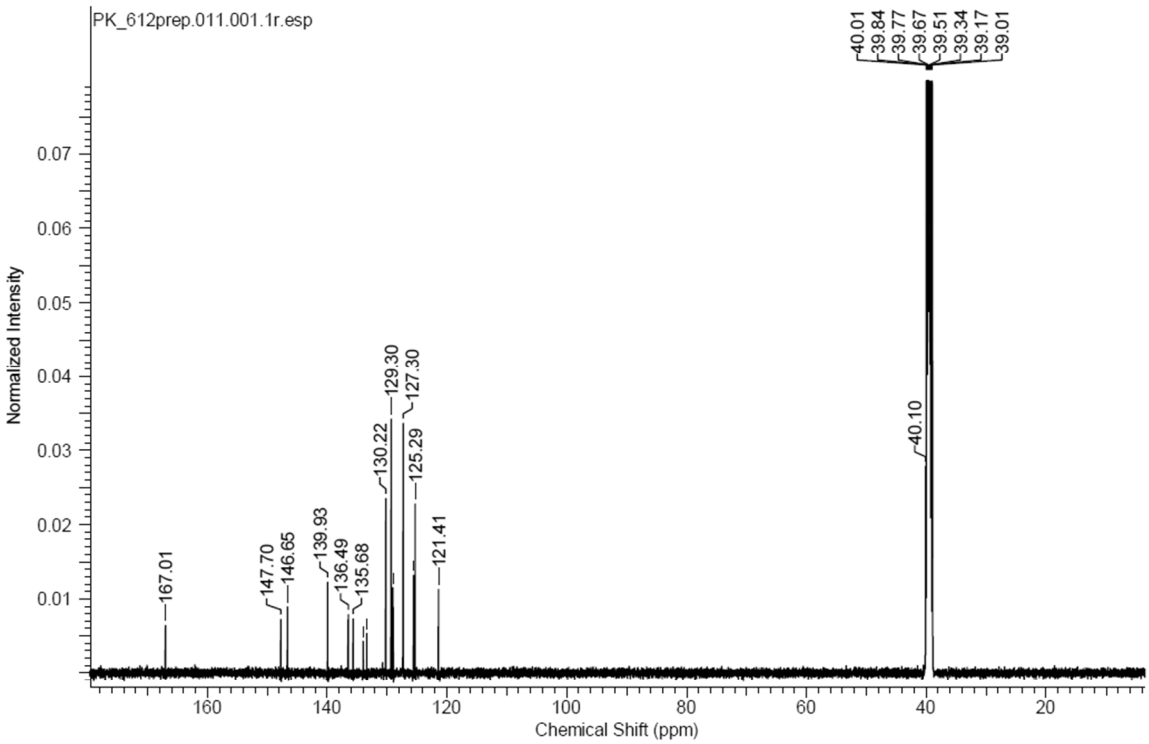

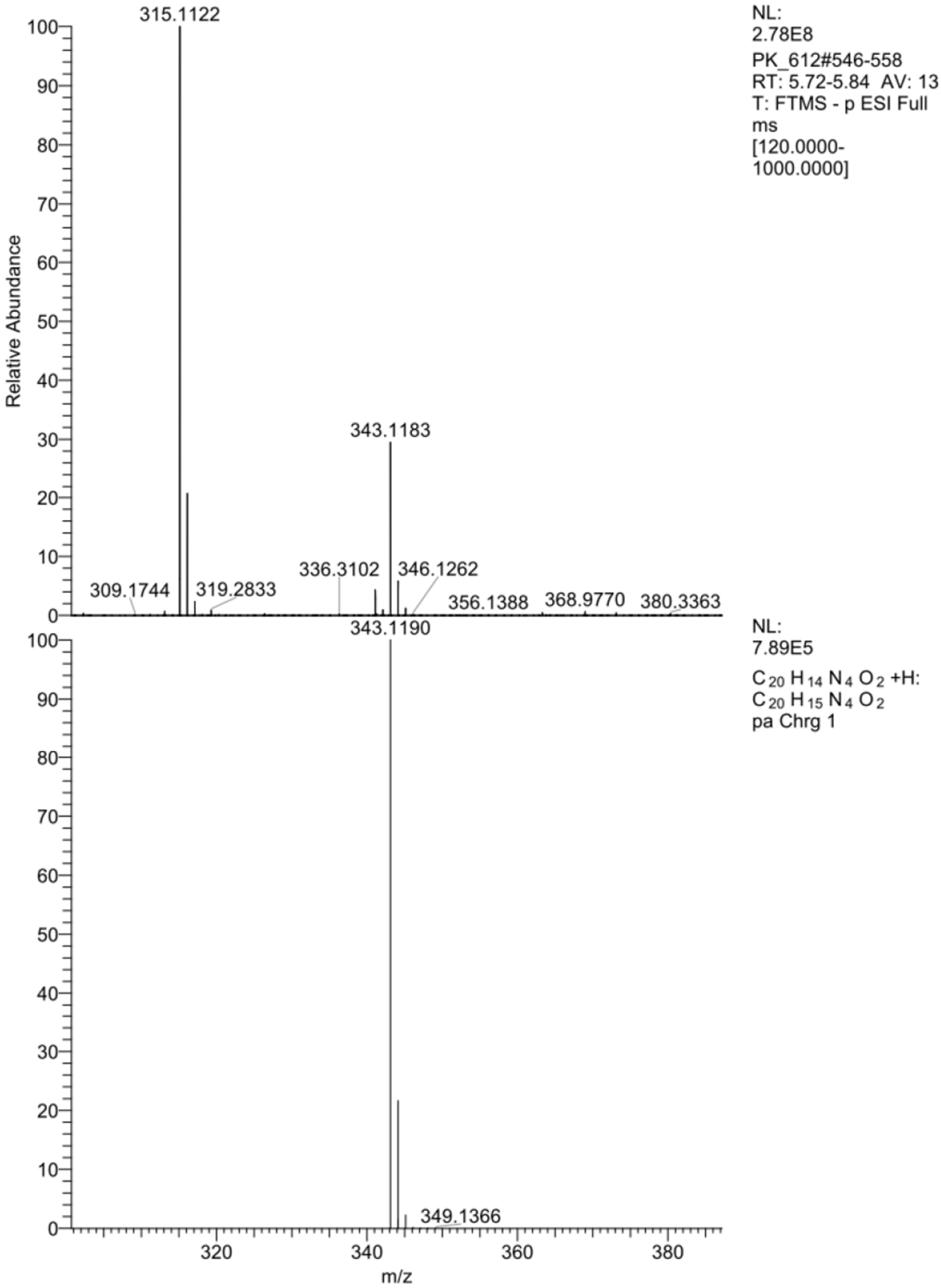
315.1122
NL:
2.78E8
PK_612#546-558
RT: 5.72-5.84 AV: 13
T: FTMS - p ESI Full
ms
[120.0000-
1000.0000]
Relative Abundance
343.1183
336.3102
346.1262
309.1744
319.2833
356.1388
368.9770
380.3363
343.1190
NL:
7.89E5
C20 H14 N4 O2 +H:
C20 H15 N4 O2
pa Chrg 1
349.1366
m/z

4-(1-(5-(2-methoxyphenyl)pyridin-3-yl)-1*H*-1,2,3-triazol-4-yl)benzoic acid (36b):

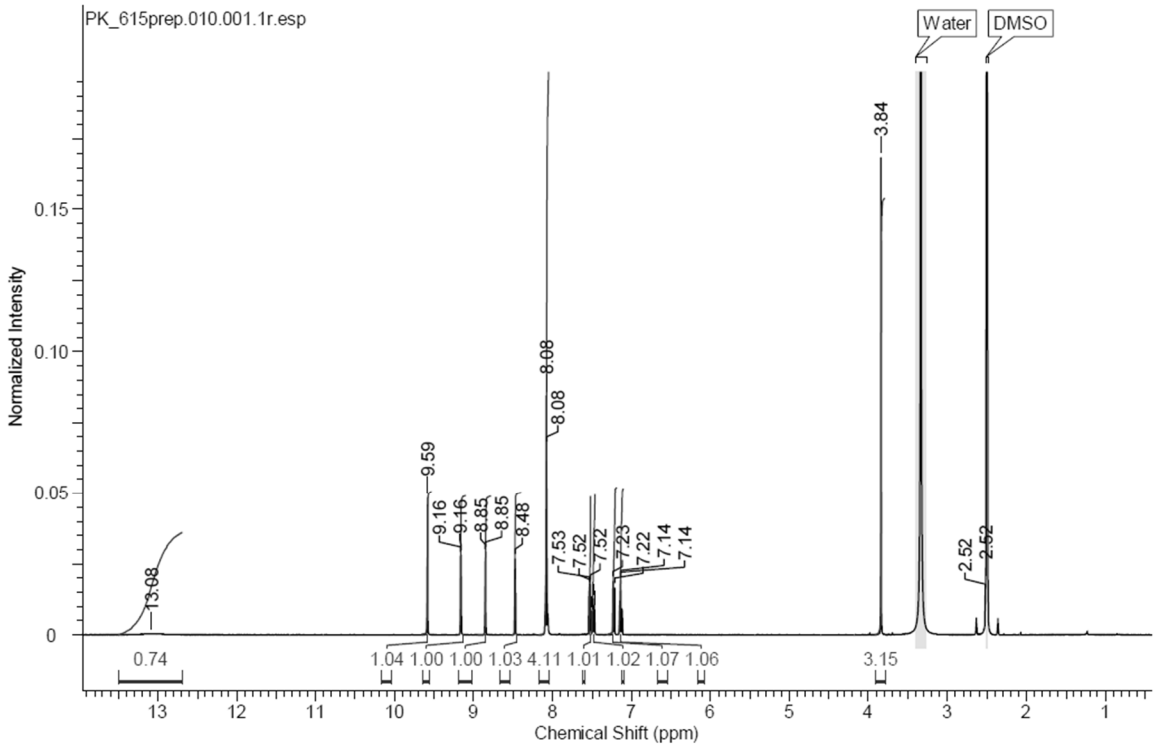

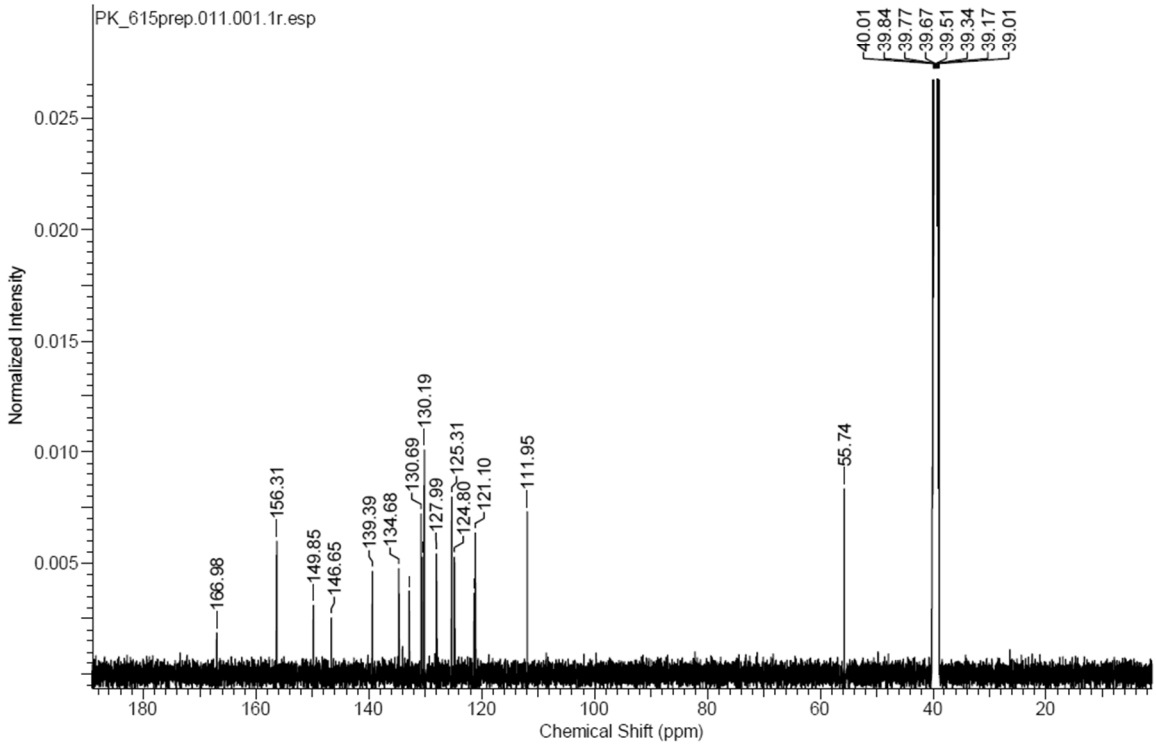

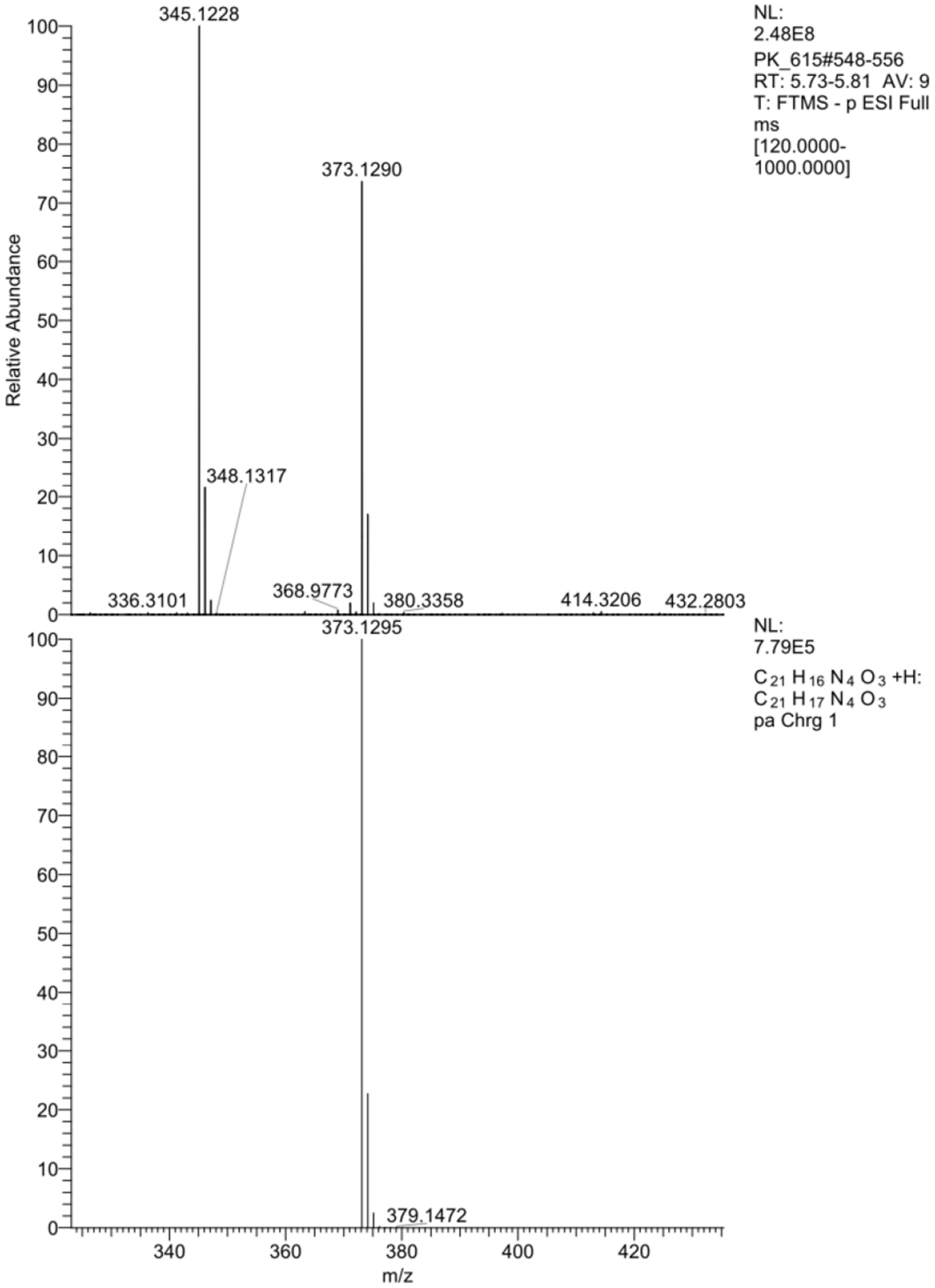
345.1228
373.1290
348.1317
336.3101
368.9773
380.3358
414.3206
432.2803
NL:
2.48E8
PK_615#548-556
RT: 5.73-5.81 AV: 9
T: FTMS - p ESI Full
ms
[120.0000-
1000.0000]
373.1295
379.1472
NL:
7.79E5
C21 H16 N4 O3 +H:
C21 H17 N4 O3
pa Chrg 1
Relative Abundance
m/z
340
360
380
400
420

4-(1-(5-(3-methoxyphenyl)pyridin-3-yl)-1*H*-1,2,3-triazol-4-yl)benzoic acid (36c):

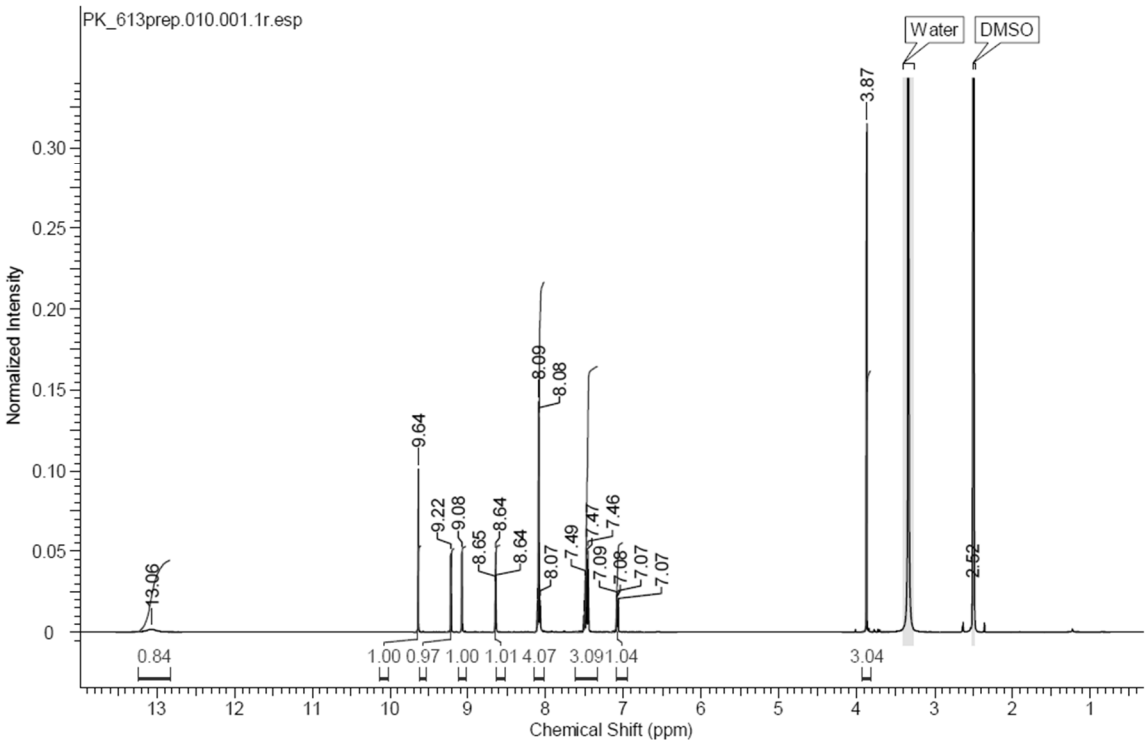

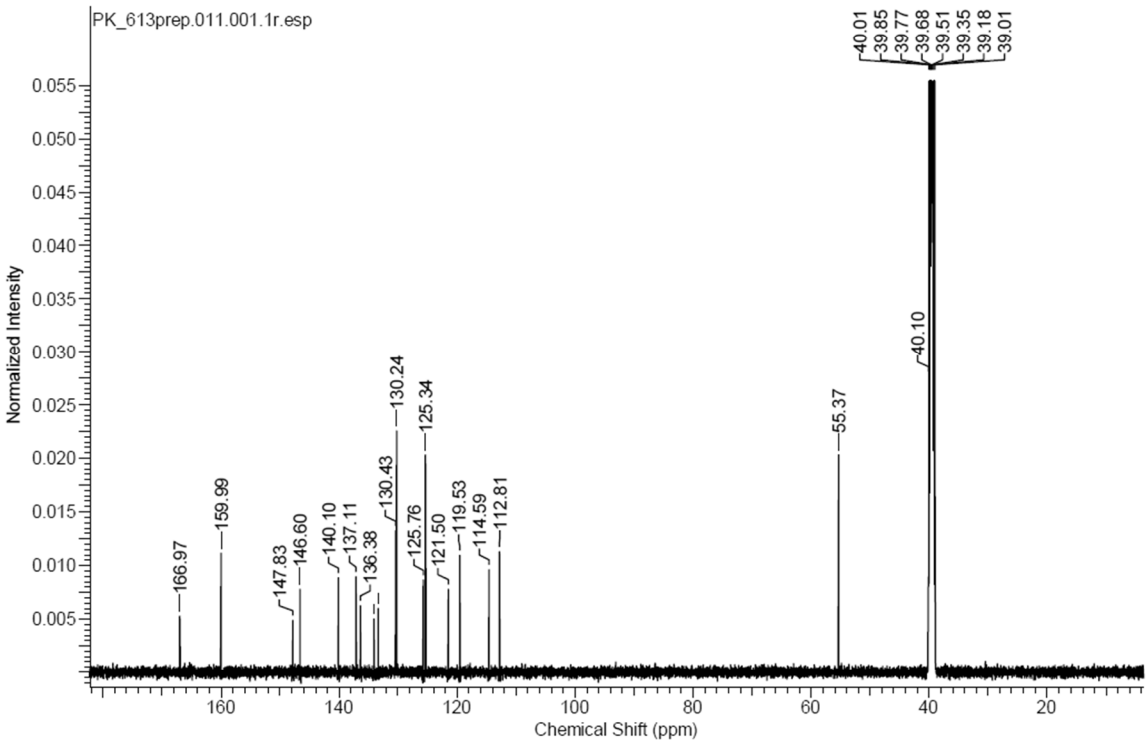

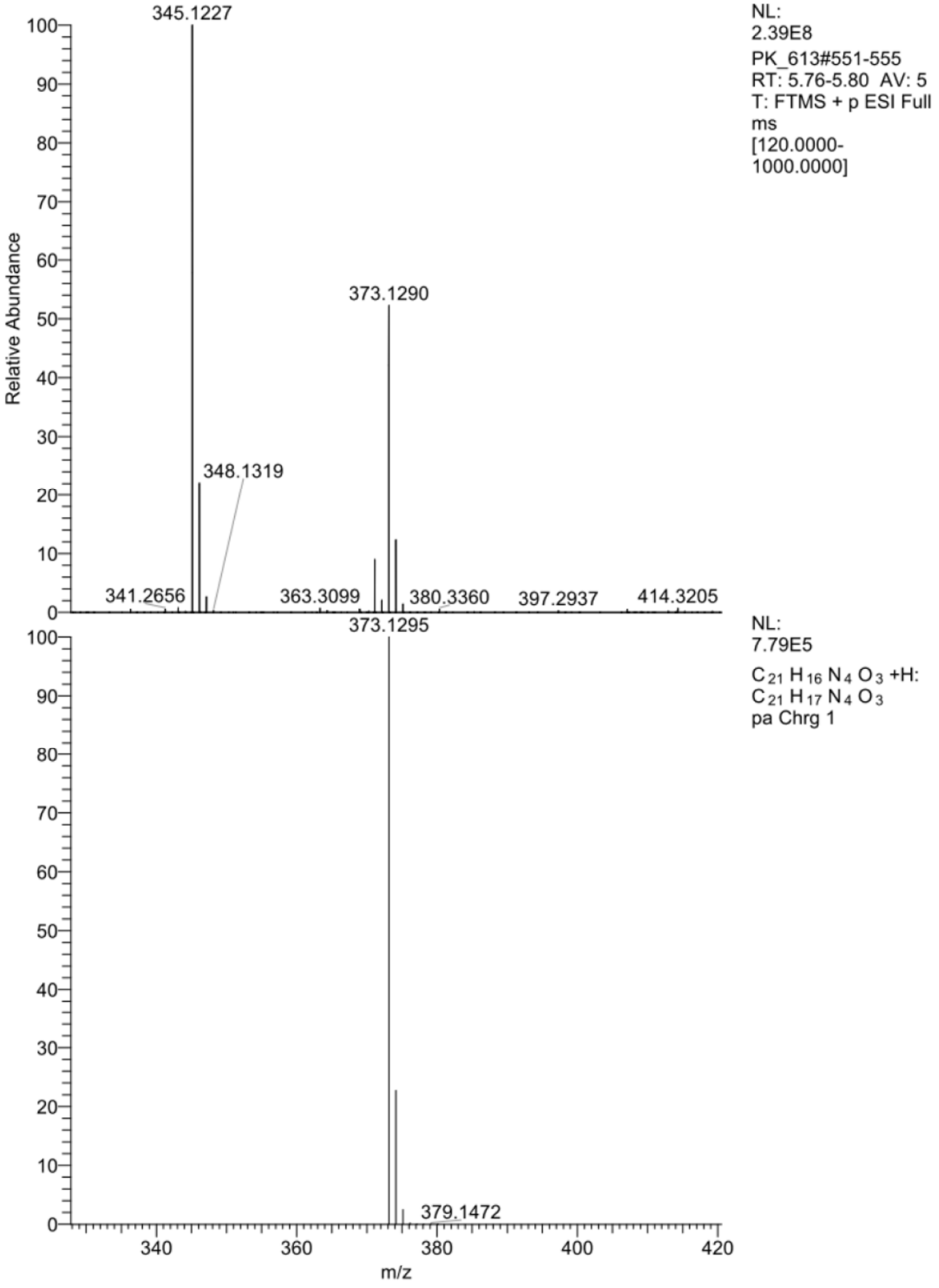
345.1227
NL:
2.39E8
PK_613#551-555
RT: 5.76-5.80 AV: 5
T: FTMS + p ESI Full
ms
[120.0000-
1000.0000]
373.1290
348.1319
341.2656
363.3099
380.3360
397.2937
414.3205
Relative Abundance
373.1295
NL:
7.79E5
C21 H16 N4 O3 +H:
C21 H17 N4 O3
pa Chrg 1
379.1472
m/z

4-(1-(5-(4-methoxyphenyl)pyridin-3-yl)-1*H*-1,2,3-triazol-4-yl)benzoic acid (36d):

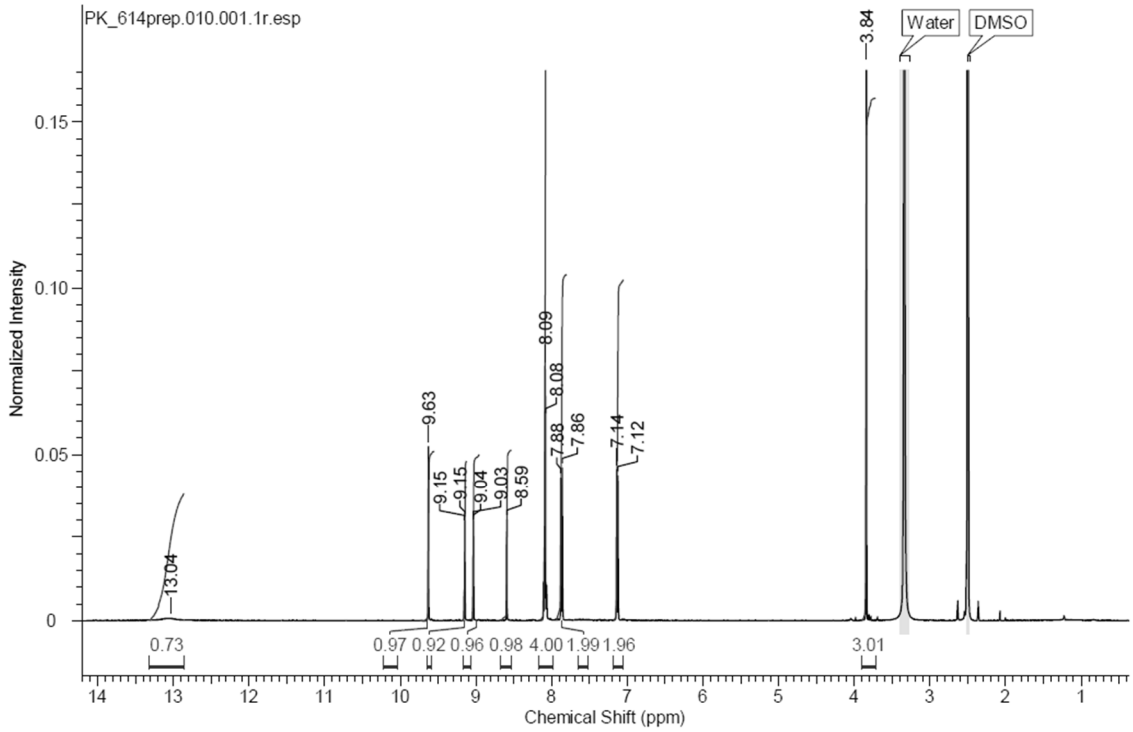

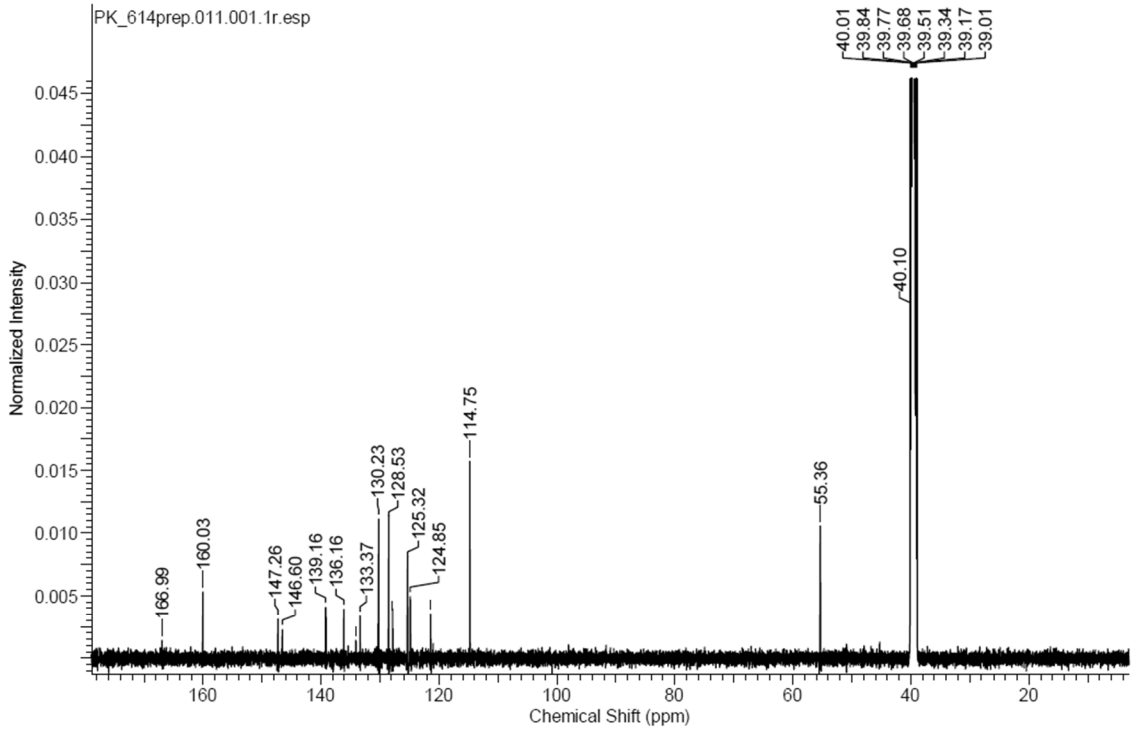

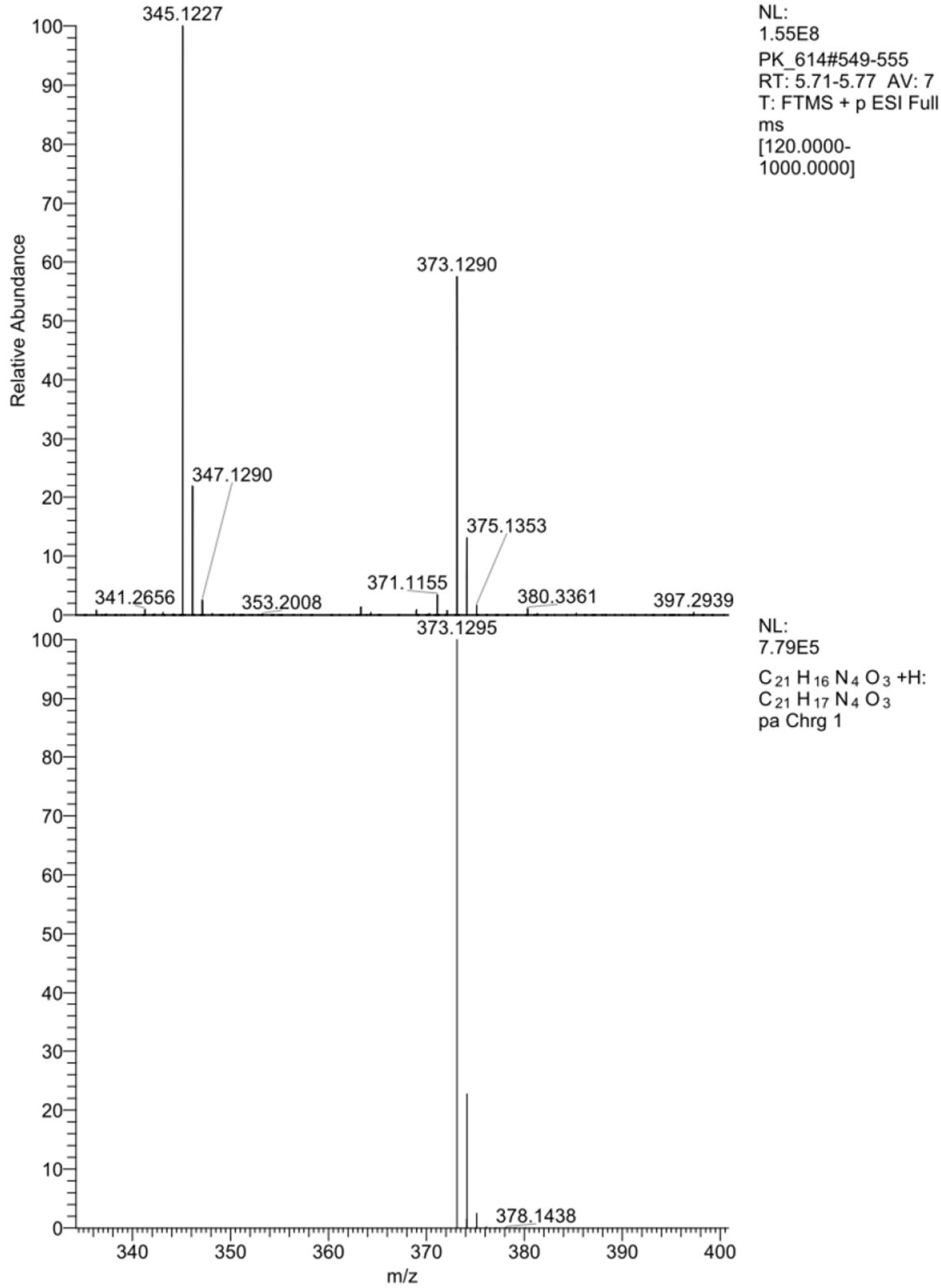
345.1227
NL:
1.55E8
PK_614#549-555
RT: 5.71-5.77 AV: 7
T: FTMS + p ESI Full
ms
[120.0000-
1000.0000]
373.1290
347.1290
375.1353
371.1155
341.2656
353.2008
380.3361
397.2939
373.1295
NL:
7.79E5
C21 H16 N4 O3 +H:
C21 H17 N4 O3
pa Chrg 1
378.1438
Relative Abundance
m/z

4-(1-(5-(3-hydroxyphenyl)pyridin-3-yl)-1*H*-1,2,3-triazol-4-yl)benzoic acid (36e):

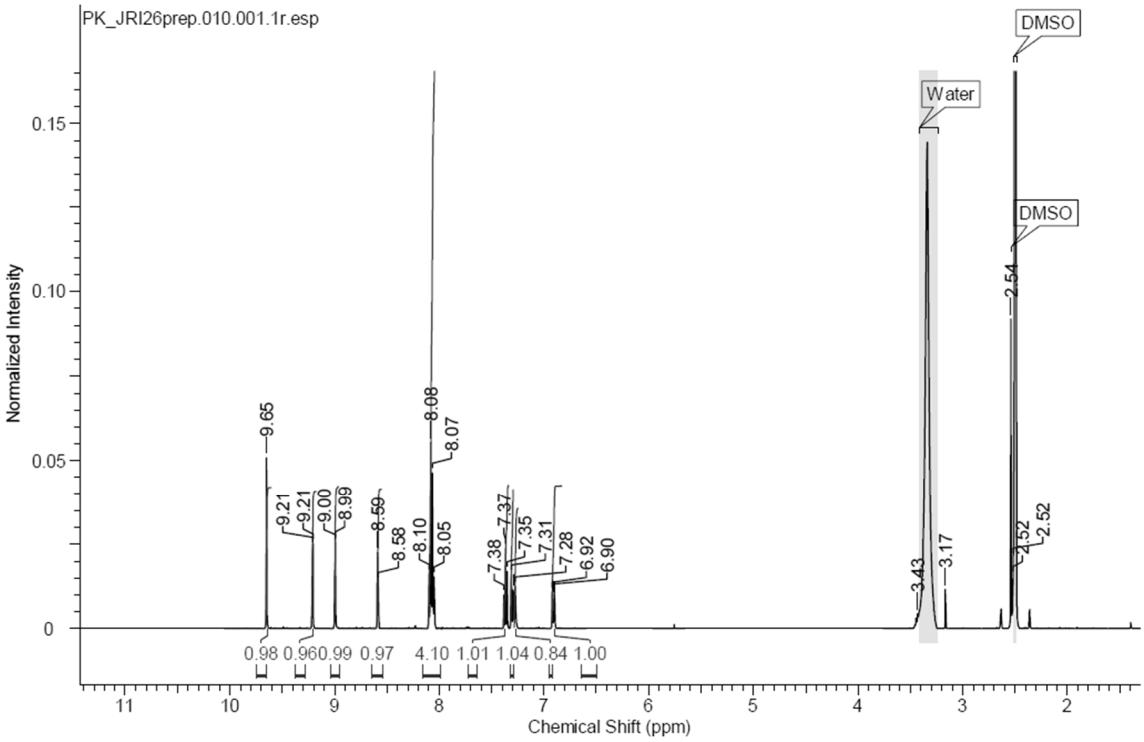

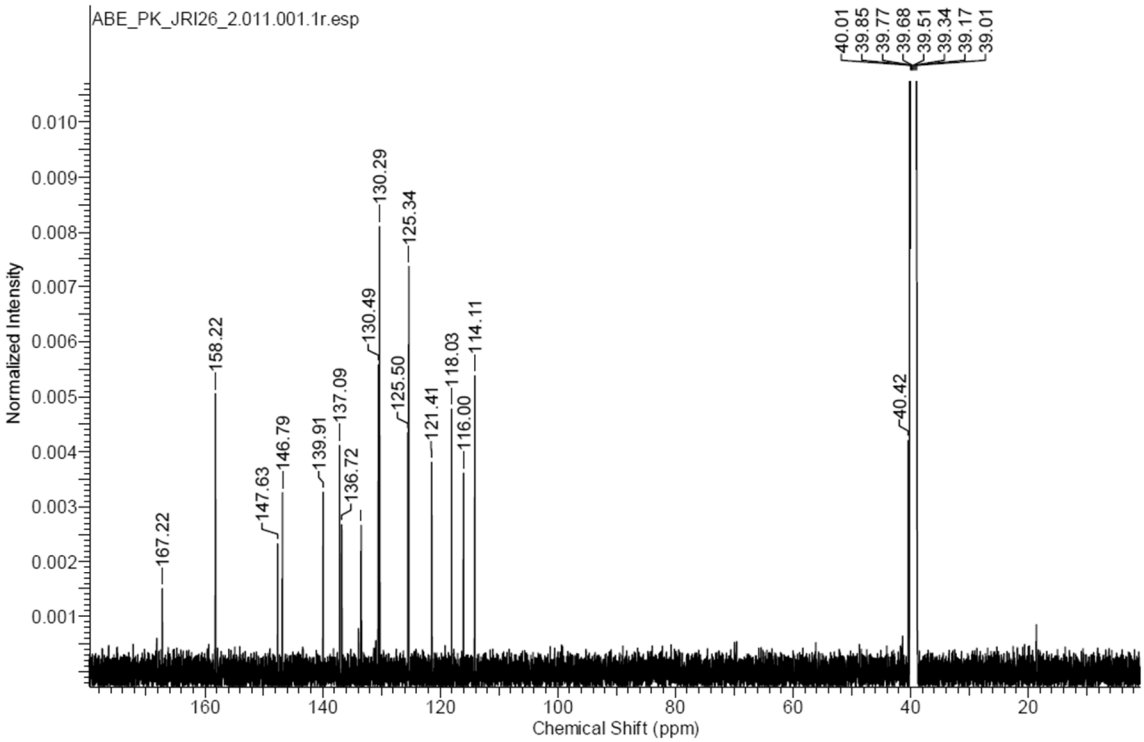

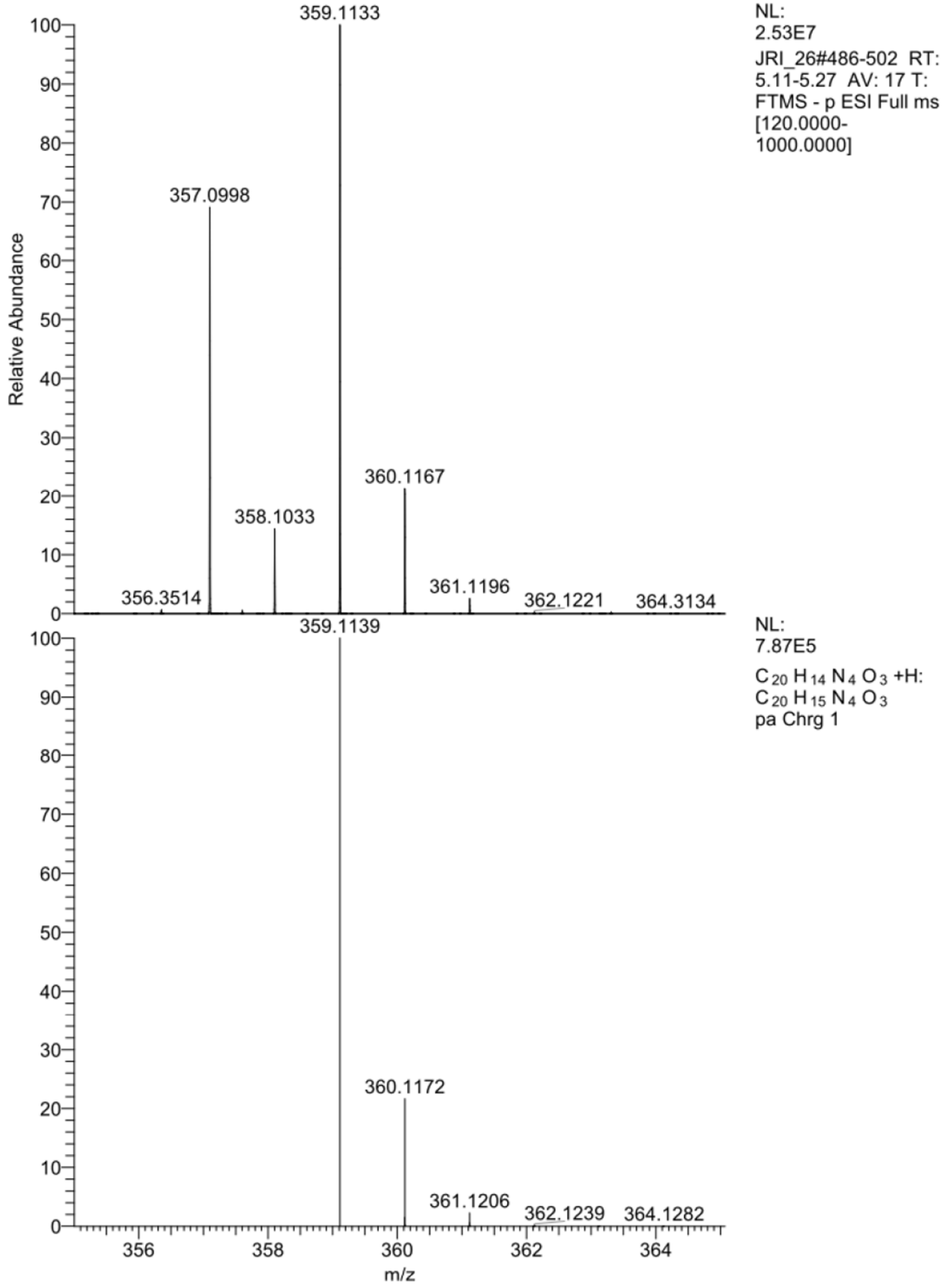
359.1133
NL:
2.53E7
JRI_26#486-502 RT:
5.11-5.27 AV: 17 T:
FTMS - p ESI Full ms
[120.0000-
1000.0000]
357.0998
360.1167
358.1033
356.3514
361.1196
362.1221
364.3134
Relative Abundance
359.1139
NL:
7.87E5
C20 H14 N4 O3 +H:
C20 H15 N4 O3
pa Chrg 1
360.1172
361.1206
362.1239
364.1282
356
358
360
362
364
m/z

4-(1-(5-(3,4-dimethylphenyl)pyridin-3-yl)-1*H*-1,2,3-triazol-4-yl)benzoic acid (36f):

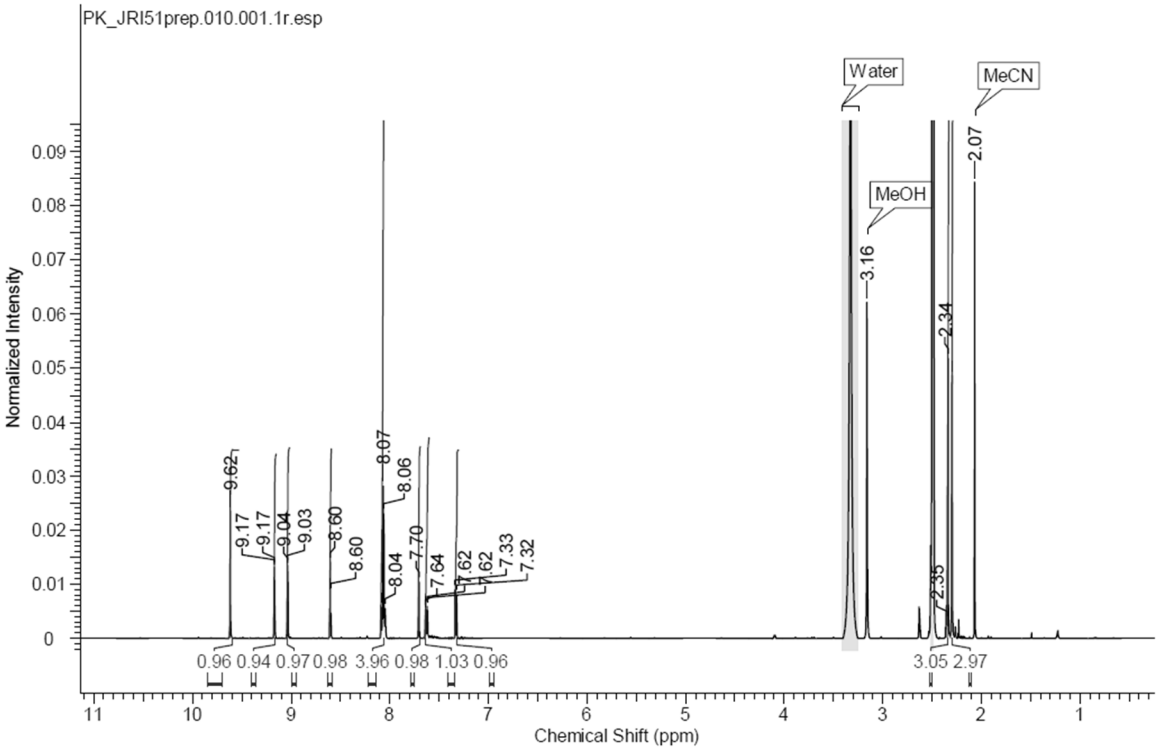

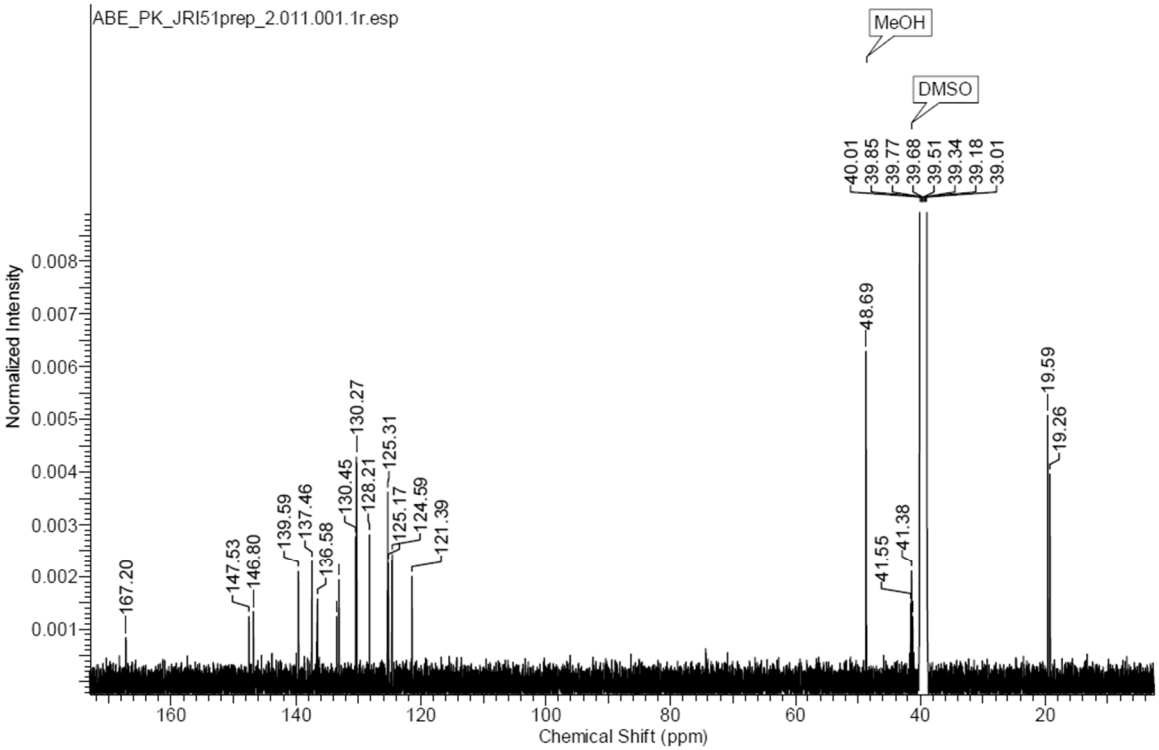

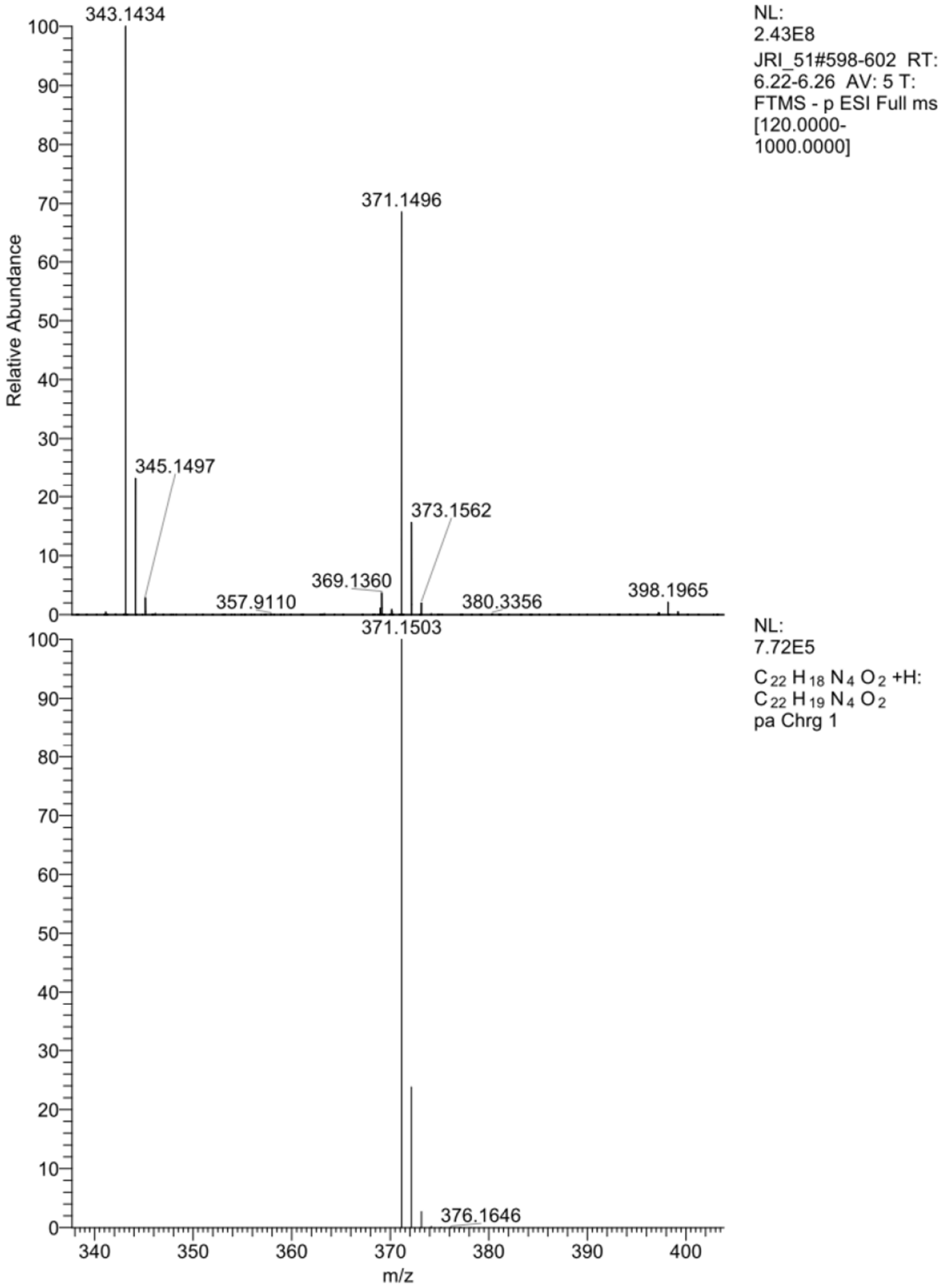
343.1434
371.1496
345.1497
373.1562
369.1360
357.9110
380.3356
398.1965
NL:
2.43E8
JRI_51#598-602 RT:
6.22-6.26 AV: 5 T:
FTMS - p ESI Full ms
[120.0000-
1000.0000]
Relative Abundance
371.1503
376.1646
NL:
7.72E5
C22 H18 N4 O2 +H:
C22 H19 N4 O2
pa Chrg 1
m/z

4-(1-(5-(3,4-difluorophenyl)pyridin-3-yl)-1*H*-1,2,3-triazol-4-yl)benzoic acid (36g):

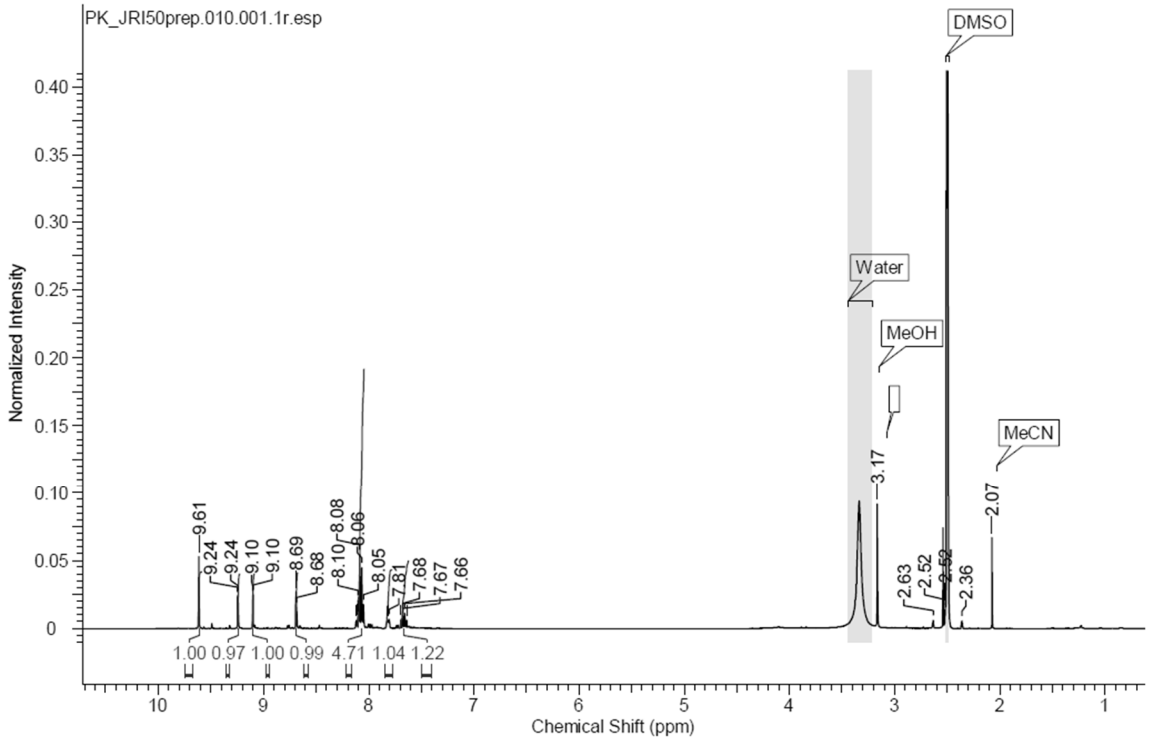

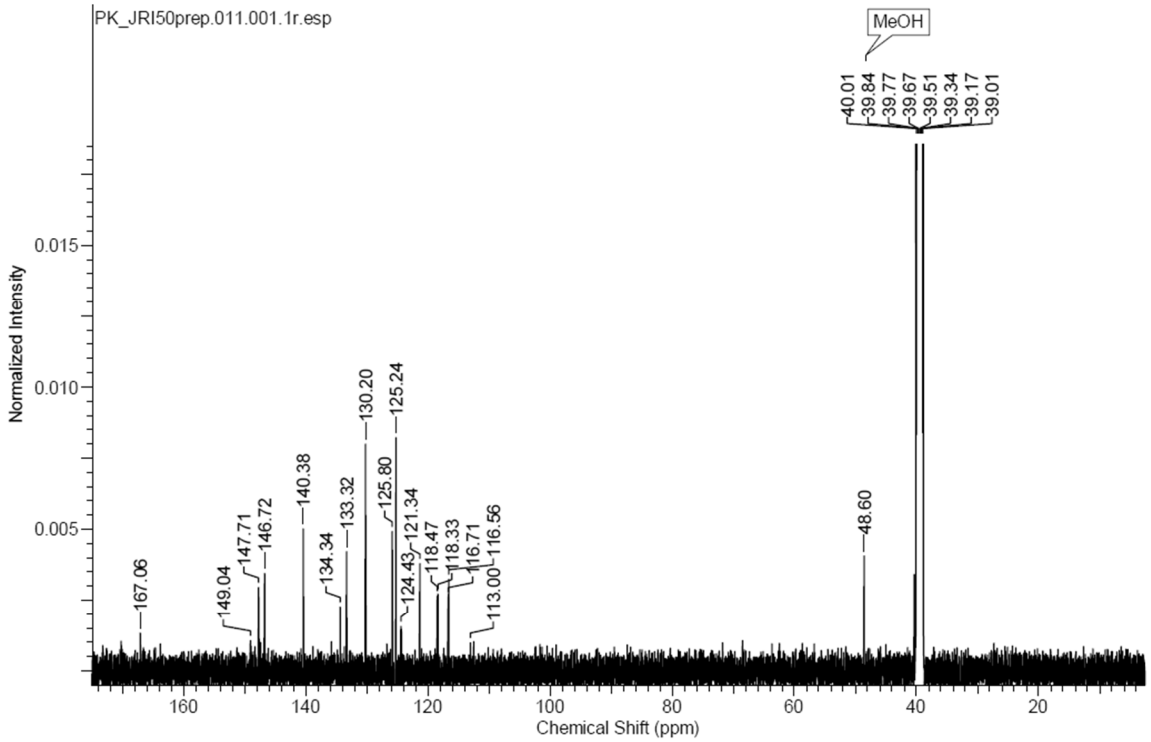

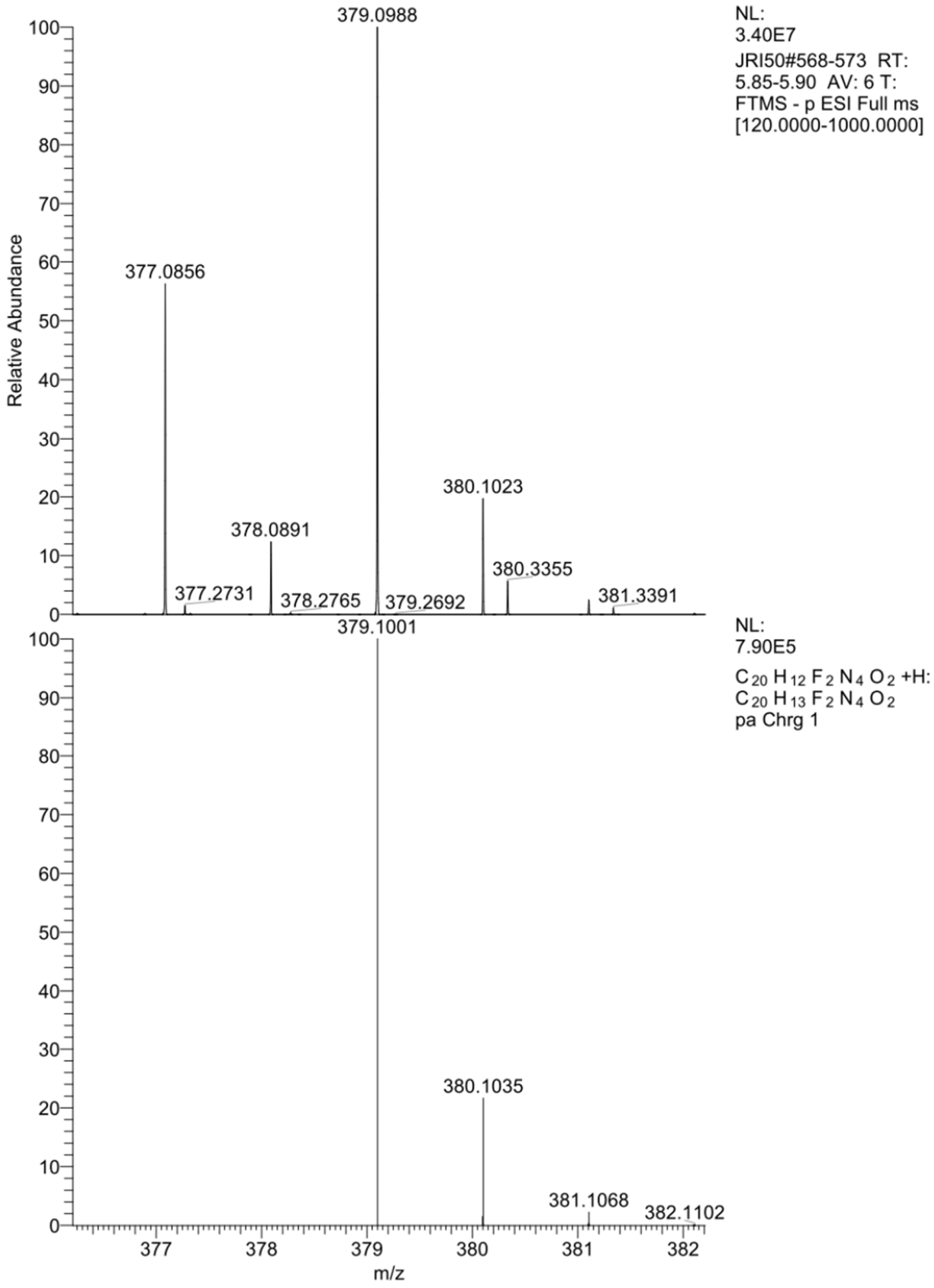
379.0988
NL:
3.40E7
JRI50#568-573 RT:
5.85-5.90 AV: 6 T:
FTMS - p ESI Full ms
[120.0000-1000.0000]
377.0856
380.1023
378.0891
380.3355
377.2731
378.2765
379.2692
381.3391
379.1001
NL:
7.90E5
C20 H12 F2 N4 O2 +H:
C20 H13 F2 N4 O2
pa Chrg 1
380.1035
381.1068
382.1102
Relative Abundance
m/z
100
90
80
70
60
50
40
30
20
10
0
377
378
379
380
381
382

4-(1-(5-(4-(hydroxymethyl)phenyl)pyridin-3-yl)-1*H*-1,2,3-triazol-4-yl)benzoic acid (36h):

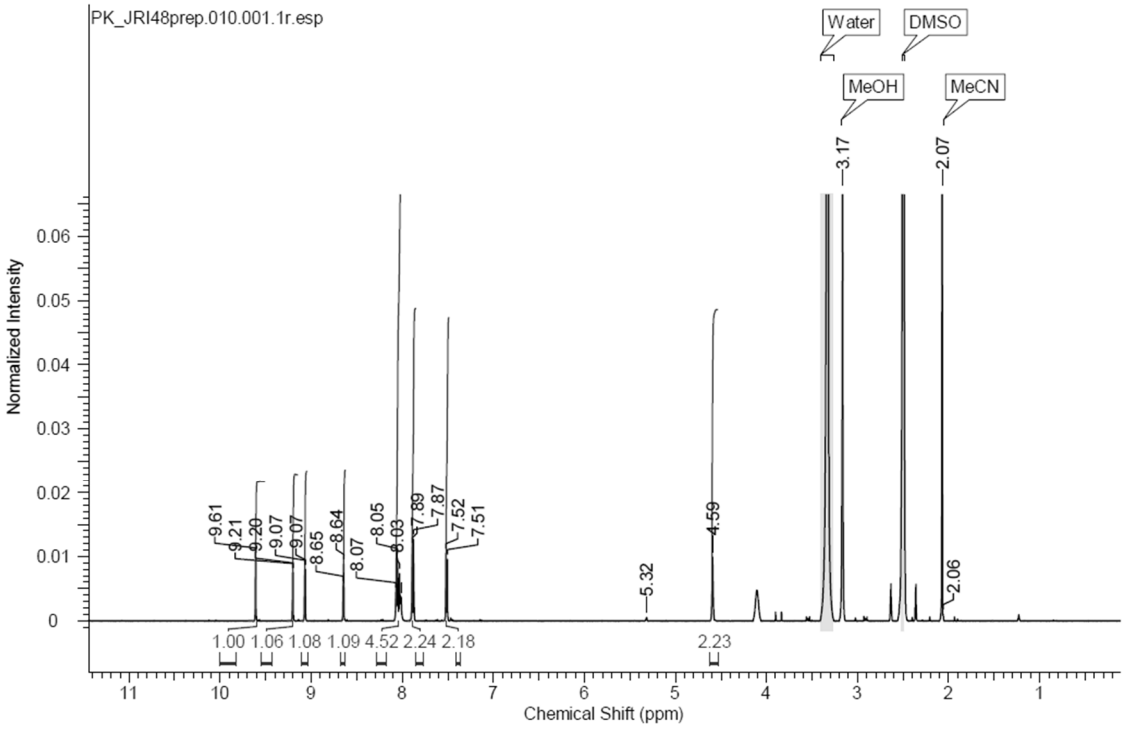

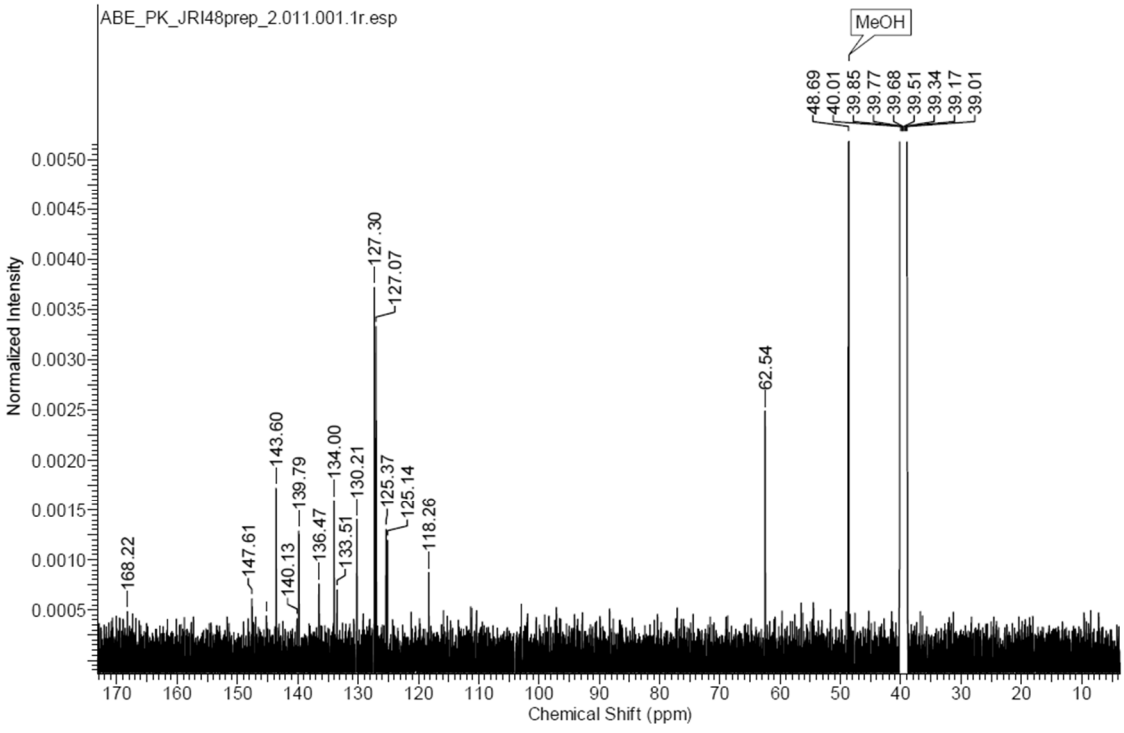

98

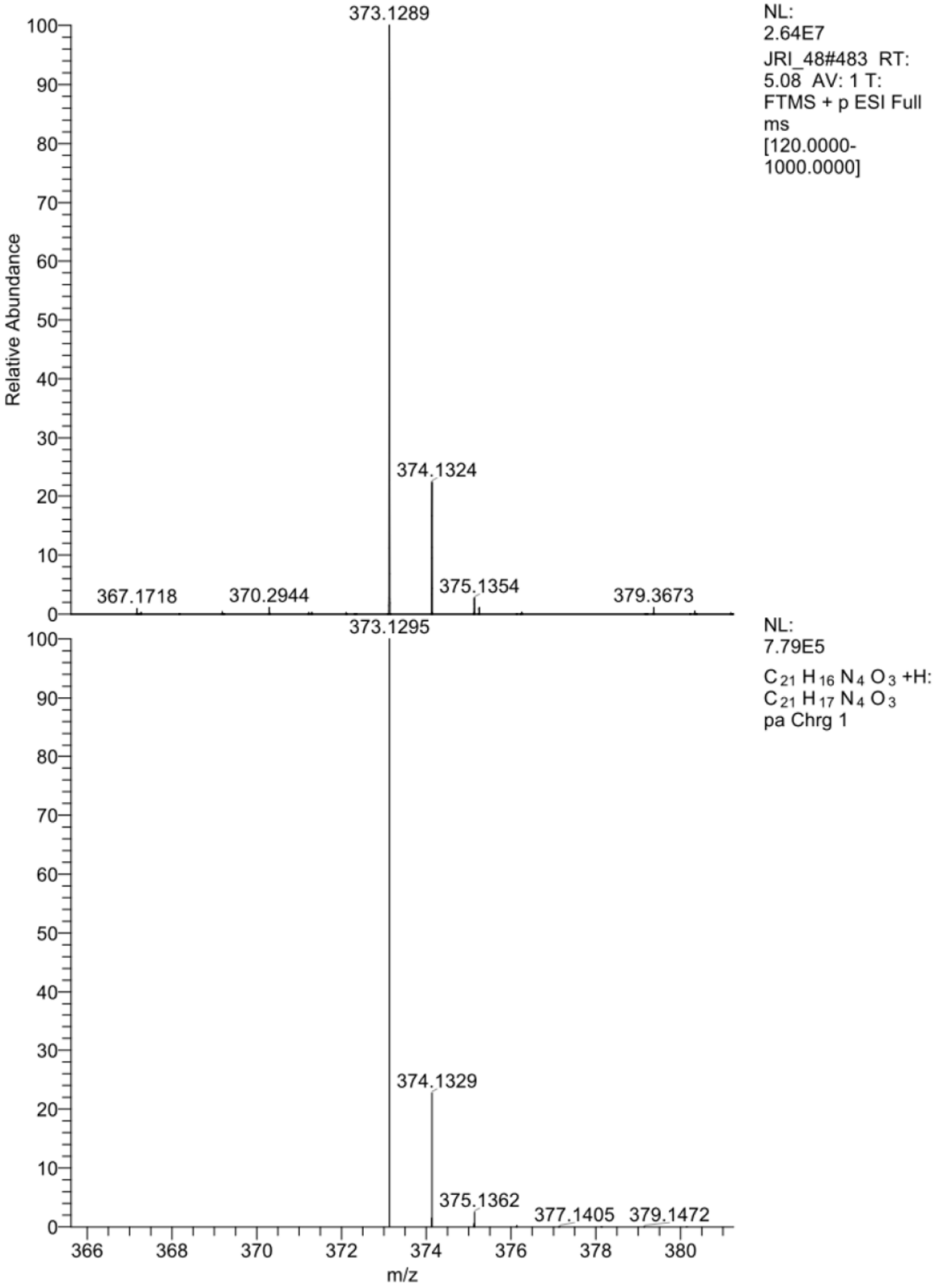
373.1289
NL:
2.64E7
JRI_48#483 RT:
5.08 AV: 1 T:
FTMS + p ESI Full
ms
[120.0000-
1000.0000]
374.1324
367.1718
370.2944
375.1354
379.3673
Relative Abundance
373.1295
NL:
7.79E5
C21 H16 N4 O3 +H:
C21 H17 N4 O3
pa Chrg 1
374.1329
375.1362
377.1405
379.1472
m/z

4-(1-(5-(3-fluoro-5-methoxyphenyl)pyridin-3-yl)-1*H*-1,2,3-triazol-4-yl)benzoic acid (36i):

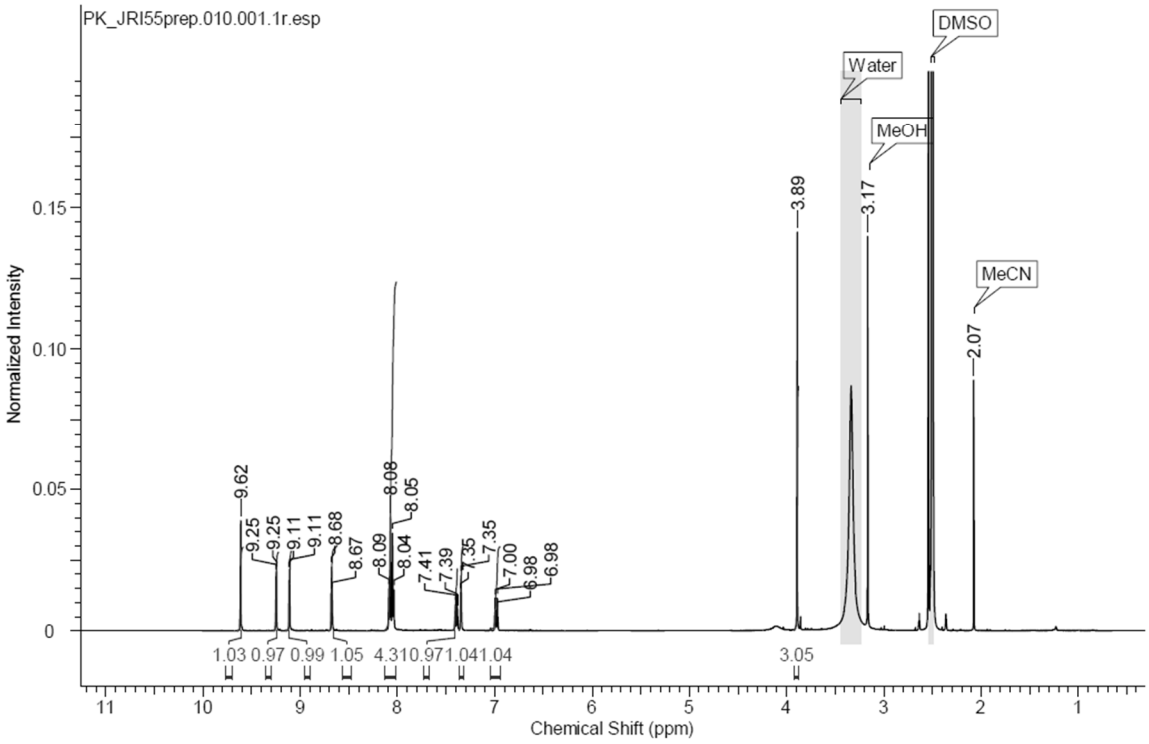

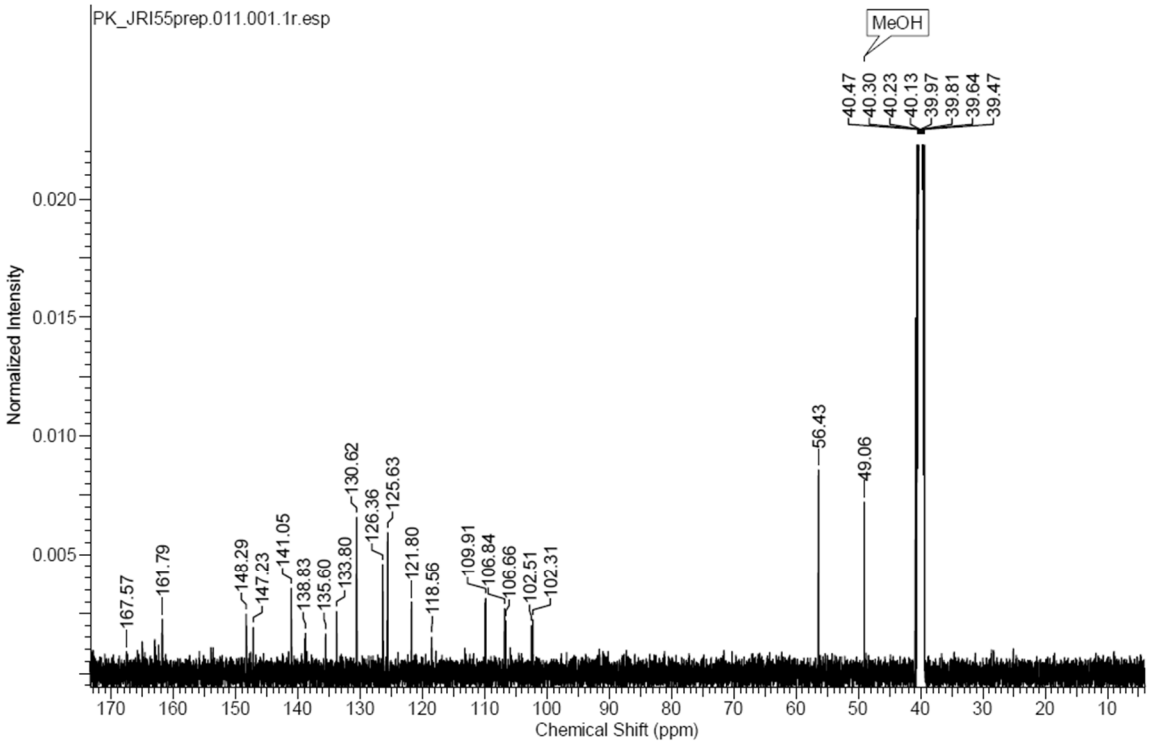

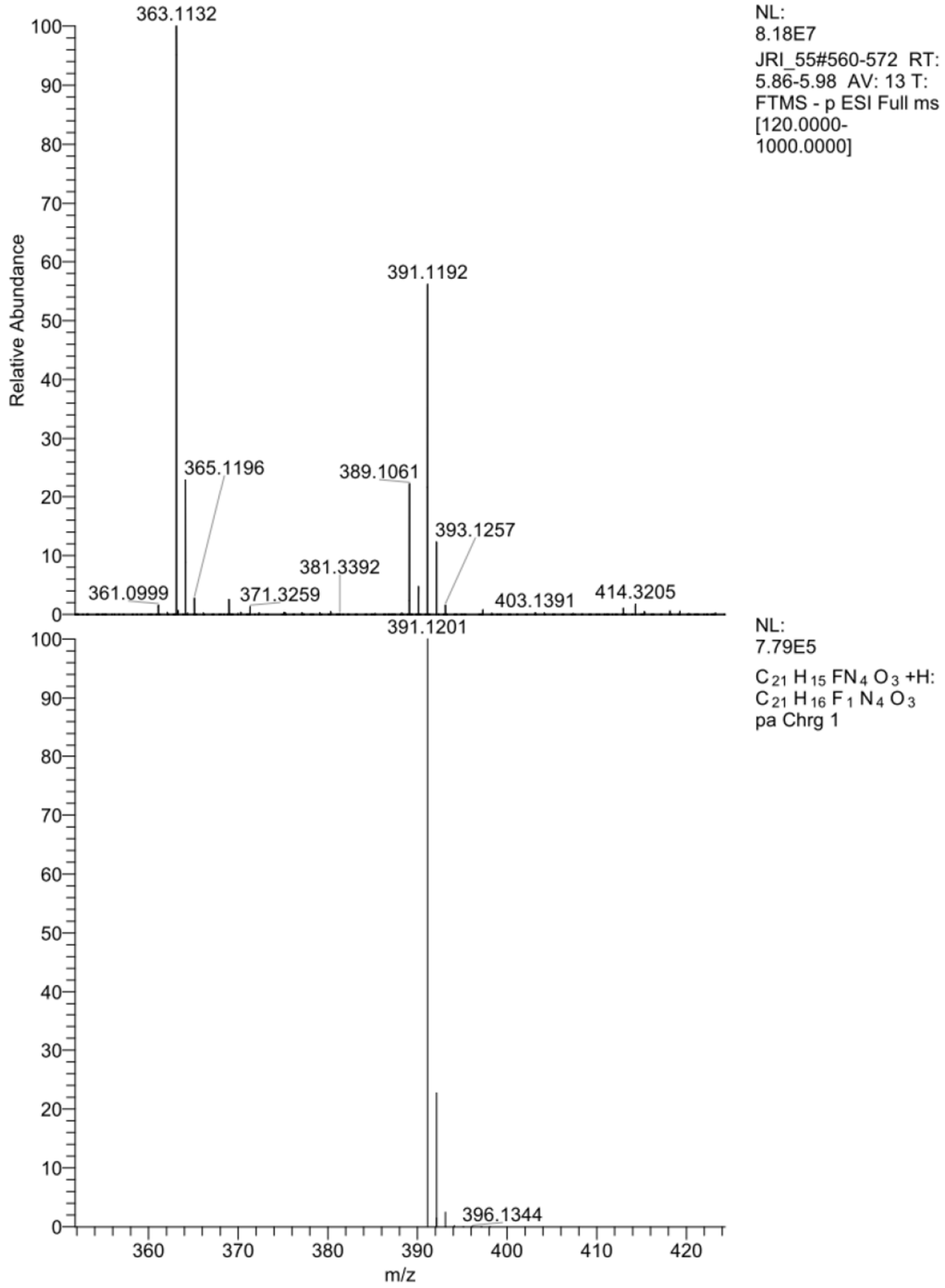
363.1132
NL:
8.18E7
JRI_55#560-572 RT:
5.86-5.98 AV: 13 T:
FTMS - p ESI Full ms
[120.0000-
1000.0000]
391.1192
365.1196
389.1061
393.1257
381.3392
361.0999
371.3259
403.1391
414.3205
Relative Abundance
391.1201
NL:
7.79E5
C21 H15 FN4 O3 +H:
C21 H16 F1 N4 O3
pa Chrg 1
396.1344
m/z

4-(1-(5-(furan-3-yl)pyridin-3-yl)-1*H*-1,2,3-triazol-4-yl)benzoic acid (36j):

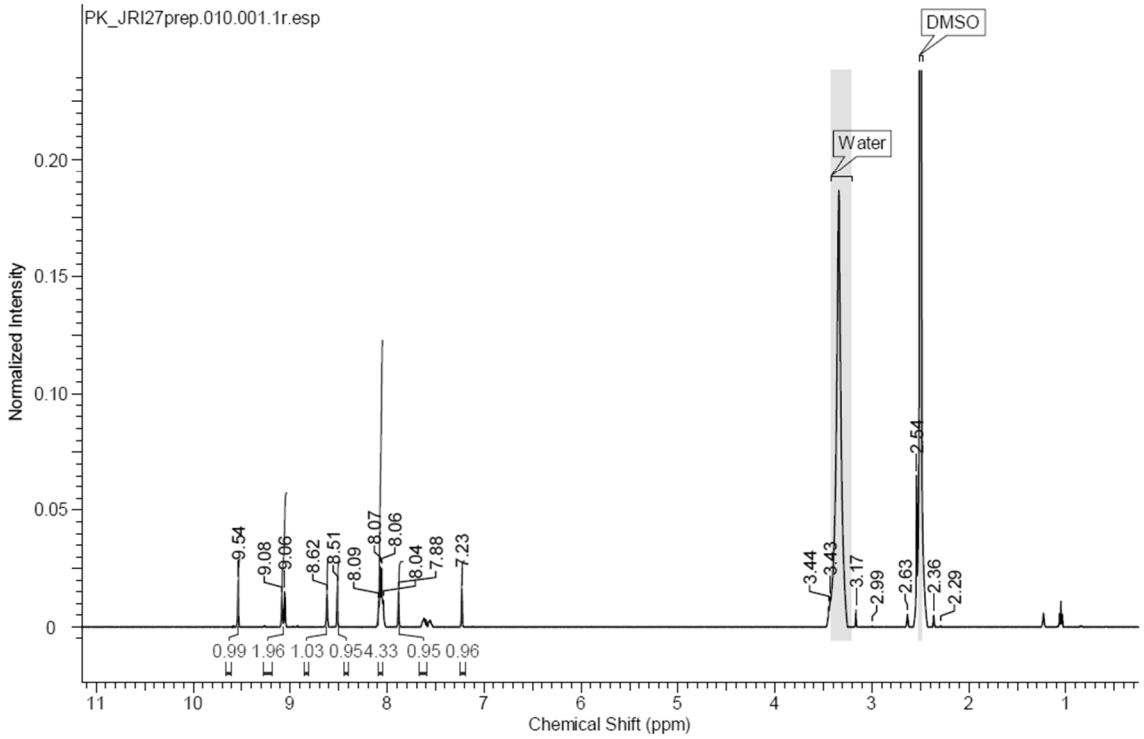

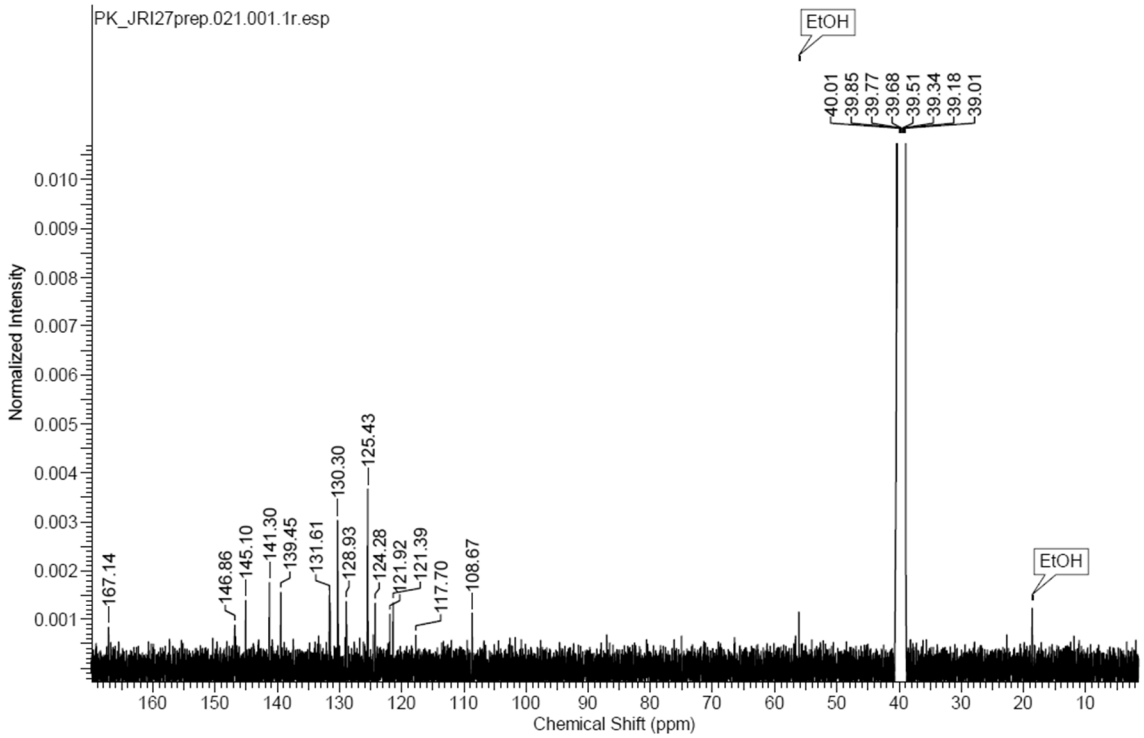

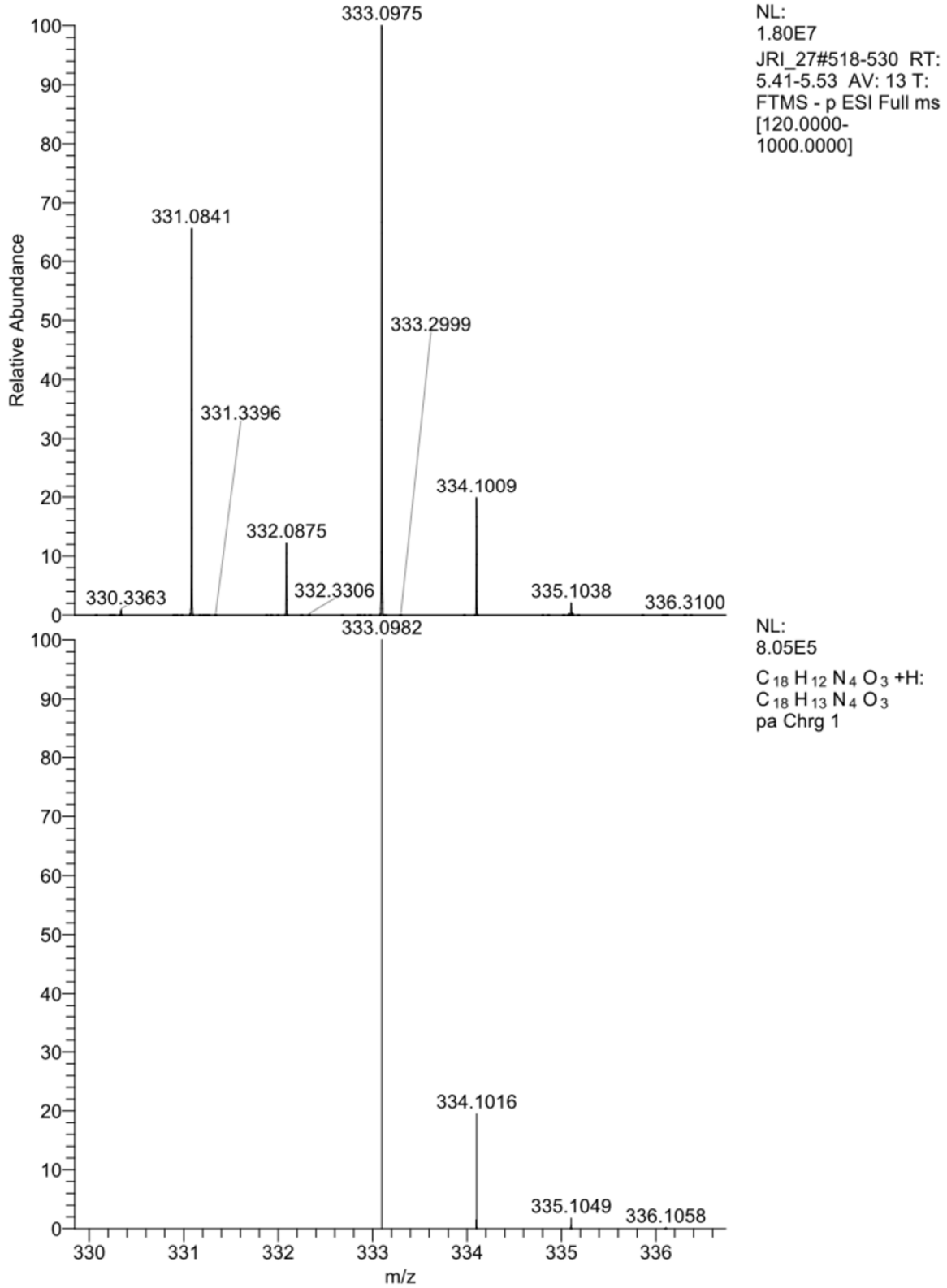
333.0975
NL:
1.80E7
JRI_27#518-530 RT:
5.41-5.53 AV: 13 T:
FTMS - p ESI Full ms
[120.0000-
1000.0000]
331.0841
333.2999
331.3396
334.1009
332.0875
330.3363
332.3306
335.1038
336.3100
Relative Abundance
333.0982
NL:
8.05E5
C18 H12 N4 O3 +H:
C18 H13 N4 O3
pa Chrg 1
334.1016
335.1049
336.1058
m/z

4-(1-(4-methyl-6-phenylpyridin-3-yl)-1*H*-1,2,3-triazol-4-yl)benzoic acid (36k):

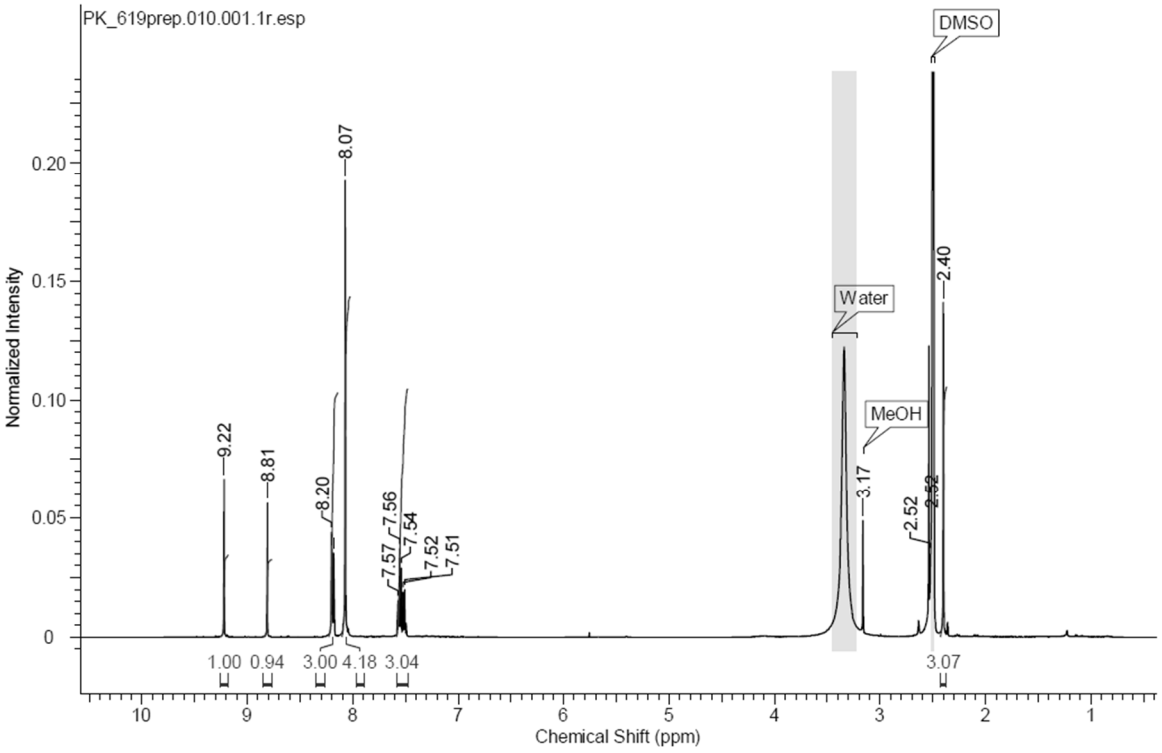

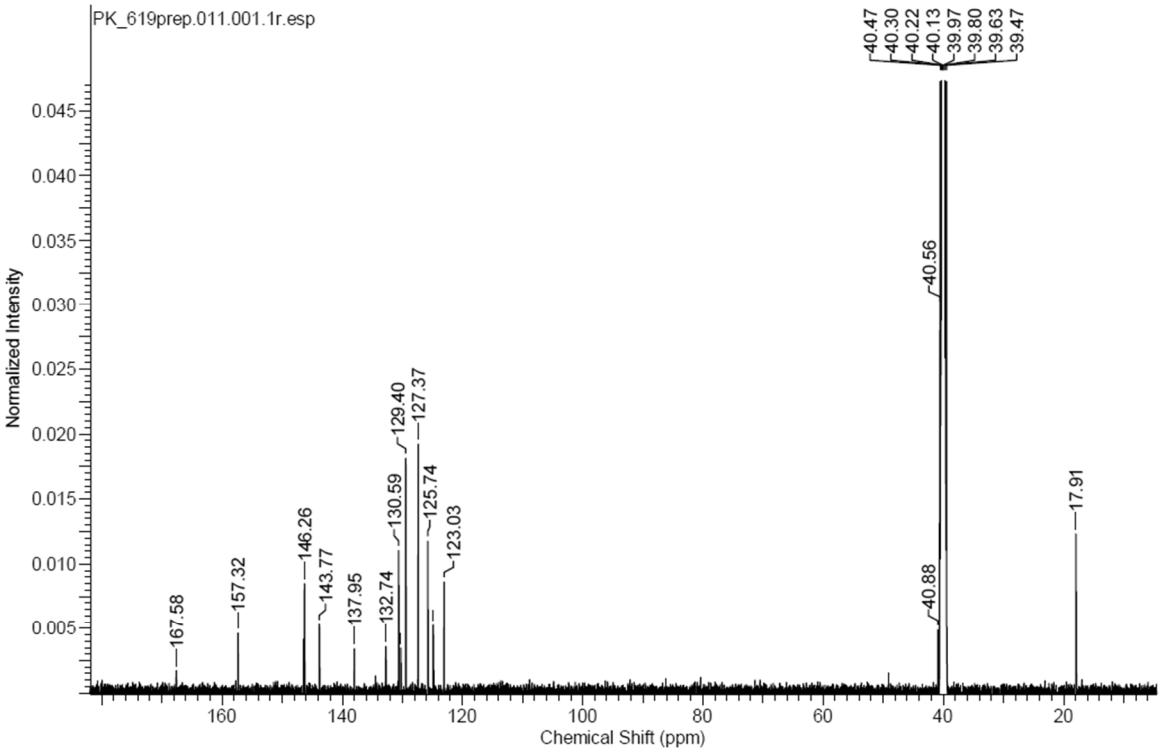

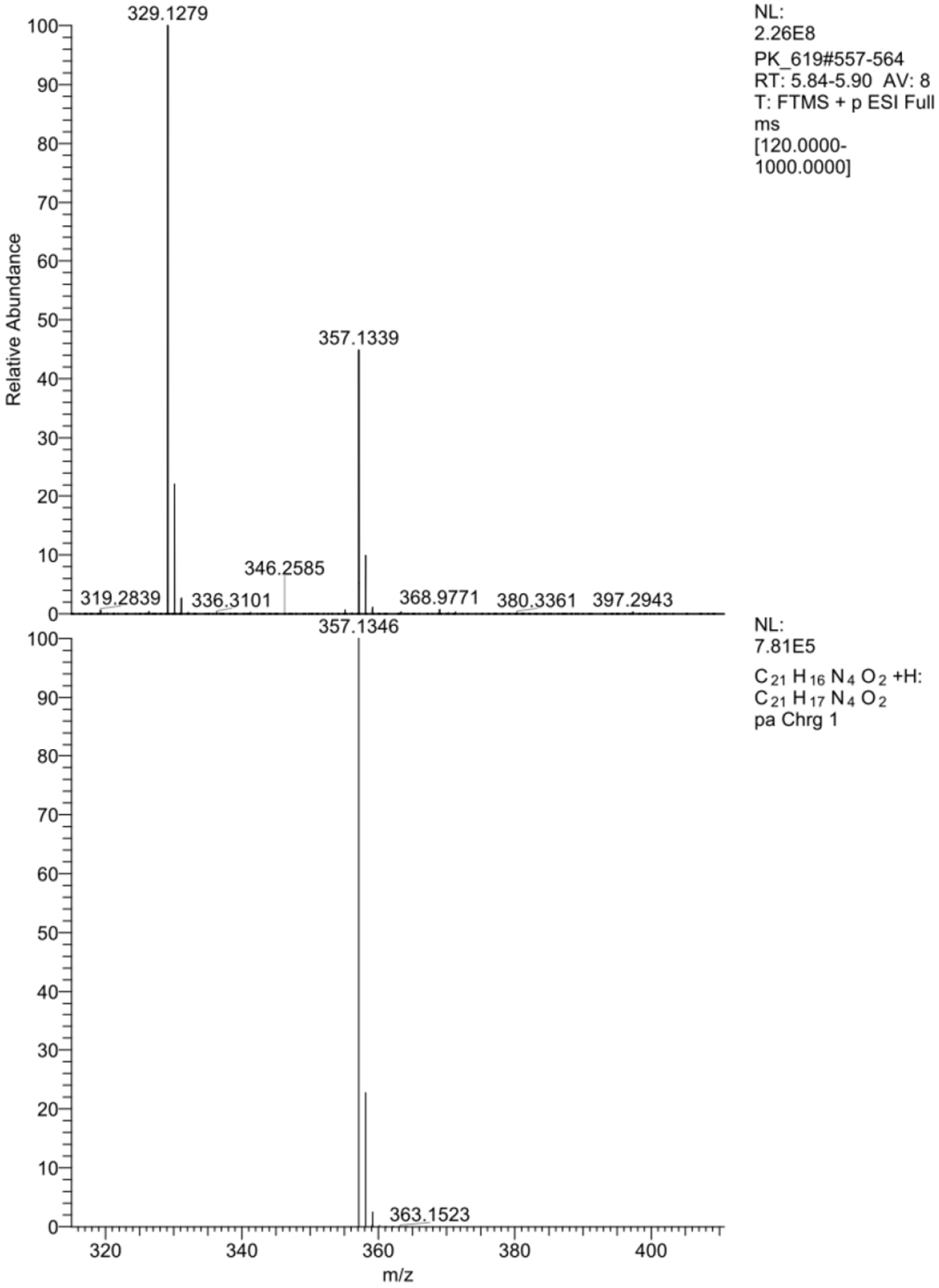
329.1279
NL:
2.26E8
PK_619#557-564
RT: 5.84-5.90 AV: 8
T: FTMS + p ESI Full
ms
[120.0000-
1000.0000]
357.1339
346.2585
319.2839
336.3101
368.9771
380.3361
397.2943
Relative Abundance
357.1346
NL:
7.81E5
C21 H16 N4 O2 +H:
C21 H17 N4 O2
pa Chrg 1
363.1523
m/z

4-(1-(6-(4-chlorophenyl)-4-methylpyridin-3-yl)-1*H*-1,2,3-triazol-4-yl)benzoic acid (36l):

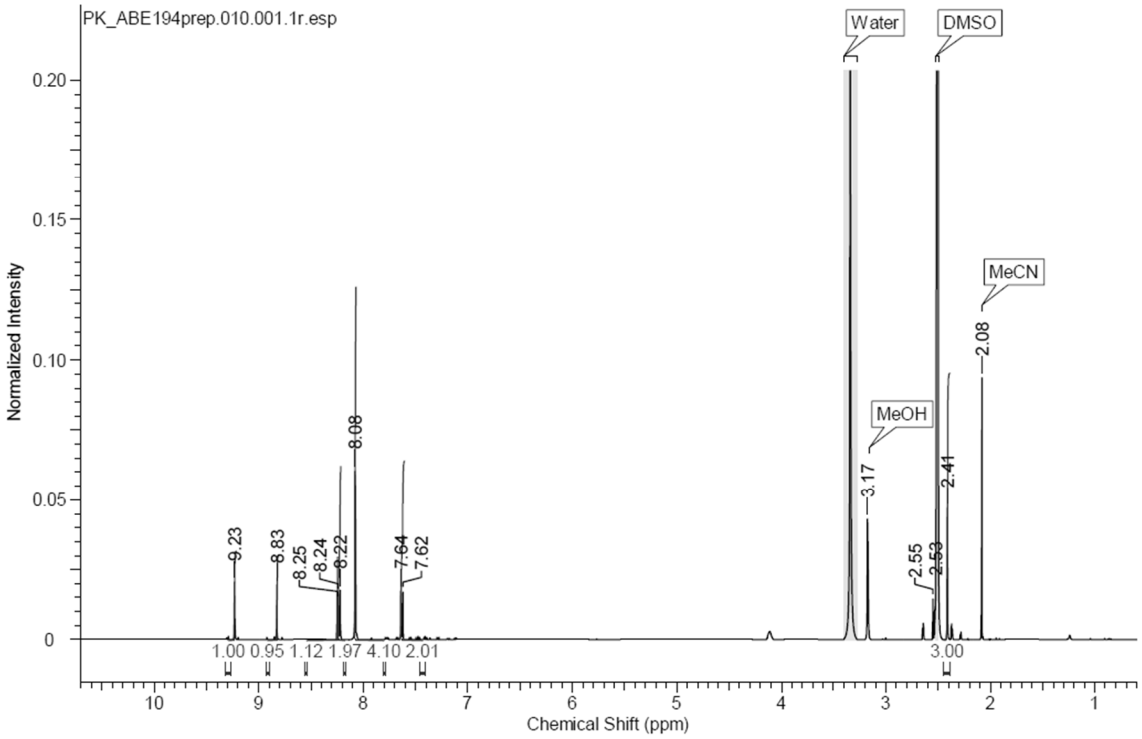

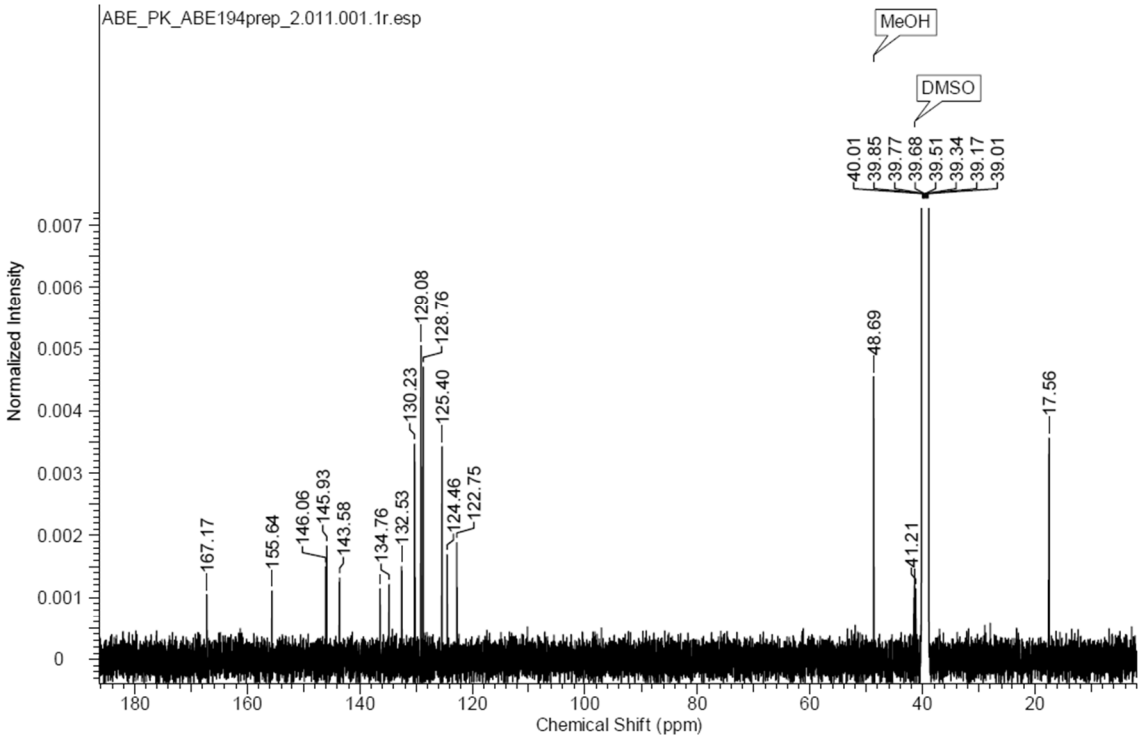

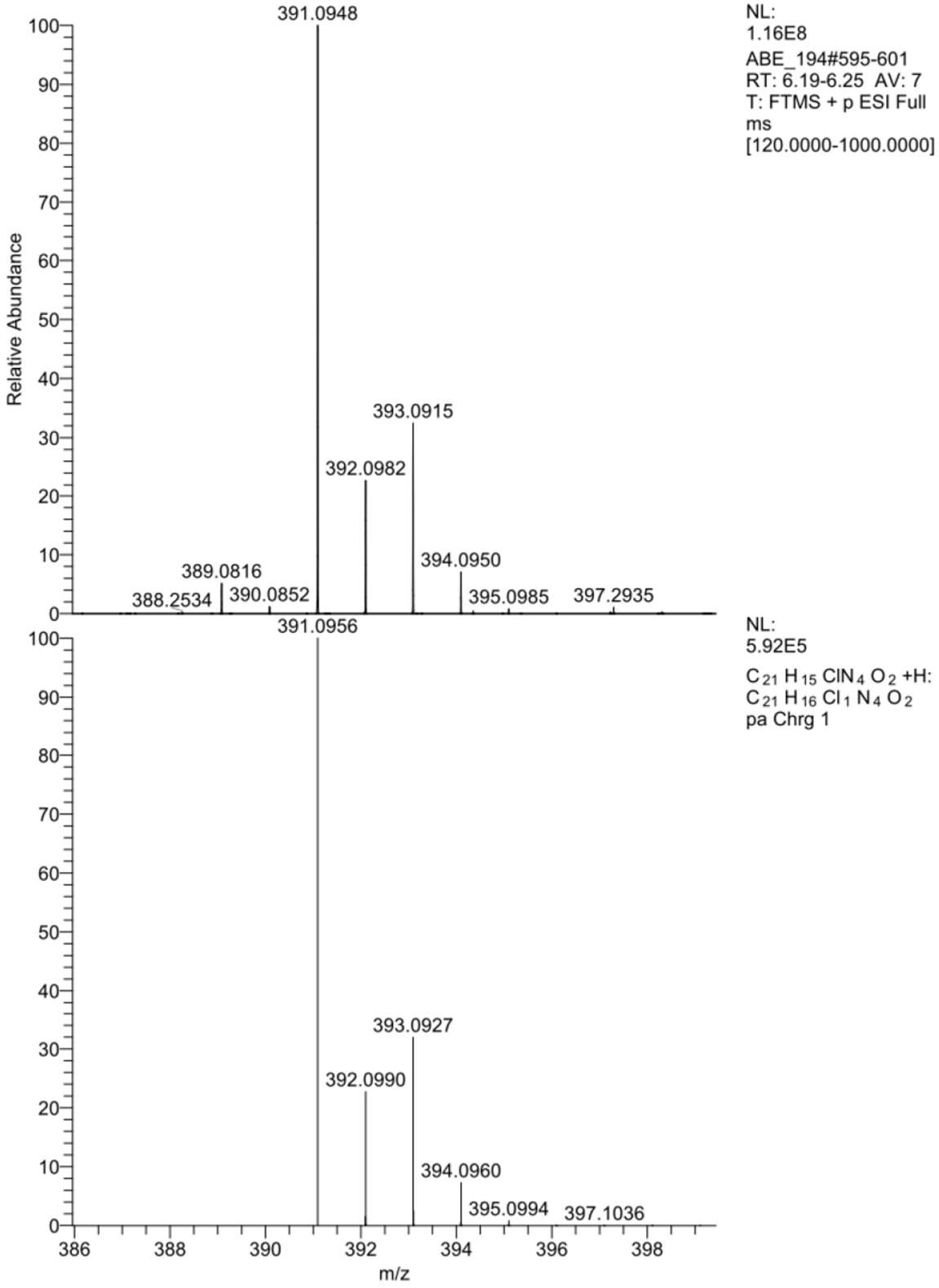
391.0948
NL:
1.16E8
ABE_194#595-601
RT: 6.19-6.25 AV: 7
T: FTMS + p ESI Full
ms
[120.0000-1000.0000]
393.0915
392.0982
394.0950
389.0816
388.2534
390.0852
395.0985
397.2935
Relative Abundance
391.0956
NL:
5.92E5
C21 H15 ClN4 O2 +H:
C21 H16 Cl1 N4 O2
pa Chrg 1
393.0927
392.0990
394.0960
395.0994
397.1036
m/z

4-(1-(4-methyl-6-phenoxypyridin-3-yl)-1*H*-1,2,3-triazol-4-yl)benzoic acid (40a):

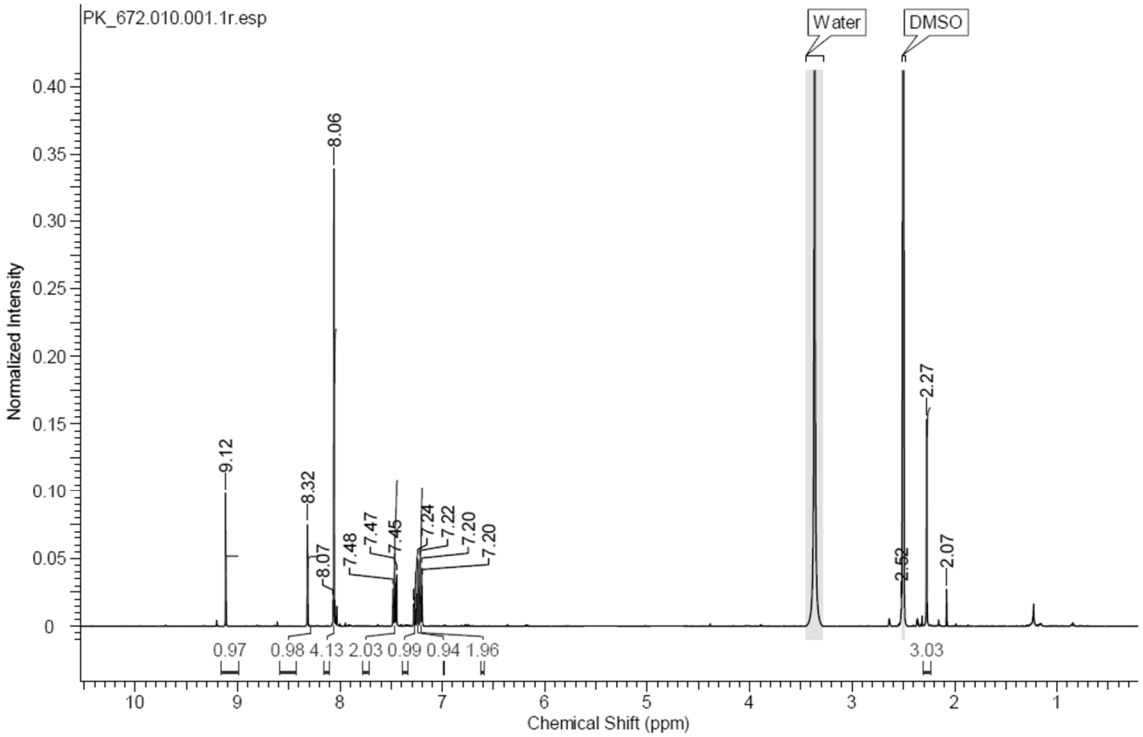

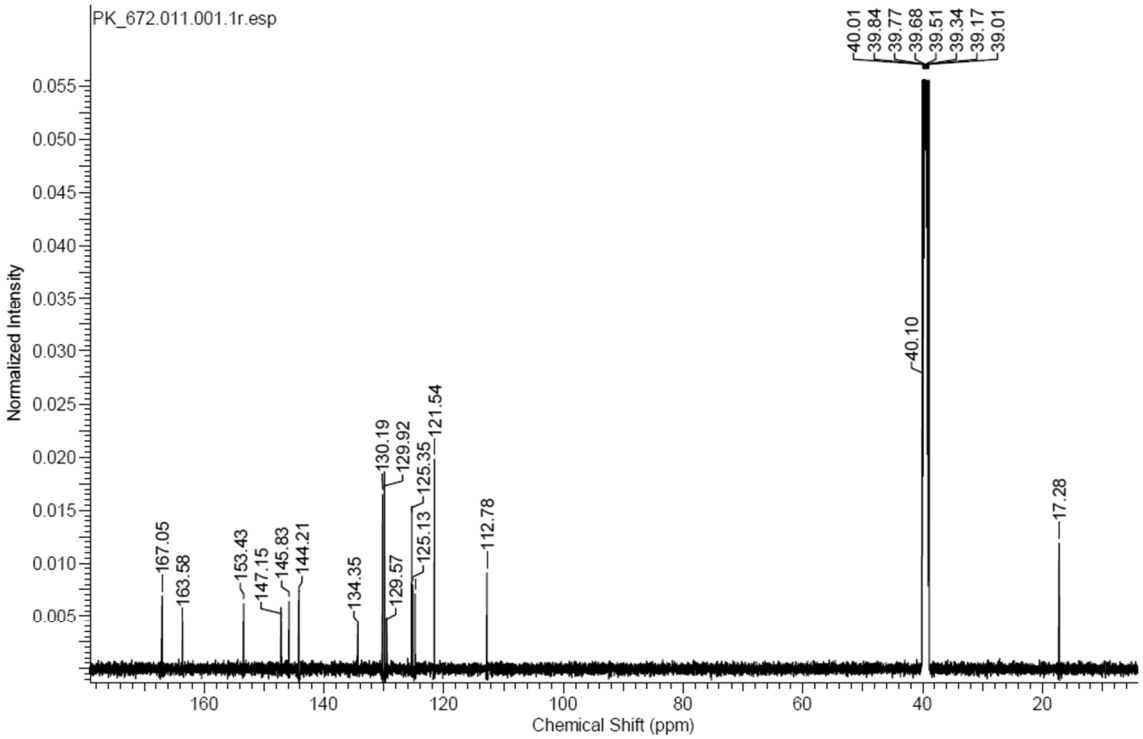

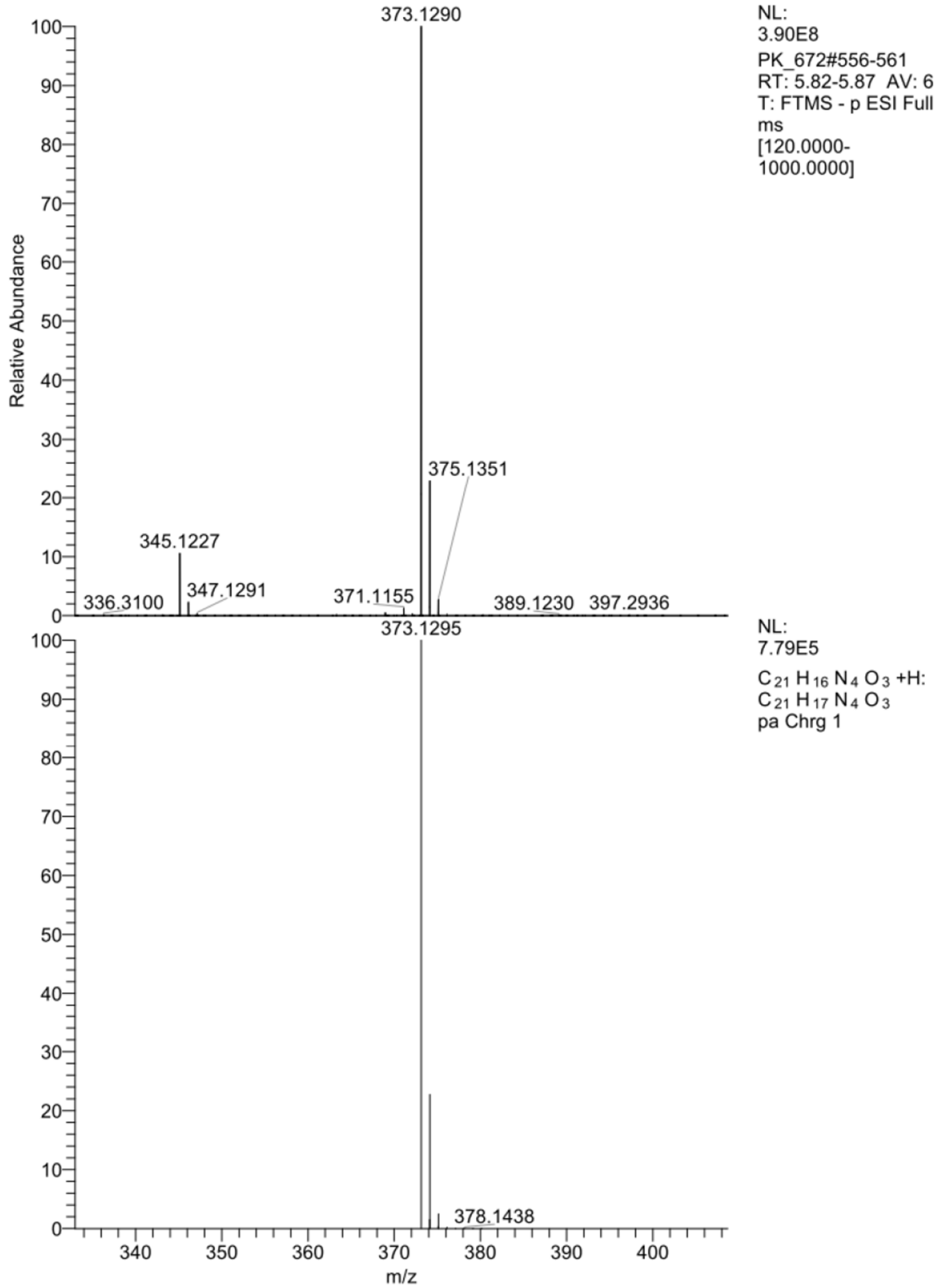
373.1290
NL:
3.90E8
PK_672#556-561
RT: 5.82-5.87 AV: 6
T: FTMS - p ESI Full
ms
[120.0000-
1000.0000]
375.1351
345.1227
347.1291
336.3100
371.1155
389.1230
397.2936
373.1295
NL:
7.79E5
C21 H16 N4 O3 +H:
C21 H17 N4 O3
pa Chrg 1
378.1438
Relative Abundance
m/z

4-(1-(6-(2-fluorophenoxy)-4-methylpyridin-3-yl)-1*H*-1,2,3-triazol-4-yl)benzoic acid (40b):

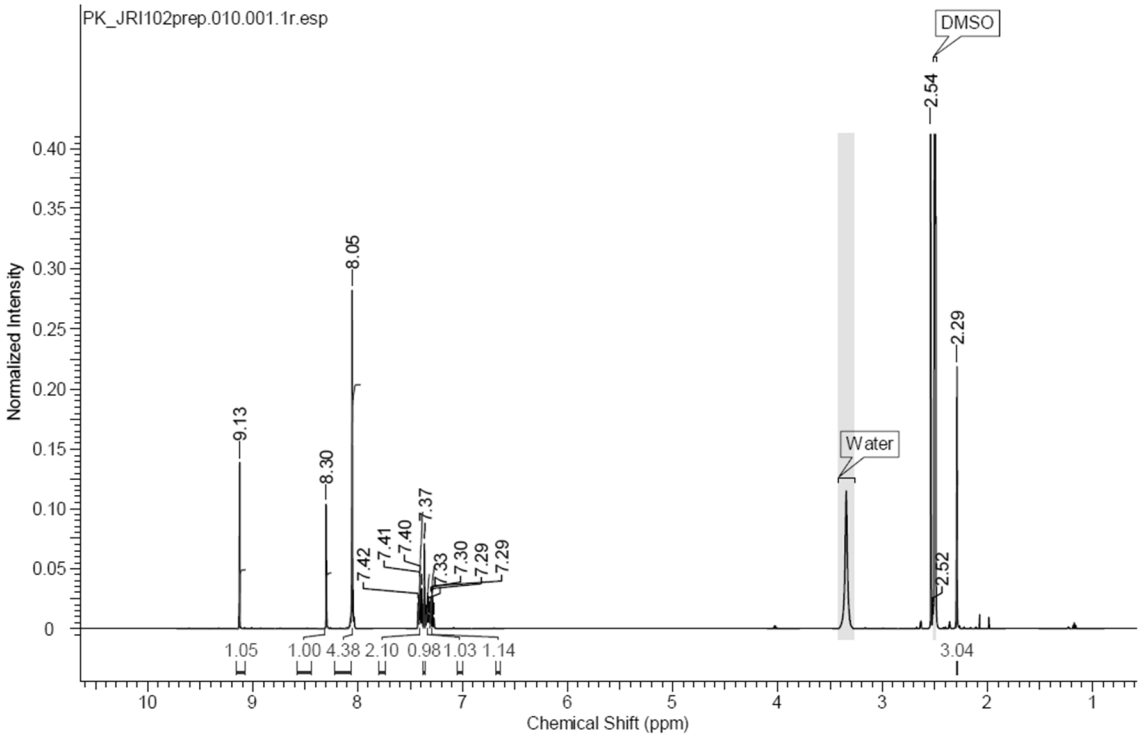

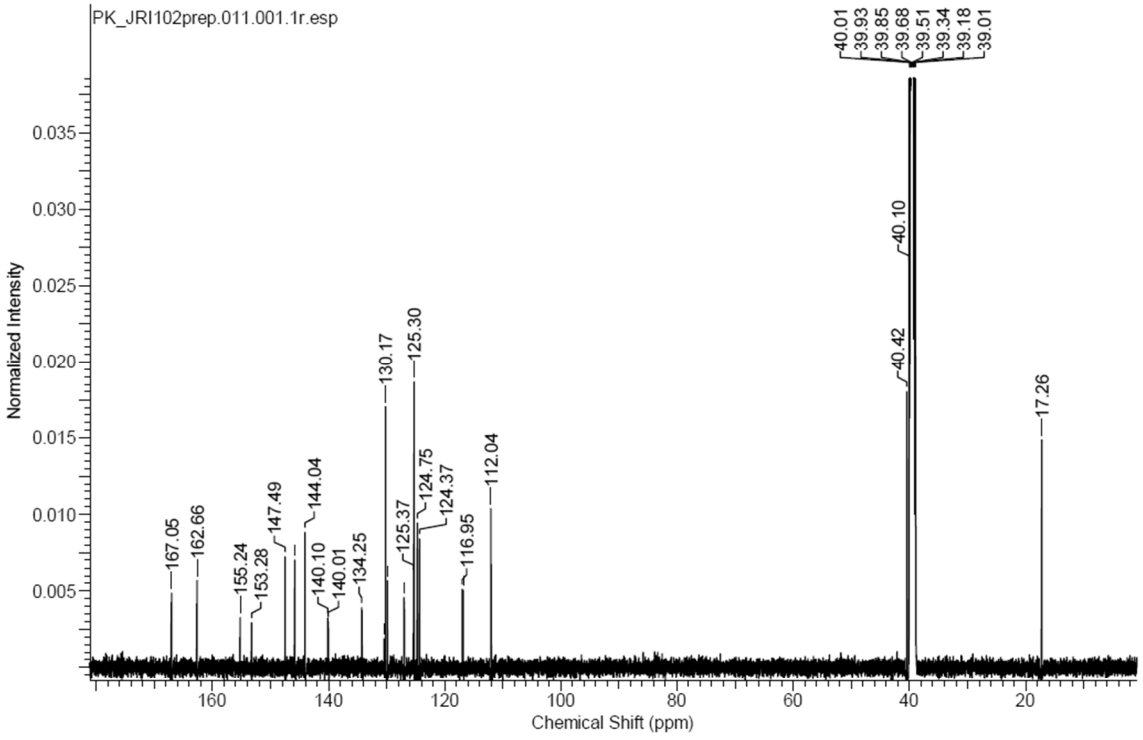

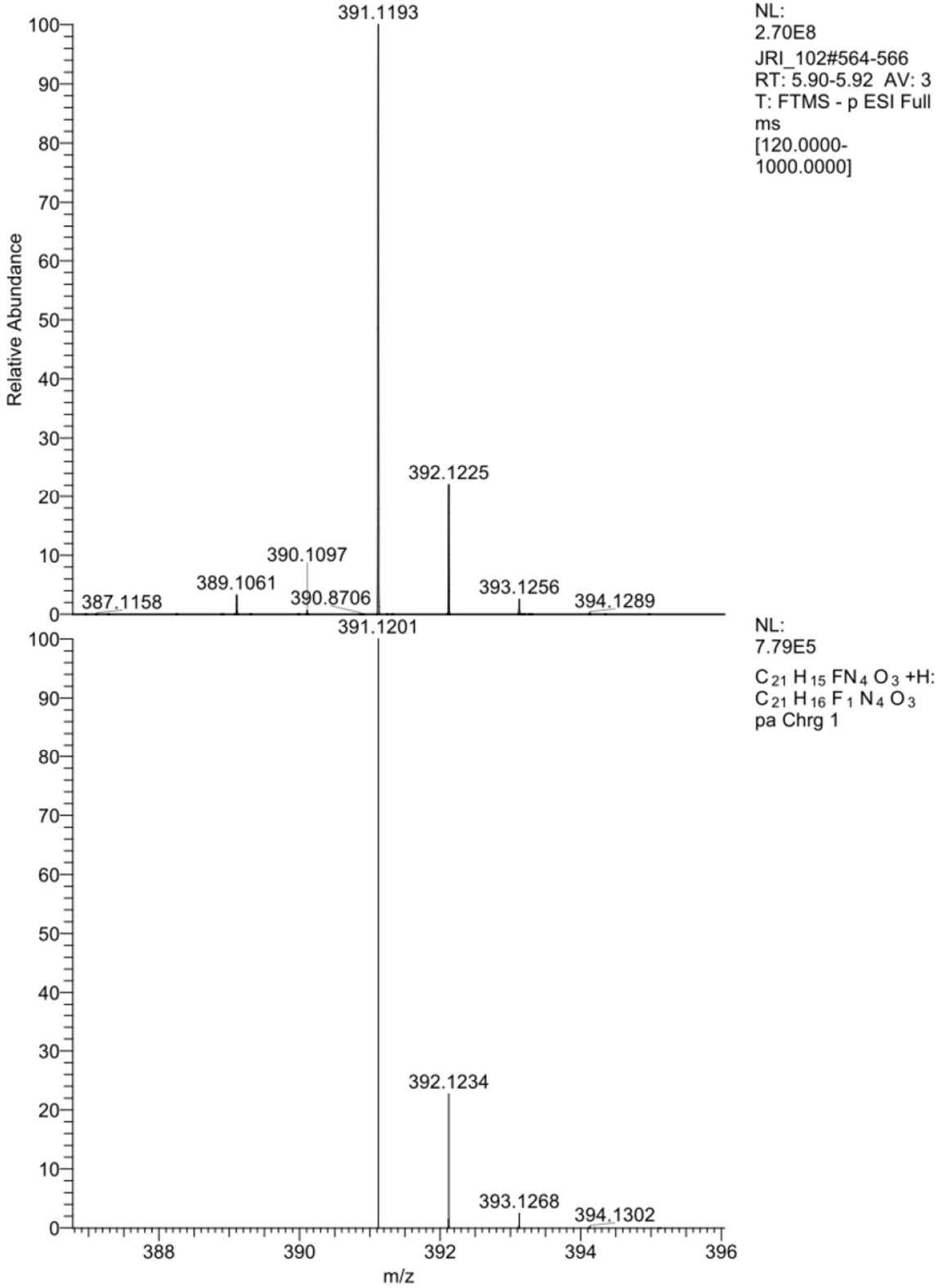
391.1193
NL:
2.70E8
JRI_102#564-566
RT: 5.90-5.92 AV: 3
T: FTMS - p ESI Full
ms
[120.0000-
1000.0000]
392.1225
390.1097
389.1061
390.8706
393.1256
387.1158
394.1289
Relative Abundance
391.1201
NL:
7.79E5
C21 H15 FN4 O3 +H:
C21 H16 F1 N4 O3
pa Chrg 1
392.1234
393.1268
394.1302
m/z

4-(1-(6-(3-fluorophenoxy)-4-methylpyridin-3-yl)-1H-1,2,3-triazol-4-yl)benzoic acid (40c):

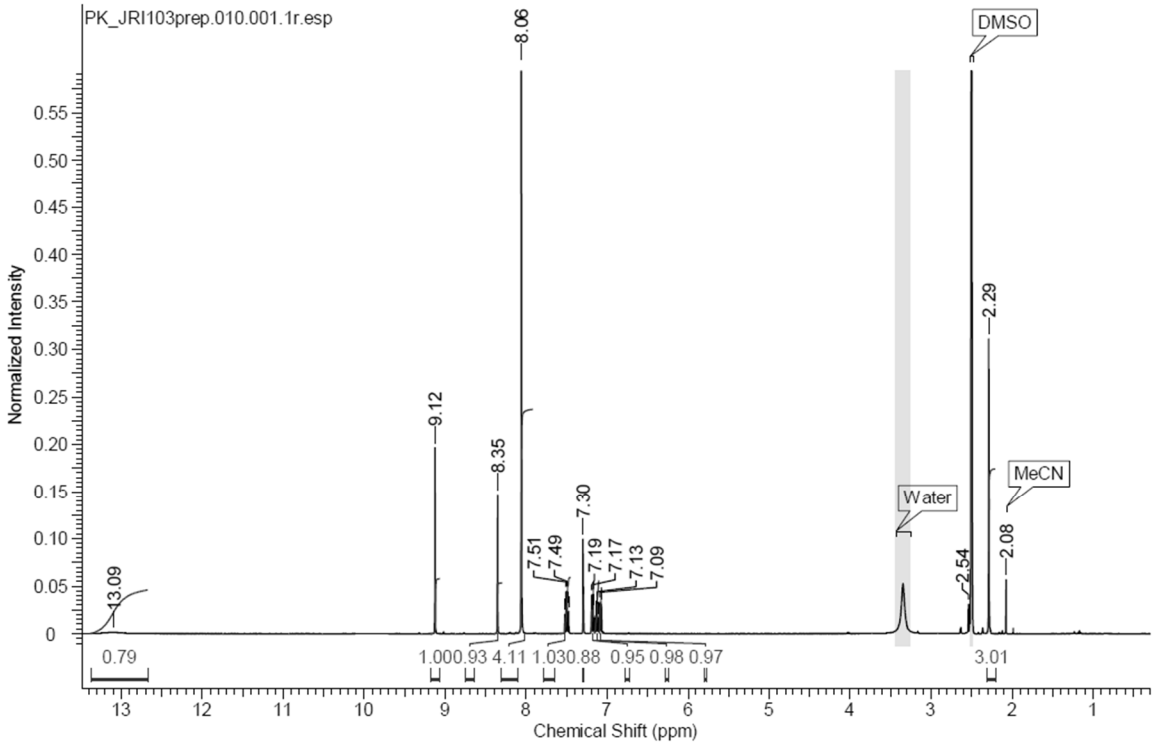

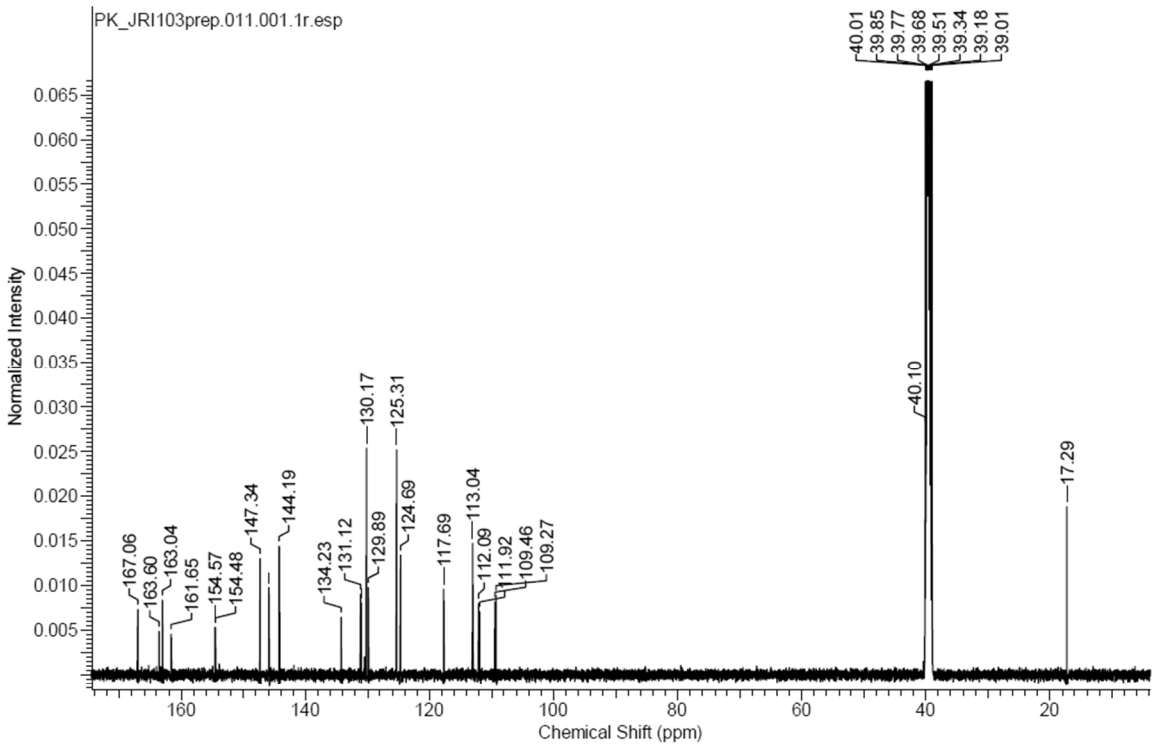

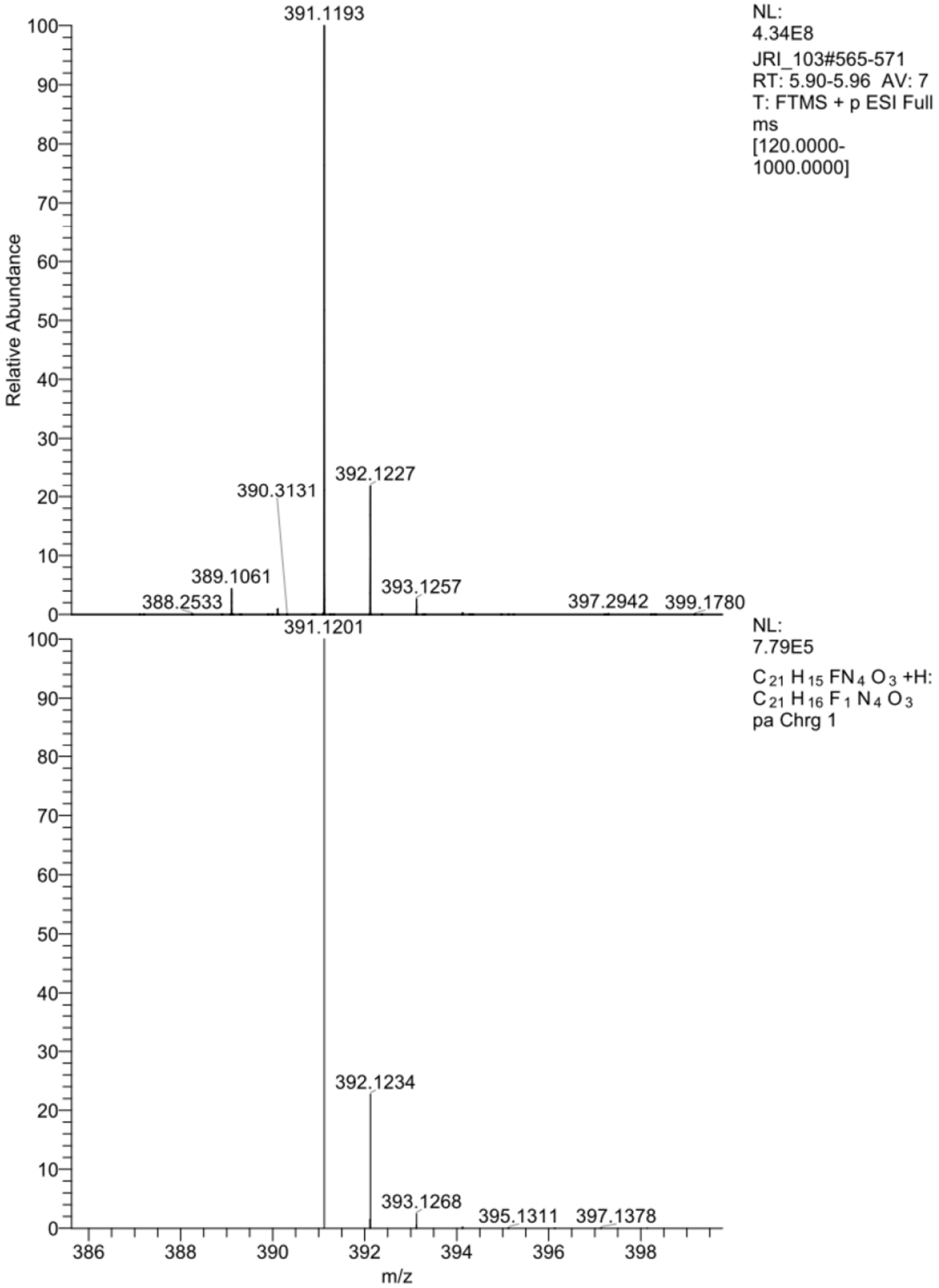
391.1193
NL:
4.34E8
JRI_103#565-571
RT: 5.90-5.96 AV: 7
T: FTMS + p ESI Full
ms
[120.0000-
1000.0000]
392.1227
390.3131
389.1061
393.1257
388.2533
397.2942
399.1780
Relative Abundance
391.1201
NL:
7.79E5
C21 H15 FN4 O3 +H:
C21 H16 F1 N4 O3
pa Chrg 1
392.1234
393.1268
395.1311
397.1378
m/z

4-(1-(6-(4-fluorophenoxy)-4-methylpyridin-3-yl)-1*H*-1,2,3-triazol-4-yl)benzoic acid (40d):

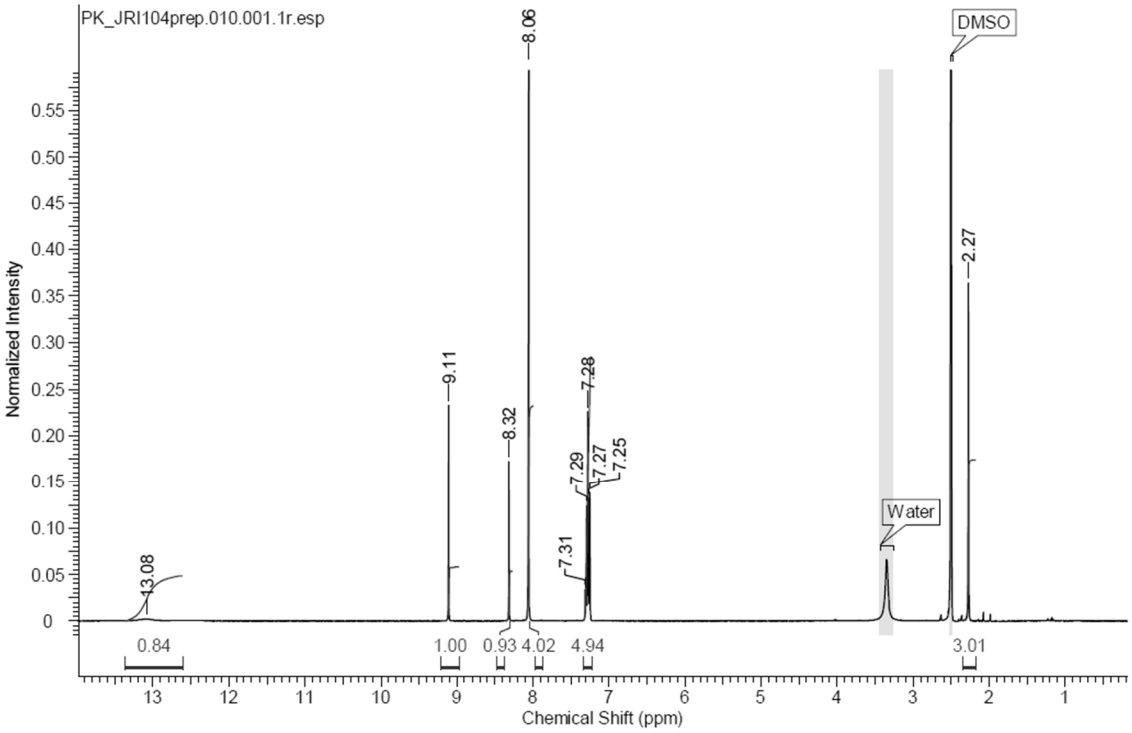

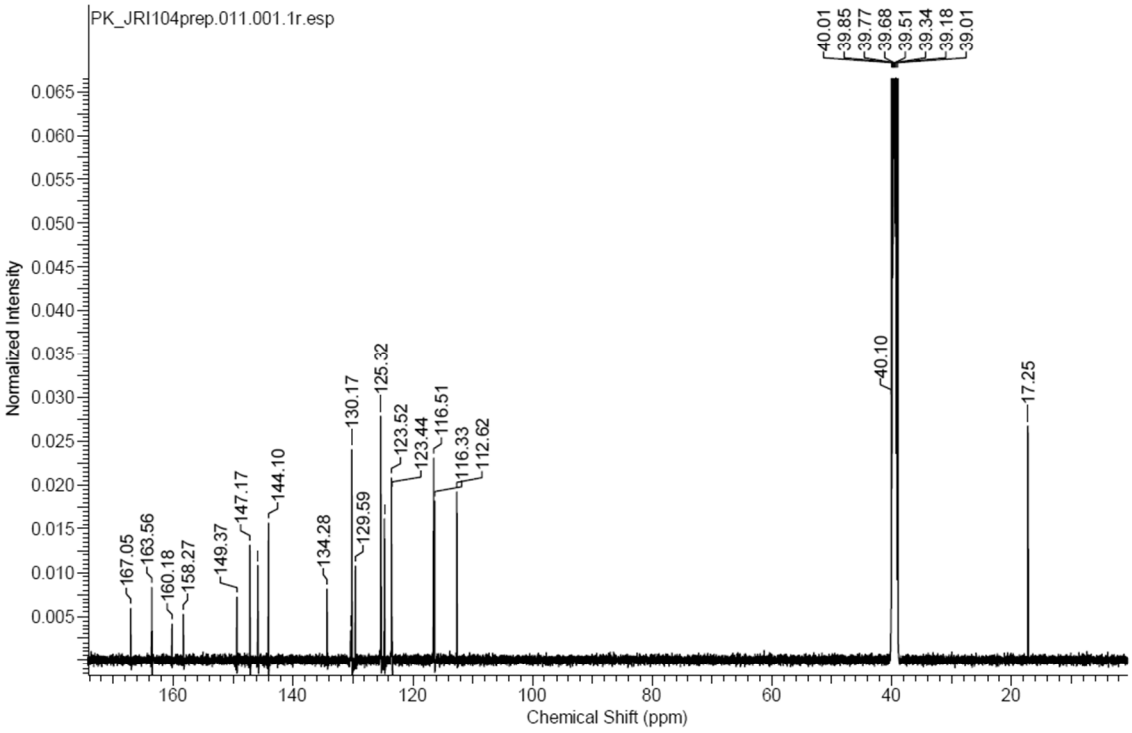

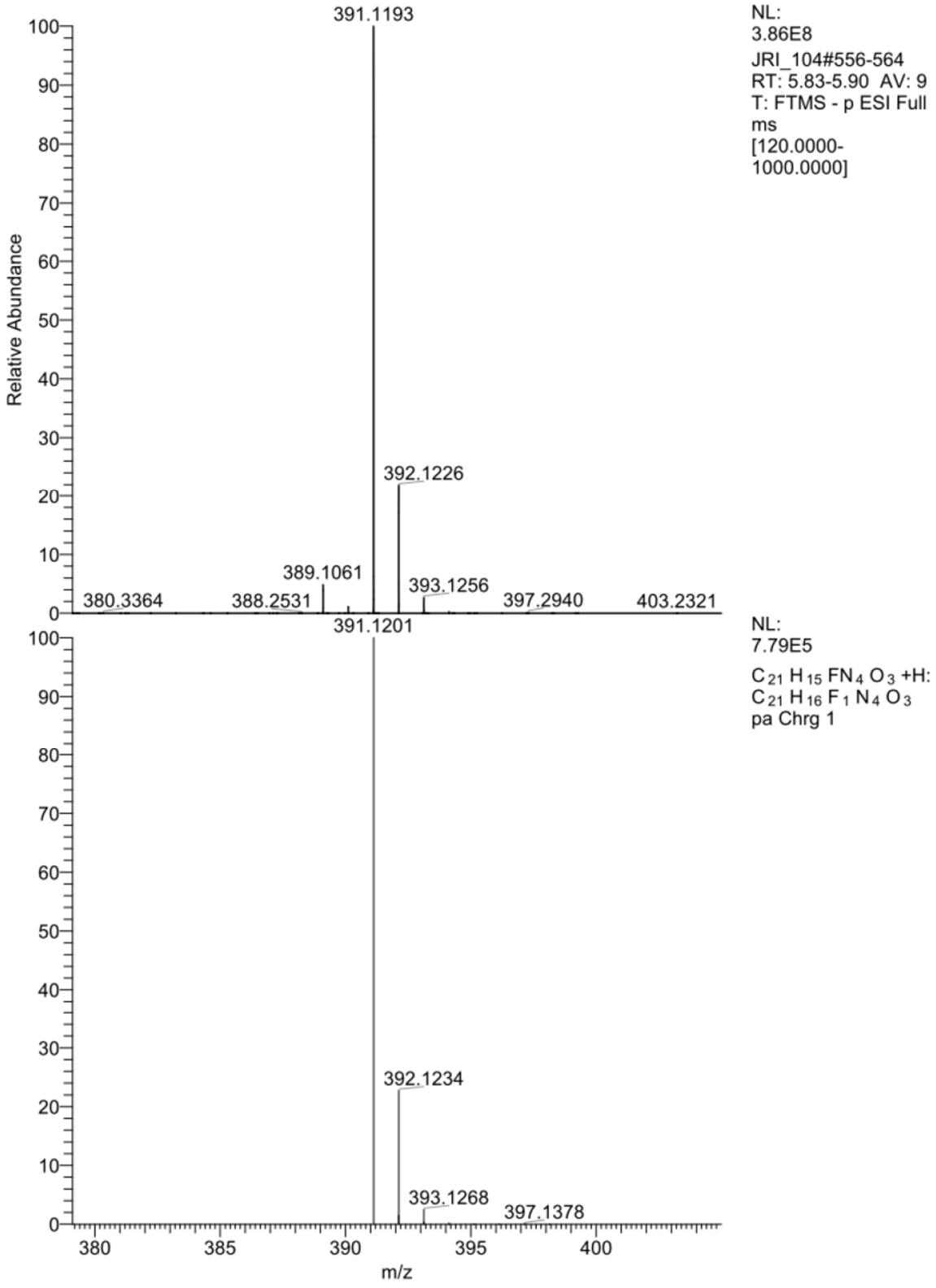
391.1193
NL:
3.86E8
JRI_104#556-564
RT: 5.83-5.90 AV: 9
T: FTMS - p ESI Full
ms
[120.0000-
1000.0000]
392.1226
389.1061
393.1256
380.3364
388.2531
397.2940
403.2321
Relative Abundance
391.1201
NL:
7.79E5
C21 H15 FN4 O3 +H:
C21 H16 F1 N4 O3
pa Chrg 1
392.1234
393.1268
397.1378
m/z

4-(1-(4-methyl-6-(phenylthio)pyridin-3-yl)-1*H*-1,2,3-triazol-4-yl)benzoic acid (40e):

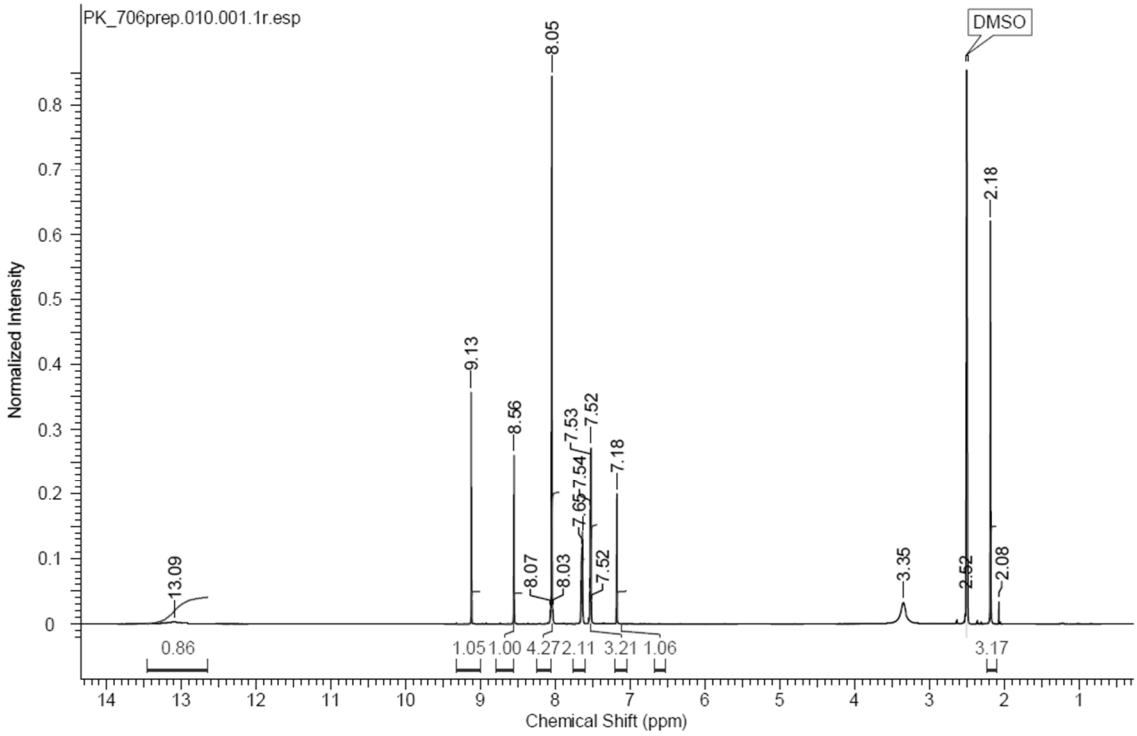

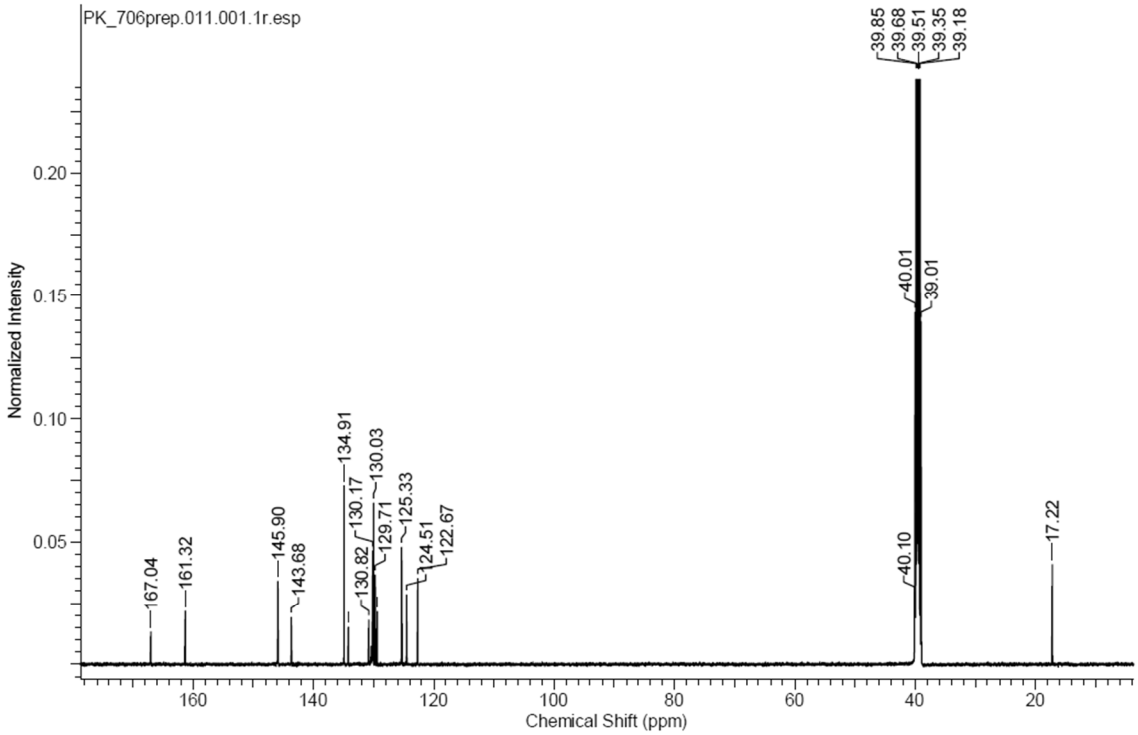

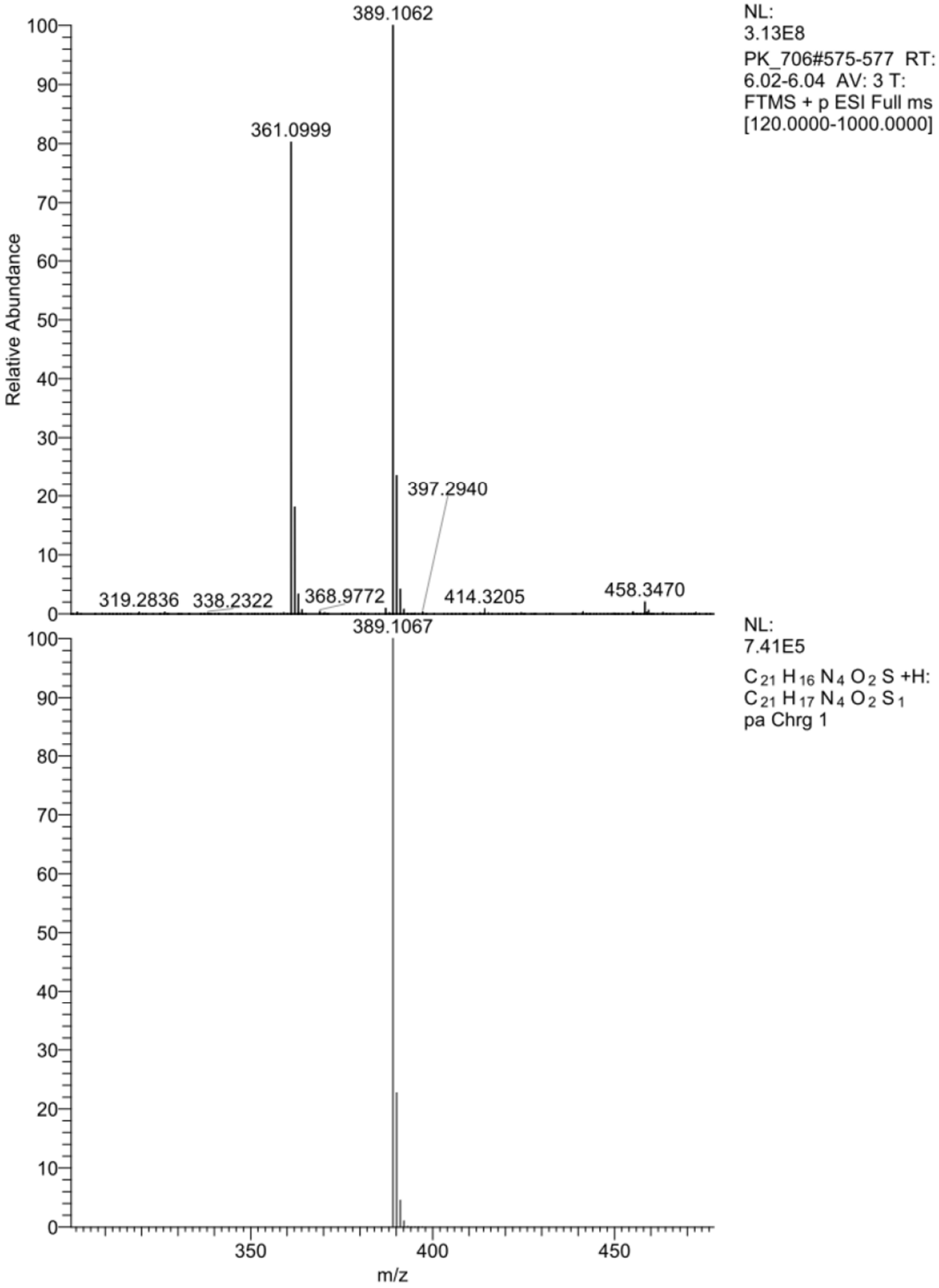
389.1062
NL:
3.13E8
PK_706#575-577 RT:
6.02-6.04 AV: 3 T:
FTMS + p ESI Full ms
[120.0000-1000.0000]
361.0999
397.2940
319.2836
338.2322
368.9772
414.3205
458.3470
Relative Abundance
389.1067
NL:
7.41E5
C21 H16 N4 O2 S +H:
C21 H17 N4 O2 S1
pa Chrg 1
m/z

4-(1-(isoquinolin-4-yl)-1*H*-1,2,3-triazol-4-yl)benzoic acid (43):

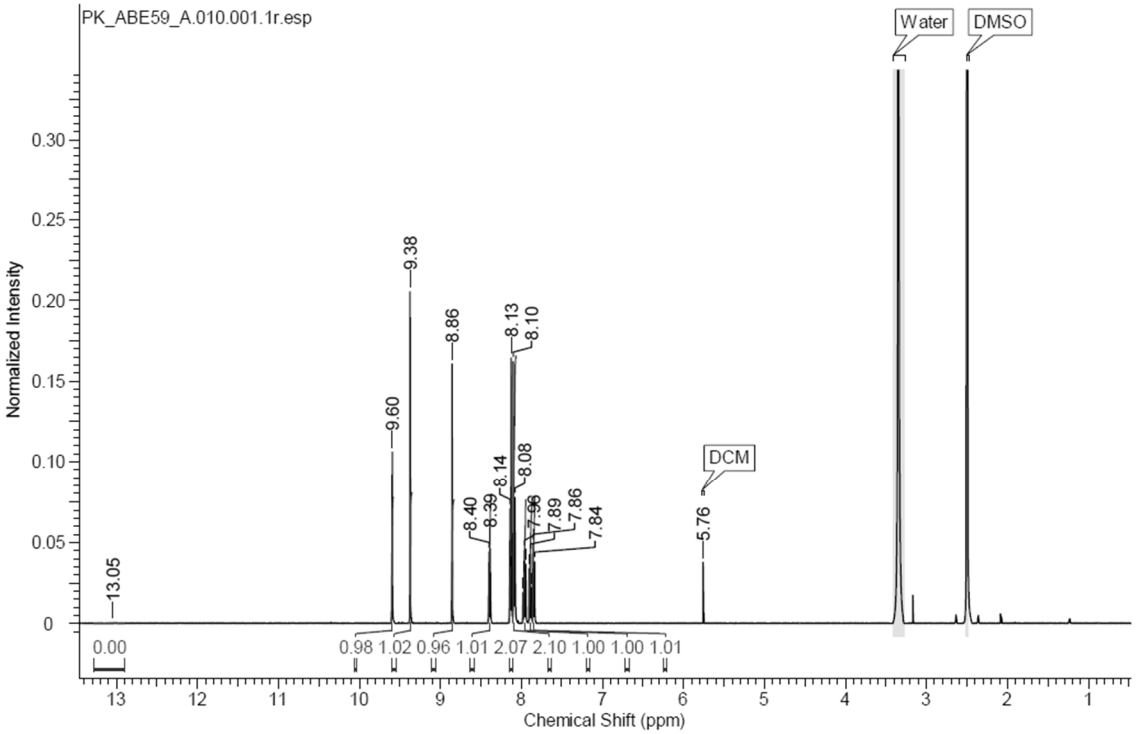

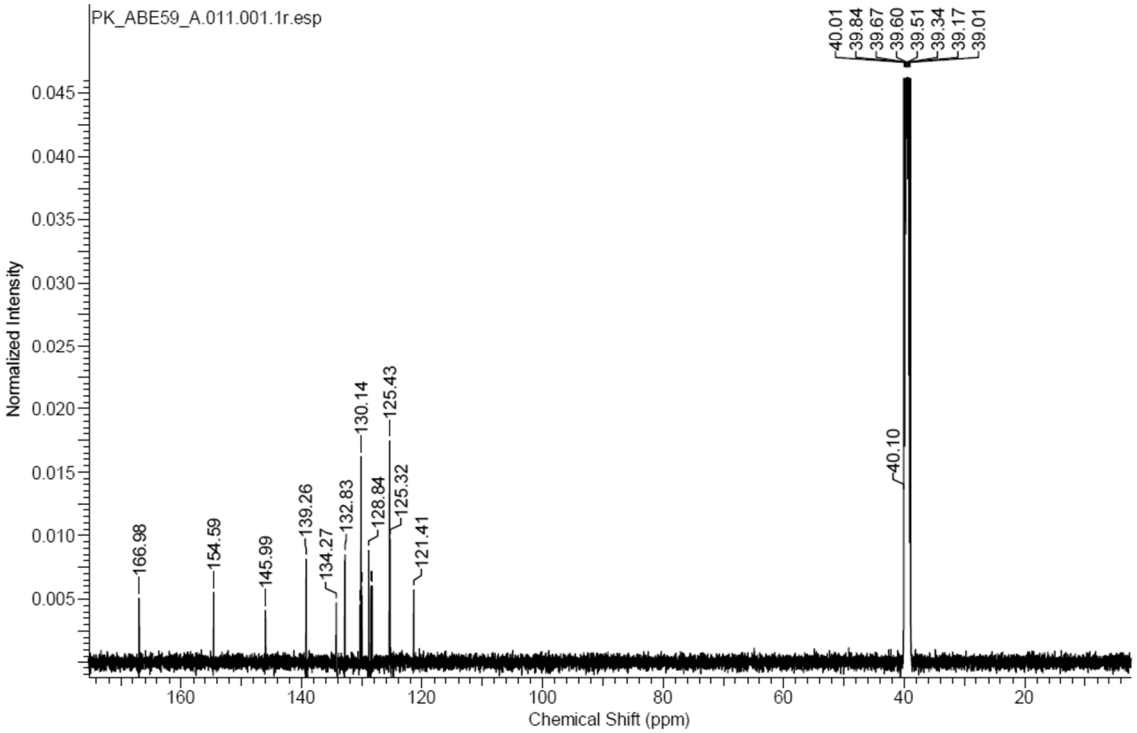

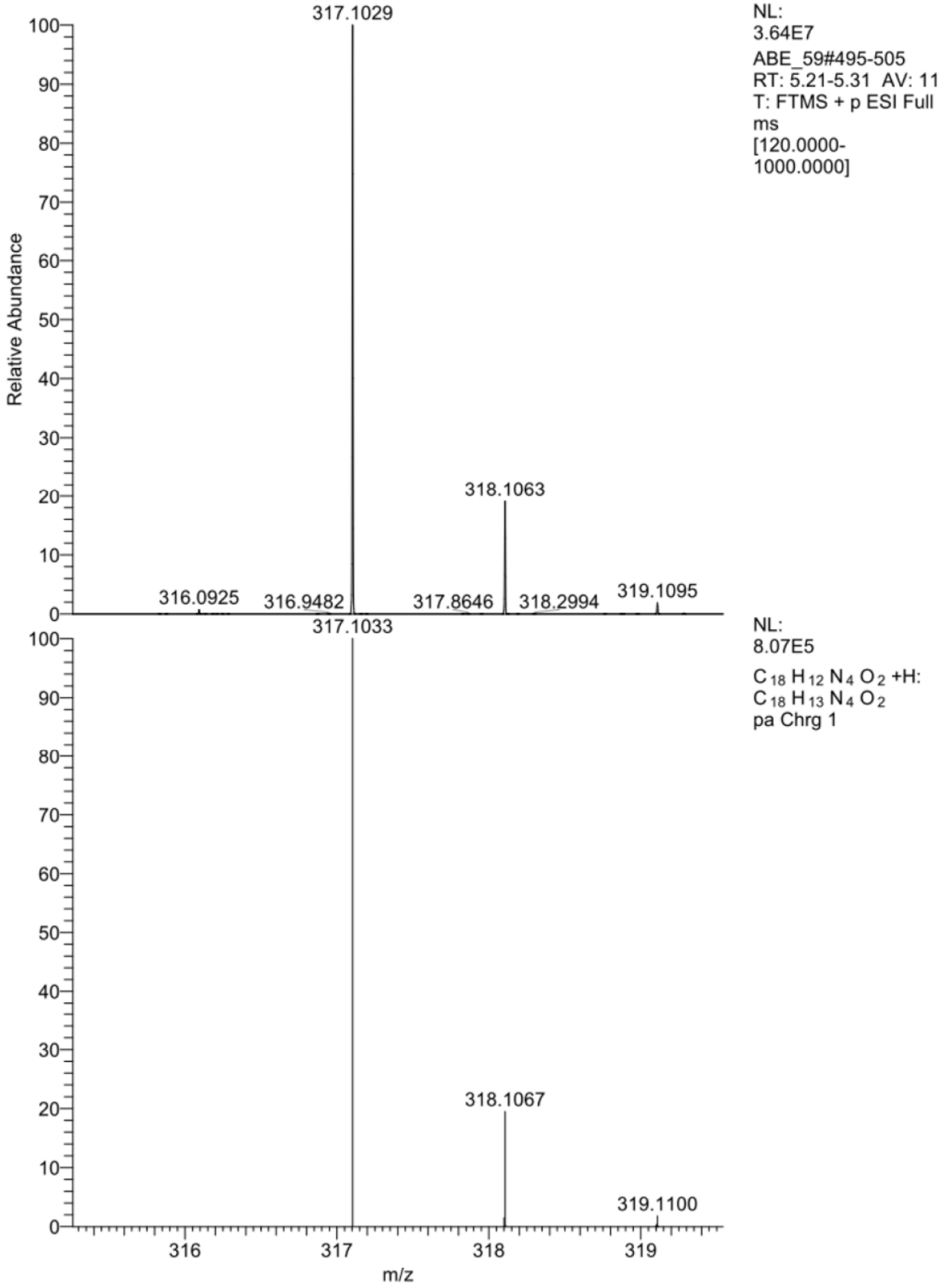
317.1029
NL:
3.64E7
ABE_59#495-505
RT: 5.21-5.31 AV: 11
T: FTMS + p ESI Full
ms
[120.0000-
1000.0000]
318.1063
316.0925
316.9482
317.8646
318.2994
319.1095
Relative Abundance
317.1033
NL:
8.07E5
C18 H12 N4 O2 +H:
C18 H13 N4 O2
pa Chrg 1
318.1067
319.1100
m/z

4-(1-(quinolin-3-yl)-1*H*-1,2,3-triazol-4-yl)benzoic acid (46):

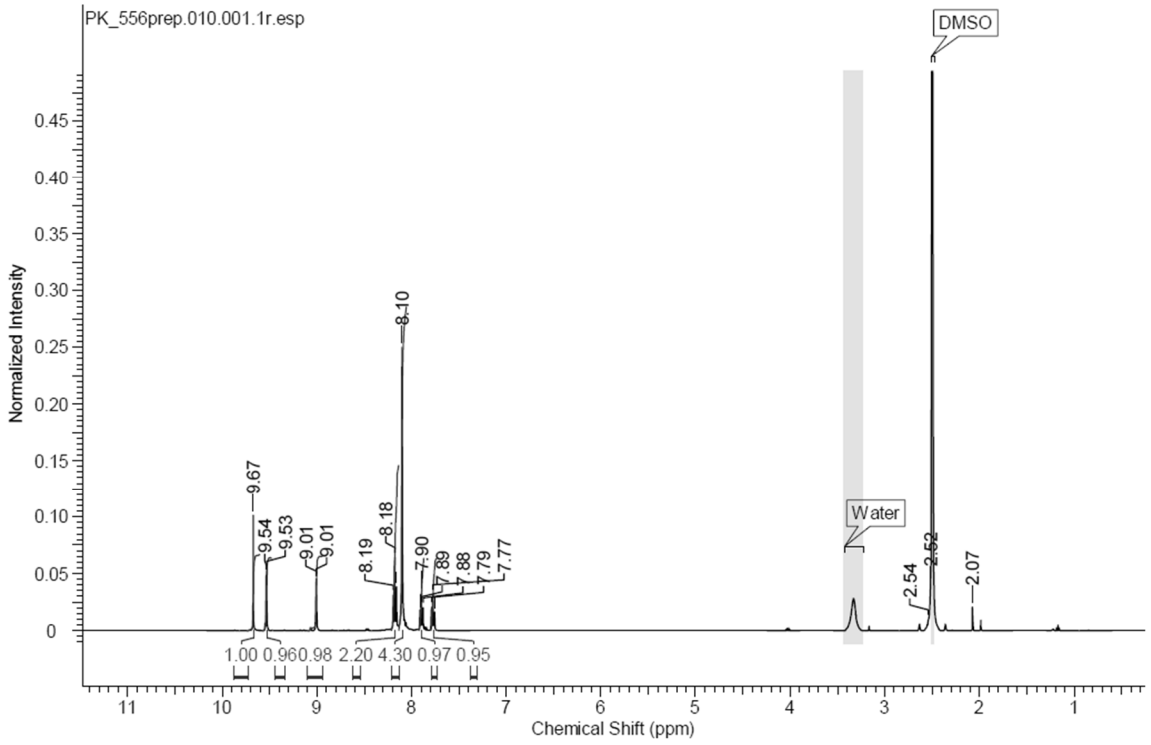

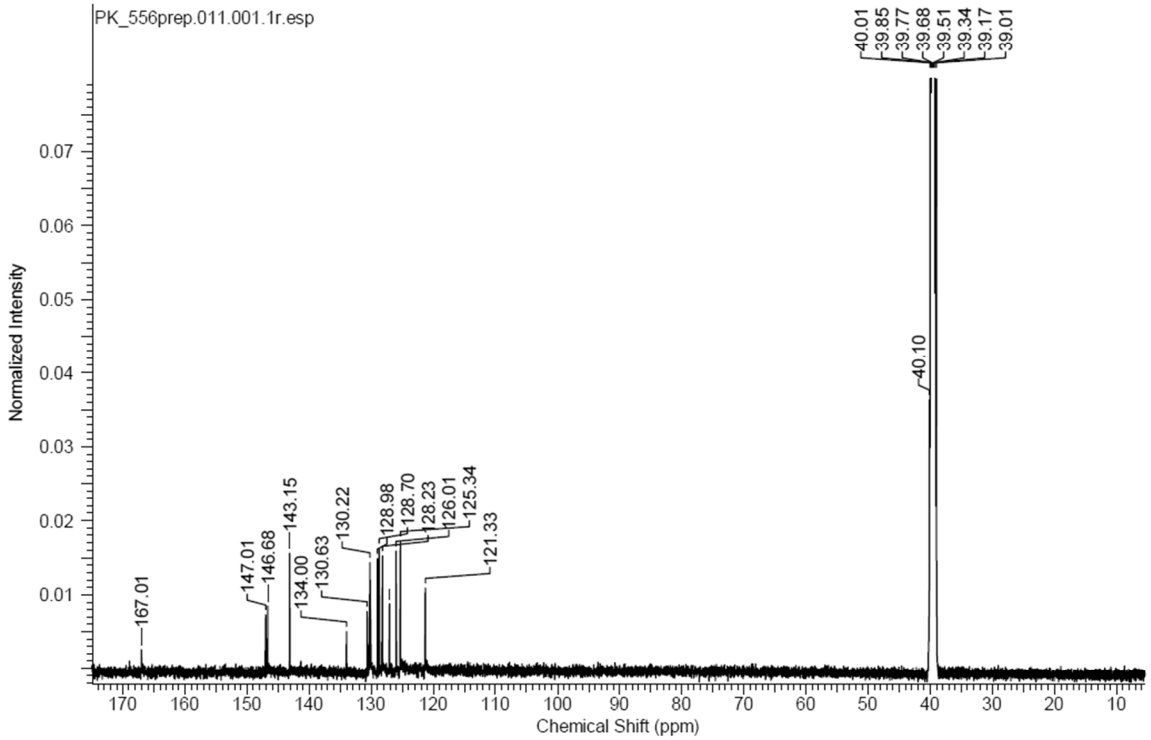

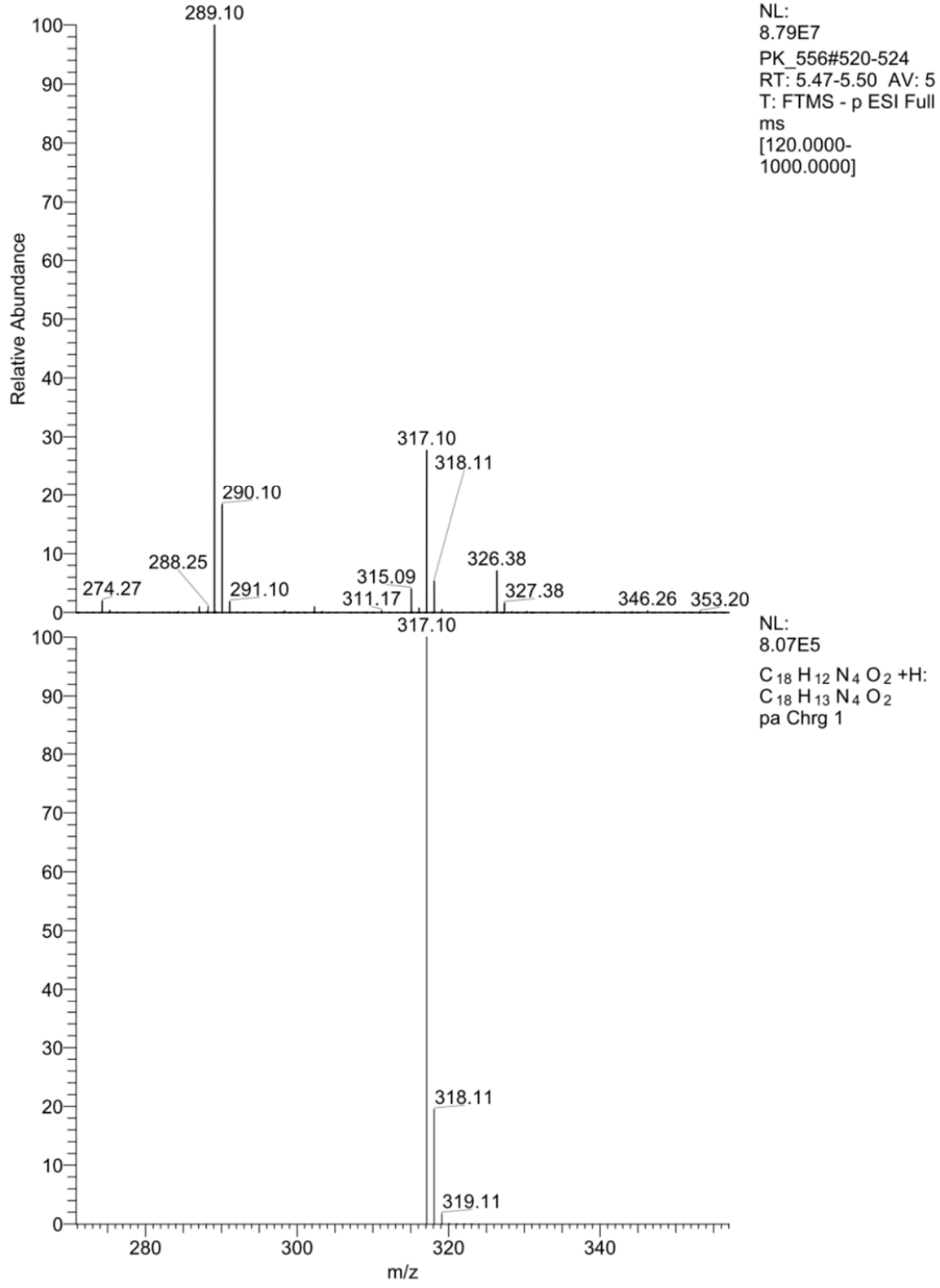
NL:
8.79E7
PK_556#520-524
RT: 5.47-5.50 AV: 5
T: FTMS - p ESI Full
ms
[120.0000-
1000.0000]
289.10
317.10
318.11
290.10
288.25
326.38
315.09
274.27
291.10
311.17
327.38
346.26
353.20
NL:
8.07E5
C18 H12 N4 O2 +H:
C18 H13 N4 O2
pa Chrg 1
317.10
318.11
319.11
Relative Abundance
m/z

4-(1-(6-methylisoquinolin-4-yl)-1*H*-1,2,3-triazol-4-yl)benzoic acid (50a):

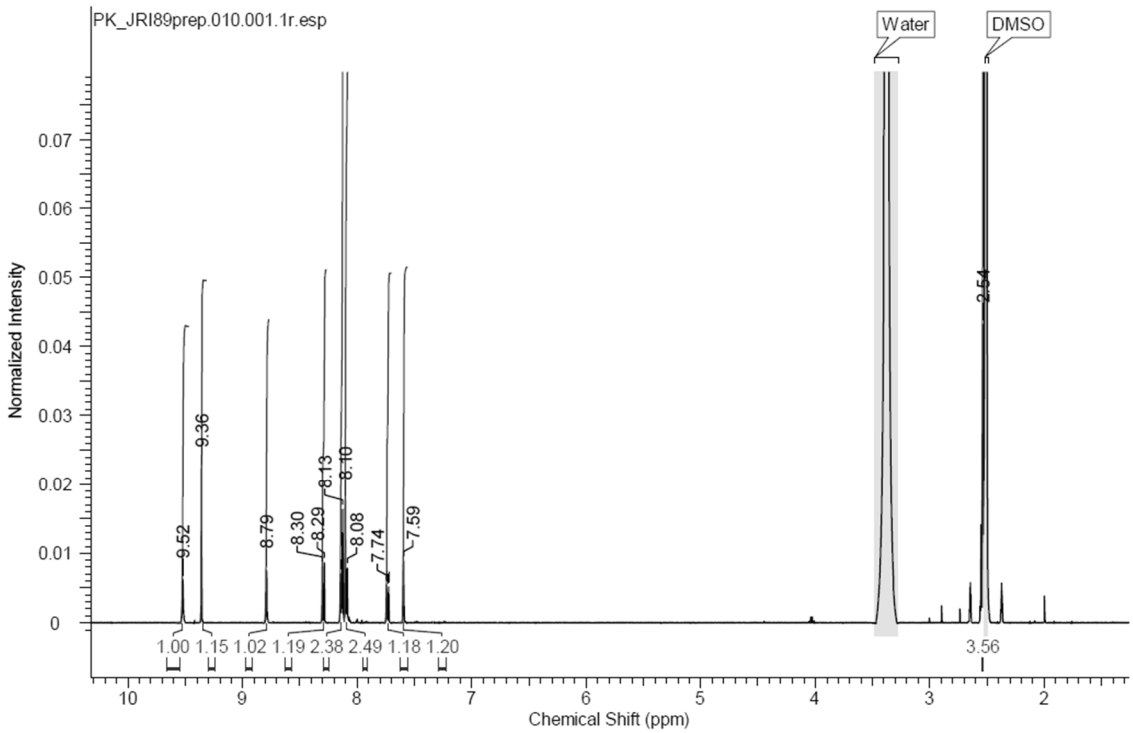

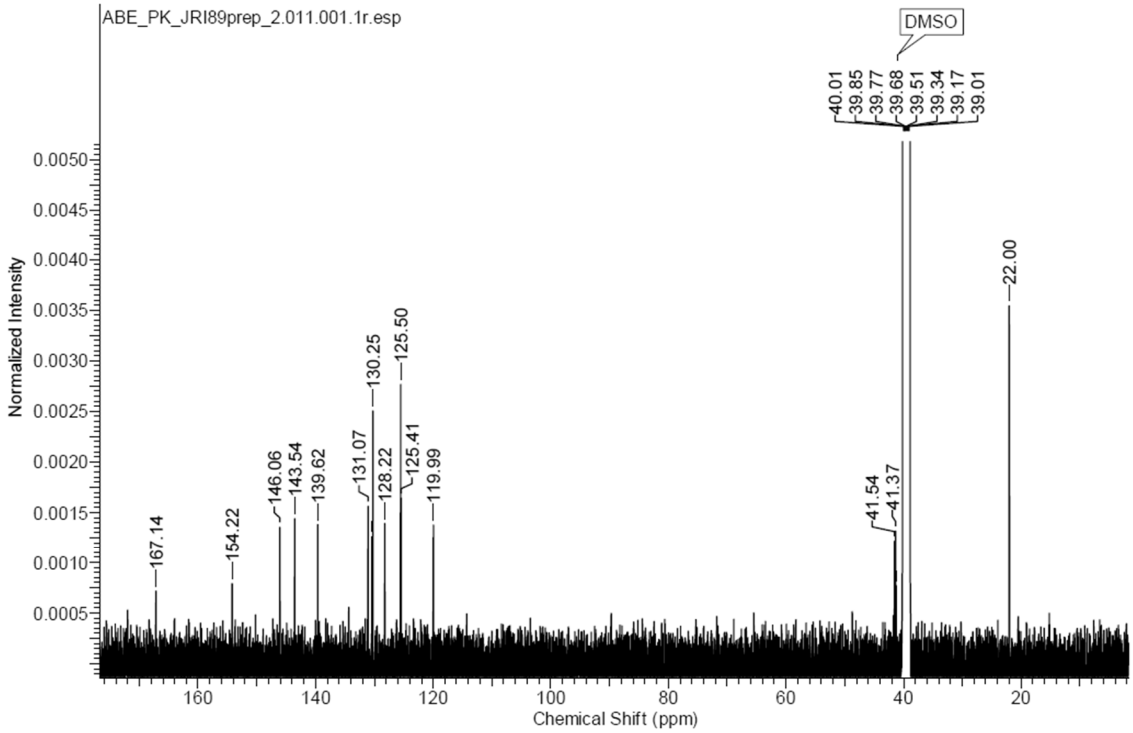

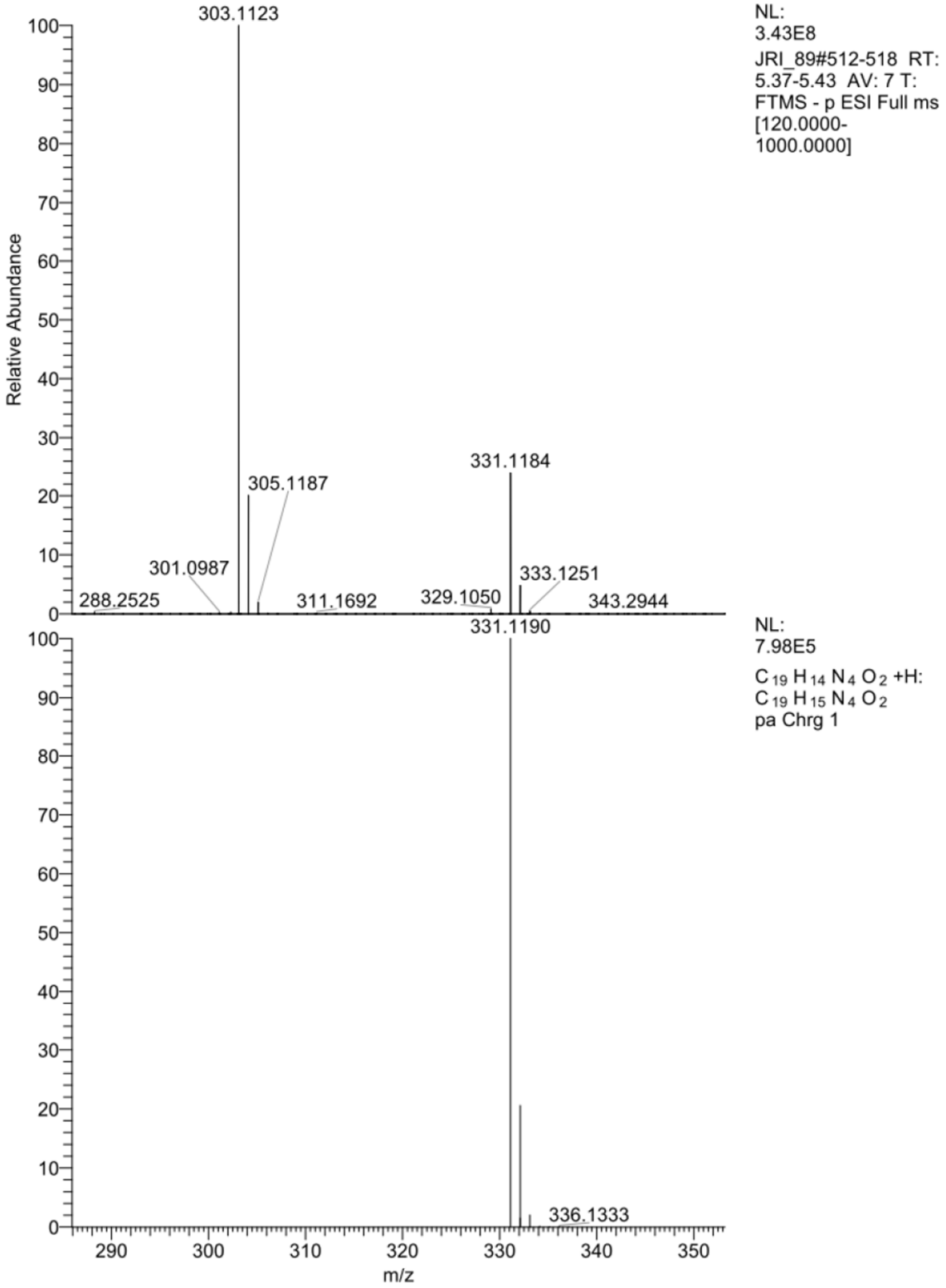
303.1123
NL:
3.43E8
JRI_89#512-518 RT:
5.37-5.43 AV: 7 T:
FTMS - p ESI Full ms
[120.0000-
1000.0000]
331.1184
305.1187
301.0987
333.1251
288.2525
311.1692
329.1050
343.2944
331.1190
NL:
7.98E5
C19 H14 N4 O2 +H:
C19 H15 N4 O2
pa Chrg 1
336.1333
Relative Abundance
m/z

4-(1-(7-chloroisoquinolin-4-yl)-1*H*-1,2,3-triazol-4-yl)benzoic acid (50b):

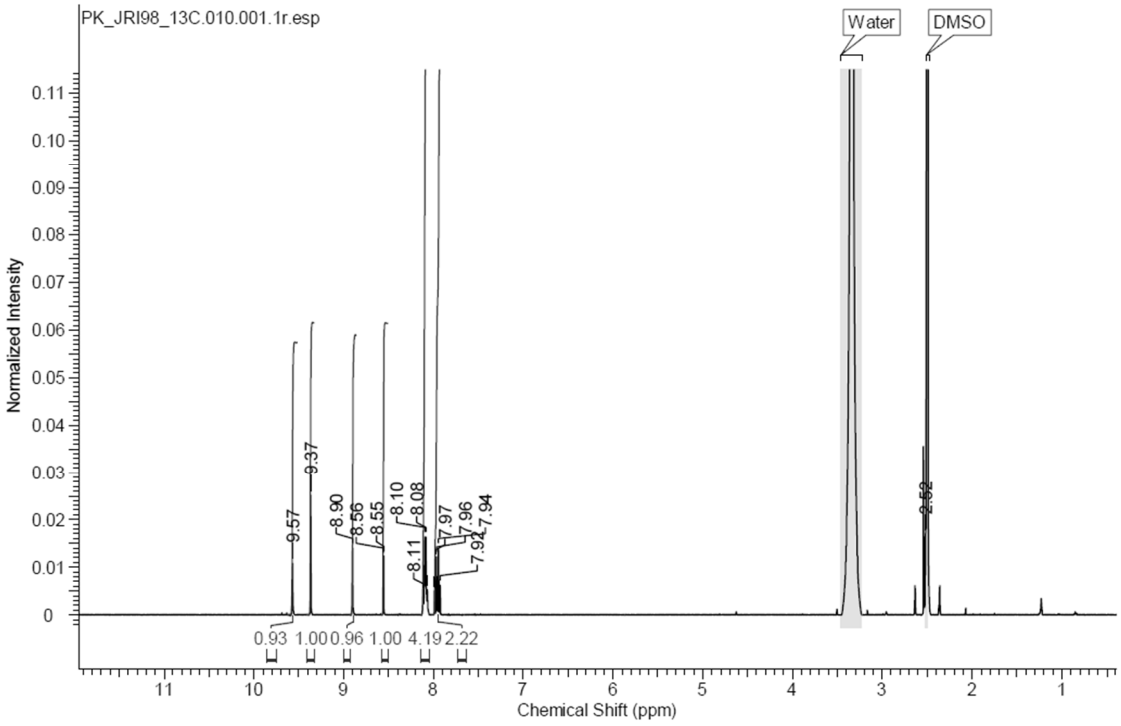

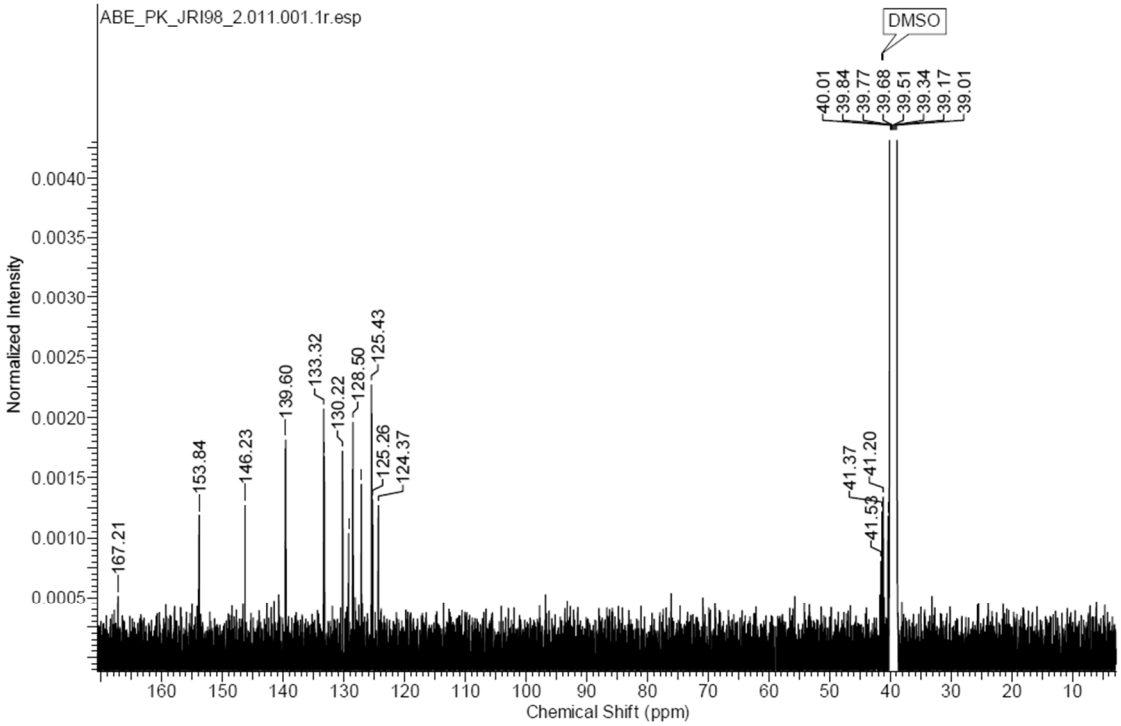

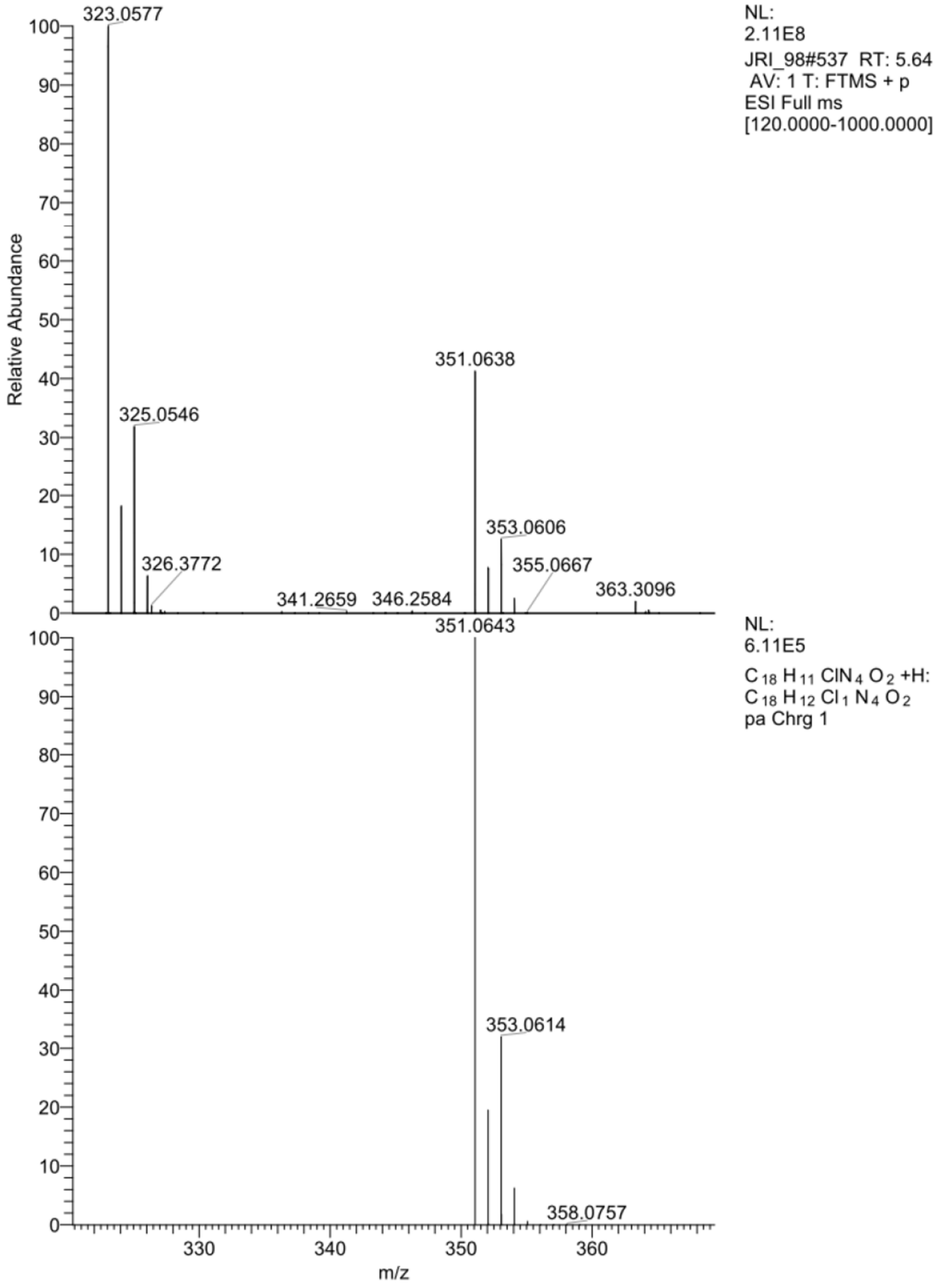
323.0577
NL:
2.11E8
JRI_98#537 RT: 5.64
AV: 1 T: FTMS + p
ESI Full ms
[120.0000-1000.0000]
Relative Abundance
351.0638
325.0546
353.0606
326.3772
355.0667
363.3096
341.2659
346.2584
351.0643
NL:
6.11E5
C18 H11 ClN4 O2 +H:
C18 H12 Cl1 N4 O2
pa Chrg 1
353.0614
358.0757
330
340
350
360
m/z

4-(1-(7-(methoxycarbonyl)isoquinolin-4-yl)-1*H*-1,2,3-triazol-4-yl)benzoic acid (50c):

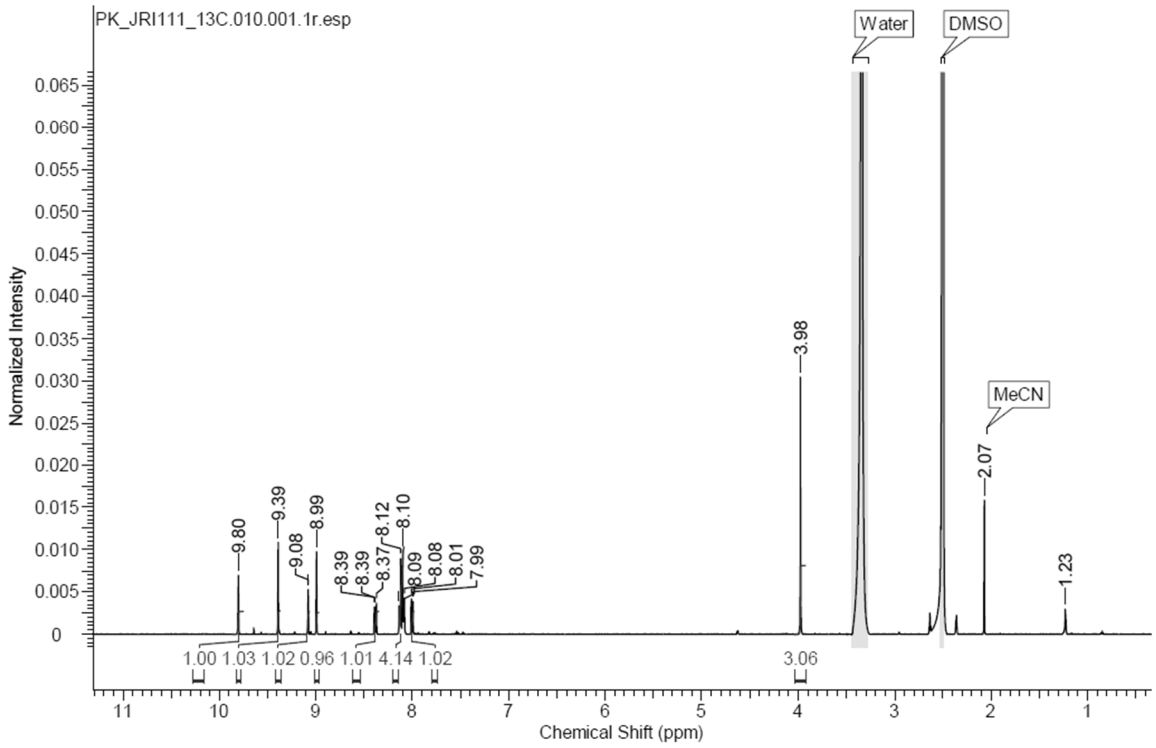

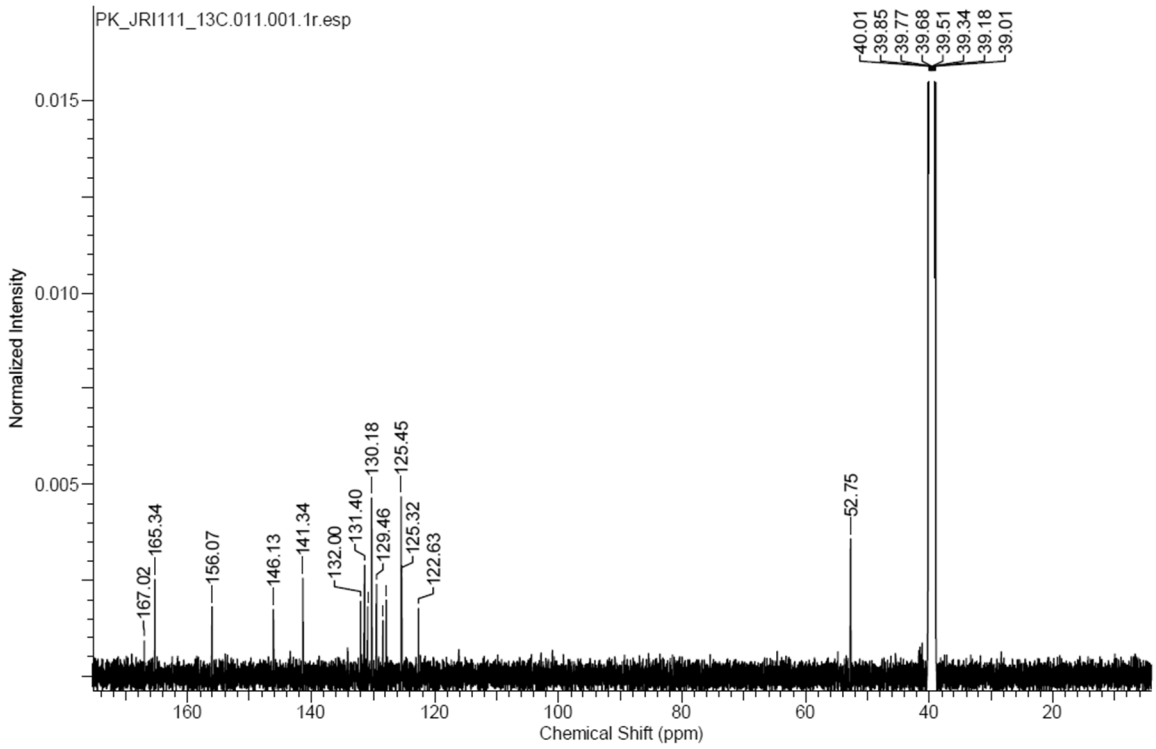

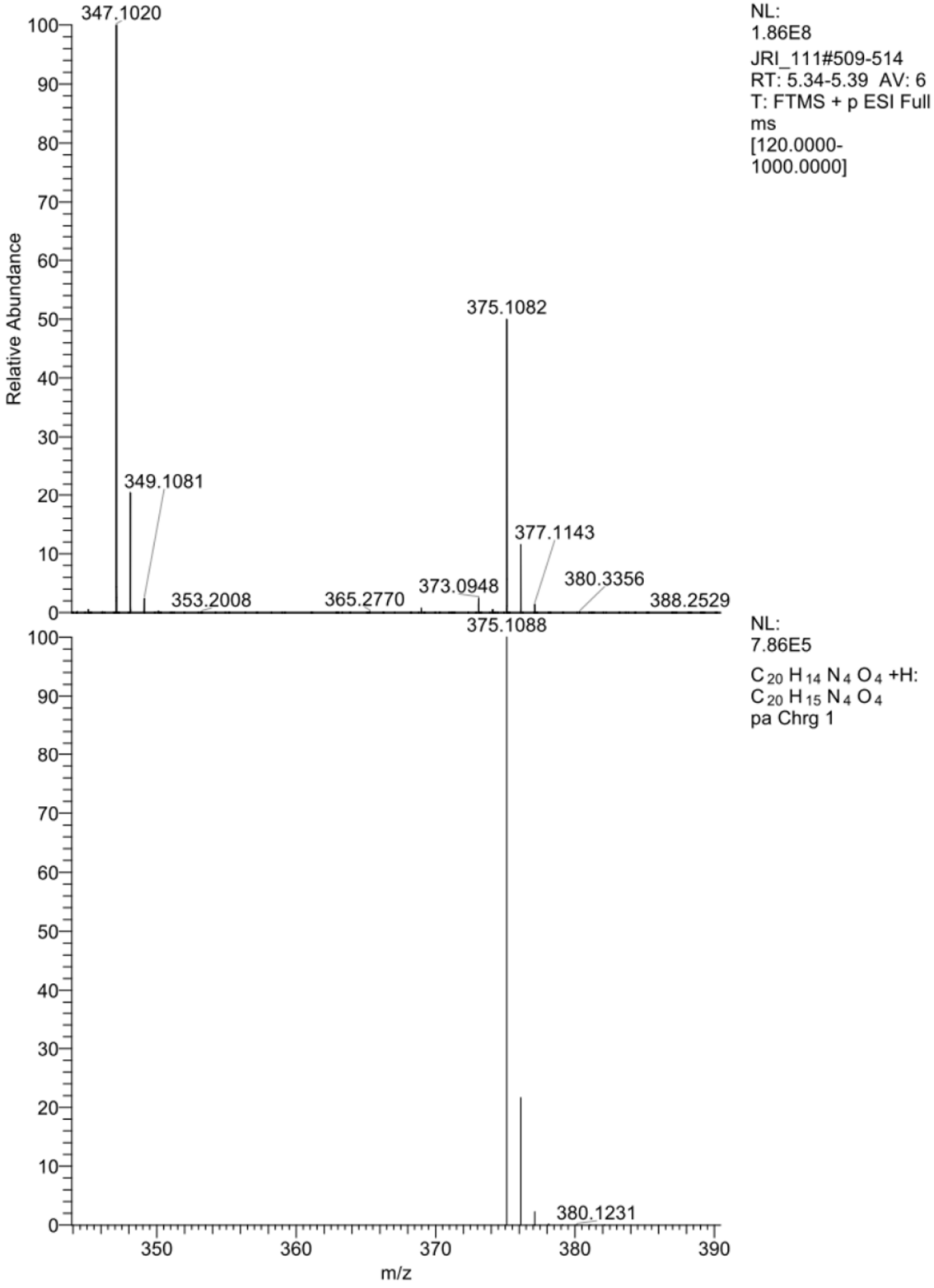
347.1020
375.1082
349.1081
377.1143
380.3356
353.2008
365.2770
373.0948
388.2529
NL:
1.86E8
JRI_111#509-514
RT: 5.34-5.39 AV: 6
T: FTMS + p ESI Full
ms
[120.0000-
1000.0000]
Relative Abundance
375.1088
380.1231
NL:
7.86E5
C20 H14 N4 O4 +H:
C20 H15 N4 O4
pa Chrg 1
m/z

2 References

1. Kirsch, P.; Jakob, V.; Oberhausen, K.; Stein, S.C.; Cucarro, I.; Schulz, T.F.; Empting, M. Fragment-Based Discovery of a Qualified Hit Targeting the Latency-Associated Nuclear Antigen of the Oncogenic Kaposi's Sarcoma-Associated Herpesvirus/Human Herpesvirus 8. *J. Med. Chem.* **2019**, *62*, 3924–3939, doi:10.1021/acs.jmedchem.8b01827.

7.4 Supporting Information Chapter E

Supporting Information

69451 Weinheim, Germany

Phage Display-based Discovery of Cyclic Peptides against the Broad Spectrum Bacterial Anti-Virulence Target CsrA.

Valentin Jakob,[a,†] Ben G. E. Zoller,[a,†] Julia Rinkes,[a] Yingwen Wu,[a] Alexander F. Kiefer,[a] Michael Hust,[b]Saskia Helmsing,[b] Andrew M. White,[c] Peta J. Harvey,[c] Thomas Durek,[c] David J. Craik,[c] Andreas Siebert,[d] Uli Kazmaier[d] and Martin Empting*

[*] Dr. M. Empting
Department of Drug Design and Optimization (DDOP)
Helmholtz-Institute for Pharmaceutical Research Saarland (HIPS) - Helmholtz Centre for Infection Research (HZI)
Campus E8.1, 66123 Saarbrücken, Germany
E-mail: martin.empting@helmholtz-hips.de

[a] V. Jakob,[†] B. G. E. Zoller,[†] J. Rinkes, Y. Wu, Dr. A. F. Kiefer
Department of Drug Design and Optimization (DDOP)
Helmholtz-Institute for Pharmaceutical Research Saarland (HIPS) - Helmholtz Centre for Infection Research (HZI)
Campus E8.1, 66123 Saarbrücken, Germany
Department of Pharmacy
Saarland University
Campus E8.1, 66123 Saarbrücken, Germany

[b] Prof. Dr. M. Hust, S. Helmsing
Abteilung Biotechnologie
Technische Universität Braunschweig, Institut für Biochemie, Biotechnologie und Bioinformatik
Spielmannstr. 7, 38106 Braunschweig, Germany

[c] Dr. A. M. White, Dr. Peta J. Harvey, Dr. T. Durek, Prof. D. J. Craik
ARC Centre of Excellence for Innovations in Peptide and Protein Science
Institute for Molecular Bioscience
The University of Queensland, Brisbane, QLD, 4072, Australia
E-mail: t.durek@uq.edu.au
d.craik@imb.uq.edu.au

[d] A. Siebert, Prof. Dr. U. Kazmaier
Institut für Organische Chemie
Saarland University
Campus C4.2, 66123 Saarbrücken, Germany

[†] These authors contributed equally to this work.

Abstract: Small macrocyclic peptides are promising candidates for new anti-infective drugs. To date, such peptides have been poorly studied in the context of anti-virulence targets. Using phage display and a self-designed peptide library, we identified a cyclic heptapeptide that can bind the carbon storage regulator A (CsrA) from *Yersinia pseudotuberculosis* and displace bound RNA. The initial disulfide-bridged peptide, showed an IC_{50} value in the low micromolar range. Upon further characterization, cyclization was found to be essential for its activity. To increase metabolic stability, a series of disulfide mimetics were designed and a redox-stable 1,4-disubstituted 1,2,3-triazole analogue displayed activity in the double-digit micromolar range. Further experiments revealed that this triazole peptidomimetic is also active against CsrA from *Escherichia coli*. This study is an ideal starting point for medicinal chemistry optimization of this macrocyclic peptide and might pave the way towards broad-acting virulence modulators.

Table of Contents

Peptide Synthesis and Macrocyclization

General information. All resins were purchased from Rapp Polymere. The azide/alkyne building blocks Fmoc-L-azidoalanine (Fmoc-Aza-OH), Fmoc-L-propargylglycine (Fmoc-Pra-OH) and Fmoc-L-homoazidoalanine (Fmoc-Aha-OH) were purchased from Carl Roth VG. Fmoc-Val-OH, Fmoc-Ala-OH, Fmoc-Glu(O*t*Bu)-OH, Fmoc-Leu-OH and Fmoc-Cys(Trt)-OH were purchased from Novabiochem. Fmoc-Ser(*t*Bu)-OH was purchased from TCI.

General Fmoc-SPPS procedure. Most peptides were synthesized manually *via* solid phase peptide synthesis (SPPS) using Fmoc chemistry. The resin was swollen for 30 min in DMF. For Fmoc deprotection piperidine/DMF (1:4, v:v) was added and shaken for 5 min, twice. It was then washed three times with DMF followed by the second round of adding piperidine/DMF (1:4) with incubating 5 min on a shaker. It was washed five times with DMF, five times with DCM and again one time with DMF. We used double coupling for each amino acid. The amino acid (4.0 eq.) was solved in DMF together with 3.9 eq. 3-[Bis(dimethylamino)methyliumyl]-*3H*-benzotriazol-1-oxide hexafluorophosphate (HBTU) followed by adding 10.0 eq. *N*-Ethyl-*N*-(propan-2-yl)propan-2-amine (DIPEA). This solution was pre-activated for 5 min on a shaker. The activated solution was added to the resin and incubated for 1 h on a shaker. After washing two times with DMF, it was added an activated amino acid/HBTU/DIPEA/DMF solution again and incubated 1 h on a shaker. The resin was washed five times with DMF and five times with DCM. This was followed by two deprotection cycles and two coupling cycles of the next amino acid.

General acetylation procedure. For Acetylation, DMF/DIPEA/Ac_2O (12:8:5, v:v:v) was added to the resin and shaken for 0.5 h. Then it was washed five times with DMF, five times with DCM and again one time with DMF.

General cleavage procedure. For protein cleavage from the solid support and removal of the side chain protecting groups a cleavage cocktail containing trifluoroacetic acid (TFA)/triisopropylsilane (TIS)/H_2O (37:1:1, v:v:v) with a spatula tip of dithiothreitol (DTT) was added to the resin and incubated 2.5 – 3.0 h on a shaker. The liquid was collected and TFA was removed under reduced pressure, followed by precipitation with cold (-20 °C) methyl *tert*-butyl ether (MTBE). The crude peptide was gained by centrifugation (4600 rpm, 4 °C, 10 min) followed by MTBE washing (3x) and repeated centrifugation.

General cyclisation procedure. For disulfide cyclisation the crude lyophilized peptide was dissolved in H_2O/ACN (1:1, v:v) with a concentration of 1 mg peptide per 1 mL solvent and 1-3 % DMSO was added. The pH was adjusted to 7.7 using 1M aq. ammonium carbonate solution. The solution was stirred for 1-4 days. The reaction was monitored by LC-MS.

General preparative HPLC procedure. The purification was done with a DIONEX UltiMate 3000 UHPLC$^+$ focused (Thermo Scientific), containing pump, diode array detector, and automated fraction collector. We used a VP 250/10 NUCLEODUR C18 Gravity, 5 µm (Macherey-Nagel) column with a gradient from 10-50 % solvent B over 25 min (solvent A: H_2O (0.05 % formic acid), solvent B: ACN (0.05 % formic acid)) and a 5 mL/min flowrate. Pure fractions were checked by LC-MS, combined and lyophilized.

***Ac*-V-[CSELC]$_{cyclic}$-W-*NH$_2$* (1); 3-((4*R*,7*S*,10*S*,13*S*,16*R*)-16-((*S*)-2-acetamido-3-methylbutanamido)-4-(((*S*)-1-amino-3-(1*H*-indol-3-yl)-1-oxopropan-2-yl)carbamoyl)-13-(hydroxymethyl)-7-isobutyl-6,9,12,15-tetraoxo-1,2-dithia-5,8,11,14-tetraazacycloheptadecan-10-yl)propanoic acid.**

The linear precursor peptide was synthesized on a Fmoc Trp(Boc) TentaGel® S RAM resin (load: 0.2 mmol/g) in a 0.2 mmol scale manually using Fmoc strategy with two coupling cycles and two deprotection cycles as described in the "general Fmoc-SPPS procedure". The cleavage of the peptide from the resin was performed by the "general cleavage procedure" protocol, where 7 mL cleavage cocktail was used with an incubation of 3 h on a shaker. After lyophilization, 45.7 mg of crude linear product was achieved, which was used for the "general cyclisation procedure" for disulfide cyclisation of the cysteines for 2 days. For purification, the "general preparative HPLC procedure" has been performed. A yield of 2.68 mg pure (≥ 98 %) cyclized peptide (3.05 µmol, 1.53 % according to initial load of the resin) was obtained and characterized by LC-MS, ^{1}H-NMR, ^{13}C-NMR and HRMS. LC-MS: Column: Phenomenex Luna C18(2), gradient: MeCN/H_2O + 0.05 % HCOOH, 5 % MeCN increase to 50% MeCN in 5.1 min, flow rate: 0.6 mL/min, t_R= 3.75 min, m/z = 878.3 ([M+H]$^+$). HRMS (ESI+) m/z calculated for $C_{38}H_{55}N_9O_{11}S_2$ [M+H]$^+$ 878.3530; found: 878.3528.

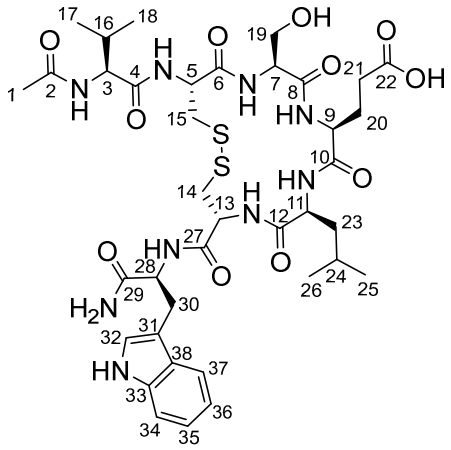

^{1}H-NMR (500 MHz, dmso-d6, δ in ppm): 10.82 (bs, 1 H, Indole NH), 8.41 (bs, 1 H, NH), 8.30 (d, ^{3}J = 7.80 Hz, 1 H, NH), 8.15 (d, ^{3}J = 8.2 Hz, 1 H, NH), 8.06 (d, ^{3}J = 6.8 Hz, 1 H, NH), 7.99 (d, ^{3}J = 6.6 Hz, 1 H, NH), 7.97–7.92 (m, 2 H, NH), 7.56 (d, $^{3}J_{37,36}$ = 7.9 Hz 1 H, H37), 7.30 (d, $^{3}J_{34,45}$ = 7.9 Hz, 2 H, H34, NH), 7.12 (m, 2 H, NH, 32H), 7.03 (t, $^{3}J_{35,36/34}$ = 7.3 Hz, 1 H, H35), 6.95 (t, $^{3}J_{36,35/37}$ = 7.4 Hz, 1 H, H36), 4.62-4.56 (m, 1 H, H5), 4.55-4.49 (m, 1H, 13-H), 4.43-4.37 (m, 1H, 28H), 4.28-4.24 (m, 1H, 7H), 4.19 (dd, ^{3}J = 8.8, 6.7 Hz, 1H, 3-H), 4-17-4.09 (m, 2H, 9H, 11H), 3.76-3.62 (m, 2H, 19H), 3.25 (dd, $^{2}J_{15a,15b}$ = 13.4, $^{3}J_{15a,5}$ = 4.2 Hz, 1H, H15$_a$), 3.13 (dd, $^{2}J_{30a,30b}$ = 13.4, $^{3}J_{30a,28}$ = 5.1 Hz, 1H, H30$_a$), 3-06-2.93 (m, 4H, H14, H15$_b$, H30$_b$), 2.23 (t, $^{3}J_{21,20}$ = 7.9 Hz, 2H, 21H), 2.00-1.90 (m, 3H, 20H, 16H), 1.88 (s, 3H, 1H), 1.60-1.53 (m, 1H, 24H), 1.52-1.47 (m, 2H, 23H), 0.87 (d, $^{3}J_{25,24}$, 3H, 25H), 0.85-0.80 (m, 9H, 17H, 18H, 26H).

^{13}C-NMR (126 MHz, dmso-d6, δ in ppm): 173.1 (C22), 172.2 (C29), 171.6 (C4), 171.5 (C10), 170.2 (C6, C8 or C12), 169.8 (C6, C8 or C12), 169.5 (C-2), 169.1 (C6, C8 or C12), 136.1 (C33), 127.4 (C38), 123.6 (C32), 120.9 (C35), 118.5 (C37), 118.3 (C36), 111.3 (C34), 110.1 (C31), 61.2 (C19), 57.6 (C3), 55.9 (C7), 54.0 (C99, 53.6 (C28), 52.8 (C13), 52.5 (C5), 52.0 (C-11), 41.9 (C15), 40.7 (C14), 40.1 (C23), 30.6 (C21), 27.7 (C30), 26.9(C20), 24.3 (C24), 23.1 (C25), 22.6 (C1), 21.6 (C26), 19.3 (C17 or C18), 18.2 (C17 or C18).

H*-V-[CSELC]$_{cyclic}$-W-*NH$_2$ **(2a); 3-((4*R*,7*S*,10*S*,13*S*,16*R*)-4-(((*S*)-1-amino-3-(1*H*-indol-3-yl)-1-oxopropan-2-yl)carbamoyl)-16-((*S*)-2-amino-3-methylbutanamido)-13-(hydroxymethyl)-7-isobutyl-6,9,12,15-tetraoxo-1,2-dithia-5,8,11,14-tetraazacycloheptadecan-10-yl)propanoic acid.**

The linear precursor peptide was synthesized on a Fmoc Trp(Boc) TentaGel® S RAM resin (load: 0.2 mmol/g) in a 0.1 mmol scale manually using Fmoc strategy with two coupling cycles and two deprotection cycles as described in the "general Fmoc-SPPS procedure". The cleavage of the peptide from the resin was done following the "general cleavage procedure" protocol, where 7 mL cleavage cocktail was used with an incubation of 2.5 h on a shaker. After lyophilization, 87.4 mg of crude linear product was achieved, which was used for the "general cyclisation procedure" for disulfide cyclisation of the cysteines for 2 days. For purification, the "general preparative HPLC procedure" has been performed. A yield of 1.03 mg pure (≥ 93 %) cyclized peptide (1.23 µmol, 1.23 % according to initial load of the resin) was obtained. LC-MS: Column: Phenomenex Luna C18(2), gradient: MeCN/H_2O + 0.05 % HCOOH, 5 % MeCN increase to 50 % MeCN in 5.1 min, flow rate: 0.6 mL/min, t_R= 3.15 min, m/z = 834.4 ([M-H]$^-$). HRMS (ESI+) m/z calculated for $C_{36}H_{53}N_9O_{10}S_2$ [M-H]$^-$ 834.3279; found: 834.3311.

Ac*-V-[CSELC]$_{cyclic}$-W-*OH **(2b); ((4*R*,7*S*,10*S*,13*S*,16*R*)-16-((*S*)-2-acetamido-3-methylbutanamido)-10-(2-carboxyethyl)-13-(hydroxymethyl)-7-isobutyl-6,9,12,15-tetraoxo-1,2-dithia-5,8,11,14-tetraazacycloheptadecane-4-carbonyl)-L-tryptophan.**

The linear precursor peptide was synthesized on a Fmoc Trp(Boc) TentaGel® S AC resin (load: 0.2 mmol/g) in a 0.05 mmol scale with a microwave-assisted peptide synthesizer (CEM Liberty Lite) using Fmoc strategy with two coupling cycles and two deprotection cycles, including acetylation of the *N*-terminus. The used coupling reagents were Oxyma (0.5 M) and DIC (0.25 M) in DMF. The cleavage of the peptide from the resin was done following the "general cleavage procedure" protocol, where 7 mL cleavage cocktail was used with an incubation of 2.5 h on a shaker. After lyophilization, 14.4 mg of crude uncyclized product was achieved, which was used for the "general cyclisation procedure" for disulfide cyclisation of the cysteines for 3 days. For purification, the "general preparative HPLC procedure" has been performed. A yield of 1.09 mg pure (≥ 98 %) cyclized peptide (1.24 µmol, 2.47 % according to initial load of the resin) was obtained. LC-MS: Column: Phenomenex Luna C18(2), gradient: MeCN/H_2O + 0.05 % HCOOH, 5 % MeCN increase to 50 % MeCN in 5.1 min, flow rate: 0.6 mL/min, t_R= 3.88 min, m/z = 879.3 ([M+H]$^+$). HRMS (ESI+) m/z calculated for $C_{38}H_{54}N_8O_{12}S_2$ [M-H]$^-$ 877.3224; found: 877.3251.

Ac*-VASELAW-*NH$_2$ **(3a); (4*S*,7*S*,10*S*,13*S*)-13-(((*S*)-1-(((*S*)-1-(((*S*)-1-amino-3-(1*H*-indol-3-yl)-1-oxopropan-2-yl)amino)-1-oxopropan-2-yl)amino)-4-methyl-1-oxopentan-2-yl)carbamoyl)-10-(hydroxymethyl)-4-isopropyl-7-methyl-2,5,8,11-tetraoxo-3,6,9,12-tetraazahexadecan-16-oic acid.** This linear peptide was synthesized on a Fmoc

Trp(Boc) TentaGel® S RAM resin (load: 0.2 mmol/g) in a 0.1 mmol scale manually using Fmoc strategy with two coupling cycles and two deprotection cycles as described in the "General Fmoc-SPPS procedure" followedby the "general acetylation procedure". The cleavage of the peptide from the resin was done following the "general cleavage procedure" protocol, where 7 mL cleavage cocktail was used with an incubation of 2.5 h on a shaker. For purification, the "general preparative HPLC procedure" has been performed. A yield of 3.24 mg pure (≥ 98 %) peptide (3.97 µmol, 3.97 % according to initial load of the resin) was obtained. LC-MS: Column: Phenomenex Luna C18(2), gradient: MeCN/H_2O + 0.05 % HCOOH, 5 % MeCN increase to 50 % MeCN in 5.1 min, flow rate: 0.6 mL/min, t_R= 3.57 min, m/z = 816.5 ($[M+H]^+$). HRMS (ESI+) m/z calculated for $C_{38}H_{57}N_9O_{11}$ $[M-H]^-$ 814.4099; found: 814.4125.

***Ac*-A-[CSELC]$_{cyclic}$-W-NH_2 (3b); 3-((4*R*,7*S*,10*S*,13*S*,16*R*)-16-((*S*)-2-acetamidopropanamido)-4-(((*S*)-1-amino-3-(1*H*-indol-3-yl)-1-oxopropan-2-yl)carbamoyl)-13-(hydroxymethyl)-7-isobutyl-6,9,12,15-tetraoxo-1,2-dithia-5,8,11,14-tetraazacycloheptadecan-10-yl)propanoic acid.** The linear precursor peptide was synthesized on a Fmoc Trp(Boc) TentaGel® S RAM resin (load: 0.2 mmol/g) in a 0.2 mmol scale manually using Fmoc strategy with two coupling cycles and two deprotection cycles as described in the "general Fmoc-SPPS procedure" followed by the "general acetylation procedure". The cleavage of the peptide from the resin was done following the "general cleavage procedure" protocol (in this case TFA/TIS/H_2O/Anisole 95:2:2:1 as cleavage cocktail), where 3 mL cleavage cocktail was used with an incubation of 3 h on a shaker. After lyophilization, the crude uncyclized product was used for the "general cyclisation procedure" for disulfide cyclisation of the cysteines for 3 days. For purification, the "general preparative HPLC procedure" has been performed. A yield of 1.07 mg pure (≥ 92 %) cyclized peptide (1.26 µmol, 0.63 % according to initial load of the resin) was obtained. LC-MS: Column: Phenomenex Luna C18(2), gradient: MeCN/H_2O + 0.05 % HCOOH, 5 % MeCN increase to 50 % MeCN in 5.1 min, flow rate: 0.6 mL/min, t_R= 3.38 min, m/z = 850.4 ($[M+H]^+$). HRMS (ESI+) m/z calculated for $C_{36}H_{51}N_9O_{11}S_2$ $[M-H]^-$ 848.3071; found: 848.3097.

***Ac*-V-[CAELC]$_{cyclic}$-W-NH_2 (3c); 3-((4*R*,7*S*,10*S*,13*S*,16*R*)-16-((*S*)-2-acetamido-3-methylbutanamido)-4-(((*S*)-1-amino-3-(1*H*-indol-3-yl)-1-oxopropan-2-yl)carbamoyl)-7-isobutyl-13-methyl-6,9,12,15-tetraoxo-1,2-dithia-5,8,11,14-tetraazacycloheptadecan-10-yl)propanoic acid.** The linear precursor peptide was synthesized on a Fmoc Trp(Boc) TentaGel® S RAM resin (load: 0.2 mmol/g) in a 0.05 mmol scale with a microwave-assisted peptide synthesizer (CEM Liberty Lite) using Fmoc strategy with two coupling cycles and two deprotection cycles as described in the "general Fmoc-SPPS procedure", including acetylation of the *N*-terminus. The used coupling reagents were Oxyma (0.5 M) and DIC (0.25 M) in DMF. The cleavage of the peptide from the resin was done following the "general cleavage procedure" protocol, where 7 mL cleavage cocktail was used with an incubation of 2.5 h on a shaker. After lyophilization, the crude uncyclized product was used for the "general cyclisation procedure" for disulfide cyclisation of the cysteines for 7 days. For purification, the "general preparative HPLC procedure" has been performed. A yield of 3.44 mg pure (≥ 98 %) cyclized peptide (3.99 µmol, 7.98 % according to initial load of the resin) was obtained. LC-MS: Column: Phenomenex Luna C18(2), gradient: MeCN/H_2O + 0.05 % HCOOH, 5 % MeCN increase to 50 % MeCN in 5.1 min, flow rate: 0.6 mL/min, t_R= 3.80 min, m/z = 862.4 ($[M+H]^+$). HRMS (ESI+) m/z calculated for $C_{38}H_{55}N_9O_{10}S_2$ $[M-H]^-$ 860.3435; found: 860.3463.

***Ac*-V-[CSALC]$_{cyclic}$-W-NH_2 (3d); (4*R*,7*S*,10*S*,13*S*,16*R*)-16-((*S*)-2-acetamido-3-methylbutanamido)-*N*-((*S*)-1-amino-3-(1*H*-indol-3-yl)-1-oxopropan-2-yl)-13-(hydroxymethyl)-7-isobutyl-10-methyl-6,9,12,15-tetraoxo-1,2-dithia-5,8,11,14-tetraazacycloheptadecane-4-carboxamide.** The linear precursor peptide was synthesized on a Fmoc Trp(Boc) TentaGel® S RAM resin (load: 0.2 mmol/g) in a 0.2 mmol scale manually using Fmoc strategy with two coupling cycles and two deprotection cycles as described in the "general Fmoc-SPPS procedure" followed by the "general acetylation procedure". The cleavage of the peptide from the resin was done following the "general cleavage procedure" protocol (in this case TFA/TIS/H_2O/Anisole 95:2:2:1 as cleavage cocktail), where 7 mL cleavage cocktail was used with an incubation of 4.5 h on a shaker. After lyophilization, 45 mg of crude uncyclized product was achieved, which was used for the "general cyclisation procedure" for disulfide cyclisation of the cysteines for 10 days. For purification, the "general preparative HPLC procedure" has been performed. A yield of 0.8 mg cyclized peptide (Purity: ≥ 71 %; 0.98 µmol,0.49 % according to initial load of the resin) was obtained. LC-MS: Column: Phenomenex Luna C18(2), gradient: MeCN/H_2O + 0.05 % HCOOH, 5 % MeCN increase to 50 % MeCN in 5.1 min, flow rate: 0.6 mL/min, t_R= 3.82 min, m/z = 820.3 ($[M+H]^+$). HRMS (ESI+) m/z calculated for $C_{36}H_{53}N_9O_9S_2$ $[M-H]^-$ 818.3329; found: 818.3356.

***Ac*-V-[CSEAC]$_{cyclic}$-W-NH_2 (3e); 3-((4*R*,7*S*,10*S*,13*S*,16*R*)-16-((*S*)-2-acetamido-3-methylbutanamido)-4-(((*S*)-1-amino-3-(1*H*-indol-3-yl)-1-oxopropan-2-yl)carbamoyl)-13-(hydroxymethyl)-7-methyl-6,9,12,15-tetraoxo-1,2-dithia-5,8,11,14-tetraazacycloheptadecan-10-yl)propanoic acid.** The linear precursor peptide was synthesized on a Fmoc Trp(Boc) TentaGel® S RAM resin (load: 0.2 mmol/g) in a 0.1 mmol scale manually using Fmoc strategy with two coupling cycles and two deprotection cycles as described in the "general Fmoc-SPPS procedure" followed by the "general acetylation procedure". The cleavage of the peptide from the resin was done following the "general cleavage procedure" protocol, where 5 mL cleavage cocktail was used with an incubation of 2 h on a shaker. After lyophilization, 44 mg of crude uncyclized product was achieved, which was used for the "general cyclisation procedure" for disulfide cyclisation of the cysteines for 3 days. For purification, the "general preparative HPLC procedure" has been performed. A yield of 1.21 mg pure (≥ 98 %) cyclized peptide (1.45 µmol, 1.45 % according to initial load of the resin) was obtained. LC-MS: Column: Phenomenex Luna C18(2), gradient: MeCN/H_2O + 0.05 % HCOOH, 5 % MeCN increase to 50 % MeCN in 5.1 min, flow

rate: 0.6 mL/min, t_R= 3.10 min, m/z = 834.3 ([M-H]$^-$). HRMS (ESI+) m/z calculated for $C_{35}H_{49}N_9O_{11}S_2$ [M-H]$^-$ 834.2915; found: 834.2944.

***Ac*-V-[CSELC]$_{cyclic}$-A-*NH$_2$* (3f); 3-((4*R*,7*S*,10*S*,13*S*,16*R*)-16-((*S*)-2-acetamido-3-methylbutanamido)-4-(((*S*)-1-amino-1-oxopropan-2-yl)carbamoyl)-13-(hydroxymethyl)-7-isobutyl-6,9,12,15-tetraoxo-1,2-dithia-5,8,11,14-tetraazacycloheptadecan-10-yl)propanoic acid.** The linear precursor peptide was synthesized on a Fmoc Ala TentaGel® S RAM resin (load: 0.2 mmol/g) in a 0.1 mmol scale manually using Fmoc strategy with two coupling cycles and two deprotection cycles as described in the "general Fmoc-SPPS procedure" followed by the "general acetylation procedure". The cleavage of the peptide from the resin was done following the "general cleavage procedure" protocol, where 5 mL cleavage cocktail was used with an incubation of 2.5 h on a shaker. After lyophilization, 63 mg of crude uncyclized product was achieved, which was used for the "general cyclisation procedure" for disulfide cyclisation of the cysteines for 3 days. For purification, the "general preparative HPLC procedure" has been performed. A yield of 6 mg pure (≥ 98 %) cyclized peptide (7.86 µmol, 7.86 % according to initial load of the resin) was obtained. LC-MS: Column: Phenomenex Luna C18(2), gradient: MeCN/H_2O + 0.05 % HCOOH, 5 % MeCN increase to 50 % MeCN in 5.1 min, flow rate: 0.6 mL/min, t_R= 2.99 min, m/z = 761.3 ([M-H]$^-$). HRMS (ESI+) m/z calculated for $C_{30}H_{50}N_8O_{11}S_2$ [M-H]$^-$ 761.2985; found: 761.2985.

***Ac*- – -[CSELC]$_{cyclic}$-W-*NH$_2$* (4a); ((4*R*,7*S*,10*S*,13*S*,16*R*)-16-acetamido-10-(2-carboxyethyl)-13-(hydroxymethyl)-7-isobutyl-6,9,12,15-tetraoxo-1,2-dithia-5,8,11,14-tetraazacycloheptadecane-4-carbonyl)-L-tryptophan.** The linear precursor peptide was synthesized on a Fmoc Trp(Boc) TentaGel® S RAM resin (load: 0.2 mmol/g) in a 0.1 mmol scale manually using Fmoc strategy with two coupling cycles and two deprotection cycles as described in the "general Fmoc-SPPS procedure" followed by the "general acetylation procedure". The cleavage of the peptide from the resin was done following the "general cleavage procedure" protocol, where 5 mL cleavage cocktail was used with an incubation of 2.75 h on a shaker. The solution was suspended in 1.5 mL DCM. At -20 °C TFA (300 µL, 40 eq.) was added and incubated overnight. After lyophilization, 24 mg of crude uncyclized product was achieved, which was used for the "general cyclisation procedure" for disulfide cyclisation of the cysteines for 2 days. For purification, the "general preparative HPLC procedure" has been performed. A yield of 0.77 mg pure (≥ 98 %) cyclized peptide (0.99 µmol, 0.99 % according to initial load of the resin) was obtained. LC-MS: Column: Phenomenex Luna C18(2), gradient: MeCN/H_2O + 0.05 % HCOOH, 5 % MeCN increase to 50 % MeCN in 5.1 min, flow rate: 0.6 mL/min, t_R= 3.39 min, m/z = 777.3 ([M-H]$^-$). HRMS (ESI+) m/z calculated for $C_{33}H_{46}N_8O_{10}S_2$ [M-H]$^-$ 877.2700; found: 877.2720.

***Ac*-V-[CSELC]$_{cyclic}$ – -*NH$_2$* (4b); (4*R*,7*S*,10*S*,13*S*,16*R*)-16-((*S*)-2-acetamido-3-methylbutanamido)-10-(2-carboxyethyl)-13-(hydroxymethyl)-7-isobutyl-6,9,12,15-tetraoxo-1,2-dithia-5,8,11,14-tetraazacycloheptadecane-4-carboxylic acid.** The linear precursor peptide was synthesized on a Fmoc Cys(Trt) TentaGel® S RAM resin (load: 0.2 mmol/g) in a 0.1 mmol scale manually using Fmoc strategy with two coupling cycles and two deprotection cycles as described in the "general Fmoc-SPPS procedure" followed by the "general acetylation procedure". The cleavage of the peptide from the resin was done following the "general cleavage procedure" protocol, where 7 mL cleavage cocktail was used with an incubation of 2.5 h on a shaker. After lyophilization, 55.9 mg of crude uncyclized product was achieved, which was used for the "general cyclisation procedure" for disulfide cyclisation of the cysteines for 3 days. For purification, the "general preparative HPLC procedure" has been performed. A yield of 0.27 mg pure (≥ 89 %) cyclized peptide (0.39 µmol, 0.39 % according to initial load of the resin) was obtained. LC-MS: Column: Phenomenex Luna C18(2), gradient: MeCN/H_2O + 0.05 % HCOOH, 5 % MeCN increase to 50 % MeCN in 5.1 min, flow rate: 0.6 mL/min, t_R= 2.99 min, m/z = 690.3 ([M-H]$^-$). HRMS (ESI+) m/z calculated for $C_{27}H_{45}N_7O_{10}S_2$ [M-H]$^-$ 690.2591; found: 690.2608.

General Fmoc-SPPS procedure for triazole-bridged peptides 5a, 5b, 5c. The amino acids were coupled *via* two coupling cycles. For proteinogenic amino acids a solution of the Fmoc protected amino acid (4.0 eq), HBTU (3.9 eq) and DIPEA (8.0 eq) was used. For non-proteinogenic amino acids a solution of the amino acid (3.5 eq), HATU (3.9 eq) and DIPEA (8.0 eq) was used. The resin was shaken 1 h at room temperature before every coupling step was followed by washing steps with DMF (5 x 6 mL) and DCM (5 x 6 mL). Fmoc deprotection was achieved by a reaction with 20 % piperidine in DMF for 5 min at room temperature, followed by a second deprotection step under same conditions. A solution of DMF/DIPEA/Ac_2O (5:3:2) was given on the resin and shook 30 min at room temperature for the Acetylation of the peptide. The cleavage of the peptide from the resin and removal of the side chain protecting groups was done with a cleavage cocktail of TFA/H_2O/anisole/TES (47:1:1:1). The mixture was shaken at room temperature for 3 h. After precipitation, the obtained solid was washed with MTBE (4 x 2 mL) and dried by freeze-drying.

Copper-catalyzed azide-alkyne cycloaddition (CuAAC). The linear peptide (1.0 eq) was dissolved in argon-flushed H_2O (1 mL/mg). $CuSO_4 \cdot 5H_2O$ (2.0 eq), Na-ascorbate (4.0 eq) and DIPEA (8.0 eq) were added and the reaction mixture stirred under argon at room temperature overnight. The solvent was removed by freeze-drying and the macrocyclic peptide was purified by preparative HPLC.

***Ac*-V-[Pra-SEL-Aza]$_{cyclic}$-W-*NH$_2$* (1,4-triazole) (5a); 3-((3*S*,6*S*,9*S*,12*S*,15*S*,*Z*)-15-((*S*)-2-acetamido-3-methylbutanamido)-3-(((*S*)-1-amino-3-(1*H*-indol-3-yl)-1-oxopropan-2-yl)carbamoyl)-12-(hydroxymethyl)-6-isobutyl-5,8,11,14-tetraoxo-11*H*-4,7,10,13-tetraaza-1(1,4)-triazolacyclohexadecaphane-9-yl)propanoic acid.** The

linear precursor peptide ***Ac*-V-Pra-SEL-Aza-W-*NH$_2$*** was synthesized manually on a Fmoc Trp(Boc) Tenta Gel S RAM resin (0.20 mmol/g) at 0.10 mmol scale. According to the general Fmoc-SPPS procedure for triazole-bridged peptides, the following amino acids and building blocks were used: Fmoc-L-Aza-OH (0.35 mmol, 3.5 eq), Fmoc-Leu-OH (0.4 mmol, 4.0 eq), Fmoc-Glu(O*t*Bu)-OH (0.4 mmol, 4.0 eq), Fmoc-Ser(*t*Bu)-OH (0.4 mmol, 4.0 eq), Fmoc-Pra-OH (0.35 mmol, 3.5 eq) and Fmoc-Val-OH (0.4 mmol, 4.0 eq). Fmoc-L-Aza-OH and Fmoc-Pra-OH were used together with HATU (0.39 mmol, 3.9 eq) and DIPEA (0.8 mmol, 8.0 eq), while all other amino acids were used together with HBTU (0.39 mmol, 3.9 eq) and DIPEA (0.8 mmol, 8.0 eq). The product was received as a white solid (32.6 mg, 37.0 µmol, 37 % according to the initial load of the resin). According to "Copper-catalyzed azide-alkyne cycloaddition" the macrocyclic peptide was prepared by a reaction of 27.0 mg (30.6 µmol, 1.0 eq) linear precursor peptide, 15.4 mg $CuSO_4 \cdot 5H_2O$ (61.2 µmol, 2.0 eq), 24.4 mg Na-ascorbate (122 µmol, 4.0 eq) and 41.5 µL DIPEA (245 µmol, 8.0 eq). The solvent was removed by freeze-drying. The macrocyclic peptide was purified by preparative HPLC (H_2O:ACN 9:1→1:1) and was received as a pure (≥ 98 %) white solid (5.10 mg, 5.79 µmol, 19 %). The characterization was done by LC-MS, IR, ^{1}H-NMR, ^{13}C-NMR, 2 D NMR and HRMS (m/z). LC-MS: Column: Phenomenex Luna C18(2), gradient: MeCN/H_2O + 0.05 % HCOOH, 5 % MeCN increase to 50 % MeCN in 5.1 min, flow rate: 0.6 mL/min, t_R= 3.49 min, m/z = 879.5 ([M-H]$^-$). HRMS (ESI+) m/z calculated for $C_{40}H_{56}N_{12}O_{11}$ $[M+H]^+$ 881.4270; found: 881.4236.

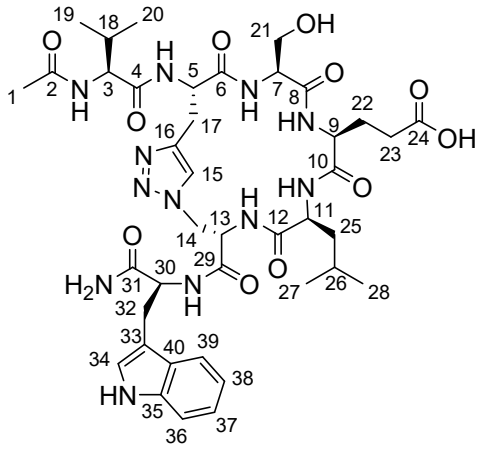

^{1}H-NMR (500 MHz, CD_3OD, δ in ppm): 10.0 (bs, 1 H, Indole NH), 8.46-8.55 (m, 1 H, NH), 8.27-8.35 (bs, 1 H, NH), 8.08 (d, $^3J_{NH,5}$ = 8.24 Hz, 1 H, NH), 7.76 – 7.81 (m, 1 H, NH), 7.65 (s, 1 H, H15), 7.60 (d, $^3J_{39,38}$ = 7.78 Hz 1 H, H39), 7.54 (d, $^3J_{NH,7}$ = 8.24 Hz, 1 H, NH), 7.34 (d, $^3J_{36,37}$ = 8.09 Hz, 1 H, H36), 7.09 (dd, $^3J_{37,36/38}$ = 7.68 Hz, 1 H, H37), 7.01-7.04 (m, 1 H, H38), 7.01 (s, 1 H, H34), 4.94-5.01 (m, 1 H, H13), 4.73-4.82 (m, 3 H, H5/H14/H30), 4.59 (bs, 1 H, NH), 4.49 (d, $^3J_{14,13}$ = 3.74 Hz, 1 H, H14), 4.30-4.34 (m, 2 H, H7/H9), 4.26-4.30 (m, 1 H, H3), 3.97-4.08 (m, 2 H, H11/H21), 3.76 (dd, $^2J_{21a,21b}$ = 3.74 Hz, $^3J_{21,7}$ = 11.4 Hz, 1 H, H21), 3.60-3.65 (m, 2 H, H23), 3.38 (dd, $^2J_{17a,17b}$ = 3.74 Hz, $^3J_{17,5}$ = 11.4 Hz,, 1 H, H17), 3.19-3.26 (m, 1 H, H17), 3.16 (dd, $^3J_{32a,30}$ = 3.66 Hz, $^3J_{32b,30}$ = 4.88 Hz, 2 H, H32), 2.02-2.19 (m, 2 H, H18/OH), 2.00 (s, 3 H, H1), 1.77-1.94 (m, 2 H, H22), 1.52-1.68 (m, 3 H, H25/H26), 0.97 (dd, $^3J_{19/20,18}$ = 6.48 Hz, 6 H, H19/H20), 0.92 (d, $^3J_{27,26}$ = 6.10 Hz. 3 H, H27), 0.87 (d, $^3J_{28,26}$ = 6.10 Hz, 3 H, H28).

^{13}C-NMR (126 MHz, CD_3OD, δ in ppm): 176.9 (C24), 175.3 (C31), 174.6 (C29), 173.8 (C2), 173.7 (C4), 173.1 (C12), 172.7 (C10), 171.1 (C6/C8), 138.2 (C16/C35), 128.9 (C40), 126.2 (C15), 125.0 (C34), 122.7 (C37), 120.1 (C39), 119.6 (C38), 112.4 (C36), 111.3 (C33), 63.5 (C21), 60.4 (C3), 57.0 (C7/C9), 55.9 (C30), 55.3 (C5), 54.3 (C11), 53.7 (C13), 51.3 (C14), 39.9 (C25), 32.1 (C18), 29.2 (C23), 28.6 (C32), 26.7 (C17/C22), 26.2 (C26), 23.5 (C27), 22.6 (C1), 21.6 (C28), 19.9 (C20), 18.8 (C19).

Ac*-V-[Aza-SEL-Pra]$_{cyclic}$-W-*NH$_2$* (1,4-triazole) (5b); 3-((3*S*,6*S*,9*S*,12*S*,15*S*,*Z*)-15-((*S*)-2-acetamido-3-methylbutanamido)-3-(((*S*)-1-amino-3-(1*H*-indol-3-yl)-1-oxopropan-2-yl)carbamoyl)-12-(hydroxymethyl)-6-isobutyl-5,8,11,14-tetraoxo-11*H*-4,7,10,13-tetraaza-1(4,1)-triazolacyclohexadecaphane-9-yl)propanoic acid.** The linear precursor peptide ***Ac*-V-Aza-SEL-Pra-W-*NH$_2$ was synthesized on a microwave-assisted peptide synthesizer (Liberty Lite) using Fmoc Trp(Boc) Tenta Gel S RAM resin (0.20 mmol/g) at 0.05 mmol scale. The engaged amino acids were used in concentrations of 0.2 M in DMF. The used coupling reagents were Oxyma (0.5 M) and DIC (0.25 M) in DMF. The product was received as a white solid (32.0 mg, 36.3 µmol, 73 % according to the initial load of the resin). According to "Copper-catalyzed azide-alkyne cycloaddition" the macrocyclic peptide was prepared by a reaction of 32.0 mg (36.3 µmol, 1.0 eq) linear precursor peptide, 18.6 mg $CuSO_4 \cdot 5H_2O$ (74.5 µmol, 2.05 eq), 28.2 mg Na-ascorbate (142 µmol, 3.92 eq) and 55 µL DIPEA (317 µmol, 8.7 eq). The solvent was removed by freeze-drying. The macrocyclic peptide was purified by preparative HPLC (H_2O:ACN 9:1→1:1) and was received as a white solid (6.42 mg, 7.29 µmol, 15 %). The characterization was done by LC-MS, ^{1}H-NMR, ^{13}C-NMR and HRMS (m/z). LC-MS: Column: Phenomenex Luna C18(2),

gradient: MeCN/H_2O + 0.05 % HCOOH, 5 % MeCN increase to 50 % MeCN in 5.1 min, flow rate: 0.6 mL/min, t_R= 3.52 min, m/z = 879.4 ([M-H]$^-$). HRMS (ESI+) m/z calculated for $C_{40}H_{56}N_{12}O_{11}$ [M+H]$^+$ 881.4270; found: 881.4253.

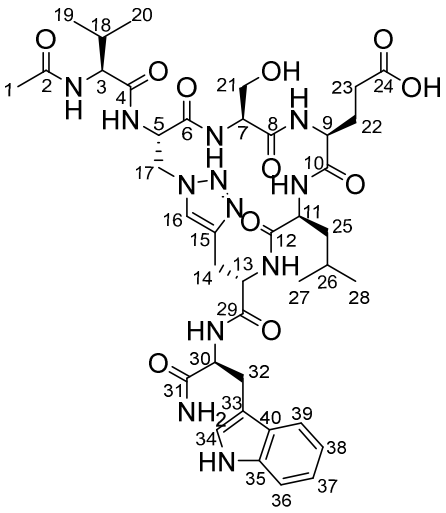

^{1}H-NMR (500 MHz, CD_3OD, δ in ppm): 7.64 (d, $^3J_{39,38}$ = 7.9 Hz, 1 H, H39), 7.58 (s, 1 H, H16), 7.34 (d, $^3J_{36,37}$ = 8.1 Hz, 1 H, H36), 7.15 (s, 1 H, H34), 7.09 (t, $^3J_{37,36/38}$ = 7.3 Hz, 1 H, H37), 7.02 (t, $^3J_{38,37/39}$ = 7.4 Hz, 1 H, H38), 5.13-5.09 (m, 1 H, H5), 4.75-4.66 (m, 3 H, H13/H17$_a$/H30), 4.62-4.55 (m, 2 H, H9, H11), 4.36 (t, $^3J_{17,5}$ = 3.5 Hz, 1 H, H17$_b$), 4.21 (d, ^{3}J = 7.3 Hz, 1 H, H3), 4.11 (dd, $^2J_{21a,21b}$ = 11.5 Hz, $^3J_{21a,7}$ = 4.2 Hz, 1H, H21$_a$), 4.03 (dd, $^2J_{32a,32b}$ = 9.5 Hz, $^3J_{32a,30}$ = 5.6 Hz, 1H, H32$_a$), 3.81-3.77 (m, 1H, H32$_b$), 3.74 (dd, $^2J_{21a,21b}$ = 11.5, $^3J_{21b,7}$ = 3.0, 1 H, H21$_b$), 3.43 (dd, $^2J_{14a,14b}$ = 15.2 Hz, $^3J_{14a,13}$ = 3.9 Hz, 1 H, H14$_a$), 3.25-3.18 (m, 1 H, H14$_b$), 2.97-2.90 (m, 1H, H23$_a$), 2.85-2.78 (m, 1H, H23$_b$), 2.31 (br.s, 2 H, H18/OH), 2.12-2.03 (m, 2H, H22), 2.01 (s, 3 H, H1), 1.69-1.61 (m, 1H, 26H), 1.58-1.54 (m, 2 H, 25H), 0.97 (dd, $^3J_{19/20,18}$ = 6.8 Hz, 6 H, H19/H20), 0.92 (d, $^3J_{27,26}$ = 6.5 Hz. 3 H, H27), 0.87 (d, $^3J_{28,26}$ = 6.4 Hz, 3 H, H28).

^{13}C-NMR (126 MHz, CD_3OD, δ in ppm): 177.1 (C24), 175.6 (C31), 174.6 (C29), 174.0 (C2), 173.9 (C4), 173.9 (C12), 173.6 (C10), 172.3 (C8), 171.1 (C6), 138.1 (C35), 138.1 (C15), 129.0 (C40), 125.0 (C34), 124.8 (C16), 122.6 (C37), 120.1 (C39), 119.7 (C38), 112.4 (C36), 111.7 (C33), 63.5 (C21), 60.7 (C3), 57.1 (C7/C9), 56.1 (C30), 55.9 (C13), 55.4 (C5), 54.8 (C11), 51.5 (C17), 41.1 (C25), 31.9 (C18), 28.8 (C23), 28.6 (C32), 28.1 (C14/C22), 26.2 (C26), 23.5 (C27), 22.5 (C1), 21.5 (C28), 19.8 (C20), 18.9 (C19).

Ac*-V-[Pra-SEL-Aha]$_{cyclic}$-W-*NH$_2$* (1,4-triazole) (5c); 3-((3*S*,6*S*,9*S*,12*S*,15*S*,*Z*)-3-((*S*)-2-acetamido-3-methylbutanamido)-15-(((*S*)-1-amino-3-(1*H*-indol-3-yl)-1-oxopropan-2-yl)carbamoyl)-6-(hydroxymethyl)-12-isobutyl-4,7,10,13-tetraoxo-11*H*-5,8,11,14-tetraaza-1(1,4)-triazolacycloheptadecaphane-9-yl)propanoic acid.** The linear precursor peptide ***Ac*-V-Pra-SEL-Aha-W-*NH$_2$ was synthesized on a microwave-assisted peptide synthesizer (Liberty Lite) using Fmoc Trp(Boc) Tenta Gel S RAM resin (0.20 mmol/g) at 0.05 mmol scale. The engaged amino acids were used in concentrations of 0.2 M in DMF. The used coupling reagents were Oxyma (0.5 M) and DIC (0.25 M) in DMF. The product was received as a white solid (35.5 mg, 39.7 µmol, 79 % according to the initial load of the resin). According to "Copper-catalyzed azide-alkyne cycloaddition" the macrocyclic peptide was prepared by a reaction of 35.5 mg (39.7 µmol, 1.0 eq) linear precursor peptide, 20.4 mg $CuSO_4 \cdot 5H_2O$ (81.7 µmol, 2.06 eq), 33.2 mg Na-ascorbate (168 µmol, 4.2 eq) and 55 µL DIPEA (317 µmol, 8.0 eq). The solvent was removed by freeze-drying. The macrocyclic peptide was purified by preparative HPLC (H_2O:ACN 9:1→1:1) and was received as a pure (≥ 98 %) white solid (8.45 mg, 9.4 µmol, 19 %). The characterization was done by LC-MS, ^{1}H-NMR, ^{13}C-NMR and HRMS (m/z). LC-MS: Column: Phenomenex Luna C18(2), gradient: MeCN/H_2O + 0.05 % HCOOH, 5 % MeCN increase to 50 % MeCN in 5.1 min, flow rate: 0.6 mL/min, t_R= 3.48 min, m/z = 895.4 ([M+H]$^+$). HRMS (ESI+) m/z calculated for $C_{40}H_{56}N_{12}O_{11}$ [M+H]$^+$ 895.4426; found: 895.4406.

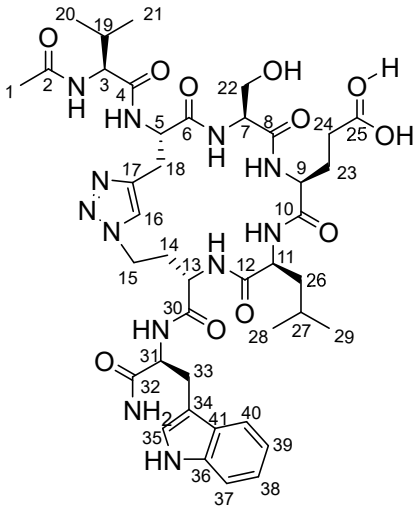

^{1}H-NMR (500 MHz, CD_3OD, δ in ppm): 7.66 (d, $^3J_{40,39}$ = 7.8 Hz, 1 H, H40), 7.39 (s, 1 H, H16), 7.32 (s, 1 H, H35), 7.05 (d, $^3J_{37,38}$ = 8.0 Hz, 1 H, H37), 7.00 (t, $^3J_{39,38/40}$ = 7.3 Hz, 1 H, H39), 6.94 (t, $^3J_{38,37/39}$ = 7.4 Hz, 1 H, H38), 4.85-4.81 (m, 1H, H5), 4.44-4.37 (m, 2H, H9, H31), 4.25-4.18 (m, 2H, H9, H31), 4.13 (d, $^3J_{13,14}$ = 6.1 Hz, 1H, H13), 4.08 (dd, $^3J_{11,26}$ = 4.1 Hz, 1H, H11), 3.89 (dd, $^2J_{22a,22b}$ = 10.3 Hz, $^3J_{22a,7}$ = 5.2 Hz, 1H, $H22_a$), 3.54-3.33 (m, 3H, $H22_b$, H15), 3.19-3.06 (m, 4H, H18, H33), 2.58 (br.s, 1H, H24), 2.49-2.40 (m, 1H, $H14_a$), 2.23 (br.s, 1H, H23), 2.06-2.00 (m, 1H, H19), 1.99 (s, 3H, H1), 1.89-1.81 (m, 1H, $H14_b$), 1.66-1.52 (m, 3H, H26, H27), 0.94 (dd, $^3J_{20,19or21,19}$ = 6.6 Hz, 4.6 Hz, 6H, H20, H21), 0.91 (d, $^3J_{29,27}$ = 5.8 Hz, 3H, H29), 0.87 (d, $^3J_{28,27}$ = 6.0 Hz, 3H, H28).

^{13}C-NMR (126 MHz, CD_3OD, δ in ppm): 176.9 (C25), 176.0 (C32), 174.8 (C4 or C8 or C30), 174.7 (C4 or C8 or C30), 173.5 (C2 or C6 or C10), 173.4 (C2 or C6 or C10), 173.3 (C2 or C6 or C10), 172.2 (C12, C4 or C8 or C30), 138.0 (C36), 128.5 (C17, C41), 125.3 (C16, C35), 122.5 (C39), 120.0 (C38), 119.6 (C40), 112.3 (C37), 111.4 (C34), 62.4 (C22), 60.0 (C3), 57.2 (C7), 56.6 (C31), 54.9 (C5 or C9 or C11), 54.8 (C5 or C9 or C11), 53.6 (C13), 45.7 (C15), 39.7 (C26), 32.0 (C19), 31.2 (C14), 28.9 (C23, C24), 28.4 (C33), 26.1 (C27), 23.4 (C29), 22.4 (C1), 19.7 (C20 or C21), 18.7 (C20 or C21).

***Ac*-V-[Pra-SEL-Aza]$_{cyclic}$-W-*NH*$_2$ (6a); (4*S*,7*S*,10*S*,13*S*)-13-(((*S*)-1-(((*S*)-1-(((*S*)-1-amino-3-(1*H*-indol-3-yl)-1-oxopropan-2-yl)amino)-3-(5-methyl-1*H*-1,2,3-triazol-1-yl)-1-oxopropan-2-yl)amino)-4-methyl-1-oxopentan-2-yl)carbamoyl)-10-(hydroxymethyl)-4-isopropyl-7-methyl-2,5,8,11-tetraoxo-3,6,9,12-tetraazahexadecan-16-oic acid, *Ac*-V-[Pra-SEL-Aha]$_{cyclic}$-W-*NH*$_2$ (6b); (4*S*,7*S*,10*S*,13*S*)-13-(((*S*)-1-(((*S*)-1-(((*S*)-1-amino-3-(1*H*-indol-3-yl)-1-oxopropan-2-yl)amino)-4-(5-methyl-1*H*-1,2,3-triazol-1-yl)-1-oxobutan-2-yl)amino)-4-methyl-1-oxopentan-2-yl)carbamoyl)-10-(hydroxymethyl)-4-isopropyl-7-methyl-2,5,8,11-tetraoxo-3,6,9,12-tetraazahexadecan-16-oic acid and *Ac*-V[Aha-SEL-Pra]$_{cyclic}$-W-*NH*$_2$ (6c); 3-((3*S*,6*S*,9*S*,12*S*,15*S*,*Z*)-15-((*S*)-2-acetamido-3-methylbutanamido)-3-(((*S*)-1-amino-3-(1*H*-indol-3-yl)-1-oxopropan-2-yl)carbamoyl)-12-(hydroxymethyl)-6-isobutyl-5,8,11,14-tetraoxo-11H-4,7,10,13-tetraaza-1(4,1)-triazolacycloheptadecaphane-9-yl)propanoic acid.**

Each peptide was manually synthesized by Fmoc-SPPS using Rink amide-MBHA resin (0.8 mmol loading, 100-200 mesh, Chempep Inc). Fmoc-protected amino acids (Fmoc-Trp(Boc)-OH, Fmoc-Leu-OH, Fmoc-Glu(OtBu)-OH, Fmoc-Ser(tBu)-OH, Fmoc-Val-OH) were purchased from either Mimotopes or CSBio, and the azide and alkyne precursors (Fmoc-Aza-OH, Fmoc-Aha-OH and Fmoc-Pra-OH) were purchased from Chem-Impex International Inc. The peptides were synthesized on a 0.25 mmol scale and the resins were first swelled in DMF for 30 min prior to Fmoc deprotection (standard condition used throughout assembly: 20 % piperidine, 5 mL, 15 min). Each amino acid was coupled using 4.0 eq. of amino acid, 4.0 eq. of benzotriazol-1-yl-oxytripyrrolidinophosphonium hexafluorophosphate (PyBOP) and 8.0 eq. of *N,N*-diisopropylethylamine (DIPEA) in 3 mL of DMF, shaken for 45 min. The resin was washed with DMF (3 x 5 mL) and DCM (3 x 5 mL) between each deprotection and coupling step. Following assembly of the sequences, the *N*-terminus was acetylated using acetic anhydride/DMF (1:4, 6 mL) and 2 eq. of DIPEA, shaken for 45 min. The resin was then washed thoroughly in DMF (5 x 5 mL) and DCM (5 x 5 mL), dried under a stream of N_2 and stored in a desiccator overnight.

The crude peptide-bound resin was next subject to ruthenium-catalyzed azide-alkyne cycloaddition (RuAAC) to install the 1,5-disubstituted 1,2,3-triazole bridge. For each analogue, 75 µmol of resin-bound peptide (**6a**: 160 mg; **6b**: 170 mg; and **6c** 170 mg; based on initial resin loading) was loaded into a glass vessel and suspended in 2 mL of anhydrous DMF. The mixture was sparged with argon for 30 min prior to the addition of 50 mol% of chloro(pentamethylcyclopentadienyl)(cyclooctadiene)ruthenium(II) (14.2 mg, 37.5 µmol). The reaction was heated to 80 °C for 18 h under an atmosphere of argon. The resin was thoroughly washed with DMF (3 x 5 mL), 0.5 % sodium diethyldithiocarbamate trihydrate in DMF (w/v, 3 x 5 mL), MeOH (3 x 5 mL), and DCM (5 x 5 mL) and dried under N_2. The peptides were next cleaved from the resin by suspending the resin in 5 mL of TFA/TIS/H_2O (95:2.5:2.5, v/v/v) for 2 h, followed by precipitation with cold Et_2O before being redissolved in 50 % MeCN and lyophilized. The peptide was next purified to >95 % purity by preparative RP-HPLC on a Shimadzu Prominence system with a Phenomenex Gemini C-18

column (5 µm, 250 x 10 mm) using a gradient of 20-50 % Solvent B (Solvent A: H_2O with 0.05 % trifluoroacetic acid; Solvent B: 95 % acetonitrile with 0.05 % trifluoroacetic acid) at 3 mL/min. The lyophilized peptides were obtained as a white solid (**6a**: purity: ≥ 95 %*, 0.67 mg, 0.76 µmol, 1.0 % overall yield based on the initial resin loading; **6b**: purity: ≥ 98 %, 1.72 mg, 1.92 µmol, 2.6 %; and **6c**: purity: ≥ 98 %, 1.40 mg, 1.56 µmol, 2.1 %) and further characterized by LC-MS, ^{1}H-NMR and HRMS.

6a: HRMS (ESI+) m/z calculated for $C_{40}H_{56}N_{12}O_{11}$ $[M+H]^+$ 881.4270; found: 881.4280.

6b: LC-MS: Column: Phenomenex Luna C18(2), gradient: MeCN/H_2O + 0.05 % HCOOH, 5 % MeCN increase to 50 % MeCN in 5.1 min, flow rate: 0.6 mL/min, t_R= 3.52 min, m/z = 895.4 ($[M+H]^+$). HRMS (ESI+) m/z calculated for $C_{41}H_{58}N_{12}O_{11}$ $[M+H]^+$ 895.4426; found: 895.4428.

6c: LC-MS: Column: Phenomenex Luna C18(2), gradient: MeCN/H_2O + 0.05 % HCOOH, 5 % MeCN increase to 50 % MeCN in 5.1 min, flow rate: 0.6 mL/min, t_R= 3.52 min, m/z = 895.4 ($[M+H]^+$). HRMS (ESI+) m/z calculated for $C_{41}H_{58}N_{12}O_{11}$ $[M+H]^+$ 895.4426; found: 895.4402.

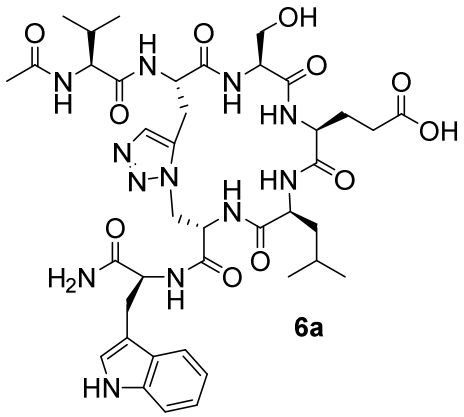

6a

Table S1. NMR chemical shifts of **6a**.

Residue	H	N	Hα	Hβ	Others
1 Val	8.08	114.1	4.04	1.97	0.88 Hγ1; 0.87 Hγ2; 59.8 Cα; 30.0 Cβ; 17.7 Cγ1; 18.3 Cγ2; Ac: 1.97 3H, 21.7 CH_3
2 Pra	8.73	123.5	4.73	3.02, 3.16	7.63 Hδ; 25.5 Cβ; 133.3 Cδ
3 Ser	7.87	118.1	4.20	3.75, 3.85	56.1 Cα; 60.3 Cβ
4 Glu	8.40	120.9	3.86	1.91 (2H)	2.16 Hγ (2H); 56.1 Cα; 26.4 Cβ; 33.3 Cγ
5 Leu	7.73	118.6	4.09	1.25 (2H)	1.39 Hγ; 0.74 Hδ1; 0.77 Hδ2; 52.5 Cα; 39.5 Cβ; 24.3 Cγ; 20.6 Cδ1; 22.2 Cδ2
6 Aza	8.08	125.5	5.04	4.39 (2H)	52.2 Cα; 47.3 Cβ
7 Trp	7.93	123.5	4.74	3.14, 3.32	128.9 Nε1; 7.13 Hδ1; 9.98 Hε1; 7.58 Hε3; 7.41 Hζ2; 7.06 Hζ3; 7.16 Hη2; 27.0 Cβ; 124.6 Cδ1; 118.4 Cε3; 112.0 Cζ2; 119.4 Cζ3; 122.03 Cη2; NH_2: 7.09 H1, 7.43 H2, 108.0 N

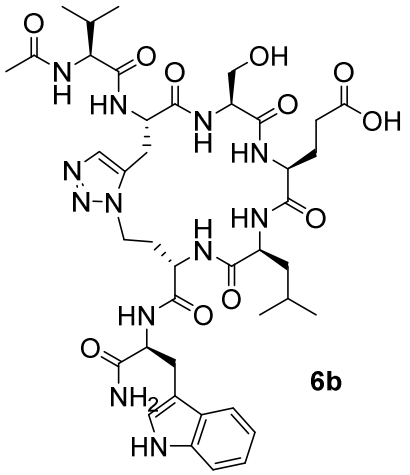

6b

Table S2. NMR chemical shifts of **6b**.

Residue	H	N	Hα	Hβ	Others
1 Val	8.07	125.6	3.94	1.91	0.81 Hγ1; 0.83 Hγ2; 60.0 Cα; 29.8 Cβ; 18.3 Cγ1; 17.9 Cγ2; Ac: 1.95 3H, 21.6 CH_3
2 Pra	8.78	123.5	4.77	3.38, 3.11	7.54 Hδ; 25.6 Cβ; 131.7 Cδ
3 Ser	8.59	118.2	4.26	3.89, 3.81	57.1 Cα; 60.7 Cβ
4 Glu	7.87	119.3	4.37	2.07, 1.85	2.29 Hγ (2H); 52.2 Cα; 27.2 Cβ; 30.5 Cγ
5 Leu	7.95	119.8	3.98	1.45, 1.35	1.41 Hγ; 0.73 Hδ1; 0.79 Hδ2; 53.9 Cα; 39.2 Cβ; 24.3 Cγ; 21.4 Cδ1; 21.7 Cδ2
6 Aha	8.33	121.8	4.40	2.24, 1.82	4.16 Hγ1; 4.25 Hγ2; 50.7 Cα; 31.7 Cβ; 44.1 Cγ
7 Trp	7.99	121.4	4.62	3.27, 3.13	129.1 Nε1; 7.14 Hδ1; 10.01 Hε1; 7.55 Hε3; 7.34 Hζ2; 7.02 Hζ3; 7.09 Hη2; 27.2 Cβ; 124.6 Cδ1; 118.3 Cε3; 112.0 Cζ2; 119.3 Cζ3; 122.0 Cη2; NH_2: 7.02 H1, 7.46 H2, 108.2 N

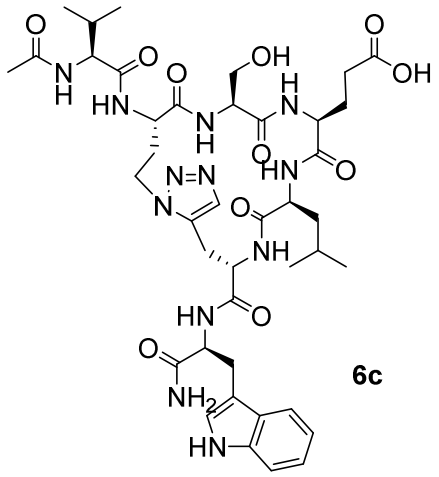

6c

Table S3. NMR chemical shifts of **6c**.

Residue	H	N	Hα	Hβ	Others
1 Val	8.02	124.5	4.07	2.02	0.87 Hγ1; 0.86 Hγ2; 62.2 Cα; 32.6 Cβ; 21.2 Cγ1; 20.1 Cγ2; Ac 1.96 3H, 24.4 CH_3
2 Aha	8.70	124.4	4.08	2.27, 2.61	3.71 Hγ (2H); 46.1 Cα; 32.3 Cβ; 54.8 Cγ
3 Ser	8.18	117.7	4.23	3.96, 3.79	59.5 Cα; 63.2 Cβ
4 Glu	7.88	118.5	4.15	2.00 (2H)	2.36 Hγ2 (2H); 57.6 Cα; 28.7 Cβ; 33.3 Cγ
5 Leu	7.58	118.1	4.11	1.02, 1.24	1.43 Hγ; 0.69 Hδ1; 0.72 Hδ2; 56.2 Cα; 42.9 Cβ; 26.8 Cγ; 24.8 Cδ1; 23.0 Cδ2
6 Pra	7.98	117.0	4.62	2.89 (2H)	7.43 Hδ; 26.84 Cβ; 134.7 Cδ
7 Trp	7.68	121.1	4.62	3.16, 3.31	128.8 Nε1; 7.14 Hδ1; 10.0 Hε1; 7.5 Hε3; 7.41 Hζ2; 7.06 Hζ3; 7.16 Hη; 29.8 Cβ; 127.3 Cδ1; 121.1 Cε3; 114.6 Cζ2; 122.1 Cζ3; 124.6 Cη2; NH_2: 7.03 H1, 7.33 H2, 107.7 N

Table S4. Key facts about the synthesis of the individual peptides. Starting from the used resin over cleavage cocktail and cyclization and yield.

Peptide	Resin	Approach	Manually/ synthesizer	Cleavage cocktail	Crude linear peptide yield	Cyclisation	Yield after prep HPLC	Purity[a]
1	Fmoc Trp(Boc) TentaGel® S RAM	0.2 mmol	Manually	TFA/TIS/H_2O (37:1:1) + DTT, 7 mL, 3 h	45.7 mg	ACN/H_2O (1:1) 1 mg/mL, 2 % DMSO, 2 days	2.68 mg	≥98%
2a	Fmoc Trp(Boc) TentaGel® S RAM	0.1 mmol	Manually	TFA/TIS/H_2O (37:1:1) + DTT, 7 mL, 2.5 h	87.4 mg	ACN/H_2O (1:1) 1 mg/mL, 2 % DMSO, 2 days	1.03 mg	≥98%
2b	Fmoc Trp(Boc) TentaGel® S AC	0.05 mmol	Synthesizer	TFA/TIS/H_2O (37:1:1) + DTT, 7 mL, 2.5 h	14.4 mg	ACN/H_2O (1:1) 1 mg/mL, 2 % DMSO, 3 days	1.09 mg	≥98%
3a	Fmoc Trp(Boc) TentaGel® S RAM	0.1 mmol	Manually	TFA/TIS/H_2O (37:1:1) + DTT, 7 mL, 2.5 h	n.d.	--	3.24 mg	≥98%
3b	Fmoc Trp(Boc) TentaGel® S RAM	0.2 mmol	Manually	TFA/TIS/H_2O/Anisole (95:2:2:1), 3 mL, 3 h	n.d.	ACN/H_2O (1:1) 1 mg/mL, 2 % DMSO, 3 days	1.07 mg	≥95%
3c	Fmoc Trp(Boc) TentaGel® S RAM	0.05 mmol	Synthesizer	TFA/TIS/H_2O (37:1:1) + DTT, 7 mL, 2.5 h	n.d.	ACN/H_2O (1:1) 1 mg/mL, 3 % DMSO, 7 days	3.44 mg	≥98%
3d	Fmoc Trp(Boc) TentaGel® S RAM	0.2 mmol	Manually	TFA/TIS/H_2O/Anisole (95:2:2:1) + DTT, 7 mL, 4.5 h	45 mg	ACN/H_2O (2:1) 0.17 mg/mL, 1 % DMSO, 10 days	0.8 mg	≥91%[b]
3e	Fmoc Trp(Boc) TentaGel® S RAM	0.1 mmol	Manually	TFA/TIS/H_2O (37:1:1) + DTT, 5 mL, 2 h	44 mg	ACN/H_2O (1:1) 1 mg/mL, 2 % DMSO, 3 days	1.21 mg	≥98%
3f	Fmoc Ala TentaGel® S RAM resin	0.1 mmol	Manually	TFA/TIS/H_2O (37:1:1) + DTT, 5 mL, 2.5 h	63 mg	ACN/H_2O (1:1) 1 mg/mL, 2 % DMSO, 3 days	6 mg	≥98%
4a	Fmoc Trp(Boc) TentaGel® S RAM	0.1 mmol	Manually	TFA/TIS/H_2O (37:1:1) + DTT, 5 mL, 2.75 h	24 mg	ACN/H_2O (1:1) 1 mg/mL, 2 % DMSO, 2 days	0.77 mg	≥98%
4b	Fmoc Cys(Trt) TentaGel® S RAM resin	0.1 mmol	Manually	TFA/TIS/H_2O (37:1:1) + DTT, 7 mL, 2.5 h	55.9 mg	ACN/H_2O (1:1) 1 mg/mL, 2 % DMSO, 3 days	0.27 mg	≥92%
5a	Fmoc Trp(Boc) TentaGel® S RAM	0.1 mmol	Manually	TFA/H_2O/anisole/TE S (47:1:1:1), 3 h	32.6 mg	CuAAC	5.1 mg	≥98%
5b	Fmoc Trp(Boc) TentaGel® S RAM	0.05 mmol	Synthesizer	TFA/H_2O/anisole/TE S (47:1:1:1), 3 h	32 mg	CuAAC	6.42 mg	≥98%
5c	Fmoc Trp(Boc) TentaGel® S RAM	0.05 mmol	Synthesizer	TFA/H_2O/anisole/TE S (47:1:1:1), 3 h	35.5 mg	CuAAC	8.45 mg	≥98%
6a/6b/6c	Rink amide-MBHA resin	0.25 mmol	Manually	TFA/TIS/H_2O (95:2.5:2.5, v/v/v), 2 h	160 mg / 170 mg / 170 mg	RuAAC	0.67 mg / 1.72 mg / 1.4 mg	≥95% / ≥98% / ≥98%

[a] Determined by LC-MS. [b] This peptide was very poorly soluble, therefore the cyclization reaction had to be diluted and carried out with a higher ACN amount. This also prolonged the cyclization time significantly. In addition, many side products were formed, which could not be separated easily, which explains the lower purity of ≥ 91 %.

Expression of *Yersinia* CsrA-biot-His_6

The expression protocol of *Yersinia* CsrA-biot-His_6 has already been published by Christine Maurer *et al*.[1] Two plasmids were transformed into electro competent *E. coli* BL21 by performing a double transformation. On the one hand pET28a with pAKH172_biotag insert for overexpression of His- and biotin-tagged CsrA and on the other hand pBirAcm for overexpression of biotin ligase for *in vivo* biotinylation at the lysine residue of the biotintag. pET28a has a kanamycin resistance, pBirAcm a chloramphenicol resistance. The amino acid sequence for the CsrA-biot-His_6 construct is MLILTRRVGE TLMIGDEVTV TVLGVKGNQV RIGVNAPKEV SVHREEIYQR IQAEKSQPTT YLEGLNDIFE AQKIEWHELE HHHHHH. Biotin tag and His tag are underlined. The molecular weight of the CsrA-biot-His_6 monomer is 10.2 kDa.

4 L of LB medium, containing 50 µg/mL kanamycin and 17 µg/mL chloramphenicol, were inoculated with an overnight preculture. This main culture was grown at 37 °C and 180 rpm until an O.D. 600 of 0.6 was reached. Then, 10 mL 5 mM biotin (50 µM end concentration), 3 mL 3 M $MgCl_2$ (10 mM end concentration) and 1.19 mL 0.84 M IPTG (1 mM end concentration) per liter of culture was added. The culture was grown again at 37 °C, 180 rpm overnight. Cells were harvested by centrifugation (4 °C, 6200 rpm, 20 min). The pellets were resuspended in 4.5 mL/g wet cells lysis buffer (50 mM dipotassium hydrogen phosphate trihydrate, 300 mM sodium chloride, 10 mM imidazole, pH 8.0) containing cOmplete™ (EDTA-free protease inhibitor cocktail, Roche). Afterwards the cells were disrupted by one passage through a microfluidizer. After centrifugation of the homogenisate (4 °C, 19000 rpm, 1 h), the supernatant was sterile-filtered through 0.22 µm membrane filter. For purification an ÄKTAxpress™ device with a 1 mL HisTrap™ HP column was used, which was equilibrated with 20 mL lysis buffer (4 mL/min flowrate). The clear lysate was loaded on the column with 1 mL/min. This was followed by two washing steps, first 15 mL of high salt buffer (50 mM dipotassium hydrogen phosphate trihydrate, 1 M sodium chloride, 10 mM imidazole, pH 8.0), second 20 mL of binding buffer (50 mM dipotassium hydrogen phosphate trihydrate, 300 mM sodium chloride, 30 mM imidazole, pH 8.0). Next, a linear gradient from 0 to 70 % elution buffer (25 mM dipotassium hydrogen phosphate trihydrate, 150 mM sodium chloride, 125 mM imidazole, pH 8.0) within 56 min was chosen. For the final elution step, it was switched to 100 % elution buffer and the fractions were collected. The CsrA-containing fractions were concentrated via Vivaspin® 20 spin filters (3 kDa MWCO, Sartorius™), before the buffer was exchanged to storage buffer (50 mM dipotassium hydrogen phosphate trihydrate, 300 mM sodium chloride, ad DEPC-treated water (RNase-free), pH 8.0) with a PD10 desalting column. The concentration was determined by UV spectroscopy with NanoDrop™ (ε_{280} = 8480 $M^{-1}cm^{-1}$, monomer). If required, the united fractions were concentrated again with Vivaspin® 20 spin filters (3 kDa MWCO, Sartorius™) to adjust a monomer concentration of about 200 µM. Glycerol (10 % end concentration) was added to the protein and divided into aliquots, flash frozen in liquid nitrogen and stored at -80 °C. About 2 mg protein per liter of main culture were yielded.

Expression of *E. coli* CsrA-His_6

The amino acid sequence for the *E. coli* CsrA-His_6 construct is MLILTRRVGE TLMIGDEVTV TVLGVKGNQV RIGVNAPKEV SVHREEIYQR IQAEKSQQSSY HHHHH. The molecular weight of the CsrA-His_6 monomer is 7.68 kDa. The construct is present in pET21a+ with an ampicillin resistance. The expression protocol of *E. coli* CsrA-His_6 is based on Dubey *et al*..[2]

TB medium, containing 100 µg/mL ampicillin, were inoculated with an overnight preculture. This main culture was grown at 37 °C and 180 rpm until an O.D. 600 of 0.6 was reached. Then, 1.19 mL 0.84 M IPTG (1 mM end concentration) per liter of culture was added. The culture was grown again at 37 °C, 180 rpm overnight. Cells were harvested by centrifugation (4 °C, 6200 rpm, 20 min). The pellets were resuspended in 4.5 mL/g wet cells lysis buffer (50 mM potassium dihydrogen phosphate, 300 mM sodium chloride, 10 mM imidazole, 10 % glycerol, pH 8.0) containing cOmplete™ (EDTA-free protease inhibitor cocktail, Roche). Afterwards the cells were disrupted by ultra-sonification (current = 50 %, every 30 sec and 5 cycles, break between every 5 cycles). After centrifugation of the homogenisate (4 °C, 19000 rpm, 1 h), the supernatant was sterile-filtered through 0.22 µm membrane filter. For purification an ÄKTAxpress™ device with a 1 mL HisTrap™ HP column was used, which was equilibrated with 20 mL lysis buffer (4 mL/min flowrate). The clear lysate was loaded on the column with 1 mL/min. This was followed by three washing steps, first washing buffer 1 (50 mM potassium dihydrogen phosphate, 300 mM sodium chloride, 20 mM imidazole, 10 % glycerol, pH 8.0), second two times washing buffer 2 (50 mM potassium dihydrogen phosphate, 300 mM sodium chloride, 50 mM imidazole, 10 % glycerol, pH 8.0). The elution was done with elution buffer (50 mM potassium dihydrogen phosphate, 300 mM sodium chloride, 250 mM imidazole, 10 % glycerol, pH 8.0) and the fractions were collected. The CsrA-containing fractions were concentrated via Vivaspin® 20 spin filters (3 kDa MWCO, Sartorius™), before the buffer was exchanged to storage buffer (50 mM dipotassium hydrogen phosphate trihydrate, 300 mM sodium chloride, ad DEPC-treated water (RNase-free), pH 8.0) with a PD10 desalting column. The concentration was determined by UV spectroscopy with NanoDrop™ (ε_{280} = 2980 $M^{-1}cm^{-1}$, monomer). If required, the united fractions were concentrated again with Vivaspin® 20 spin filters (3 kDa MWCO, Sartorius™) to adjust a monomer concentration of about 200 µM. Glycerol (10 % end concentration) was added to the protein and divided into aliquots, flash frozen in liquid nitrogen and stored at -80 °C.

Phage Display

A more detailed description of oligomer design, cloning, library packaging and phage display can be found in Jakob *et al.* methods book chapter.[3]
In brief, an oligomer was designed, which encodes for a very small peptide library, which has the structure XCXXXCX. There are two fixed cysteine positions in it and X encodes for any amino acid except cysteine. The oligomer was synthesized by Ella Biotech GmbH. This library was cloned into the phagemid pHAL30[4] (Figure S1) where it displays $2.48 \cdot 10^6$ different peptides. The library was packed into M13K07 phages, which are able to present the peptides on their surface to a protein target.

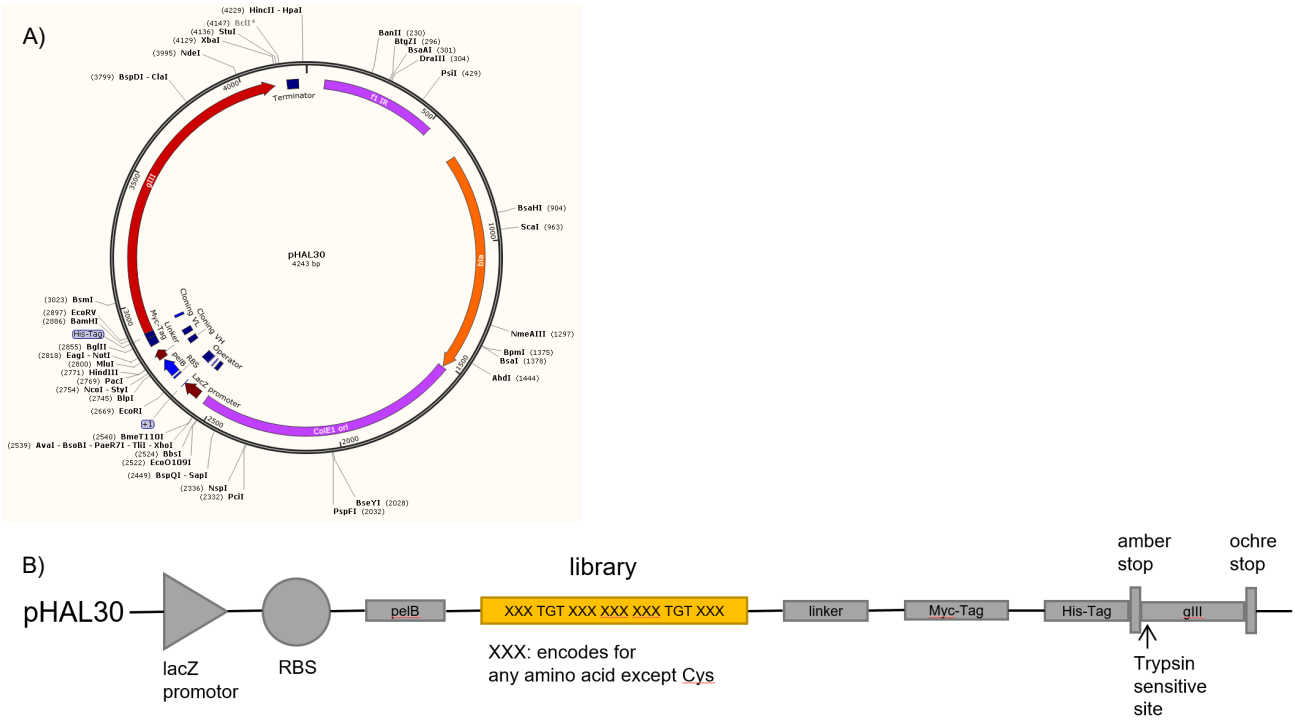

Figure S1. A) Vector map of pHAL30, B) Schematic drawing of pHAL30 with cloned peptide library. lacZ promoter: promoter of the bacterial lac operon; RBS: ribosome binding site; pelB: signal peptide sequence of bacterial pectate lyase *Erwinia caratovora*, mediating secretion into the periplasmic space; gIII: gene encoding for the phage protein III.[4]

Under oxidative conditions, the cysteines are forming a macrocycle over the disulfide bond. For selection of potential CsrA binders, phage display was established. For this process, CsrA_biot_His_6 was bound to a streptavidin-coated ELISA plate well. After blocking with BSA / milk powder, the pre-selected library, where BSA and streptavidin binders were excluded, was added. Unspecific binders were eliminated with a plate washer (Tecan Hydroflex), where PBS pH 7.4 containing Tween-20 was used. After the third panning round the clones were separated on agar plates. 32 clones were sequenced and checked for plausibility. Criteria for selection were an intact sequence with low tryptophane content and one glutamic acid, while carboxyl groups are beneficial for binding to positively charged surfaces on CsrA. We identified two interesting sequences containing a glutamate residue within the macrocycle. Peptide **1** (*Ac*-V-[CSELC]$_{cyclic}$-W-NH_2) could be successfully synthesized. Synthesis and macrocyclization of the alternative sequence *Ac*-H-[CQEVC]$_{cyclic}$-P-NH_2 yielded only dimerized product (data not shown). Nevertheless, this finding underscores the potential ionic interaction between the glutamate side chain and basic residues on the protein surface.
CsrA coating amount of the wells, detergent amount in PBS buffer as well as washing stringency with the plate washer were optimized. Before each panning round, the wells were coated with either 4 µg or 40 µg CsrA_biot_His_6. The better results were obtained with 4 µg. 0 µg CsrA was used as negative control. Before phage elution with trypsin, PBS containing different amounts of Tween-20 (0.05 %, 0.1 % or 0.2 %) was tried to rinse the wells with the plate washer. Since the variation effect was not significant, 0.1 % Tween-20 was chosen as the detergent amount. The number of washing cycles, however, had a significant impact on the results. Tested were 2/4/6, 4/8/10 and 10/10/10 washing cycles. The first number corresponds to the number of washing cycles after the first panning round, the second after the second and the third after the third round. The more washing rounds were used, the more sequences containing frame shifts or predominantly hydrophobic amino acids (i.e., more than one tryptophan residues) were found. This was the case for the 4/8/10 and 10/10/10 variant. If, on the other hand, fewer washing cycles were used (2/4/6), a large proportion of pHAL30 origin empty vector containing no peptide encoding sequence was found, but also a few desired peptide sequences as potential binders. Peptide **1** was one of those useful sequences.

Fluorescence Polarization Assay

The fluorescence polarization assay has been established by Maurer et al.[1] Fluorescence polarization was recorded using a CLARIOstar microplate reader (BMG LABTECH, Ortenberg, Germany) with an extinction filter at 485 nm and emission filter at 520 nm. Gain adjustment was performed before starting each measurement to achieve maximum sensitivity. The FP values were measured in millipolarization units (mP). The assay was performed two times in duplicates and the IC_{50} value was calculated using sigmoidal logistic fit in Origin. Fluorescein-labeled RNA (for *Yersinia* CsrA: 5'-UUCACGGAGAA[flc]; for *E. coli* CsrA: 5'-AGACAAGGAUGU[flc]) was obtained from Sigma Aldrich in HPLC purity. The results of the dose-dependent measurement are shown in Figure S3 and S4.

A 20 mM peptide in DMSO stock solution was diluted with assay buffer (10 mM HEPES, 150 mM NaCl, 0.005 % (v/v) Tween-20, ad DEPC-treated H_2O (RNase free water), pH 7.4) in a way that 3 mM peptide in 15 % DMSO was achieved (21 µL 20 mM peptide in DMSO + 119 µL assay buffer). Afterwards, a 1:2 dilution series containing 12 steps was utilized by diluting 70 µL of assay buffer containing 15 % DMSO with 70 µL of the peptide in assay buffer with 15 % DMSO from this solution, starting from 3 mM ended in 1,46 µM. Using a 12-channel pipette, 10 µL of each concentration were transferred to a 384 well microtiter plate (black, flat bottom, Greiner Bio-One) in two replicates and another 10 µL of 1.2 µM (2.4 µM for *E. coli* CsrA) of the corresponding CsrA-biot-His_6 protein (in assay buffer) were added to each well and quickly centrifuged to be preincubated for 1 h on a Duomax 1030 shaker under light exclusion. 10 µM fluorescein-labelled RNA (RNAflc) was diluted with assay buffer to a concentration of 45 nM obtaining an end concentration of 15 nM in the assay. After short centrifugation the plate was incubated for 1.5 h on the shaker under light exclusion. The final concentrations in the assay were 400 nM (800 nM for *E. coli* CsrA) CsrA-biot-His_6 (monomer concentration), 5 % DMSO, 15 nM RNAflc and 1000 µM to 0.49 µM peptide.
Furthermore, a high control was prepared to check for the homogeneity of fluorescence for the complex between protein and RNAflc, a low control to verify the homogeneity of fluorescence for the free RNAflc as well as a blank to exclude any deviation due to the matrix of the assay. For the high control components were 10 µL of 15 % DMSO in assay buffer, 10 µL of protein and 10 µL of RNAflc, for the low control corresponding 10 µL of 15 % DMSO in assay buffer, 10 µL of assay buffer and 10 µL of RNAflc and the blank consisted of 10 µL of 15 % DMSO in assay buffer and two times 10 µL of assay buffer. These three controls were measured in 24-lets.
Moreover, a fluorescence control was performed for the peptides measured to check for the possibility of fluorescence quenching. Therefore, the first component was 10 µL of the dilution series of the corresponding peptide, second component was 10 µL of assay buffer and third component was 10 µL of RNAflc.
Thereby, fluorescence intensity was calculated by determination of the sum of blank corrected based on raw data parallel and perpendicular for the highest concentration on the one hand and for the lowest concentration on the other hand. Afterwards, the average of these two values was determined and the deviation from fluorescence intensity to the average value should be under 20 % for no fluorescence quenching. This was the reason why the 1000 µM and 500 µM value was not included in the assay for **3d** and **5a**.

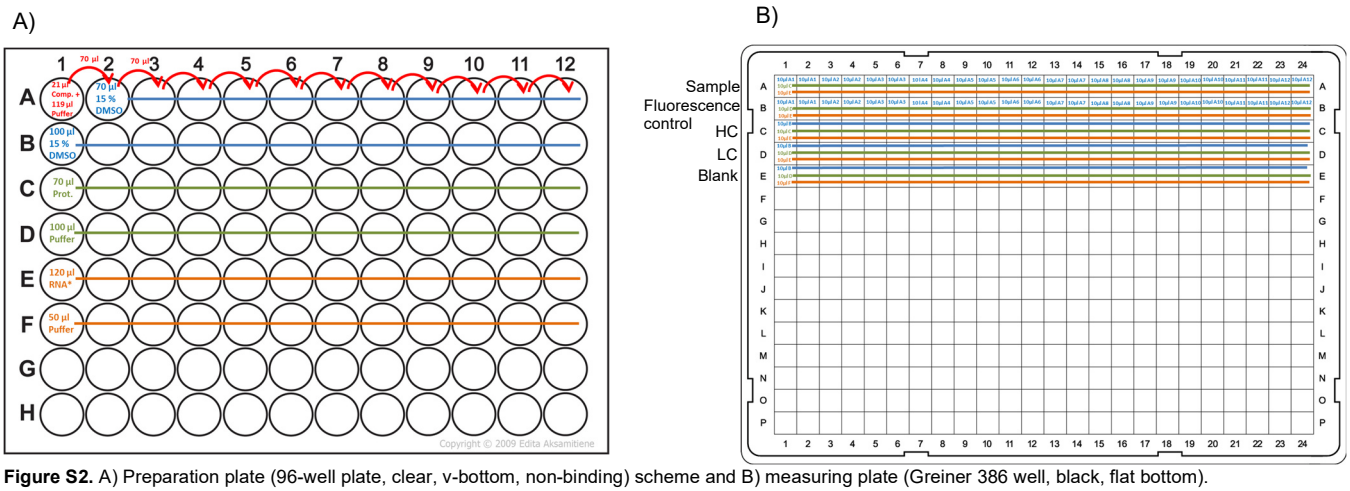

Figure S2. A) Preparation plate (96-well plate, clear, v-bottom, non-binding) scheme and B) measuring plate (Greiner 386 well, black, flat bottom). Transferring in duplicates with 12-channel pipette from preparation plate to measuring plate

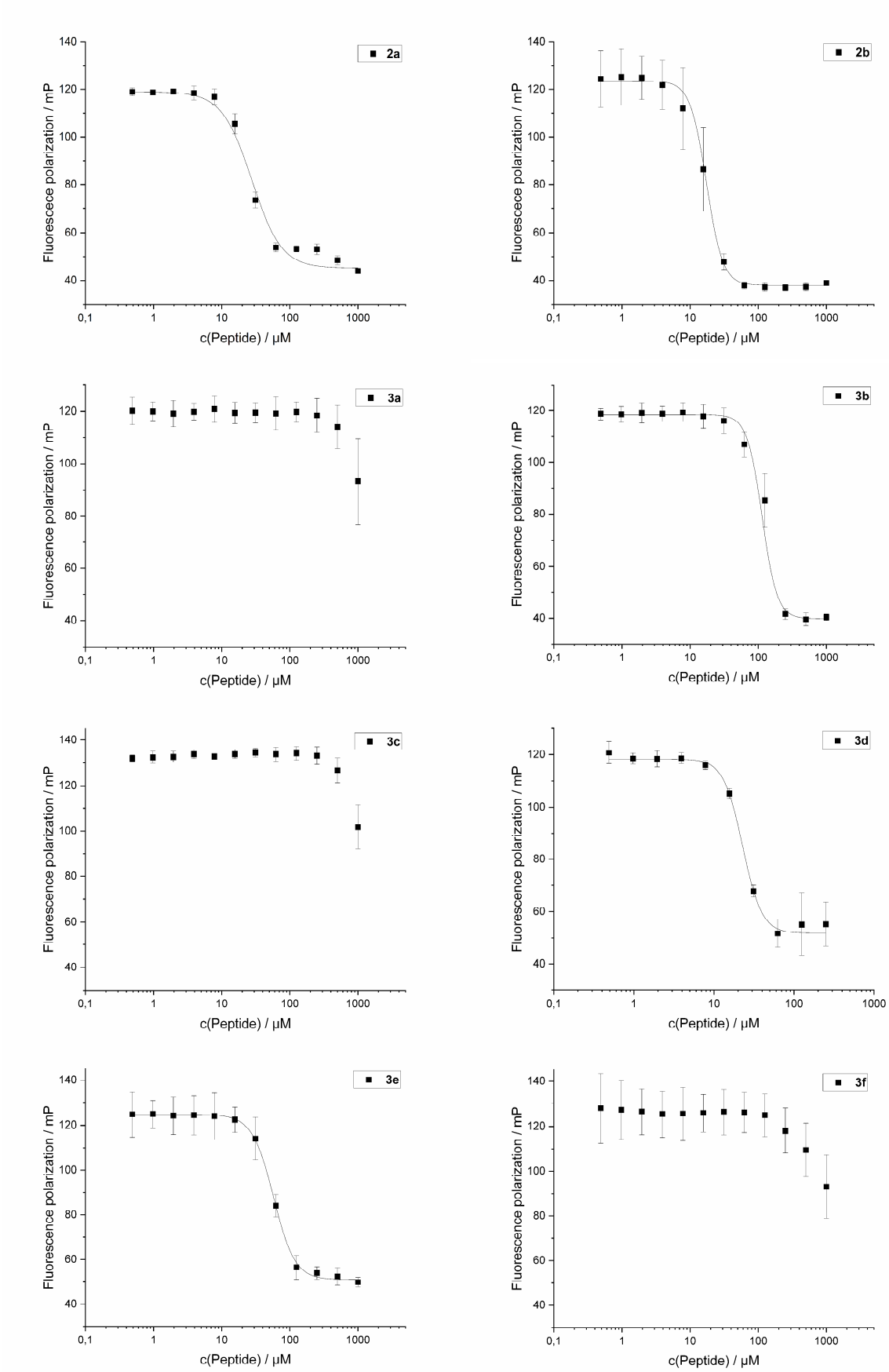

Figure S3 (part 1). Results of the dose-dependent fluorescence polarization assay with competition inhibition curves used to determine the half maximal inhibitory concentration (IC_{50}) for **peptides 2a-3f** with *Yersinia* CsrA_biot_His_6**.** The assay has been performed two times in duplicates.

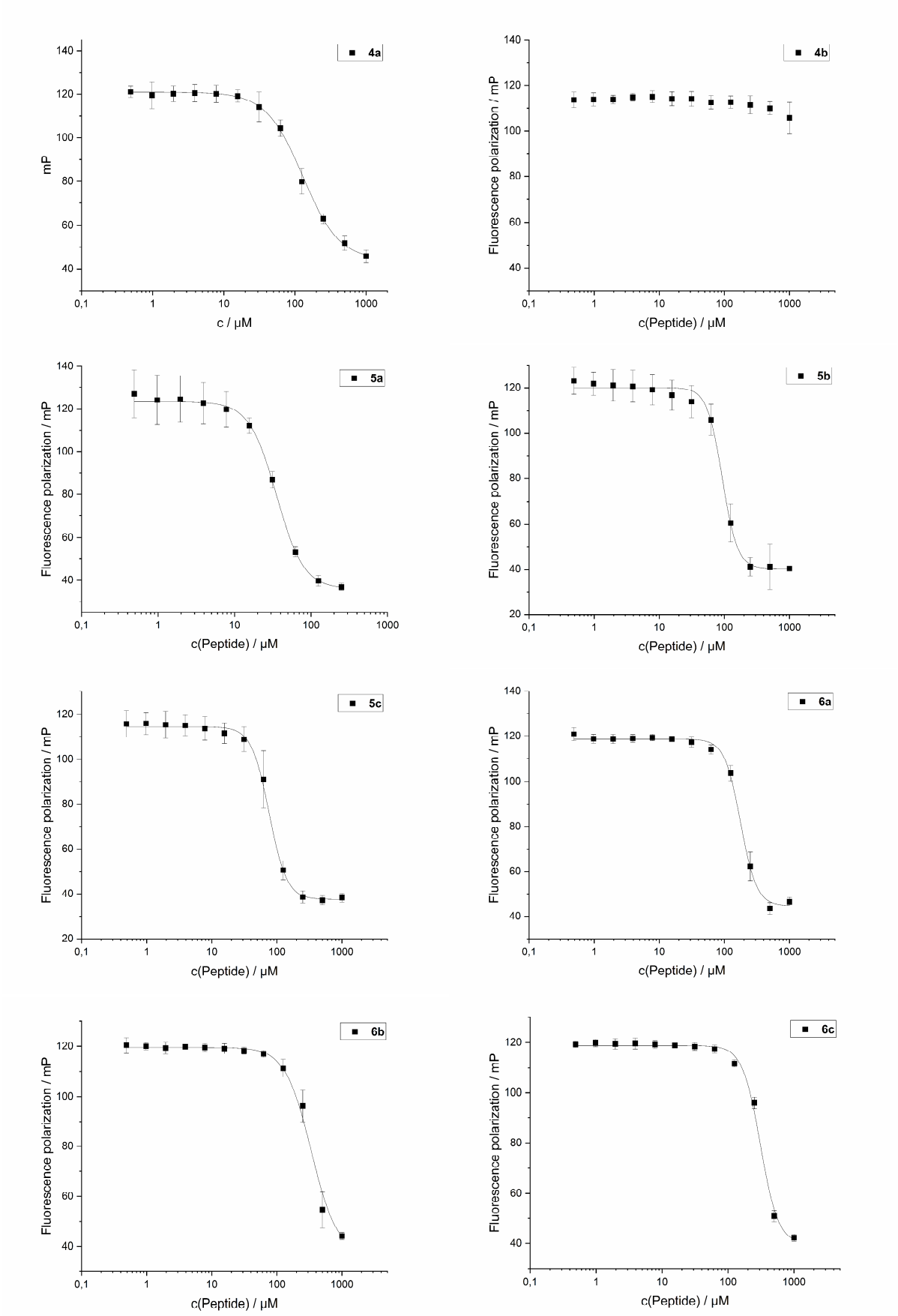

Figure S3 (part 2). Results of the dose-dependent fluorescence polarization assay with competition inhibition curves used to determine the half maximal inhibitory concentration (IC_{50}) for **peptides 4a-6c** with *Yersinia* CsrA_biot_His_6**.** The assay has been performed two times in duplicates.

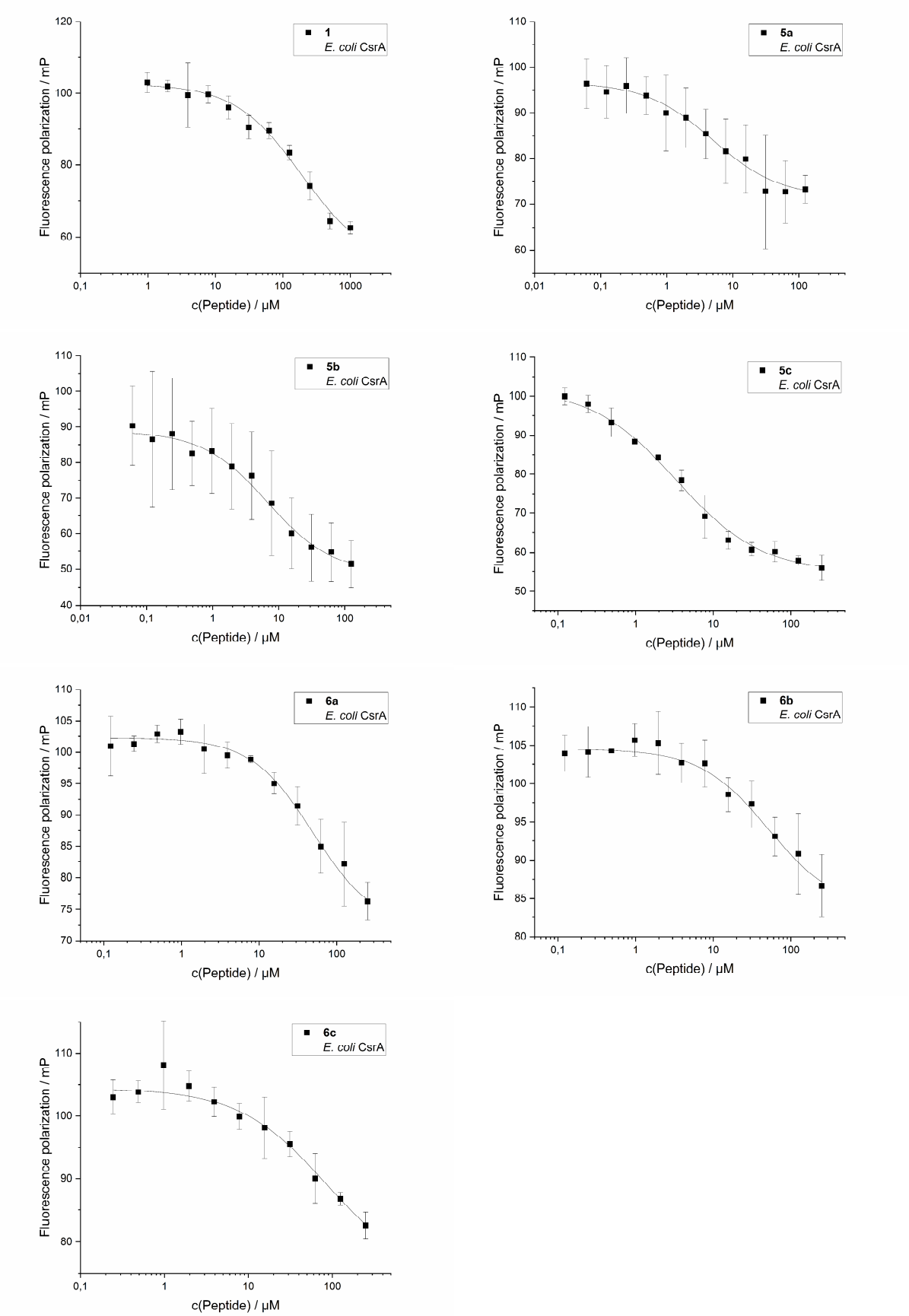

Figure S4. Result of the dose-dependent fluorescence polarization assay with competition inhibition curve used to determine the half maximal inhibitory concentration for peptide **5a** and **5b** with *E. coli* CsrA_His_6 as target. The assay has been performed two times in duplicates.

Microscale Thermophoresis Assay (MST)

The MST assay was performed according to the protocol of the Monolith NT™ His-Tag labelling Kit RED-tris-NTA and was used for Peptide **1** only. The *Yersinia* CsrA-biot-His_6 monomer concentration was adjusted with assay buffer (10 mM HEPES, 150 mM NaCl, 0.005 % (v/v) Tween-20, ad DEPC-treated H_2O (RNase free water), pH 7.4) to 200 nM in a volume of 100 µL, mixed with 100 µL 100 nM dye (Nano RED) and incubated for 30 min in the dark at room temperature. The sample was centrifuged for 10 min at 4 °C and 15000 g. This was the ready-labelled protein. A 20 mM peptide DMSO stock solution was diluted with assay buffer to 2 mM, that the highest end concentration in the assay was 1000 µM with 5 % DMSO. 20 µL of the 2 mM peptide was transferred into a first PCR tube and 10 µL of assay buffer containing 10 % DMSO was transferred into each next PCR tube 2-16. For the serial dilution series of the peptide, 10 µL of the ligand from tube 1 were transferred to tube 2 with a pipette and mixed by pipetting up-and-down several times. The procedure was repeated for tube 3-16 and 10 µL from tube 16 were discarded. Finally, 10 µL of the labelled protein were added to each PCR tube, mixed with a pipette and incubated in the dark for 45 min. All 16 dilutions were loaded into Monolith NT™ Standard Capillaries and measured in the Monolith NT.115™ device with 60 % excitation power and 40 % MST power. The protein concentration in the assay was 50 nM. The assay was performed three times in duplicates and the K_d value of 10.5 ± 1.4 µM was calculated using sigmoidal logistic fit in Origin.

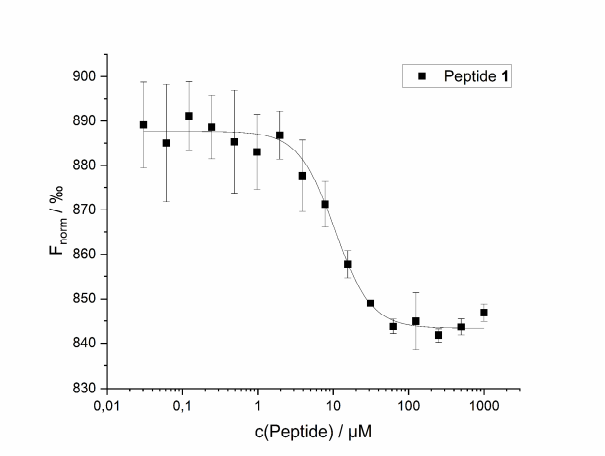

Figure S5. Dose-dependent MST interaction curve of peptide **1** with *Yersinia* CsrA_biot_His_6 used to determine the dissociation constant (K_d).

Calculation of the Error Bars in Fluorescence Polarization and MST Assay

Error bars are calculated with TINV function of Microsoft Excel, which returns the two-tailed inverse of the Student's t-distribution multiplied with the standard deviation of the mean of the measurements:

TINV(probability, deg_freedom) · (STDEV of the mean)

The argument probability is set to 95 % and the degree of freedom to 4.

NMR analysis and structure calculations

NMR analysis of peptide **1** was performed with a 2 mM solution in 50 % H_2O/50 % d3-acetonitrile (298 K, pH 3.4) on a Bruker Avance III 600 MHz spectrometer. 2D Spectra included TOCSY, ROESY, and natural abundance heteronuclear correlation spectroscopy (^{15}N- and ^{13}C-HSQC). TOCSY spectra were also recorded at variable temperatures (283 – 303 K) to determine amide proton temperature coefficients. Spectra were referenced to residual acetonitrile at 1.94 ppm. All spectra were processed using TopSpin v3.6 and assigned using CcpNMR Analysis.
Preliminary structures were calculated in CYANA based upon ROESY-derived distance restraints. Several dihedral angle restraints were also added as predicted by TALOS-N[5] along with a single hydrogen bond pair after consideration of preliminary structures and amide proton temperature coefficients. A final ensemble of 20 structures were generated within CNS[6] using torsion angle dynamics and refinement and energy minimization in explicit water solvent. MolProbity[7] was used to assess stereochemical quality (summarised in Table S5).

Table S5. Statistical analysis of peptide **1** structures[a]

Experimental restraints	
total no. distance restraints	45
intraresidue	22
sequential	23
medium range, *i-j*<5	2
hydrogen bond restraints	2
dihedral angle restraints	
phi	5
psi	1
Deviations from idealized geometry	
bond lengths (Å)	0.012 ± 0.001
bond angles (deg)	1.161 ± 0.107
impropers (deg)	1.14 ± 0.15
NOE (Å)	0.033 ± 0.005
cDih (deg)	0.032 ± 0.104
Mean energies (kcal/mol)	
overall	-194 ± 13
bonds	3.9 ± 0.4
angles	9.0 ± 1.8
improper	3.3 ± 0.7
van Der Waals	-14.5 ± 2.2
NOE	0.05 ± 0.02
cDih	0.01 ±0.03
electrostatic	-977 ± 33
Violations	
NOE violations exceeding 0.2 Å	0
Dihedral violations exceeding 2.0 Å	0
Rms deviation from mean structure, Å	
backbone atoms	0.79 ± 0.37
all heavy atoms	1.81 ± 0.70
Stereochemical quality[b]	
Residues in most favoured Ramachandran region, %	80.0 ± 11.0
Ramachandran outliers, %	0 ± 0
Unfavourable sidechain rotamers, %	0.0 ± 0.0
Clashscore, all atoms	0.0 ± 0.0
Overall MolProbity score	1.2 ± 0.3

[a] All statistics are given as mean ± SD.
[b] According to MolProbity[7]

In silico Investigations

General. All *in silico* experiments were performed with Molecular Operating Environment (MOE) by Chemical Computing Group (CCG) release 2020.09 employing the Amber10:EHT force field.[8]

Homology Model Building. Homology model of *Yersinia pseudotuberculosis* CsrA in complex with RNA was built using the first entry of NMR-solution structure 2MFH from *Pseudomonas fluorescens* in complex with RNA-oligo ucaggacau.[9] The template structure 2MFH was chosen from the available structures in the PDB based on the following requirements: resolved *C*-terminal residues and complex with short RNA oligo.
The sequence of the template structure (*P. fluorescens*, Sec1) and the target sequence (*Y. pseudotuberculosis*, Sec2) share an identity of 71% and homology of 89% as shown by following blast result:

Score	Expect	Method	Identities	Positives	Gaps
91.7 bits(226)	3e-32	Compositional matrix adjust.	41/58(71%)	52/58(89%)	0/58(0%)

```
Sec2        MLILTRRVGETLMIGDEVTVTVLGVKGNQVRIGVNAPKEVSVHREEIYQRIQAEKSQP  58
            MLILTR+VGE++ IGD++T+T+LGV G QVRIG+NAPK+V+VHREEIYQRIQA  + P
Sec1        MLILTRKVGESINIGDDITITILGVSGQQVRIGINAPKDVAVHREEIYQRIQAGLTAP  58
```

The built-in “homology model” function of MOE was used with standard parameters, while RNA atoms were used as environment to successfully yield a model in complex with RNA.

Docking. Docking was performed using the built-in “Docking” function of MOE. NMR structures of peptide **1** (all 20 entries of PDB ID 7M7X, BMRB ID 30895) were used as “ligand” structures and the above-mentioned homology model as “receptor”. The docking site was defined by involving protein residues in 4.5 Å proximity to the RNA atoms as well as the *C*-terminal residues of one of the two identical RNA-interaction sites. The resulting selection was as follows:

```
>CsrAYP_1|Chain A|Translational repressor|Y.pseudotuberculosis HomologyModel
MLILTRR--E---------------------------------------------
>CsrAYP_1|Chain B|Translational repressor|Y.pseudotuberculosis HomologyModel
--------------------T-L--K--Q-R----APK-VSVHR-EIYQRIQAEKSQPT
```

Placement algorithm was “Triangle Matcher” with “London dG” as Scoring function generating 10 initial poses for every peptide **1** conformer (entry). Refinement method was “Induced Fit” with “GBVI/WSA dG” as Scoring function and 5 keeper poses.
The resulting 100 docking poses (5 poses × 20 entries) were sorted according to the refinement/binding score. The 10 best-scoring poses were sorted according to the “rmsd_refine” parameter indicating binding hypothesis with minimal deviation from the initial (experimental) solution geometry. By this means, we selected the optimal pose scoring in number 8 of 100 regarding refinement/binding score and 3 of 100 regarding the “rmsd_refine” parameter.

Analysis and Visualisation. The pose derived by the docking procedure described above was analysed using the “Ligand Interactions” function of MOE for generating a 2D depiction of the interaction profile (see Figure 3c from the main text). Graphic processing for manuscript figures was done using YASARA structure (YASARA Biosciences GmbH)[139] and POV-Ray 3.7.0.

Analytical LC-MS

For analytical LC-MS, all samples were solved in Methanol. The measurements of compounds **1**-**5c** and **6b**, **6c** were done with a DIONEX UltiMate 3000 UHPLC$^+$ focused (Thermo Scientific), containing RS Pump, RS Autosampler, Diode Array Detector, Column Compartment (heated to 40 °C) and ISQ EC Mass Spectrometer. We used a HYPERSIL GOLD 1.9UM 100 x 2.1MM COLUMN (Thermo Scientific). The gradient was 5-50 % solvent B over 4.2 min (solvent A: H_2O containing 0.05 % formic acid, solvent B: ACN containing 0.05 % formic acid followed by 50 % solvent B for 0.8 min all with a flowrate of 0.6 mL/min.
The graphs show the HPLC chromatogram measured at 220 nm and the total ion count in the mass track. The chromatogram was used to determine the purity of the respective peptide. The mass spectrum from the main peak of the mass track is also shown.

Compounds **6b** and **6c** were additionally analysed and **6a** was only analysed on a Shimadzu Prominence LC-MS system using an Agilent Zorbax 300SB-C18 column (5 µm, 150 x 2.1 mm) with a flow rate of 0.6 mL/min. The samples were analysed using a linear gradient of 0-60 % solvent B in 30 min (Solvent A: H_2O with 0.05 % formic acid; Solvent B: 95 % acetonitrile with 0.05 % formic acid) and the elutants were monitored by absorbance at 214 nm and 280 nm and low resolution ESI-MS.

Ac-V-[CSELC]$_{cyclic}$-W-*NH*$_2$ (**1**)

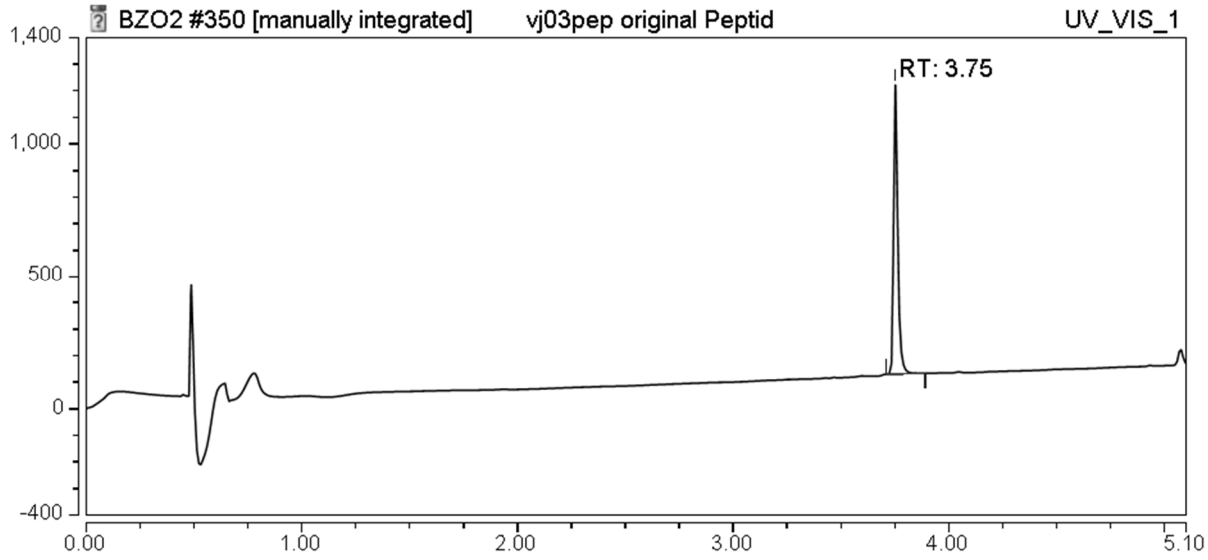

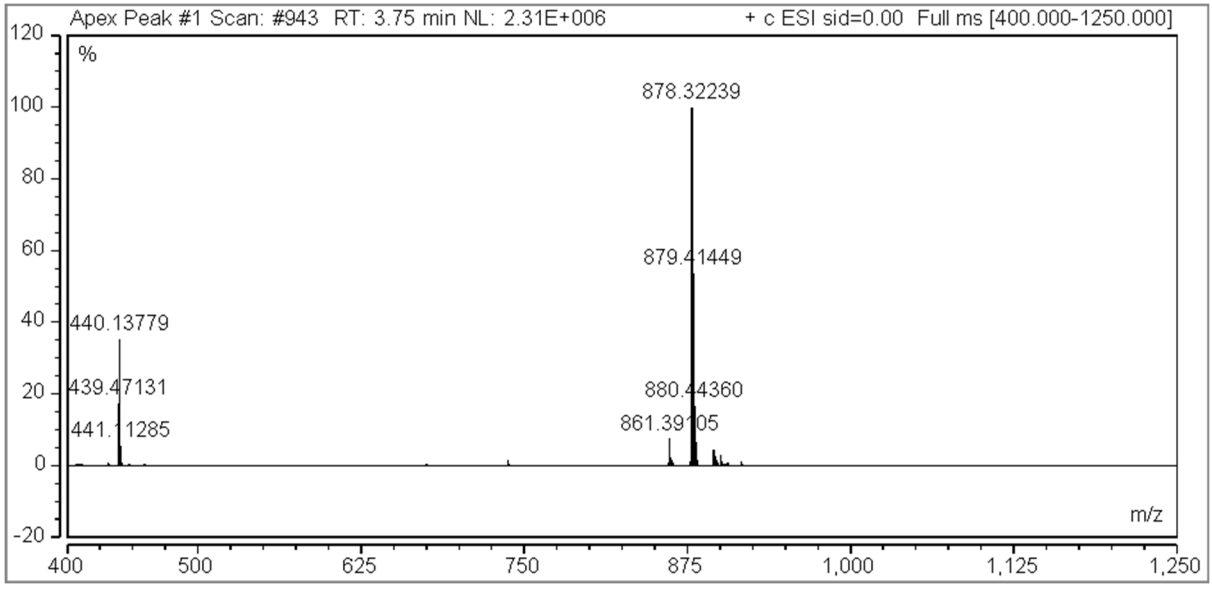

H-V-[CSELC]$_{cyclic}$-W-*NH*$_2$ (**2a**)

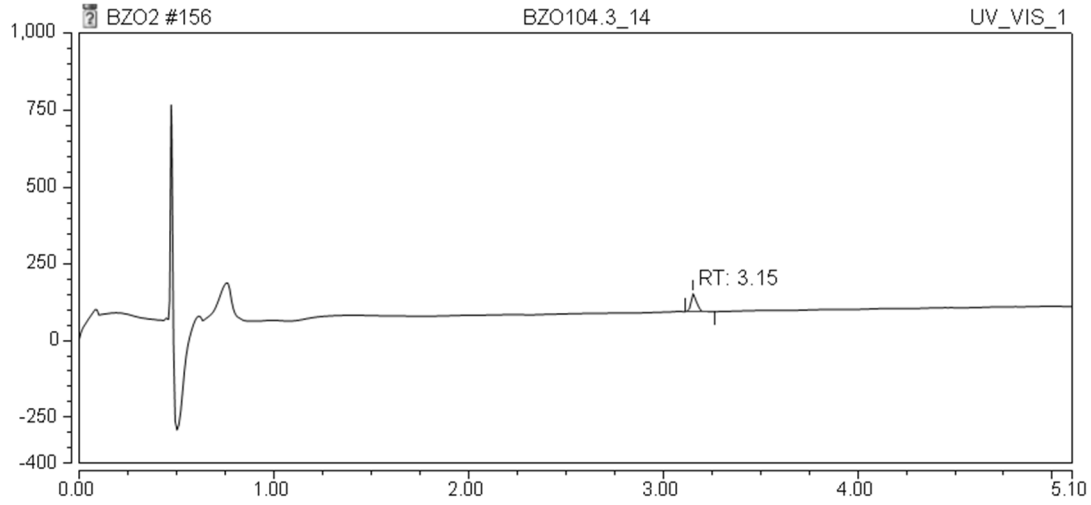

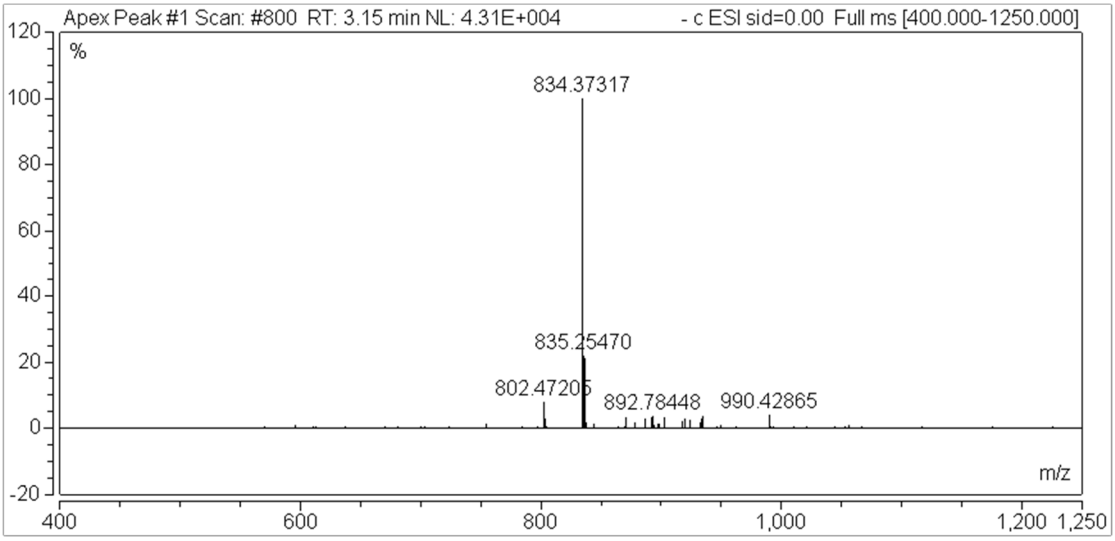

Ac-V-[CSELC]$_{cyclic}$-W-***OH*** (**2b**)

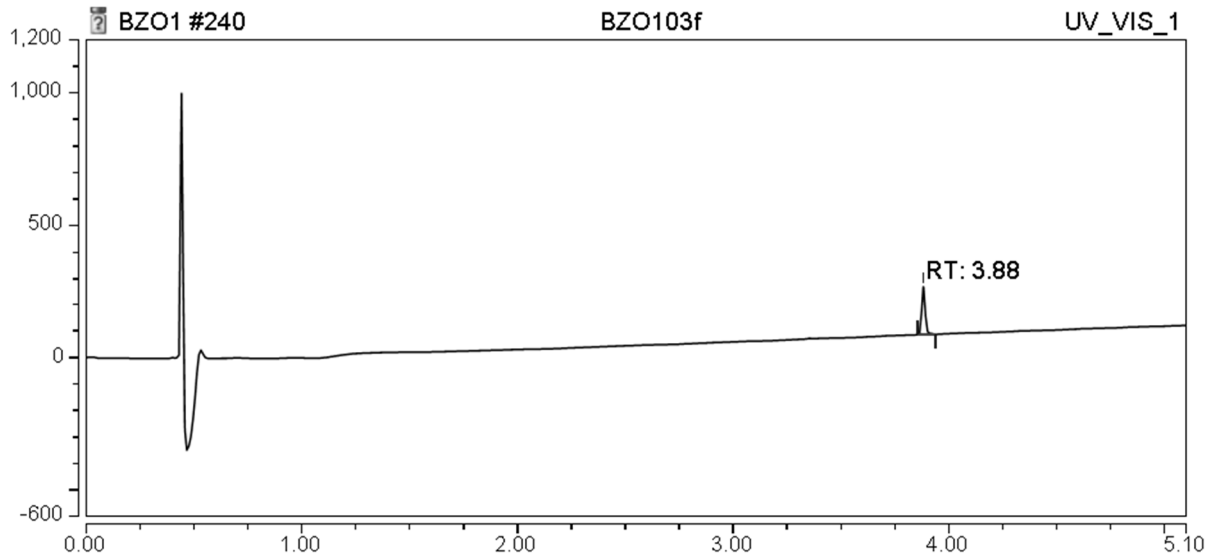

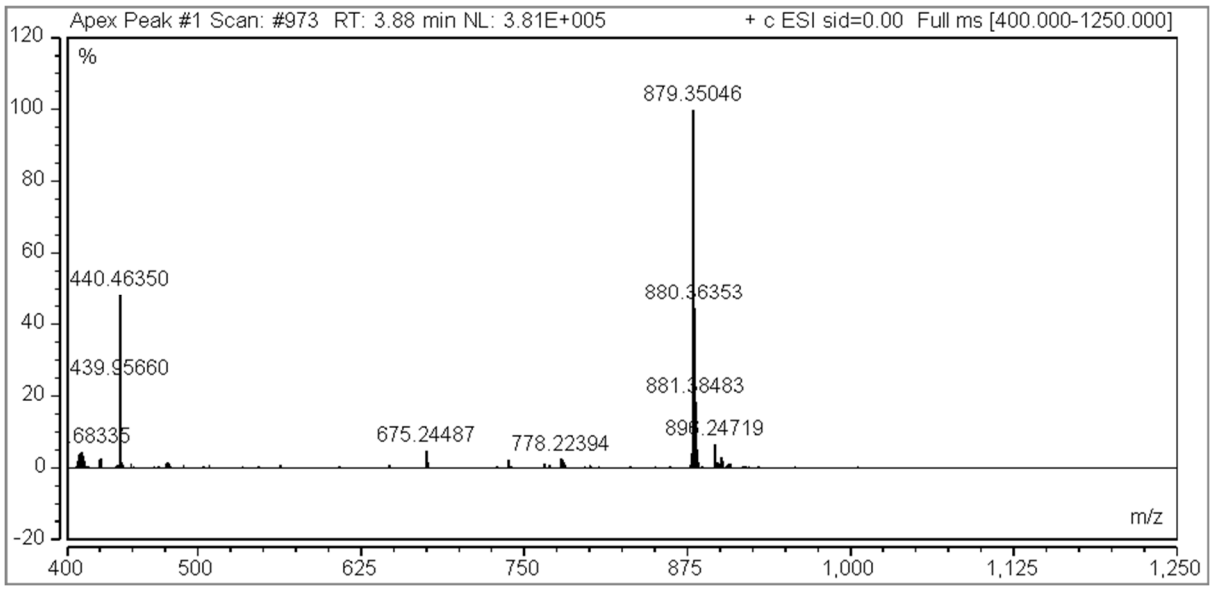

Ac-V**A**SEL**A**W-*NH*$_2$ (**3a**)

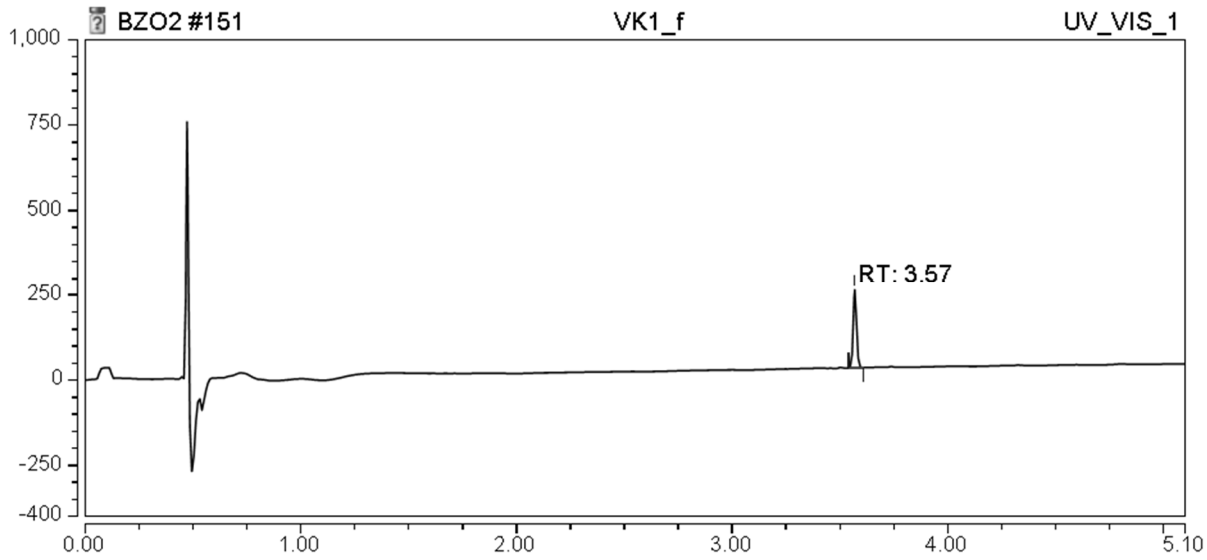

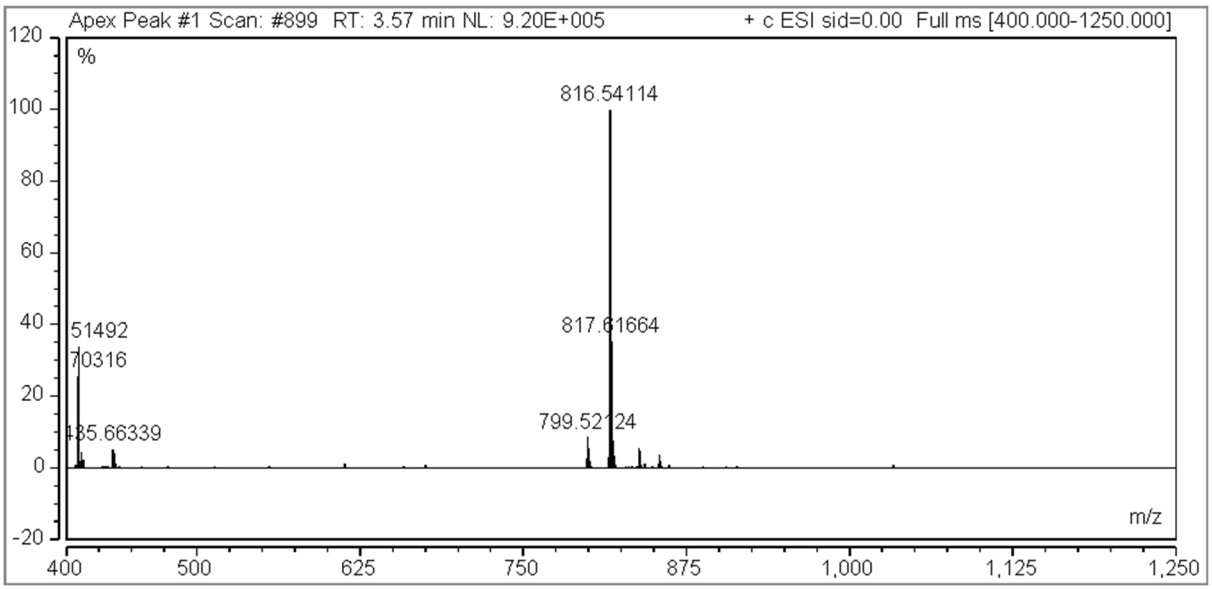

Ac-**A**-[CSELC]$_{cyclic}$-W-NH_2 (**3b**)

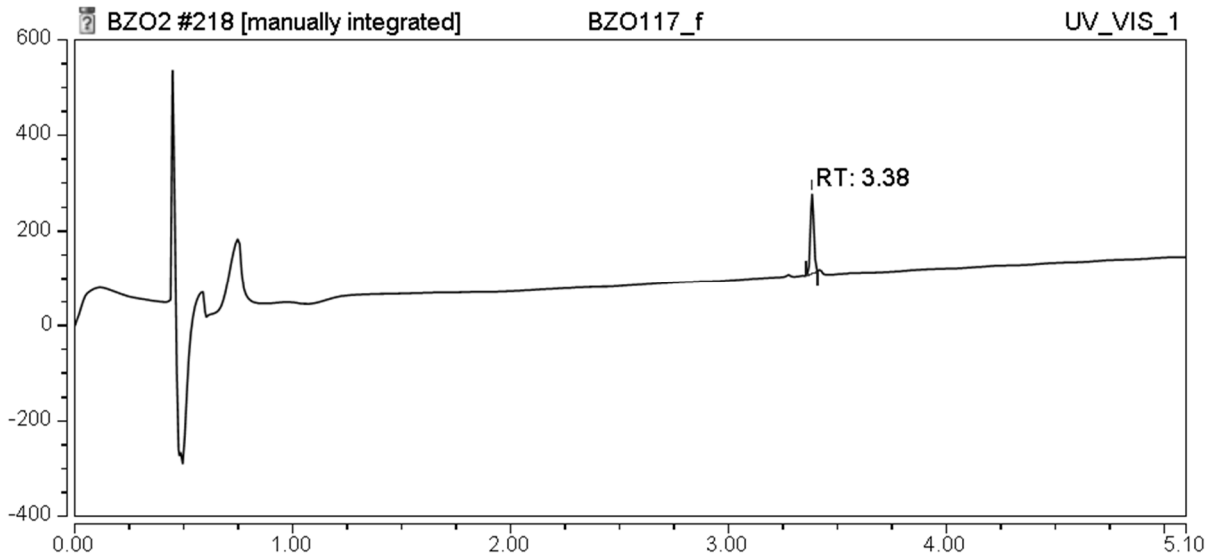

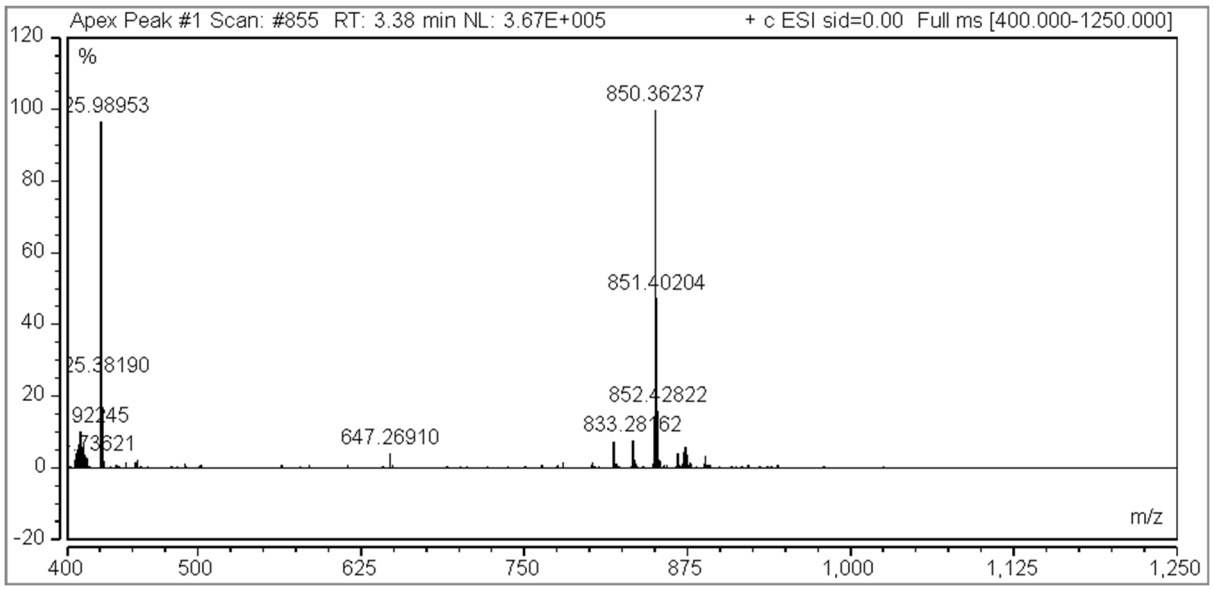

Ac-V-[C**A**ELC]$_{cyclic}$-W-NH_2 (**3c**)

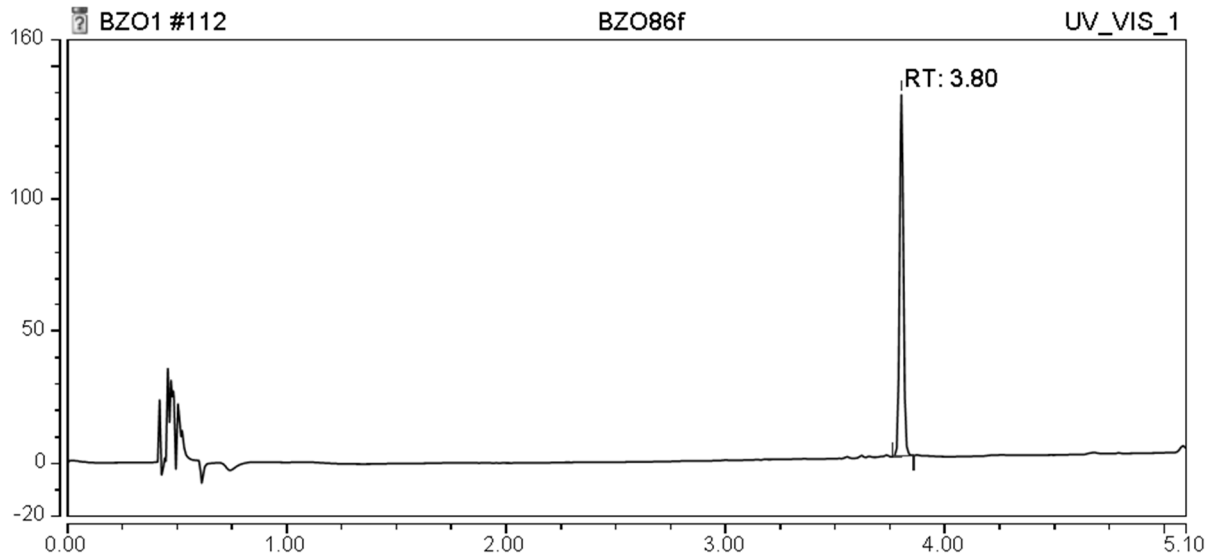

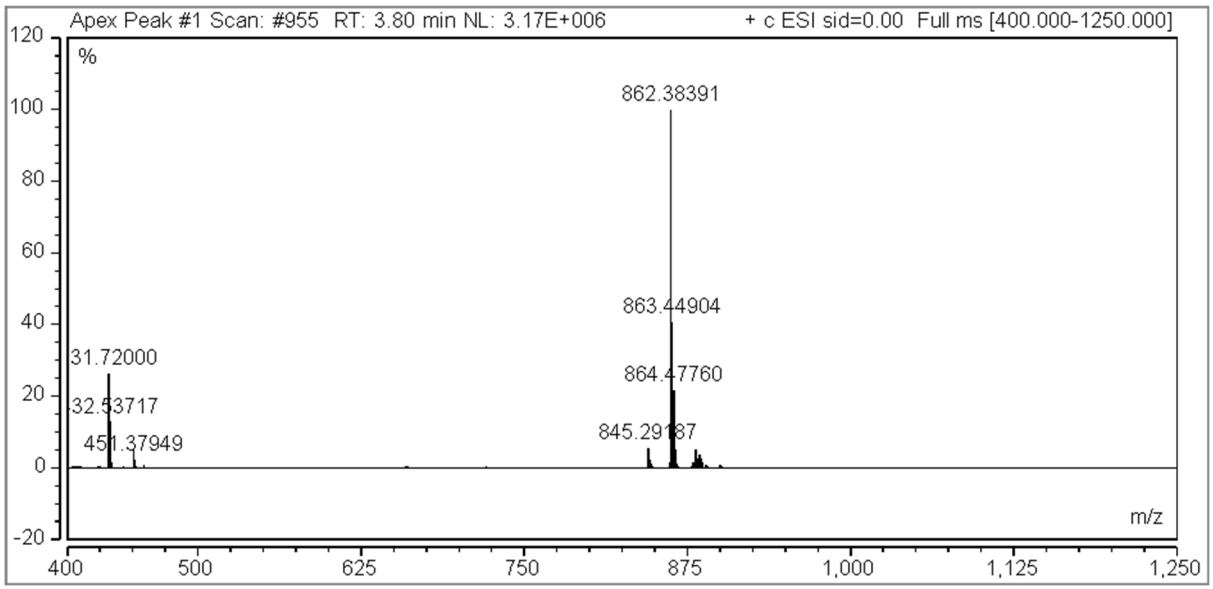

Ac-V-[CS**A**LC]$_{cyclic}$-W-NH_2 (**3d**)

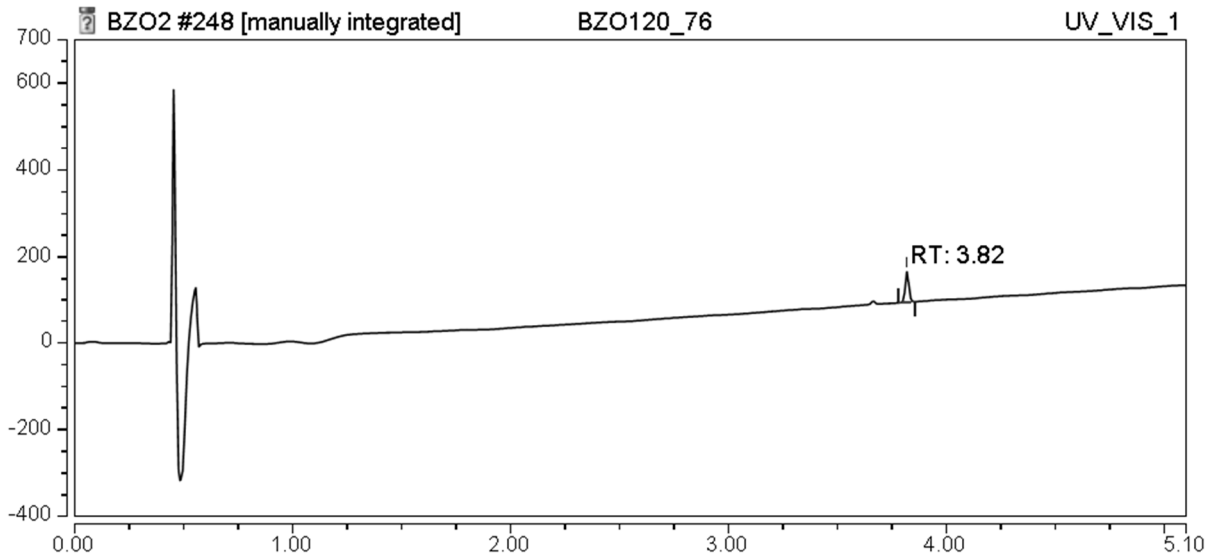

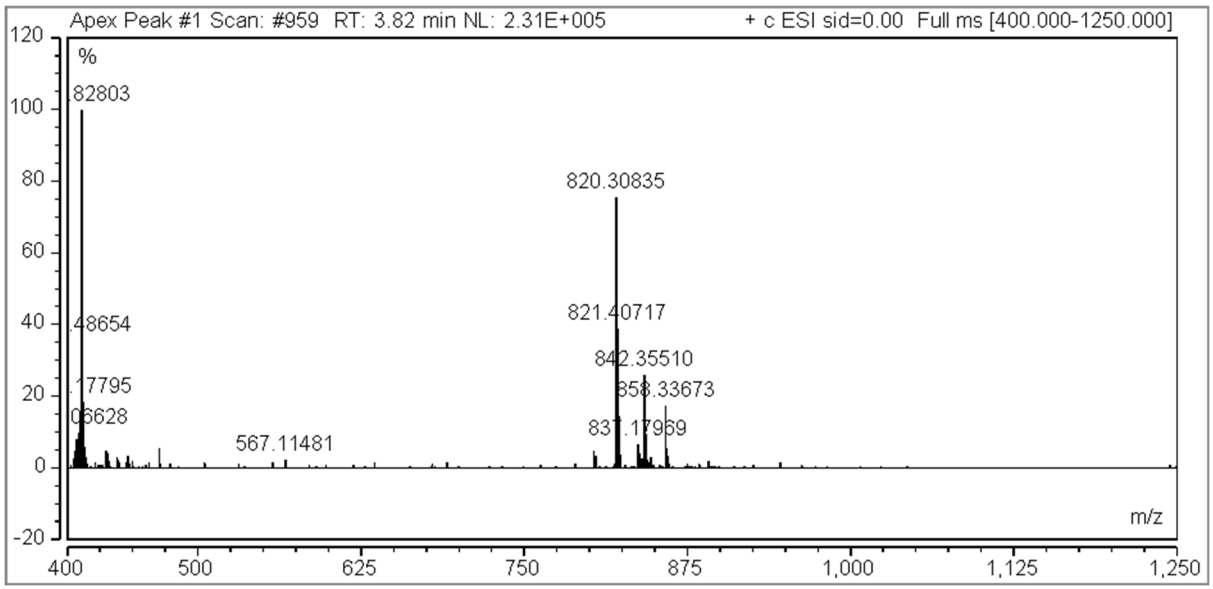

Ac-V-[CSE**A**C]$_{cyclic}$-W-NH_2 (**3e**)

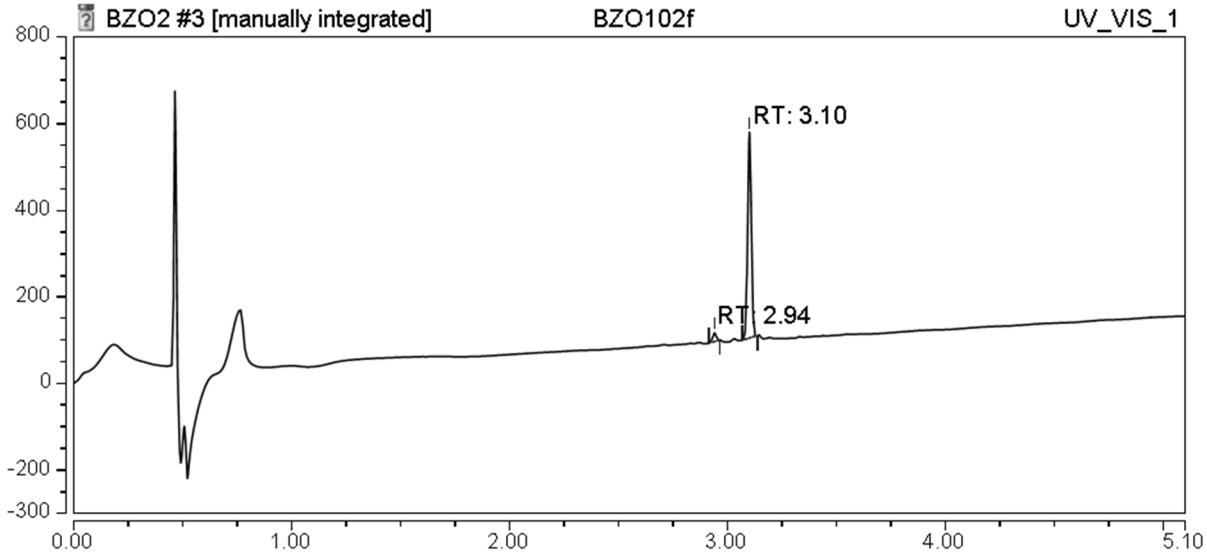

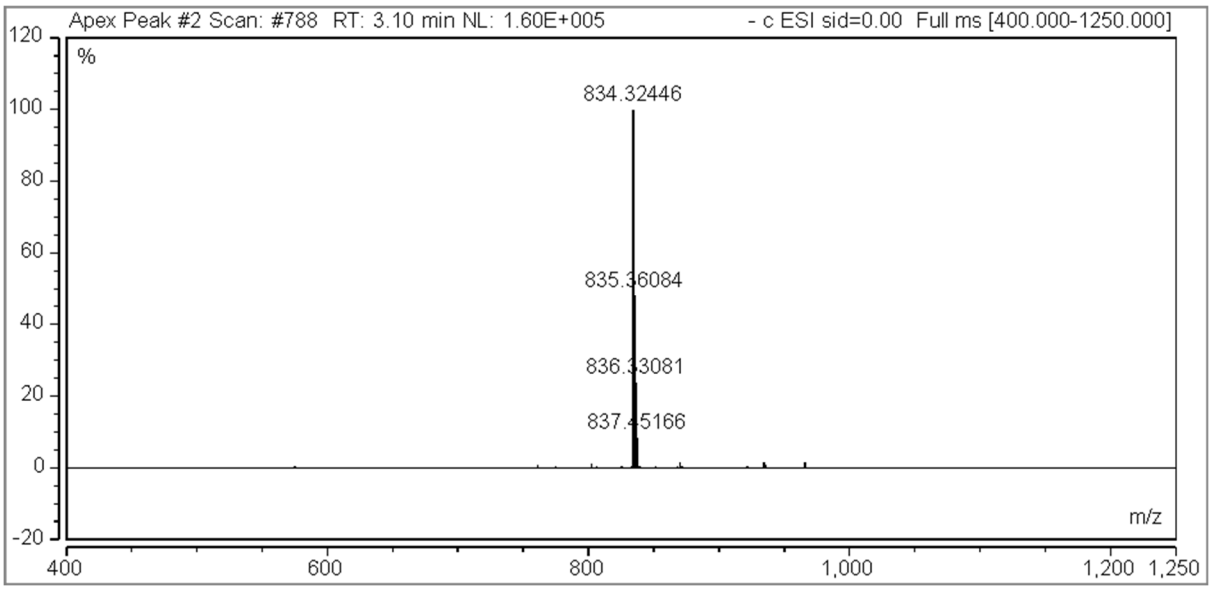

Ac-V-[CSELC]$_{cyclic}$-**A**-NH_2 (**3f**)

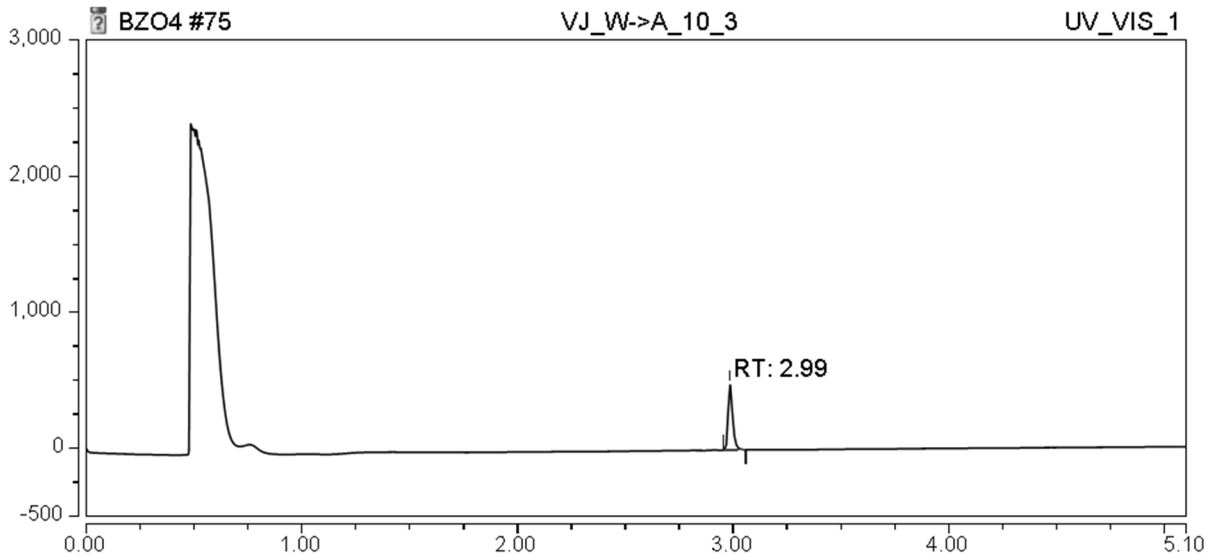

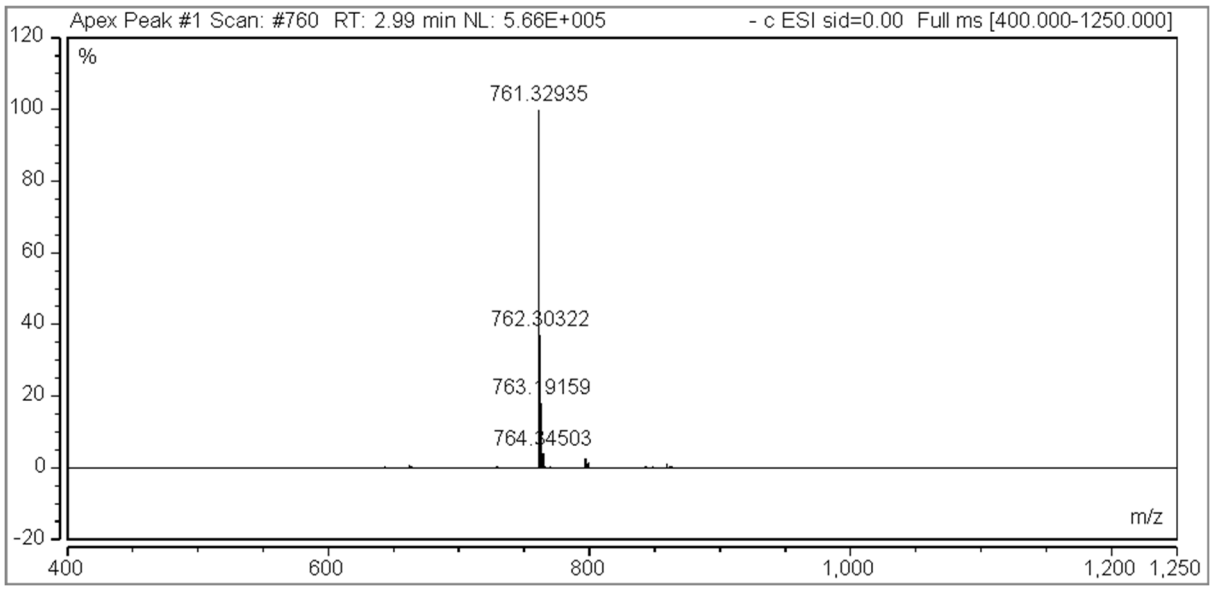

Ac- **–** -[CSELC]$_{cyclic}$-W-NH_2 (**4a**)

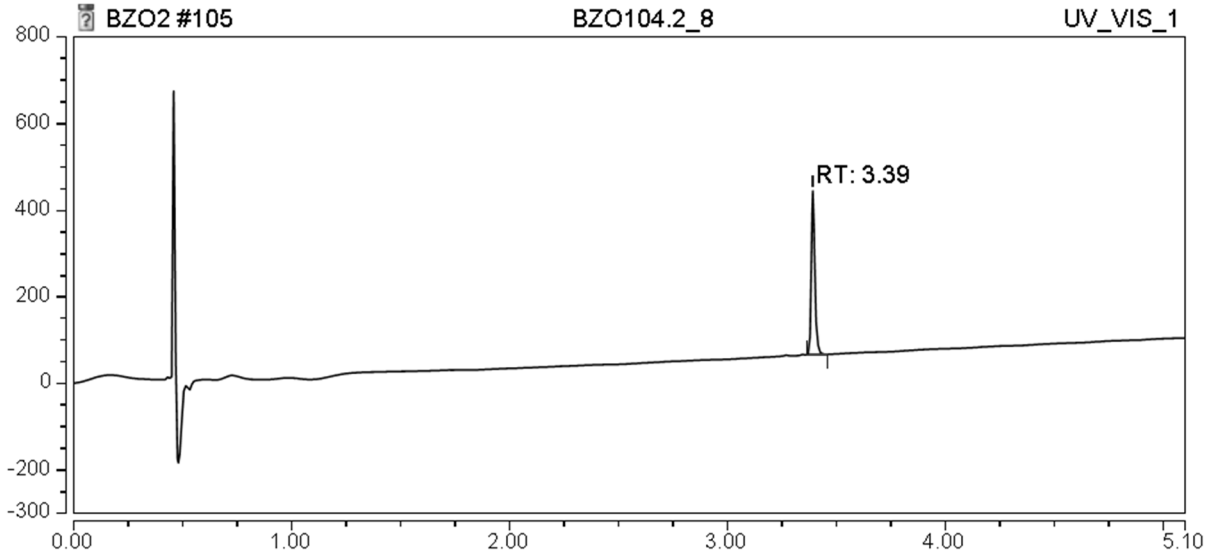

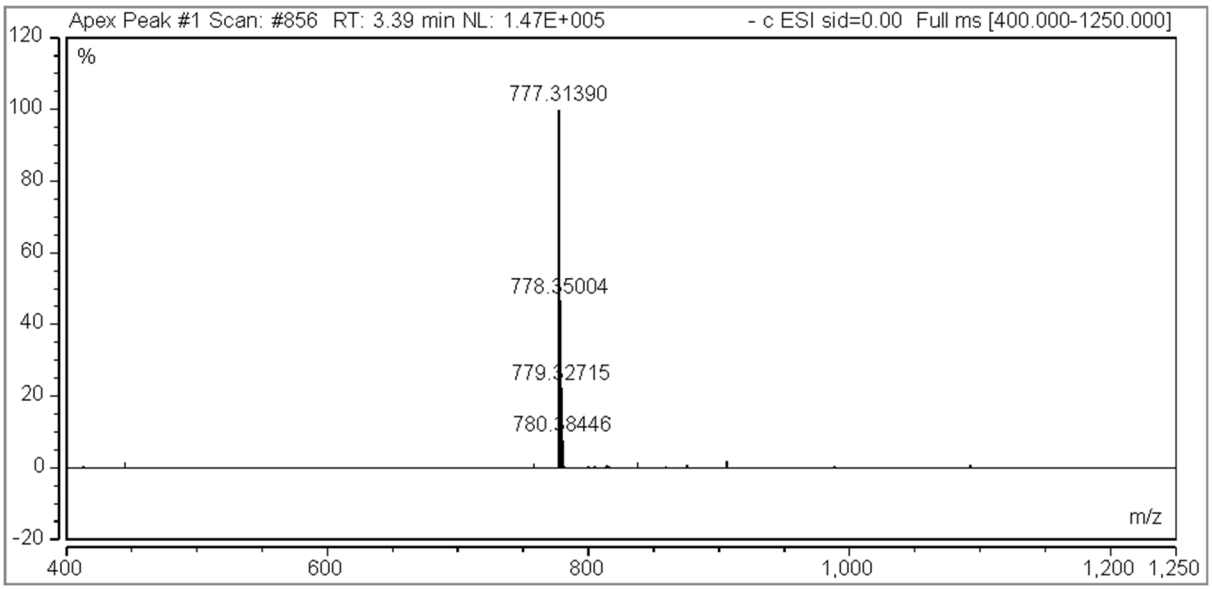

Ac-V-[CSELC]$_{cyclic}$ – -NH_2 (**4b**)

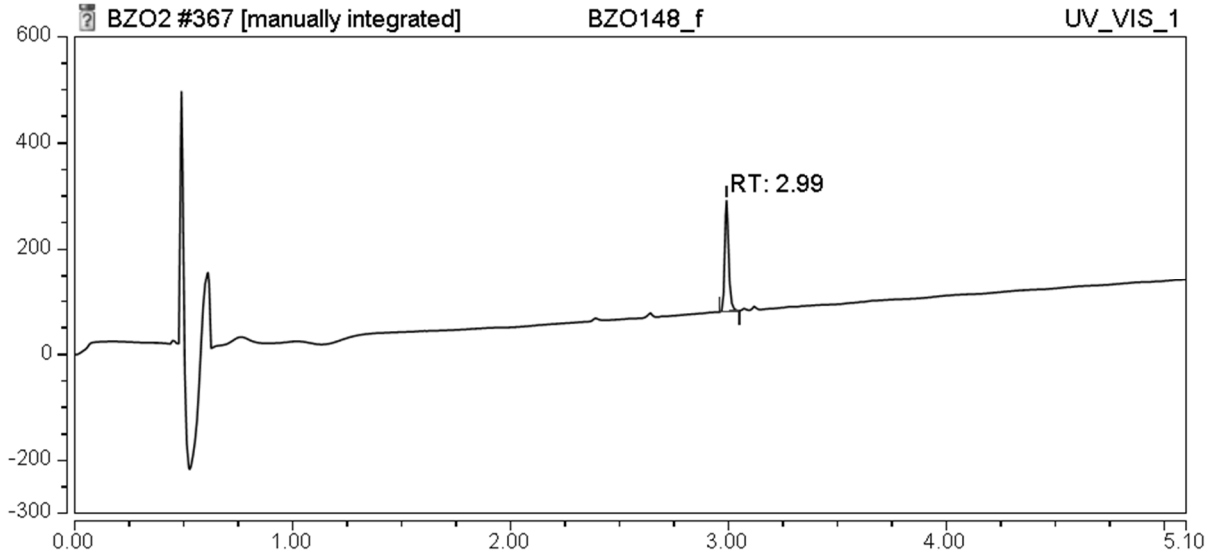

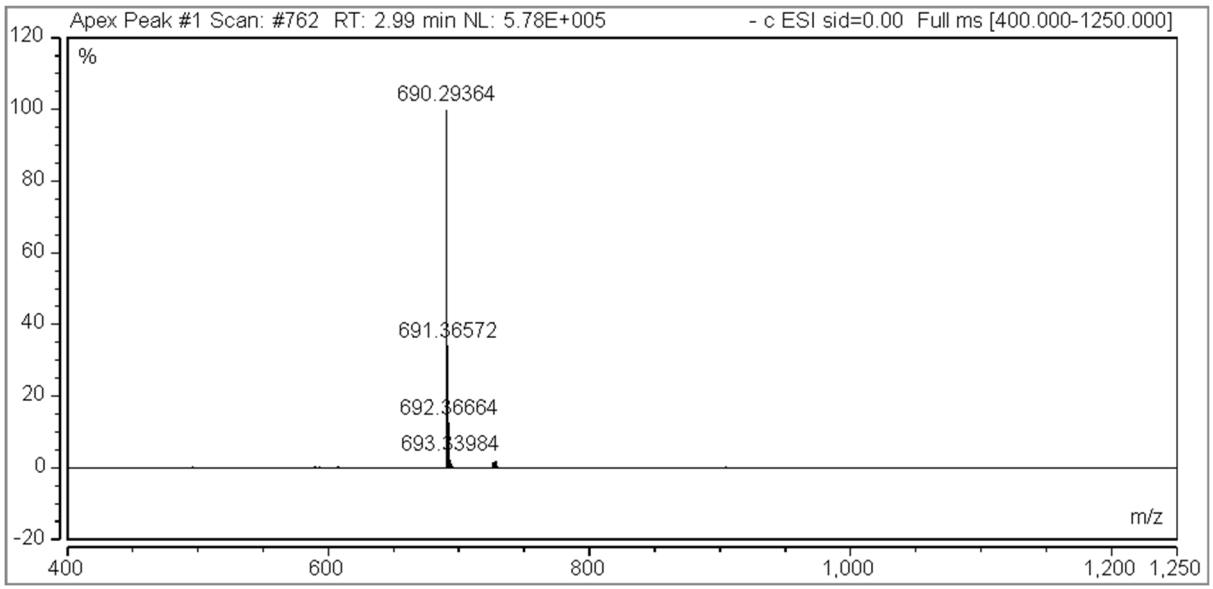

Ac-V-[**Pra**-SEL-**Aza**]$_{cyclic}$-W-NH_2 (1,4-triazole) (**5a**)

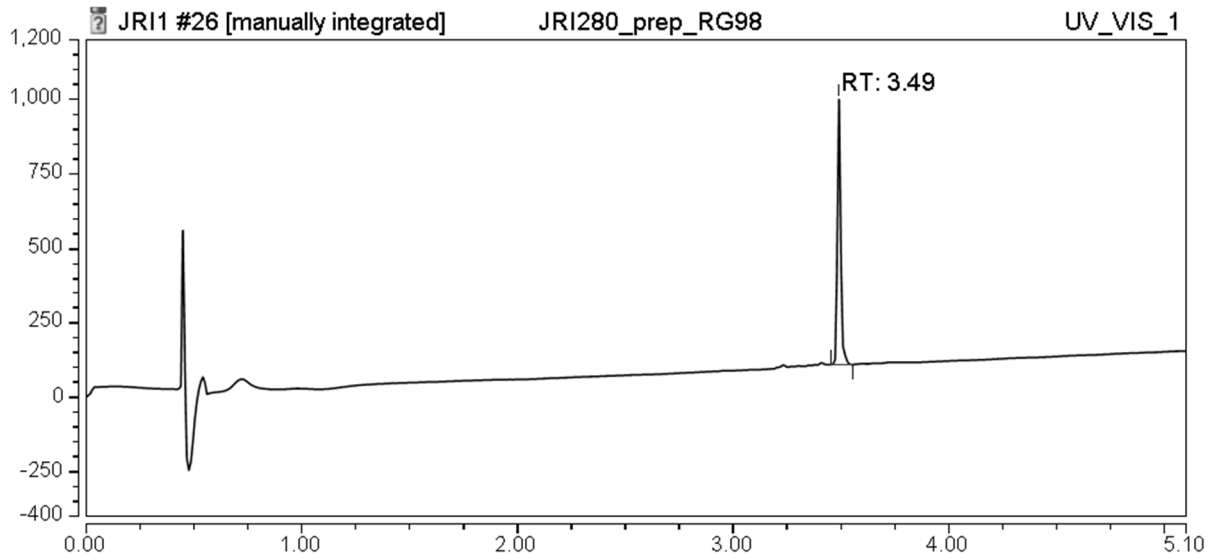

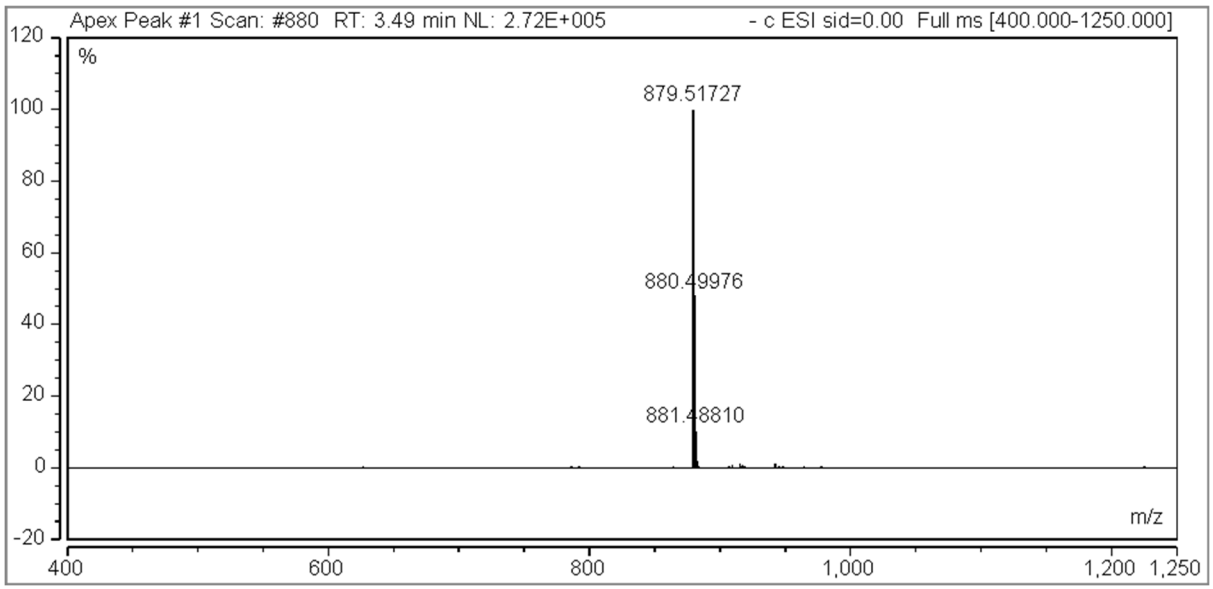

Ac-V-[**Aza**-SEL-**Pra**]$_{cyclic}$-W-NH_2 (1,4-triazole) (**5b**)

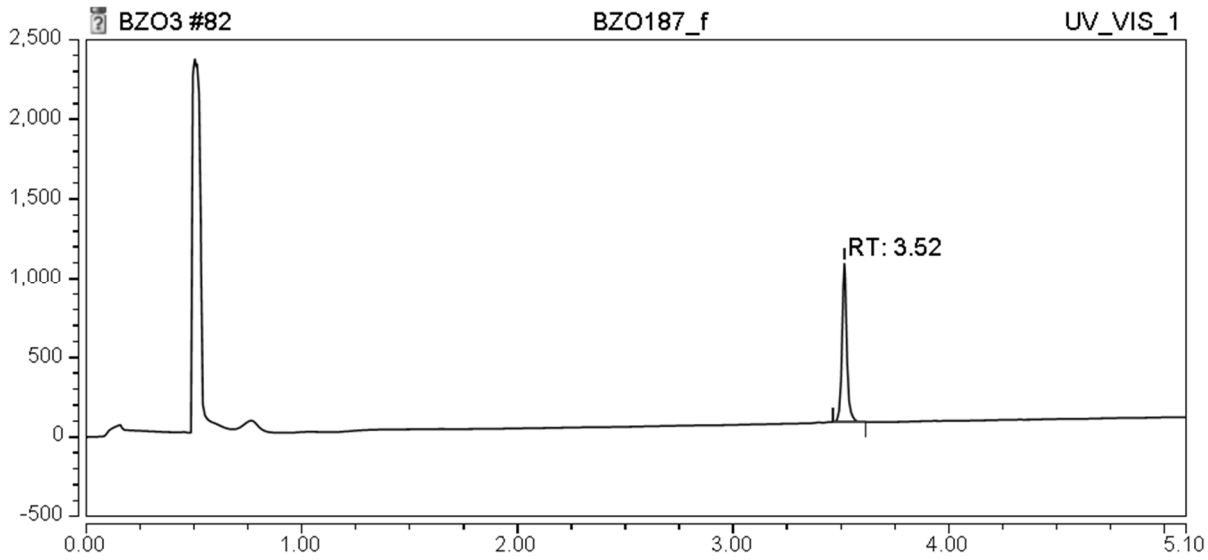

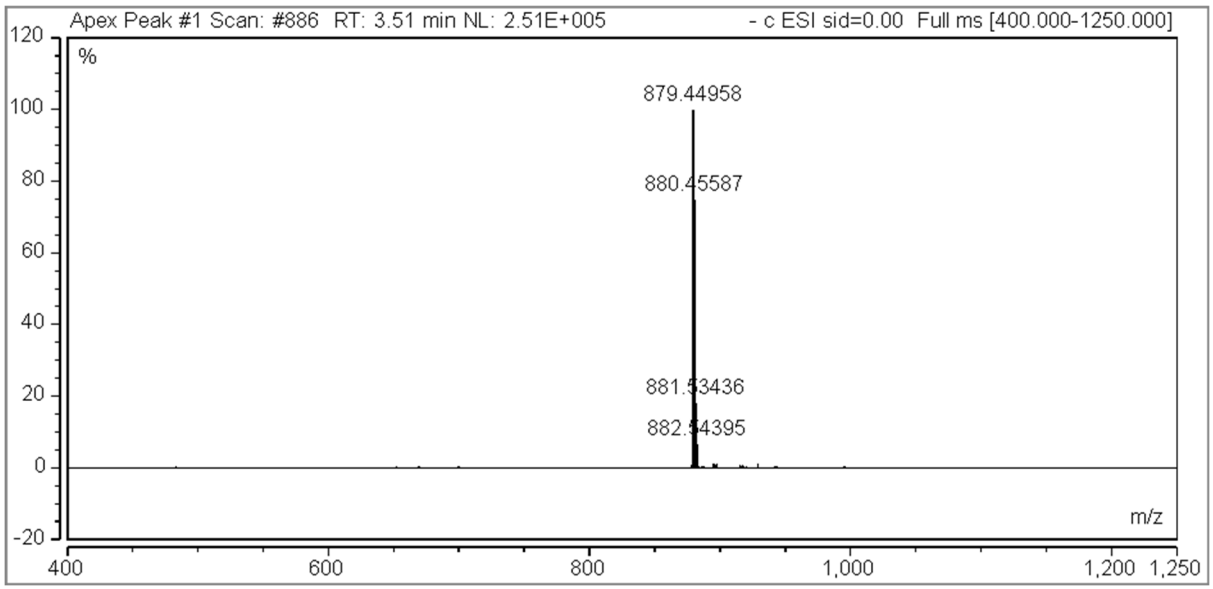

Ac-V-[**Pra**-SEL-**Aha**]$_{cyclic}$-W-*NH*$_2$ (1,4-triazole) (**5c**)

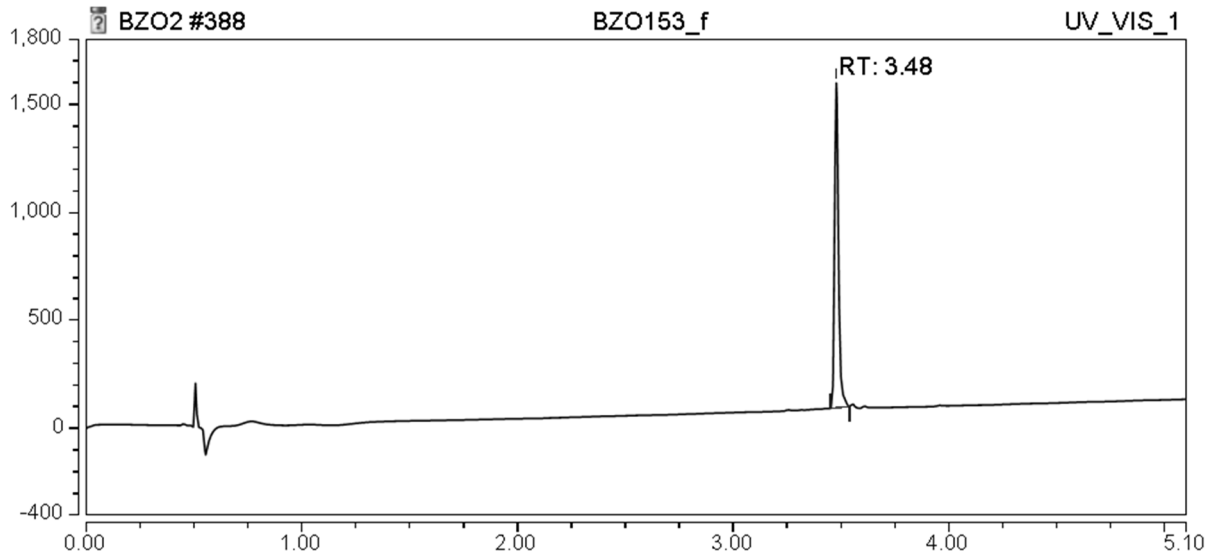

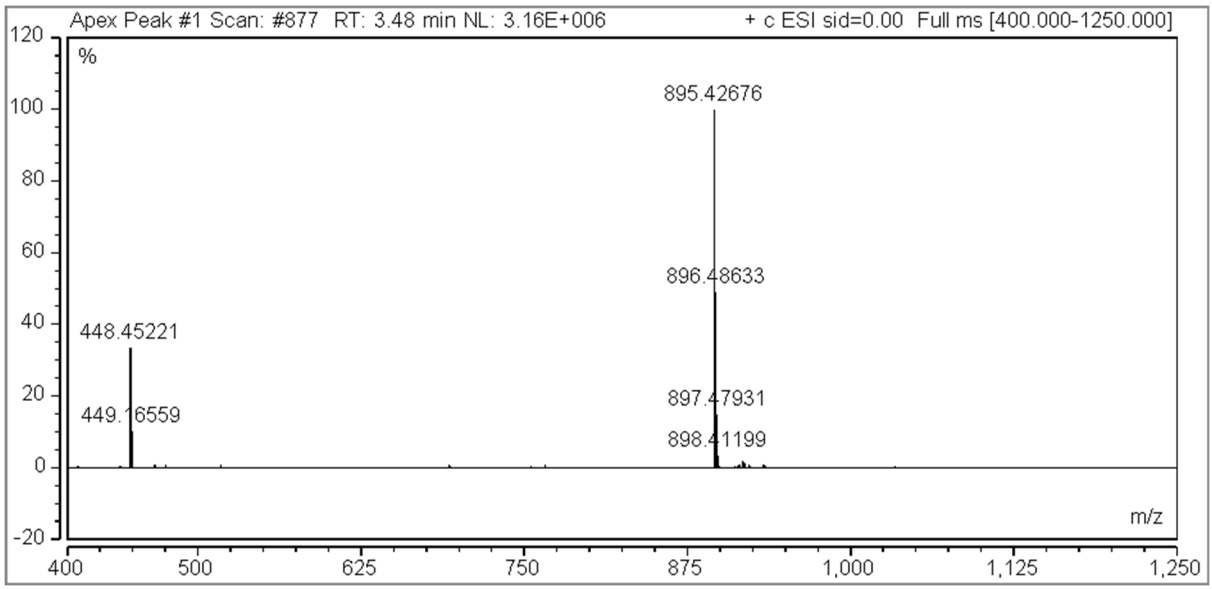

Ac-V-[**Pra**-SEL-**Aza**]$_{cyclic}$-W-*NH*$_2$ (1,5-triazole) (**6a**)

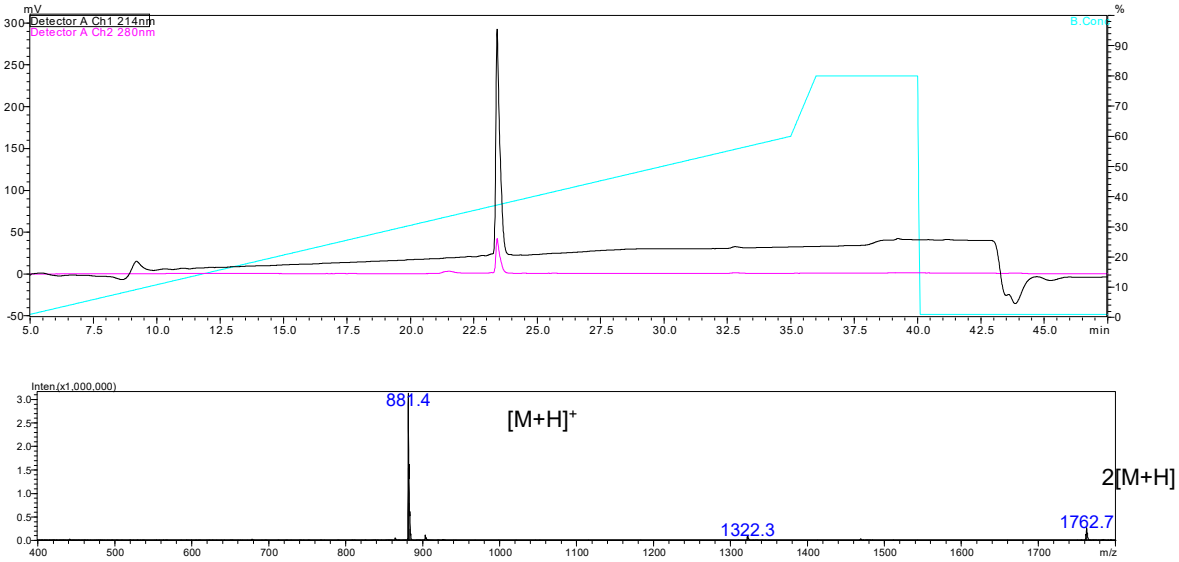

Ac-V-[**Pra**-SEL-**Aha**]$_{cyclic}$-W-*NH*$_2$ (1,5-triazole) (**6b**)

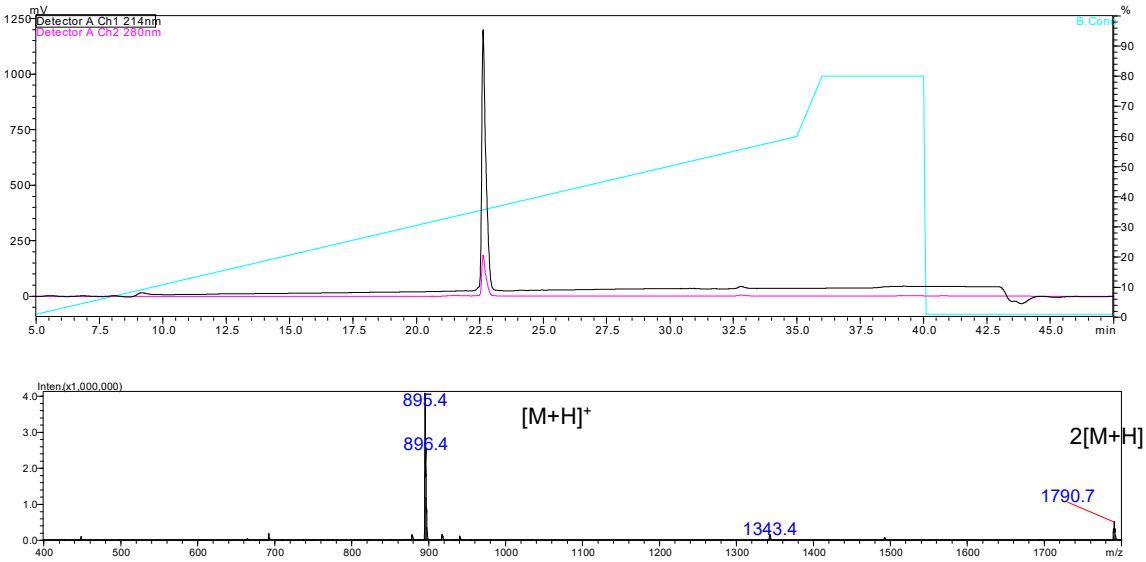

Ac-V-[**Aha**-SEL-**Pra**]$_{cyclic}$-W-*NH*$_2$ (1,5-triazole) (**6c**)

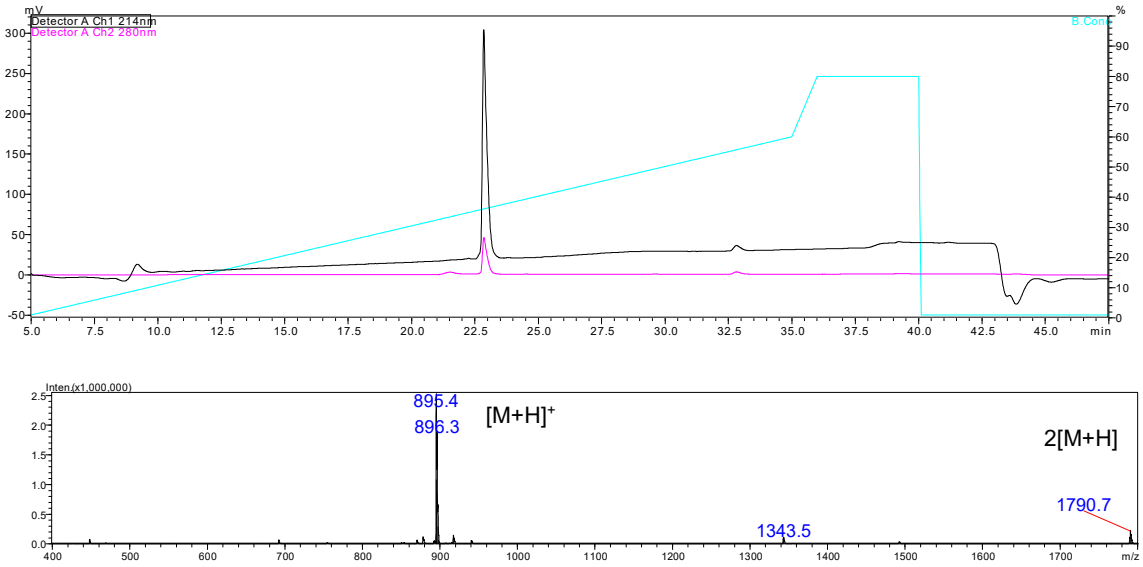

Purity

No.	Purity / %
1	100
2a	100
2b	100
3a	100
3b	95
3c	100
3d	91
3e	98
3f	100
4a	100
4b	92
5a	100
5b	100
5c	100
6a	100
6b	100
6c	100

^{1}H-NMR and ^{13}C-NMR Spectra

Compounds **1**, **5a**-**5c** were dissolved in 0.5 mL DMSO-d6 and measured with Bruker Fourier spectrometer model Ultrashield Plus 500 (500 MHz for ^{1}H-NMR and 126 MHz for ^{13}C-NMR). Chemical shifts are given in parts per million (ppm) and referenced against the residual proton or carbon resonances of the >99% deuterated solvents as internal standard. Coupling constants (*J*) are given in Hertz (Hz). Data are reported as follows: chemical shift, multiplicity (s = singlet, d = doublet, t =triplet, q = quartet, m = multiplet, dd = doublet of doublets, dt =doublet of triplets, br = broad and combinations of these) coupling constants, and integration. NMR spectra were evaluated using MestReNova.

The 1,5-triazole analogues **6a**, **6b**, and **6c** were analyzed on a Bruker AVANCE III 600 MHz spectrometer equipped with a cryogenically cooled probe. The samples were prepared in 500 µL of H_2O/D_2O (9:1 v/v, ~2 mM, pH 3.4) and ^{1}H and ^{13}C experiments were acquired at 298 K (referencing to H_2O at 4.70 ppm). The spectra were manually assigned using CCPNMR analysis 2.4.2.

Ac-V-[CSELC]$_{cyclic}$-W-*NH*$_2$ (**1**)

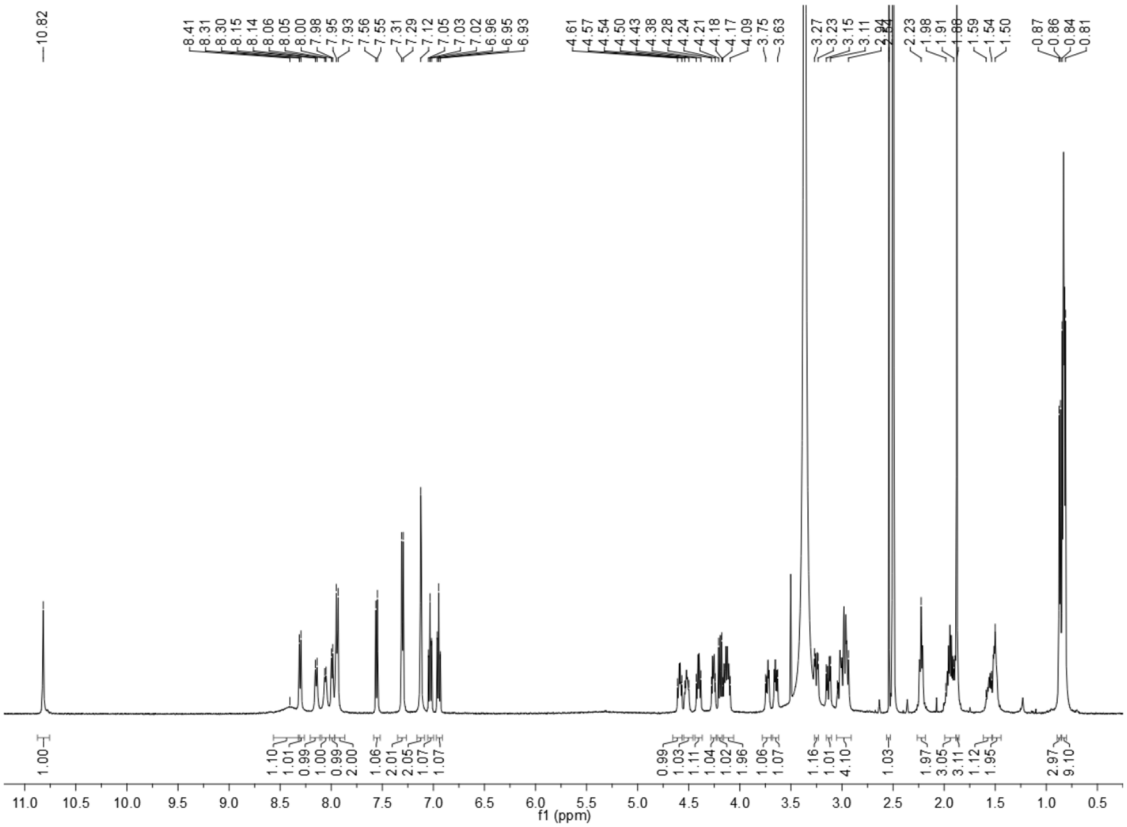

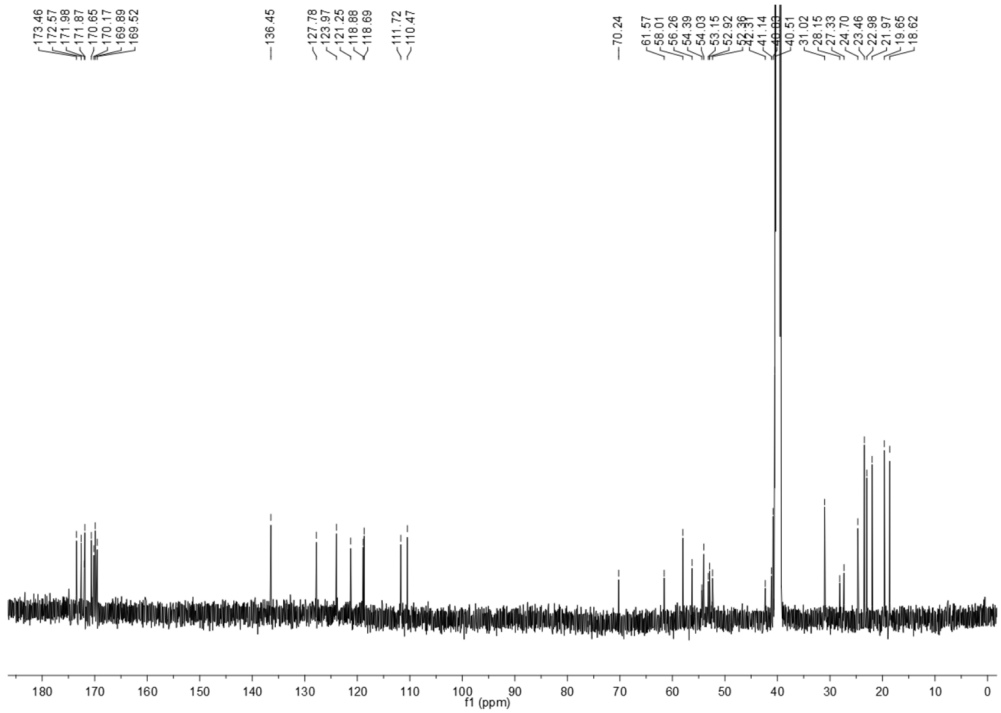

Ac-V-[**Pra**-SEL-**Aza**]$_{cyclic}$-W-*NH*$_2$ (1,4-triazole) (**5a**)

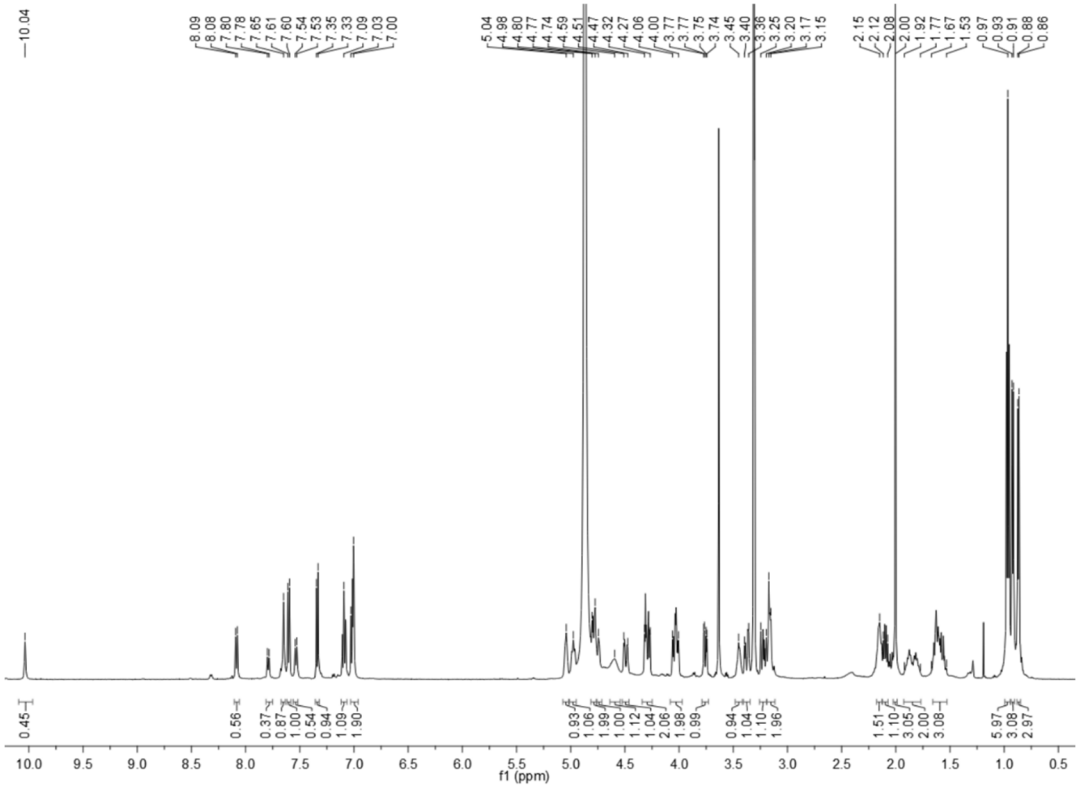

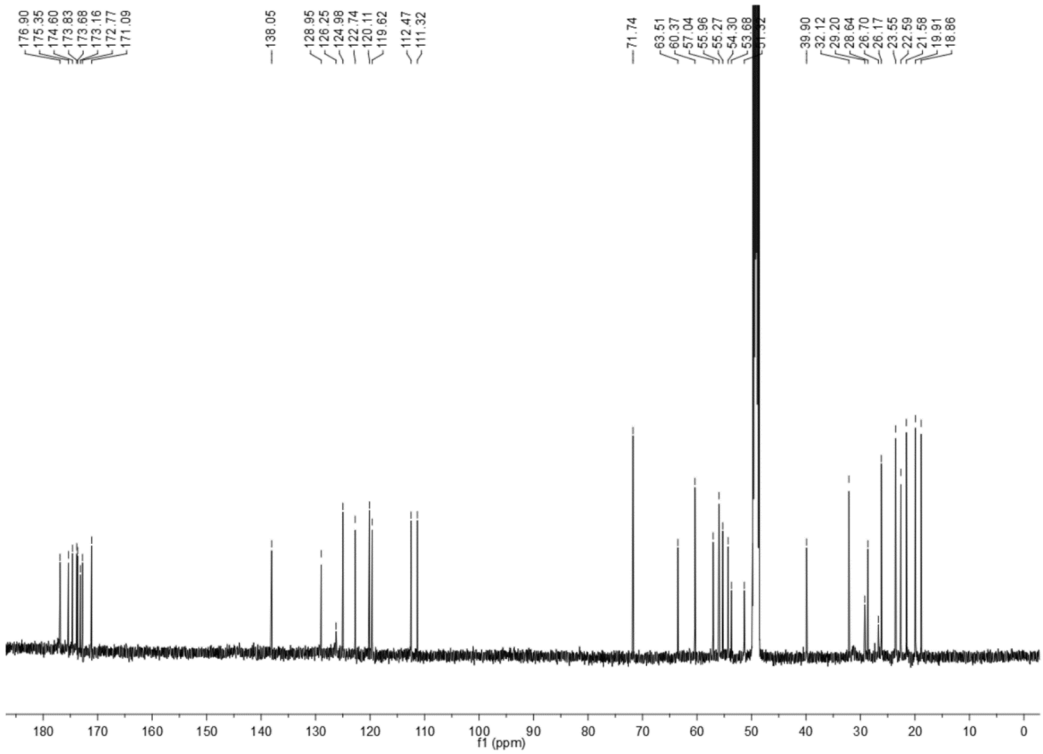

Ac-V-[**Aza**-SEL-**Pra**]$_{cyclic}$-W-*NH*$_2$ (1,4-triazole) (**5b**)

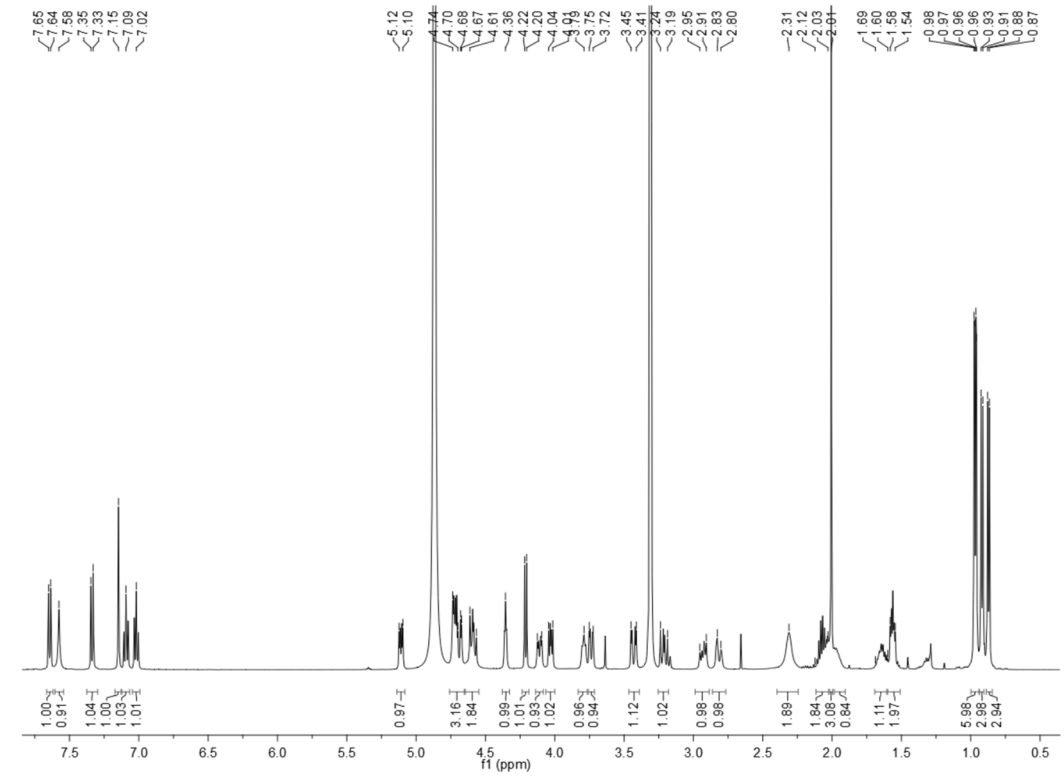

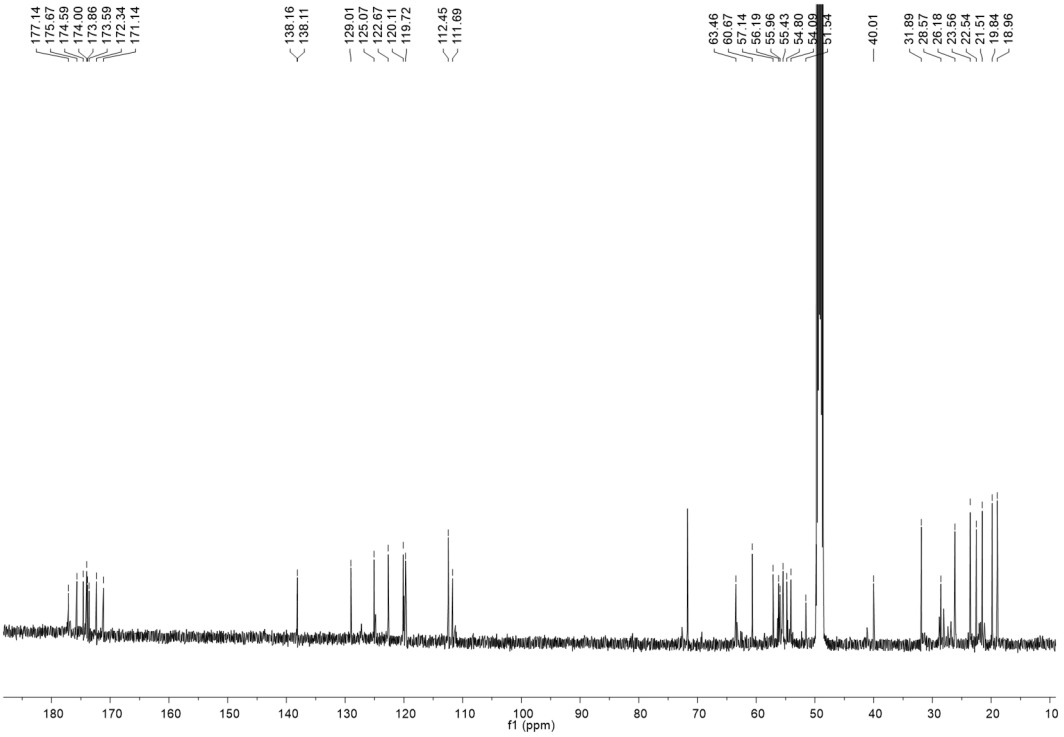

Ac-V-[**Pra**-SEL-**Aha**]$_{cyclic}$-W-*NH*$_2$ (1,4-triazole) (**5c**)

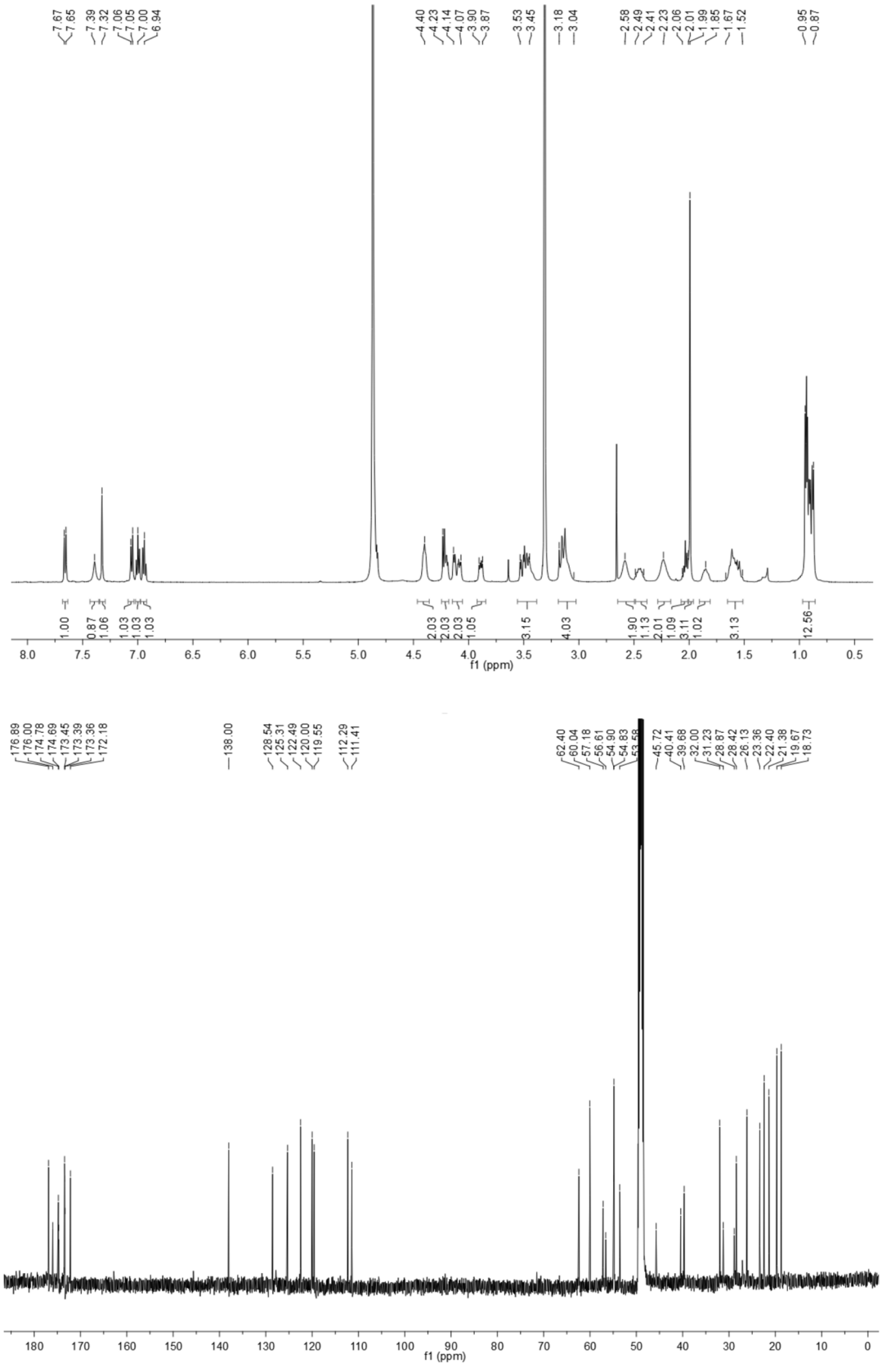

Ac-V-[**Pra**-SEL-**Aza**]$_{cyclic}$-W-*NH*$_2$ (1,5-triazole) (**6a**)

^{1}H NMR spectra of **6a** (600 MHz, H_2O/D_2O (9:1), pH 3.4)

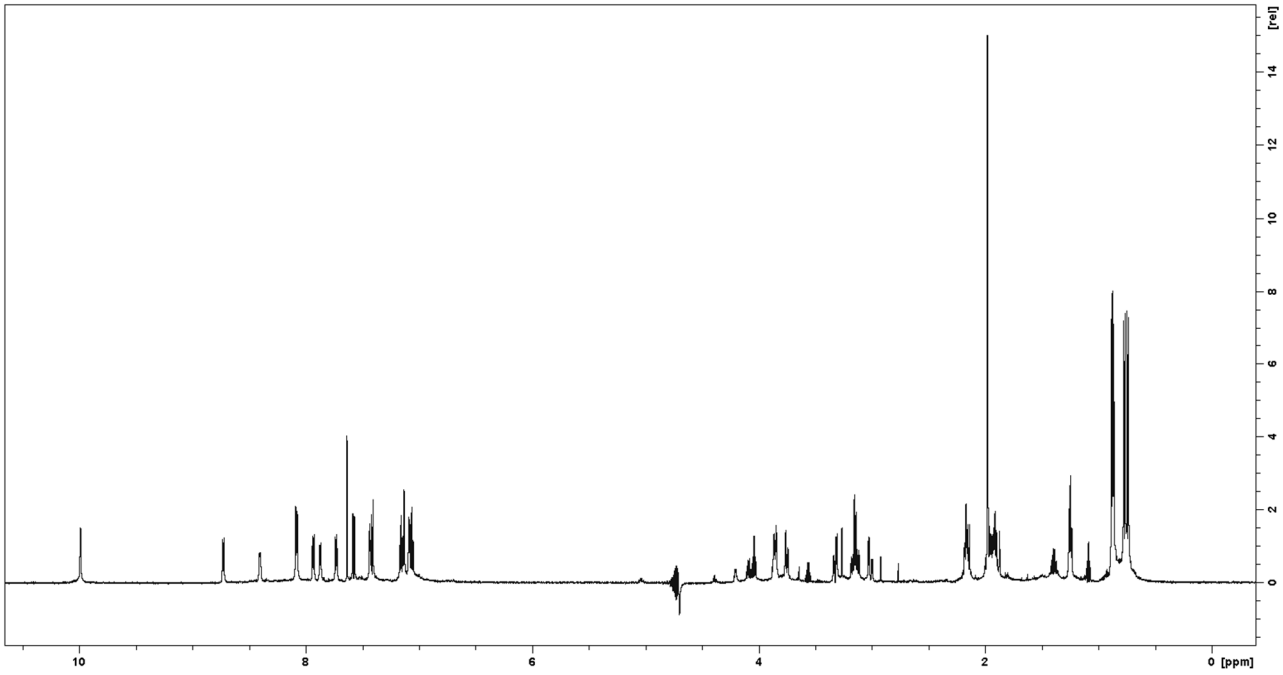

Ac-V-[**Pra**-SEL-]$_{cyclic}$-W-*NH*$_2$ (1,5-triazole) (**6b**)

^{1}H NMR spectra of **6b** (600 MHz, H_2O/D_2O (9:1), pH 3.4)

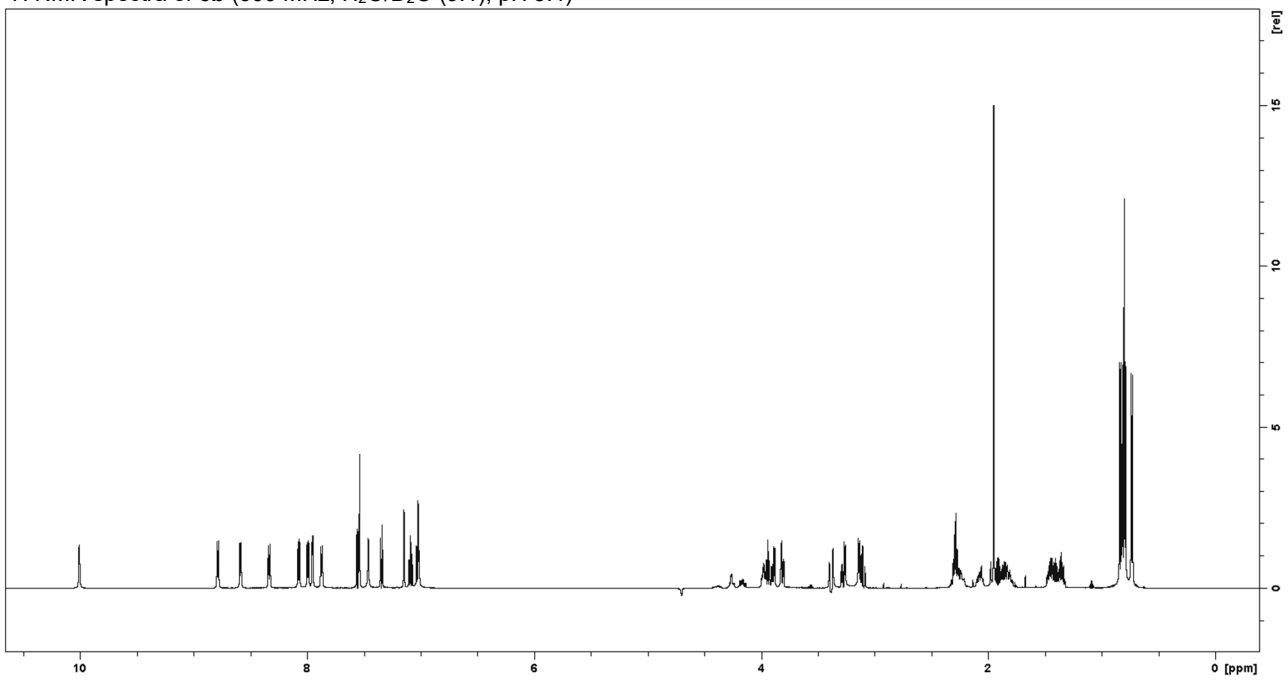

Ac-V-[**Aha**-SEL-**Pra**]$_{cyclic}$-W-*NH*$_2$ (1,5-triazole) (**6c**)

^{1}H NMR spectra of **6c** (600 MHz, H_2O/D_2O (9:1), pH 3.4)

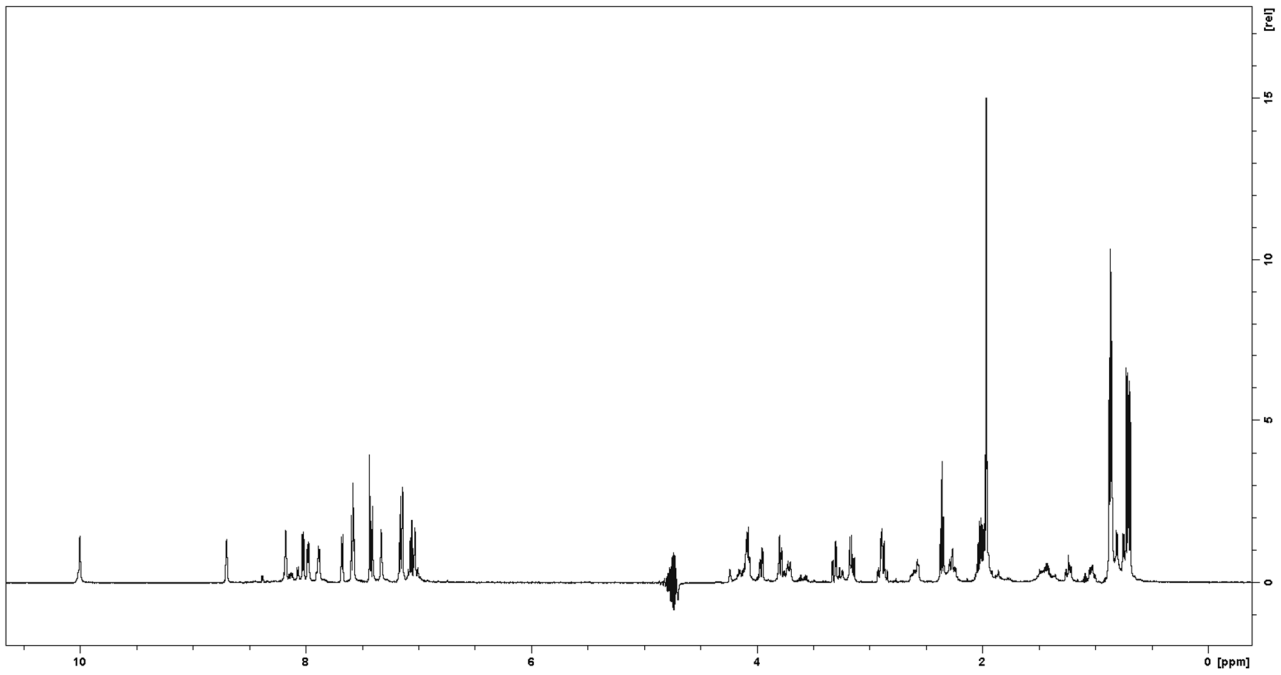

2D NMR Spectra

Ac-V-[**Pra**-SEL-**Aza**]$_{cyclic}$-W-*NH*$_2$ (1,4-triazole) (**5a**)

[^{1}H, ^{13}C]-HSQC (full)

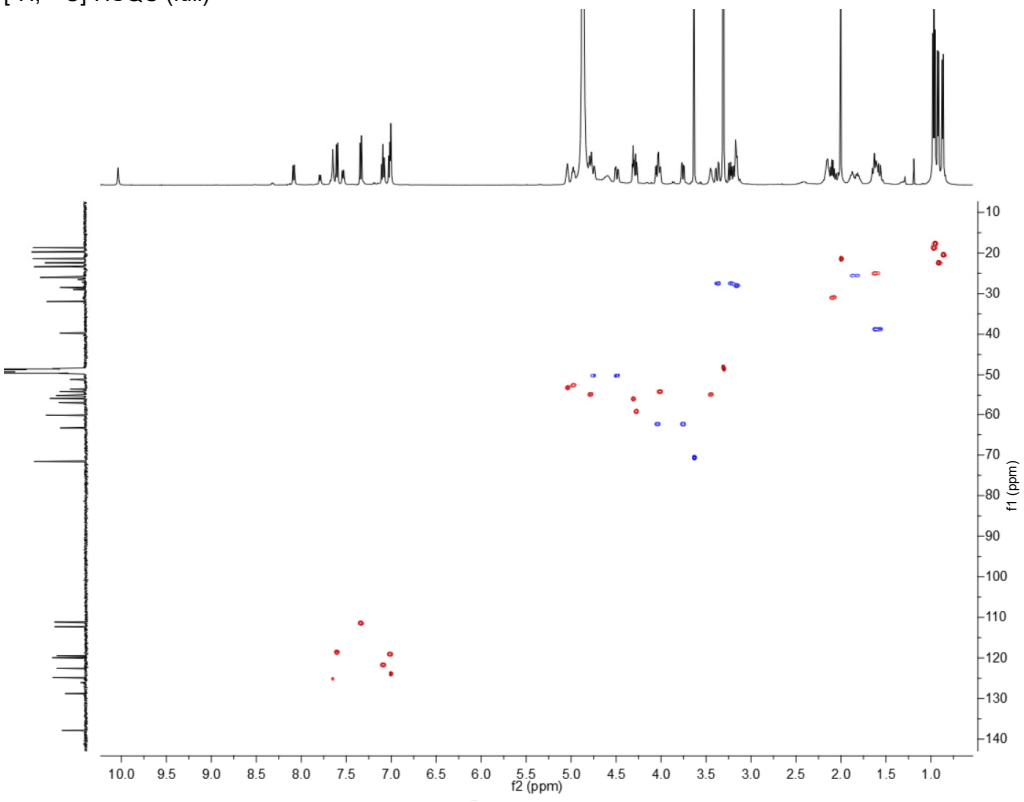

[^{1}H, ^{13}C]-HSQC (7.65, 126.2 C/H 15) Triazole

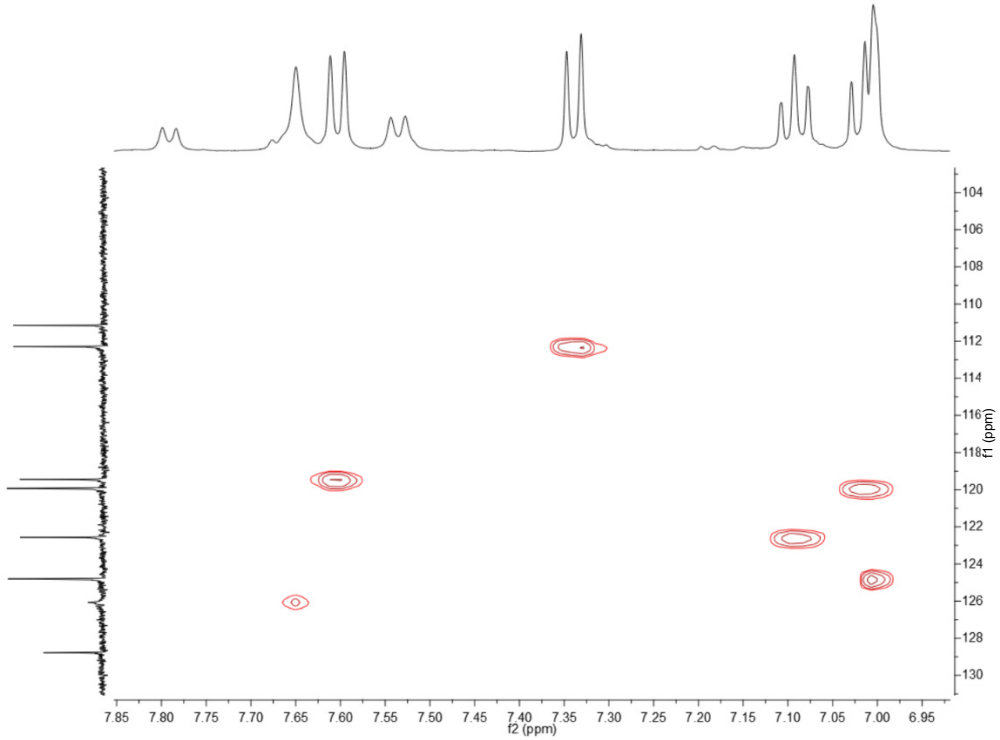

[^{1}H, ^{13}C]-HMBC (full)

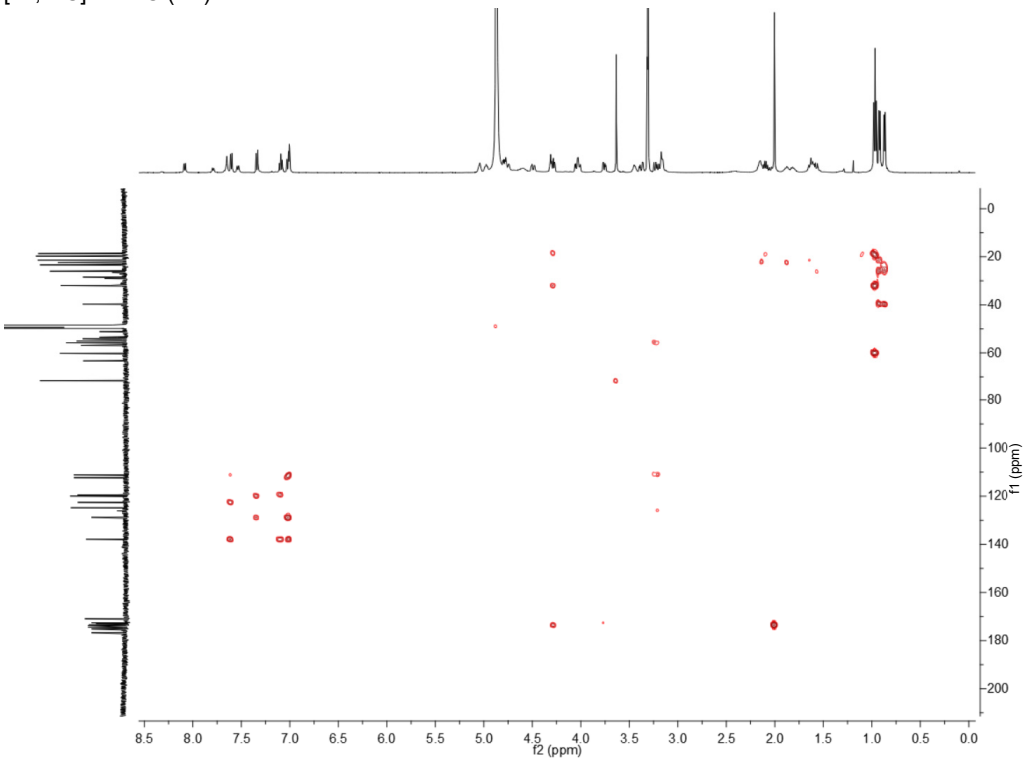

[^{1}H, ^{13}C]-HMBC (C15/H17)

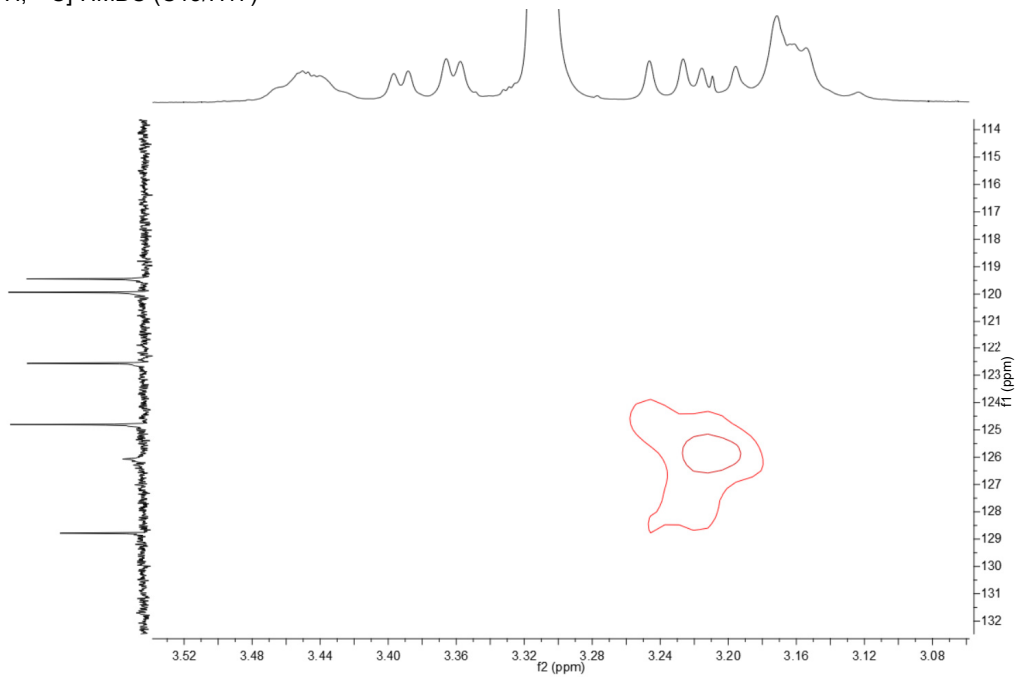

FTIR Spectra

IR spectra were measured on a PerkinElmer Spectrum 100 FT-IR Spectrometer. The samples were measured as solid.

Ac-V-[**Pra**-SEL-**Aza**]$_{cyclic}$-W-*NH*$_2$ (1,4-triazole) (**5a**)

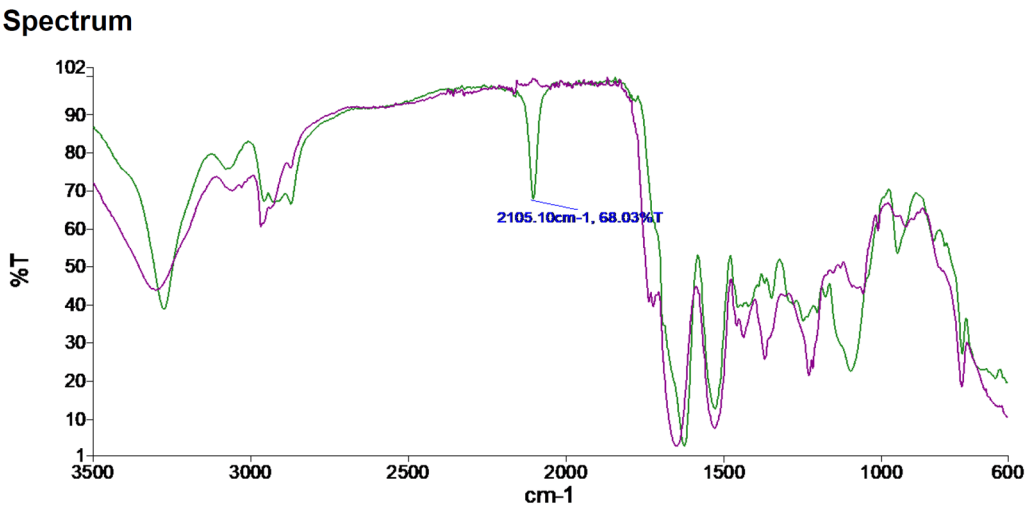

Green curve: before CuAAC
Purple curve: after CuAAC

HRMS

Compounds **1** and **5a**-**5c** were solved in H_2O/ACN (1:1) (v/v). HRMS was done with a DIONEX UltiMate 3000 UHPLC$^+$ focused (Thermo Scientific), containing pump, autosampler, column compartment heated to 30 °C, diode array detector, and Q exactive focus. We used an EC 150/2 NUCLEODUR C18 Pyramid, 3 µm (Macherey-Nagel) column with a gradient from 90-5 % solvent B over 9 min and 1.5 min constant 5 % solvent B (solvent A: H_2O (0.05 % formic acid), solvent B: ACN (0.05 % formic acid)) and a 0.5 mL/min flowrate.

Compounds **6a**, **6b** and **6c** were analyzed by HRMS on a Shimadzu interfaced UPLC coupled to an AB Sciex 5600 TripleTOF MS using time-of-flight-MS (TOF-MS) scanning. The samples were run over a linear gradient of 20-40% acetonitrile in H_2O (v/v) on an Agilent Zorbax C18 column (100 x 2.1 mm, 1.8 µm) at 40 °C and a flow rate of 0.2 mL/min. The electrospray voltage was 5500 V with a source temperature of 500 °C. The data was processed using Analyst v1.6.3 software by AB Sciex.

Ac-V-[CSELC]$_{cyclic}$-W-*NH*$_2$ (**1**)

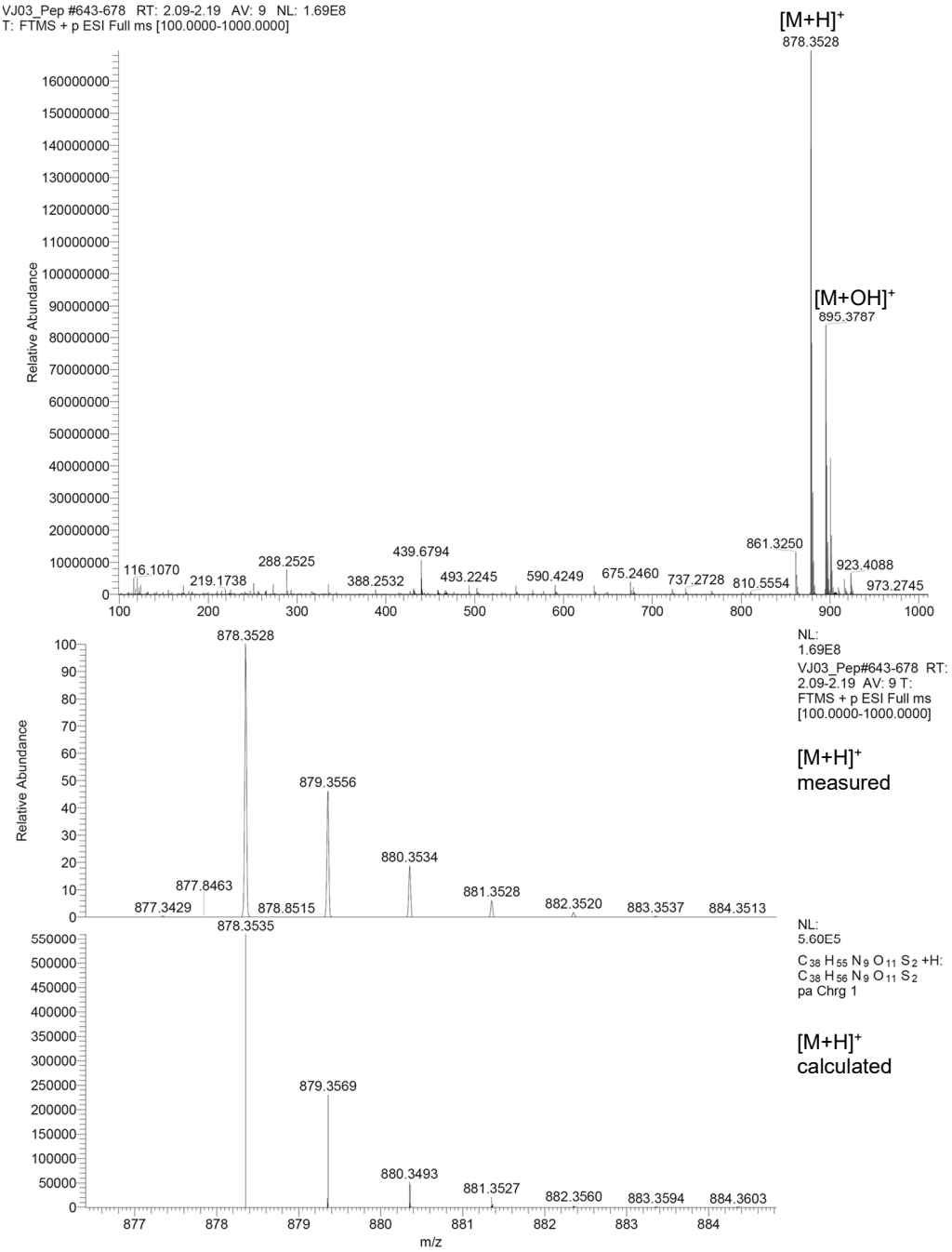

H-V-[CSELC]$_{cyclic}$-W-NH_2 (**2a**)

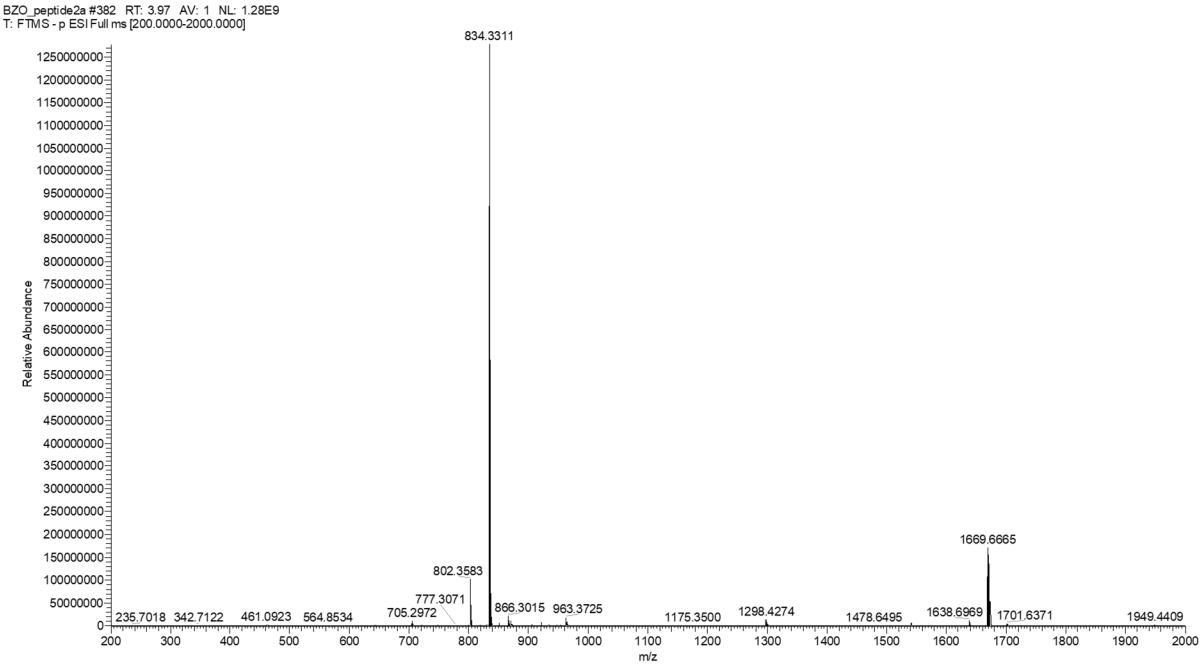

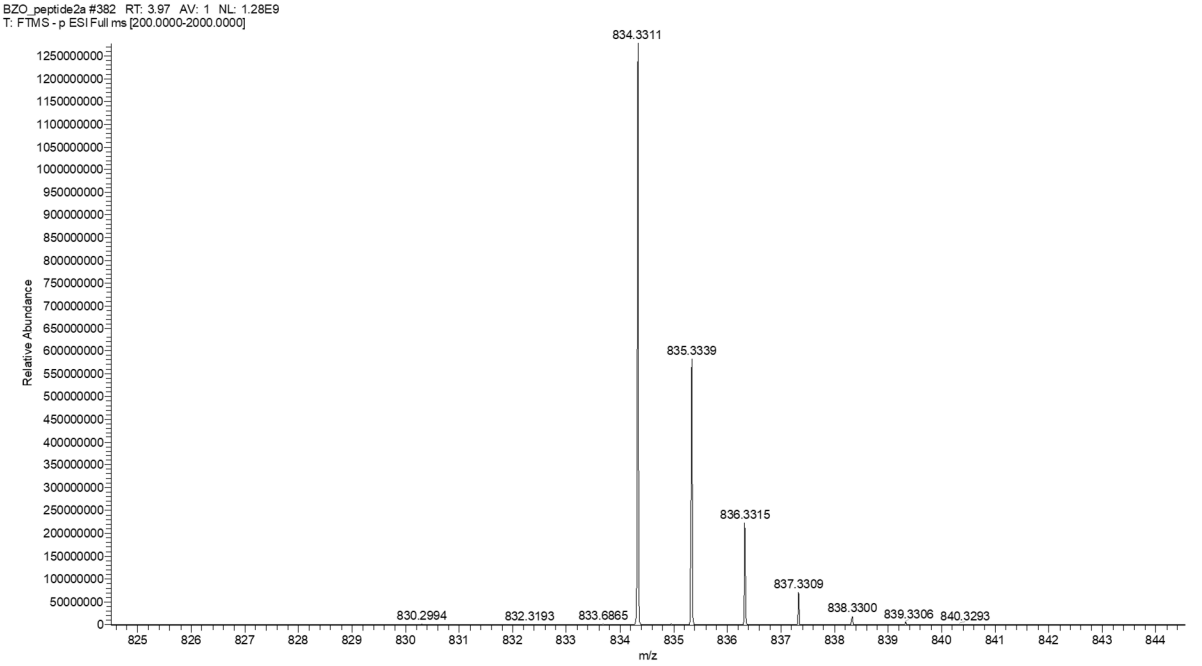

Ac-V-[CSELC]$_{cyclic}$-W-***OH*** (**2b**)

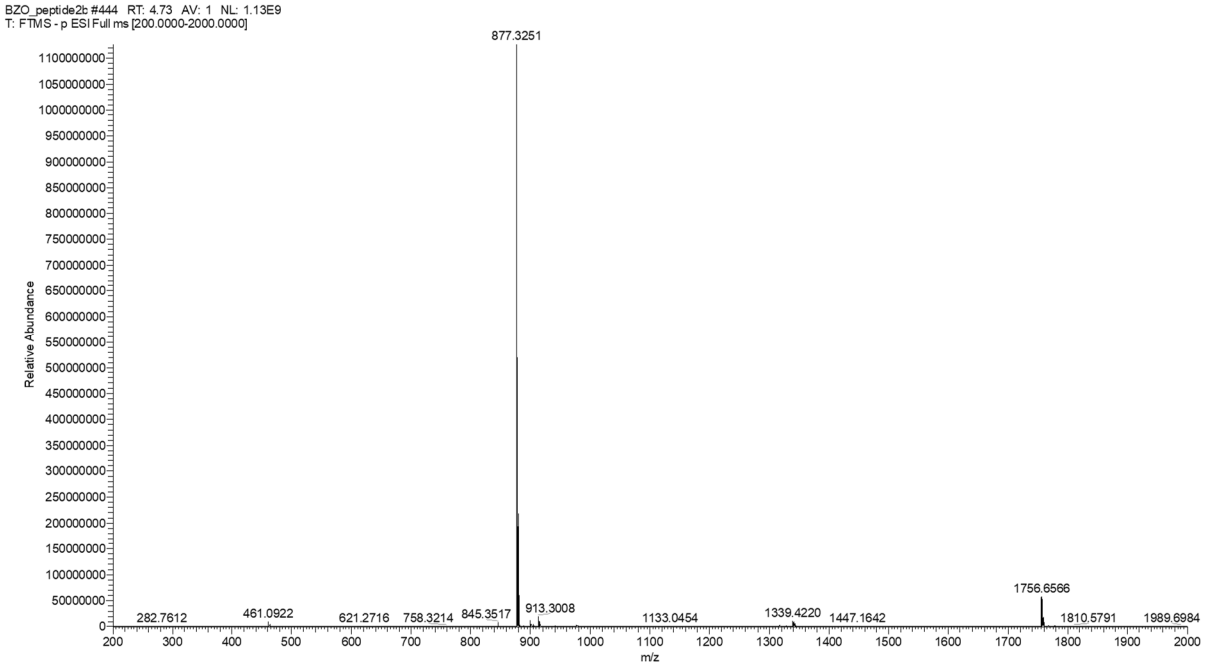

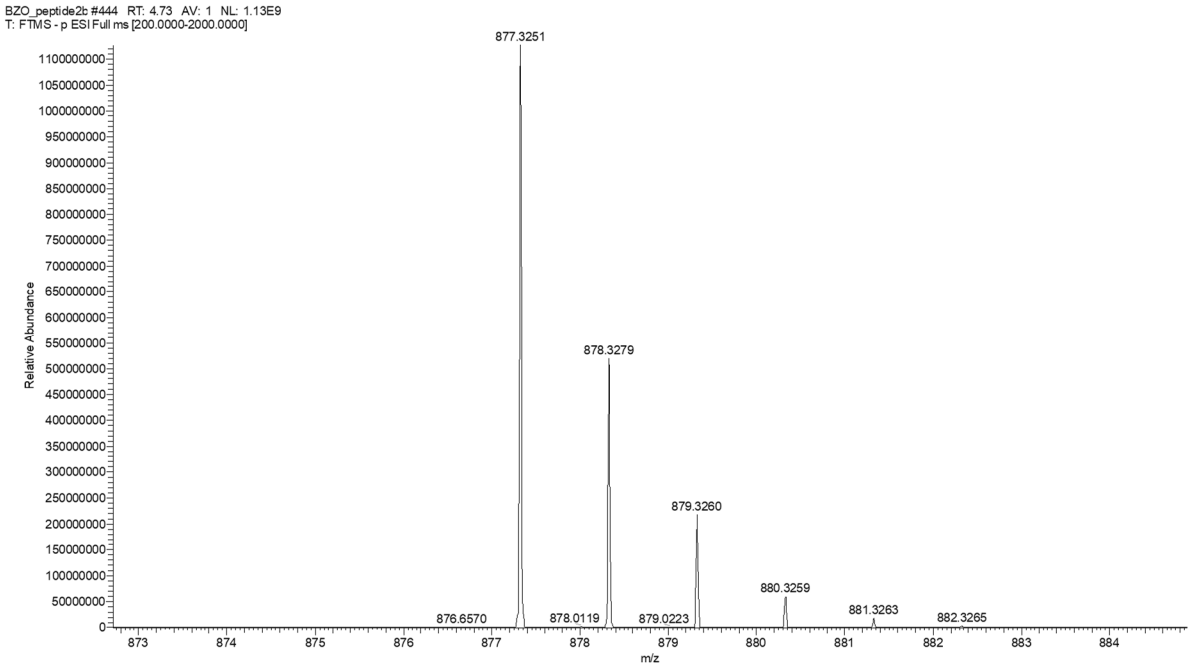

Ac-V**A**SEL**A**W-*NH*$_2$ (**3a**)

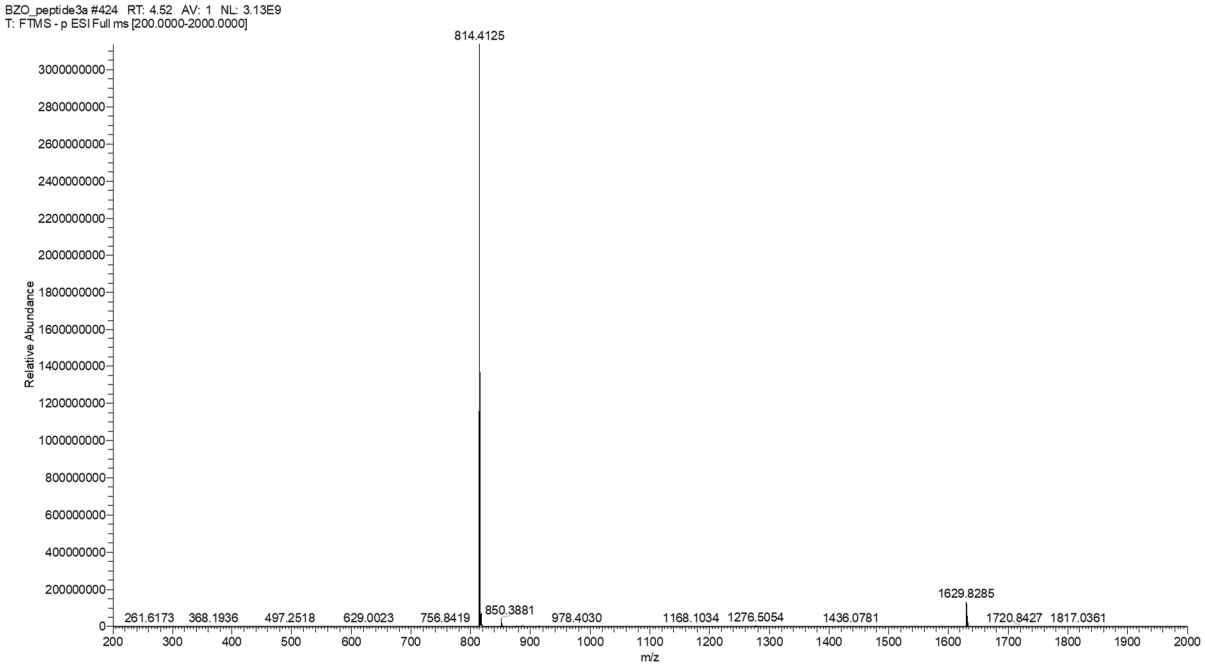

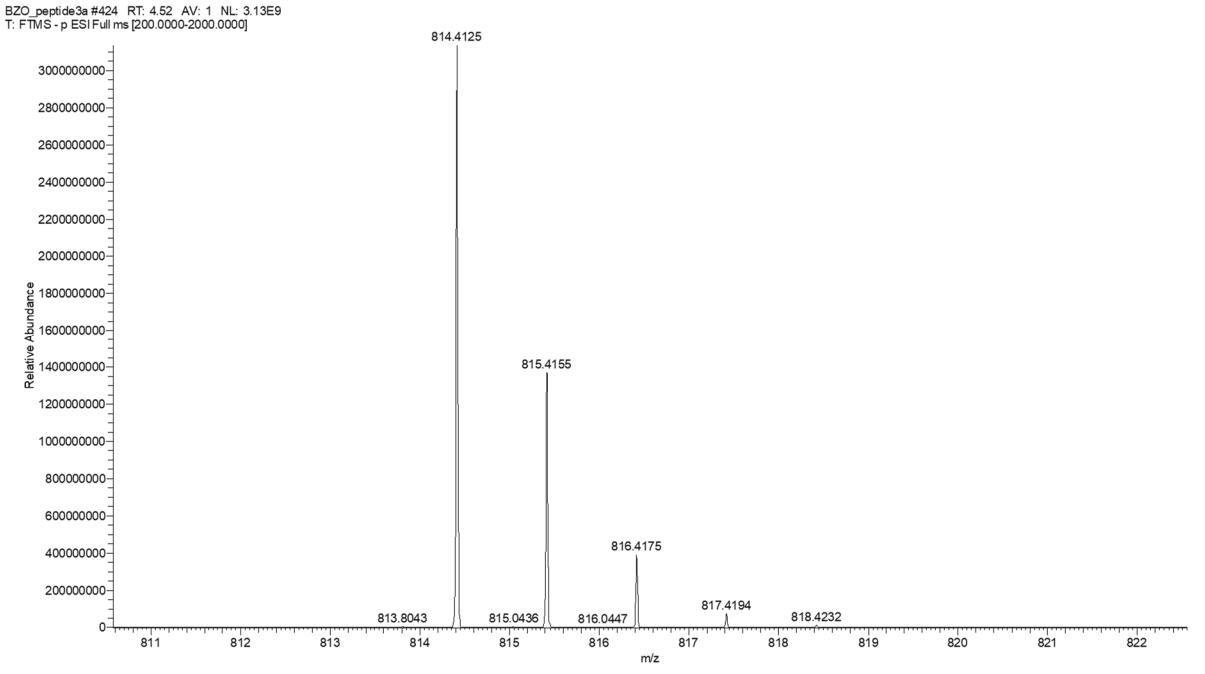

Ac-**A**-[CSELC]$_{cyclic}$-W-NH_2 (**3b**)

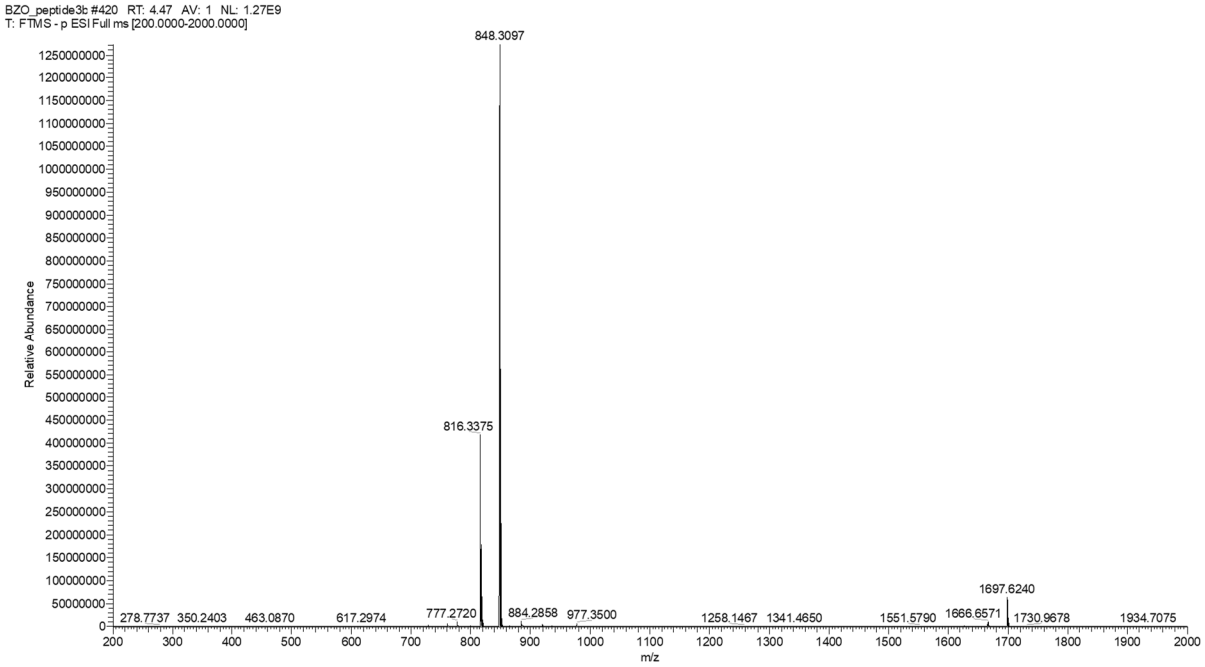

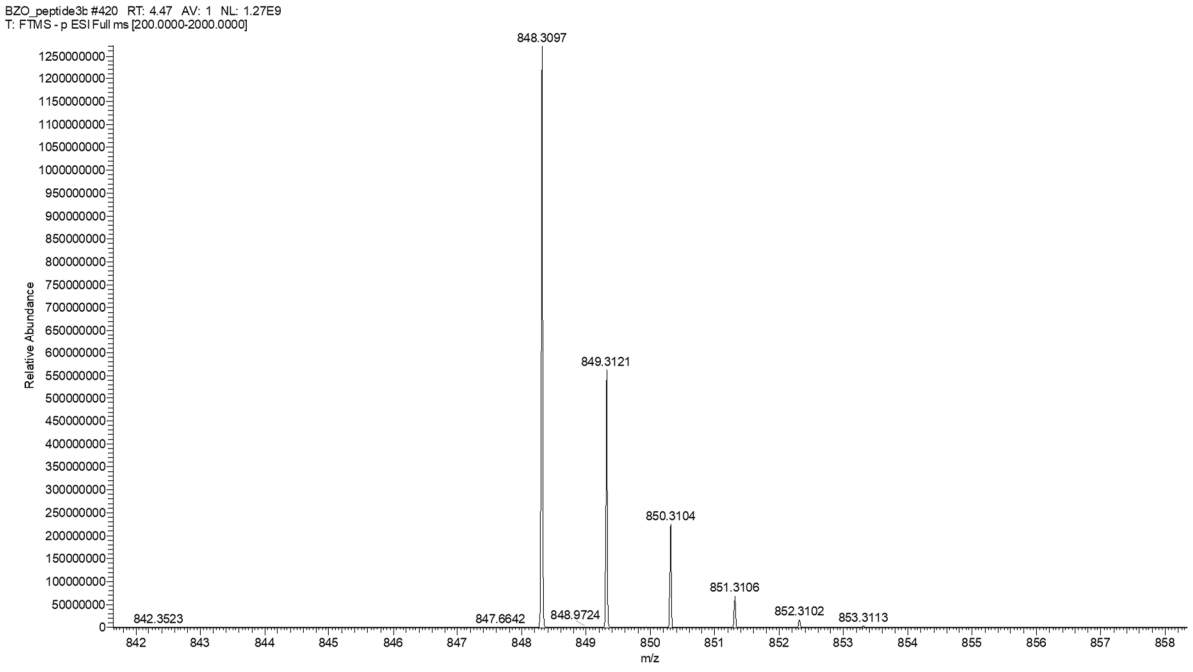

Ac-V-[C**A**ELC]$_{cyclic}$-W-NH_2 (**3c**)

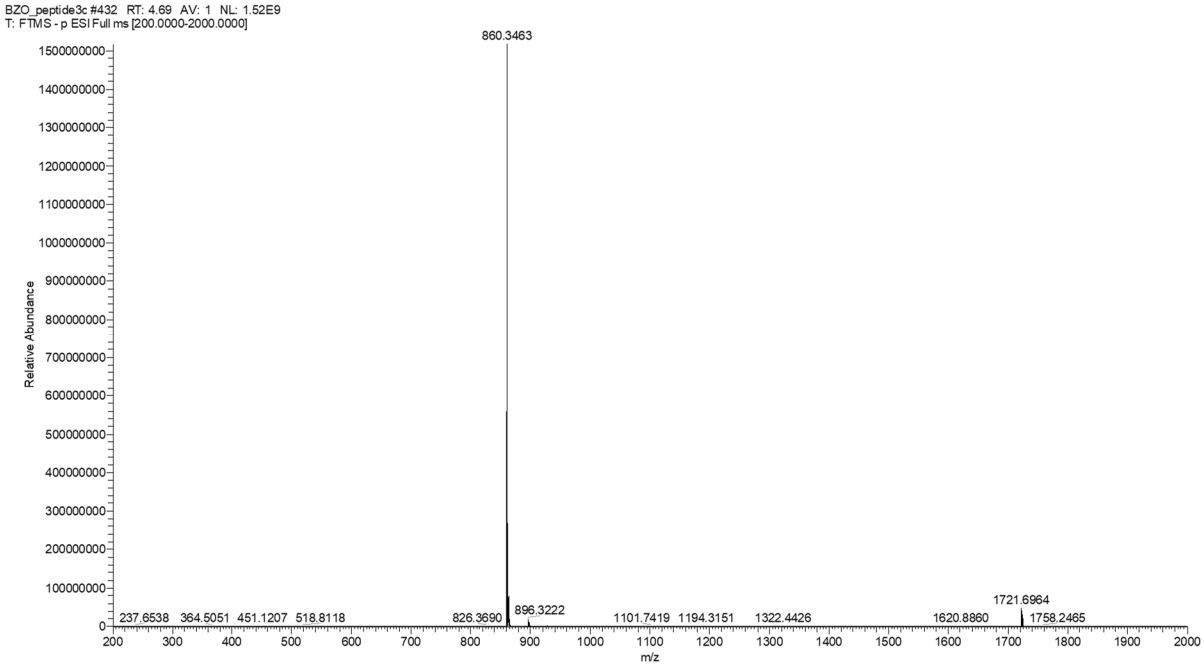

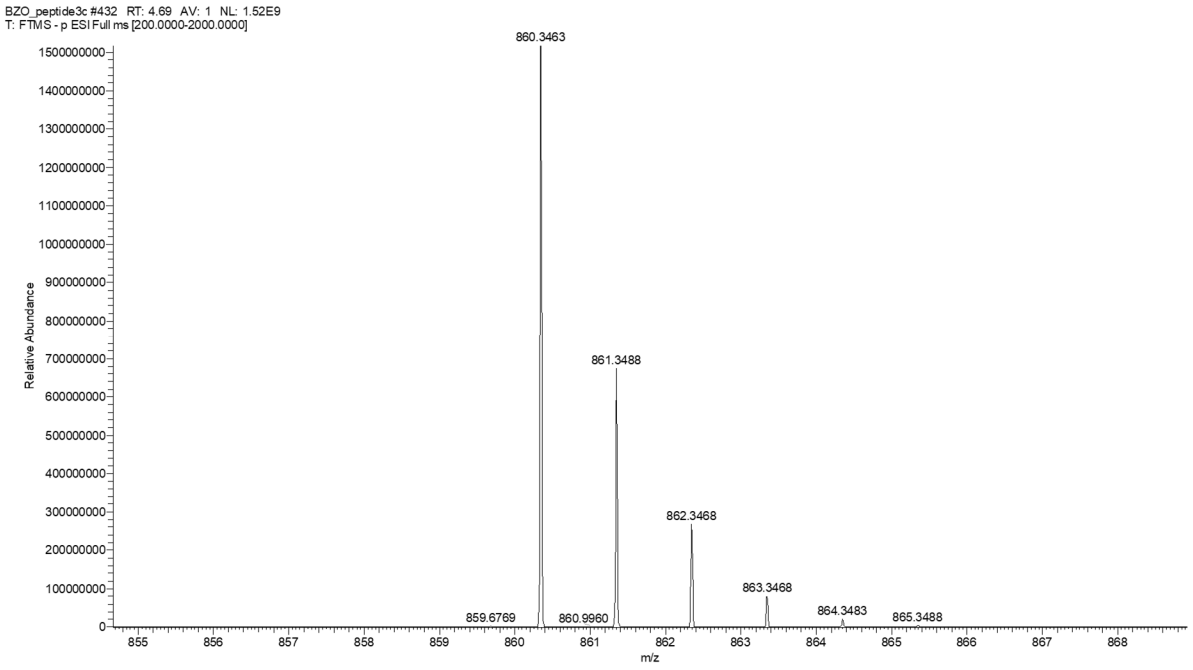

Ac-V-[CS**A**LC]$_{cyclic}$-W-NH_2 (**3d**)

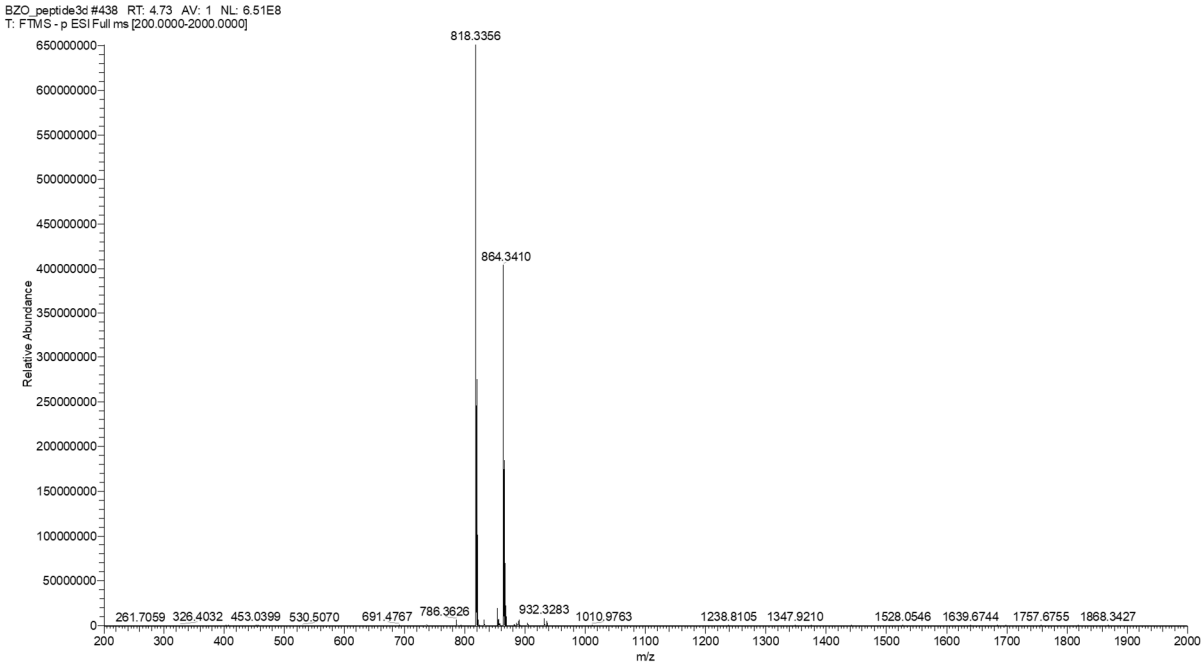

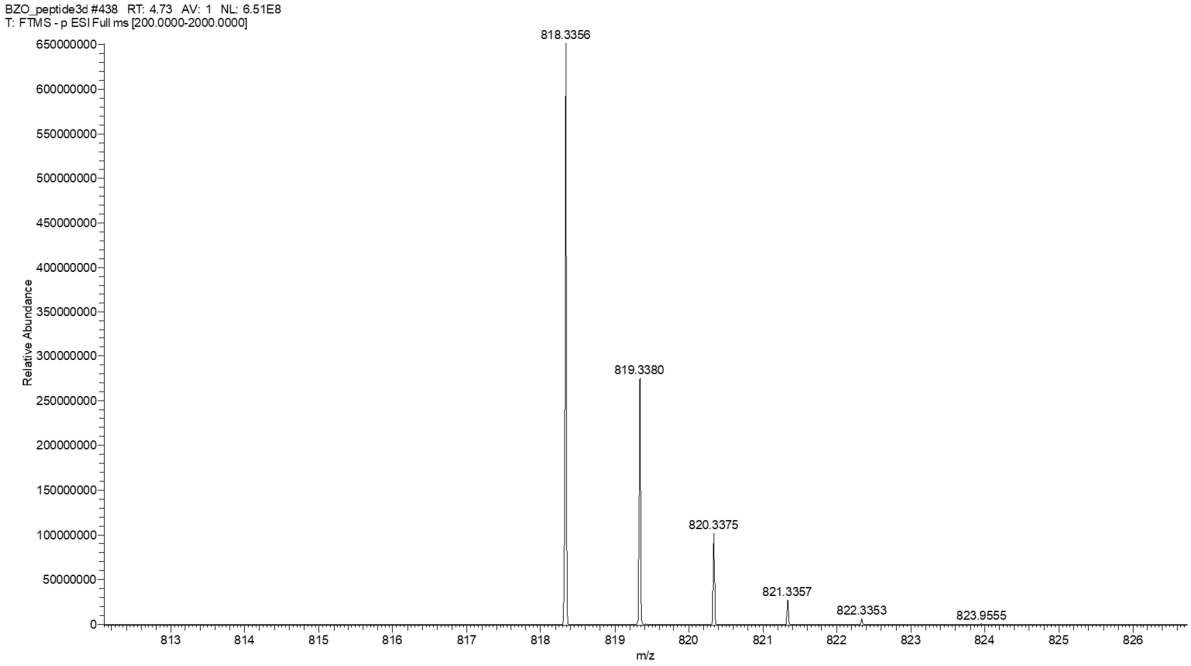

Ac-V-[CSE**A**C]$_{cyclic}$-W-NH_2 (**3e**)

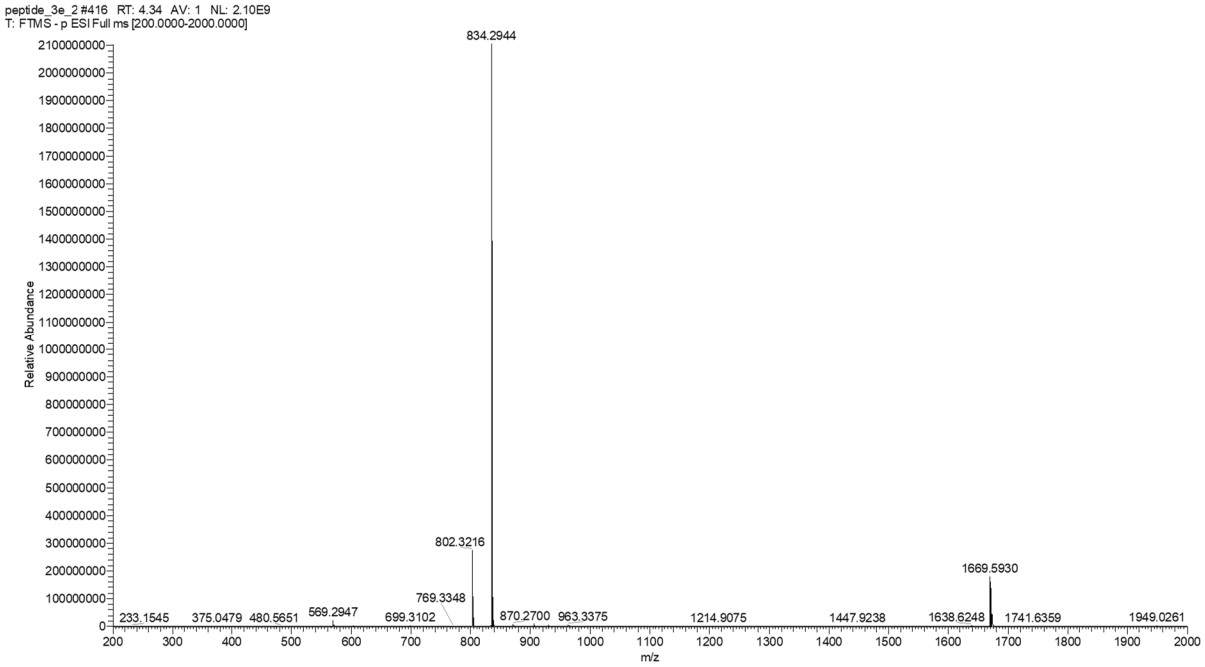

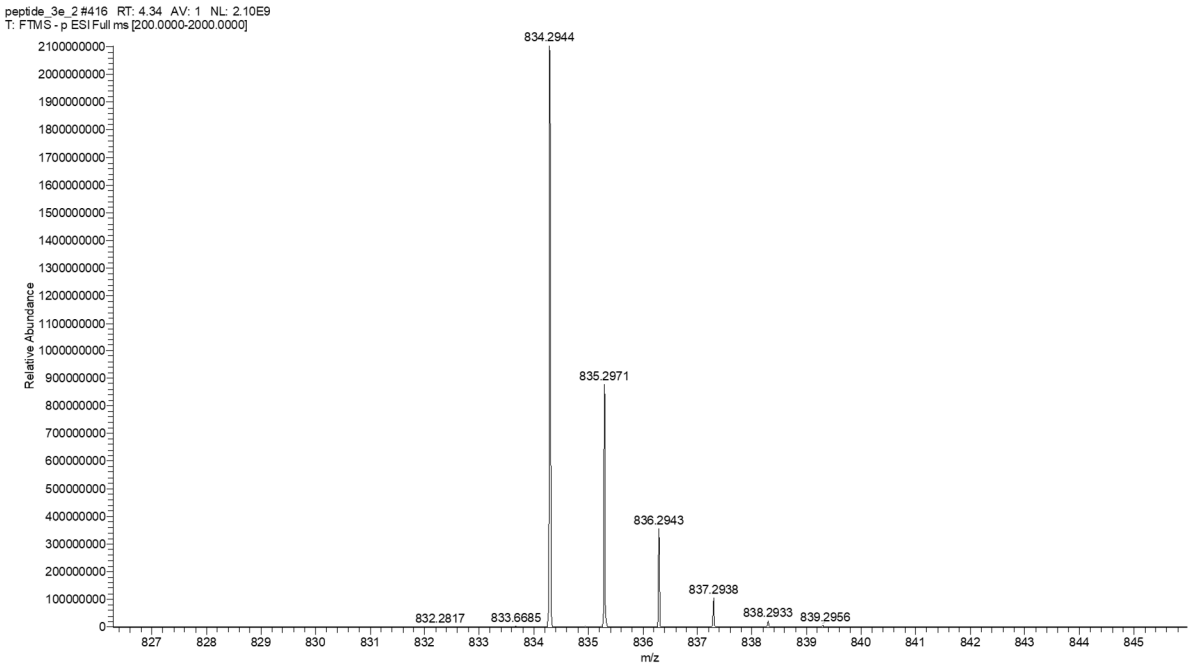

Ac-V-[CSELC]$_{cyclic}$-**A**-NH_2 (**3f**)

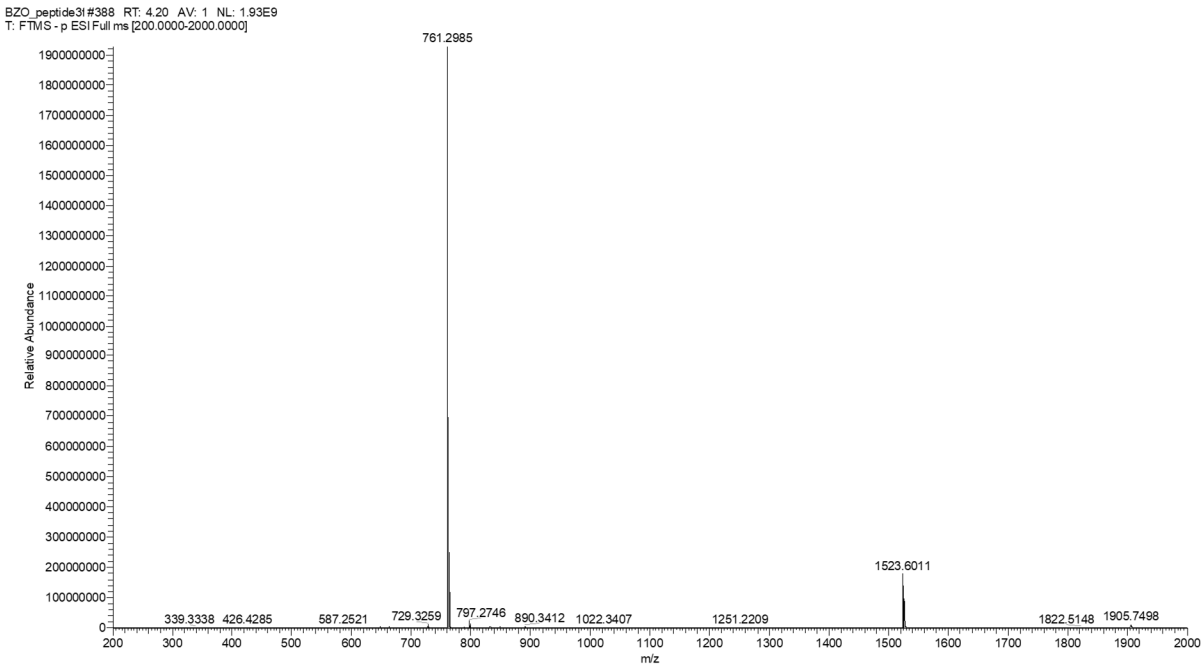

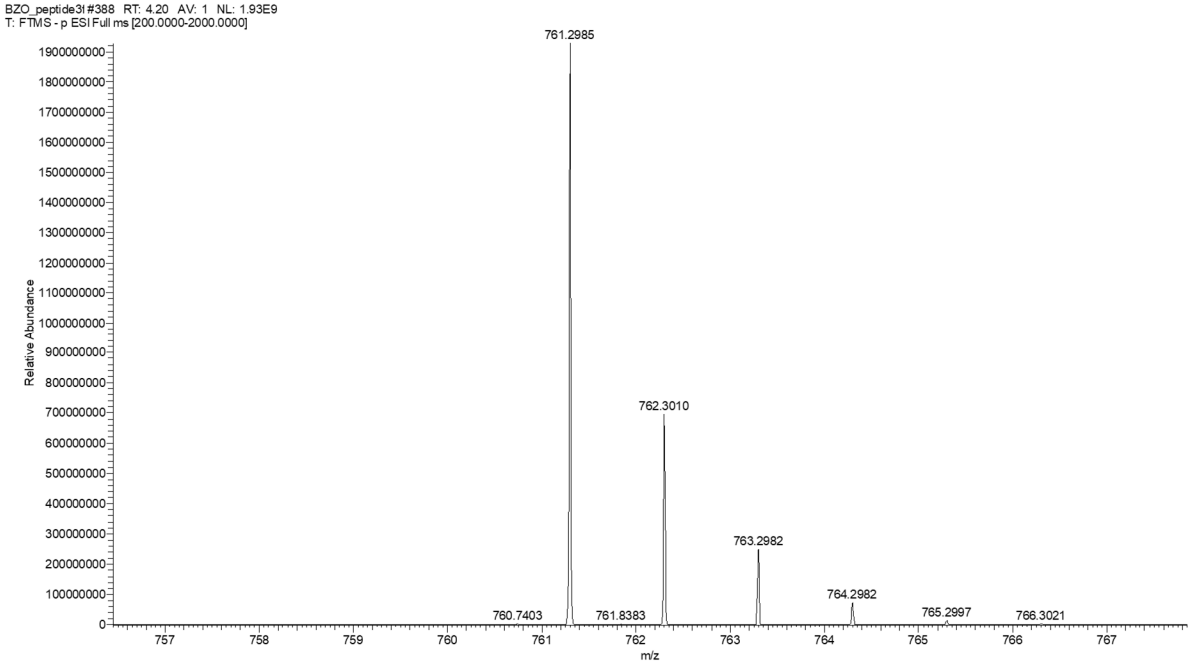

Ac- **–** -[CSELC]$_{cyclic}$-W-NH_2 (**4a**)

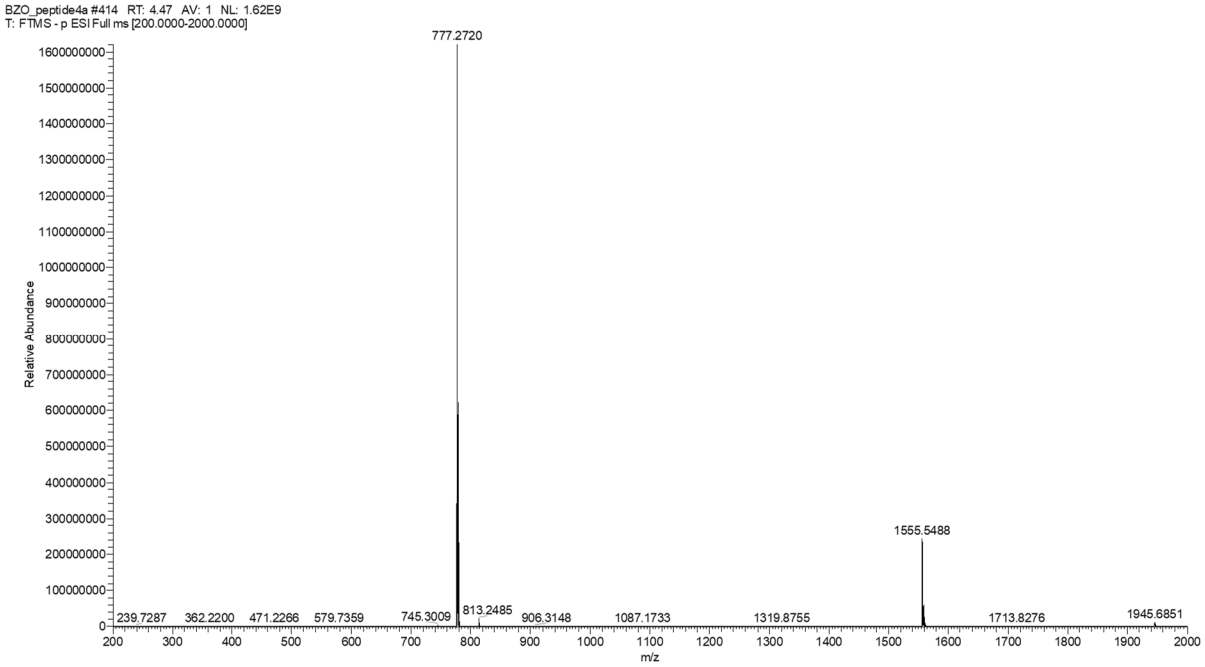

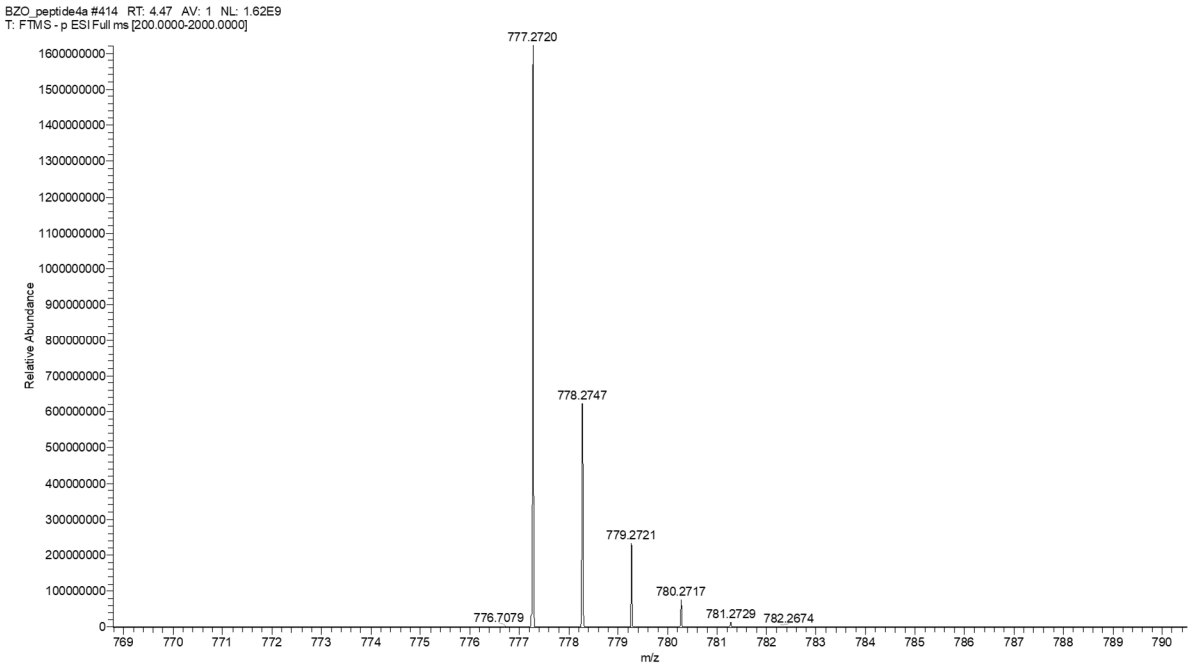

Ac-V-[CSELC]$_{cyclic}$ **–** -NH_2 (**4b**)

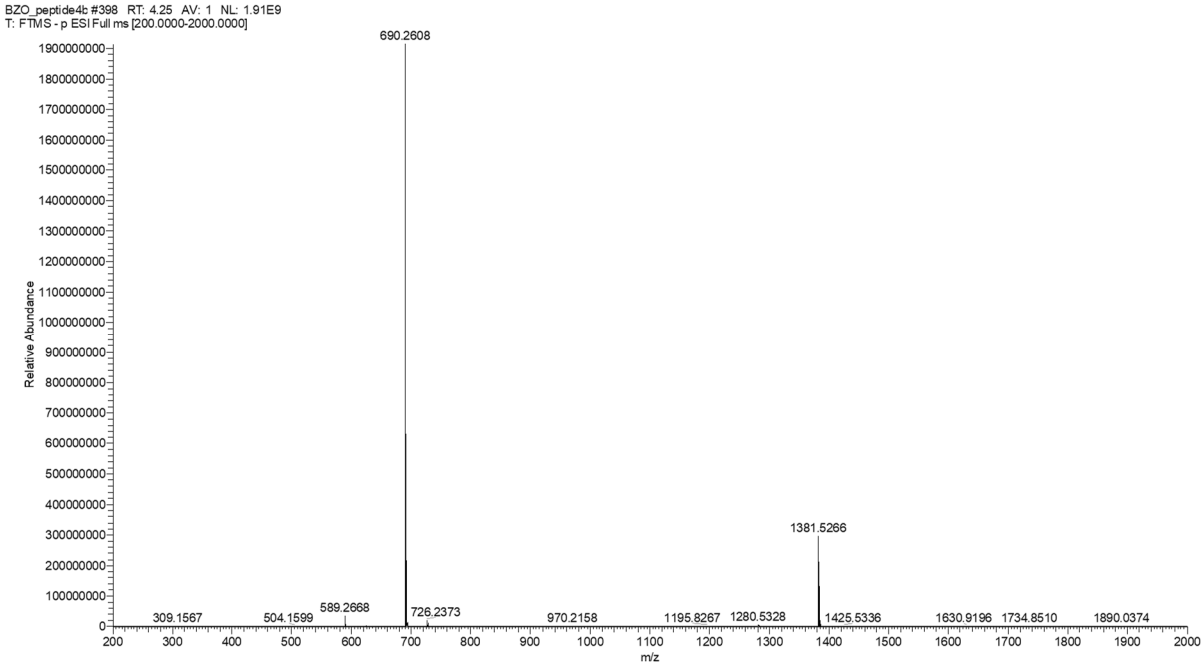

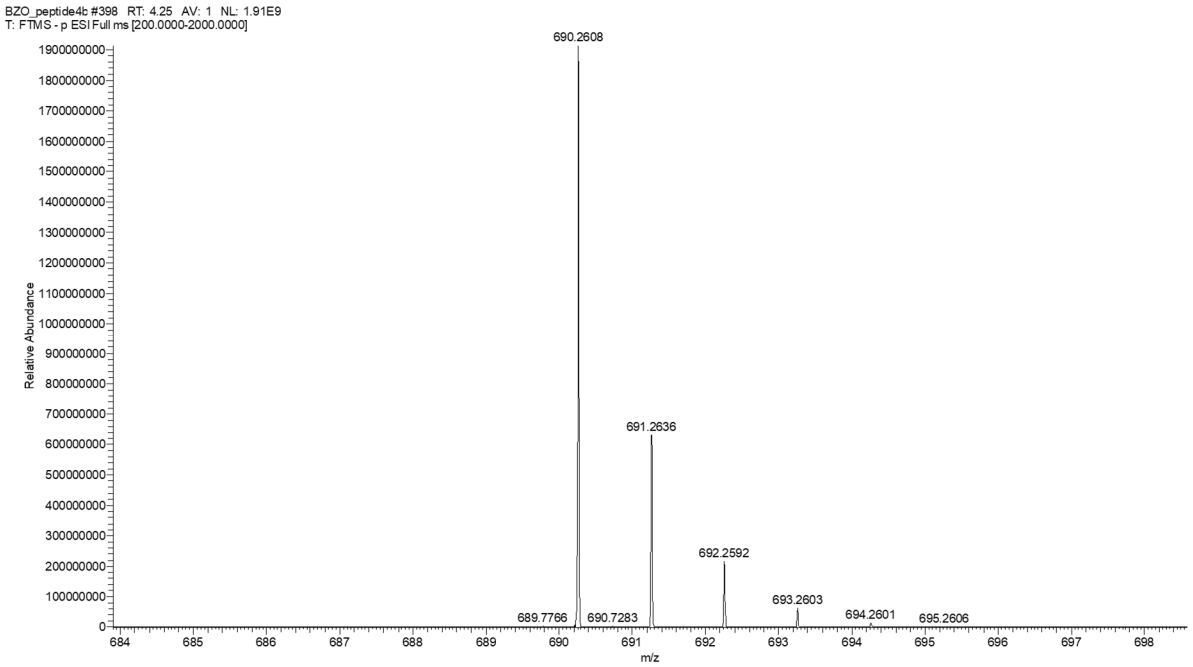

Ac-V-[**Pra**-SEL-**Aza**]$_{cyclic}$-W-*NH*$_2$ (1,4-triazole) (**5a**)

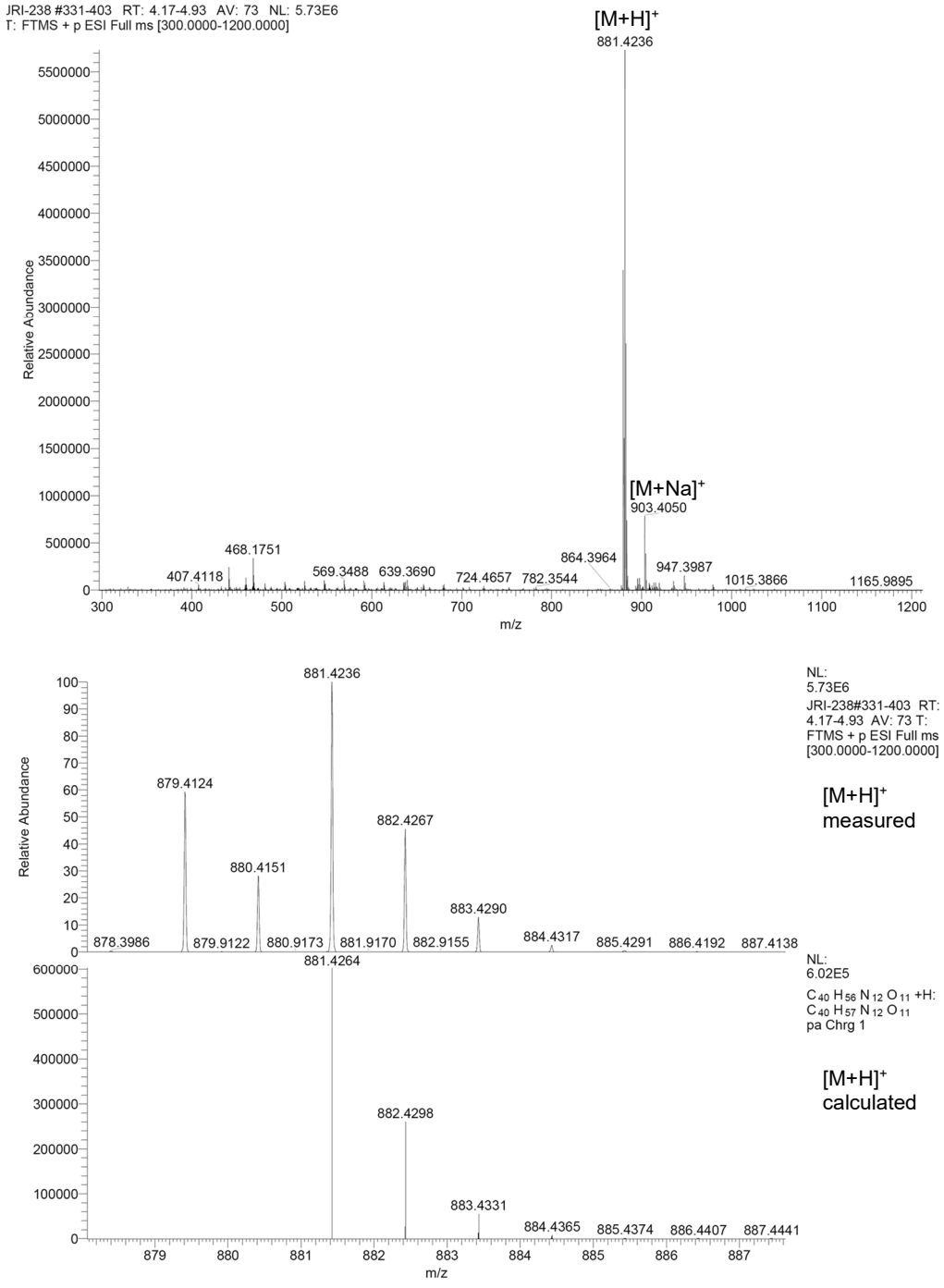

Ac-V-[**Aza**-SEL-**Pra**]$_{cyclic}$-W-*NH*$_2$ (1,4-triazole) (**5b**)

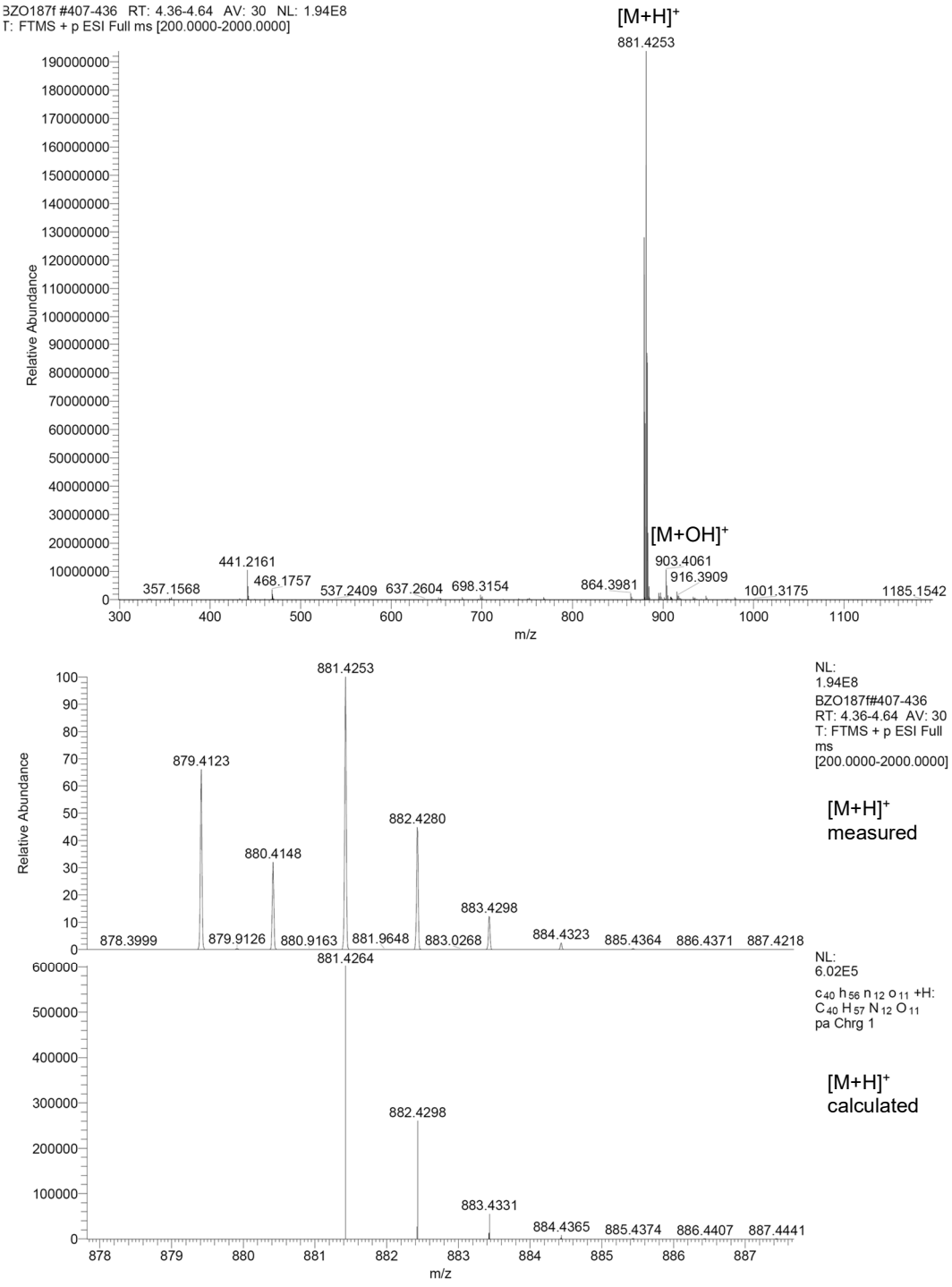

Ac-V-[**Pra**-SEL-**Aha**]$_{cyclic}$-W-NH_2 (1,4-triazole) (**5c**)

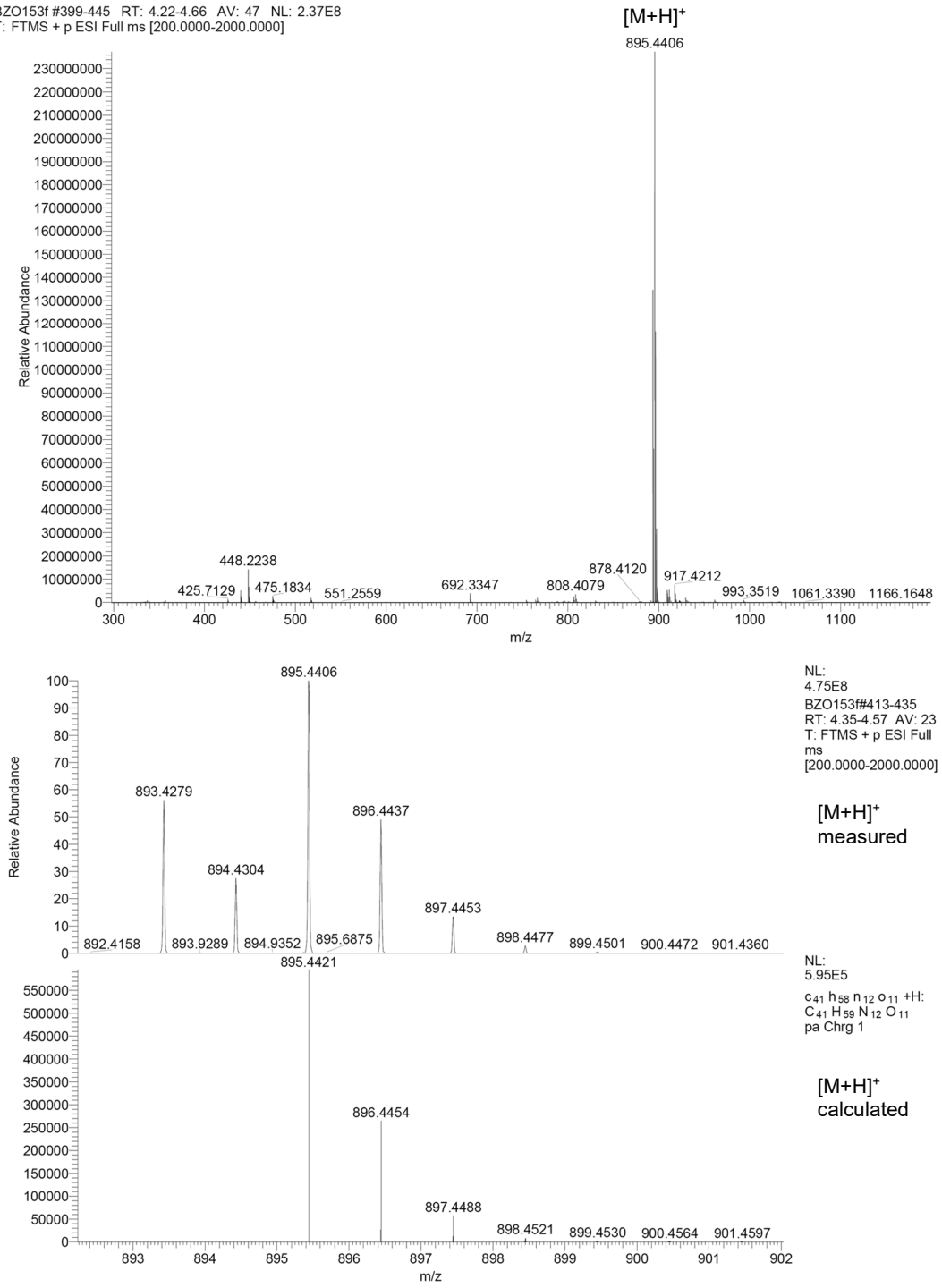

Ac-V-[**Pra**-SEL-**Aza**]$_{cyclic}$-W-NH_2 (1,5-triazole) (**6a**)

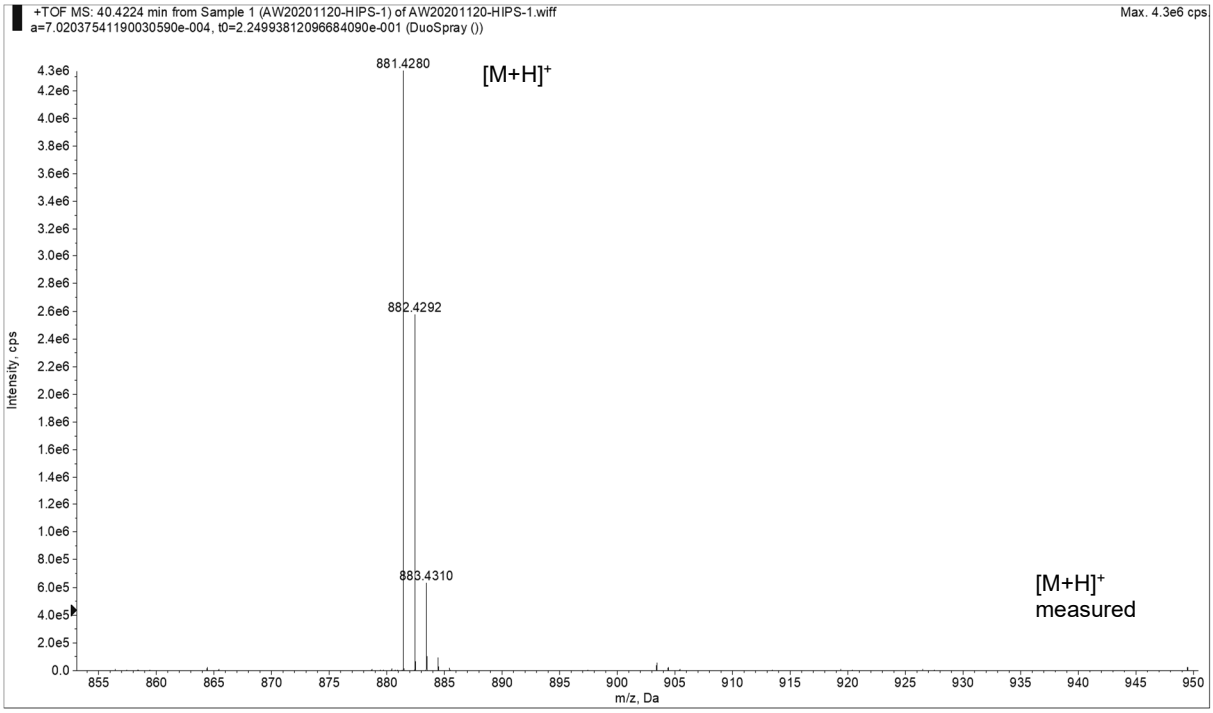

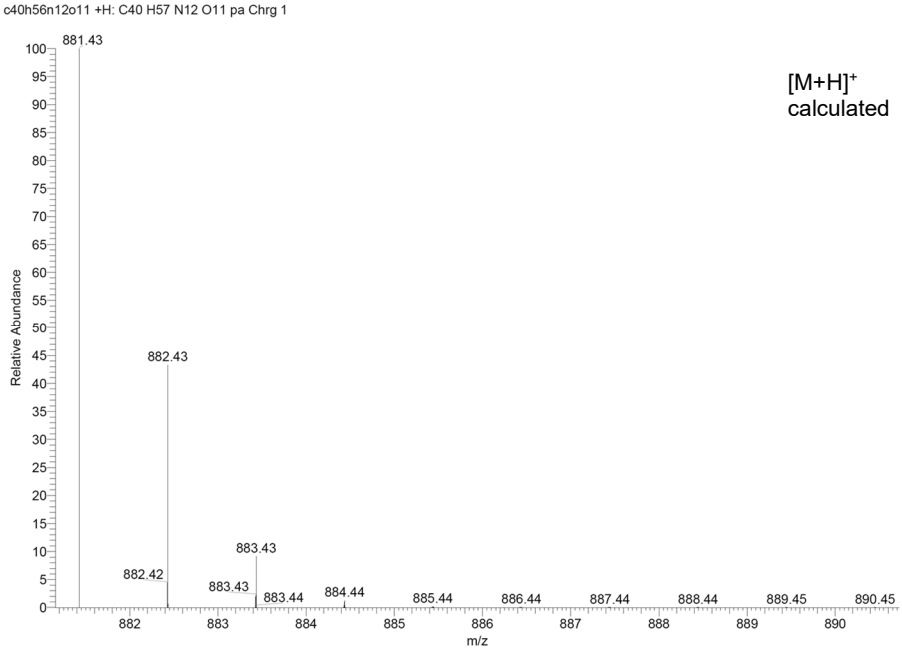

Ac-V-[**Pra**-SEL-**Aha**]$_{cyclic}$-W-*NH*$_2$ (1,5-triazole) (**6b**)

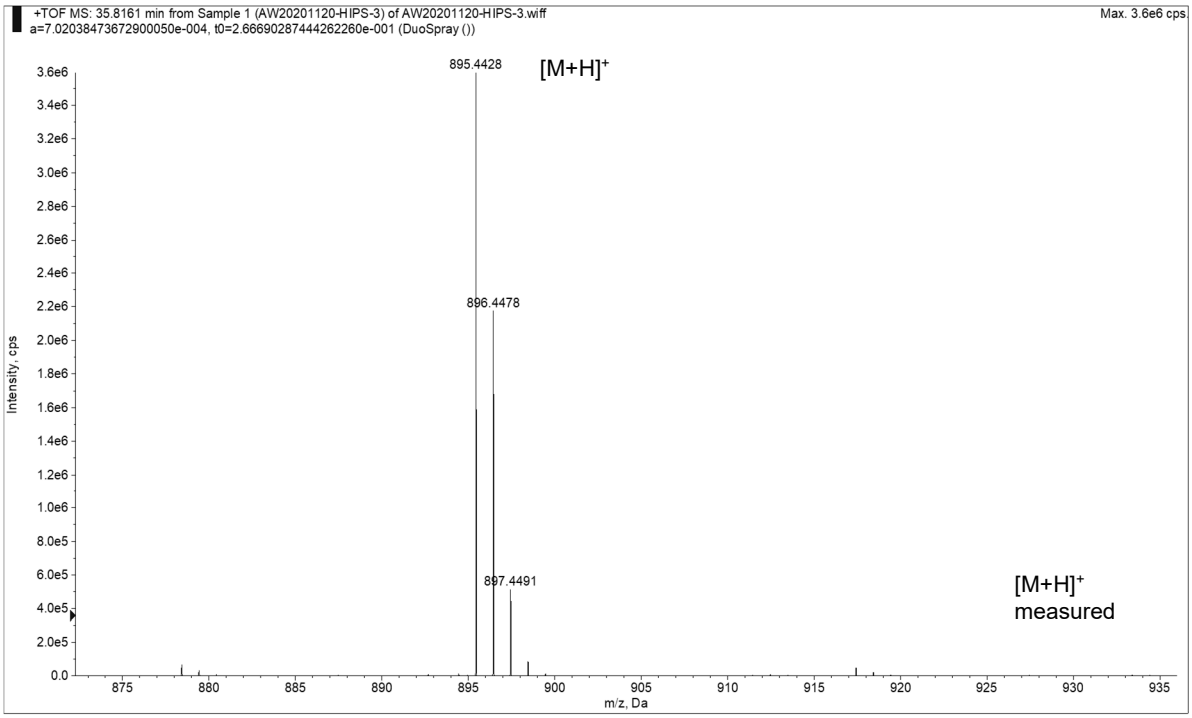

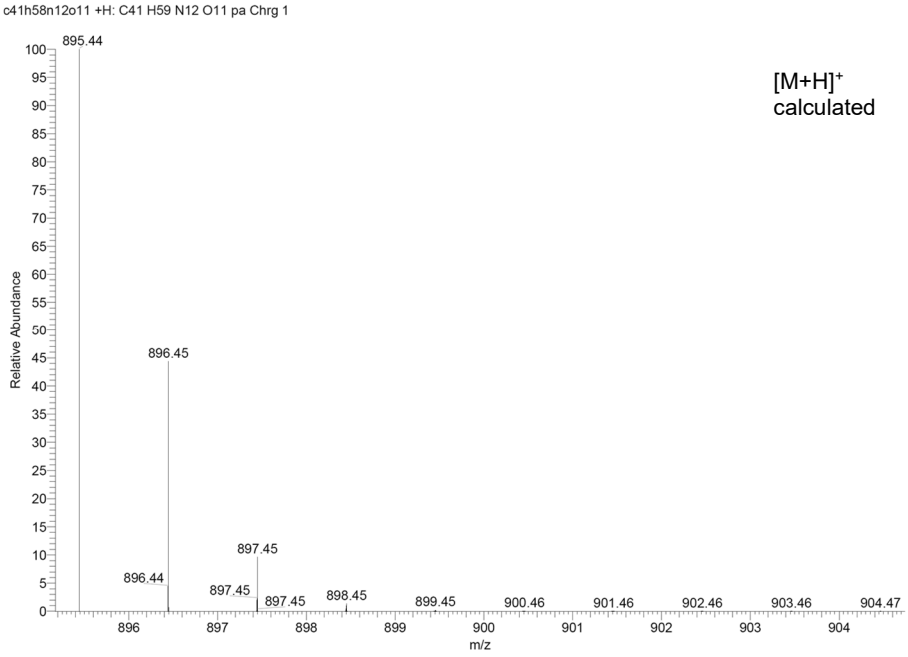

Ac-V-[**Aha**-SEL-**Pra**]$_{cyclic}$-W-*NH*$_2$ (1,5-triazole) (**6c**)

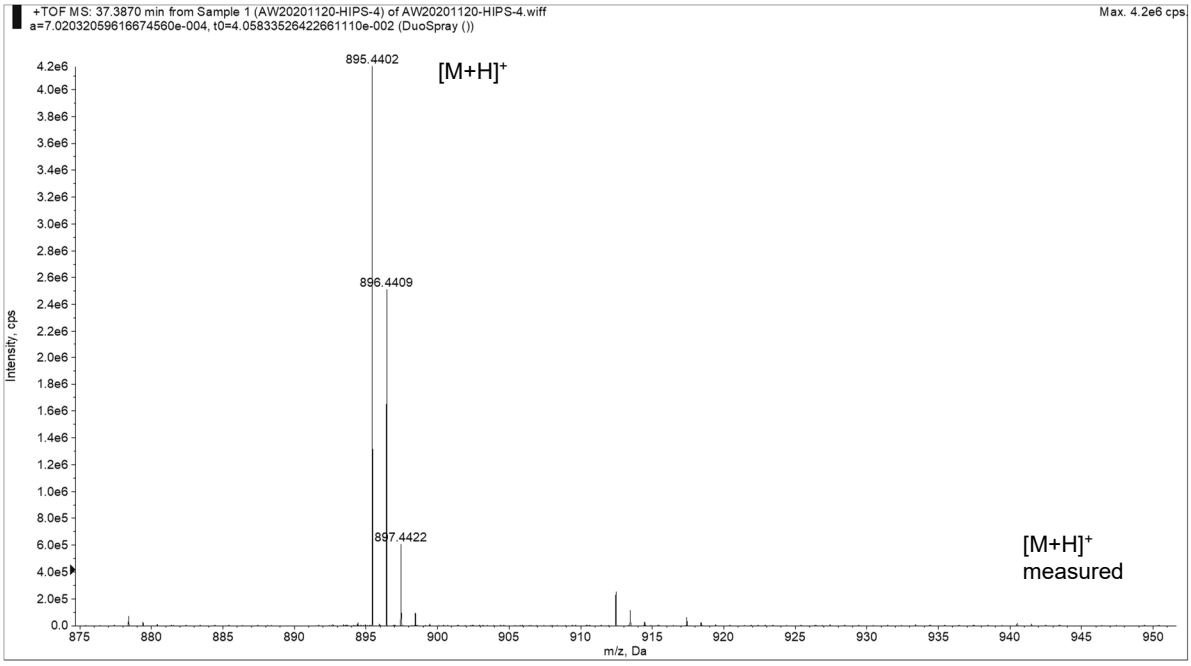

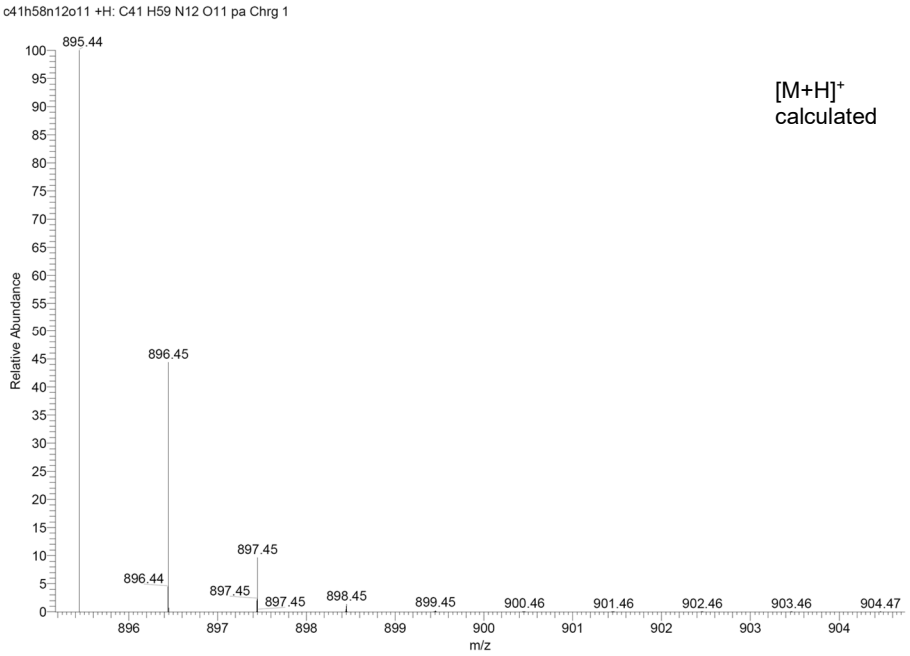

References

[1] C. K. Maurer, M. Fruth, M. Empting, O. Avrutina, J. Hoßmann, S. Nadmid, J. Gorges, J. Herrmann, U. Kazmaier, P. Dersch et al., *Future Med. Chem.* **2016**, *8*, 931–947.
[2] A. K. Dubey, C. S. Baker, T. Romeo, P. Babitzke, *RNA* **2005**, *11*, 1579–1587.
[3] V. Jakob, S. Helmsing, M. Hust, M. Empting in *Genotype Phenotype Coupling*, Springer US, New York, NY, **2020**, pp. 95–113.
[4] J. Kügler, S. Wilke, D. Meier, F. Tomszak, A. Frenzel, T. Schirrmann, S. Dübel, H. Garritsen, B. Hock, L. Toleikis et al., *BMC Biotechnol.* **2015**, *15*, 10.
[5] Y. Shen, A. Bax, *J. Biomol. NMR* **2013**, *56*, 227–241.
[6] A. T. Brünger, P. D. Adams, G. M. Clore, W. L. DeLano, P. Gros, R. W. Grosse-Kunstleve, J. S. Jiang, J. Kuszewski, M. Nilges, N. S. Pannu et al., *Acta Cryst.* **1998**, *D54*, 905–921.
[7] V. B. Chen, W. B. Arendall, J. J. Headd, D. A. Keedy, R. M. Immormino, G. J. Kapral, L. W. Murray, J. S. Richardson, D. C. Richardson, *Acta Cryst.* **2010**, *D66*, 12–21.
[8] Molecular Operating Environment (MOE), 2020.09 Chemical computing group ULC 2020.
[9] O. Duss, E. Michel, N. Diarra dit Konté, M. Schubert, F. H.-T. Allain, *Nucleic Acids Res.* **2014**, *42*, 5332–5346.
[10] E. Krieger, G. Koraimann, G. Vriend, *Proteins* **2002**, *47*, 393–402.

Author Contributions

Dr. Martin Empting conceived the concept of the study, interpreted the data of the presented idea and wrote parts of the manuscript.

Valentin Jakob wrote the manuscript, has done CsrA expression, performed the assays and involved in peptide synthesis and analytics.

Ben G. E. Zoller synthesized the peptides, performed the analytics and wrote parts of the manuscript.

Julia Rinkes involved in peptide synthesis and analytics and wrote some parts of the SI.

Yingwen Wu was involved in CsrA expression and in some assays, especially *E. coli* CsrA.

Dr. Alexander F. Kiefer contributed to peptide synthesis, data evaluation and processing and wrote parts of the manuscript.

Prof. Dr. Michael Hust and Saskia Helmsing taught us how to perform Phage Display and gave continuous support.

Andreas Siebert gave us an introduction how to handle the peptide synthesizer and was always a great help during the experiments with it.

The group of Prof. Dr. Uli Kazmaier provided the peptide synthesizer.

Dr. Andrew M. White synthesized compounds 6a, 6b and 6c, made parts of the analytics of these and wrote some parts of the SI.

Dr. Thomas Durek and Prof. David J. Craik were involved in planning and wrote parts of the manuscript.

Dr. Peta J. Harvey generated and deposited the NMR structures.